Pure

Bangor University

DOCTOR OF PHILOSOPHY

The identification of phytoplankton groups using in-water optical techniques

Shon, Dong Hyun

Award date:
2005

Awarding institution:
University of Wales, Bangor

Link to publication

General rights
Copyright and moral rights for the publications made accessible in the public portal are retained by the authors and/or other copyright owners and it is a condition of accessing publications that users recognise and abide by the legal requirements associated with these rights.

- Users may download and print one copy of any publication from the public portal for the purpose of private study or research.
- You may not further distribute the material or use it for any profit-making activity or commercial gain
- You may freely distribute the URL identifying the publication in the public portal ?

Take down policy
If you believe that this document breaches copyright please contact us providing details, and we will remove access to the work immediately and investigate your claim.

Download date: 18. Jun. 2024

The Identification of phytoplankton groups using in-water optical techniques

by

Dong Hyun Shon, B.Sc., M.Sc.

A thesis partial fulfilment of the requirements of the University of Wales for the degree of Doctor of Philosophy

May 2005

University of Wales, Bangor
School of Ocean Sciences
Menai Bridge
Anglesey LL59 5AB
UK

U.W.B LIBRARY
P.C.B. LLYFRGELL

ABSTRACT

The detection of an algal bloom from ocean colour sensors depends on the concentration of phytoplankton pigments when pigments, such as chlorophylls, produce a significant change in the optical properties of water. The pigment composition results in a characteristic colour, which can be measured using absorption spectra and spectral reflectance signatures. An Individual phytoplankton group contains a number of accessory pigments and has its own characteristic composition. Several of these pigments are restricted to 1 or 2 phytoplankton classes. As these marker pigments have distinctive absorption spectra, which determine a characteristic spectral signature for phytoplankton, they can be used as indicators of different phytoplankton classes. Using the High Performance Liquid Chromatography (HPLC) system, major accessory pigments contained in phytoplankton samples were analysed. *In situ* measurements of remote sensing reflectance were obtained at wavelengths coincident with the SeaWiFS visible wavebands using a Profiling Reflectance Radiometer (PRR600, Biospherical Instruments Inc). Group specific absorption spectra were generated according to the proportion of one of the marker pigment, fucoxanthin in the sum of pigments measured by HPLC. Remote sensing reflectance was modelled based on phytoplankton group specific absorption spectra and compared to the *in situ* remote sensing reflectance signatures.

CONTENTS

APPENDIX

ACKNOWLEDGEMENTS

I would like to express a sincere gratitude to Dr. Gay Mitchelson-Jacob for her supportive supervision. I am also grateful to Dr. Steve Mudge, Dr. Ian Lucas and Dr. Dave Bowers for taking parts in the committee. Special thanks to Dr. Dave Bowers for his invaluable advice and encouragement. Thanks to all the members of crew of the *R.V. Prince Madog* and the technical staff for their support. My appreciation goes to Caren Binding for letting me use the fluorometric chlorophyll *a* data from the Clyde Sea cruise in April 2001, the Irish Sea cruise in August 2001 and the Irish Sea cruise in November 2001. Thanks to Sean Gaffney for the CTD data from the cruises. Finally thanks to my wife, Wha-Young for her endless support and encouragement.

I dedicate this thesis to my wife, my parents in Seoul and newly born daughter, Ju-Hee, who gives me the greatest joy in the world.

나의 아내와 서울에 계신 부모님 그리고 세상에서 가장 커다란 기쁨을 선사한 새로 태어난 딸 주희에게 이 논문을 바칩니다.

1. GENERAL INTRODUCTION

The continuous observation of phytoplankton blooms from space greatly extends the knowledge of their spatial and seasonal succession trends. Information on the spatial and temporal distribution of phytoplankton is important for the global marine environment as they are the predominant primary producers. Such information also aids our understanding of the role of the ocean in the uptake of carbon dioxide ($CO_{2)}$.

The abundance and distribution of phytoplankton and other light attenuating components in the water can be estimated from ocean colour (Gordon and Morel, 1983). Phytoplankton have biochemical structures, containing pigments that allow them to absorb light energy and convert it through photosynthesis for growth and reproduction. Chlorophyll *a* is the major pigment for all algal groups and is used as a convenient measure of phytoplankton biomass (Gordon and Morel, 1983).

Remote sensing technology and *in-situ* optical measurements have improved the accuracy to which phytoplankton pigment concentration can be derived. Recent works have tried to distinguish between phytoplankton groups using optical instruments which measure changes in the optical properties of the in-water light field in natural assemblages (Cullen *et al.*, 1997). There are three major pigment groups that determine bio-optical properties; these are the chlorophylls, carotenoids and phycobiliproteins. Apart from chlorophyll *a*, the rest of the pigments are called accessory pigments. Each individual phytoplankton group has its own characteristic accessory pigment composition. Therefore it should be possible to differentiate a particular group of phytoplankton using the different composition of accessory pigments which creates distinct in-water optical properties, such as absorption, *a*, which influences reflectance,

R. Those optical parameters are described in the following chapter.

1.1. The principal characteristics of dominant phytoplankton classes in the U.K. shelf seas

The representative phytoplankton classes in north temperate seas are Bacillariophyceae (diatoms) and Dinophyceae (dinoflagellates) (Boney, 1989), while microbial blue-green (Cyanophyceae or Cyanobacteria), green (Chlorophyceae, Prochlorophyceae and Prasinophyceae), brown (Chrysophyceae and Prymnesiophyceae) coloured unicellular flagellates and Cryptophyceae are present in small numbers (Bold and Wynne, 1985). Most phytoplankton cells are covered by a dense wall. The wall is made of cellulose in some dinoflagellate and chlorophyceae; silica in diatoms and chrysophyceae; calcite or organic scales or both in Prymnesiophyceae; and protein for Cryptophyceae (Jeffery and Vesk, 1997). In this section, the characteristics of dominant groups of phytoplankton in the U.K. Shelf Seas are described. These are Bacillariophyceae, Dinophyceae, Prymnesiophyceae and Chrysophyceae.

1.1.1 Bacillariophyceae (Diatoms)

Bacillariophyceae, known as diatoms, are unicellular, although chains of cells and colonial aggregation may occur. Diatoms have a range of cell size from 2 μm to over 200 μm, while some tropical species and Antarctic *Thalassiothrix* have a size of 2 mm and 4 mm, respectively (Jeffery and Vesk, 1997). Diatoms are found in all aquatic (fresh and marine) and terrestrial or subaerial habitats, that have at least periodic moisture

(Bold and Wynne, 1985). All species have an external skeleton, or frustule, made of silica and fundamentally composed of two valves (Boney, 1989; Lalli and Parsons, 1997). The frustule is usually sculptured into patterns of spines, pores, channels, and ribs, which are distinctive to individual species. There are two types of diatoms: the pennate and centric forms. Pennate diatoms have on elongated shape and are mostly benthic (e.g. *Gyrosigma wormleyi*, Figure 1.1(a)). Centric diatoms have valves that are arranged radially or concentrically around a point, and they are much more common (e.g. *Cerataulina pelagica*, Figure 1.1 (b)). Centric diatoms do not have any locomotor structures and are normally incapable of independent movement. As diatoms and other plankton need to remain on the surface for photosynthesis, a variety of mechanisms and structures are developed. To retard sinking from the surface, their size and structure increase the ratio of cell surface area to volume. Colony or chain formation also increases surface area and slows sinking. The components of the frustule are divided into a variety of structures which can be visualised with the light microscope (Bold and Wynne, 1985). An elevation is a raised area of the valve wall which does not project laterally outside the margin of the valve. If the outgrowth of the valve projects beyond the valve margin, it is called a seta, and the structure is different from that of the valve. Setae are significant in increasing the surface area and enhance the ability to float (Bold and Wynne, 1985).

1.1.2. Dinophyceae (Dinoflagellates)

Dinophyceae comprise the dinoflagellates, a diverse assemblage of unicellular organisms (Bold and Wynne, 1985). The class is characterised by the presence of

chlorophyll *a*, and *c*; β -carotene; and the xanthophylls peridinin, neoperidinin, dinoxanthin, neodinoxanthin, and diatoxanthin. Dinoflagellate have a range of cell size from 2 μm to over 200 μm while, some species are 2 mm in diameter (Jeffery and Vesk, 1997). The cells may be unarmoured (naked) or armoured (thecate). The wall of armoured dinoflagellates is arranged in thecal plates, thin plates present in some apparently naked cells. Whether naked or armoured, the cell covering (amphiesma) consists of several membranes. The important constituent of the armour is a polysaccharide, apparently cellulose, whereas in the diatoms the wall elements are made of silica (Hoek *et al.*, 1995). The margins of these plates are slightly beveled and increase the cell size. The plates of dinophyceae armour resemble the silica elements of the diatom wall. However one difference is that in the dinophyceae the membrane outside the armour is intact, while in the diatoms the silica elements are exocytosed to lie outside the cell. One Dinophycean, *Ceratium furca,* found in the Menai Strait is presented in Figure 1.2. Species of the genus *Ceratium* are characterised by the presence of several horns. The apical half of the cell extends up into a single horn, while the antapical half bears one to three horns (Bold and Wynne, 1985).

1.1.3 Prymnesiophyceae (Haptophyceae)

The size of most Prymnesiophyceae is between 5 μm and 20 μm (Jeffery and Vesk, 1997). This class comprises organisms that produce motile cells bearing two equal, subequal, or unequal acronematic flagella, with homodynamic or heterodynamic motion. The composition of scales is organic and cellulosic. A deposition of calcite (coccoliths) may be present on the surface of a second type of scale produced in the

coccolithophores, which constitute a large group within this class. For example, the cells of *Pleurochrysis carterae* are covered by several layers of organic scales with an outer layer of coccoliths (Hoek *et al.*, 1995). Coccolithophore blooms produce a bright reflectance signature because the calcareous scales (or liths) are highly reflective. As a result, this bloom can be distinguished from other blooms using ocean colour imagery in the red region of spectrum. Figure 1.3 (a) shows one of the representative coccolithophores, *Emiliania huxleyi*. Scales are produced within Golgi vesicles for all prymnesiophytes. The form of the Golgi body is very distinctive and regarded as one of the diagnostic features of the class. The single polarised Golgi body is always located between the base of the flagella and the nucleus (Bold and Wynne, 1985). Silica is not produced in Prymnesiophyceae. Almost all members of this class have at least some type of cell covering. In some of the filamentous or packet-forming genera, such as *Gloeothamnion* and *Chrysotila*, the cell covering changes with the age of the culture.

Phaeocystis pouchetii (Figure 1.3 (b)) have been found in the North Sea (Bold and Wynne, 1985). There are two phases of life cycle in this species; a unicellular flagellate phase and a gelatinous colonial phase, the latter being the bloom-forming stage. Figure 1.3 (b) shows a gelatinous colony which contains a large number of cells. Both phases, colonies and flagellated cells, can be simultaneously present in the same culture and can reproduce independently (Bold and Wynne, 1985). In the North Sea, the *Phaeocystis* bloom develops in mid-April or in May, after the spring diatom bloom, which is brought to an end by the depletion of silicate used by the diatoms for the construction of their frustules. The *Phaeocystis* bloom in the Menai Strait occurs in June and July (Newton, 1986).

1.1.4 Chrysophyceae

The class Chrysophyceae comprises unicellular and colonial organisms, but there are also some filamentous forms and multicellular types. The size of Chrysophyceae is from 2 μm to 100 μm (Jeffery and Vesk, 1997). This class has a golden yellow to brown colour in their chloroplasts. The green colour of the chlorophyll is masked by the principal accessory pigment fucoxanthin. Other xanthophylls are also present, including zeaxanthin, antheraxanthin, violaxanthin, diatoxanthin and diadinoxanthin (Hoek *et al.*, 1995). Many chrysophycean algae have naked protoplasts, while others have various cell coverings, including scales, loricas, and close-fitting cell walls. One of the most distinctive features of this class is the internal formation of a characteristic cyst, or statospore. The statospore (Figure 1.4 (a)) consists of two pieces of different size. The larger portion is first developed within the cytoplasm, and the cytoplasm external to this bottle-shaped piece migrates into it. A plug is finally formed at the mouth (Bold and Wynne, 1985). The wall of the statospore is always siliceous unlike the lorica of vegetative cells, which are cellulosic in composition, with or without the addition of calcium carbonate or iron compounds (Bold and Wynne, 1985). A chrysophyceae, *Meringosphaera mediterranea*, is shown in Figure 1.4 (b).

1.2 Phytoplankton variability in specific areas of study

In north temperate seas, the phytoplankton succession starts with small celled fast growing diatoms, such as the members of the genera *Thalassiosira*, *Chaetoceros* and *Skeletonema* (Boney, 1989). They are capable of high photosynthetic rates and rapid cell

division, as well as requiring high nutrient levels. Phytoplankton populations at the early stage are followed by medium sized and slow growing diatoms (e.g. *Rhizosolenia* species and *Guinardia flaccida*) and by dinoflagellates (e.g. species of *Ceratium* and *Protoperidinium*) (Hoek *et al.*, 1995). Other flagellate groups with more complex nutritional requirements (e.g. green algae, blue-green algae) occur later the year (Bold and Wynne, 1985; Boney, 1989; Hoek *et al.*, 1995). This section describes the succession of phytoplankton population in the Menai Strait, the Clyde Sea, the Irish Sea and the Celtic Sea.

1.2.1 The Menai Strait.

In the Menai Strait there is normally a multi-species bloom in April or May followed by a secondary bloom later in the year dominated by individual species such as *Phaeocystis pouchetti*. This pattern of increasing concentration of phytoplankton is closely related to the coastal temperature (Jones and Spencer, 1970; Blight, 1996). During the spring, a bloom of various *Rhizosolenia* species (diatoms) is observed in May, while *Phaeocystis* species, which dominate phytoplankton composition for extended periods in the early summer, succeeds the spring diatom bloom in June (Jones and Spencer, 1970; Blight, 1996). Lennox (1979) investigated the triggers of the *Phaeocystis* bloom in relation to the influence of seasonal micronutrients and physical variables. One of the reasons of decrease in small sized early diatom population is the depletion of silica, which is one of the main nutrients for diatoms, while another reason is the increase in grazing rate of herbivorous zooplankton (Boney, 1989). After a *Phaeocystis* bloom, the summer decline in phytoplankton population may be less attributable to zooplankton grazing because the

larger diatoms, dinoflagellates and flagellates are less subject to predation (Boney, 1989). The *Phaeocystis* bloom, which normally occurs in May or June, has considerable impact on the east coast of Anglesey because once *Phaeocystis* starts to decompose it forms mats and smothers area of the sea bed (Young 1993). During the autumn, the population of phytoplankton (predominantly dinoflagellates) is less abundant than in earlier blooms due to the lower concentration of nutrients and differences in light exposure (Jones and Spencer, 1970). However, if the autumn growth is measured in terms of biomass or volume, it may equal that of spring (Boney, 1989).

Four classes of phytoplankton species have been found in the Menai Strait (Lennox, 1979; Newton, 1986); these are Dinophyceae (dinoflagellates), Prymnesiophyceae (Haptophyceae), Chrysophyceae and Bacillariophyceae (diatom). Newton (1986) studied the succession of phytoplankton and made counts of phytoplankton cell numbers and measured cell volumes, to determine the relative importance of the various species. Sixty-one species were found in 1983. Three diatoms, *Fragilaria oceanica*, *Coscinodiscus* species, and *Rhizosolenia fragilissima* were predominant species for both counts and volume, while the Prymnesiophyceae (Haptophyceae), *Phaeocystis pouchetti* has a large number but low volume of cells. However, the annual highest concentration of chlorophyll *a* was found during *Phaeocystis pouchetti* bloom (Blight, 1996).

1.2.2 The Irish Sea

Vertically mixed and stratified water zones are present in the Irish Sea, like the rest of the UK and European shelf seas, during the main spring-summer phytoplankton growth

season. These boundaries at the sea surface between the mixed and stratified zones are sharply delineated and are called fronts or frontal zones. The location of fronts is related to the velocity of the local tidal streams (Simpson, 1971). In the mixed zone phytoplankton growth is limited by availability of light as the mixing restricts the residence time of phytoplankton within the well lit surface layers of the sea, while in the stratified zone phytoplankton growth is restricted by limited nutrient input from the deep water to the surface layer of the sea through the thermocline. Phytoplankton increases are closely related to the physical structure of the frontal region, where the availability of nutrient and light is optimised as a result of accumulations of biological material due to the physical convergence of waters on either side of the front (Simpson *et al.*, 1979).

Voltolina (1980) and Spencer (1988) studied phytoplankton species composition in Liverpool Bay. They found that diatoms, such as *Skeletonema costatum*, *Thalassiosira decipiens*, *Asterionella septentrionalis* and *Navicula pelagica* are dominant species during the spring bloom in the eastern Irish Sea.
Silicate depletion following the early diatom bloom contributes to the dominance of flagellates and especially *Phaeocystis* species which may form large blooms in May (Voltolina, 1980). *Phaeocystis* is generally common from North Wales to the Solway Firth and can become a nuisance through foam generation in coastal areas.

Blooms of red-tide organisms, in particular the dinoflagellate, *Gyrodinium aureolum*, which are linked to the increase in organic pollution, have been reported in the inshore water of south-east Liverpool Bay (Helm *et al.*, 1974). Red-tide blooms in Liverpool Bay occur mostly in the late summer-autumn period. In addition, the heterotrophic dinoflagellate *Noctiluca scintillans* has been frequently observed in

Liverpool Bay (Helm *et al.*, 1974). The presence of *Noctiluca scintillans* has also been reported locally in the Irish inshore water (Savidge and Kain, 1990).

In the western Irish Sea, diatoms, *Chaetoceros debilus* and *Chaetoceros compressus*; *Thalassiosira decipiens* and *Thalassiosira rotula*; and *Skeletonema costatum* are commonly found during the spring bloom (McKinney *et al.*, 1997). During the summer *Leptocylindrus danicus* and *Rhizosolenia delicatula* dominate the diatom population. In general, dinoflagellates do not appear to dominate the summer phytoplankton in the western Irish Sea. *Noctiluca scintillans* and *Phaeocystis pouchetti* have been observed in the western Irish Sea. (McKinney, *et al.*, 1997)

1.2.3 The Clyde Sea

Commonly found diatoms in the first stages in the spring outburst in March 1973 were *Skeletonema costatum* and *Thalassiosira nordenskioldii* in the Firth of Clyde (Boney, 1989). In the middle of March 1973, *Thalassiosira nordenskioldii* was more prominent. However, within a few days the faster growing *Skeletonema costatum* overtook *Thalassiosira nordenskioldii*, reaching maximum numbers (10.7×10^6 cells l^{-1}) on the 23rd of March, thereafter declining rapidly (Boney, 1989). The decline of spring growth was reflected in the fall in the levels of nutrients, with that of dissolved silica being especially decreased (Bold and Wynne, 1985). Species of *Chaetoceros*, *Coscinodiscus* and *Biddulphia* are also prominent in north temperate coastal localities during the spring (Bold and Wynne, 1985; Hoek *et al.*, 1995).

1.2.4 The Celtic Sea

Martinjezequel and Videau (1992) investigated the phytoplankton population and productivity over the transient area of the continental-slope of the Celtic Sea in May 1987. They found that chlorophyll biomass and primary productivity increased proportionally to the stratification in the stratified zone, while the highest biomass of diatom and dinoflagellates were observed in the transitional water. Diatoms tend to dominate the population in the mixed water, while flagellates are more abundant in the surface water on the stratified side (Boney, 1989; Martinjezequel and Videau, 1992) In the Celtic Sea, the dinoflagellates *Gonyaulax verior*, *Ceratium furca*, *Ceratium fusus and Prorocetrum micans*, *Protoperidinium steinii* are dominant in the summer (Johnson and Costello, 2002). Commonly found diatoms during the spring are *Thalassionema nitzschioides*, *Cylindrotheca closterium* and *Rhizosolenia* species (Fasham *et al.*, 1983; Prestidge and Taylor, 1995).

1.3 The aims of the study

The combination of accessory pigments within phytoplankton cells can provide valuable information for the identification of taxonomic groups. Using the High Performance Liquid Chromatography (HPLC) system major accessory pigments contained in phytoplankton samples have been analysed. The pigment composition of phytoplankton produce a characteristic colour, that can be measured using absorption spectra and spectral reflectance signatures. Absorption spectra are to be measured and divided into four groups according to the proportion of a marker pigment for diatom in

the sum of all marker pigments. Then the chlorophyll specific absorption coefficients are to be used to develop modelled remote sensing reflectance.

The aim of this study is to optically differentiate phytoplankton groups classified due to the proportion of a marker pigment, fucoxanthin in the sum of all marker pigments used in the study.

To achieve the aim, specific objectives are as follows. Firstly, different taxonomic groups of phytoplankton will be identified using visual microscopy and marker pigments for dominant group of phytoplankton will be determined using HPLC (High Performance Liquid Chromatography). Secondly, *in situ* remote sensing reflectance signatures will be collected using a profiling radiometer, and absorption spectra will be measured using a spectrophotometer. Finally, grouped specific absorption spectra will be used to derive modelled remote sensing reflectance ratio.

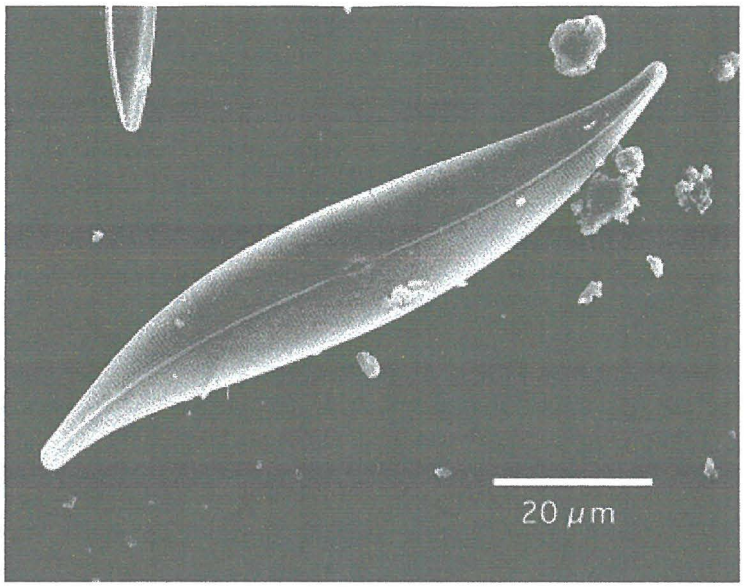

Figure 1.1 (a) Examples of Bacillariophyceae found in the Menai Strait *Gyrosigma wormleyi* (from Tiffany and Lange, 2000)

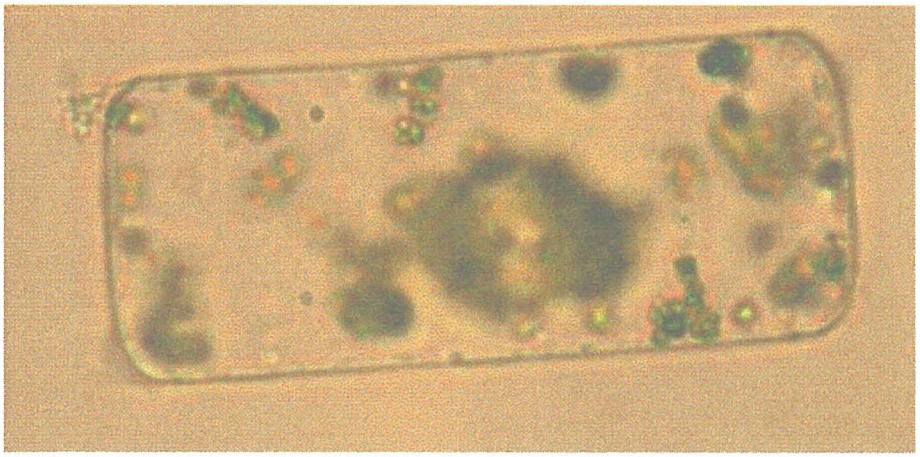

Figure 1.1 (b) Examples of Bacillariophyceae found in the Menai Strait *Cerataulina pelagica* (from Embleton, 2000)

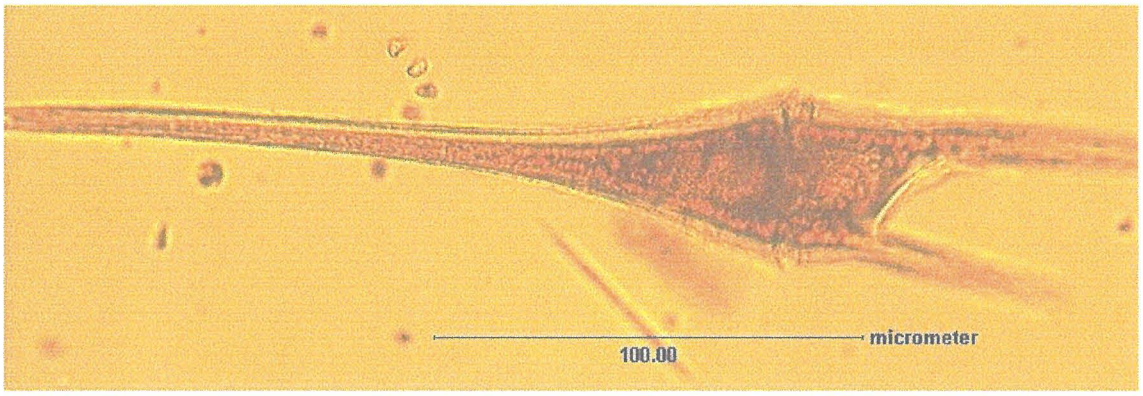

Figure 1.2 *Ceratium furca* (from Embleton, 2000)

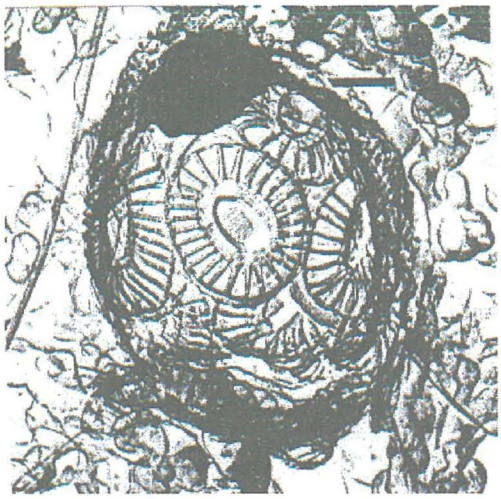

Figure 1.3 (a) Examples of Prymnesiophyceae found in the Menai Strait *Emiliania huxleyi* (from Hoek *et al.*, 1995)

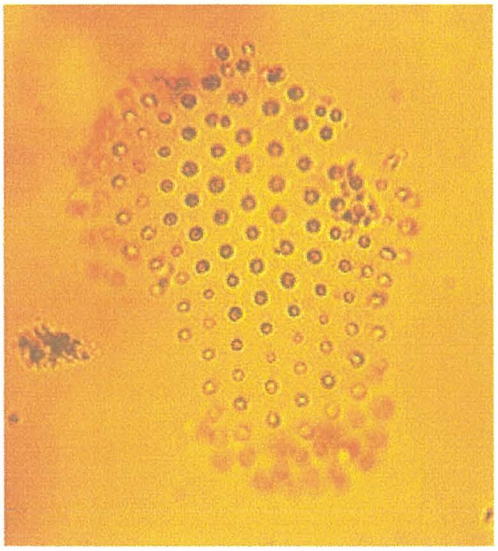

Figure 1.3 (b) Examples of Prymnesiophyceae found in the Menai Strait *Phaeocystis pouchetii* (from Embleton, 2000)

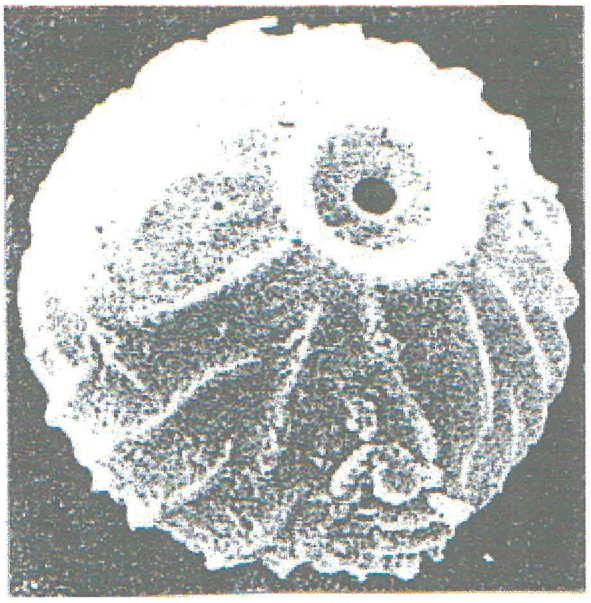

Figure 1.4 (a) Examples of Chrysophycean statospore (from Bold and Wynne, 1985)

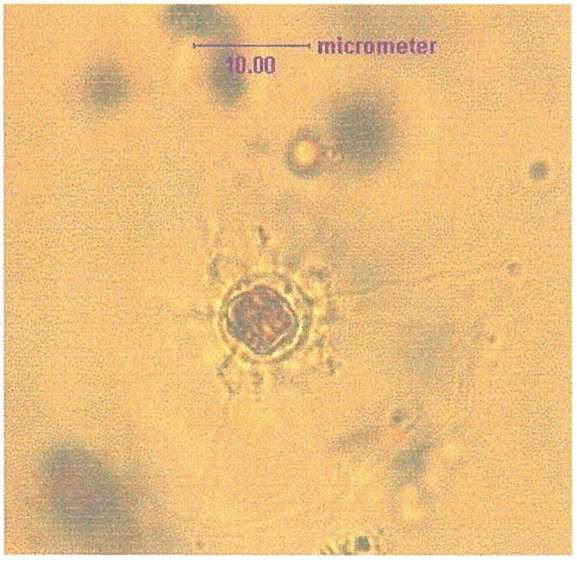

Figure 1.4 (b) Examples of Chrysophyceae, *Meringosphaera mediterranea* (from Embleton, 2000)

2. PIGMENT COMPOSITION AND SPECTRAL CHARACTERISATION

2.1 Introduction

This chapter reviews optical properties and parameters of marine environments. The effects of sea water and its constituents on the absorption spectral signal, with particular emphasis on the influence of phytoplankton are defined, while algorithms for the phytoplankton biomass measurement are briefly introduced. In addition, optical determination of phytoplankton groups using their unique pigment composition is discussed. The past and current ocean colour sensors are described in the final part of this chapter.

2.2 The derivation of radiance, irradiance and reflectance

This section defines optical parameters, radiance, irradiance and reflectance. The definition of zenith angel, θ, is the angle between a downward beam light and the upward vertical, while the azimuth angle, ϕ, is defined as the angle between a vertical plane incorporating the light beam and other reference vertical plane (e.g. the vertical plane of the Sun) (Jerlov, 1976; Preisendorfer, 1976; Kirk, 1994). The radiant intensity, I, is described as follow (Kirk, 1994);

$$I = d\Phi/d\omega \qquad (2.1)$$

where $d\Phi$ is the radiant flux and $d\omega$ is a unit solid angle. Radiance $L(\theta,\phi)$, which

indicates a function of direction (i.e. both zenith and azimuth angle), is defined as the flux per the projected area of surface, dS $\cos\theta$, and the unit solid angle dω (Kirk, 1994);

$$L(\theta,\phi) = d^2\Phi / dS \cos\theta \, d\omega \tag{2.2}$$

The irradiance due to radiant flux within dω, is defined as, $L(\theta,\phi) \cos\theta \, d\omega$, as the area of the element of surface is dS. The total downwelling irradiance, E_d, or upwelling irradiance, E_u, can be described by integrating with respect to solid angle over the whole upper or lower hemisphere (Kirk, 1994). They are defined as;

$$E_d = \int_{2\pi} L(\theta,\phi) \cos\theta \, d\omega \tag{2.3}$$

$$E_u = \int_{-2\pi} L(\theta,\phi) \cos\theta \, d\omega \tag{2.4}$$

For the irradiance, the contribution of the radiation flux at different angles depends on proportion to the cosine of the zenith angle of incidence of the radiation, while the scalar irradiance, E_0, receives the radiant flux from all directions equally. The scalar irradiance is described as the integral of the radiance distribution at a point over all directions (Kirk, 1994);

$$E_0 = \int_{4\pi} L(\theta,\phi) \, d\omega \tag{2.5}$$

The scalar irradiance is divided into down welling and upwelling scalar irradiance. The

down welling scalar irradiance, E_{0d}, is the integral of the radiance distribution over the upper hemisphere and upwelling scalar irradiance, E_{0u}, is the integral of the radiance distribution over the lower hemisphere;

$$E_{0d} = \int_{2\pi} L(\theta,\phi)\, d\omega \tag{2.6}$$

$$E_{0u} = \int_{-2\pi} L(\theta,\phi)\, d\omega \tag{2.7}$$

The irradiance reflectance, R, which provides information about the angular structure of the light field, is defined as the ratio between upwelling and down welling irradiance, while the remote sensing reflectance R_{rs}, is defined as the ratio between upwelling nadir radiance, L_u, and down welling irradiance (Kirk, 1994);

$$R = E_u / E_d \tag{2.8}$$

$$R_{rs} = L_u / E_d \tag{2.9}$$

2.3 The relationship between reflectance, R and absorption coefficient, a

A photon can be absorbed or scattered underwater. The absorption coefficient, a, and the scattering coefficient, b, are the inherent optical properties of particular interest in ocean optics (Kirk, 1994). The absorption coefficient, a, is defined as the proportion of incident photons absorbed by a thin slab of water divided by the thickness of the slab, while the scattering coefficient, b, is defined as the proportion of photons scattered by a

thin slab divided by the thickness of the slab. A third inherent property, the beam attenuation coefficient, c, is equal to the amount of the light lost due to absorption and scattering, and is expressed as follows.

$$c = a + b \tag{2.10}$$

The vertical attenuation coefficient for down welling irradiance, K_d can be related to inherent optical properties using the equation, which links the average cosine of the light field and the absorption coefficient (Kirk, 1994);

$$K_d = \frac{1}{\mu_d}\ a \tag{2.11}$$

The mean cosine of the angle of photons from the vertical, μ_d, is defined as the ratio between the downwelling irradiance, E_d, and scalar downwelling irradiance, E_{0d};

$$\mu_d = \frac{E_d}{E_{0d}} \tag{2.12}$$

The range of the mean cosine is from 0.6 to 1 in the ocean. Therefore without information about the shape of the light field, and assuming the mean cosine has a value of 0.8, downwelling attenuation coefficient, K_d, can be estimated from a with a maximum error of 25 %. The mean cosine can be determined accurately from the refracted solar zenith angle near the surface of the ocean. It provides more accurate

determination of K_d from a (Kirk, 1994). A useful result of μ_d from computer modeling can be given as follows (Kirk, 1994);

$$\mu_d = \frac{1}{(1 + 0.256\, b/a)^{1/2}} \tag{2.13}$$

From the equation above K_d can also be described;

$$\frac{K_d}{a} = \frac{1}{\mu_0}\left(1 + 0.256\ \frac{b}{a}\right)^{1/2} \tag{2.14}$$

where μ_0 is the mean cosine just beneath the surface.

The relationship between near-surface reflectance, $R(0)$, and absorption, a, and backscattering, b_b, can be described as follows using a Monte Carlo study (Gordon *et al.*, 1975).

$$R(0) = E_u/E_d = C(\mu_0)\, b_b / a \tag{2.15}$$

where E_u is upwelling irradiance, E_d is downwelling irradiance. The constant of proportionality, $C(\mu_0)$, is a function of solar altitude, which can be expressed in terms of μ_0, the cosine of the zenith angle of the refracted solar beam, below the surface. For the zenith sun, when μ_0 is 1 the coefficient $C(1.0)$ is approximately equal to 0.33 (Gordon *et al.*, 1975).

The ratio between upwelling irradiance, E_u, and upwelling radiance, L_u, is approximately 5 for intermediate solar altitudes (Kirk, 1994). An equation relating

remote sensing reflectance, R_{rs} (L_u/E_d) to backscattering coefficient, b_b, and absorption coefficient a may be derived from equation 2.15 by dividing the constant of proportionality, C, by 5. R_{rs} for a solar altitude of 45° gives the relation as follows (Kirk, 1994).

$$R_{rs} = L_u / E_d \approx 0.083\ b_b / a \qquad (2.16)$$

From this relationship (equation 2.16), both remotely-sensed and *in situ* reflectance measurements can be used to estimate absorption a, and vice versa.
Gordon *et al.* (1988), and Garver and Siegel (1997) developed a model for waters where the optical properties are dominated by the presence of phytoplankton to define the relationship between, R_{rs}, and a and b_b;

$$R_{rs} = L_u / E_d \cong \sum_{i=1}^{2} l_i [\, b_b / (b_b + a)]^i \qquad (2.17)$$

where $l_1 = 0.0945$ steradian^{-1}, and $l_2 = 0.0794$ steradian^{-1} (Gordon *et al.*, 1988).

2.4 Absorption spectra of diverse phytoplankton

Higher chlorophyll concentration indicates more phytoplankton presence and greener water colour appearance from blue as pigments, such as chlorophyll *a* and other plant pigments, absorb the light mainly at the blue and red regions of the spectrum. Chlorophyll *a* is taken as an index of phytoplankton concentration. Specific coefficients of absorption and scattering for phytoplankton are estimated relative to chlorophyll *a*

concentration.

The bio-optical properties of the water column can be used to estimate phytoplankton pigment concentration and additional information, such as the phytoplankton species composition if they are in abundance with characteristic absorption and scattering properties (Smith, 1999). Individual photosynthetic pigments have distinctive absorption spectra, which determine a characteristic spectral signature for every phytoplankton species. An individual phytoplankton species contains a number of accessory pigments and has its own characteristic composition. Several of these pigments are restricted to 1 or 2 phytoplankton classes (Sathyendranath *et al.*, 1987; Everitt, 1990). Therefore these marker pigments can be used as indicators of different phytoplankton classes. However, the determination of phytoplankton composition using optical properties of the water is not yet reliable as the individual pigment absorption bands can overlap. In addition, the presence of coloured dissolved organic material (CDOM) and suspended particulate material (SPM) might mask the signal. Figure 2.1 shows the specific absorption curves of SPM, and CDOM. Both are closely located with chlorophylls in the blue and green region of spectrum (440-550 nm).

Bricaud *et al.* (1983) and Bricaud *et al.* (1988) measured absorption spectra of several phytoplankton species in the laboratory to distinguish different genera from the variability of their spectra. They found that the variability of absorption spectra for living cells in suspension is due to variations in the pigment composition of the species, and to differences in cell size and intracellular chlorophyll *a* concentration, leading to the so-called 'package' effect. The package effect lessens the effectiveness of specific absorption as the pigment molecules are contained within discrete packages, such as

chloroplasts, cells and cell colonies, instead of being uniformly distributed.

The absorption spectrum of a cell or colony suspension is noticeably weaker than that of dispersed thylakoid fragments (Kirk, 1994). Bricaud *et al.* (1988) tried to eliminate the package effect theoretically by computing the spectral absorption values of a hypothetical aqueous solution of the absorbing cell material. Figure 2.2 shows computed absorption spectra of phytoplankton species for a hypothetical aqueous solution of the cell material compared with absorption spectra of phytoplankton measured from intact cells (in suspension) and after acetone extraction (Bricaud *et al.*, 1988). The species studied were Bacillariophyceae (diatoms) (*Chaetoceros curvisetum, Chaetoceros lauderi*), Prymnesiophyceae (or Haptophyceae) (*Pavlova pinguis, Pavlova lutheri, Prymnesium parvum*), Chlorophyceae (*Dunaliella salina*), Rhodophyceae (*Porphyridium cruentum*) *and* Cyanophyceae (cyanobacteria) (*Synechococcus sp., Synechocystis sp.*).

The differences of absorption spectra of five species after acetone extraction are presented with absorption spectra of chlorophyll *a* as another example in Figure 2.3 (Sathyendranath, 1981). These were Bacillariophyceae (*Chaetoceros didymus, Chaetoceros curvisetus*), Chlorophyceae (*Dunaliella marina, Platymonas suecica*), and Prymnesiophyceae (*Cricosphaera elongata*).

Cullen *et al.* (1997) and Millie *et al.* (1997) distinguished phytoplankton species using optical measurements under certain conditions. Millie *et al.* (1997) used *in vivo* absorption by accessory chlorophylls and carotenoids to discern spectra of the fucoxanthin-containing *Gymnodinium breve* from spectra of peridinin-containing dinoflagellates, a diatom, a haptophyte, and a prasinophyte.

The specific absorption spectra of phytoplankton blooms are dependent on the

algal species that make up the phytoplankton population, and on their physiological state. With changes in the growth environment, such as light, the absorption characteristics of a phytoplankton culture varies. (Johnsen *et al.*, 1994).

2.4.1 Pigments

There are three main pigment groups which determine the bio-optical properties; these are chlorophylls, carotenoids, which are both lipid pigments, and phycobiliproteins, which are water soluble (Everitt *et al.*, 1990; Paerl and Millie, 1991; Barlow *et al* ., 1993; Weaver and Wrigley, 1994)

The chlorophyll group includes chlorophyll *a*, *b*, and c_1, c_2, c_3 with phaeopigments, which are known as chlorophyll degradation products. There are two major absorption peaks for each of the chlorophyll pigments. The red region of the spectrum, called the alpha peak, occurs at approximately 670 nm and the blue, called the Soret band, is at approximately 450 nm (Bidigare *et al.*, 1990). Figure 2.4 shows the absorption spectra of chlorophyll *a*, *b*, *c*. The peak in the blue region is always higher than in the red in all chlorophylls. As absorption in the green region is lower than the blue and red, the green colour of the chlorophyll pigments are observed for most algal blooms. The alpha peak of chlorophyll *a* at 670 nm is prominent for all phytoplankton species.

The second pigment group, the carotenoids, can be divided into two categories; these are photosynthetic and the photoprotectant carotenoids (Figure 2.4). Photosynthetic carotenoids include fucoxanthin, peridinin, prasinoxanthin and 19'-hexanoyloxyfucoxanthin while photoprotectant carotenoids include diadinoxanthin and

diatoxanthin (Vernet *et al.*, 1989). As photosynthetic carotenoids emit a fluorescent signal, they are important in the study of the fluorescent properties of the algae (Johnsen *et al.*, 1992). Some carotenoids are indicators of a particular phytoplankton group, for example, the pigment peridinin indicates the presence of dinoflagellates (e.g. those which are from red tides), while fucoxanthin is associated with the diatoms and chrysophytes (Jeffrey *et al.*, 1975).

Millie *et al.* (1997) studied major pigments (marker pigments) from globally important toxic dinophyceae (dinoflagellates) and prymnesiophyceae; these classes are also commonly found in the Menai Strait. They found that dinoflagellates, of the *Gymnodinium* sp. contain chlorophyll *a*, c_2, c_3, fucoxanthin, 19'-hexanoyloxyfucoxanthin, 19'-butanoyloxyfucoxanthin, diatoxanthin, dinoxanthin, gyroxanthin-diester, and β-carotene, while other dinoflagellates, *Dinophysis* sp., contain chlorophyll *a*, c_2, peridinin, diatoxanthin, dinoxanthin, β-carotene. The prymnesiophyceae, *Phaeocystis pouchetii* contains chlorophyll *a*, c_2, c_3, fucoxanthin, 19'-hexanoyloxyfucoxanthin, 19'-butanoyloxyfucoxanthin, diatoxanthin, dinoxanthin, and β-carotene.

The third pigment group, the phycobilins, exist in the cyanobacteria (cyanophyceae), red algae (rhodophyceae) and some flagellates of the class cryptophyceae (Vernet *et al.*, 1989; Smith, 1999). There are three classes of phycobilins: phycoerythrins, phycocyanins and allophycocyanins. Phycoerythrins is red in colour with the main absorption peaks between 510 nm and 590 nm while phycocyanins and allophycocyanins are blue in colour with the absorption peaks around 600 nm and 640 nm respectively (Figure 2.5) (Kirk, 1994; Lalli and Parsons, 1997). Absorption spectra of chlorophyll *a*, one of carotenoids, fucoxanthin and phycobilins; phycocyanin and

phycoerythrin, are presented in Figure 2.5.

Allophycocyanin and one or other of the phycocyanins occur in all red and blue-green algae. Phycoerythrin is mostly present in the red algae but is frequently absent in the blue-green algae. While phycoerythrin constitutes most of the phycobilins present in the red algae, phycocyanin, or less commonly phycoerythrin, is the major component. Allophycocyanin is nearly always a minor component in the phycobilins (Kirk, 1994).

The major pigments present can be identified using different absorption spectra of individual phytoplankton species as different species of photosynthetic phytoplankton contain different accessory pigments and produce a characteristic absorption spectra. Therefore, by using these bio-optical differences between the light absorption spectra, the major species during the phytoplankton bloom can be anticipated (Johnsen *et al.*, 1994).

High Performance Liquid Chromatography (HPLC) analysis is commonly applied to identify minor accessory pigments, which are difficult to identify and quantify from absorption spectra (Wright *et al.*, 1991). An array of chlorophylls and carotenoids which can be used as biological markers for algal groups, can be separated giving 50 chlorophylls, carotenoids and their derivatives (Wright *et al.*, 1991). Absorption signatures of the chlorophylls are generally observed in the blue (400-500 nm) and red (580-700 nm) region of the spectrum. The carotenoids absorb mainly between 450-550 nm (Johnsen *et al.*, 1992), while the phycobilin pigments absorb in the green to orange (480-600 nm) (Bidigare *et al.*, 1987).

Photosynthetic pigments re-emit some portion of absorbed radiation, called fluorescence. Chlorophyll fluorescence occurs at a longer wavelength in the red region

of the spectrum between 682 and 688 nm (Boxall *et al.*, 1993) while the phycobilins fluoresce in the green between 560 and 570 nm (Wood *et al.*, 1998). Natural chlorophyll fluorescence measurements are highly correlated with photosynthesis. Although there is variation between fluorescence and pigment concentration due to the size and species of the organism, chlorophyll fluorescence provides valuable information, such as the physiological state of algae (Prezelin and Boczar, 1986). Chlorophyll fluorescence occurs in the red region at wavelengths where the reflectance due to SPM has decreased, *i.e.* the SPM does not interfere with the fluorescence signature for the detection of photosynthetic phytoplankton. On the contrary, the presence of CDOM can enhance and exaggerate the chlorophyll-derived fluorescence signatures. As Figure 2.1 shows, the absorption curve of SPM increases in the region of chlorophyll fluorescence peak at 685 nm. However, the absorption coefficient of CDOM at 685 nm is negligible. Therefore, if there is a CDOM presence in the water, it will enhance the chlorophyll-derived fluorescence peak as it might emit strong reflectance signals at the same wavelength as chlorophyll fluorescence, suggesting a higher than actual level of chlorophyll biomass (Kirk, 1994).

2.5 Absorption spectra of sea water and other constituents

The light is scattered and absorbed by the sea water and the suspended and dissolved materials. The contribution of the light absorption by constituents apart from phytoplankton are described in this section.

2.5.1 Pure sea water

Pure sea water absorbs light weakly in the blue and green region of the spectrum (Figure 2.6). The absorption increases greatly after a wavelength at 550 nm in the red region. At a wavelength 680 nm, 1 m depth of sea water absorbs 35% of incident light (Kirk, 1994). Morel and Prieur (1977), Smith and Baker (1981) and Pope and Fry (1997) studied inherent optical properties of pure sea water and measured its absorption and scattering coefficients.

2.5.2 Suspended particulate matter (SPM)

As the sources of sediment tend to be diverse due to varying colour and size, it is difficult to produce a characteristic absorption spectra for SPM. Nova *et al.* (1989) tested various types of sediment to define the relationship between reflectance and SPM. They found that a narrow reflectance signature might be detected at the wavelength corresponding to the colour of sediment. Figure 2.1 shows the specific absorption curve of SPM.

2.5.3 Coloured dissolved organic matter (CDOM)

CDOM absorbs the light mainly in the blue wavelengths (See Figure 2.1). The absorption by CDOM is described by an exponential function (Morel and Prieur, 1977; Bricaud *et al.*, 1981).

$$a(\lambda) = C\exp(-0.014\lambda) \quad (2.18)$$

where $a(\lambda)$ is the absorption at wavelength, λ, and C is a constant.

As CDOM fluoresces over the entire visible spectrum, fluorescence by CDOM enhances the red peaks of the phytoplankton fluorescence spectrum.

CDOM is produced more rapidly in coastal waters than in the open sea as the input of freshwater accelerates phytoplankton decay. CDOM is inversely proportional to the salinity of the water. In oceanic waters, CDOM is produced by the algal cell degradation, which is a long-term biological activity. (Blough and Vecchio, 2002; Nelson and Siegel, 2002)

2.6 Algorithms for phytoplankton biomass

As chlorophyll *a* is the major pigment present in all photosynthetic phytoplankton, it can be used as a measure of the phytoplankton biomass (Gordon and Morel, 1983). Chlorophyll *a* absorbs light strongly in the red and blue portions of the spectrum. The absorption spectra of chlorophyllous pigments is shown in Figure 2.1 and chlorophyll *a* is in Figure 2.4.

The measurement of chlorophyll *a* is based on the colour ratio between blue (443 nm) and green (555 nm). If there is a high concentration of chlorophyll (more than 1.5 mg m^{-3}), the blue channel at 443 nm yields very low water-leaving radiance due to the high absorption. A channel near 500 nm, which is the region of high carotenoid and low chlorophyll *a* absorption, can substitute for the blue channel at 443 nm. A regression between the log of the chlorophyll concentration, C, and colour ratio is used

to estimate the phytoplankton biomass (Gordon and Morel, 1983),

$$C = A(R_x/R_y)^B \tag{2.19}$$

where R is the reflectance at waveband *X* and *Y*, and *A* and *B* are constants derived from sea truth data. Reflectance, *R*, may be substituted for irradiance, *E*, or the subsurface radiance, L_{ss}, as spectral ratios are used. The algorithms given below are an example for case 1 waters (Gordon *et al.*, 1983),

$$C = 1.13\ (L_{ss}(443)/\ L_{ss}\ (550))^{-1.71} \qquad (C<1.5\ mg\ m^{-3}) \tag{2.20}$$

$$C = 3.326(L_{ss}(520)/\ L_{ss}\ (550))^{-2.439} \qquad (C>1.5\ mg\ m^{-3}) \tag{2.21}$$

These algorithms are based on *in-situ* data from the Mid-Atlantic Bight, and have been used in Coastal Zone Color Scanner (CZCS) data processing for case 1 type waters. It is possible to retrieve chlorophyll concentrations from optical measurements in case 2 waters. However site and time specific *in situ* measurement are required to calibrate the data (Mitchelson *et al.*, 1986). Water types were classified into two cases by Morel and Prieur (1977) in which case 1 waters are those where the optical properties are dominated by biological matter, *i.e.* by the presence of phytoplankton and its associated degradation products, and case 2 waters are those where the optical properties are dominated by the presence of SPM or CDOM. Mueller and Austin (1995) define case 1 waters as those that have high phytoplankton concentrations relative to other particles, so that phytoplankton pigments are the major constituent in light absorption. In case 2

waters, inorganic particles are dominant, and pigment absorption is of comparatively minor importance. For both water types, CDOM is present in variable concentrations and also contributes to total absorption.

Sathyendranath *et al.* (1994) developed multiwavelength algorithms based on SeaWiFS channels to investigate chlorophyll *a* concentration in the New York Bight. The chlorophyll fluorescence peak at 685 nm has also been used to study surface chlorophyll distribution. Forrest and Neil (1994) used a narrow bandwidth between 673 nm and 685 nm to detect chlorophyll *a* fluorescence in the Tennessee River in the United States. An algorithm using the chlorophyll *a* fluorescence obtained using the Compact Airborne Spectrographic Imager (CASI) in the Barkley Sound on the west coast of Canada was used by Gower and Borstad (1990). The form of the algorithm is:

$$\text{Fluorescence Line Height (FLH)} = (L_b - L_c) - \left(\frac{(\lambda_b - \lambda_c)}{(\lambda_a - \lambda_c)}\right) \times (L_a - L_c) \qquad (2.22)$$

where L_λ is the water-leaving radiance in channel *a*, *b* and *c* and λ is the central wavelength of channel *a*, *b* and *c*. The bands *a*, *b*, and *c* are; Band *a*: 659-673nm, Band *b*: 673-687nm, and Band *c*: 713-718nm. Using regression analysis, the chlorophyll *a* concentration can be estimated from its fluorescence signals as chlorophyll *a* fluorescence signal with *in-situ* chlorophyll *a* data is comparable by linear relationship (Gower, 1979).

2.7 Determination of phytoplankton groups

Pigments are used as diagnostic markers for distinguishing the various classes of

phytoplankton (Hooks *et al.*, 1988). The presence or absence of the major accessory pigments in natural waters provides valuable information on the composition of photosynthetic phytoplankton. The pigment composition results in a characteristic colour, which can be measured using absorption spectra and spectral reflectance signatures. Using algal absorption and reflectance spectra, the phytoplankton group specific optical algorithm might be developed from the various combination of band ratio. Ocean colour satellites, such as SeaWiFS (Sea-viewing Wide Field-of-view Sensor), and dedicated in-water instruments have bands, tuned particularly to the accessory pigment absorption; chlorophylls: 400-500 nm, carotenoids: 450-550 nm, and phycobilins: 480-600 nm. With suitable band selection for remote sensing sensors, the major phytoplankton groups in the natural environment may be distinguishable where there is a large proportion of a particular group in the population (Millie *et al.*, 1995; 1997), e.g. during bloom conditions.

High Performance Liquid Chromatography (HPLC) analysis has made it possible to correlate the accessory pigments with the major phytoplankton groups. The presence of major marker pigments can indicate the algal types. Table 2.1 shows the major pigments, which distinguish specific algal groups. However, there are a few exceptions to the general pigment patterns. For example, peridinin, a marker pigment for dinoflagellates, is not found in all dinoflagellate species (Barlow *et al.* 1993). One of the dinoflagellates, *Gyrodinium aureolum,* contains 19'-hexanoyloxyfucoxanthin as main carotenoid (Barlow *et al.* 1993). Johnsen *et al.* (1994) used HPLC analysis to determine the spectral light absorption characteristics of 31 species of phytoplankton and identified phytoplankton classes during blooms using *in situ* bio-optical measurements at 3 to 5 appropriately chosen wavelengths.

Table 2.1 Summary of major signature pigments for algal types (after Everitt *et al.*, 1990; Paerl and Millie, 1991; Barlow *et al* ., 1993; Weaver and Wrigley, 1994).

Pigment	Phytoplankton Group
Chlorophylls	
Chlorophyll *a*	Sole chlorophyll in cyanobacteria; can be used in proportion to chl *b* and *c* in other groups
Chlorophyll *b*	Green flagellates (chlorophytes, prochlorophytes, prasinophytes, and euglenophytes)
Chlorophyll c_1	Chrysophytes and diatoms
Chlorophyll c_2	Dinoflagellates, cryptophytes and some diatoms
no accessory chlorophyll	Cyanobacteria
Carotenoids	
Peridinin	Dinoflagellates (most)
Alloxanthin	Cryptophytes
Fucoxanthin	Diatoms, prymnesiophytes, some dinoflagellates
Prasinoxanthin	Prasinophytes
Zeaxanthin	Prochlorophytes, cyanobacteria
Lutein	Chlorophytes
19'-hexanoyloxyfucoxanthin	Prymnesiophytes
19'-butanoylfucoxanthin	Chrysophytes
Beta-carotein	In all groups, proportions vary
Phycoblins	
Allophycocyanin	Cyanobacteria
Phycocyanin	Cyanobacteria
Phycoerythrin	Cyanobacteria

2.8 Ocean colour sensors

The Multispectral Scanner (MSS) on board the Landsat series of satellites and the Thematic Mapper (TM), which succeeded the MSS, are the earliest instruments to measure ocean colour from space. Landsat D, launched in 1982, carried an MSS scanner as well as TM. As they had few broad wavelength bands, they had a limited capability to measure the radiance of the ocean, being designed to detect radiance changes on the land.

The Coastal Zone Color Scanner (CZCS) was the first designated instrument to acquire ocean colour data from space, from 1978 to 1986. The CZCS had four visible spectral bands specifically formulated for the detection of chlorophyll. The bandset of

visible radiometry was as follows band 1 (433-553 nm) to observe chlorophyll absorption, band 2 (510-530 nm) to observe chlorophyll concentration, band 3 (540-560 nm) to observe CDOM, and band 4 (660-680 nm) to observe chlorophyll absorption (Gordon and Morel, 1983). There was also a near infrared band at 750 nm (band 5) and an infrared band at 11.5 μm (band 6) which were designed to detect the surface vegetation and temperature respectively. The CZCS clearly demonstrated the feasibility of determining phytoplankton pigment concentration from remotely-sensed data as the data has been used for the development of algorithms through the determination of the relationship between water-leaving radiance and pigment concentration (Gordon *et al.*, 1983). The sensor had a daily repeat pattern over the same ground point and a spatial resolution of 825 m.

The Advanced Very High Resolution Radiometer (AVHRR), which is on board the NOAA (National Oceanic and Atmospheric Administration) polar orbiting satellite, has five wavebands in the visible and infrared. This has a spatial resolution of 1.1 km and has provided data on bright phytoplankton blooms. The AVHRR sensors can not offer spectral information as they have a single broad band for ocean colour at the red end of the visible spectrum.

The Sea-viewing Wide Field-of-view Sensor (SeaWiFS) was launched in 1997. SeaWiFS has extra bands which offer great benefit for the development of multiband algorithms compared with the bandset of CZCS (Hooker *et al.*, 1992). The bandset of the instrument and major parameters are given in Table 2.2.

Table 2.2 The bandset of SeaWiFS ocean colour sensor. (from Hooker *et al.*, 1992)

Band	Wavelength (nm)	Saturation Radiance ($mW\ cm^{-2}\ \mu m^{-1}\ sr^{-1}$)	Scientific Observation
1	402-422	13.63	CDOM and turbidity
2	433-453	13.25	Chlorophyll absorption
3	480-500	10.50	Chlorophyll and other pigment concentrations
4	500-520	9.08	Chlorophyll and other pigment concentrations
5	545-565	7.44	Chlorophyll baseline (absorption minimum)
6	660-680	4.20	Chlorophyll absorption
7	745-785	3.00	Oxygen absorption and vegetation
8	845-885	2.13	Aerosols, water vapour and vegetation

The selection of SeaWiFS bands was based on previous sensors, especially the CZCS and the spectral absorption characteristics of in-water optical constituents. Figure 2.6 shows the bandset of SeaWiFS and absorption spectrum of chlorophytes, diatoms, gelbstoff (CDOM), and pure sea water, a phycobilin pigment (phycoerythrin). As absorption curves between chlorophytes and diatoms are different in the SeaWiFS channels at 3 (490 nm), 4 (510 nm), 5 (555 nm), and 6 (670 nm), the reflectance signatures between these two groups are also expected to be different at these channels. Various combination of bands, for example between 443 nm to 510 nm, and 490 nm to 510 nm will derive distinct ratios of reflectance value between chlorophytes and diatoms due to the difference of their absorption (Hooker *et al.*, 1992). The SeaWiFS sensor has a nadir resolution of 1.1 km for LAC (Local Area Coverage) and 4.6 km for GAC (Global Area Coverage; GAC = 4 × LAC). The swath width at the equator is 2801 km for LAC and 1502 km for GAC.

The Moderate-resolution Imaging Spectroradiometer (MODIS) on board the Terra and Aqua satellites and the Medium Resolution Imaging Spectrometer (MERIS), which was launched on the Envisat platform in 2001, have a number of advantages over SeaWiFS.

Terra MODIS, launched in December 1999, is viewing the entire Earth's surface

every 1 to 2 days, acquiring data in 36 spectral bands (Esaias, *et al.*, 1998). From these bands, ocean colour, Sea Surface Temperature (SST) and atmospheric parameters can be observed simultaneously. The full bandset of Terra MODIS is given in Table 2.3 (Esaias, *et al.*, 1998). Particular interests for the relationship between in-water optical properties and reflectance signature to build phytoplankton group specific algorithms can be studied from bands 8 to 16. The MODIS sensor has a nadir resolution of 250 m (bands 1-2), 500 m (bands 3-7), 1000 m (bands 8-36) and a swath width of 2330 km.

The MERIS has high spectral and radiometric resolution and a dual spatial resolution, 1.2 km globally and 300 m regionally. Thus, MERIS can be useful to acquire accurate data for small patches of bloom and near-shore environments (Rast, *et al.*, 1999). One of the most outstanding features of MERIS is the programmability of its spectral bands. There are 15 wavebands that can be programmed in width and location (Table 2.4). The specific channels can be constructed from the programmable bands to observe specific phenomena, such as red tides, through their absorption feature near 520 nm.

Table 2.3 The bandset of Terra MODIS (Bands 1 to 19 are in nm; Bands 20 to 36 are in μm) (from Esaias, *et al.*, 1998)

Primary Use	Band	Bandwidth	Primary Use	Band	Bandwidth
Land/Cloud/Aerosols Boundaries	1	620 - 670	Surface/Cloud Temperature	20	3.660 - 3.840
	2	841 - 876		21	3.929 - 3.989
Land/Cloud/Aerosols Properties	3	459 - 479		22	3.929 - 3.989
	4	545 - 565		23	4.020 - 4.080
	5	1230 - 1250	Atmospheric Temperature	24	4.433 - 4.498
	6	1628 - 1652		25	4.482 - 4.549
	7	2105 - 2155	Cirrus Clouds Water Vapor	26	1.360 - 1.390
Ocean Color/ Phytoplankton/ Biogeochemistry	8	405 - 420		27	6.535 - 6.895
	9	438 - 448		28	7.175 - 7.475
	10	483 - 493	Cloud Properties	29	8.400 - 8.700
	11	526 - 536	Ozone	30	9.580 - 9.880
	12	546 - 556	Surface/Cloud Temperature	31	10.780 - 11.280
	13	662 - 672		32	11.770 - 12.270
	14	673 - 683	Cloud Top Altitude	33	13.185 - 13.485
	15	743 - 753		34	13.485 - 13.785
	16	862 - 877		35	13.785 - 14.085
Atmospheric Water Vapor	17	890 - 920		36	14.085 - 14.385
	18	931 - 941			
	19	915 - 965			

Table 2.4 The bandset of MERIS (from Rast, *et al.*, 1999)

Band	Band centre (nm)	Bandwidth (nm)	Scientific Observation
1	412.5	10	CDOM, turbidity
2	442.5	10	Chlorophyll absorption maximum
3	490	10	Chlorophyll, other pigments
4	510	10	Turbidity, suspended sediment, red tides
5	560	10	Chlorophyll reference, suspended sediment
6	620	10	Suspended sediment
7	665	10	Chlorophyll absorption
8	681.25	7.5	Chlorophyll fluorescence
9	705	10	Atmospheric correction, red edge
10	753.75	7.5	Oxygen absorption reference
11	760	2.5	Oxygen absorption R-branch
12	775	15	Aerosols, vegetation
13	865	20	Aerosols corrections over ocean
14	890	10	Water vapour absorption reference
15	900	10	Water vapour absorption, vegetation

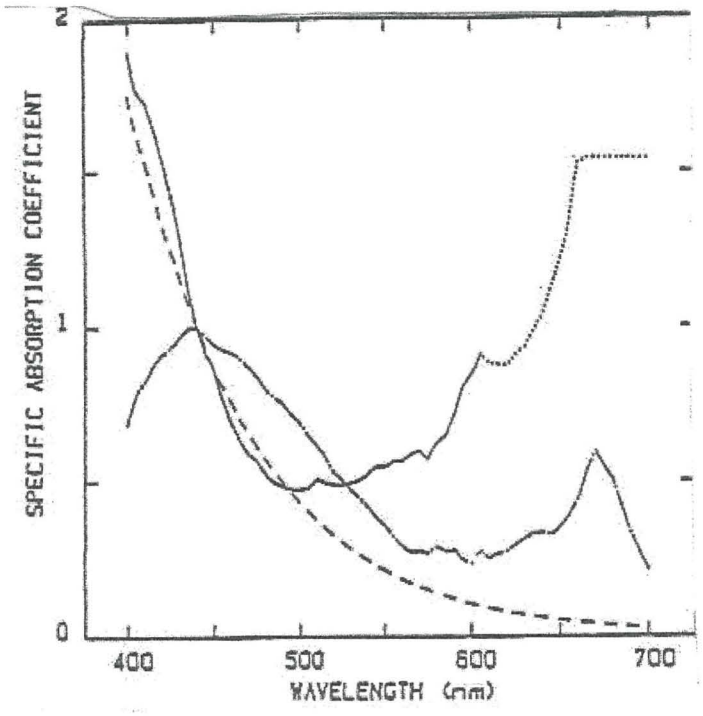

Figure 2.1 Normalised specific absorption spectra of chlorophyllous pigments $a_c^*(\lambda)$ (— · —), non-chlorophyllous particles (SPM) $a_p^*(\lambda)$ (——) and yellow substance (CDOM) $a_y^*(\lambda)$ (---) (Prieur and Sathyendranath, 1981).

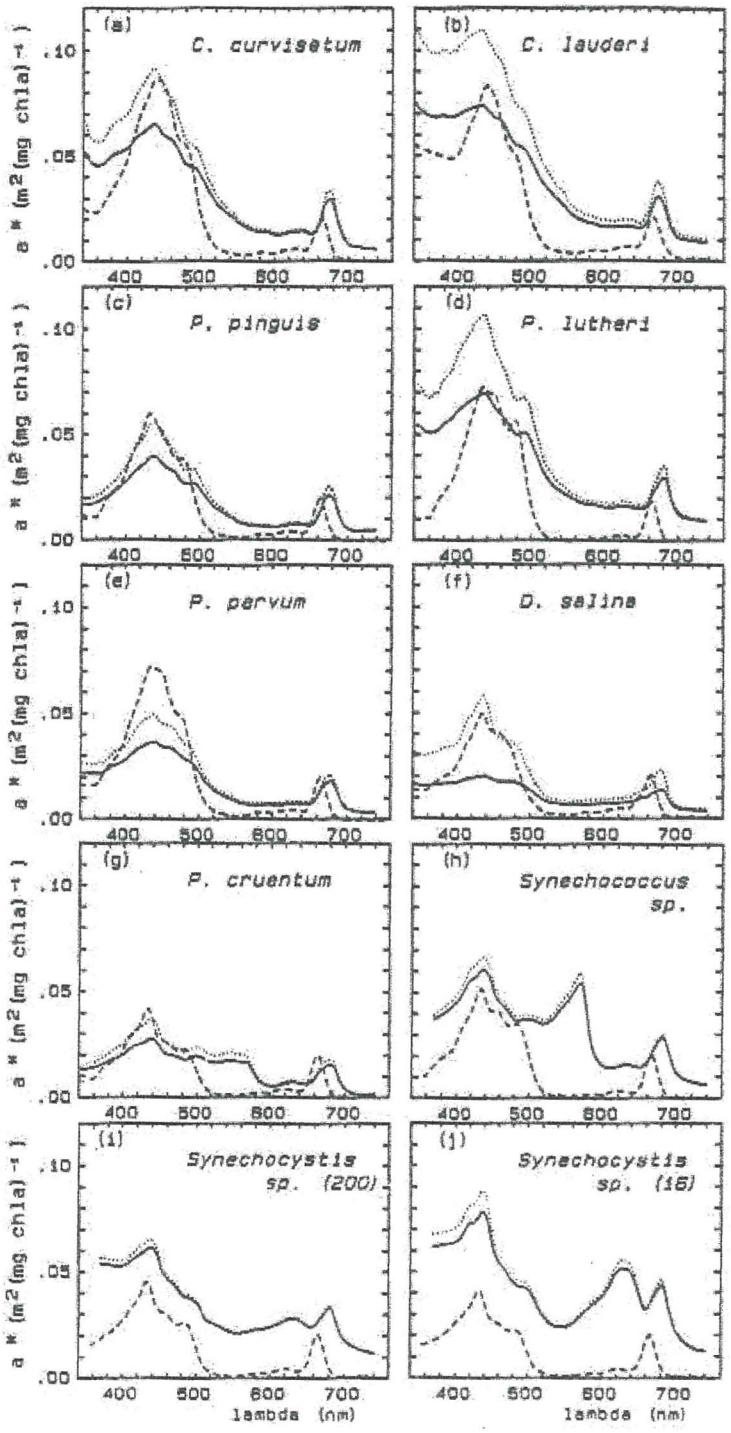

- **Figure 2.2 (a)** absorption spectra of 10 phytoplankton species after acetone extraction (dashed line). *Solid and dotted lines are intact cells and computed spectra, respectively* (Bricaud *et al.*, 1988).

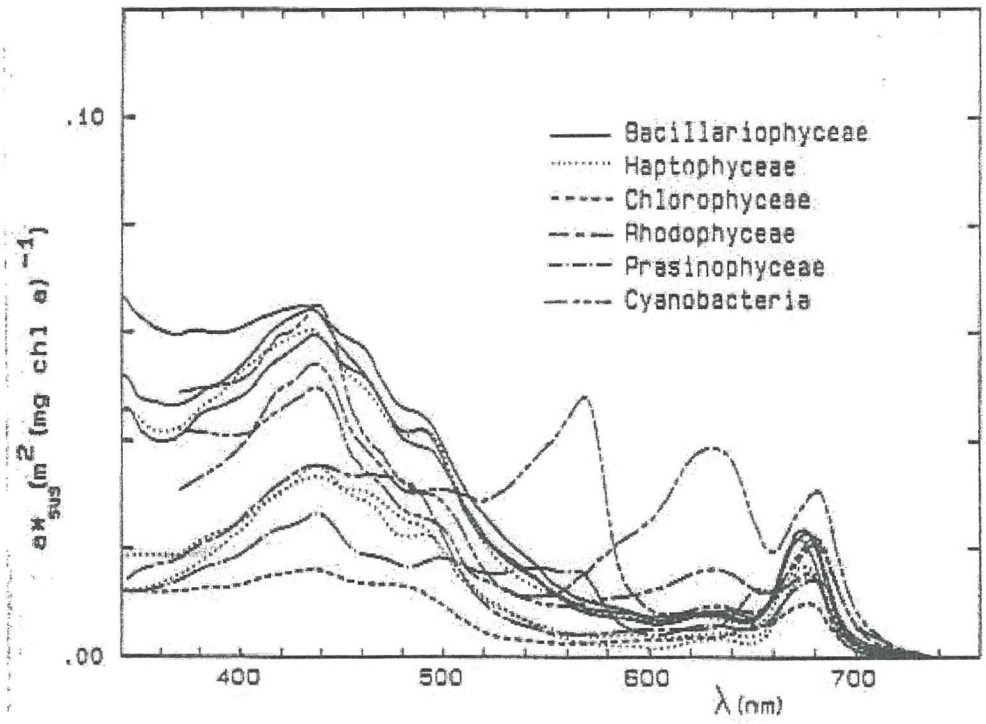

Figure 2.2 (b) absorption spectra of 6 classes for intact cells in suspension. (Bricaud *et al.*, 1988)

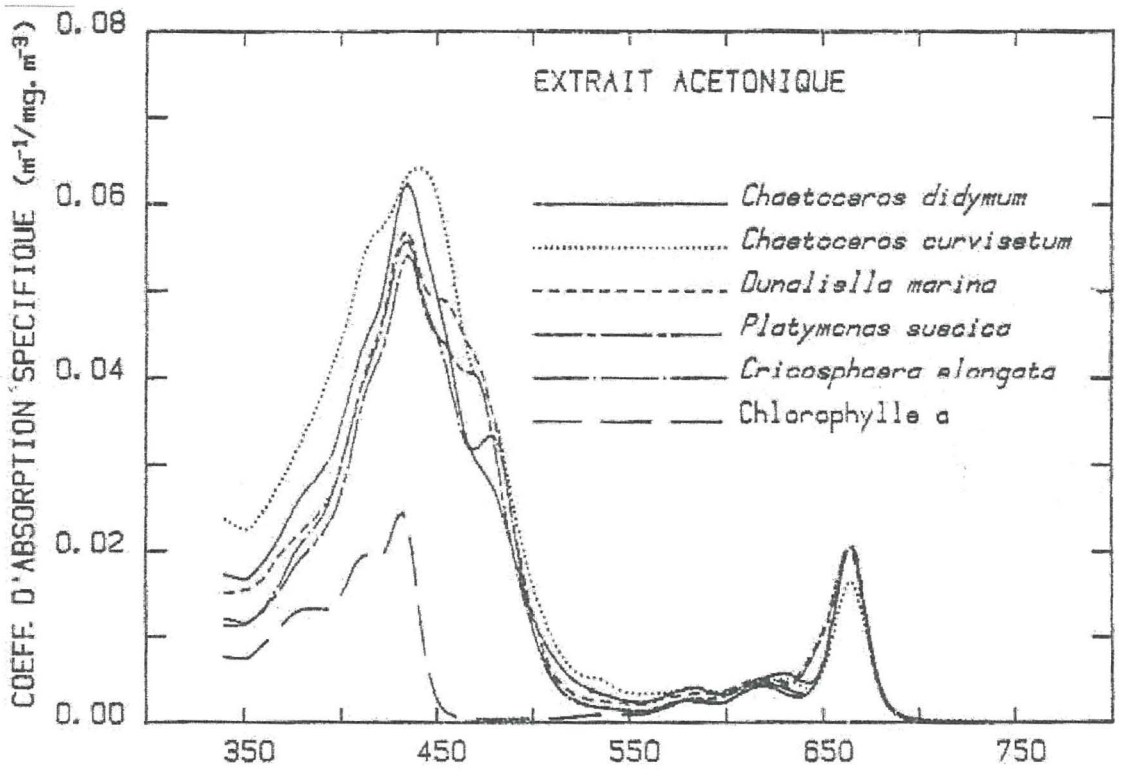

Figure 2.3 absorption spectra of five species (source Sathyendranath, 1981)

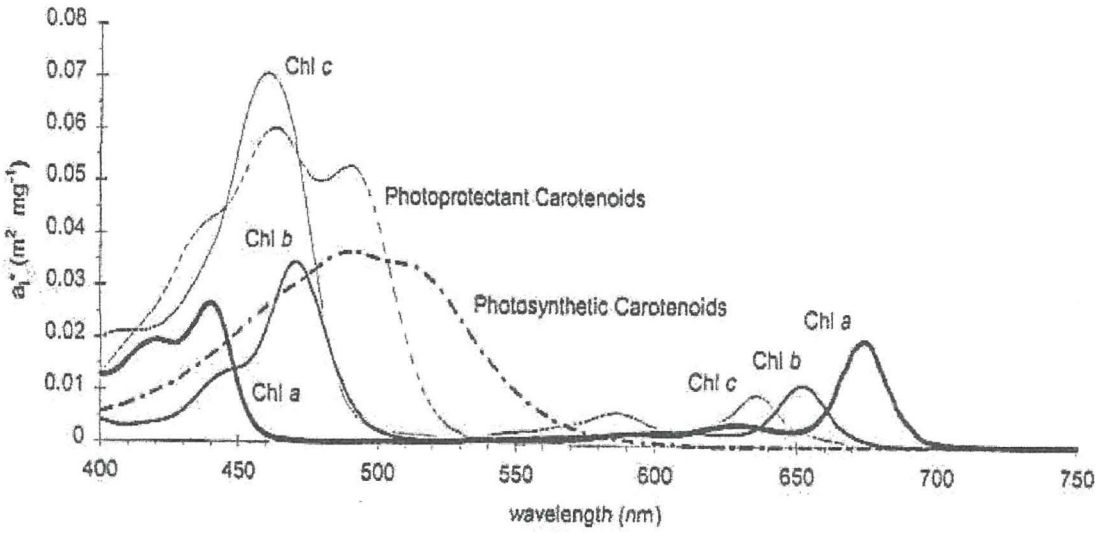

Figure 2.4 Weight-specific absorption coefficients ($a_i^*(\lambda)$, m^2 mg^{-1}) of major pigments found in marine phytoplankton - chlorophyll *a*, *b*, *c*, and photosynthetic and photoprotectant carotenoids (Bidigare *et al.*, 1990).

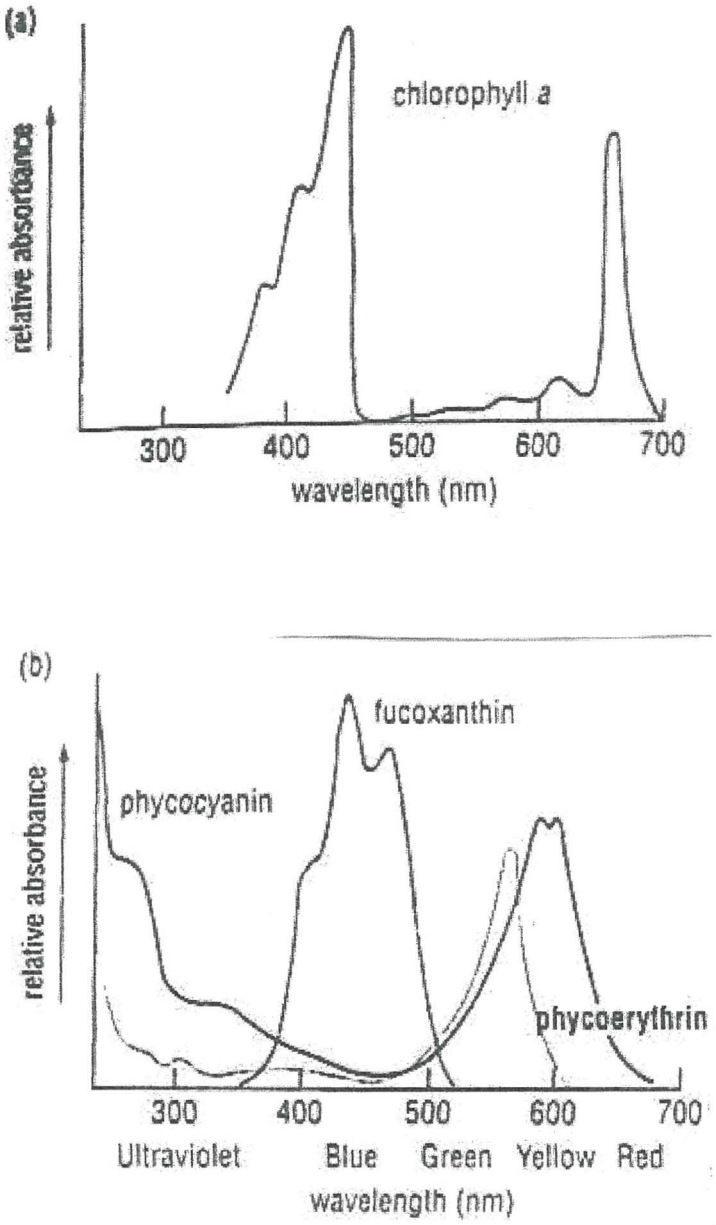

Figure 2.5 the absorption spectrum of chlorophyll *a* (a) and the accessory pigments fucoxanthin (carotenoid), and phycocyanin and phycoerythrin (phycobilins) (b) (Lalli and Parsons, 1997).

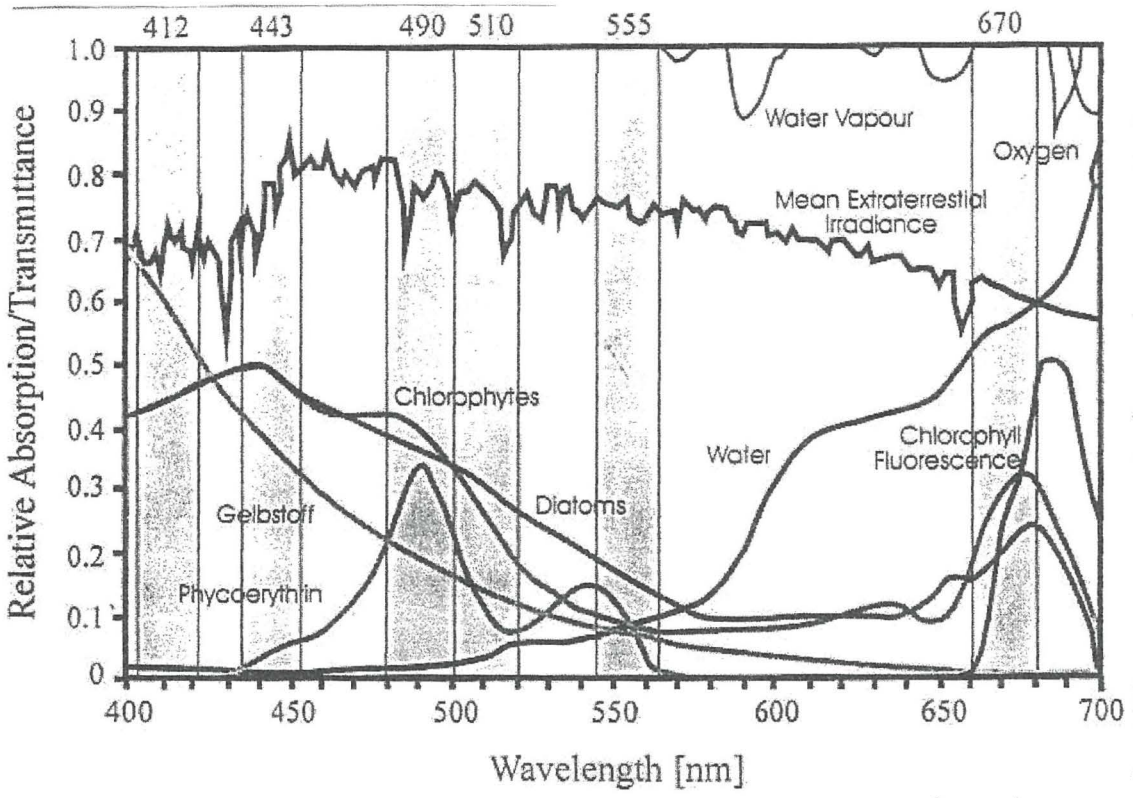

Figure 2.6 The SeaWiFS bands and spectral absorption characteristics of some in-water optical constituents (Hooker *et al.*, 1992).

3. METHODOLOGY

3.1 Introduction

This chapter details the methodology and measurement techniques to be used in this project. *In situ* optical data were collected to measure absorption and remote sensing reflectance of phytoplankton with water samples for taxonomic analysis from the 25th of May 2001 to the 21st of October 2002 in the Menai Strait and from five cruises around the U.K. Shelf Seas (Table 3.1). The total pigment (chlorophyll *a* + phaeopigments) was measured fluorometrically while the accessory pigments which represent major group of phytoplankton, fucoxanthin (diatoms), peridinin (dinoflagellates), 19' hexanoyloxyfucoxanthin (prymnesiophyceae) and chlorophyll *b* (green flagellates) were measured using High Performance Liquid Chromatography (HPLC). Table 3.1 shows the period of each cruise and Menai Strait sampling, and measurements made from studies. Maps of areas of study and sampling stations are presented in figure 3.1 a-e.

Table 3.1 Sampling details: Number of samples taken from five cruises between 2001 and 2002, and from Menai Strait. Number of samples processed for chlorophyll *a* using fluorometer, marker pigments including chlorophyll *a* using HPLC and absorption spectra, microscopic taxonomy data for cell identification, and reflectance radiance signature are on the lists.

			fluoro metric	HPLC								
Cruises	periods	No. of samples	chla[1]	peri[2]	fuco[3]	19' hex[4]	Chlb[5]	chla	phaeo a[6]	a*C[7]	Cell ID[8]	R[9]
Clyde Sea	23/04-27/04/01	52		42	42	42	42	42	42		48	14
Irish Sea 1	06/08-10/08/01	54	54	54	54	54	54	54	54	16	54	16
Irish Sea 2	26/11-30/11/01	65	65	60	60	60	60	60	60	19	64	19
Irish Sea 3	02/04-05/04/02	95	95	95	95	95	95	95	95	28	95	28
Celtic Sea	13/07-20/0702	148	148	148	148	148	148	148	148	44	148	44
Menai Strait	25/05/01-21/10/02	27	27	27	27	27	27	27	27	19	27	19

1 chlorophyll a; 2 peridinin; 3 fucoxanthin; 4 19' hexanoyloxyfucoxanthin; 5 chlorophyll b; 6 phaeophytin a; 7 absorption spectra; 8 cell identification; 9 remote sensing reflectance measurement

3.2 CTD profiles

During the cruises on R.V. Calanus (the Clyde Sea) and R.V. Prince Madog (the Irish Sea and the Celtic Sea), water samples were taken at two depths at most stations, with the sampling depth chosen based upon the CTD (conductivity, temperature and depth) profile. These depths were chosen where thermal stratification might occur, and under the thermal stratification. 30 litres of water were taken at each of two depths using the CTD rosette sampler. The surface water samples were obtained using a bucket.

3.3 Phytoplankton preservation and microscopic analysis

Water samples were taken for taxonomic analysis. 100-125 ml was immediately fixed with a few drops of 0.5 % Lugol's iodine solution with acetic acid (Willén, 1976). Then, the samples were stored in capped glass bottles, in the dark at 4 °C

The inverted light microscope was used for cell counting and identification. The sample bottles were allowed to equilibrate to room temperature and then shaken gently for even distribution of particles before pouring into settling chambers. Chamber volumes of 10 ml sample require a settling time of 8 hours (Edler, 1979; Hoek, *et al.*, 1995). The cell numbers of individual species were recorded to estimate each taxon and total phytoplankton population. Most diatom and dinoflagellate species were identified at the species level, while the rest of classes were classified as flagellates. Following references used as guides for the phytoplankton identification; these are Sykes (1981), Sournia (1986), Ricard (1987) and Chretiennot - Dinet (1990).

3.4 Spectral radiometer measurement

Spectral radiance reflectance signatures, irradiance reflectance, remote sensing reflectance, attenuation coefficient of downwelling irradiance, and water-leaving radiance, can be measured using a PRR-600 profiling radiometer (Biospherical instruments). The PRR-600 measured vertical profiles of in-water downwelling spectral irradiance, E_d, and upwelling spectral radiance, L_u, while upwelling irradiance, E_u, was measured by inverting the PRR-600 deployment frame. These profiles were normalised to the surface incident spectral irradiance, which was measured by the PRR-610. The PRR-600 and PRR-610 have a spectral response of 10 nm bandwidth ± 1nm with centre wavelengths, which coincide to the SeaWiFS bands (Table 2.2). Table 3.2 shows the waveband selection for the PRR-600 and 610.

Table 3.2 The bandset of PRR-600 and 610. The PRR-600 and 610 irradiance sensors can measure irradiance of Photosynthetically Active Radiation (PAR), bandwidth ranging 400-700nm. The natural fluorescence productivity measurement can also be made on the PRR-600 radiance sensor at 683 nm.

Channel	PRR-600/610 Irradiance sensor (nm)	PRR-600 Radiance sensor (nm)
1	412	412
2	443	443
3	490	490
4	510	510
5	555	555
6	665	665
7	PAR	683

Primary optical parameters measured by the PRR-600, E_d, E_u and L_u derive

irradiance reflectance, R, and remote sensing reflectance, R_{rs}, from the relation $R = E_u / E_d$, and $R_{rs} = L_u / E_d$ respectively (Gordon *et al.*, 1975; Gordon *et al.*, 1988). Table 3.3 shows the parameters measured by the PRR-600 and 610 with irradiance and remote sensing reflectance derived from these parameters. The units of each parameter are also listed.

Table 3.3 Optical measurements using PRR-600 and 610 with units.

Parameter	Unit
Downwelling spectral irradiance (E_d)	$\mu W\ cm^{-2}\ nm^{-1}$
Upwelling spectral irradiance (E_u)	$\mu W\ cm^{-2}\ nm^{-1}$
Upwelling spectral radiance (L_u)	$\mu W\ cm^{-2}\ nm^{-1}\ steradian^{-1}$
Irradiance reflectance (R)	-
Remote sensing reflectance (R_{rs})	$steradian^{-1}$

3.5 Pigment determination

The total pigment (chlorophyll *a* + phaeopigments) was measured using a Turner design bench fluorometer. Chlorophyll *a* measurements provide a useful estimate of algal biomass, while phaeopigment is used as an index of the amount of dead plant material present. High Performance Liquid Chromatography (HPLC) analysis allows measurements of individual phytoplankton pigments and determines the pigment composition of the phytoplankton population. The accessory pigments which represent major group of phytoplankton, fucoxanthin (diatoms), peridinin (dinoflagellates), 19' hexanoyloxyfucoxanthin (prymnesiophyceae) and chlorophyll *b* (green flagellates) were measured using HPLC.

3.5.1 Fluorometric measurement

The concentration of chlorophyll *a* and phaeopigments were determined with a fluorometer using the Joint Global Ocean Flux Studies protocols (JGOFS, 1994). Water samples were taken from niskin bottles into clean polyethylene bottles. 1 to 4 litres of sea water were immediately filtered on board through a 47 mm GF/F filter with a nominal pore size of 0.7 μm. Filter samples were stored under –20 °C or using liquid nitrogen at –196 °C. The pigment extraction of filter samples may last in 90 % acetone from 18 to 72 hours in darkness at 4 °C for complete extraction (Tett, 1987). However, in this study, the pigment extraction took 4 hours in 90 % acetone in the dark at –20 °C (JGOFS, 1994). The extraction volume of 5.8 ml was used. However, additional 5.0 ml acetone can be used to completely submerge 47 mm GF/F filter in 15 ml centrifuge tubes (JGOFS, 1994). Samples were sonicated at 0 °C under subdued light. As sample extracts were vortexed, filters were pressed down to the bottom of the tube with a stainless spatula. The sample was centrifuged for 5 minutes to separate the extracted pigment solution from the filter completely.

A Turner Designs Model 10 fluorometer was calibrated every six months with a commercially available chlorophyll *a* standard. The chlorophyll *a* standard was dissolved in 90 % acetone and measured spectrophotometrically (JGOFS, 1994);

$$\text{Chl } a = [(A_{max} - A_{750nm}) / (E \times l)] \times [1000 \text{ mg} / 1 \text{ g}] \qquad (3.1)$$

where A_{max} and A_{750nm} are absorbance maximum at 664 nm (for chlorophyll *a*) and

absorbance at 750 nm to correct for light scattering, respectively. E is extinction coefficient for chlorophyll *a* in 90 % acetone at 664 nm (87.67 L g^{-1} cm^{-1}) (Table 3.6) and l is cuvette path length (cm).

The fluorescence of chlorophyll *a* and phaeopigments were measured by acidifying the sample with 2 drops of 1.2 M HCl (100 ml HCl in 900 ml de-ionised water), which converts all the chlorophyll to phaeopigments. 90 % acetone blanks were measured to zero the instrument to give a correction factor. The concentration of chlorophyll *a* and phaeopigments in the sample were calculated using the equations as follows (JGOFS, 1994). For coefficients F_m and K_x, a minimum of five dilutions of pure chlorophyll *a* standards were prepared;

$$\text{Chl } a = [(F_m / (F_m\text{-}1)] \times (F_0 - F_a) \times K_x \times (V_e / V_s) \quad (3.2)$$

$$\text{Phaeo} = [(F_m / (F_m\text{-}1)] \times [(F_m \times F_a) - F_0] \times K_x \times (V_e / V_s) \quad (3.3)$$

where F_m is acidification coefficient, the average ratio between unacidified and acidified readings of pure chlorophyll *a* standards. F_0 and F_a are fluorometer readings of samples before and after acidification, respectively. K_x is linear calibration factor calculated as the slope of the unacidified fluorometric readings for pure chlorophyll *a* standards against the concentrations of chlorophyll *a* standards measured by spectrophotometer. V_e is the extraction volume and V_s is the sample volume filtered.

3.5.2 High Performance Liquid Chromatography (HPLC) analysis

Pigments contained in phytoplankton, over 50 carotenoids and chlorophylls, can be separated using the HPLC method (Wright *et al.*, 1991). Measurement of the light absorbing pigment composition allows optical determination of phytoplankton species. The HPLC method can separate important phytoplankton pigments with detection limits to the order of 1 ng (Bidigare, 1991; JGOFS, 1994). 1 to 6 litres of water sample were filtered through 47 mm GF/F filters. Filters were folded in half twice and wrapped in aluminium foil, and stored in liquid nitrogen (–196 °C) to avoid the formation of degradation products. The storage of filter samples is important as pigments degrade if they are stored for long periods in the freezer. A mixture of cultured microalgae stored under – 20 °C recovers 75 % of the original chlorophyll *a* after four weeks (Mantoura *et al.*, 1997). The storage of filter samples under liquid nitrogen is highly recommended as it preserves and recovers 96 % of pigments from filter samples for up to 328 days (Mantoura *et al.*, 1997). Frozen filters were extracted in 5.8 ml of 90 % acetone. Additional 5.0 ml acetone can be used to completely submerge 47 mm GF/F filter in 15 ml centrifuge tubes (JGOFS, 1994). Samples were sonicated at 0 °C under subdued light. The extraction took 4 hours in the dark at –20 °C (JGOFS, 1994). Samples were then centrifuged for 5 minutes to remove filter debris. 1 ml of the extract was prepared in the 1.5 ml of vial, and 100 µl was injected into the HPLC system.

The HPLC instrument at the University of Wales, Bangor (UWB) is equipped with a Tsp AS 3000 automated injector, a Tsp P4000 pump, a reverse phase chromatographic Phenomenex ODS(2) column (250 x 4.6 mm, 5µm particle size) and a Tsp UV 3000Hr UV/visible detector. The HPLC uses the solvent systems as follows:

Solvent A: 80:20 methanol : 0.5 M ammonium acetate (aq., pH 7.2 v/v)

Solvent B: 90:10 acetonitrile (210 nm UV cut-off grade) : water (v/v)

Solvent C: ethyl acetate (HPLC grade)

Flow rate is 1 ml min^{-1}. The gradient systems used are shown in Table 3.4.

The individual peaks on the chromatograms can be identified by comparing the retention times with pure pigment standards, extracts from algal culture and literature spectra, for example from Wright *et al.* (1991).

Table 3.4 HPLC solvent program.

Time (Min.)	Flow Rate	Solvent A (%)	Solvent B (%)	Solvent C (%)	Conditions
0.0	1.0	100	0	0	Injection
2.0	1.0	0	100	0	Linear gradient
2.6	1.0	0	90	10	Linear gradient
13.6	1.0	0	65	35	Linear gradient
18.0	1.0	0	31	69	Hold
23.0	1.0	0	31	69	Linear gradient
25.0	1.0	0	100	0	Linear gradient
26.0	1.0	100	0	0	Hold
34.0	1.0	100	0	0	Equilibration

Wright *et al.* (1991) listed the pigments separated in increasing elution order with retention time (Table 3.5). Using retention time and the sequence from Table 3.5, most pigments composition on the chromatograms can be identified. Pigments standards were obtained commercially to calibrate the HPLC system (Chlorophyll *a* and *b* can be purchased from Sigma Chemical Co., and fucoxanthin, peridinin, 19' hexanoyloxyfucoxanthin and phaeophytin *a* from DHI environmental Co.). Concentration of pigment standards were measured spectrophotometrically before the HPLC calibration (JGOFS, 1994);

$$Cs = [(A_{max} - A_{750nm}) / (E \times l)] \times [1000 \text{ mg} / 1 \text{ g}] \quad (3.4)$$

Where Cs is pigment concentration. A_{max} and A_{750nm} are absorbance maximum of individual standard pigments and absorbance at 750 nm to correct for light scattering, respectively. E is extinction coefficient of individual standard pigments and l is cuvette path length (in cm). Absorbance maximum and extinction coefficient of pigment standards are listed in Table 3.6

Pigment standards measured spectrophotometrically were injected onto the HPLC system to derive standard response factor (Rf). Response factor were calculated using the equation below (JGOFS, 1994);

$$Rf = W_s / (A_s + A_i) \tag{3.5}$$

where W_s is the weigh of standard injected (determined spectrophotometrically). A_s is the area of the pigment standard from HPLC reading and A_i is areas of structurally related isomer, if present.

The pigment concentrations in the sample were measured using HPLC as follows (JGOFS, 1994);

$$Ci = A \times Rf \times (1 / V_i) \times V_e \times (1 / V_s) \tag{3.6}$$

where Ci is individual pigment concentration. A is the integrated peak area. Rf is the standard response factor. V_i, V_e and V_s are the injected sample volume, extraction volume and the sample volume filtered, respectively.

Table 3.5 Elution order of pigments from standard cultures and their visible absorption characteristics (Wright *et al.*, 1991).

Peak	Pigment	Retention time (min)	Acetone Maxima (nm)			% III : II[a]	Eluant Maxima (nm)			% III : II[a]
0	(Solvent front)	2.56								
1	Chlorophyllide *b*	4.48	453	598	645					
2	Carotenoid P468[b]	4.50						470		
3	Chlorophyllide *a*	5.01	430 663	577	617					
4	Carotenoid P457[b]	5.11						458		
5	Chlorophyll c_3	5.38	452	584	627					
6a	Chlorophyll c_2	6.40	449	581	629		446	580	626	
6b	Chlorophyll $c_1 + c_2$	6.40		- - -						
6c	Mg2,4D	6.40	437	575	625					
6d	Chlorophyll $c_1 + c_2$ + Mg2,4D	6.40		- - -						
7	Peridinin	7.42		474				472		
8	Siphonaxanthin	8.11		445				442	(466)	
9	19'-butanoyloxyfucoxanthin	8.11		445	470	44	(415)	444	469	42
10	Fucoxanthin	8.70		446				446	(466)	
11	*trans*-neoxanthin	9.11					416	441	470	100
12	9'-*cis*-19'-butanoyloxy-fucoxanthin	9.12		440	464	33				
13	Neochrome	9.21					400	422	450	90
14	9'-*cis*-neoxanthin	9.31	415	439	467	65	412	436	466	88
15	19'-hexanoyloxyfucoxanthin	9.31		444	470	48	418	445	469	38
16	*cis*-fucoxanthin	9.68						444	(464)	
17	*cis*-19'-hexanoyloxy-fucoxanthin	9.97								
18	Unknown siphonaxanthin-like	10.12						453		
19	Prasinoxanthin	10.20		451				450	(470)	
20	Phaeophorbide *a*	10.39	410 669	505 666	535					
21	Violaxanthin	10.59	419	443	472	96	416	440	470	101
22	Phaeophorbide *a*-like[c]	10.62	410 669	505 666	535					
23	Dinoxanthin	10.76	418	442	471	86	415	440	470	87
24	*cis*-prasinoxanthin	11.11								
25	Unknown siphonaxanthin-like	11.15						456		
26	Diadinoxanthin	11.61					422	446	476	64
27	Diadinochrome I	11.79		431	458	63	406	430	458	76
28	Diadinochrome II	11.96					406	428	458	76
29	Antheraxanthin	12.24					(423)	446	476	67
30	Alloxanthin	12.51		454	484	48	(428)	454	484	63
31	Monadoxanthin	12.78					(428)	448	480	40
32	Diatoxanthin	13.08		454	484	42	(424)	452	482	33
33	Lutein	13.36	425	446	476	68	(422)	446	476	64
34	Zeaxanthin	13.59		454	481	32	(428)	454	478	11
35	Canthaxanthin	14.00		472				472		
35b	*trans*-β-apo-8'-carotenal	14.00		456						
36	Siphonein	14.36		452				455		34
37	Chlorophyll *b*	15.15	453	598	645		456	596	646	
38	Ethyl 8'-β-apocarotenoate	15.43		444				446	(467)	–
39	Crocoxanthin	15.87					(427)	449	480	58
40	Chlorophyll *a* allomer	15.87					425	616	664	
41	Chlorophyll *a*	16.15	412	431 616	581 663		431	618	665	
42	Chlorophyll *a* epimer	16.53					431	618	666	
43	Echinenone	16.74		461				464		
44	Unknown carotenoid	16.99					420	443	471	59
45	Lycopene	17.59	448	474	505	77	438	472	505	70
46	Phaeophytin *b*	17.66								
47	*cis*-lycopene	17.84					365, 444	470	502	
48	Phaeophytin *a*	18.56	410 669	505 666	535		408 504	534 608	666	
49	β,Ψ-carotene	18.26		464	493	54	438	462	496	44
50	ε,ε-carotene	18.40					416	440	471	94
51	β,ε-carotene	18.64		447	475	55	(425)	448	476	60
52	β,β-carotene	18.76		453	480	13	427	452	480	18
53	*cis*-β,ε-carotene	18.83					(419)	442	470	37
54	*cis*-β,β-carotene	18.94					(422)	446	470	

[a] Sue Ke et al. (1970)
[b] Following the nomenclature of Johansen et al. (1974)
[c] Probably pyrophaeophorbide *a* (unverified)

Table 3.6 The absorbance maximums and recommended extinction coefficients for algal pigments. Chlorophyllous pigments were prepared in 90% acetone and carotenoids were prepared in 100 % ethanol (from Bidigare, 1991).

Pigment	Absorbance maximums (nm) (solvent)	Extinction coefficients (Litres g^{-1} cm^{-1})
Chlorophyll *a*	664 (90% acetone)	87.67
Chlorophyll *b*	647 (90% acetone)	51.36
Fucoxanthin,	449 (ethanol)	160.0
19' hexanoyloxyfucoxanthin	447 (ethanol)	160.0
Peridinin	472 (ethanol)	132.5
Phaeophytin *a*	665 (90% acetone)	49.5

3.6 Measurements of spectrophotometric absorption

1-4 litres of sea water containing phytoplankton particles were filtered through a GF/F filter. The filter was placed on a microscopic slide which was fixed by a magnet over the exit window of the spectrophotometer. The particle side of the filter faced the light source. Few drops of filtered sea water held the wet filters to the glass slide. The spectrum of the particles on the GF/F filter was scanned from 350 to 750 nm. A wet GF/F filter with filtered sea water was used as a filter blank (or reference) for all scans. Blank filters were prepared by soaking in filtered sea water for 20 minutes (Smith, 1999). The reference spectrum was measured by placing two wetted reference filter blanks using the dual beam spectrophotometer. One was then left in the reference beam during the sample scans. The absorption of light by particles, $a_p(\lambda)$, was derived by the following relation (Kiefer and SooHoo, 1982; Mitchell and Kiefer, 1984);

$$a_p(\lambda) = (2.3\ S / \beta V) \times [(A_p(\lambda) - A_r(\lambda)) - (A_p(750) - A_r(750))] \qquad (3.7)$$

where the conversion factor 2.3 is for *ln* from $\log_{10}$ units. $A_p(\lambda)$ and $A_r(\lambda)$ are the sample and reference absorbances measured by spectrophotometer between 400 and 750 nm.

$A_p(750)$ and $A_r(750)$ are the sample and reference absorbances at 750 nm. S is the solid area of the filter and V is the volume of water filtered. β is the path length amplification factor, which can be calculated using equation 3.9. The value of $A_p(750)$ is assumed to represent loss of light by scattering as phytoplankton pigments do not absorb at this wavelength. Therefore, subtracting $A_p(750)$ from all wavelengths is the correction for scattering, assuming that it is constant across the spectrum (Bowers *et al.*, 1996). After the measurement, the filter sample was de-colourised with 100 % methanol for 30 to 60 minutes (Kishino *et al.*, 1985). The absorption spectra of extracted filter samples, $a_d(\lambda)$, was measured in the same manner as $a_p(\lambda)$

$$a_d(\lambda) = (2.3\ S / \beta V) \times [(A_d(\lambda) - A_r(\lambda)) - (A_d(750) - A_r(750))] \qquad (3.8)$$

where $A_d(\lambda)$ and $A_r(\lambda)$ are the sample and reference absorbances measured by spectrophotometer between 400 and 750 nm. $A_d(750)$ and $A_r(750)$ are the sample and reference absorbances at 750 nm. Kishino *et al.*, (1985) calculated the path length amplification factor, β, as the ratio between absorption of light by particles on the filter, $a_p(\lambda)$, and absorption of suspended particles, $a_s(\lambda)$. For three different cultures of phytoplankton and one field sample, β for phytoplankton cells ranged between 2.43 and 4.71 (Kishino *et al.*, 1985). The path length amplification factor β for phytoplankton cells was estimated empirically using a polynomial regression (Mitchell, 1990; Cleveland and Weidemann, 1993; Mueller and Austin, 1995);

$$\beta^{-1} = C_1 + C_2\,(A_p(\lambda) - A_r(\lambda)) \qquad (3.9)$$

where C_1 and C_2 are coefficients of polynomial regression. These coefficients were defined by Cleveland and Weidemann (1993) as $C_1 = 0.378$ and $C_2 = 0.523$. Using these coefficients, the absorption spectra of light by particles, $a_p(\lambda)$, and the absorption spectra of extracted filter samples, $a_d(\lambda)$, can be expressed as follow, assuming that the absorption by the particles at 750 nm, A(750), is zero;

$$a_p(\lambda) = (2.3\ S / V) \times [C_1\ (A_p(\lambda) - A_r(\lambda)) + C_2\ (A_p(\lambda) - A_r(\lambda))^2] \quad (3.10)$$

$$a_d(\lambda) = (2.3\ S / V) \times [C_1\ (A_d(\lambda) - A_r(\lambda)) + C_2\ (A_d(\lambda) - A_r(\lambda))^2] \quad (3.11)$$

The difference between the two readings $a_p(\lambda)$ and $a_d(\lambda)$ was considered to be the light absorption related to phytoplankton, $a_{ph}(\lambda)$, (Kishino *et al.*, 1985);

$$a_{ph}(\lambda) = a_p(\lambda) - a_d(\lambda) \quad (3.12)$$

The specific absorption coefficient of phytoplankton, $a_{ph}^*(\lambda)$, was determined by regressing $a_{ph}(\lambda)$ against the concentration of chlorophyll *a*. the relationship can be described as follow;

$$a_{ph}(\lambda) = a_{ph}^*(\lambda) \times \text{Chl } a \quad (3.13)$$

where Chl *a* is the Chlorophyll *a* concentration. The specific absorption coefficient of

phytoplankton, $a_{ph}^{*}(\lambda)$ was used for the direct comparison of absorption spectra between samples.

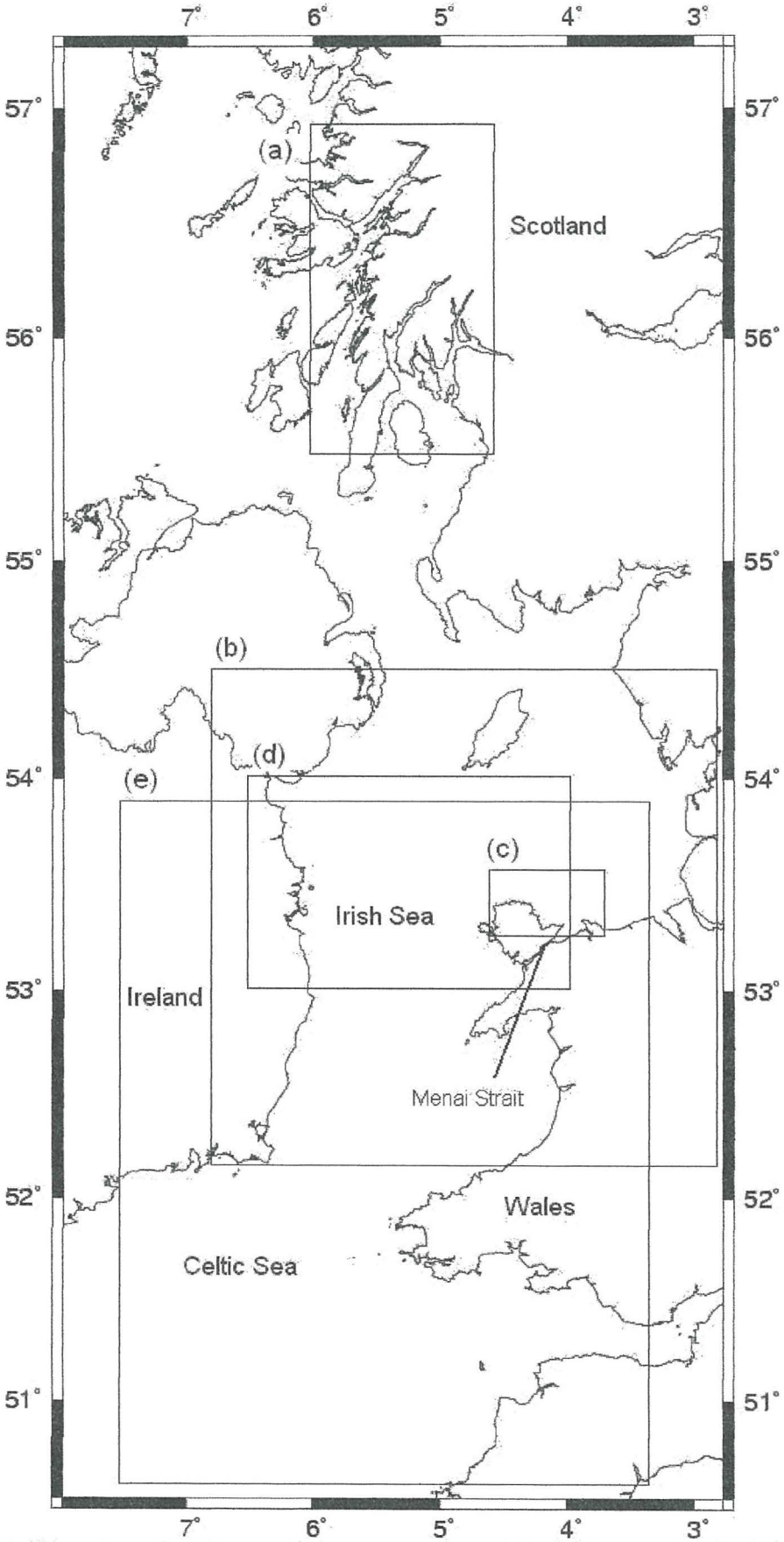

Figure 3.1 Map of sampling sites; (a) Clyde Sea cruise in April 2001, (b) Irish Sea cruise in August 2001, (c) Irish Sea cruise in November 2001, (d) Irish Sea cruise in April 2002, (e) Celtic Sea cruise in July 2002. The Menai Strait where the Menai Bridge Pier is located is also on the map

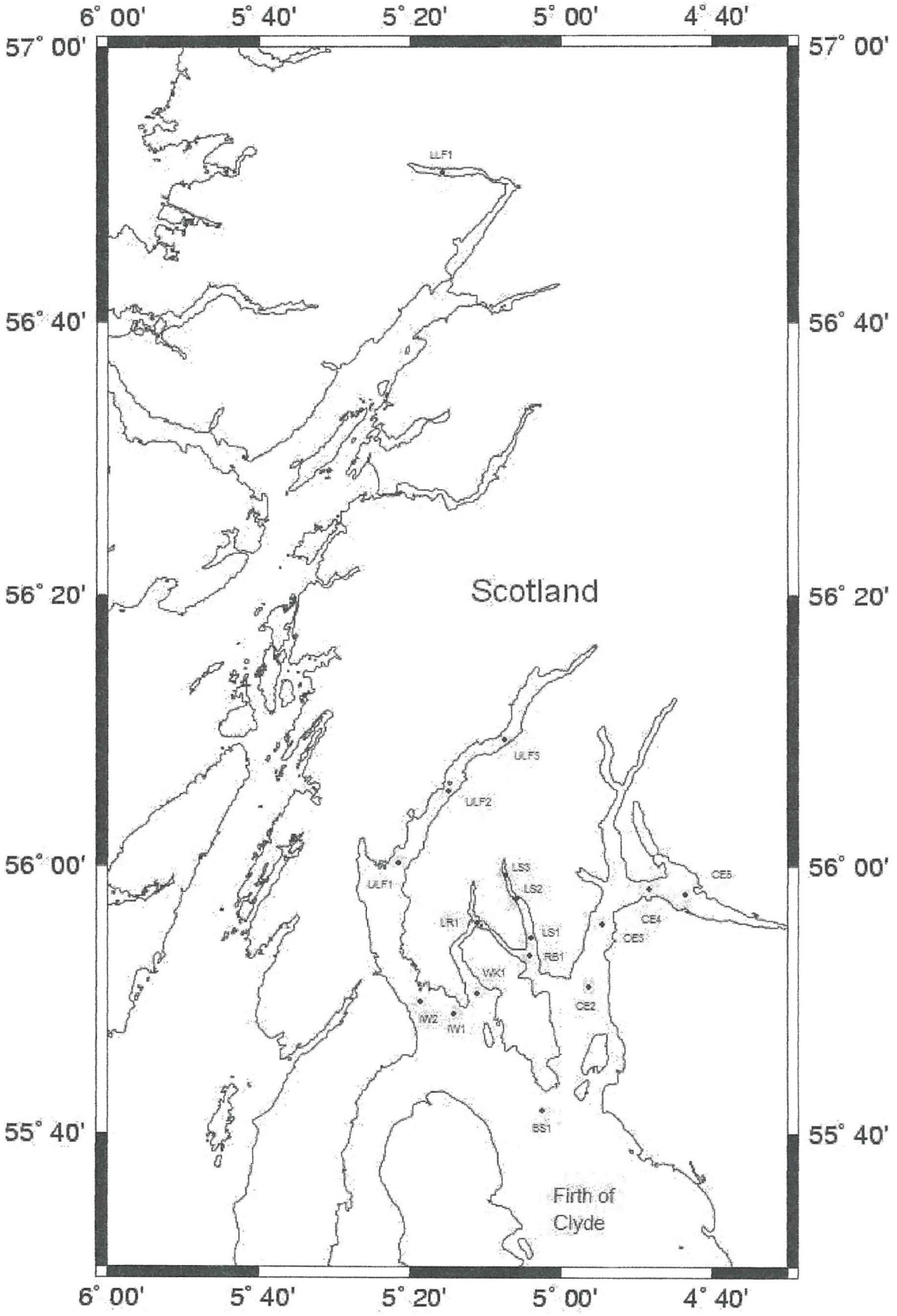

Figure 3.1a Map of sampling stations during the Clyde Sea cruise in April 2001

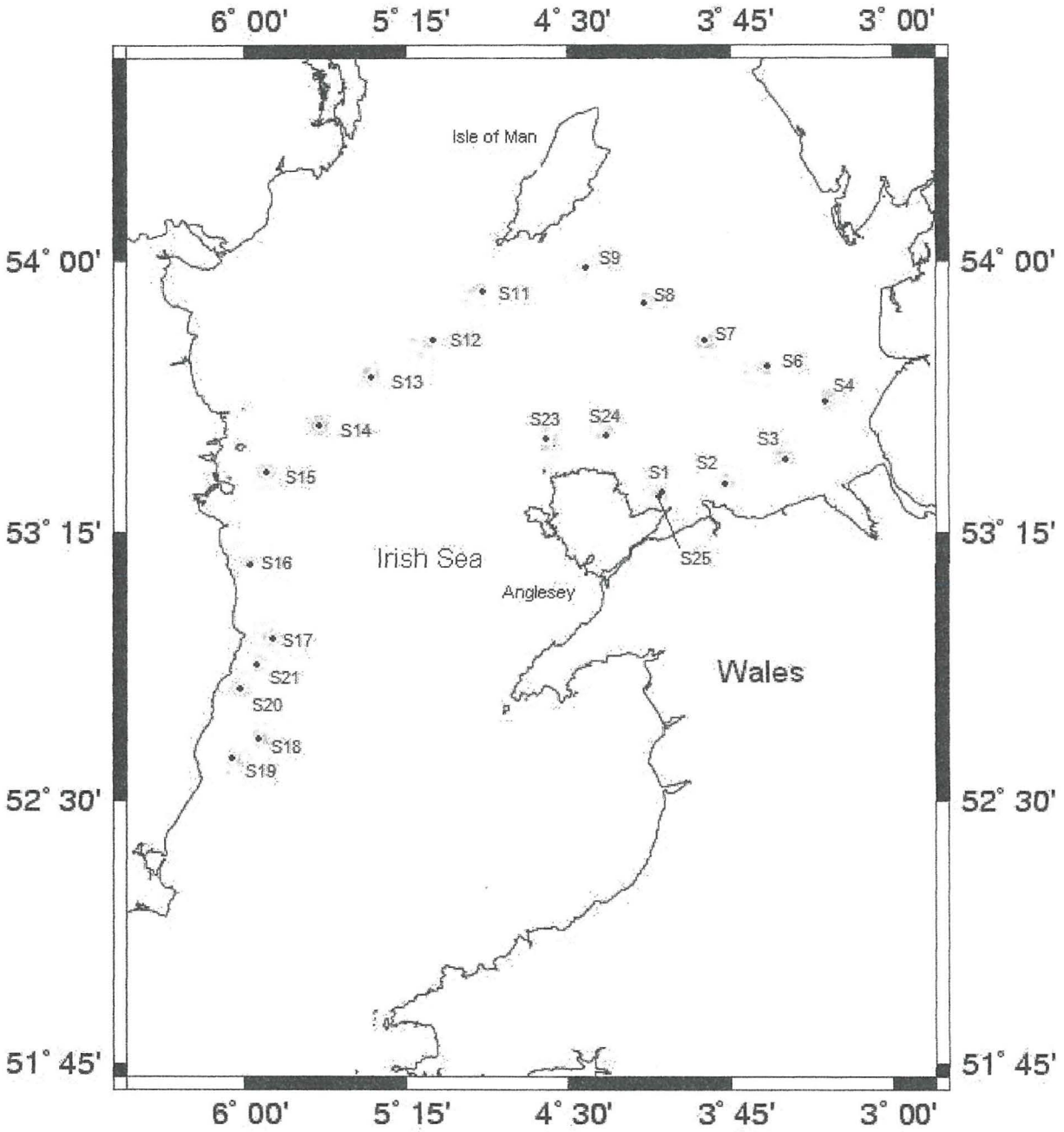

Figure 3.1b Map of sampling stations during the Irish Sea cruise in August 2001

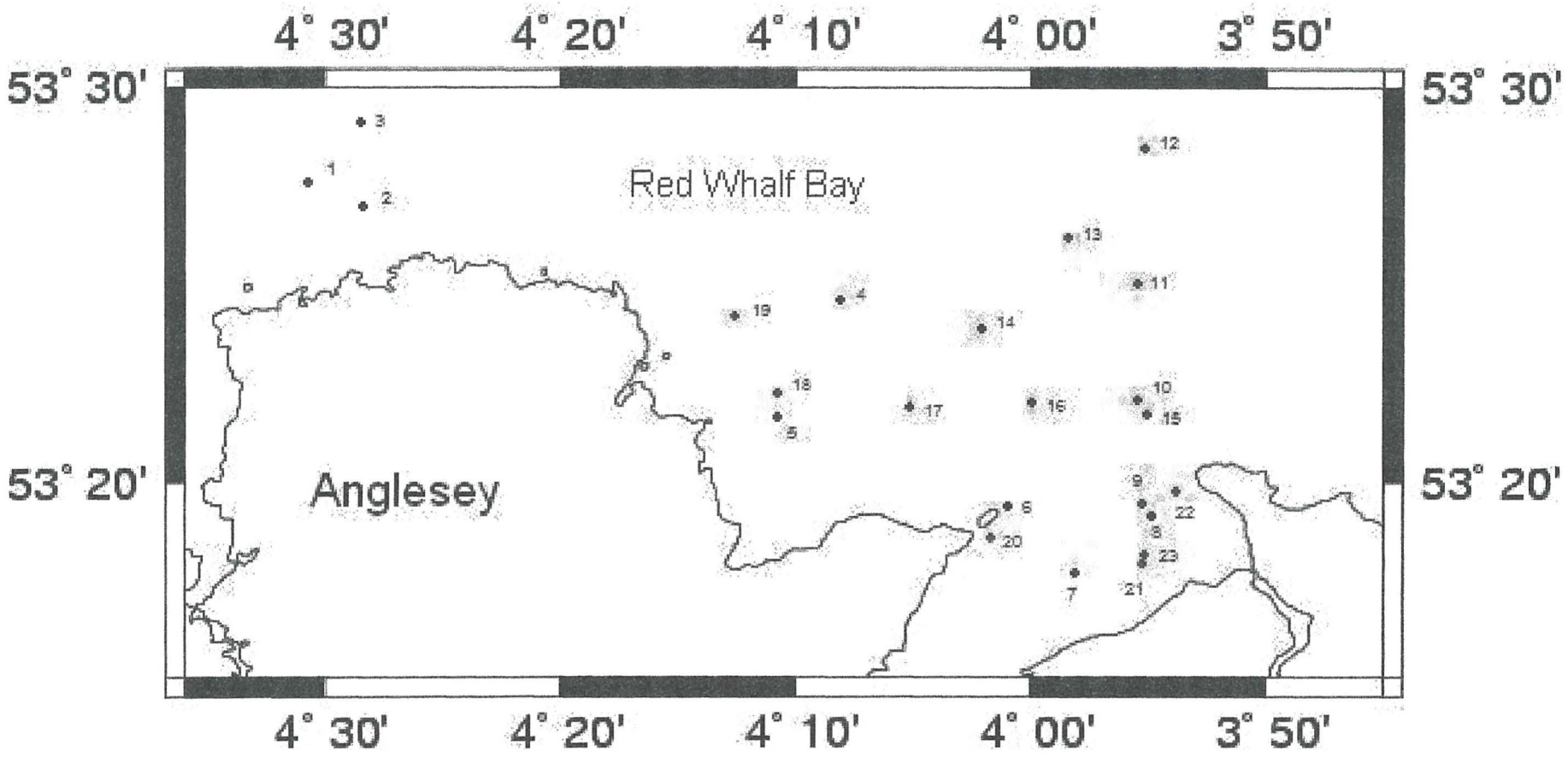

Figure 3.1c Map of sampling stations during the Irish Sea cruise in November 2001

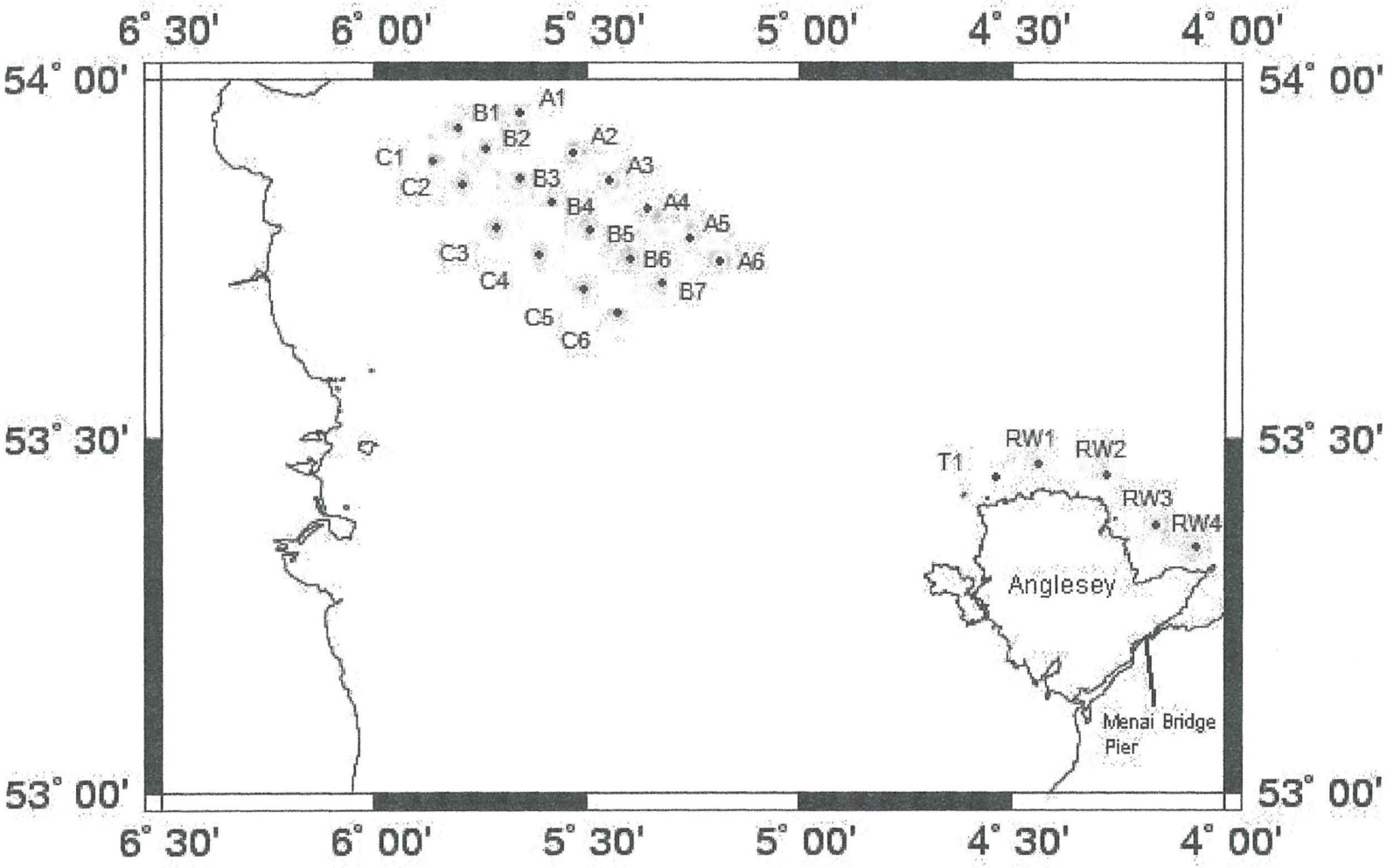

Figure 3.1d Map of sampling stations during the Irish Sea cruise in April 2002

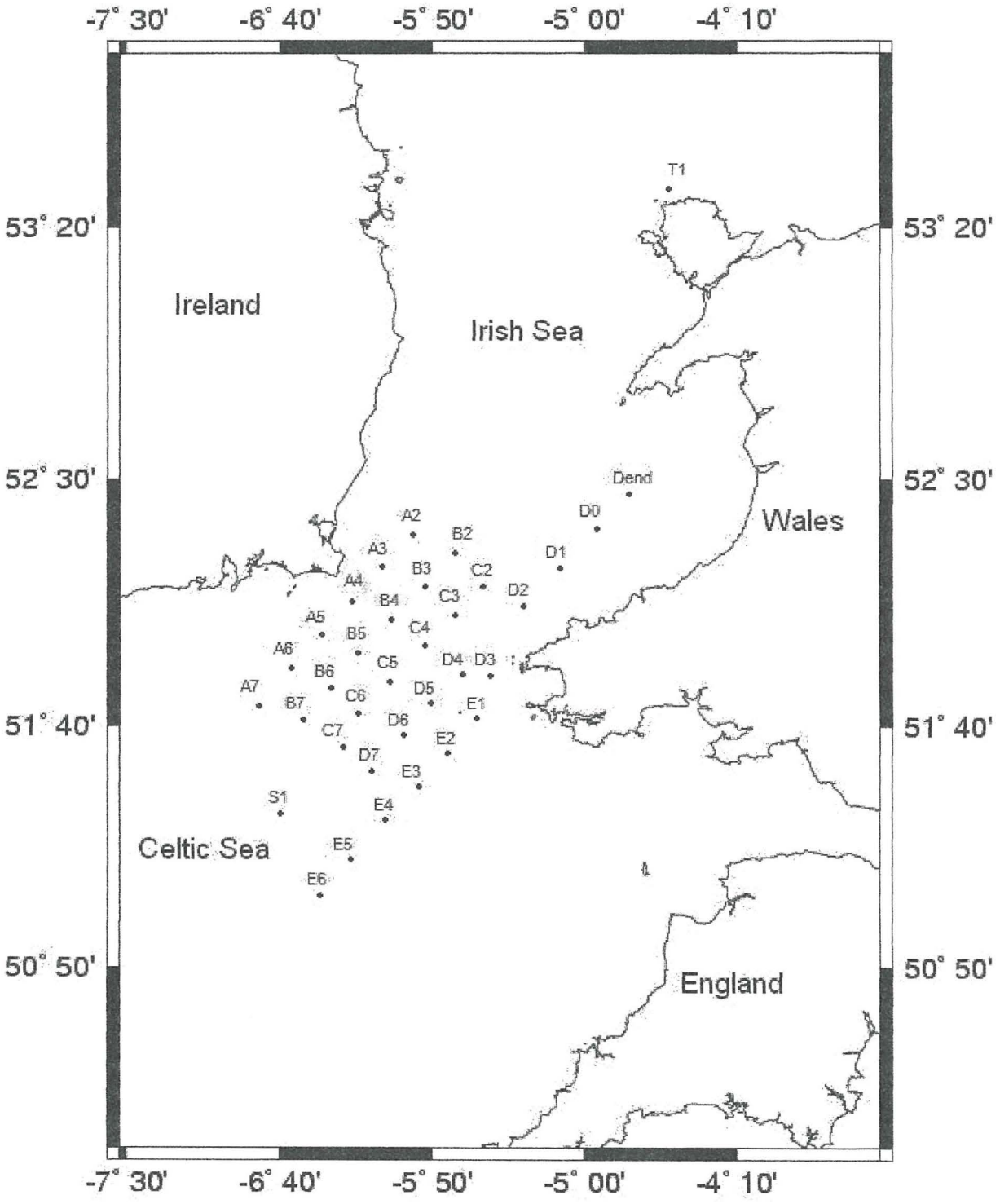

Figure 3.1e Map of sampling stations during the Celtic Sea cruise in July 2002

4. PHYTOPLANKTON POPULATION CHANGES AND PIGMENT DETERMINATION

4.1 Introduction

This chapter describes the result of microscopic taxonomic analysis to identify and obtain cell counts for the dominant phytoplankton species present, and the determination of pigment biomass using HPLC and fluorometric techniques. Samples were taken from the Menai Strait at the Menai Bridge pier between May 2001 and October 2002. There were five cruises around the U.K. shelf seas: the Clyde Sea in April 2001; the Irish Sea in August and November 2001, and in April 2002; and the Celtic Sea in July 2002. The areas of study are shown in Figures 3.1

4.2 Taxonomic analysis of phytoplankton

Phytoplankton species found at each station are presented in Appendix A. The counts were used to determine the major phytoplankton groups. Phytoplankton groups found were divided into three categories; diatoms, dinoflagellates, and the other flagellates. The other flagellates are indicated as 'flagellates' in Appendix A. As diatoms and dinoflagellates were the predominant groups of phytoplankton and individual flagellate groups rarely represented a significant proportion of the population from the areas of study, the rest of phytoplankton groups, such as cryptophytes, prymnesiophytes, chrysophytes, and cyanobacteria, green flagellates were all combined into a single group (flagellates). Green flagellates were assumed to include chlorophytes,

prochlorophytes, prasinophytes, and euglenophytes (Barlow *et al.*, 1993). The cell densities of phytoplankton counted for diatoms, dinoflagellates and flagellates for the areas of study are presented in Figures 4.1-6.

4.2.1 The Menai Strait

In the Menai Strait, apart from diatom and dinoflagellate species, a prymnesiophyte, *Phaeocystis pouchetti* and a chrysophytes, *Distephanus speculum* were the only species found during the study (Appendix A-1).

The sampling for taxonomic analysis initiated on the 25th of May 2001 when one of the prymnesiophytes, *Phaeocystis pouchetti* began to flourish. A seasonal pattern of algal blooms in the Menai Strait seen in the cell counts (Appendix A-1) suggested that *Phaeocystis pouchetti*, which succeeded spring diatom blooms, dominated phytoplankton composition for extended periods in the early summer in the year 2001 and 2002. The population density of *Phaeocystis pouchetti* reached over 650 x 10^3 cells l^{-1} on the 15th of June 2001. *Skeletonema costatum* was the dominant diatom species from late May to mid June 2001 with various *Chaetoceros*, *Lauderia*, *Nitzschia* and *Thalassiosira* species.

Phaeocystis pouchetti's predominance in the phytoplankton population lasted until the 2nd of July. There were more than 350 x 10^3 cells l^{-1} of *Phaeocystis pouchetti* and around 480 x 10^3 cells l^{-1} of diatoms on the 2nd of July (Figure 4.1). There was a decline in the cell density of diatoms in early summer after the 15th of June. These diatoms were *Chaetoceros*, *Skeletonema and Thalassionema* species. However other diatoms such as, *Nitzschia* and *Rhizosolenia* species increased during the summer

bloom in 2001. Their cell densities were around 130 x 10^3 cells l^{-1} and 8 x 10^3 cells l^{-1} respectively, on the 15th of June, and 170 x 10^3 cells l^{-1} and 100 x 10^3 cells l^{-1} respectively, on the 2nd of July (Appendix A-1). Dinoflagellates were found from the 2nd of July 2001. *Ceratium* species, especially *Ceratium furca* were a commonly found dinoflagellates through the summer and autumn of 2001. The population density of *Ceratium* species reached over 230 x 10^3 cells l^{-1} on the 12th of September. The cell density of phytoplankton decreased dramatically to 14 x 10^3 cells l^{-1} on the 13th of December 2001 (Figure 4.1). Diatoms, such as *Biddulphia regia*, *Coscinodiscus lineatus*, and *Nitzschia* species were found on the 13th of December 2001.

Diatoms require silica in soluble form for wall silicification (Boney, 1989). As a result, at times of maximum diatom growth in spring, there is a decline in dissolved silica content. The spring diatom bloom is ended after the depletion of silica in north temperate waters (Lalli and Parsons, 1997). One of the diatoms, *Skeletonema costatum* dominated early spring phytoplankton population in the Menai Strait from February to mid May 2002. As *Skeletonema costatum* is able to grow with very thin siliceous walls, this organism appears in great numbers at the early stage of spring algal bloom in temperate seas (e.g. the Clyde Sea and Southampton Water) (Boney, 1989). The population density of *Skeletonema costatum* was 16 x 10^3 cells l^{-1} on the 22nd of February while it reached 65 x 10^3 cells l^{-1} on the 17th of May 2002. On the 24th of May, the population density of *Skeletonema costatum* began to decrease to 61 x 10^3 cells l^{-1}. The other major diatoms which were present during the early spring bloom were *Nitzschia* species, *Asterionella glacialis*, *Fragilaria oceanica* and *Thalassiosira* species. *Nitzschia* species were found during the spring bloom, however, higher cell density of *Nitzschia* species was observed during the *Phaeocystis pouchetti* bloom in June. The

cell density of *Nitzschia* species reached around 200 x 10^3 cells l^{-1} on the 7th of June 2002 and it began to decrease afterwards. The population density of *Asterionella glacialis* increased sharply from 10 x 10^3 cells l^{-1} on the 22nd of March 2002 to 45 x 10^3 cells l^{-1} on the 12th of April 2002. The highest cell concentration of *Asterionella glacialis* was 95 x 10^3 cells l^{-1} on the 3rd of May 2002. *Fragilaria oceanica* was the dominant diatom on the 15th of March. The cell density of *Fragilaria oceanica* was 47 x 10^3 cells l^{-1}. However it decreased to 15 x 10^3 cells l^{-1} in late March. The cell density of *Fragilaria oceanica* reached 66 x 10^3 cells l^{-1} on the 17th of May 2002 during the period of the highest diatom outburst. The population density of *Thalassiosira* species increased steadily and reached around 25 x 10^3 cells l^{-1} on the 22nd of March 2002. It decreased below 7 x 10^3 cells l^{-1} on the 12th of April and increased again on the 17th of May, reaching around 150 x 10^3 cells l^{-1}.

The presence of *Phaeocystis pouchetti* was detected on the 24th of May 2002. There were more diatoms than *Phaeocystis pouchetti* on the 24th and 31st of May. The population densities of *Phaeocystis pouchetti* found on the 24th and 31st of May were 147 x 10^3 cells l^{-1} and 209 x 10^3 cells l^{-1} respectively. However, the cell density of *Phaeocystis pouchetti* increased sharply over 1100 x 10^3 cells l^{-1}, while there was around 600 x 10^3 cells l^{-1} of diatoms on the 7th of June 2002. The cell density of *Phaeocystis pouchetti* decreased to 654 x 10^3 cells l^{-1} on the 21st of June and less than 100 x 10^3 cells l^{-1} on the 3rd of July, respectively.

During the dinoflagellate bloom between August and September 2002, *Ceratium furca* and *Ceratium fusus* were the predominant dinoflagellates, while *Guinardia flaccida* was one of the major diatoms. The population density of *Ceratium* species increased from 4 x 10^3 cells l^{-1} on the 3rd of July to 268 x 10^3 cells l^{-1} on the 19th

of August. The cell density of diatom, *Guinardia flaccida*, increased from 10 x 10^3 cells l^{-1} on the 3rd of July to 182 x 10^3 cells l^{-1} on the19th of August 2002. *Gyrodinium aureolum* was the second largest group of dinoflagellates on the19th of August and the number reached around 90 x 10^3 cells l^{-1}

A small population of *Distephanus speculum*, which is one of the silicoflagellate, was found between late July and early September 2002. While dinoflagellates dominated the phytoplankton population on the 19th of August, the cell density of *Distephanus speculum* reached around 45 x 10^3 cells l^{-1}. The population density of phytoplankton decreased below 130 x 10^3 cells l^{-1} on the 21st of October 2002 with diatoms dominating the population.

4.2.2 The Clyde Sea; April 2001

Commonly found diatoms in the first stages in the spring outburst in March 1973 were *Skeletonema costatum* and *Thalassiosira nordenskioldii* in the Firth of Clyde (Boney, 1989). In the middle of March 1973, *Thalassiosira nordenskioldii* was more prominent. However, within a few days the faster growing *Skeletonema costatum* overtook *Thalassiosira nordenskioldii*, reaching maximum numbers (10.7 x 10^6 cells l^{-1}) on the 23rd of March, thereafter declining rapidly (Boney, 1989). The decline of spring growth was reflected in the fall in the levels of nutrients, with that of dissolved silica being especially decreased (Bold and Wynne, 1985). Species of *Chaetoceros*, *Coscinodiscus* and *Biddulphia* are also prominent in north temperate coastal localities during the spring (Bold and Wynne, 1985; Hoek *et al.*, 1995).

The diatoms were the predominant phytoplankton group during the Clyde Sea

cruise from the 23rd to 27th of April 2001 (Figure 4.2). Although, the spring outburst of *Skeletonema costatum* and *Thalassiosira nordenskioldii* were observed to end in March 1973 (Boney, 1989), there was a significant presence of both species during the cruise.

4.2.2.1 23rd April

The Clyde Sea cruise started at the stations ULF1, ULF2 and ULF3 on the 23rd of April (Figure 3.1a). The population densities of *Thalassiosira nordenskioldii* at ULF3 were 381 x 10^3 cells l^{-1}, 1010 x 10^3 cells l^{-1} and 60 x 10^3 cells l^{-1}, at the depth of 0 m, 5 m and 15 m, respectively, while there was less than 260 x 10^3 cells l^{-1} of *Skeletonema costatum* at the surface (Appendix A-2).

More *Skeletonema costatum* were found than *Thalassiosira nordenskioldii* at ULF2. There were 506 x 10^3 cells l^{-1} of *Skeletonema costatum*, while there were 146 x 10^3 cells l^{-1} of *Thalassiosira nordenskioldii* at the surface of ULF2. There were 436 x 10^3 cells l^{-1} of *Thalassiosira nordenskioldii*, while the population densities of other *Thalassiosira* species, *T. nitzschoides*, and *T. mendiolana* were 18 x 10^3 cells l^{-1} and 169 x 10^3 cells l^{-1} respectively at the surface of ULF1. The cell density of *Skeletonema costatum* at the surface of ULF1 were 469 x 10^3 cells l^{-1}. The population density of *Coscinodiscus lineatus* at the surface of ULF3 and ULF2 were 117 x 10^3 cells l^{-1} and 89 x 10^3 cells l^{-1}, respectively, while there was no *Coscinodiscus lineatus* at the surface at ULF1.

The higher cell concentrations of *Thalassiosira nordenskioldii* were found at the depth of 5 m than at the depth of 0 m at stations ULF3, ULF2 and ULF1. The cell densities of *Thalassiosira nordenskioldii* at the depth of 5 m at ULF3, ULF2 and ULF1

were 1010 x 10^3 cells l^{-1}, 232 x 10^3 cells $l^{-1}$and 584 x 10^3 cells l^{-1}, respectively.

4.2.2.2 24th April

Samples were taken at stations LLF1, IW1 and BS1 on the 24th of April (Figure 3.1a). The population densities of *Skeletonema costatum* and *Thalassiosira nordenskioldii* at the depth of 10 m were 269 x 10^3 cells l^{-1} and 334 x 10^3 cells l^{-1}, respectively, at LLF1, while the population densities of *Skeletonema costatum* and *Thalassiosira nordenskioldii* at the surface were 232 x 10^3 cells l^{-1} and 289 x 10^3 cells l^{-1}, respectively (Appendix A-2). *Chaetoceros* species, *Detonula confervacea*, *Navicula* species and *Rhizosolenia delicatula* were also major diatoms at LLF1. Their population densities at the depth of 10 m were 89 x 10^3 cells l^{-1}, 99 x 10^3 cells l^{-1}, 110 x 10^3 cells l^{-1} and 107 x 10^3 cells l^{-1}, respectively.

The cell density of *Skeletonema costatum* reached 349 x 10^3 cells l^{-1} at the depth of 5 m at IW1, while the cell density of *Thalassiosira nordenskioldii* was below 90 x 10^3 cells l^{-1}. The cell density of *Paralia sulcata* at the depth of 5 m were 156 x 10^3 cells l^{-1} at IW1, while the cell density of *Chaetoceros* species at the depth of 40 m reached 117 x 10^3 cells l^{-1}.

There were over 310 x 10^3 cells l^{-1} of *Thalassiosira nordenskioldii* at the surface at BS1, while there were 143 x 10^3 cells l^{-1} of *Skeletonema costatum*. The population density of *Thalassiosira nordenskioldii* were 175 x 10^3 cells l^{-1} at the depth of 15 m, and 18 x 10^3 cells l^{-1} at the depth of 45 m at BS1. The cell density of Navicula species reached 112 x 10^3 cells l^{-1} at the surface of BS1, while the cell density of *Detonula confervacea* was around 60 x 10^3 cells l^{-1} at the depth of 15 m. One of the

dinoflagellates, *Ceratium furca* was found at the surface of LLF1 and BS1. There were 13 x 10^3 cells l^{-1} and 8 x 10^3 cells l^{-1}, respectively.

4.2.2.3 25th April

Samples were taken at stations CE5, CE4, CE3 and CE2 on the 25th of April (Figure 3.1a). Station CE5 was sampled twice at 0916 BST and 0955 BST. At CE5, there was a decrease in the cell density of *Skeletonema costatum* from 563 x 10^3 cells l^{-1} at 0916 BST to 482 x 10^3 cells l^{-1} at 0955 BST at the surface, whereas there was a slight increase in the cell density of *Thalassiosira nordenskioldii* from 125 x 10^3 cells l^{-1} at 0916 BST to 149 x 10^3 cells l^{-1} at 0955 BST at the surface (Appendix A-2). The population density of phytoplankton decreased from 1610 x 10^3 cells l^{-1} at 0916 BST to 1440 x 10^3 cells l^{-1} at 0955 BST at the surface of CE5 (Figure 4.2).

The population density of *Skeletonema costatum* at the surface of CE4, CE3 and CE2 were 386 x 10^3 cells l^{-1}, 430 x 10^3 cells l^{-1}, and 227 x 10^3 cells l^{-1} respectively, while the population density of *Thalassiosira nordenskioldii* at the surface of CE4, CE3 and CE2 were 289 x 10^3 cells l^{-1}, 141 x 10^3 cells l^{-1}, and 329 x 10^3 cells l^{-1}, respectively. The cell density of *Lauderia annulata* reached 177 x 10^3 cells l^{-1} at the depth of 12 m at CE4, while the cell density of *Rhizosolenia delicatula* was around 100 x 10^3 cells l^{-1} at the surface. The population densities of *Bacillaria paxillifera* , *Coscinodiscus lineatus* and *Lauderia annulata* at the depth of 5 m were 100 x 10^3 cells l^{-1}, 96 x 10^3 cells l^{-1}, and 91 x 10^3 cells l^{-1}, respectively at CE3.

There was an increase in the population density of dinoflagellates at stations CE4 and CE3. The cell density of *Ceratium furca* at the depth of 12 m at CE4 and at the

depth of 5 m at CE3 were 86 x 10^3 cells l^{-1}, and 29 x 10^3 cells l^{-1}, respectively, while the cell concentrations of *Gyrodinium* species at the surface at CE4 and CE3 reached 120 x 10^3 cells l^{-1}, and 63 x 10^3 cells l^{-1}, respectively. The population densities of *Chaetoceros* species, *Detonula confervacea* and *Melosira moniliformis* at the surface of CE2 were 87 x 10^3 cells l^{-1}, 50 x 10^3 cells l^{-1}, and 71 x 10^3 cells l^{-1}, respectively.

4.2.2.4 26th April

Samples were taken at stations LS3, LS2, LS1 and RB1, LR1on the 26th of April (Figure 3.1a). The population densities of *Skeletonema costatum* at the surface increased seaward, being 203 x 10^3 cells l^{-1}, 279 x 10^3 cells l^{-1}, 428 x 10^3 cells l^{-1}, and 639 x 10^3 cells l^{-1} at LS3, LS2, LS1 and RB1, respectively (Appendix A-2). The population densities of *Coscinodiscus lineatus*, *Lauderia annulata* and *Nitzschia* species at the surface of LS3 were 86 x 10^3 cells l^{-1}, 83 x 10^3 cells l^{-1}, and 82 x 10^3 cells l^{-1} respectively, while the population density of *Thalassiosira nordenskioldii* reached 117 x 10^3 cells l^{-1}.

At LS2, the cell densities of *Skeletonema costatum* and *Thalassiosira nordenskioldii* at the depth of 20 m was larger than at the depth of 5 m. Their population density were 407 x 10^3 cells l^{-1}, and 175 x 10^3 cells l^{-1} respectively, at 20 m, and, 83 x 10^3 cells l^{-1}, and 86 x 10^3 cells l^{-1} respectively, at 5 m. The cell density of *Minidiscus trioculatus* at the depth of 20 m at LS2 was 141 x 10^3 cells l^{-1}, while the cell density of it at the surface was 29 x 10^3 cells l^{-1}. In addition, there were 83 x 10^3 cells l^{-1} of *Chaetoceros* species and 112 x 10^3 cells l^{-1} of *Detonula confervacea* at the surface at LS2.

The population density of *Skeletonema costatum* at 10m at LS1 reached 696 x

10^3 cells l^{-1}, while the population density of *Thalassiosira nordenskioldii* was 378 x 10^3 cells l^{-1}. The population densities of *Chaetoceros* species, *Ditylum brightwellii* and *Melosira moniliformis* at the depth of 10 m at LS1 were around 60 x 10^3 cells l^{-1} respectively, while the population density of dinoflagellates, *Gyrodinium* species, was 47 x 10^3 cells l^{-1}.

The largest population density of *Skeletonema costatum* was found at RB1 at the depth of 7 m, with the cell concentration reaching 814 x 10^3 cells l^{-1} on the 26th of April. The cell densities of *Asterionella kariana* and *Chaetoceros* species at the surface of RB1 reached around 60 x 10^3 cells l^{-1} respectively, while the cell density of *Minidiscus trioculatus* was 83 x 10^3 cells l^{-1}. The cell densities of dinoflagellates at the depth of 0 m, 7 m and 20 m at RB1 were 65 x 10^3 cells l^{-1}, 128 x 10^3 cells l^{-1}, and 55 x 10^3 cells l^{-1} respectively.

At LR1, there were around 232 x 10^3 cells l^{-1}, and 271 x 10^3 cells l^{-1} of *Skeletonema costatum* at the surface and 10 m, respectively, while there were 279 x 10^3 cells l^{-1}, and 313 x 10^3 cells l^{-1} of *Thalassiosira nordenskioldii*, respectively. The cell density of *Chaetoceros* species reached 84 x 10^3 cells l^{-1} at the surface of LR1, while the cell densities of *Ditylum brightwellii*, *Lauderia borealis* and *Paralia sulcata* were around 55 x 10^3 cells l^{-1} respectively at the depth of 10 m.

4.2.2.5 27th April

Samples were taken at stations WK1 and IW2 on the 27th of April. The cell densities of *Skeletonema costatum* and *Thalassiosira nordenskioldii* at the depth of 15 m at WK1 were 401 x 10^3 cells l^{-1}, and 269 x 10^3 cells l^{-1} respectively, while their cell densities at

the depth of 10 m at IW2 reached 389 x 10^3 cells l^{-1}, and 282 x 10^3 cells l^{-1} respectively (Appendix A-2). The population density of *Thalassiosira nordenskioldii* at the surface of IW2 was higher than at the surface of WK1. The cell densities of *Thalassiosira nordenskioldii* were 386 x 10^3 cells l^{-1} at the surface of IW2 and 31 x 10^3 cells l^{-1} at the surface of WK1, respectively. However, the cell density of *Skeletonema costatum* at the surface of WK1 (316 x 10^3 cells l^{-1}) was larger than at the surface of IW2 (172 x 10^3 cells l^{-1}). The population densities of *Chaetoceros* species and *Fragilaria* species at 15 m at WK1 were 112 x 10^3 cells l^{-1}, and 60 x 10^3 cells l^{-1} respectively, while their cell densities at 10 m at IW2 were 83 x 10^3 cells l^{-1}, and 57 x 10^3 cells l^{-1} respectively. The population density of dinoflagellates at 15 m at WK1 was 120 x 10^3 cells l^{-1} (Figure 4.2). There were 81 x 10^3 cells l^{-1} of *Gyrodinium* species and 39 x 10^3 cells l^{-1} of *Ceratium furca* at 15 m at WK1.

4.2.3 The Irish Sea; August 2001

A mixed population of diatoms and dinoflagellates was observed during the Irish Sea cruise from the 6th to 10th of August 2001 (Figure 4.3). Diatoms, such as *Detonula confervacea* and *Rhizosolenia* species were found from Liverpool Bay to the western Irish Sea through the cruise, whereas *Leptocylindrus danicus* was mainly found in the western Irish Sea. One of dinoflagellates, *Gyrodinium aureolum* was found in the eastern Irish Sea, while other dinoflagellates, such as *Ceratium* species and *Noctiluca scintillans* were found at all sampling stations during the cruise.

Previous works showed that *Leptocylindrus danicus* and *Rhizosolenia delicatula* were the dominant diatoms during the summer in the Irish inshore water

(Hallegraeff, 1993; McKinney *et al.*, 1997), while a dinoflagellate, *Gyrodinium aureolum* was reported in the inshore water of south-east Liverpool Bay (Helm *et al.*, 1974).

4.2.3.1 6th August 2001

The cruise worked a line of stations (1, 2 and 3) on the 6th of August 2001 from Red Wharf Bay along the coast of North Wales to Liverpool Bay (Figure 3.1b). *Rhizosolenia shrubsolei* was the dominant diatom at station 1, with the population densities of 26 x 10^3 cells l^{-1} at the surface, and 47 x 10^3 cells l^{-1} at the depth of 10 m, respectively (Appendix A-3). The population density of *Coscinodiscus lineatus* at the surface of station 1 was 23 x 10^3 cells l^{-1}, while that of *Detonula confervacea* was 16 x 10^3 cells l^{-1}. The dominant dinoflagellates at station 1 were *Ceratium furca* and *Gyrodinium aureolum*, with a population density of 21 x 10^3 cells l^{-1}, and 18 x 10^3 cells l^{-1} at the surface, respectively.

The population density of *Rhizosolenia setigera* at the surface of station 2 was 34 x 10^3 cells l^{-1}, while the population density of *Rhizosolenia delicatula* was 23 x 10^3 cells l^{-1}. The population densities of *Chaetoceros danicum*, *Coscinodiscus* species and *Rhizosolenia shrubsolei* at the depth of 7 m at station 2 were 15 x 10^3 cells l^{-1}, 23 x 10^3 cells l^{-1}, and 16 x 10^3 cells l^{-1} respectively. *Ceratium* species were the dominant dinoflagellates at station 2. There were 31 x 10^3 cells l^{-1} of *Ceratium furca*, 21 x 10^3 cells l^{-1} of *Ceratium fusus*, and 13 x 10^3 cells l^{-1} of *Ceratium lineatum*, respectively at 7 m at station 2. The cell densities of other dinoflagellates, *Gyrodinium aureolum* and *Prorocentrum micans* were 10 x 10^3 cells l^{-1} and 16 x 10^3 cells l^{-1} respectively, at the

surface, and 18 x 10^3 cells l^{-1} and 10 x 10^3 cells l^{-1} respectively, at the depth of 7 m at station 2.

The diatom of the genus *Rhizosolenia* were dominant with the population density of 84 x 10^3 cells l^{-1} at the surface and 31 x 10^3 cells l^{-1} at the depth of 11 m at station 3. The population density of *Chaetoceros danicum* at 11 m at station 3 was 23 x 10^3 cells l^{-1}, while the population density of *Leptocylindrus danicus* was 5 x 10^3 cells l^{-1}. *Dictyocha fibula* and *Protoperidinium depressum* were the dominant dinoflagellates at station 3. There were 18 x 10^3 cells l^{-1} of *Dictyocha fibula* and 16 x 10^3 cells l^{-1} of *Protoperidinium depressum* at the surface. In addition, the population density of *Gyrodinium aureolum* at the surface of station 3 was 10 x 10^3 cells l^{-1}, while the population density of *Noctiluca scintillans* was 8 x 10^3 cells l^{-1}.

The population density of diatoms was higher than that of the dinoflagellates at station 1 and 3 (Figure 4.3). There were 89 x 10^3 cells l^{-1} and 96 x 10^3 cells l^{-1} of diatoms, at the surface of station 1 and 3, respectively, while there were 73 x 10^3 cells l^{-1} and 87 x 10^3 cells l^{-1} of dinoflagellates, respectively. However, the population density of dinoflagellates at station 2 was higher than that of the diatoms. The population density of dinoflagellates at station 2 was 81 x 10^3 cells l^{-1} at the surface, while that of diatoms was 73 x 10^3 cells l^{-1}. The population densities of individual flagellate groups were 16 x 10^3 cells l^{-1}, 39 x 10^3 cells l^{-1}, and 47 x 10^3 cells l^{-1} at the surface of stations 1, 2 and 3, respectively. Flagellate groups included prymnesiophytes, chrysophytes and chlorophytes at stations 1, 2, and 3.

4.2.3.2 7th August 2001

Samples were taken from Liverpool Bay toward the Isle of Man at the stations 4, 6, 7 and 8, 9 on the 7th of August 2001 (Figure 3.1b). The dominant genus of diatoms were *Rhizosolenia* species from station 4 to 9, while the dominant genus of dinoflagellates were *Ceratium* and *Gyrodinium* species (Appendix A-3). The cell densities of *Rhizosolenia* species and *Ceratium* species at the surface of station 4 reached 133 x 10^3 cells l^{-1}, and 86 x 10^3 cells l^{-1} respectively, while the cell densities of both genus at station 6 were 29 x 10^3 cells l^{-1}, and 44 x 10^3 cells l^{-1} respectively. There were 18 x 10^3 cells l^{-1} of *Gyrodinium aureolum* and 8 x 10^3 cells l^{-1} of *Noctiluca scintillans* at the surface of station 6.

At station 7, *Rhizosolenia setigera* was the dominant species within the diatom population with the cell densities reaching 23 x 10^3 cells l^{-1}, 29 x 10^3 cells l^{-1}, and 37 x 10^3 cells l^{-1} at the depths of 0 m, 10 m and 25 m, respectively. The population densities of *Coscinodiscus lineatus* and *Guinardia flaccida* at the surface were 13 x 10^3 cells l^{-1} and 10 x 10^3 cells l^{-1} respectively, while that of *Detonula confervacea* at 10 m was 23 x 10^3 cells l^{-1}. There were 44 x 10^3 cells l^{-1} of *Ceratium* species and 29 x 10^3 cells l^{-1} of *Gyrodinium aureolum* at the surface of station 7.

Rhizosolenia species were the prominent groups of diatoms at stations 8 with population densities of 95 x 10^3 cells l^{-1}, 125 x 10^3 cells l^{-1}, and 139 x 10^3 cells l^{-1} at the depths of 0 m, 10 m and 25 m, respectively. However the population density of *Ceratium* species decreased to 5 x 10^3 cells l^{-1}, 19 x 10^3 cells l^{-1} and 8 x 10^3 cells l^{-1} at the depths of 0 m, 10 m and 25 m, respectively at station 8. The population densities of *Gyrodinium aureolum* and *Noctiluca scintillans* at station 8 were 10 x 10^3 cells l^{-1} and 8

x 10^3 cells l^{-1} respectively, at the surface, and 21 x 10^3 cells l^{-1} and 13 x 10^3 cells l^{-1} respectively, at the depth of 10 m.

Rhizosolenia species were the dominant diatoms at station 9. The population densities of *Rhizosolenia delicatula* and *Rhizosolenia setigera* were 55 x 10^3 cells l^{-1} and 31 x 10^3 cells l^{-1} respectively at the depth of 10 m, while there were 13 x 10^3 cells l^{-1} of *Ceratium furca* and 15 x 10^3 cells l^{-1} of *Noctiluca scintillans* at the surface.

The largest population of phytoplankton during the cruise was recorded at the surface of station 4 with cell densities of 389 x 10^3 cells l^{-1} (Figure 4.3). There were 193 x 10^3 cells l^{-1} of dinoflagellates and 172 x 10^3 cells l^{-1} of diatoms, with 23 x 10^3 cells l^{-1} of flagellates at the surface of station 4. The population density of dinoflagellates was higher than that of diatoms at the surface and 10 m at station 6, and at all depths of station 7. There were 86 x 10^3 cells l^{-1} of dinoflagellates, and 44 x 10^3 cells l^{-1} of diatoms, respectively at the surface of station 6, while there were 94 x 10^3 cells l^{-1} of dinoflagellates and 55 x 10^3 cells l^{-1} of diatoms, respectively at the surface of station 7. However, diatoms dominated the phytoplankton population at station 8 and 9. The cell densities of diatoms and dinoflagellates reached 164 x 10^3 cells l^{-1} and 55 x 10^3 cells l^{-1} respectively, at the surface of station 8, and 86 x 10^3 cells l^{-1} and 50 x 10^3 cells l^{-1} respectively, at the surface of station 9. The cell densities of flagellates increased from 8 x 10^3 cells l^{-1} at the surface of station 6 to 41 x 10^3 cells l^{-1} at the surface of station 8 (Figure 4.3).

4.2.3.3 8th August 2001

Samples were taken across the western Irish Sea from the Isle of Man to the Irish

inshore water at stations 11, 12, 13 and 14, 15 on the 8th of August (figure 3.1b). *Rhizosolenia setigera* and *Detonula confervacea* were the dominant diatoms at the surface of station 11 with population densities of 73 x 10^3 cells l^{-1} and 47 x 10^3 cells l^{-1} respectively, while the population densities of *Leptocylindrus danicus* and *Rhizosolenia styliformis* at the depth of 10 m reached around 23 x 10^3 cells l^{-1} respectively (Appendix A-3). The major dinoflagellates at station 11 were *Ceratium furca, Ceratium lineatum, Dinophysis acuta* and *Noctiluca scintillans* with population densities of 34 x 10^3 cells l^{-1}, 16 x 10^3 cells l^{-1}, 23 x 10^3 cells l^{-1}, and 29 x 10^3 cells l^{-1} respectively, at the surface.

The cell densities of *Rhizosolenia delicatula, Rhizosolenia setigera* and *Rhizosolenia shrubsolei* at 15 m at station 12 were 31 x 10^3 cells l^{-1}, 39 x 10^3 cells l^{-1}, and 23 x 10^3 cells l^{-1} respectively, while those of *Detonula confervacea, Leptocylindrus danicus* reached 26 x 10^3 cells l^{-1}, 13 x 10^3 cells l^{-1} respectively. The prominent species of dinoflagellates at station 12 was *Ceratium lineatum* with the cell densities reaching 96 x 10^3 cells l^{-1}, 60 x 10^3 cells l^{-1}, and 31 x 10^3 cells l^{-1} at the depths of 0 m, 15 m and 30m, respectively. The population densities of *Ceratium furca* and *Ceratium fusus* were 39 x 10^3 cells l^{-1} and 31 x 10^3 cells l^{-1} respectively at the surface, and 23 x 10^3 cells l^{-1} and 8 x 10^3 cells l^{-1} respectively at 15 m, while those of *Gonyaulax spinifera, Gyrodinium spirale*, and *Pyrodinium bahamense* were 23 x 10^3 cells l^{-1}, 15 x 10^3 cells l^{-1}, and 15 x 10^3 cells l^{-1} respectively at the surface.

Rhizosolenia species, *Detonula confervacea* and *Leptocylindrus danicus* were the dominant diatom groups at station 13, while *Ceratium* species and *Noctiluca scintillans* were the dominant dinoflagellates. There were 55 x 10^3 cells l^{-1} of *Rhizosolenia delicatula*, 16 x 10^3 cells l^{-1} of *Rhizosolenia setigera*, and 15 x 10^3 cells l^{-1} of *Rhizosolenia shrubsolei* respectively, at the depth of 15 m at station 13, while the cell

densities of *Detonula confervacea* and *Leptocylindrus danicus* were 31 x 10^3 cells l^{-1} and 23 x 10^3 cells l^{-1} respectively. The population densities of *Ceratium furca* and *Ceratium lineatum* at station 13 were 39 x 10^3 cells l^{-1} and 23 x 10^3 cells l^{-1} respectively, at the surface, and 16 x 10^3 cells l^{-1} and 63 x 10^3 cells l^{-1} respectively, at the depth of 15 m. The cell density of *Noctiluca scintillans* was 5 x 10^3 cells l^{-1} at the surface of station 13, whereas it reached 23 x 10^3 cells l^{-1} at 15 m.

Only surface samples were obtained at stations 14 and 15 due to the malfunction of the CTD. *Leptocylindrus danicus* with cell densities of 37 x 10^3 cells l^{-1} was the dominant diatom species, while *Ceratium lineatum* with cell densities of 31 x 10^3 cells l^{-1} was the major dinoflagellate at surface of station 14.

The population densities of *Detonula confervacea* and *Leptocylindrus danicus* were 23 x 10^3 cells l^{-1} and 26 x 10^3 cells l^{-1} respectively at the surface of station 15, while that of *Rhizosolenia* species was 46 x 10^3 cells l^{-1}. The population densities of *Ceratium furca* was 39 x 10^3 cells l^{-1} and *Prorocentrum micans* was 26 x 10^3 cells l^{-1} respectively, at the surface of station 15.

The population density of diatoms was 172 x 10^3 cells l^{-1} while that of dinoflagellates was 128 x 10^3 cells l^{-1} at the surface of station 11 (Figure 4.3). However, the population density of dinoflagellates was higher than diatoms at the surface of station 12. There were 196 x 10^3 cells l^{-1} of dinoflagellates and 94 x 10^3 cells l^{-1} of diatoms, with 16 x 10^3 cells l^{-1} of flagellates at the surface of station 12. The cell density of phytoplankton at the surface of station 13 decreased to 211 x 10^3 cells l^{-1}; there were 110 x 10^3 cells l^{-1} of diatoms, 86 x 10^3 cells l^{-1} of dinoflagellates, and 15 x 10^3 cells l^{-1} of flagellates. The cell densities of diatoms and dinoflagellates at the surface were 86 x 10^3 cells l^{-1} and 94 x 10^3 cells l^{-1} respectively at station 14, and 125 x 10^3 cells l^{-1} and 110 x

10^3 cells l^{-1} respectively, at station 15.

4.2.3.4 9th August 2001

Samples were taken along the Irish inshore water at stations 16, 17, 18, 19 and 20, 21 on the 9th of August (Figure 3.1b). The dominant diatoms were *Rhizosolenia* species, *Detonula confervacea* and *Leptocylindrus danicus* in the Irish inshore water, while *Ceratium* species and *Noctiluca scintillans* were commonly found dinoflagellates in all stations on the 9th of August (Appendix A-3).

Rhizosolenia species were the major diatoms with population densities of 72 x 10^3 cells l^{-1}, 61 x 10^3 cells l^{-1}, and 50 x 10^3 cells l^{-1} respectively at the depths of 0 m, 15 m and 30 m at station 16, whereas *Ceratium* species were the prominent dinoflagellates with population densities of 86 x 10^3 cells l^{-1}, 109 x 10^3 cells l^{-1}, and 117 x 10^3 cells l^{-1} respectively. The population densities of *Leptocylindrus danicus* at station 16 were 37 x 10^3 cells l^{-1}, 23 x 10^3 cells l^{-1}, and 42 x 10^3 cells l^{-1} respectively, at the depths of 0 m, 15 m and 30 m, while those of *Detonula confervacea* were 21 x 10^3 cells l^{-1}, 13 x 10^3 cells l^{-1}, and 18 x 10^3 cells l^{-1} respectively. The cell densities of *Noctiluca scintillans* at station 16 were 23 x 10^3 cells l^{-1}, 10 x 10^3 cells l^{-1}, and 8 x 10^3 cells l^{-1} respectively, at the depths of 0 m, 15 m and 30 m, while there were 26 x 10^3 cells l^{-1} of *Gymnodinium fuscum* at the surface.

The population densities of *Leptocylindrus danicus* and *Detonula confervacea* at the surface of station 17 were 29 x 10^3 cells l^{-1} and 16 x 10^3 cells l^{-1} respectively, while those of *Rhizosolenia setigera* and *Coscinodiscus lineatus* were 10 x 10^3 cells l^{-1} and 16 x 10^3 cells l^{-1} respectively. The cell densities of *Ceratium furca*, *Ceratium fusus*

and *Ceratium lineatum* at the depth of 10 m at station 17 were 16 x 10^3 cells l^{-1}, 8 x 10^3 cells l^{-1}, and 16 x 10^3 cells l^{-1} respectively, while there were 10 x 10^3 cells l^{-1} of *Noctiluca scintillans*.

Leptocylindrus danicus and *Detonula confervacea* were the dominant diatoms at station 18 with *Coscinodiscus eccentrica* and *Nitzschia* species. The population densities of *Leptocylindrus danicus* and *Detonula confervacea* reached 29 x 10^3 cells l^{-1} and 21 x 10^3 cells l^{-1} at 15 m, respectively, while there were 18 x 10^3 cells l^{-1} of *Coscinodiscus eccentrica* at 15 m, and 23 x 10^3 cells l^{-1} of *Nitzschia* species at 30 m, respectively. The population densities of *Rhizosolenia* species and *Ceratium* species at station 18 were larger at the depth of 30 m than at the surface and 15 m. There were 26 x 10^3 cells l^{-1}, 25 x 10^3 cells l^{-1}, and 91 x 10^3 cells l^{-1} of *Rhizosolenia* species at the depths of 0 m, 15 m and 30 m, respectively, while there were 63 x 10^3 cells l^{-1}, 40 x 10^3 cells l^{-1}, and 91 x 10^3 cells l^{-1} of *Ceratium* species, respectively. The population densities of *Gymnodinium fuscum* at station 18 were 8 x 10^3 cells l^{-1}, 16 x 10^3 cells l^{-1}, and 23 x 10^3 cells l^{-1} at the depths of 0 m, 15 m and 30 m, respectively, while those of *Prorocentrum micans* were 16 x 10^3 cells l^{-1} and 23 x 10^3 cells l^{-1} at the depths of 0 m and 30 m, respectively. There were over 23 x 10^3 cells l^{-1} of *Pyrodinium bahamense* at 15 m at station 18.

The cell densities of *Leptocylindrus danicus* were 13 x 10^3 cells l^{-1}, 21 x 10^3 cells l^{-1}, and 29 x 10^3 cells l^{-1} at the depths of 0 m, 15 m, and 25 m at station 19, respectively, while those of *Detonula confervacea* were 16 x 10^3 cells l^{-1}, 8 x 10^3 cells l^{-1}, and 18 x 10^3 cells l^{-1} respectively. There were 18 x 10^3 cells l^{-1} of *Rhizosolenia delicatula* and 13 x 10^3 cells l^{-1} of *Coscinodiscus lineatus* at 15 m at station 19. The cell densities of *Ceratium* species at station 19 were 24 x 10^3 cells l^{-1}, 23 x 10^3 cells l^{-1}, and

46 x 10^3 cells l^{-1} respectively, at the depths of 0 m, 15 m, and 25 m.

Leptocylindrus danicus, *Detonula confervacea* and *Rhizosolenia delicatula* were the dominant diatoms at stations 20 and 21. The population densities of *Leptocylindrus danicus* at the surface and 10 m were 18 x 10^3 cells l^{-1}, and 31 x 10^3 cells l^{-1} respectively, at station 20, while they were 16 x 10^3 cells l^{-1} and 29 x 10^3 cells l^{-1} at the surface and 15 m, respectively, at station 21. The population densities of *Detonula confervacea* were 23 x 10^3 cells l^{-1} at 10 m at station 20, and 21 x 10^3 cells l^{-1} at 15 m at station 21, respectively, while those of *Rhizosolenia delicatula* were 16 x 10^3 cells l^{-1} at the surface of station 20 and 23 x 10^3 cells l^{-1} at the surface of station 21, respectively. The cell densities of *Ceratium* species were 16 x 10^3 cells l^{-1} at the surface and 32 x 10^3 cells l^{-1} at 10 m, respectively, at station 20, and 39 x 10^3 cells l^{-1} at the surface and 16 x 10^3 cells l^{-1} at 15 m, respectively, at station 21, while there were 23 x 10^3 cells l^{-1} of *Noctiluca scintillans* at the surface of station 20 with 8 x 10^3 cells l^{-1} of *Noctiluca scintillans* at the surface of station 21.

The population densities of dinoflagellates were greater than diatoms at the surface and at the depth of 30 m at station 16 (Figure 4.3). The cell density of dinoflagellates at the surface of station 16 was 141 x 10^3 cells l^{-1}, and that of diatoms was 133 x 10^3 cells l^{-1} respectively, with 8 x 10^3 cells l^{-1} of flagellates, while there were 125 x 10^3 cells l^{-1} of dinoflagellates, 141 x 10^3 cells l^{-1} of diatoms, and 23 x 10^3 cells l^{-1} of flagellates respectively at 15 m at station 16. There were more diatoms than dinoflagellates at station 17, The cell densities of diatoms and dinoflagellates at the surface of station 17 were 86 x 10^3 cells l^{-1} and 47 x 10^3 cells l^{-1} respectively, with 23 x 10^3 cells l^{-1} of flagellates. The cell density of phytoplankton at the depth of 30m at station 18 reached 352 x 10^3 cells l^{-1}, while it was 211 x 10^3 cells l^{-1} at the surface. There

were 146 x 10^3 cells l^{-1} of dinoflagellates, 183 x 10^3 cells l^{-1} of diatoms, and 23 x 10^3 cells l^{-1} of flagellates, respectively, at 30 m at station 18. The population densities of phytoplankton increased from the surface of station 19 with cell concentrations of 110 x 10^3 cells l^{-1}, to the surface of station 21 with cell concentrations of 164 x 10^3 cells l^{-1}. The cell densities of flagellates at the surface of station 19, 20 and 21 were 8 x 10^3 cells l^{-1}, 31 x 10^3 cells l^{-1}, and 23 x 10^3 cells l^{-1} respectively.

4.2.3.5 10th August 2001

Samples were taken in Red Wharf Bay along the north coast of Anglesey at station 23, 24 and 25 on the 10th of August 2001 (Figure 3.1b). The major diatom at stations 23, 24 and 25 was *Rhizosolenia setigera*, while the prominent dinoflagellate was *Ceratium furca* (Appendix A-3). The cell densities of *Rhizosolenia setigera* at station 23 were 26 x 10^3 cells l^{-1}, 13 x 10^3 cells l^{-1}, and 16 x 10^3 cells l^{-1} respectively at the depths of 0 m, 10 m and 25 m, while there were 16 x 10^3 cells l^{-1} of *Coscinodiscus* species at the depth of 10 m. There were 13 x 10^3 cells l^{-1} of *Ceratium furca* and 10 x 10^3 cells l^{-1} of *Gyrodinium aureolum*, respectively, at the depth of 10 m at station 23.

The population densities of *Rhizosolenia setigera* at station 24 at the depths of 0 m, 15m and 25 m were 16 x 10^3 cells l^{-1}, 18 x 10^3 cells l^{-1}, and 13 x 10^3 cells l^{-1} respectively, while those of *Detonula confervacea* were 10 x 10^3 cells l^{-1}, 8 x 10^3 cells l^{-1}, and 5 x 10^3 cells l^{-1} repectively. There were 52 x 10^3 cells l^{-1} of *Ceratium* species, 18 x 10^3 cells l^{-1} of *Gyrodinium aureolum*, and 13 x 10^3 cells l^{-1} of *Noctiluca scintillans* at the surface of station 24.

The population densities of *Rhizosolenia setigera* at the depths of 0 m and 5 m

at station 25 were 39 x 10^3 cells l^{-1}, and 23 x 10^3 cells l^{-1} respectively. The dominant dinoflagellate at the depths of 0 m and 5 m at station 25 was *Noctiluca scintillans* with cell concentrations of 34 x 10^3 cells l^{-1}, and 29 x 10^3 cells l^{-1} respectively. The cell density of *Nitzschia* species at the surface of station 25 was 23 x 10^3 cells l^{-1}, whereas that of *Ceratium furca* at the depth of 5 m was 21 x 10^3 cells l^{-1} respectively.

The diatom population was larger than the dinoflagellate population at station 23 and 25 (Figure 4.3). There were 63 x 10^3 cells l^{-1} of diatoms and 29 x 10^3 cells l^{-1} of dinoflagellates with 3 x 10^3 cells l^{-1} of flagellates at the surface of station 23, while there were 55 x 10^3 cells l^{-1} of diatoms and 86 x 10^3 cells l^{-1} of dinoflagellates, with 8 x 10^3 cells l^{-1} of flagellates at the surface of station 24. The population density of diatoms was 128 x 10^3 cells l^{-1} at the surface of station 25, while that of dinoflagellates was 102 x 10^3 cells l^{-1} respectively. There were 16 x 10^3 cells $l^{-1}$of flagellates at the surface of station 25.

4.2.4 The Irish Sea; November 2001

Species of *Biddulphia* and *Coscinodiscus* were commonly found diatoms together with a few dinoflagellates during the cruise from the 26th to 30th of November in Red Wharf Bay (Figure 3.1c). Phytoplankton was sparsely populated during this period compared to spring and summer cruises in other areas. The fall in population after autumn is due to grazing by zooplankton, greater mixing of water column, reduced light and shorter days (Boney, 1989).

4.2.4.1 26th November 2001

The cruise started at stations 1, 2 and 3 in the north coast of Anglesey on the 26th of November 2001 (Figure 3.1c). Diatoms, especially *Biddulphia sinensis* and *Coscinodiscus lineatus* were the prominent phytoplankton species at stations 1, 2 and 3 (Appendix A-4). The population densities of *Biddulphia sinensis* at the depths of 0 m, 17 m and 37 m at station 1 were 21 x 10^3 cells l^{-1}, 23 x 10^3 cells l^{-1}, and 18 x 10^3 cells l^{-1} respectively, while those of *Coscinodiscus lineatus* were 10 x 10^3 cells l^{-1}, 10 x 10^3 cells l^{-1}, and 5 x 10^3 cells l^{-1} respectively. There were 8 x 10^3 cells l^{-1} of *Biddulphiopsis titiana* and 10 x 10^3 cells l^{-1} of *Pleurosigma* species, respectively at the depth of 17 m at station 1.

The population densities of *Biddulphia sinensis* at the depths of 0 m, 12 m and 41 m at station 2 were 16 x 10^3 cells l^{-1}, 37 x 10^3 cells l^{-1}, and 39 x 10^3 cells l^{-1} respectively, while there were 18 x 10^3 cells l^{-1}, 21 x 10^3 cells l^{-1}, and 23 x 10^3 cells l^{-1} of *Coscinodiscus lineatus*, respectively. The cell density of *Navicula* species increased to 21 x 10^3 cells l^{-1} at the surface of station 2. There were 8 x 10^3 cells l^{-1} and 3 x 10^3 cells l^{-1} of *Navicula* species at the depths of 12 m and 41 m, respectively at station 2.

The population density of *Biddulphia sinensis* at 46 m at station 3 reached 37 x 10^3 cells l^{-1}, while there were 16 x 10^3 cells l^{-1} and 18 x 10^3 cells l^{-1} of *Biddulphia sinensis* at the surface and 12 m, respectively. *Coscinodiscus lineatus* was the second largest group of diatoms at station 3 with the population densities reaching 21 x 10^3 cells l^{-1}, 5 x 10^3 cells l^{-1}, and 13 x 10^3 cells l^{-1} at the depths of 0 m, 12 m and 46 m, respectively. There were 16 x 10^3 cells l^{-1} of *Paralia sulcata* and 10 x 10^3 cells l^{-1} of *Leptocylindrus danicus* at 12 m at station 3.

Diatoms predominated at stations 1, 2 and 3. The population densities of phytoplankton at station 1 were 78 x 10^3 cells l^{-1}, 73 x 10^3 cells l^{-1}, and 10 x 10^3 cells l^{-1} respectively, at the depths of 0 m, 17m and 37 m, while those of phytoplankton at station 2 were 57 x 10^3 cells l^{-1}, 89 x 10^3 cells l^{-1}, and 86 x 10^3 cells l^{-1} respectively at the depths of 0 m, 12 m, 41 m (Figure 4.4). The cell density of phytoplankton at 46 m at station 3 was 73 x 10^3 cells l^{-1}, while the cell densities of phytoplankton at 0 m and 12 m at station 3 were 55 x 10^3 cells l^{-1} respectively. There were 8 x 10^3 cells l^{-1} and 5 x 10^3 cells l^{-1} of dinoflagellates at the surface of station 1 and at 12 m at station 3, respectively.

4.2.4.2 27th November 2001

Samples were taken at stations 4, 5, 6 and 7, 8 on the 27th of November (Figure 3.1c). The population densities of *Biddulphia sinensis* and *Thalassiosira mendiolana* reached over 20 x 10^3 cells l^{-1} at the depth of 31 m at station 4, respectively, while there were 18 x 10^3 cells l^{-1} of *Coscinodiscus lineatus* (Appendix A-4). The cell density of *Coscinodiscus lineatus* at 8 m at station 5 was around 31 x 10^3 cells l^{-1}, whereas they reached 73 x 10^3 cells l^{-1}, and 47 x 10^3 cells l^{-1} at 10 m at station 6 and at 4 m at station 7, respectively.

The cell densities of *Biddulphia sinensis* were lower than those of *Coscinodiscus lineatus* at stations 5, 6 and 7. There were 8 x 10^3 cells l^{-1}, 31 x 10^3 cells l^{-1}, and 26 x 10^3 cells l^{-1} of *Biddulphia sinensis* at the surface of stations 5, 6, and 7, respectively. The cell densities of *Biddulphia sinensis* at 0m and 3.5 m at station 8 were 39 x 10^3 cells l^{-1}, and 37 x 10^3 cells l^{-1} respectively, while those of *Coscinodiscus lineatus* were 34 x 10^3 cells l^{-1} and 23 x 10^3 cells l^{-1} respectively.

Apart from *Biddulphia sinensis* and *Coscinodiscus lineatus*, the dominant diatom at the depth of 8 m at station 5 was *Paralia sulcata* (31 x 10^3 cells l^{-1}) and at the surface of station 7 was *Pleurosigma* species (37 x 10^3 cells l^{-1}), while *Navicula* species was the major diatom at the surface of station 8 (31 x 10^3 cells l^{-1}).

The population density of phytoplankton increased from 86 x 10^3 cells l^{-1} at the surface of station 4 to 190 x 10^3 cells l^{-1} at the surface of station 8 (Figure 4.4). The dinoflagellates, *Ceratium* species were observed at the surface of station 4 and 8 with cell densities of 16 x 10^3 cells l^{-1} and 13 x 10^3 cells l^{-1} respectively, while there were 5 x 10^3 cells l^{-1}, 10 x 10^3 cells l^{-1}, and 8 x 10^3 cells l^{-1} of flagellates at the surface of stations 6, 7 and 8, respectively.

4.2.4.3 28th November 2001

Samples were taken from the northern reaches of Beaumaris Bay (stations 9 to 12), and from Red Wharf Bay (stations 13 and 14) on the 28th of November (Figure 3.1c). The population densities of *Coscinodiscus lineatus* at the depths of 0 m, 4 m and 8 m at station 9 were 55 x 10^3 cells l^{-1}, 50 x 10^3 cells l^{-1}, and 47 x 10^3 cells l^{-1} respectively, while those of *Biddulphia sinensis* were 29 x 10^3 cells l^{-1}, 37 x 10^3 cells l^{-1}, and 44 x 10^3 cells l^{-1} respectively (Appendix A-4). There were 18 x 10^3 cells l^{-1} of *Biddulphiopsis titiana* and 16 x 10^3 cells l^{-1} of *Leptocylindrus danicus*, respectively, at the surface of station 9, while there were 21 x 10^3 cells l^{-1} of *Detonula confervacea*, and 13 x 10^3 cells l^{-1} of *Paralia sulcata*, respectively at the depth of 4 m.

The cell densities of *Coscinodiscus lineatus* were higher than *Biddulphia sinensis* at all stations on the 28th of November 2001. There were 18 x 10^3 cells l^{-1}, 21 x

10^3 cells l^{-1}, and 13 x 10^3 cells l^{-1} of *Biddulphia sinensis*, respectively, at the surface of station 10, 11 and 12, while there were 23 x 10^3 cells l^{-1}, 29 x 10^3 cells l^{-1}, and 18 x 10^3 cells l^{-1} of *Coscinodiscus lineatus*, respectively.

The population densities of *Coscinodiscus lineatus* at the depths of 0 m, 11 m and 32 m at station 13 were 31 x 10^3 cells l^{-1}, 26 x 10^3 cells l^{-1}, and 23 x 10^3 cells l^{-1} respectively while *Biddulphia sinensis* was still second largest diatoms after *Coscinodiscus lineatus* with cell concentrations of 16 x 10^3 cells l^{-1}, 13 x 10^3 cells l^{-1}, and 10 x 10^3 cells l^{-1} respectively.

Paralia sulcata was the second dominant diatoms after *Coscinodiscus lineatus* at station 14. The population densities of *Paralia sulcata* at 0 m, 12 m and 21 m at station 14 were 21 x 10^3 cells l^{-1}, 16 x 10^3 cells l^{-1}, and 18 x 10^3 cells l^{-1} respectively, while those of *Coscinodiscus lineatus* were 26 x 10^3 cells l^{-1}, 21 x 10^3 cells l^{-1}, and 23 x 10^3 cells l^{-1} respectively. There were 8 x 10^3 cells l^{-1}, 3 x 10^3 cells l^{-1}, and 5 x 10^3 cells l^{-1} of *Biddulphia sinensis* at 0 m, 12 m and 21 m, respectively, at station 14.

The small number of dinoflagellates was observed at stations 9, 13 and 14 (Figure 4.4). The population densities of *Ceratium* species at the depth of 0 m, 4 m and 8 m at station 9 were 13 x 10^3 cells l^{-1}, 10 x 10^3 cells l^{-1}, and 5 x 10^3 cells l^{-1} respectively, while there were 3 x 10^3 cells l^{-1} and 5 x 10^3 cells l^{-1} of flagellates at the surface and 8 m, respectively. There were 8 x 10^3 cells l^{-1} of *Ceratium fusus* at the depth of 32 m at station 13, while the population densities of *Ceratium fusus* at station 14 were 5 x 10^3 cells l^{-1} at the surface, and 10 x 10^3 cells l^{-1} at the depth of 21 m, respectively.

4.2.4.4 29th November 2001

Samples were taken at stations 15, 16, 17 and 18, 19 on the 29th of November (Figure 3.1c). *Coscinodiscus lineatus* at the surface and at the depth of 21 m at station 15 dominated the phytoplankton population, while the cell density of *Biddulphia sinensis* at 5 m was the highest (Appendix A-4). The population densities of *Coscinodiscus lineatus* at the depths of 0 m, 5 m, and 21 m at station 15 were 34 x 10^3 cells l^{-1}, 23 x 10^3 cells l^{-1}, and 18 x 10^3 cells l^{-1} respectively, while those of *Biddulphia sinensis* were 21 x 10^3 cells l^{-1}, 26 x 10^3 cells l^{-1}, and 13 x 10^3 cells l^{-1} respectively. There were 16 x 10^3 cells l^{-1} of *Navicula* species and 10 x 10^3 cells l^{-1} of *Leptocylindrus danicus* at 21 m at station 15.

The cell density of *Biddulphiopsis titiana* at the depth of 21 m at station 16 reached 26 x 10^3 cells l^{-1}, while there were 8 x 10^3 cells l^{-1} of *Biddulphia sinensis* and 21 x 10^3 cells l^{-1} of *Coscinodiscus lineatus*, respectively. There were 18 x 10^3 cells l^{-1} and 21 x 10^3 cells l^{-1} of *Pleurosigma* species at the surface and at the depth of 10 m, respectively at station 16, while there were 16 x 10^3 cells l^{-1} and 5 x 10^3 cells l^{-1} of *Detonula confervacea* respectively.

The population densities of *Coscinodiscus lineatus* at the depths of 0 m, 8 m, and 22 m at station 17 were 26 x 10^3 cells l^{-1}, 37 x 10^3 cells l^{-1}, and 18 x 10^3 cells l^{-1} respectively, while those of *Biddulphia sinensis* were 16 x 10^3 cells l^{-1}, 26 x 10^3 cells l^{-1}, and 21 x 10^3 cells l^{-1} respectively. The cell densities of *Biddulphia sinensis* were higher than *Coscinodiscus lineatus* at station 18. There were 23 x 10^3 cells l^{-1}, 44 x 10^3 cells l^{-1}, and 37 x 10^3 cells l^{-1} of *Biddulphia sinensis*, respectively and 5 x 10^3 cells l^{-1}, 18 x 10^3 cells l^{-1}, and 21 x 10^3 cells l^{-1} of *Coscinodiscus lineatus*, respectively at the depths of 0 m,

8 m and 17 m at station 18.

Coscinodiscus lineatus was the dominant diatom at station 19, with cell densities of 29 x 10^3 cells l^{-1}, 34 x 10^3 cells l^{-1}, and 16 x 10^3 cells l^{-1} respectively at the depths of 0 m, 4.5 m and 23 m, while there were 21 x 10^3 cells l^{-1}, 18 x 10^3 cells l^{-1}, and 10 x 10^3 cells l^{-1} of *Biddulphia sinensis*, respectively. The cell density of *Navicula* species was 13 x 10^3 cells l^{-1} at the depth of 4.5 m at station 19, while there were 10 x 10^3 cells l^{-1} of *Pleurosigma* species. There were 13 x 10^3 cells l^{-1}, 21 x 10^3 cells l^{-1}, and 16 x 10^3 cells l^{-1} of *Paralia sulcata* at the surface of stations 17, 18 and 19, respectively.

In addition to diatoms, dinoflagellates were present at stations 15, 17 and 18. There were 8 x 10^3 cells l^{-1} of *Ceratium* species at the depth of 5 m at station 15, while there were 3 x 10^3 cells l^{-1} of *Gymnodinium fuscum* and 10 x 10^3 cells l^{-1} of *Gyrodinium* species at the depth of 21 m, respectively. There were around 10 x 10^3 cells l^{-1} of *Ceratium lineatum* at all depths and 5 x 10^3 cells l^{-1} of *Gymnodinium fuscum* at 8 m at station 17, while there were 10 x 10^3 cells l^{-1} of *Ceratium fusus* and 5 x 10^3 cells l^{-1} of *Ceratium lineatum* at 17 m at station 18.

4.2.4.5 30th November 2001

The phytoplankton population was dominated by diatoms throughout the cruise (Appendix A-4). However, the presence of dinoflagellates were detected in all samples on the 30th of November 2001 at stations 20 to 23 (Figure 4.4). There were 26 x 10^3 cells l^{-1}, 13 x 10^3 cells l^{-1}, 34 x 10^3 cells l^{-1}, and 21 x 10^3 cells l^{-1} of dinoflagellates, and 63 x 10^3 cells l^{-1}, 60 x 10^3 cells l^{-1}, 89 x 10^3 cells l^{-1}, and 107 x 10^3 cells l^{-1} of diatoms at the surface of stations 20, 21, 22 and 23 respectively. The dominant phytoplankton at

stations 20, 21 and 22 were the diatoms, *Biddulphia sinensis* and *Coscinodiscus lineatus*. The population density of *Biddulphia sinensis* reached 34 x 10^3 cells l^{-1} at the depth of 10 m and that of *Coscinodiscus lineatus* was 44 x 10^3 cells l^{-1} at the depth of 5.5 m at station 22. However, the dominant phytoplankton at station 23 was *Paralia sulcata*. The population density of *Paralia sulcata* at the depth of 4 m at station 23 was 39 x 10^3 cells l^{-1}, while that of *Coscinodiscus lineatus* was 37 x 10^3 cells l^{-1}.

The dominant dinoflagellates at station 20, 21, 22 and 23 were *Ceratium* species. There were 34 x 10^3 cells l^{-1}, 15 x 10^3 cells l^{-1}, and 21 x 10^3 cells l^{-1} of *Ceratium* species at the depths of 0 m, 5.5 m and 10 m, respectively, at station 22. There were 3 x 10^3 cells l^{-1}, 8 x 10^3 cells l^{-1}, and 5 x 10^3 cells l^{-1} of flagellates at the surface of station 20, 21 and 22, respectively.

4.2.5 The Irish Sea; April 2002

In total, there were 34 stations during the cruise between the 2nd and 5th of April 2002 in the north coast of Anglesey and in the western Irish Sea (Figure 3.1d). 11 stations were the same station repeated over a tidal cycle. The station used for monitoring over a tidal cycle (T1) was positioned off the northwest coast of Anglesey. The stations in the Western Irish Sea (transects 'A', 'B' and 'C') were chosen to provide detailed spatial coverage on both sides of the region where the Western Irish Sea front is known to form (Simpson, 1971) in order to determine the differences between stratified and mixed area. The final four stations (RW1 – RW4) were positioned off the north coast of Anglesey (Red Wharf Bay).

Diatoms were the dominant group of phytoplankton during the cruise

(Appendix A-5) (Figure 4.5). *Bacillaria paxillifer* and *Skeletonema costatum* were commonly found diatoms at most stations, while *Ceratium* species were the commonly found dinoflagellates at many stations. *Bacillaria paxillifer* was the major diatom at station T1, whereas *Chaetoceros debilus* was the dominant diatom at the stations in the Western Irish Sea. *Skeletonema costatum* and *Thalassiosira decipiens* were the predominant phytoplankton species from station RW1 to station RW4. *Skeletonema costatum* and *Thalassiosira decipiens* have previously been observed during the spring diatom bloom in Liverpool Bay (Voltolina, 1980; Spencer, 1988) and in the Western Irish Sea (McKinney *et al.*, 1997).

4.2.5.1 2nd April 2002

Samples were taken hourly for 11 times over a tidal cycle at station T1, northwest of Anglesey on the 2nd of April 2002 (Figure 3.1d). Sampling started from 0800 HRS BST at low water slack tide to 1800 HRS BST. Diatoms, such as *Bacillaria paxillifer* and *Skeletonema costatum* predominated the phytoplankton population at station T1 (Appendix A-5). The population densities of *Bacillaria paxillifer* at the depths of 0 m and 20 m at station T1C1 at 0800 HRS BST reached 39 x 10^3 cells l^{-1} and 11 x 10^3 cells l^{-1} respectively, whereas the population densities of *Skeletonema costatum* were 17 x 10^3 cells l^{-1} and 11 x 10^3 cells l^{-1} respectively. The population densities of *Bacillaria paxillifer* and *Skeletonema costatum* at the surface of station T1C6 at 1300 HRS BST decreased to 11 x 10^3 cells l^{-1} and 8 x 10^3 cells l^{-1} respectively, then, they reached 28 x 10^3 cells l^{-1} and 15 x 10^3 cells l^{-1} respectively at the surface of station T1C11 at 1800 HRS BST.

The cell density of phytoplankton decreased from 72 x 10^3 cells l^{-1} at the surface of station T1C1 at 0800 HRS BST to 37 x 10^3 cells l^{-1} at the surface of station T1C5 at 1200 HRS BST (Figure 4.5a). The cell density of phytoplankton increased to 78 x 10^3 cells l^{-1} at the surface of station T1C8 at 1500 HRS BST, one hour after high water, while it decreased again to 62 x 10^3 cells l^{-1} at the surface of station T1C10 at 1700 HRS BST. The population density of phytoplankton at the surface of T1C11 at 1800 HRS BST reached 69 x 10^3 cells l^{-1}.

4.2.5.2 3rd April 2002

All stations on the 'A' transect were sampled on the 3rd of April 2002, from station A6 (east) to station A1 (west) (Figure 3.1d). Stations B2, B1 and C1 were also sampled, in that order. *Chaetoceros debilus*, *Bacillaria paxillifer*, *Paralia sulcata* and *Skeletonema costatum*, *Thalassiosira decipiens* were commonly found diatoms in the transect 'A' (Appendix A-5). There were 25 x 10^3 cells l^{-1}, 11 x 10^3 cells l^{-1}, and 10 x 10^3 cells l^{-1} of *Chaetoceros debilus*, *Bacillaria paxillifer* and *Thalassiosira decipiens*, respectively, at the surface of station A6. The cell density of *Chaetoceros debilus* reached 36 x 10^3 cells l^{-1} at the surface of station A3. However, the dominant phytoplankton species at the surface of station A1 was *Melosira nummuloides* with cell densities of 30 x 10^3 cells l^{-1}, while there were 18 x 10^3 cells l^{-1} and 19 x 10^3 cells l^{-1} of *Chaetoceros debilus* and *Ditylum brightwellii*, respectively.

Few dinoflagellates and flagellates were found in the transect 'A'. There were 33 x 10^3 cells l^{-1} and 8 x 10^3 cells l^{-1} of *Ceratium* species and *Dictyocha* species at the surface of station A3, while there were 28 x 10^3 cells l^{-1} of flagellate groups at the

surface of station A1. The population densities of phytoplankton at the surface of stations A3, A2 and A1 were higher than those from deeper water samples and surface samples at stations A6, A5 and A4 as transect 'A' passed through a mixed zone (A6) to a stratified zone (A1) (Figure 4.5b).

The dominant phytoplankton at stations B2, B1 and C1 were *Chaetoceros debilus* and *Bacillaria paxillifer*. The population densities of *Chaetoceros debilus* and *Bacillaria paxillifer* at the surface of station B2 were 30 x 10^3 cells l^{-1} and 19 x 10^3 cells l^{-1} respectively, while there were 43 x 10^3 cells l^{-1} and 48 x 10^3 cells l^{-1} at the surface of station B1, respectively. The population density of *Chaetoceros debilus* at the surface at station C1 reached 58 x 10^3 cells l^{-1}, while that of *Bacillaria paxillifer* were 17 x 10^3 cells l^{-1}.

There were 25 x 10^3 cells l^{-1}, 14 x 10^3 cells l^{-1}, and 33 x 10^3 cells l^{-1} of dinoflagellates, respectively and there were 94 x 10^3 cells l^{-1}, 149 x 10^3 cells l^{-1}, and 127 x 10^3 cells l^{-1} of diatoms, respectively at surface of stations B2, B1 and C1, while there were 19 x 10^3 cells l^{-1} of flagellates at the surface of station C1 (Figure 4.5b).

4.2.5.3 4th April 2002

Chaetoceros debilus was the predominant phytoplankton with *Bacillaria paxillifer*, *Skeletonema costatum* and *Thalassiosira decipiens* at all stations sampled on the 4th of April 2002 (Appendix A-5). The remaining stations in the transect 'C' from C2 to C6 and transect 'B' from B3 to B7 were sampled (Figure 3.1d). The cell densities of *Chaetoceros debilus* reached 56 x 10^3 cells l^{-1} and 63 x 10^3 cells l^{-1} at the surface of station C5 and B6, respectively, while those of *Bacillaria paxillifer* and *Skeletonema*

costatum were 32 x 10^3 cells l^{-1} and 15 x 10^3 cells l^{-1} respectively, at the surface of station C5 and 14 x 10^3 cells l^{-1} and 39 x 10^3 cells l^{-1} respectively at the surface of station B6.

The cell density of phytoplankton decreased from 72 x 10^3 cells l^{-1} at the surface of station C2 to 50 x 10^3 cells l^{-1} at the surface of station C3, then it increased to 162 x 10^3 cells l^{-1} at the surface of station C6 (Figure 4.5b). The population density of phytoplankton at the surface of station B6 reached 240 x 10^3 cells l^{-1}. There were 193 x 10^3 cells l^{-1}, 28 x 10^3 cells l^{-1}, and 19 x 10^3 cells l^{-1} of diatoms, dinoflagellates and flagellates of phytoplankton at the surface of station B6 respectively. The population density of dinoflagellates at the surface of station B4 was the highest on the 4th of April 2002. It reached 39 x 10^3 cells l^{-1}, while the population density of diatoms at the surface of station B4 were 91 x 10^3 cells l^{-1} respectively. There were 34 x 10^3 cells l^{-1} and 5 x 10^3 cells l^{-1} of dinoflagellates, *Ceratium* species and *Gymnodinium fuscum* respectively, at the surface of station B4.

4.2.5.4 5th April 2002

Samples were taken at stations RW1 through RW4 along the north coast of Anglesey on the 5th of April 2002 (Figure 3.1d). *Skeletonema costatum* and *Thalassiosira decipiens* were the predominant phytoplankton species from station RW1 to station RW4 (Appendix A-5). The cell densities of *Skeletonema costatum* and *Thalassiosira decipiens* were 39 x 10^3 cells l^{-1} and 11 x 10^3 cells l^{-1} respectively, at the surface of station RW1 and, 58 x 10^3 cells l^{-1} and 25 x 10^3 cells l^{-1} respectively, at the surface of station RW2, while those of *Skeletonema costatum* and *Thalassiosira decipiens*

increased to 143 x 10^3 cells l^{-1} and 112 x 10^3 cells l^{-1} respectively, at the surface of station RW3. There were 146 x 10^3 cells l^{-1} of *Skeletonema costatum* and 109 x 10^3 cells l^{-1} of *Thalassiosira decipiens* at the surface of station RW4. *Bacillaria paxillifer* was the third largest in the phytoplankton population from stations RW1 to RW4. There were 11 x 10^3 cells l^{-1}, 19 x 10^3 cells l^{-1}, 88 x 10^3 cells l^{-1}, and 114 x 10^3 cells l^{-1} of *Bacillaria paxillifer* at the surface of stations RW1, RW2, RW3 and RW4 respectively.

The population densities of phytoplankton at stations RW1 and RW2 ranged between 100 x 10^3 cells l^{-1} and 150 x 10^3 cells l^{-1} (Figure 4.5b). However, those at RW3 and RW4 increased to around 700 x 10^3 cells l^{-1} and 800 x 10^3 cells l^{-1} at the surface, respectively. There were 642 x 10^3 cells l^{-1}, 32 x 10^3 cells l^{-1}, and 18 x 10^3 cells l^{-1} of diatoms, dinoflagellates and flagellates, respectively, at the surface of station RW3, while there were 785 x 10^3 cells l^{-1}, 34 x 10^3 cells l^{-1}, and 17 x 10^3 cells l^{-1} of diatoms, dinoflagellates and flagellates, respectively, at the surface of station RW4.

4.2.6 The Celtic Sea; July 2002

The station used for monitoring over a tidal cycle (T1) during the Irish Sea cruise in April 2002 was sampled again on the 13th of July 2002 on the first day of the cruise. It was positioned off the northwest coast of Anglesey and 12 samples were taken over one tidal cycle (see Figure. 3.1e and Figure 4.6). The stations in the Celtic Sea (transects 'A', 'B', 'C' and 'D', 'E') were chosen to provide detailed spatial coverage on both sides of the frontal region in which the Celtic Sea front is known to form. The final three stations were positioned at station T1 off the north coast of Anglesey on the 20th of 2002.

Diatoms, such as *Rhizosolenia shrubsolei*, were the dominant phytoplankton at station T1, while dinoflagellates, *Ceratium* species dominated samples taken across the Celtic Sea front (Appendix A-6). Chrysophytes (*Dictyocha speculum*, *Mallomonas* species) and prymnesiophytes (*Chrysochromulina species*) composed the flagellate population at most stations, while cyanophyceae, *Oscillatoria nigra*, was found at stations T1.

4.2.6.1 13th July 2002

Sampling initiated at station T1, northwest of Anglesey at 0800 BST when it was low water slack tide on the 13th of July 2002 (Figure 3.1e). Samples were taken hourly afterwards at the same position for 12 times over a tidal cycle until 1900 BST. Diatoms, *Rhizosolenia shrubsolei*, dominated the phytoplankton population at station T1 (Appendix A-6). Other diatoms, such as *Leptocylindrus danicus* and *Nitzschia seriata* were also present, and some dinoflagellates, *Ceratium lineatum* and *Prorocentrum micans*. The population densities of *Rhizosolenia shrubsolei* at the depths of 0 m, 25 m and 50 m at station T1C1 at 0800 BST were 18 x 10^3 cells l^{-1}, 23 x 10^3 cells l^{-1}, and 5 x 10^3 cells l^{-1} respectively, while those of *Ceratium lineatum* were 10 x 10^3 cells l^{-1}, 8 x 10^3 cells l^{-1}, and 5 x 10^3 cells l^{-1} respectively. The population densities of *Rhizosolenia shrubsolei* at the depths of 0 m, 26 m and 47 m at station T1C8 at 1500 BST reached 44 x 10^3 cells l^{-1}, 37 x 10^3 cells l^{-1}, and 42 x 10^3 cells l^{-1} respectively, There were 13 x 10^3 cells l^{-1} of *Leptocylindrus danicus*, 8 x 10^3 cells l^{-1} of *Ceratium lineatum*, and 13 x 10^3 cells l^{-1} of *Prorocentrum micans*, respectively at the surface of station T1C8. The cell densities of *Rhizosolenia shrubsolei* decreased to 21 x 10^3 cells l^{-1}, 23 x 10^3 cells l^{-1}, and

18 x 10^3 cells l^{-1} at the depths of 0 m, 26 m and 50 m, respectively at station T1C11 at 1800 BST, then they increased to 34 x 10^3 cells l^{-1}, 42 x 10^3 cells l^{-1}, and 39 x 10^3 cells l^{-1} at the depths of 0 m, 25 m and 53 m, respectively at station T1C12 at 1900 BST.

The population density of phytoplankton decreased from 117 x 10^3 cells l^{-1} at the surface of station T1C4 at 1100 BST to 86 x 10^3 cells l^{-1} at the surface of station T1C5 at 1200 BST (Figure 4.6a). Then, it increased to 133 x 10^3 cells l^{-1} at the surface of station T1C8 at 1500 BST, one hour after high water slack tide. The population density of phytoplankton decreased again to 102 x 10^3 cells l^{-1} at the surface of station T1C11 at 1800 BST, while it reached 123 x 10^3 cells l^{-1} at the surface of station T1C12 at 1900 BST.

4.2.6.2 14th July 2002

Samples were taken in the transect 'B' from stations B7 to B2 towards northeast into the Irish Sea on the 14th of July 2002 (Figure 3.1e). Dinoflagellates, *Ceratium lineatum* and *Prorocentrum micans*, and diatoms, *Nitzschia seriata* and *Rhizosolenia setigera* were the prominent phytoplankton species (Appendix A-6). The cell densities of *Ceratium lineatum* decreased from 47 x 10^3 cells l^{-1} at the depth of 31 m at station B7 to 10 x 10^3 cells l^{-1} at the depth of 43 m at station B2, while there were 29 x 10^3 cells l^{-1} of *Prorocentrum micans* at the depth of 16 m at station B5. The population density of *Prorocentrum micans* was the highest in the phytoplankton population at the surface of station B2 with cell concentrations of 23 x 10^3 cells l^{-1}, while there were 21 x 10^3 cells l^{-1} of *Ceratium lineatum*. The cell density of *Rhizosolenia setigera* reached 42 x 10^3 cells l^{-1} at the depth of 31 m at station B7, while that of *Nitzschia seriata* were 39 x 10^3 cells l^{-1}

at the surface of station B5. The cell densities of *Rhizosolenia setigera* and *Nitzschia seriata* were higher at 31 m at station B7 and at 20 m at station B6 than at the surfaces of either station (Appendix A-6). However the cell densities of *Rhizosolenia setigera* and *Nitzschia seriata* at station 5 were higher at the surface than at the depth of 16 m. There were 29 x 10^3 cells l^{-1} and 39 x 10^3 cells l^{-1} of *Rhizosolenia setigera* and *Nitzschia seriata* respectively, at the surface of station B5, while there were 8 x 10^3 cells l^{-1} and 31 x 10^3 cells l^{-1} of *Rhizosolenia setigera* and *Nitzschia seriata* respectively at the depth of 16 m.

In the Celtic Sea, a thermal front was detected in the CTD temperature data (Figure 4.15 and 4.16). As transect 'B' passed through the frontal region from the stratified zone in the Celtic Sea side (B7) to the mixed zone in the Irish Sea side (B2), the cell densities of phytoplankton at the depths of 31 m, 20 m and 16 m at stations B7, B6 and B5, respectively were the highest due to the thermal stratification (Figure 4.6b). The depths of 31 m, 20 m and 16 m at stations B7, B6 and B5, respectively formed the thermocline, where the growth conditions of phytoplankton were optimised in the stratified side of the front. The cell densities of phytoplankton at the surface increased from 164 x 10^3 cells l^{-1} at station B7 to 198 x 10^3 cells l^{-1} at station B5, whereas the cell densities of phytoplankton decreased from 250 x 10^3 cells l^{-1} at 31 m at station B7 to 237 x 10^3 cells l^{-1} at 16 m at station B5. The population densities of phytoplankton ranged between 70 x 10^3 cells l^{-1} and 110 x 10^3 cells l^{-1} at all depths from stations B4 to B2 on the mixed side of the front.

A mixed population of diatoms, dinoflagellates and flagellates was observed at station B7. Diatoms and dinoflagellates dominated at all stations in the transect 'B', while the flagellate population was more abundant at the surface water in the stratified

zone (stations B7, B6) as described in Boney (1989). There were 47 x 10^3 cells l^{-1}, 39 x 10^3 cells l^{-1}, and 34 x 10^3 cells l^{-1} of diatoms, dinoflagellates and flagellates, respectively at the surface of station B7, while there were 60 x 10^3 cells l^{-1}, 68 x 10^3 cells l^{-1}, and 37 x 10^3 cells l^{-1} of diatoms, dinoflagellates and flagellates, respectively at the surface of station B6.

4.2.6.3 15th July 2002

Samples were taken through stations A2 to A7 (transect 'A') and station S1, working southwest into the Celtic Sea on the 15th of July 2002 (Figure 3.1e). A mixed population of diatoms and dinoflagellates was observed through the transect 'A' (Figure 4.6c). Flagellates abundance increased at the depth of 26 m at station A7 with cell densities of 31 x 10^3 cells l^{-1}, while there were 133 x 10^3 cells l^{-1} of diatoms and 37 x 10^3 cells l^{-1} of dinoflagellates.

Nitzschia seriata and *Rhizosolenia setigera* were the dominant diatoms (Appendix A-6). The population densities of *Rhizosolenia setigera* were higher than the population densities of *Nitzschia seriata* at 40 m at station A2 and at 0 m at station A4, while those of *Nitzschia seriata* were the highest in the phytoplankton population at 28 m at station A6 and at 26 m at station A7 with cell concentrations of 29 x 10^3 cells l^{-1} and 34 x 10^3 cells l^{-1} respectively.

Dinoflagellates, *Ceratium lineatum* and *Prorocentrum micans* were commonly found along transect 'A'. The cell density of *Ceratium lineatum* at the depth of 40 m at station A2 reached 34 x 10^3 cells l^{-1}, while *Prorocentrum micans* had the highest population density at the depth of 64 m at station A5 with cell concentrations of 31 x

10^3 cells l^{-1}.

The population densities of phytoplankton at 28 m at station A6 and at 28 m at station A7 were the highest as the thermocline formed with cell concentrations of 151 x 10^3 cells l^{-1} and 201 x 10^3 cells l^{-1} respectively (Figure 4.6c).

Station S1 was positioned southwards from station A7 in the Celtic Sea (Figure). The cell density of phytoplankton at 26m at station A7 decreased to 86 x 10^3 cells l^{-1}. The cell density of *Ceratium lineatum* was the highest in the phytoplankton population with cell concentrations of 18 x 10^3 cells l^{-1} at 26 m at station A7, while there were 16 x 10^3 cells l^{-1} of *Nitzschia seriata* at 0m.

4.2.6.4 16th July 2002

Stations C7 through C2 were sampled on the 16th of July, working northeast towards the Irish Sea (Figure 3.1e). *Nitzschia seriata*, *Rhizosolenia setigera* and *Detonula confervacea* were the commonly found diatoms, while *Ceratium lineatum*, *Prorocentrum micans* and *Dinophysis acuta* were the major dinoflagellates in the transect 'C' (Appendix A-6). The population density of *Nitzschia seriata* reached 63 x 10^3 cells l^{-1} at the depth of 17 m at station C6, while the population density of *Ceratium lineatum* reached 50 x 10^3 cells l^{-1} at the depth of 9 m at station C5. The cell densities of *Nitzschia seriata* and *Ceratium lineatum* decreased to 13 x 10^3 cells l^{-1} and 8 x 10^3 cells l^{-1} respectively at the surface of station C2.

The thermal stratification was detected in the CTD temperature profile at the depth of 14 m, 17 m and 9 m at stations C7, C6 and C5, respectively. The population densities of phytoplankton at the depths of 14 m, 17 m and 9 m at stations C7, C6 and

C5, respectively were 263 x 10^3 cells l^{-1}, 271 x 10^3 cells l^{-1}, and 339 x 10^3 cells l^{-1} (Figure 4.6d). The cell densities of phytoplankton increased at the surface from station C7 (151 x 10^3 cells l^{-1}) to station C5 (232 x 10^3 cells l^{-1}). The cell densities of diatoms and dinoflagellates increased from 76 x 10^3 cells l^{-1} and 47 x 10^3 cells l^{-1} respectively, at the surface of station C7 to 149 x 10^3 cells l^{-1} and 68 x 10^3 cells l^{-1} respectively, at the surface of station C5. However, the cell densities of flagellates at the surface decreased from 29 x 10^3 cells l^{-1} at station C7 to 16 x 10^3 cells l^{-1} at station C5. The population densities of phytoplankton at station C2 decreased to 78 x 10^3 cells l^{-1}, 60 x 10^3 cells l^{-1}, and 63 x 10^3 cells l^{-1} at the depths of 0 m, 46 m and 93 m, respectively.

4.2.6.5 17th and 18th July 2002

Station E2 and station E1 were sampled on the 17th of July and stations E3 through E6 were sampled on the 18th of July, working southwest into the Celtic Sea. (Figure 3.1e). The dinoflagellate *Ceratium lineatum* was the dominant phytoplankton species at the depth of 16m at station E2 (21 x 10^3 cells l^{-1}) and at the depth of 0 m at station E3 (34 x 10^3 cells l^{-1}), while the cell density of *Nitzschia seriata* at the depth of 24 m at station E5 reached 29 x 10^3 cells l^{-1} (Appendix A-6). *Rhizosolenia setigera* was the major species at the depth of 41 m at station E6, with cell concentrations of 18 x 10^3 cells l^{-1}, while there were 10 x 10^3 cells l^{-1} of *Nitzschia seriata* and 16 x 10^3 cells l^{-1} of *Ceratium lineatum*.

Diatoms and dinoflagellates composed the phytoplankton population in the transect 'E' (Figure 4.6e). There were 52 x 10^3 cells l^{-1} and 18 x 10^3 cells l^{-1} of diatoms and dinoflagellates, respectively, at the surface of station E1, while there were 44 x 10^3

cells l^{-1} and 39 x 10^3 cells l^{-1} of diatoms and dinoflagellates, respectively, at the surface of station E2. However, the cell density of dinoflagellates (52 x 10^3 cells l^{-1}) were higher than that of diatoms (44 x 10^3 cells l^{-1}) at the surface of station E3. The population densities of phytoplankton at 32 m at station E4, at 24 m at station E5, and at 41 m at station E6 were high, with cell concentrations of 83 x 10^3 cells l^{-1}, 143 x 10^3 cells l^{-1}, and 102 x 10^3 cells l^{-1} respectively. The cell densities of phytoplankton at the surface of stations E4, E5 and E6 were 16 x 10^3 cells l^{-1}, 34 x 10^3 cells l^{-1}, and 55 x 10^3 cells l^{-1} respectively.

4.2.6.6 19th July 2002

Samples were taken from stations D7 to Dend on the transect 'D' on the 19th of July 2002, towards northeast into the Irish Sea (Figure 3.1e). Diatoms and dinoflagellates dominated the population in the transect 'D', while there were a few flagellates at stations D7, D5, D4 and D1, D0 (Figure 4.6f).

The dominant diatoms were *Nitzschia seriata*, *Rhizosolenia setigera* and *Detonula confervacea*, while *Ceratium lineatum* and *Prorocentrum micans* were commonly found dinoflagellates in the transect 'D' (Appendix A-6). The major phytoplankton species at station D7 were *Nitzschia seriata* and *Prorocentrum micans*, with cell concentrations of 21 x 10^3 cells l^{-1} and 18 x 10^3 cells l^{-1} respectively at the surface, while *Leptocylindrus danicus* had the highest cell density at the surface of station D6, with cell concentrations of 18 x 10^3 cells l^{-1}. *Prorocentrum micans* was the prominent dinoflagellate species at the surface of station D5, with cell densities of 29 x 10^3 cells l^{-1}. However, the population density of *Ceratium lineatum* was higher than that

of *Prorocentrum micans* at station D4. There were 21 x 10^3 cells l^{-1} of *Ceratium lineatum* and 13 x 10^3 cells l^{-1} of *Prorocentrum micans*, respectively, at the depth of 50 m at station D4. The population density of *Nitzschia seriata* at the surface of station D3 was 18 x 10^3 cells l^{-1}, while there were 16 x 10^3 cells l^{-1} of *Detonula confervacea* and 10 x 10^3 cells l^{-1} of *Ceratium lineatum*, respectively. The population densities of *Nitzschia seriata* increased from station D2 to station D1, while the population densities of *Rhizosolenia setigera* decreased. There were 26 x 10^3 cells l^{-1}, 39 x 10^3 cells l^{-1}, 23 x 10^3 cells l^{-1}, and 21 x 10^3 cells l^{-1} of *Nitzschia seriata*, *Rhizosolenia setigera*, *Ceratium lineatum* and *Prorocentrum micans*, respectively at the depth of 33 m at station D2. The dominant phytoplankton at station D1 were diatoms, *Nitzschia seriata* and *Rhizosolenia setigera*, with cell densities of 57 x 10^3 cells l^{-1} and 37 x 10^3 cells l^{-1} at the depth of 29 m, respectively. The cell density of *Rhizosolenia setigera* at the surface of station D0 was 29 x 10^3 cells l^{-1}, while there was 26 x 10^3 cells l^{-1} of *Nitzschia seriata* at the depth of 51 m at station Dend. The cell density of *Prorocentrum micans* decreased from 18 x 10^3 cells l^{-1} at 29 m at station D0 to 13 x 10^3 cells l^{-1} at 25 m at station Dend.

The cell densities of phytoplankton at the surface were higher than at the depth of 41 m at stations D7 and D6 (Figure 4.6f). There were 136 x 10^3 cells l^{-1} and 55 x 10^3 cells l^{-1} of phytoplankton at 0 m and 41 m, respectively, at station D7, and 70 x 10^3 cells l^{-1} and 39 x 10^3 cells l^{-1} of phytoplankton at 0 m and 41 m, respectively, at stations D6. The population density of phytoplankton reached 287 x 10^3 cells l^{-1} at the depth of 29 m at station D1. There were 203 x 10^3 cells l^{-1}, 76 x 10^3 cells l^{-1}, and 8 x 10^3 cells l^{-1} of diatoms, dinoflagellate, and flagellates respectively, at the depth of 29 m at station D1. The population density of phytoplankton decreased to 65 x 10^3 cells l^{-1} at the surface of station Dend.

4.2.6.7 20th July 2002

The final three stations were positioned at station T1 off the north coast of Anglesey at 0750 BST (T1A-C1), 0850 BST (T1A-C2) and 0940 BST (T1A-C3) on the 20th of July 2002 (Figure 3.1e). The names of casts at T1 on the 20th of July had 'A' appended to differentiate from the samples taken on the 13th of July.

The dominant phytoplankton at station T1 on the 20th of July was still *Rhizosolenia shrubsolei* (Appendix A-6). The population densities of *Rhizosolenia shrubsolei* increased from 29 x 10^3 cells l^{-1} at the surface of T1A-C1 to 37 x 10^3 cells l^{-1} at the surface of T1A-C3, while there were 21 x 10^3 cells l^{-1}, 13 x 10^3 cells l^{-1}, and 18 x 10^3 cells l^{-1} of *Ceratium lineatum* at the surface of stations T1A-C1, T1A-C2 and T1A-C3, respectively. The population densities of phytoplankton at the surface of stations T1A-C1, T1A-C2 and T1A-C3 were 125 x 10^3 cells l^{-1}, 110 x 10^3 cells l^{-1}, and 128 x 10^3 cells l^{-1} respectively (Figure 4.6g). The population density of phytoplankton reached 162 x 10^3 cells l^{-1} at 20 m at station T1A-C3. There were 117 x 10^3 cells l^{-1}, 42 x 10^3 cells l^{-1}, and 3 x 10^3 cells l^{-1} of diatoms, dinoflagellates and flagellates respectively, at 20 m at station T1A-C3.

4.3 HPLC pigment results

Pigment concentrations were measured using High Performance Liquid Chromatography (HPLC). Standard pigment markers, which characterise each of the major phytoplankton groups found during the studies, were used. These were peridinin (dinoflagellates), fucoxanthin (diatoms), 19' – hexanoyloxyfucoxanthin

(prymnesiophytes) and chlorophyll *b* (green flagellates) (Wright and Jeffery, 1987; Paerl and Millie, 1991; Barlow *et al.*, 1993; Weaver and Wrigley, 1994). Figure 4.7 shows results from HPLC analysis in the Menai Straits, while Figures 4.8-4.12 show results from HPLC analysis for each cruise.

The HPLC data from the Menai Strait between May 2001 and October 2002 (Figure 4.7) shows the highest pigment concentrations on the 15th of June 2001 and the 7th of June 2002, during the *Phaeocystis pouchetti* bloom. The marker pigment for prymnesiophytes, 19' – hexanoyloxyfucoxanthin was prominent, with concentrations of 5.13 μg l^{-1} on the 15th of June 2001 and 6.54 μg l^{-1} on the 7th of June 2002. The presence of prymnesiophytes, *Phaeocystis* species, contributes fucoxanthin to the diatom group, as it contains both marker pigments, 19' – hexanoyloxyfucoxanthin and fucoxanthin (Wright and Jeffrey, 1987). However, there was a significant cell density of *Phaeocystis pouchetti* on the 15th of June 2001 (662 x 10^3 cells l^{-1}) and on the 7th of June 2002 (1115 x 10^3 cells l^{-1}). As a result, the concentration of 19' – hexanoyloxyfucoxanthin was still higher than the concentration of fucoxanthin on the 15th of June 2001 and on the 7th of June 2002. The marker pigment for diatoms, fucoxanthin dominated in spring 2002. The highest concentration of fucoxanthin was observed on the 24th of May 2002, with the concentration of 4.90 μg l^{-1}. The marker pigment for dinoflagellates, peridinin was observed after the *Phaeocystis pouchetti* bloom. The highest concentration of peridinin was 2.02 μg l^{-1} on the 19th of August 2002.

Figure 4.8 shows the HPLC data from the Clyde Sea cruise in April 2001. Diatoms predominated the population during the study, with *Skeletonema costatum* and *Thalassiosira nordenskioldii* most common. A marker pigment, fucoxanthin, which represents the presence of diatoms reached the highest concentration of 8.33 μg l^{-1} at the

depth of 12 m at station CE4. The presence of peridinin, the marker pigment for dinoflagellates was observed at stations LLF1, IW1, BS1, CE4, CE3 and CE2, LS1, RB1, WK1. The concentration of peridinin reached 2.08 $\mu g\ l^{-1}$ at 7 m at station RB1 and at 15 m at station WK1, respectively.

The pigment data from the Irish Sea cruise in August 2001 (Figure 4.9) displays a mixed population of diatoms and dinoflagellates with few flagellates. The highest concentration of peridinin was observed at the surface of station 4, with a concentration of 1.17 $\mu g\ l^{-1}$, while the concentration of fucoxanthin reached 0.91 $\mu g\ l^{-1}$ at the depth of 30 m at station 16. The highest concentration of 19' – hexanoyloxyfucoxanthin was found at the surface of station 8, with a concentration of 0.48 $\mu g\ l^{-1}$. The marker pigment, 19' – hexanoyloxyfucoxanthin may have been supplemented by the presence of the dinoflagellate, *Gyrodinium aureolum* in Liverpool Bay as it has a higher concentration of prymnesiophyte marker pigment, 19' – hexanoyloxyfucoxanthin than dinoflagellate marker pigment, peridinin (Tangen and Björnland, 1981; Millie *et al.*, 1997) (see Figure 3.1b and Appendix A-3).

Figure 4.10 shows the Irish Sea cruise data in November 2001. Diatom dominated the phytoplankton population, with *Coscinodiscus lineatus* and *Biddulphia sinensis*. The concentration of fucoxanthin reached 1.05 $\mu g\ l^{-1}$ at the surface of station 8, while there was 0.24 $\mu g\ l^{-1}$ of peridinin at the surface of station 22. The major dinoflagellate was *Ceratium* species.

Figure 4.11 shows the HPLC samples for the Irish Sea Cruise in April 2002. The dominant group of phytoplankton was diatoms. The highest concentration of fucoxanthin during the tidal cycle at station T1 on the 2nd of April was 0.28 $\mu g\ l^{-1}$ at the surface of station T1C10 (Figure 4.11a). The concentration of fucoxanthin reached 0.78

$\mu g\ l^{-1}$ at the surface of station B6, while the concentration of peridinin reached 0.32 $\mu g\ l^{-1}$ at the surface of station C1 (Figure 4.11b). The concentration of pigments in Red Wharf Bay increased dramatically at stations RW3 and RW4. There were 2.83 $\mu g\ l^{-1}$ of fucoxanthin, 0.52 $\mu g\ l^{-1}$ of peridinin and 0.30 $\mu g\ l^{-1}$ of 19' – hexanoyloxyfucoxanthin at the surface of station RW4.

Figure 4.12 shows HPLC data from the Celtic Sea cruise in July 2002. Diatoms and dinoflagellates dominated the phytoplankton population. The highest concentration of fucoxanthin at station T1 over a tidal cycle on the13th of July was 0.42 $\mu g\ l^{-1}$ at the depth of 25 m at station T1C9, while there was 0.24 $\mu g\ l^{-1}$ of peridinin at the surface of station T1C8 (Figure 4.12a). The highest concentration of 19'-hexanoyloxyfucoxanthinin in the Celtic Sea was found at the depth of 26 m at station A7, with a concentration of 0.19 $\mu g\ l^{-1}$ (Figure 4.12c). The highest concentration of fucoxanthin and peridinin in the Celtic Sea were observed at the depth of 9 m at station C5, with a concentration of 0.83 $\mu g\ l^{-1}$ and 0.58 $\mu g\ l^{-1}$, respectively (Figure 4.12d). The samples were taken at station T1 one more time on the 20th of July. There were 0.38 $\mu g\ l^{-1}$ of fucoxanthin and 0.19 $\mu g\ l^{-1}$ of peridinin at the surface of station T1A-C1, while there were 0.31 $\mu g\ l^{-1}$ of fucoxanthin and 0.21 $\mu g\ l^{-1}$ of peridinin at the surface of station T1A-C3 (Figure 4.12g).

4.4 Fluorometric and HPLC measurement

Chlorophyll *a* measurement by fluorometer and HPLC were compared. As chlorophyll *a* is contained all phytoplankton taxa as a major pigment, it is used as a universal indicator of phytoplankton biomass. The regression lines for the comparison of chlorophyll *a* measured by fluorometer and HPLC from the Menai Strait and each

cruise are plotted in Figure 4.13a-e and regression coefficients are presented in Table 4.1, showing high R^2 values (> 0.80).

The all data from the Menai Strait and each cruise are plotted together in Figure 4.14. It shows a good correlation with high R^2 values over the range of chlorophyll *a* measurements made (0-12 $\mu g\ l^{-1}$).

Table 4.1 regression between Chlorophyll *a* measurement by fluorometer and HPLC. R^2 is the coefficient of determination and n is number of samples. F statistic is given with the probability.

	R^2	n	F-statistic	Probability
Menai Strait	0.98	25	1298.21	0.00
Irish Sea Aug. 01	0.91	54	530.58	0.00
Irish Sea Nov. 01	0.80	65	257.23	0.00
Irish Sea Apr. 02	0.98	95	5318.10	0.00
Celtic Sea July 02	0.93	146	1815.08	0.00
All data	0.99	385	25927.20	0.00

4.5 Result of taxonomic data

Taxonomic data collected in the Menai Strait over a year between the 25th of May 2001 and the 21st of October 2002 were showed a seasonal variation of phytoplankton succession. Small celled and fast growing diatoms (e.g. *Thalassiosira*, *Chaetoceros* and *Skeletonema* species) dominated the early spring diatom population, while medium sized and slow growing diatoms (e.g. *Rhizosolenia* species, *Fragilaria oceanica* and *Guinardia flaccida*) dominated the later diatom population. This pattern of diatom succession in the Menai Strait was observed in the previous work (Newton, 1986). However, the large number of *Skeletonema costatum* was still found until June 2001 and May 2002. This reflects that phytoplankton cycles observed over several years may not

typical of more than that period (Bold and Wynne, 1985; Boney, 1989). One of the prymnesiophyte, *Phaeocystis pouchetti*, which follows the spring diatom bloom after depletion of silicate, formed the largest bloom in the early summer in the year 2001 and 2002. The *Phaeocystis* bloom, which normally occurs in May or June, has considerable impact on the east coast of Anglesey as it forms mats and smothers area of sea bed (Young 1993). Dinoflagellates became the dominant group of phytoplankton in September 2001 and August 2002 in Menai Strait. After autumnal bloom the population decreased. Diatoms, *Coscinodiscus* and *Biddulphia* species were dominant during the winter. These diatoms are commonly found in the winter in north temperate seas (Boney, 1989).

The phytoplankton population during the Clyde Sea cruise in April 2001 were predominated by diatoms. *Skeletonema costatum* and *Thalassiosira nordenskioldii* were dominant species at all stations. However, during the Irish Sea cruise in August 2001 *Rhizosolenia* species were commonly found diatoms. McKinney *et al.* (1997) identified *Rhizosolenia danicus* as a common diatom in the north-west Irish Sea in the summer. Dinoflagellates, *Ceratium* species and *Noctiluca scintillans* were found at all sampling stations during the cruise and *Gyrodinium aureolum* was found in the eastern Irish Sea. The sampling stations for the Irish Sea cruise in November 2001 were located in Red Wharf Bay. Diatoms, *Coscinodiscus* and *Biddulphia* species were the major phytoplankton species found during the cruise. During the Irish Sea cruise in April 2002, commonly found phytoplankton at all sampling stations were diatoms (e.g. *Bacillaria paxillifer* and *Skeletonema costatum*). *Chaetoceros debilus* was one of the major diatom in the Western Irish Sea, while *Thalassiosira decipiens* were the predominant phytoplankton species in Red Wharf Bay. Few dinoflagellates, such as *Ceratium* species

were also found. During the Celtic Sea cruise in July 2002, dinoflagellates, *Ceratium* species and *Prorocentrum micans* dominated many sampling station across the Celtic Sea front, while diatom, *Rhizosolenia shrubsolei* was commonly found diatom in the northwest coast of Anglesey. *Nitzschia seriata* and *Rhizosolenia setigera* were also commonly found diatoms in the Celtic Sea. Samples taken over a tidal cycle at station T1 in the northwest of Anglesey during the Irish Sea cruise in April 2002 and the Celtic Sea cruise in July 2002 (Figure 3.1d and Figure 3.1e). Sampling began at low water slack tide for both cruises. The highest cell densities of phytoplankton from both cruises were found just after the high water slack tide.

Figure 4.15 shows the surface temperature plot measured by the CTD profile during the Celtic Sea cruise in July 2002. The temperature ranged between 17 °C on the Celtic Sea side and 13 °C on the Irish Sea side. Figure 4.16 is the plot of the temperature differences between surface and bottom samples during the Celtic Sea cruise in July 2002. Bottom temperatures were measured at depths deeper than 50m. The temperature differences between surface and bottom were over 6 °C on the Celtic Sea side, while there were less than 1 °C or no differences detected on the Irish Sea side. In other words, there was a thermal stratification on the Celtic Sea side and mixed area on the Irish Sea side. The highest population densities of phytoplankton were observed in the transitional water (Figure 4.6b-f). Diatoms dominated the population at most sampling stations across the frontal region. As diatoms can grow in the colder condition of spring, they tend to be abundant in the mixed zone, which is colder than the surface of stratified zone (Martinjezequel and Videau, 1992). However, this trend could not be conformed from the data. The larger phytoplankton population were found along the thermocline and upper layer of the stratified side. The warmer conditions enable

flagellates to compete more effectively with diatoms and dinoflagellates (Boney, 1989; Hoek *et al.*, 1995). As a result, flagellates were more abundant at the surface water of the stratified side (Boney, 1989; Martinjezequel and Videau, 1992).

4.6 Comparison of taxonomic data and HPLC results

Phytoplankton group division was simplified to diatoms and dinoflagellates with remaining groups, classed as flagellates. Marker pigments for individual group of phytoplankton peridinin (dinoflagellates), fucoxanthin (diatoms), 19' – hexanoyloxyfucoxanthin (prymnesiophytes) and chlorophyll *b* (green flagellates) were used to determine the presence of dominant group of phytoplankton (Everitt, 1990; Barlow *et al.*, 1993). Only 19' – hexanoyloxyfucoxanthin and chlorophyll *b*, which represent prymnesiophytes and green flagellates respectively, were used as marker pigments for flagellates. Therefore, if flagellates present other than prymnesiophytes and green flagellates, the estimation of flagellates using HPLC might underestimate their presence. However, the flagellate population during the study rarely represented a significant proportion of the phytoplankton population.

The presence of *Phaeocystis pouchetti*, one of the prymnesiophytes, enhanced the concentration of fucoxanthin as it contains both marker pigments, fucoxanthin and 19' – hexanoyloxyfucoxanthin, while dinoflagellate, *Gyrodinium aureolum* contributed fucoxanthin rather than marker pigment for dinoflagellate, peridinin.

HPLC pigment measurements and taxonomic cell identification data were normalised and compared in Figure 4.17 and 4.18. The relationship between HPLC data and cell identification data shows generally a good agreement in the Menai Strait

(Figure 4.17a), and during all cruises; the Clyde Sea cruise in April 2001 (Figure 4.17b), the Irish Sea cruise in August 2001 (Figure 4.17c), the Irish Sea cruise in November 2001 (Figure 4.18a) and the Irish Sea cruise in April 2002 (Figure 4.18b), the Celtic Sea cruise in July 2002 (Figure 4.18c). Although the plot for the Irish Sea cruise in August 2001 (Figure 4.17c) shows R^2 value of 0.502, the relationship between HPLC and taxonomic data was significant (at $P < 0.001$). Low R^2 values were also found during the Irish Sea cruise in April 2002 (Figure 4.18b) and the Celtic Sea cruise in July 2002 (Figure 4.18c), showing 0.753 and 0.833, respectively. These lesser agreements between cell identification and HPLC data may be explained due to the mixed population of the phytoplankton population. The mixed population may cause low pigment concentration and contain a number of different accessory pigments. As marker pigments for flagellates used in the study were 19' – hexanoyloxyfucoxanthin and chlorophyll *b* only, other marker pigments, which may be present, were not included in the sum of pigments for flagellates, resulting the underestimation of flagellate population.

The samples in the Menai Strait (Figure 4.17a) were taken over a year between May 2001 and October 2002. As a result, the normalised data for the comparison between HPLC and taxonomic cell identification for diatoms, dinoflagellates and flagellates were distributed across the range of zero to one. Flagellates found in the Menai Strait was predominantly prymnesiophyte, *Phaeocystis pouchetti*. Diatoms dominated the phytoplankton population during all cruises. During the Clyde Sea cruise in April 2001 (Figure 4.17b), the Irish Sea cruise in November 2001 (Figure 4.18a) and the Irish Sea cruise in April 2002 (Figure 4.18b), diatoms and other phytoplankton groups were divided at the opposite ends of the scale. During the Irish Sea cruise in August 2001 (Figure 4.17c) and the Celtic Sea cruise in July 2002 (Figure 4.18c), there

was a mixed population of diatoms and dinoflagellates with few flagellates.

The HPLC samples collected during the Celtic Sea cruise in July 2002 were used for the principle component analysis (PCA) (Figure 4.19) (Schlens, 2004). Samples from surface, mid-depth (8 - 49 m) and the deepest depth (>50m) are presented in Figure 4.19. Diatoms tend to be abundant in the mixed zone where the temperature is colder than stratified zone (Martinjezequel and Videau, 1992), while the warmer conditions enable flagellates tend to grow more effectively than diatoms (Boney, 1989; Hoek *et al.*, 1995). Fucoxanthin, which represents diatoms, was enriched in the mixed zone at all three depths while Peridinin which represents dinoflagellates, was enriched in the mid-depth at most stations during the cruise (Figure 4.19). As flagellate populations were more abundant in the surface water on the stratified side (Boney, 1989; Hoek *et al.*, 1995), marker pigments, 19' – hexanoyloxyfucoxanthin and chlorophyll *b* were more enriched at stations located on the surface of the stratified side (stations A7, C7 and E6) (Figure 4.19).

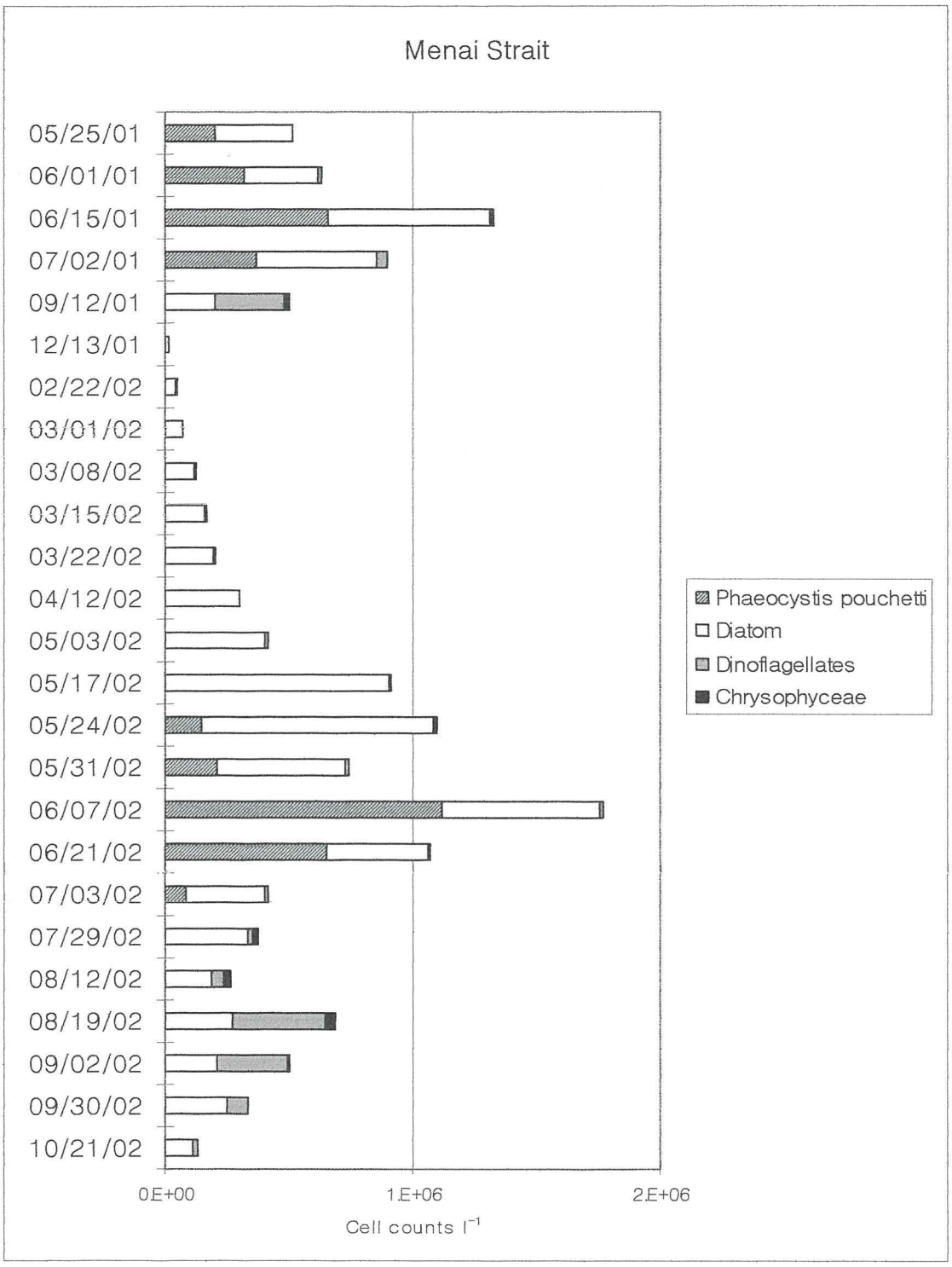

Figure 4.1 Phytoplankton cell counts data from the Menai Strait between 25 May 2001 and 21 October 2002. Phytoplankton were classified into four groups; *Phaeocystis pouchetti* (Prymnesiophyceae), dinoflagellates, diatoms and Chrysophyceae.

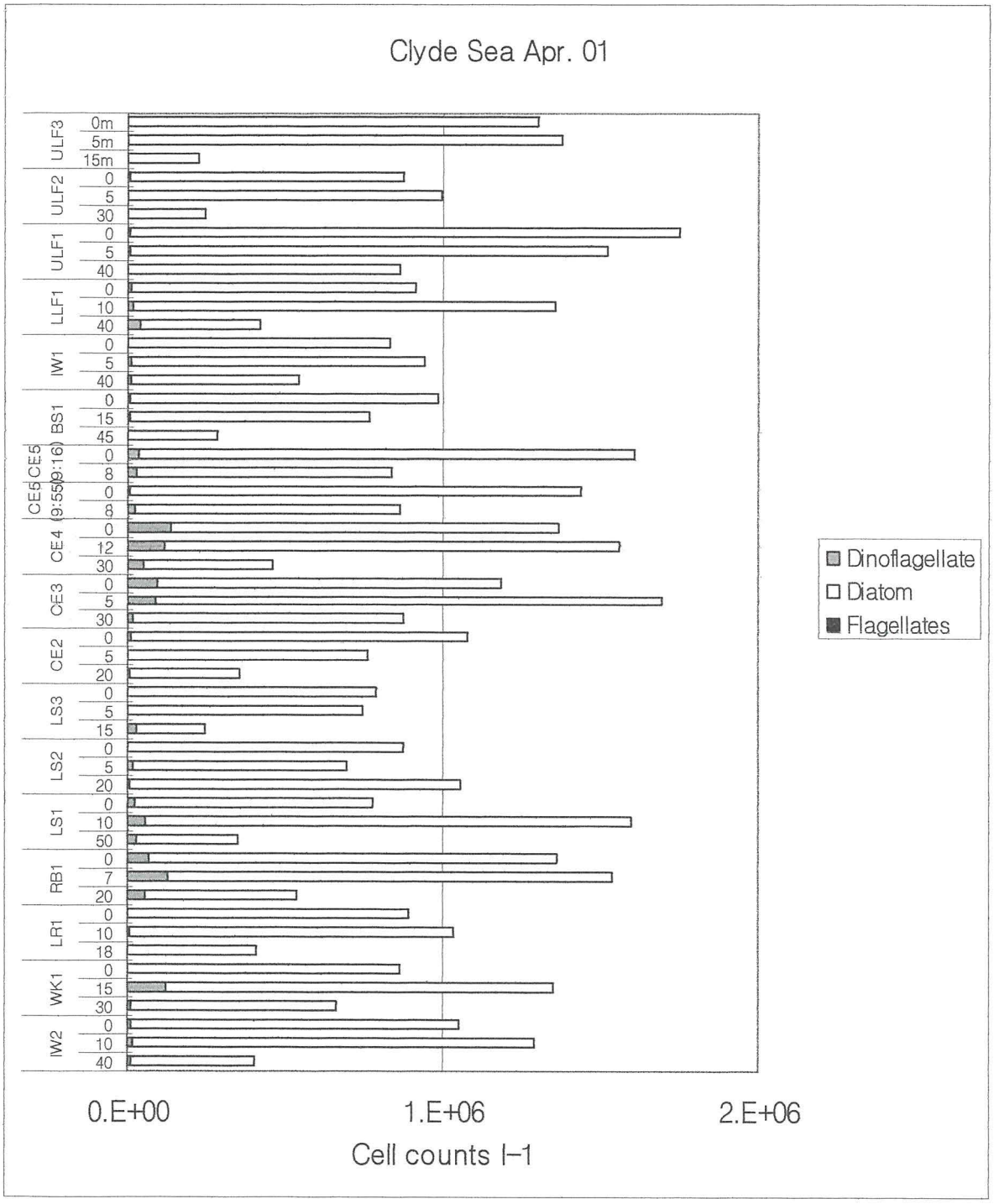

Figure 4.2 Phytoplankton cell counts data during the Clyde Sea cruise (23-27 April 2001). Phytoplankton were classified into three groups; dinoflagellates, diatoms and flagellates.

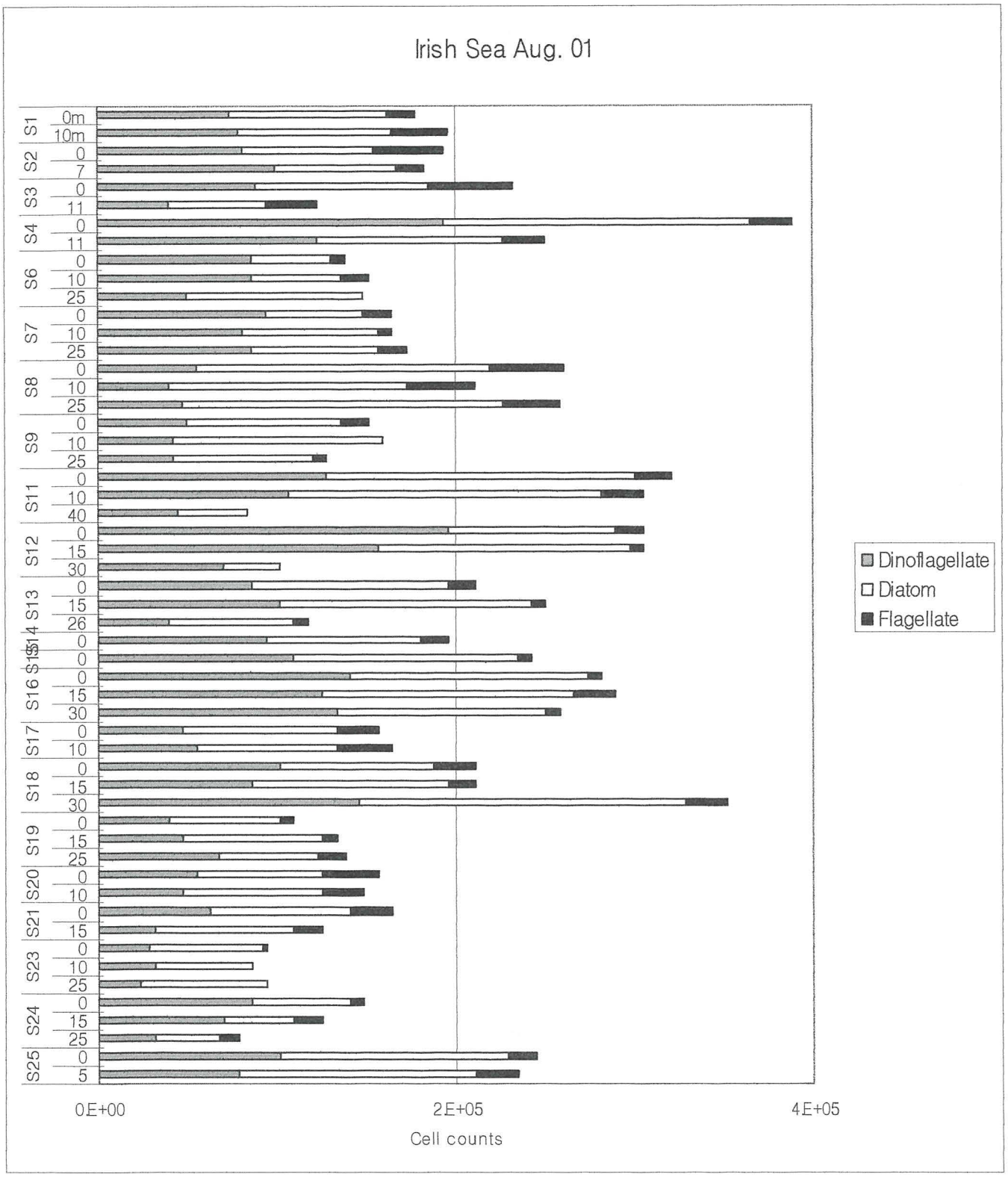

Figure 4.3 Phytoplankton cell counts data during the Irish Sea cruise (6-10 August 2001). Phytoplankton were classified into three groups; dinoflagellates, diatoms and flagellates.

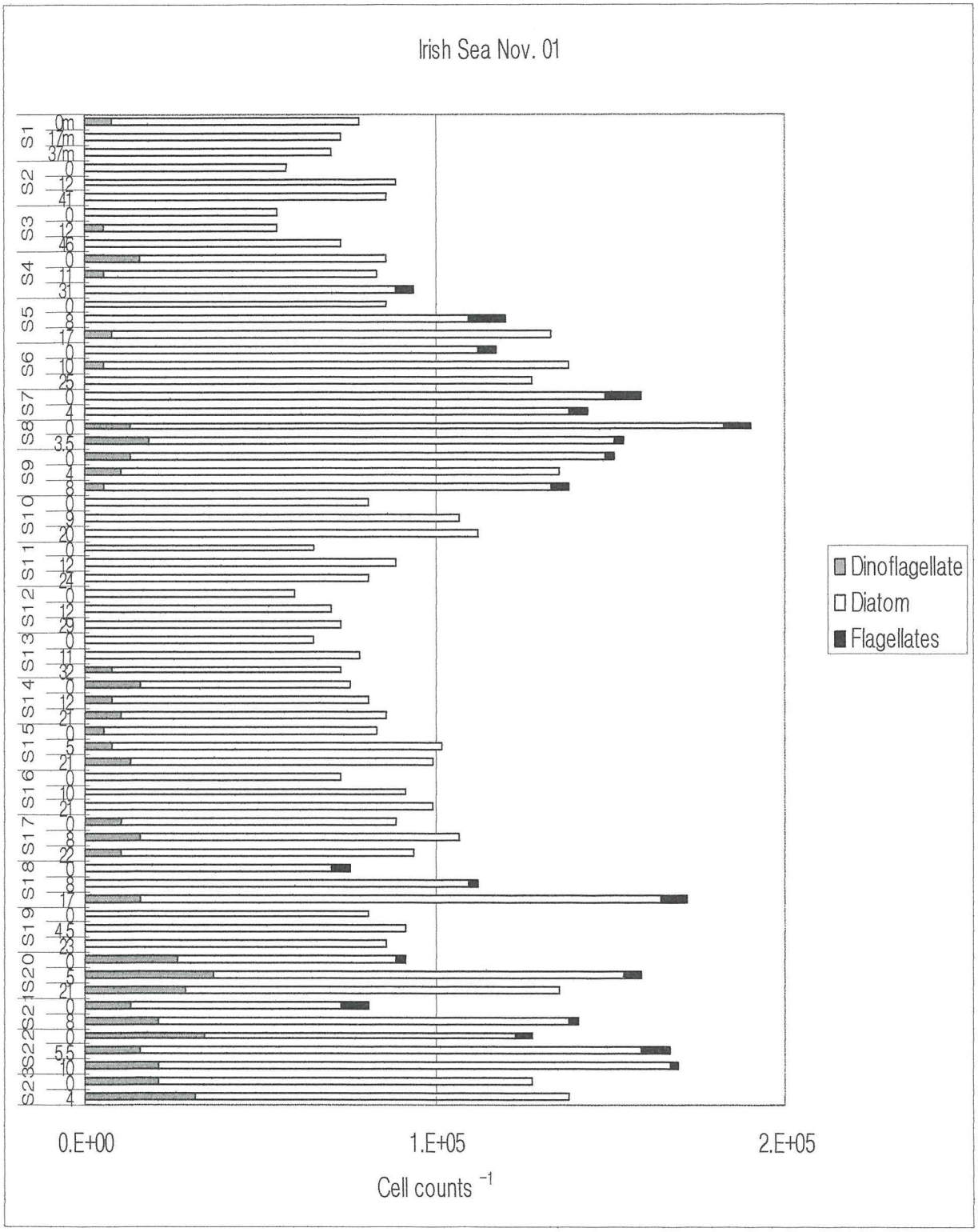

Figure 4.4 Phytoplankton cell counts data during the Irish Sea cruise (26-30 November 2001). Phytoplankton were classified into three groups; dinoflagellates, diatoms and flagellates.

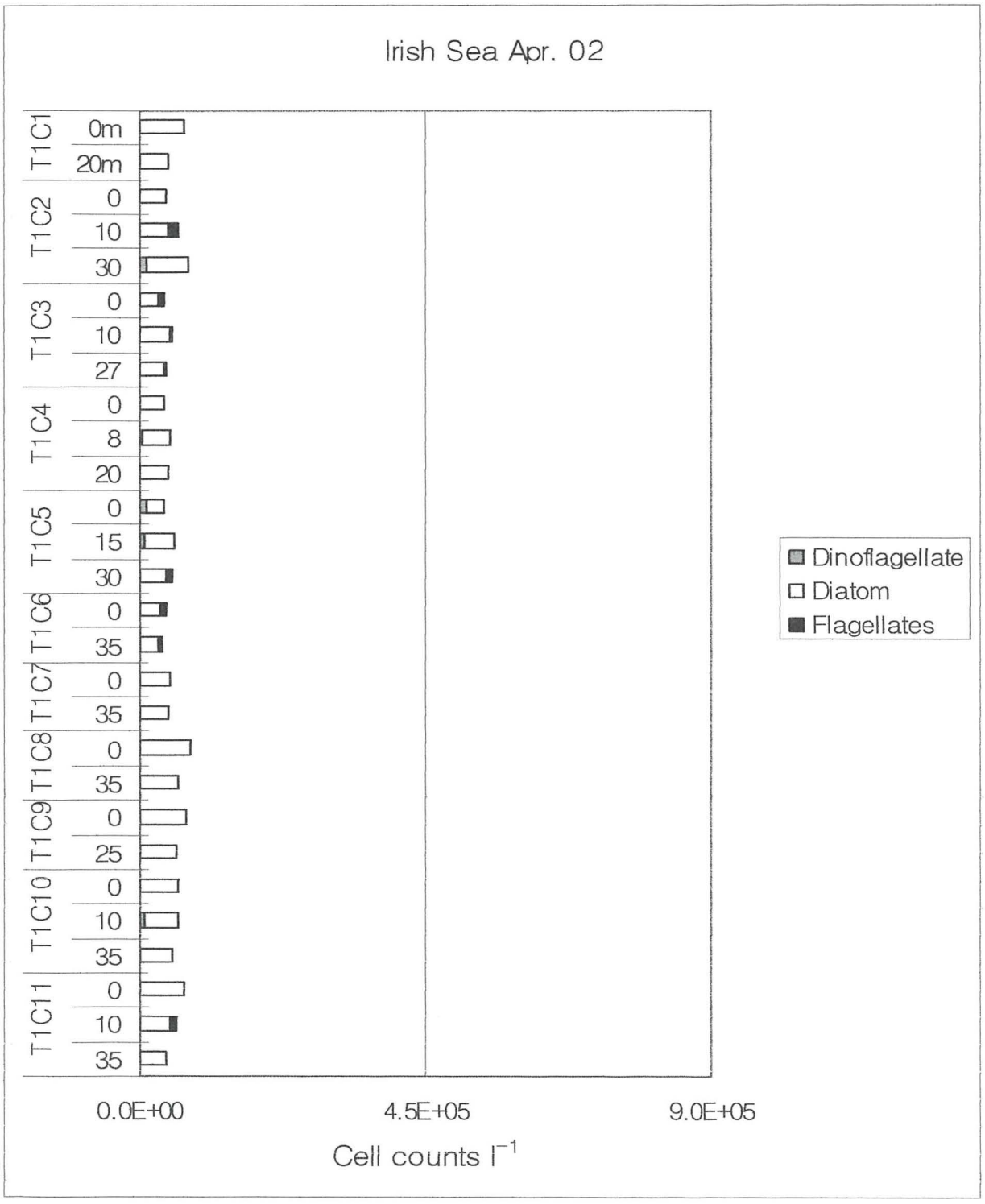

Figure 4.5a Phytoplankton cell counts data during the Irish Sea cruise (2 April 2002). Samples were taken at station T1 over a tidal cycle. Phytoplankton were classified into three groups; dinoflagellates, diatoms and flagellates.

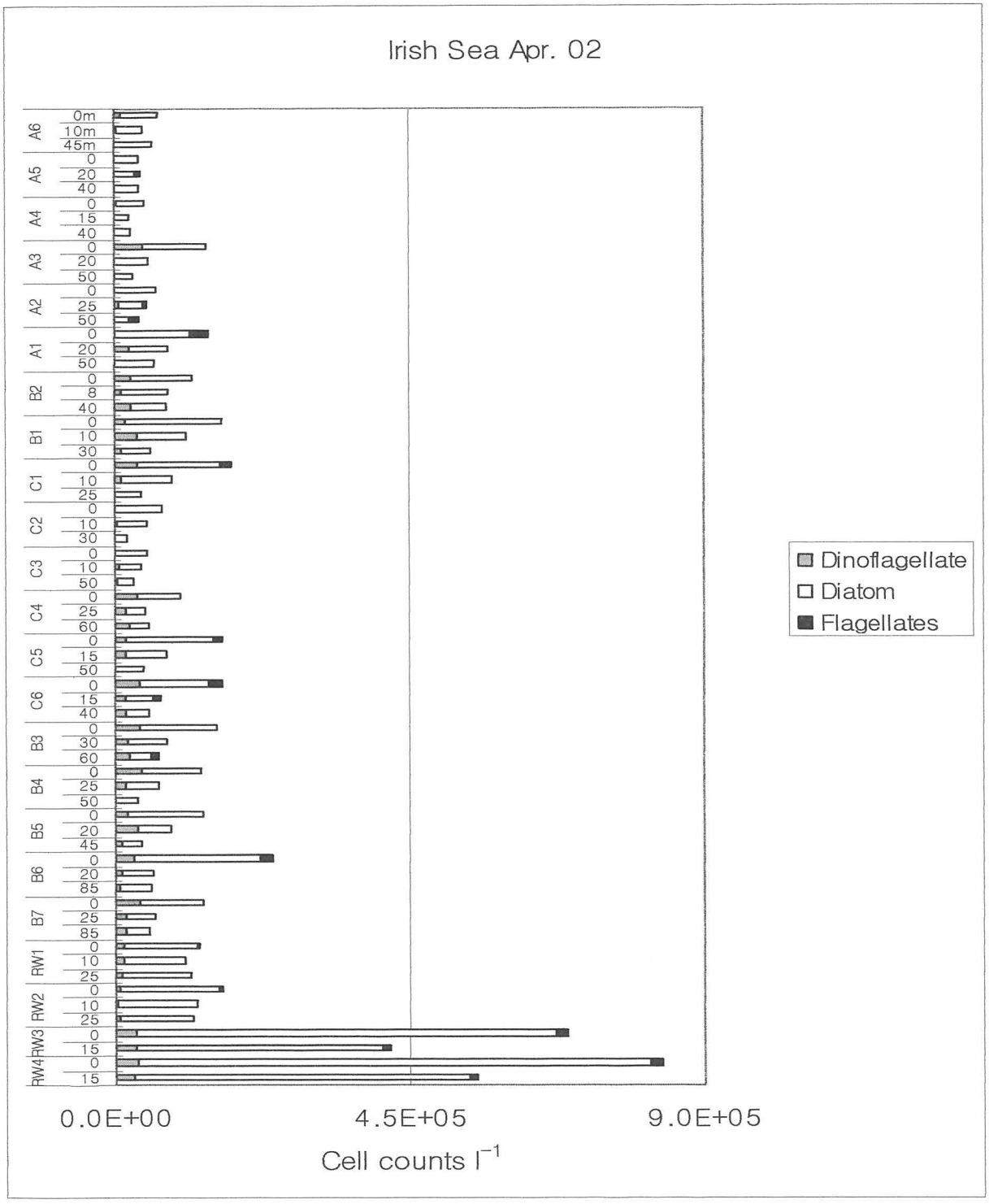

Figure 4.5b Phytoplankton cell counts data during the Irish Sea cruise (3-5 April 2002). Phytoplankton were classified into three groups; dinoflagellates, diatoms and flagellates.

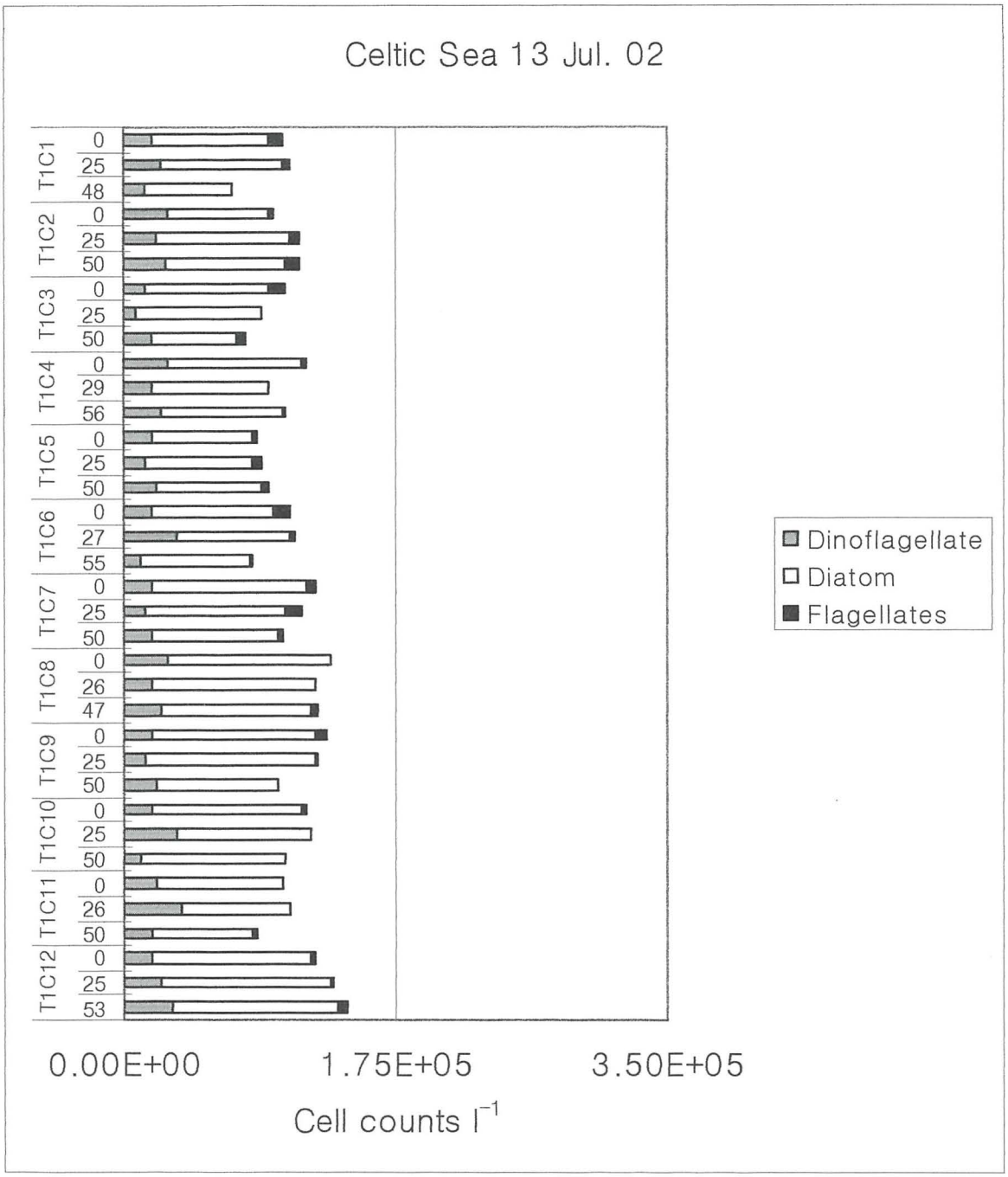

Figure 4.6a Phytoplankton cell counts data during the Celtic Sea cruise on 13 July 2002. Samples were taken at station T1 over a tidal cycle. Phytoplankton were classified into three groups; dinoflagellates, diatoms and flagellates.

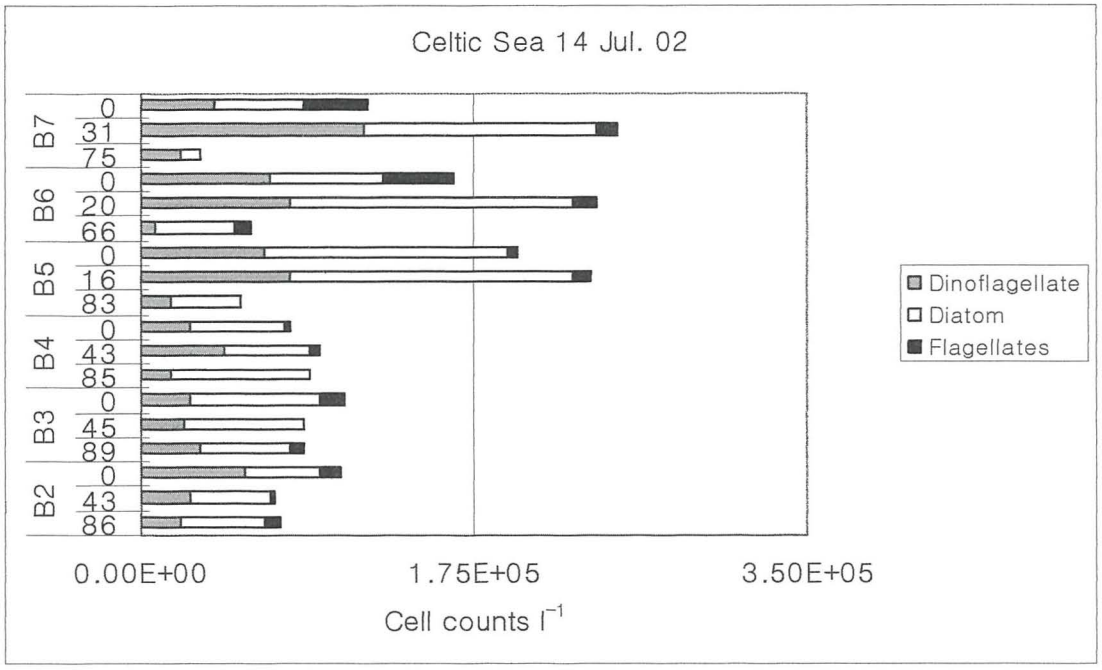

Figure 4.6b Phytoplankton cell counts data during the Celtic Sea cruise on 14 July 2002. Phytoplankton were classified into three groups; dinoflagellates, diatoms and flagellates.

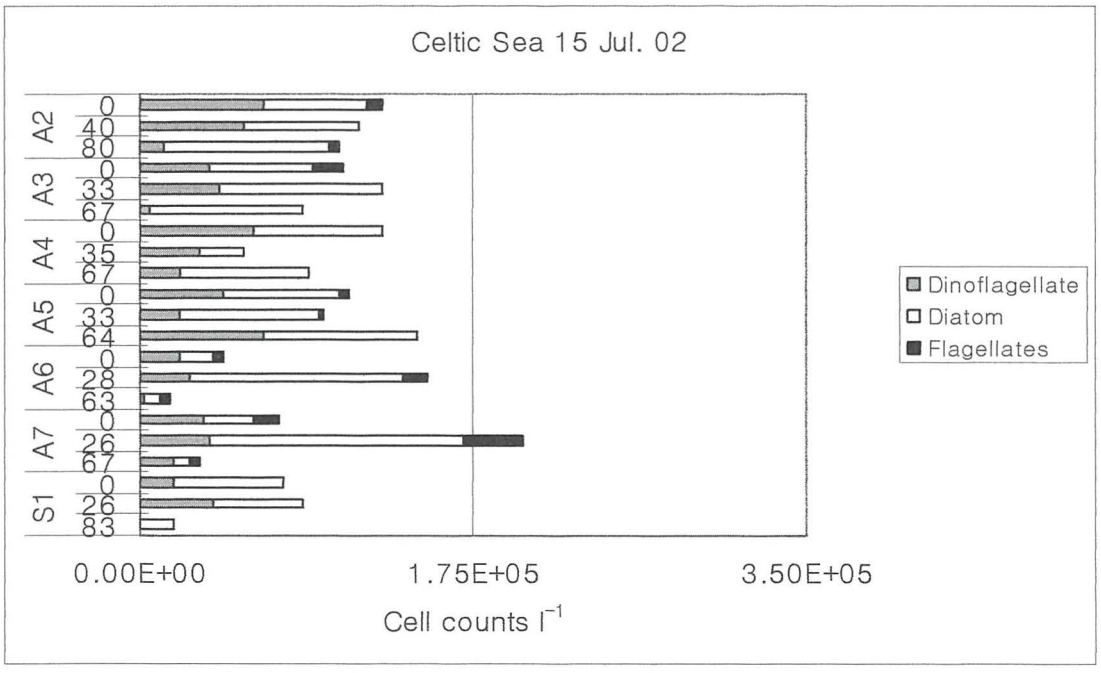

Figure 4.6c Phytoplankton cell counts data during the Celtic Sea cruise on 15 July 2002. Phytoplankton were classified into three groups; dinoflagellates, diatoms and flagellates.

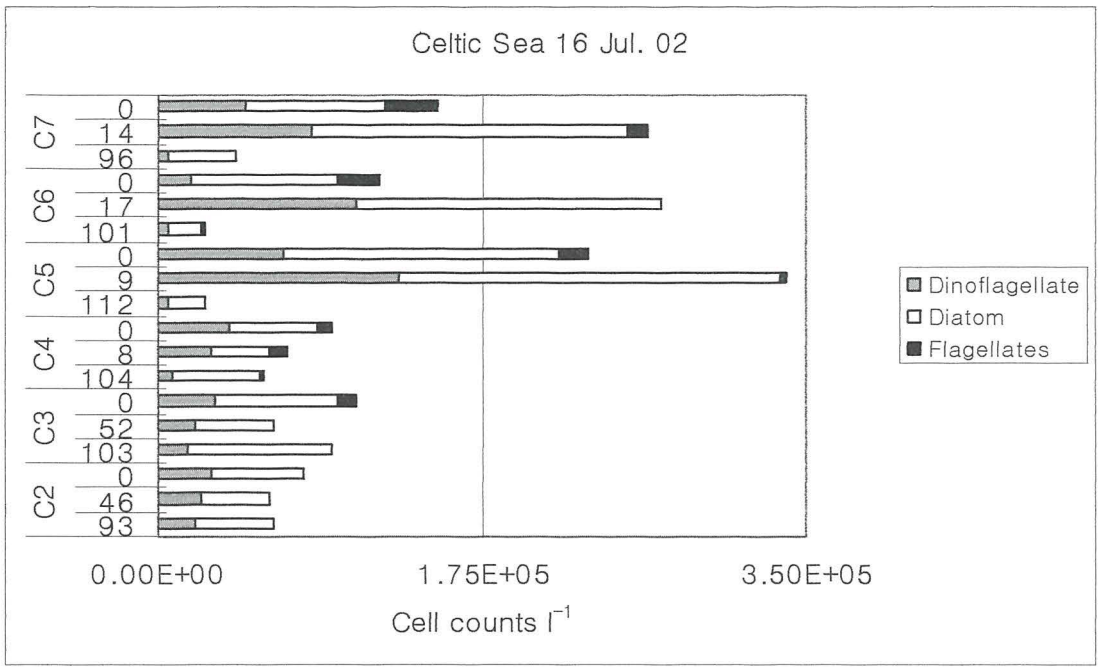

Figure 4.6d Phytoplankton cell counts data during the Celtic Sea cruise on 16 July 2002. Phytoplankton were classified into three groups; dinoflagellates, diatoms and flagellates.

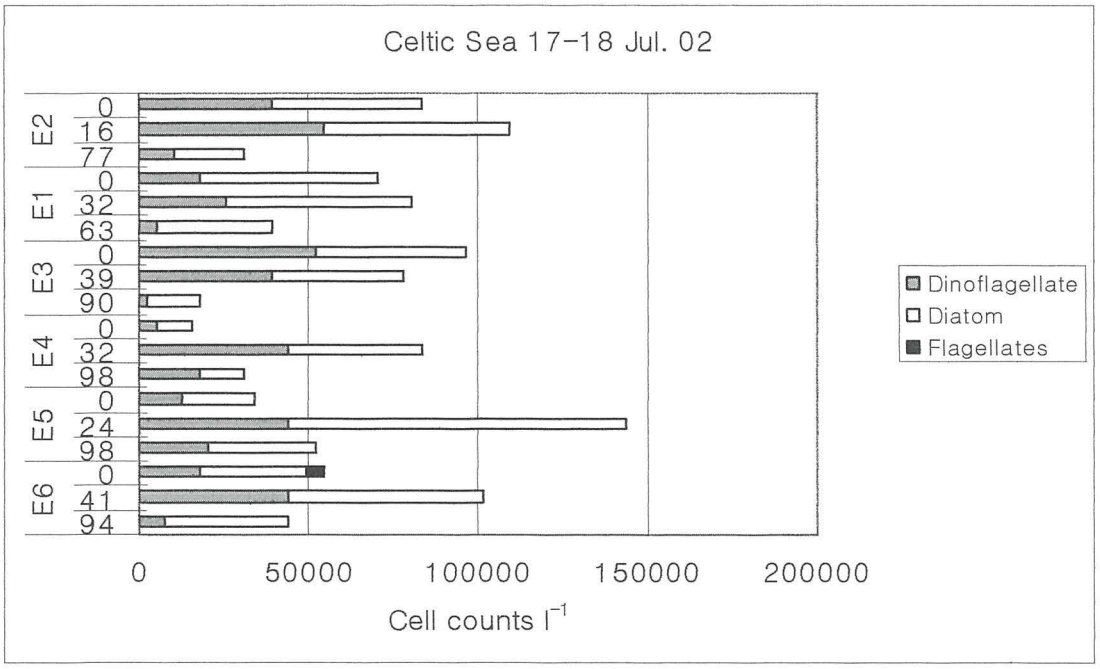

Figure 4.6e Phytoplankton cell counts data during the Celtic Sea cruise on 17 and 18 July 2002. Phytoplankton were classified into three groups; dinoflagellates, diatoms and flagellates.

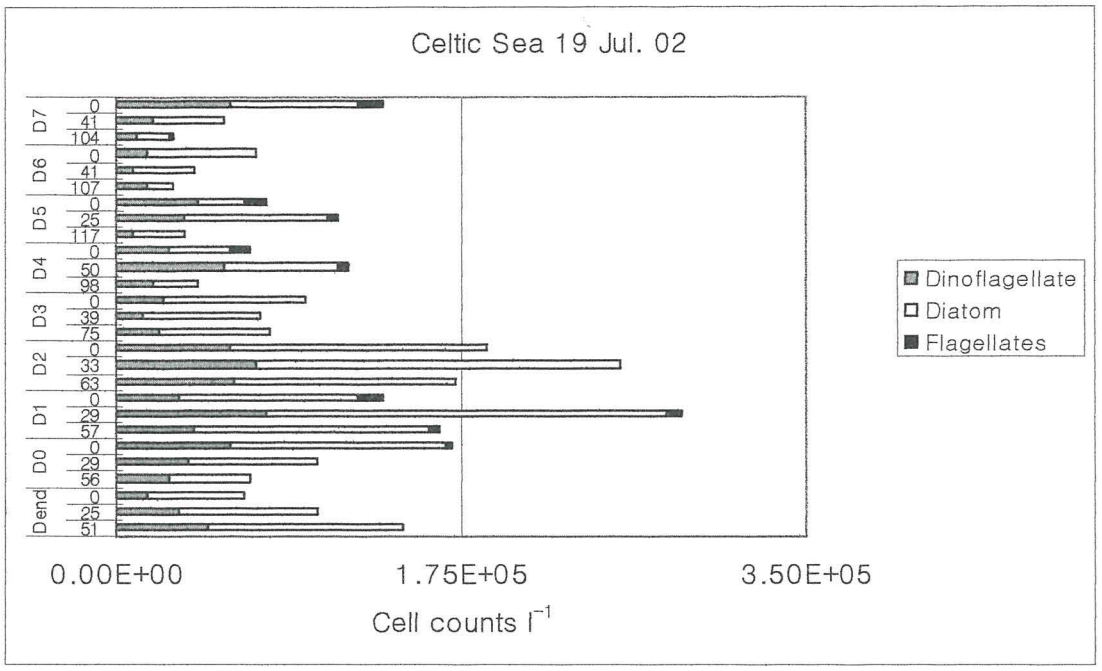

Figure 4.6f Phytoplankton cell counts data during the Celtic Sea cruise on 19 July 2002. Phytoplankton were classified into three groups; dinoflagellates, diatoms and flagellates.

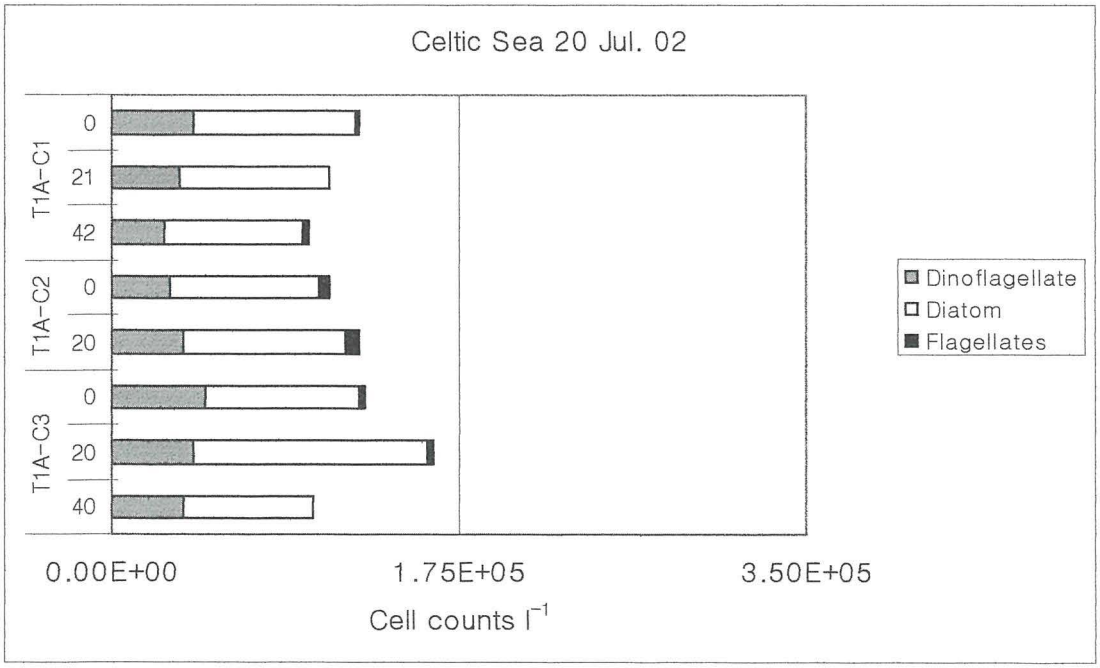

Figure 4.6g Phytoplankton cell counts data during the Celtic Sea cruise on 20 July 2002. Phytoplankton were classified into three groups; dinoflagellates, diatoms and flagellates.

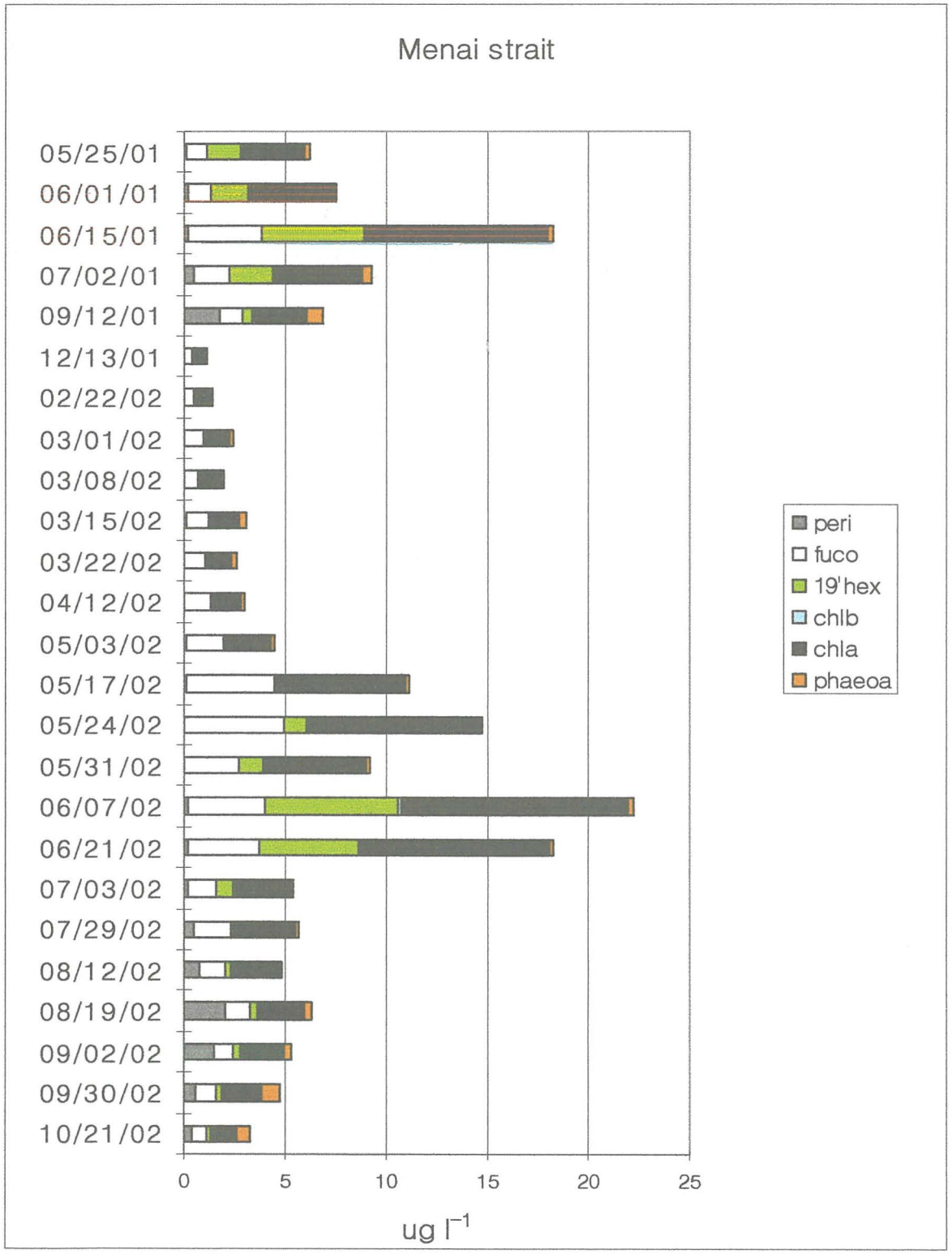

Figure 4.7 HPLC pigment measurements from the Menai Strait between 25 May 2001 and 21 October 2002. peri (peridinin), fuco (fucoxanthin), 19 hex (19' – hexanoyloxyfucoxanthin), chl b (chlorophyll *b*), chl a (chlorophyll *a*), phaeo (phaeophytin *a*).

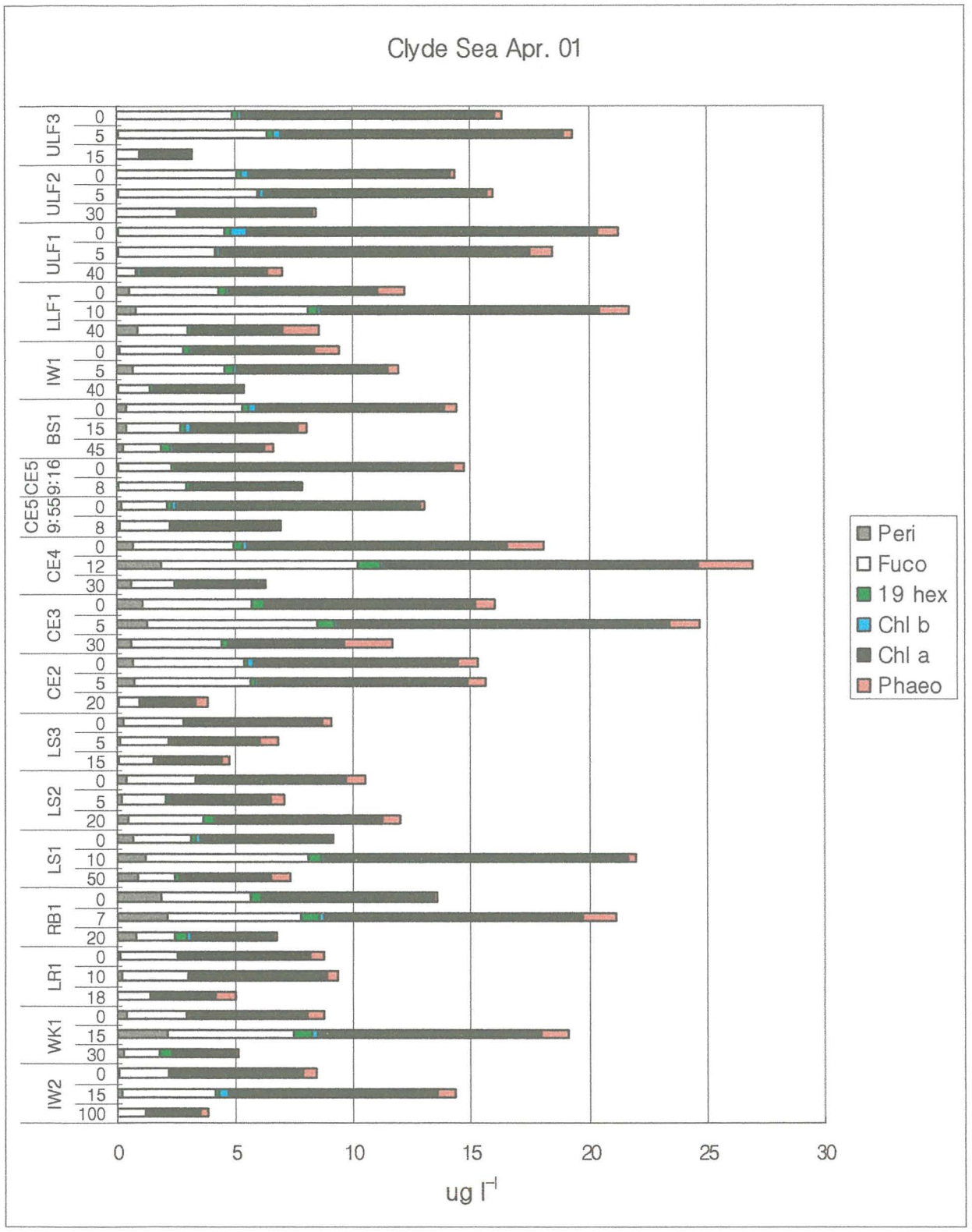

Figure 4.8 HPLC pigment measurements from the Clyde Sea cruise (23–27 April 2001). peri (peridinin), fuco (fucoxanthin), 19 hex (19' – hexanoyloxyfucoxanthin), chl b (chlorophyll *b*), chl a (chlorophyll *a*), phaeo (phaeophytin *a*).

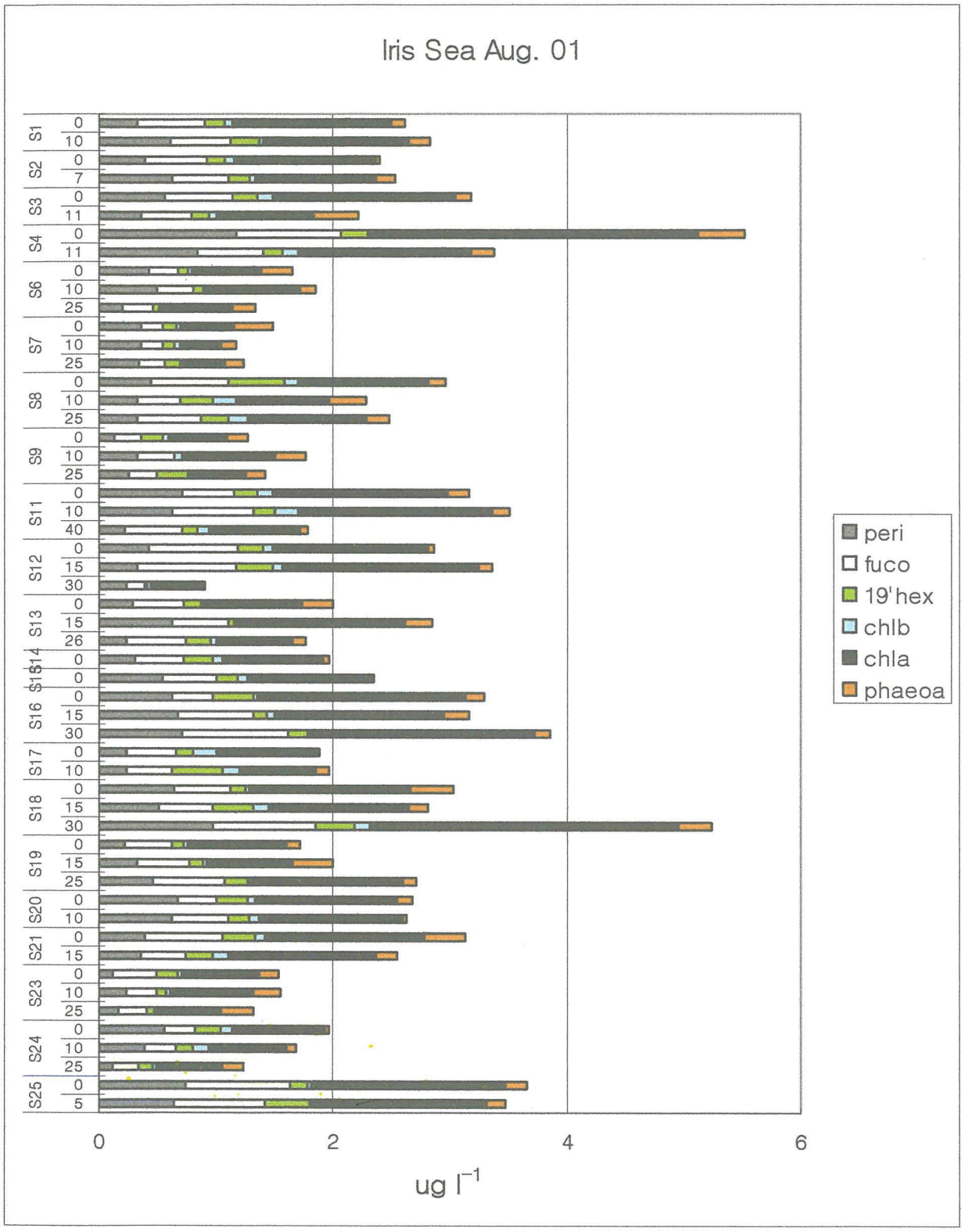

Figure 4.9 HPLC pigment measurements from the Irish Sea cruise (6–10 August 2001). peri (peridinin), fuco (fucoxanthin), 19 hex (19' – hexanoyloxyfucoxanthin), chl b (chlorophyll *b*), chl a (chlorophyll *a*), phaeo (phaeophytin *a*).

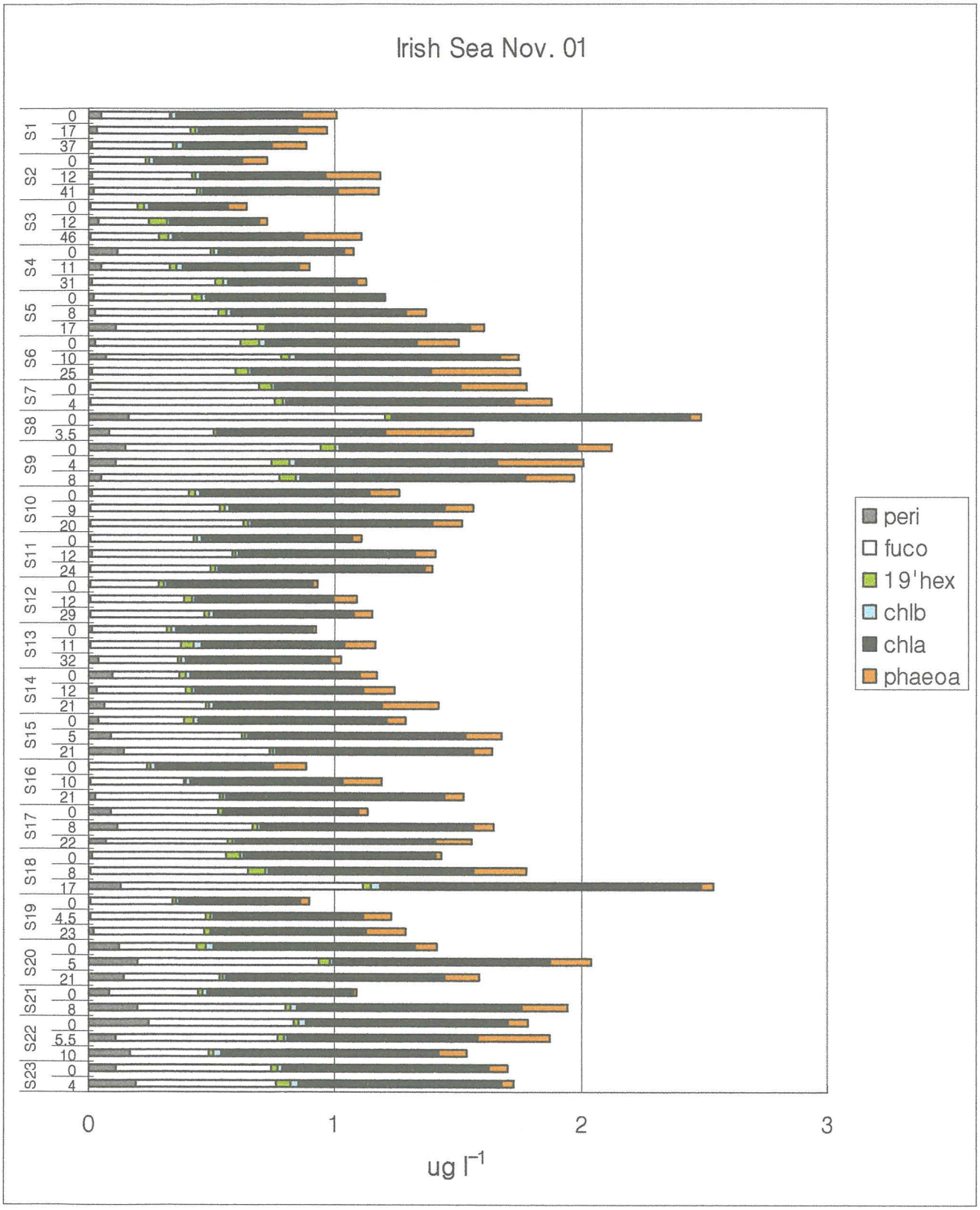

Figure 4.10 HPLC pigment measurements from the Irish Sea cruise (26–30 November 2001). peri (peridinin), fuco (fucoxanthin), 19 hex (19' – hexanoyloxyfucoxanthin), chl b (chlorophyll *b*), chl a (chlorophyll *a*), phaeo (phaeophytin *a*).

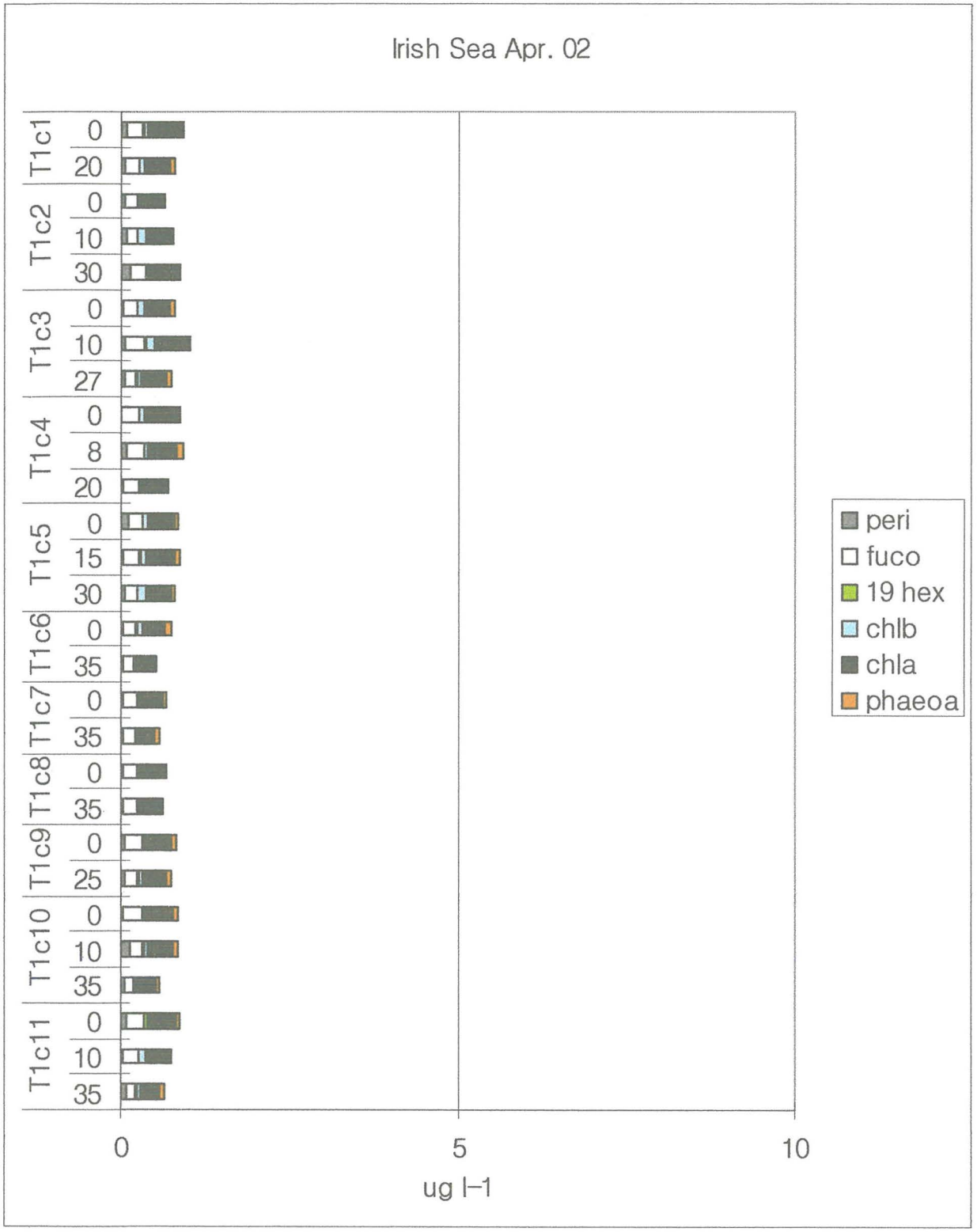

Figure 4.11a HPLC pigment measurements from the Irish Sea cruise on 2 April 2002. Samples were taken at station T1 over a tidal cycle.
peri (peridinin), fuco (fucoxanthin), 19 hex (19' – hexanoyloxyfucoxanthin), chl b (chlorophyll *b*), chl a (chlorophyll *a*), phaeo (phaeophytin *a*).

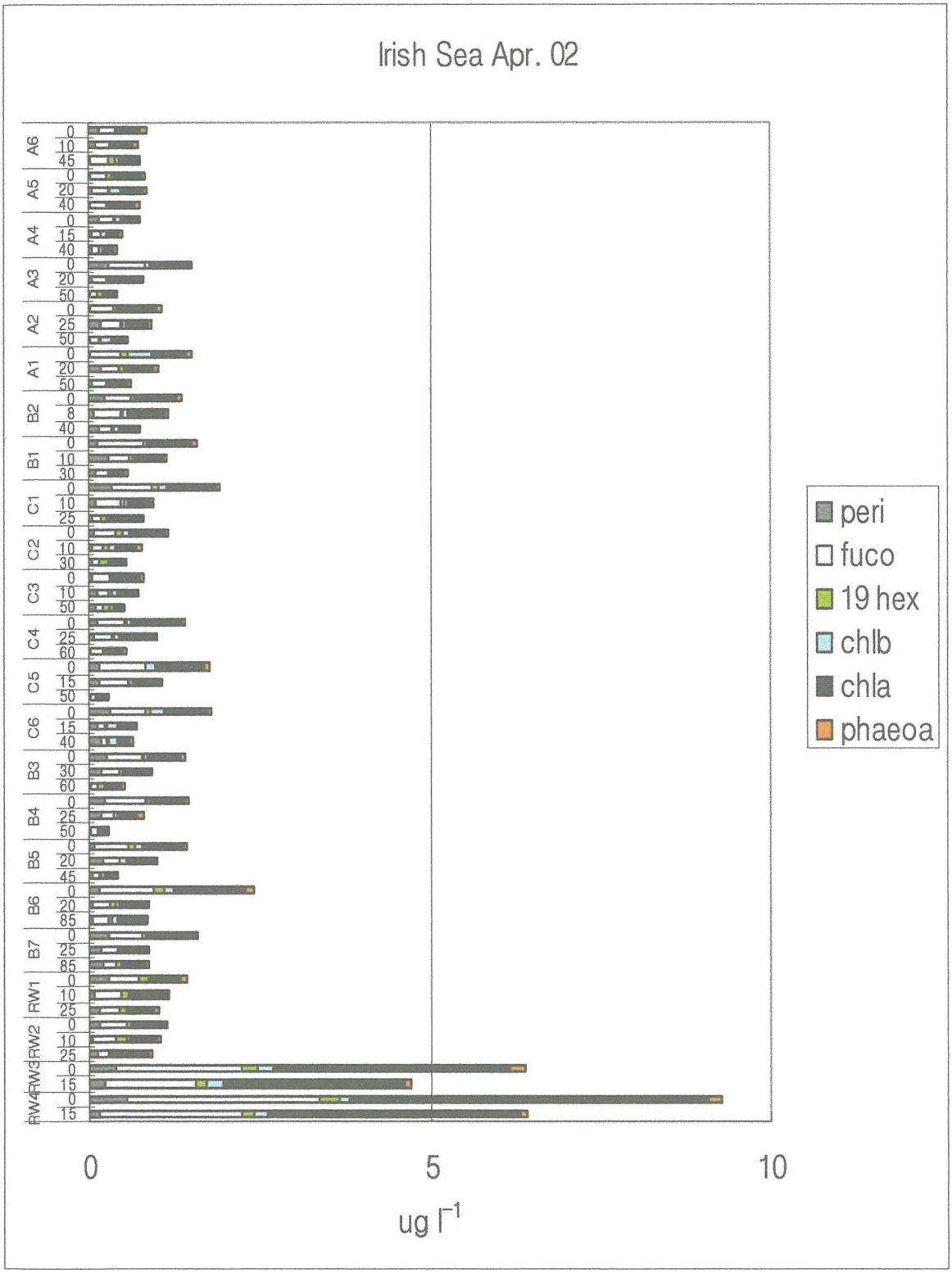

Figure 4.11b HPLC pigment measurements from the Irish Sea cruise (3–5 April 2002).

peri (peridinin), fuco (fucoxanthin), 19 hex (19' – hexanoyloxyfucoxanthin), chl b (chlorophyll *b*), chl a (chlorophyll *a*), phaeo (phaeophytin *a*).

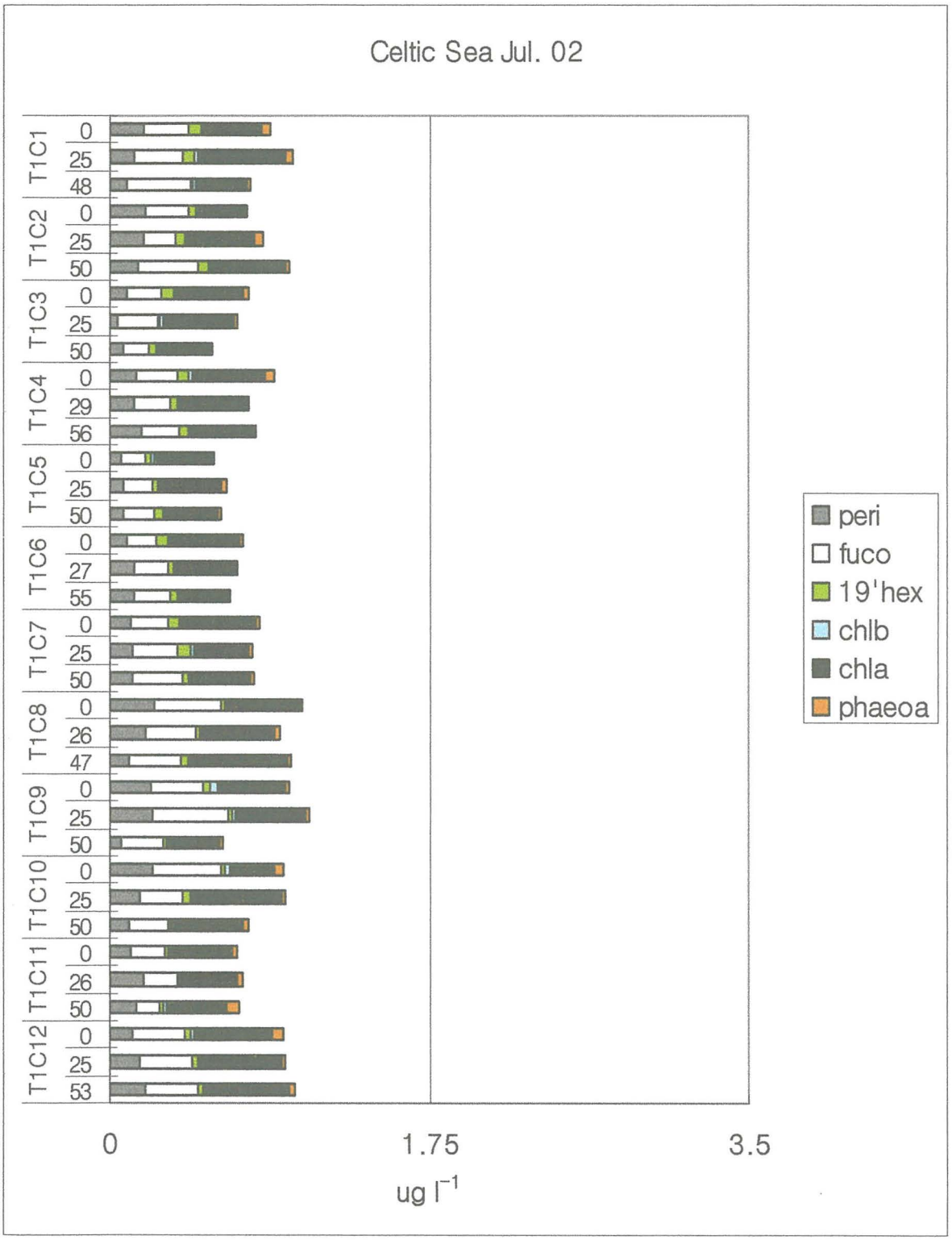

Figure 4.12a HPLC pigment measurements from the Celtic Sea cruise on 13 July 2002. Samples were taken at station T1 over a tidal cycle.
peri (peridinin), fuco (fucoxanthin), 19 hex (19' – hexanoyloxyfucoxanthin), chl b (chlorophyll *b*), chl a (chlorophyll *a*), phaeo (phaeophytin *a*).

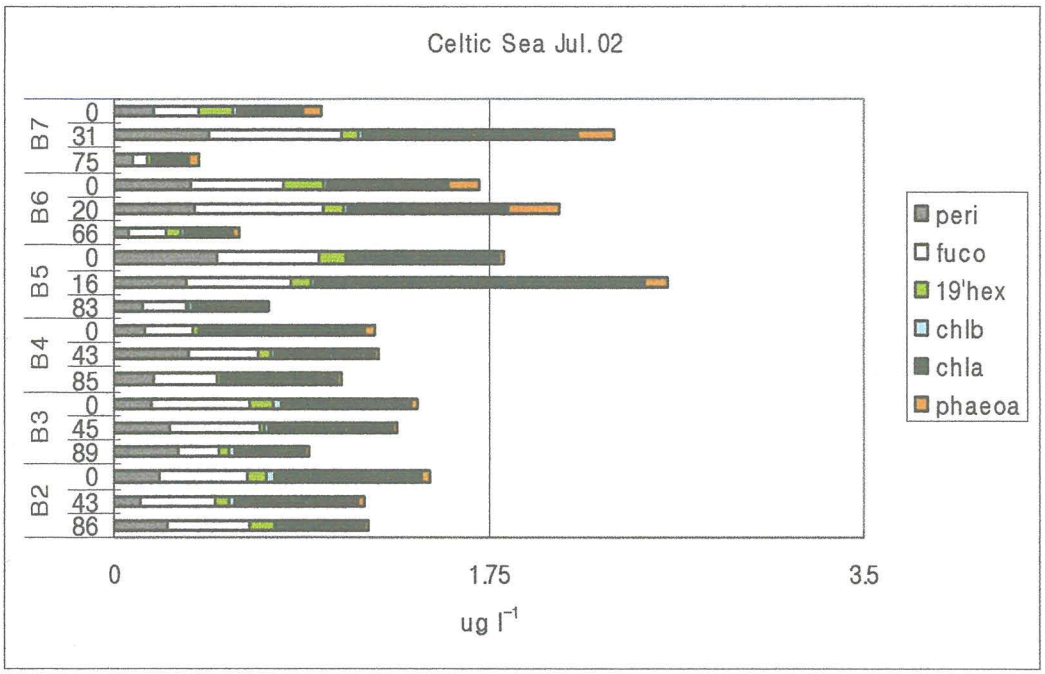

Figure 4.12b HPLC pigment measurements from the Celtic Sea cruise on 14 July 2002. peri (peridinin), fuco (fucoxanthin), 19 hex (19' – hexanoyloxyfucoxanthin), chl b (chlorophyll *b*), chl a (chlorophyll *a*), phaeo (phaeophytin *a*).

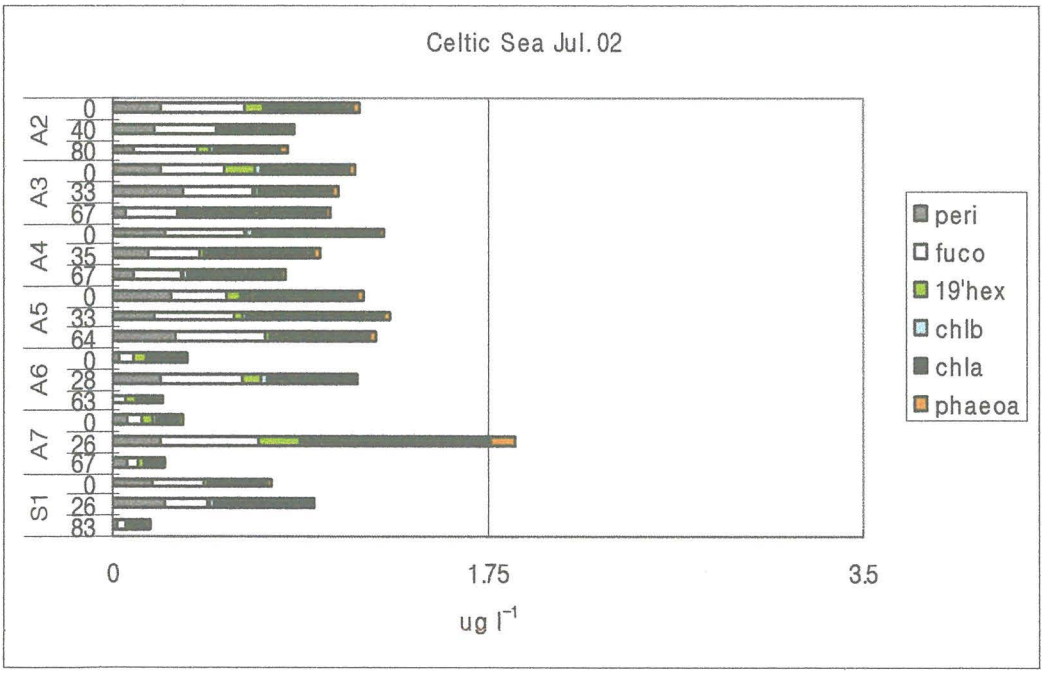

Figure 4.12c HPLC pigment measurements from the Celtic Sea cruise on 15 July 2002. peri (peridinin), fuco (fucoxanthin), 19 hex (19' – hexanoyloxyfucoxanthin), chl b (chlorophyll *b*), chl a (chlorophyll *a*), phaeo (phaeophytin *a*).

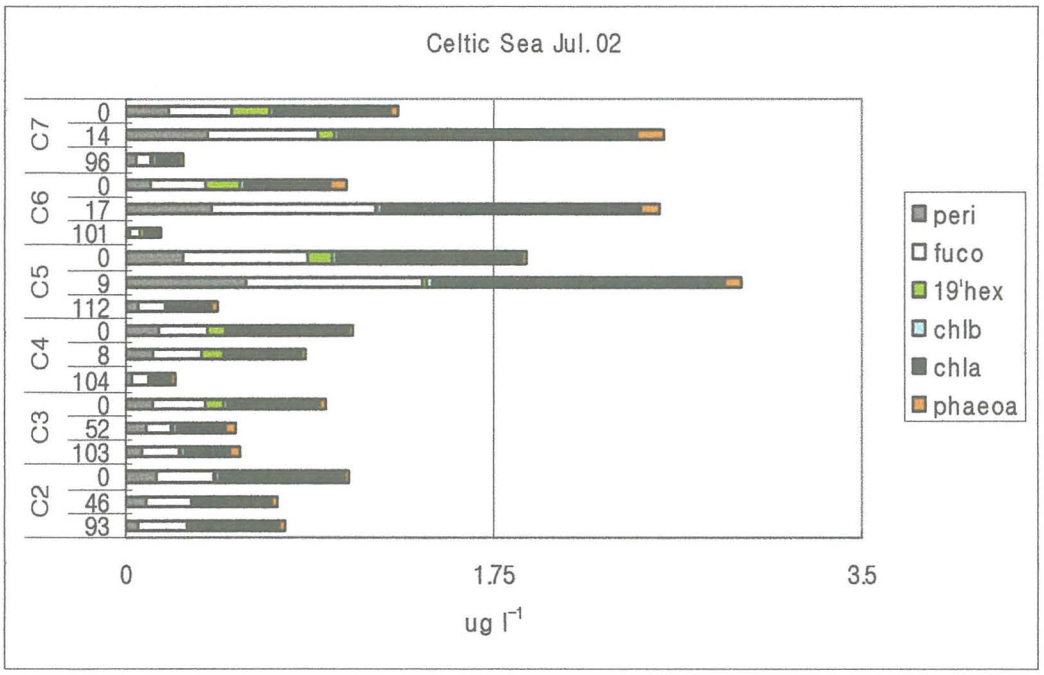

Figure 4.12d HPLC pigment measurements from the Celtic Sea cruise on 16 July 2002. peri (peridinin), fuco (fucoxanthin), 19 hex (19' – hexanoyloxyfucoxanthin), chl b (chlorophyll *b*), chl a (chlorophyll *a*), phaeo (phaeophytin *a*).

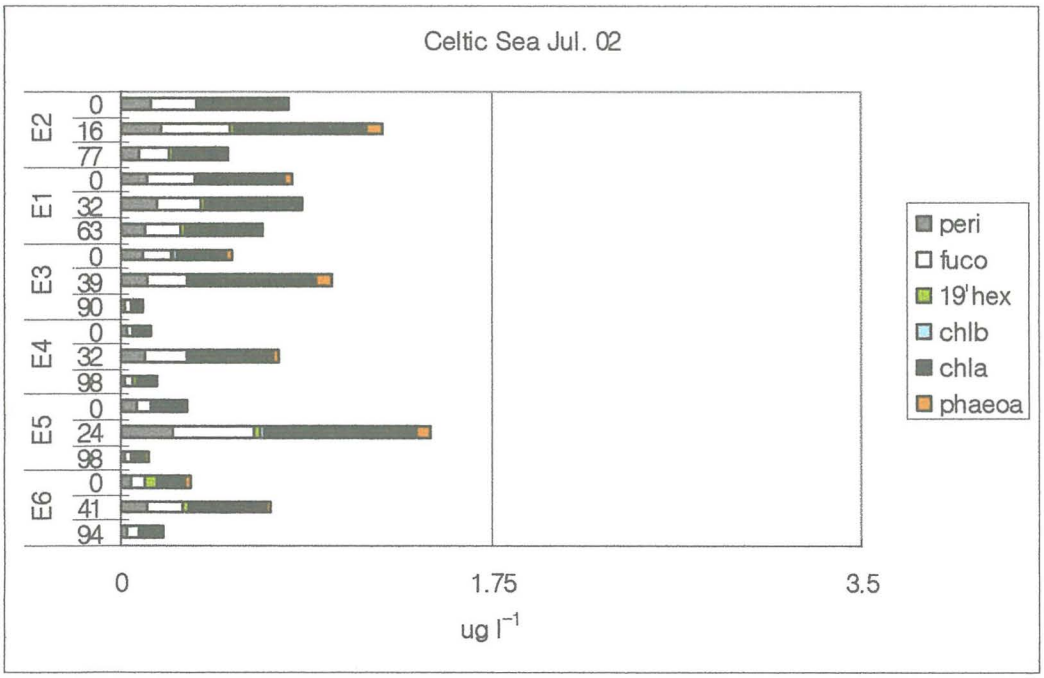

Figure 4.12e HPLC pigment measurements from the Celtic Sea cruise on 17 abd 18 July 2002. peri (peridinin), fuco (fucoxanthin), 19 hex (19' – hexanoyloxyfucoxanthin), chl b (chlorophyll *b*), chl a (chlorophyll *a*), phaeo (phaeophytin *a*).

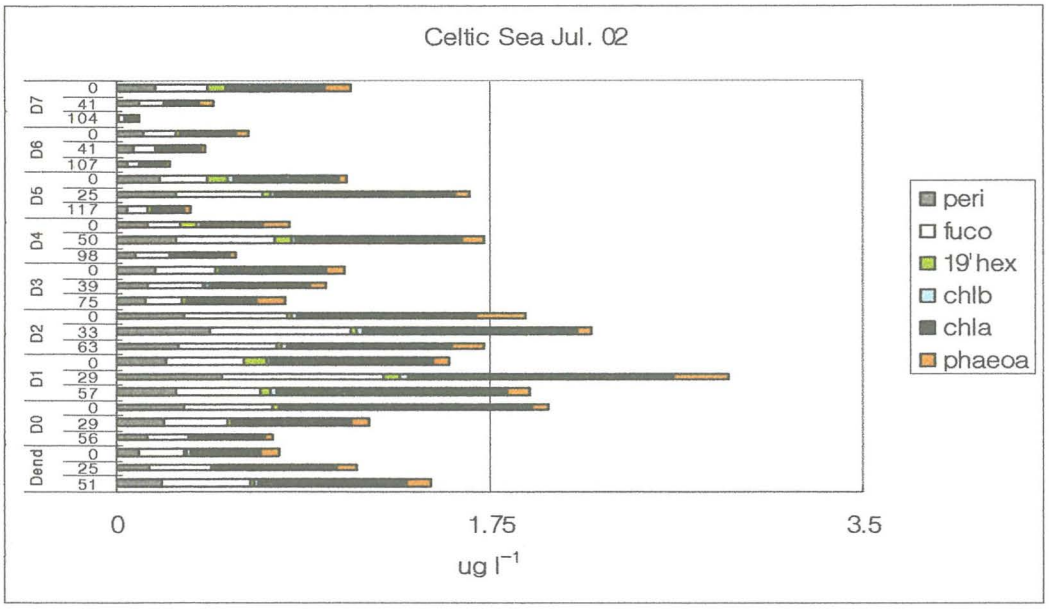

Figure 4.12f HPLC pigment measurements from the Celtic Sea cruise on 19 July 2002. peri (peridinin), fuco (fucoxanthin), 19 hex (19' – hexanoyloxyfucoxanthin), chl b (chlorophyll *b*), chl a (chlorophyll *a*), phaeo (phaeophytin *a*).

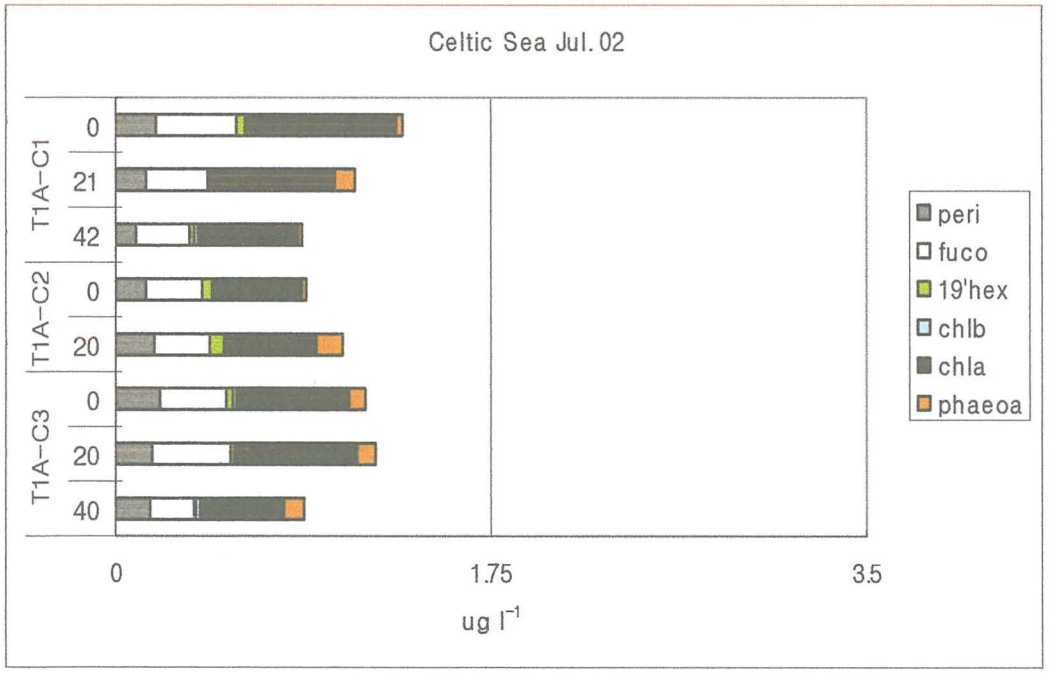

Figure 4.12g HPLC pigment measurements from the Celtic Sea cruise on 20 July 2002. peri (peridinin), fuco (fucoxanthin), 19 hex (19' – hexanoyloxyfucoxanthin), chl b (chlorophyll *b*), chl a (chlorophyll *a*), phaeo (phaeophytin *a*).

(a)

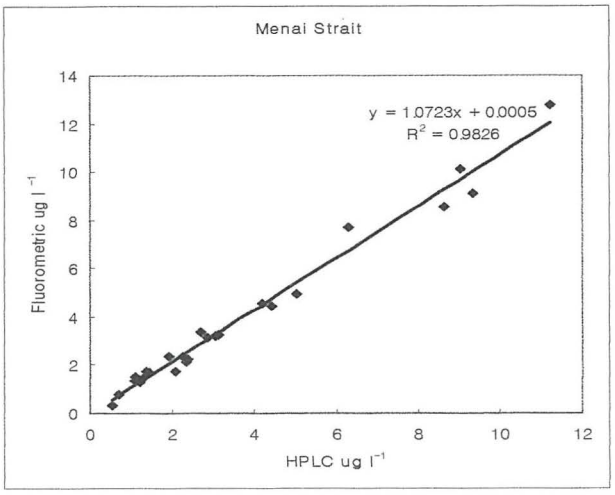

(b)

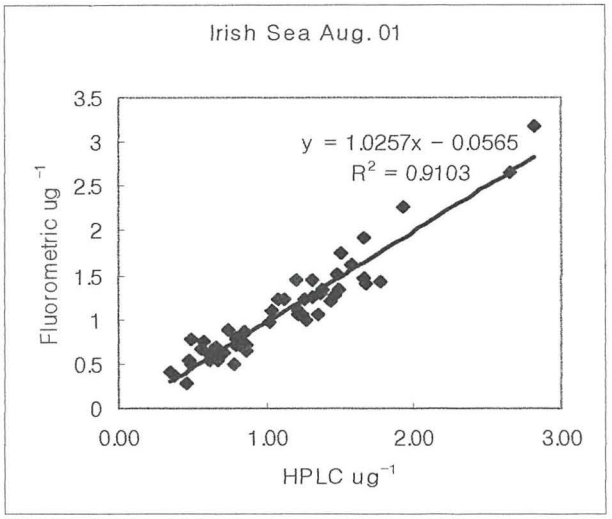

(c)

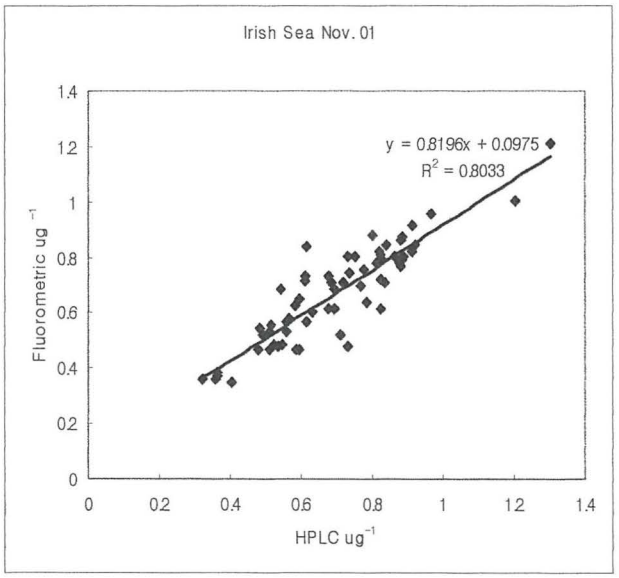

Figure 4.13 a,b,c Regression of the chlorophyll a concentration measurement by fluorometer against the chlorophyll a measurement by HPLC in the Menai Strait (a), and during the Irish Sea cruise in August 2001 (b) and November 2001 (c).

(d)

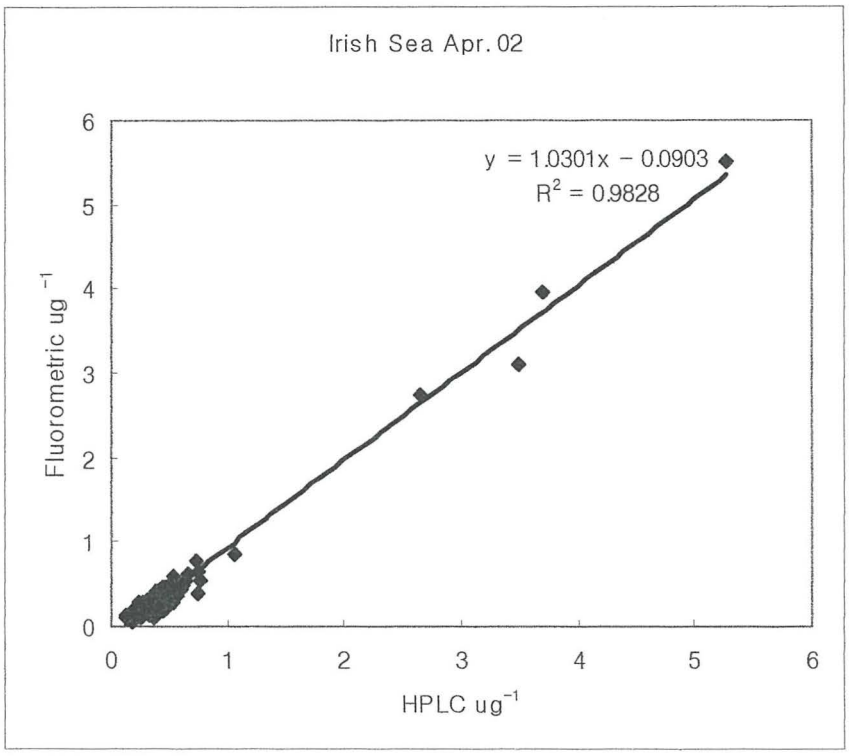

(e)

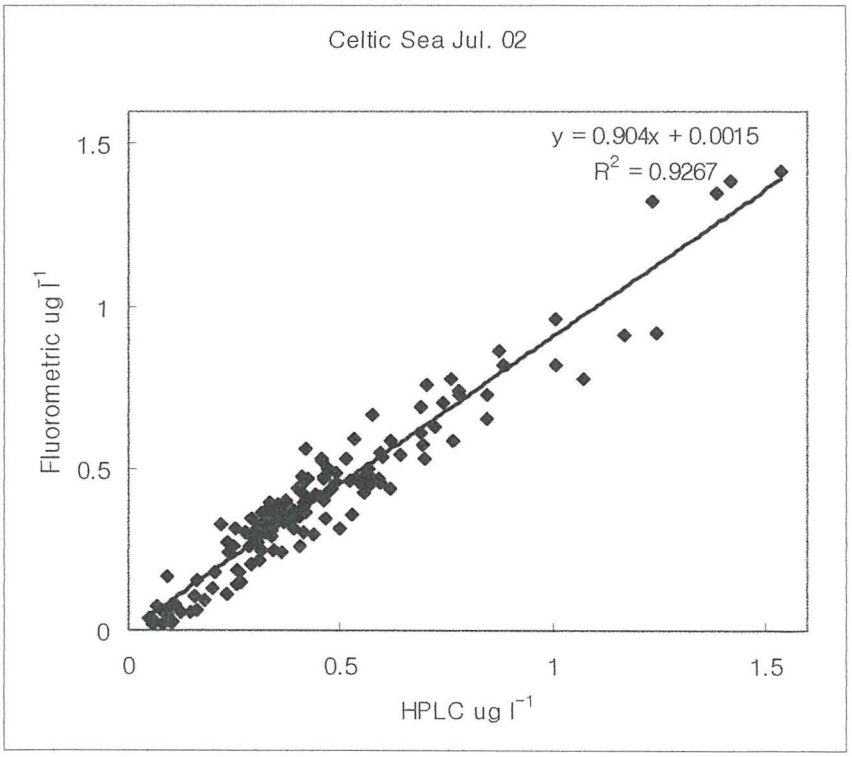

Figure 4.13 d,e Regression of the chlorophyll a concentration measurement by fluorometer against the chlorophyll a measurement by HPLC during the Irish Sea cruise in April 2002 (d) and the Celtic Sea cruise in July 2002 (e).

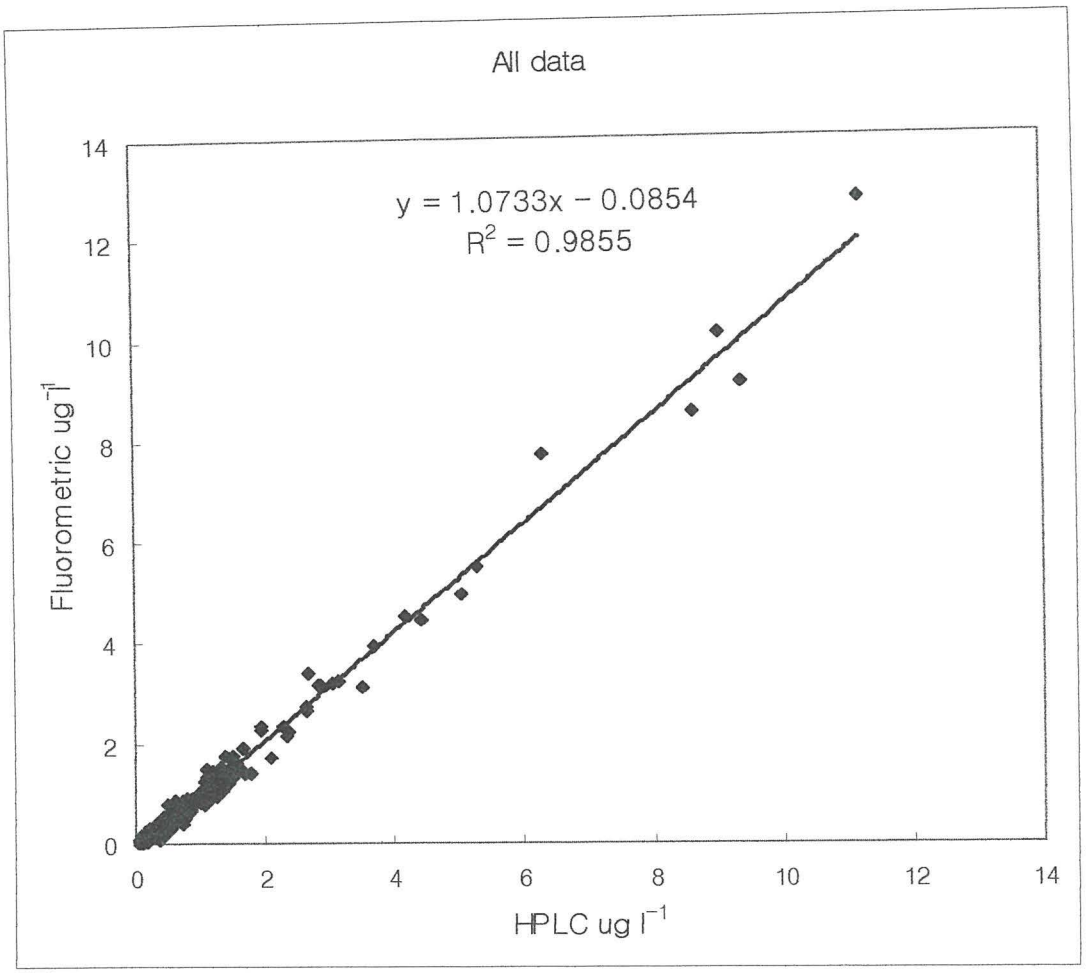

Figure 4.14 Regression of the chlorophyll a concentration measurement by fluorometer against the chlorophyll a measurement by HPLC for all data set from the Menai Strait and five cruises around the U.K. shelf seas.

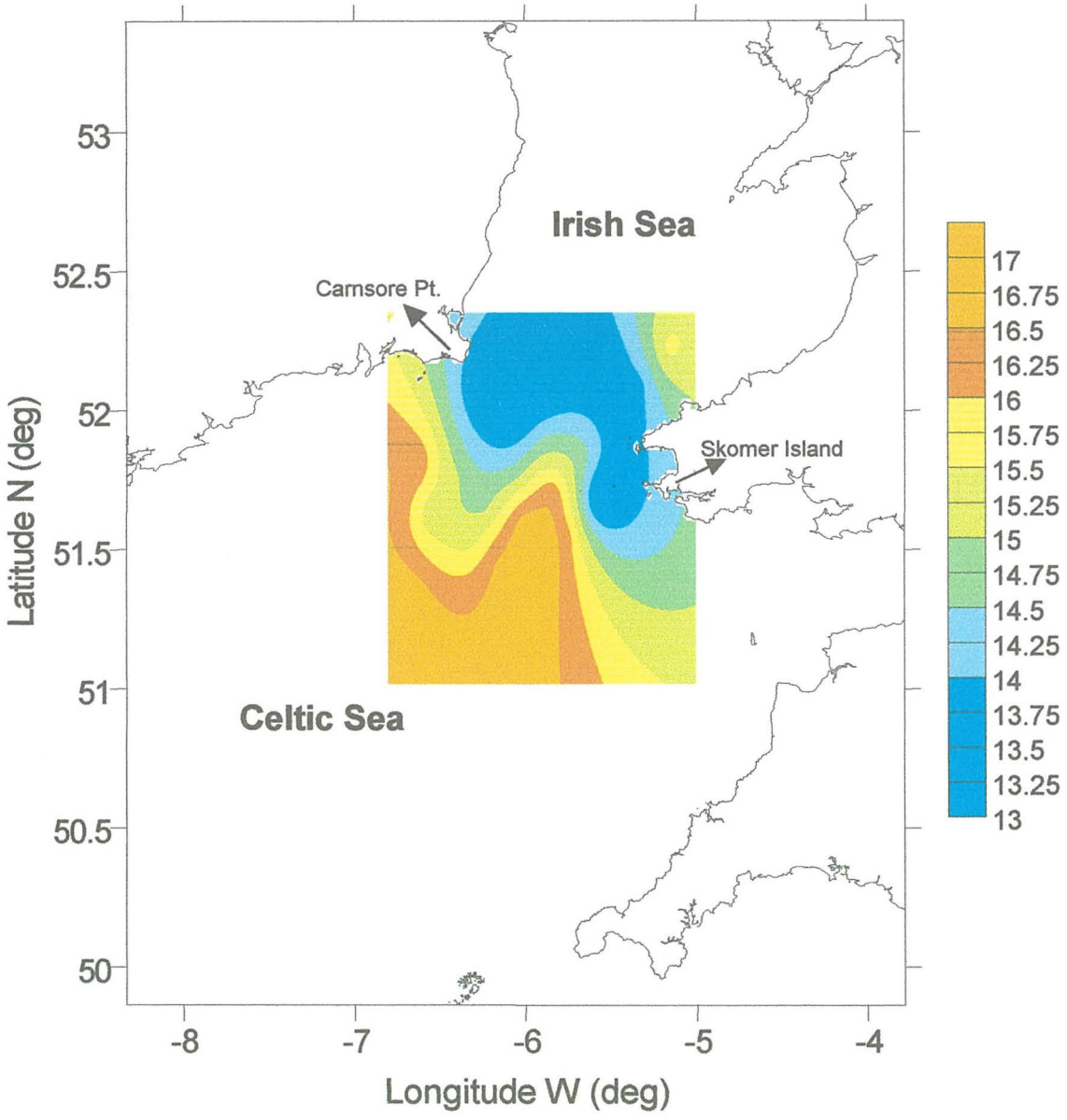

Figure 4.15 Surface water temperature (degrees C) variation in the Celtic Sea. Result obtained from CTD measurements on R.V Prince Madog cruise, 13 - 20 July 2002

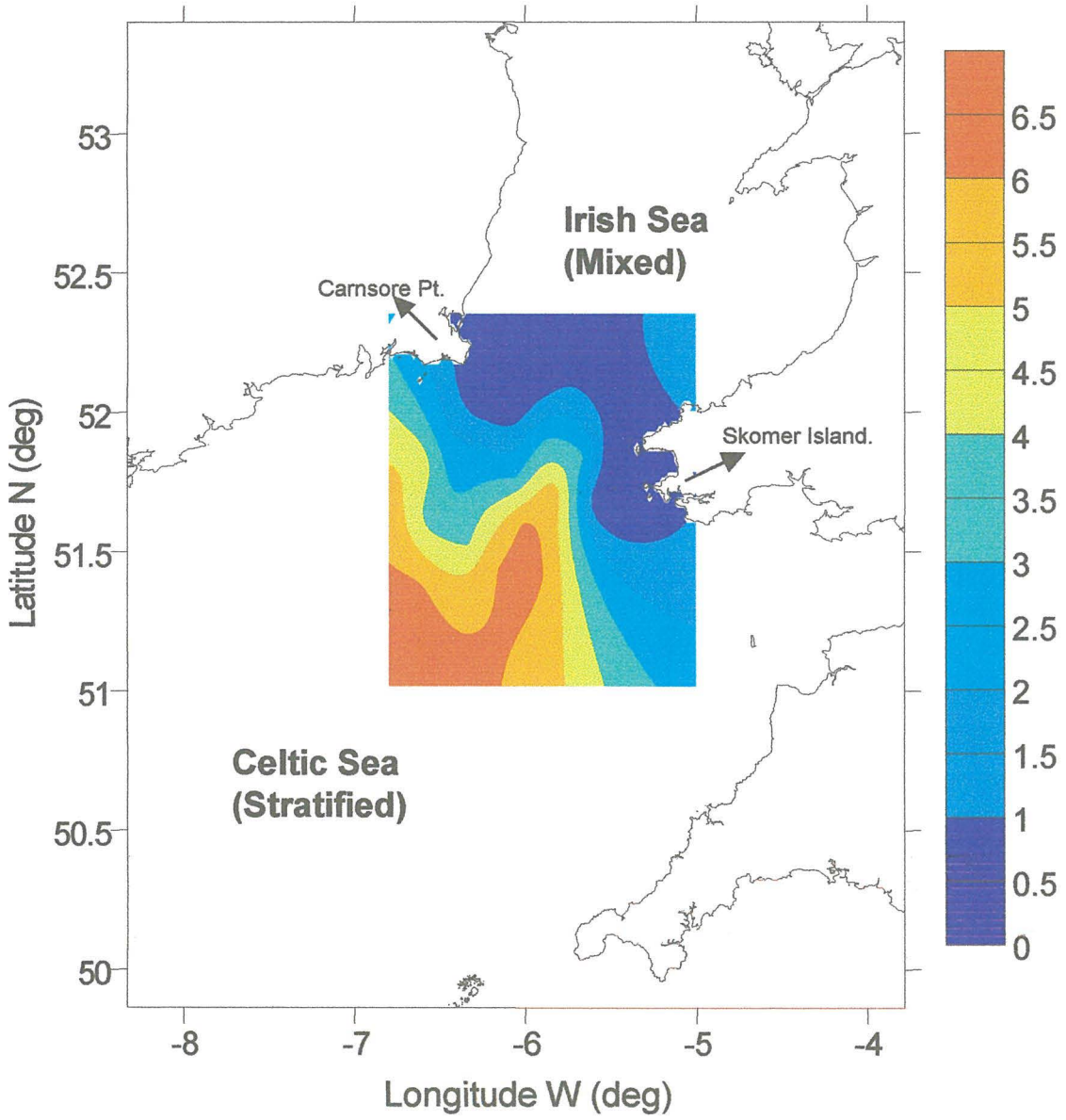

Figure 4.16 Surface and bottom temperature differences (degrees C) in the Celtic Sea, measured during R.V Prince Madog cruise, 13 - 20 July 2002, showing the stratified side in the Celtic Sea (south-east) and the mixed side in the Irish Sea (north-west).

(a)

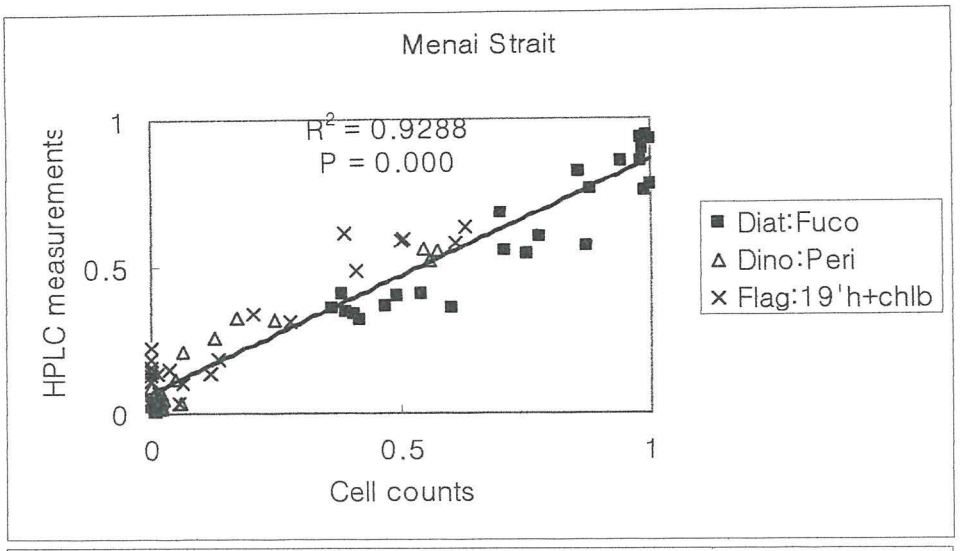

(b)

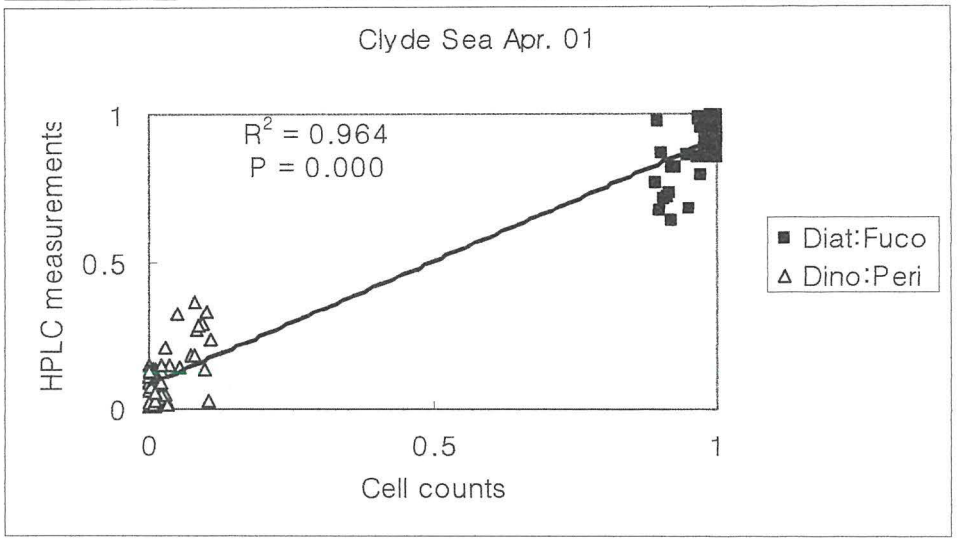

(c)

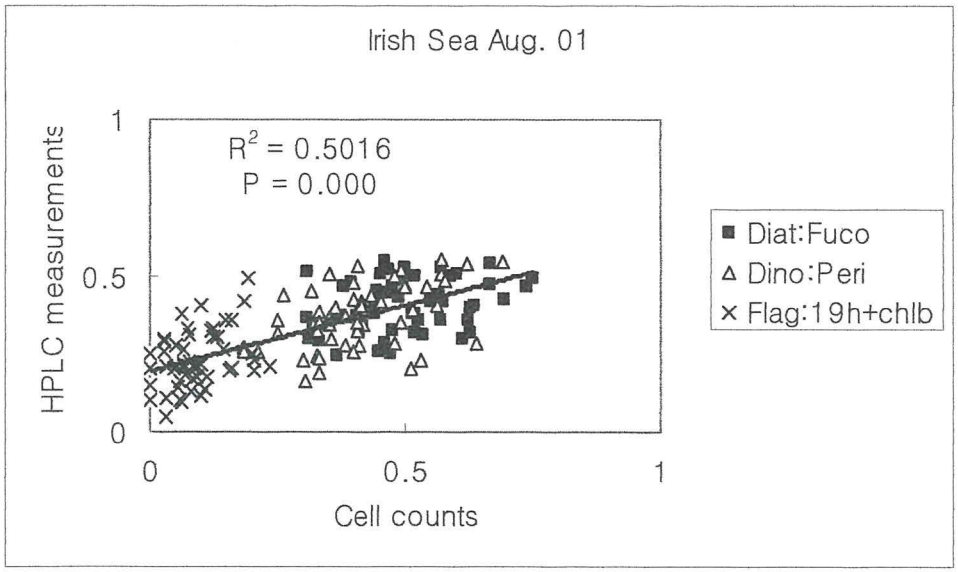

igure4.17 Comparison between HPLC pigment measurements and Taxonomic identification ata in the Menai Strait (a), the Clyde Sea April 2001(b) and the Irish Sea August 2001(c). lgal groups divided into three groups and compared to their marker pigments; diatoms vs. ucoxanthin, dinoflagellates vs. peridinin and flagellates vs. 19' hexanolyloxyfucoxanthin with hlorophyll b.The scale of both axis were proportionalised to 1

(a)

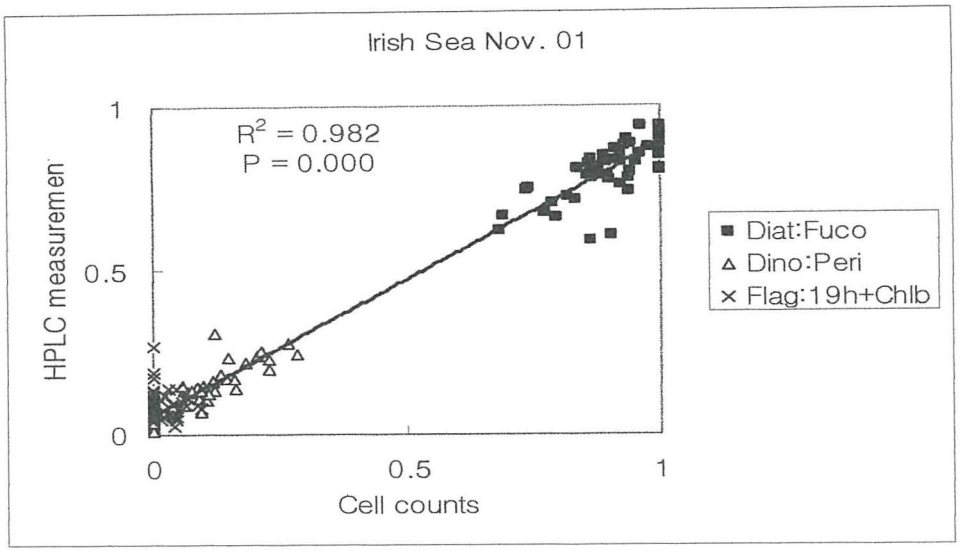

(b)

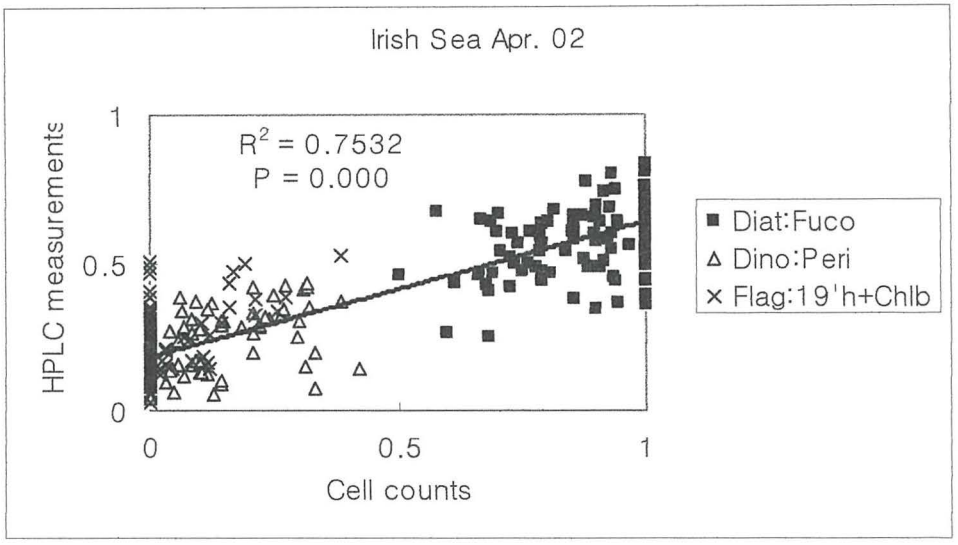

(c)

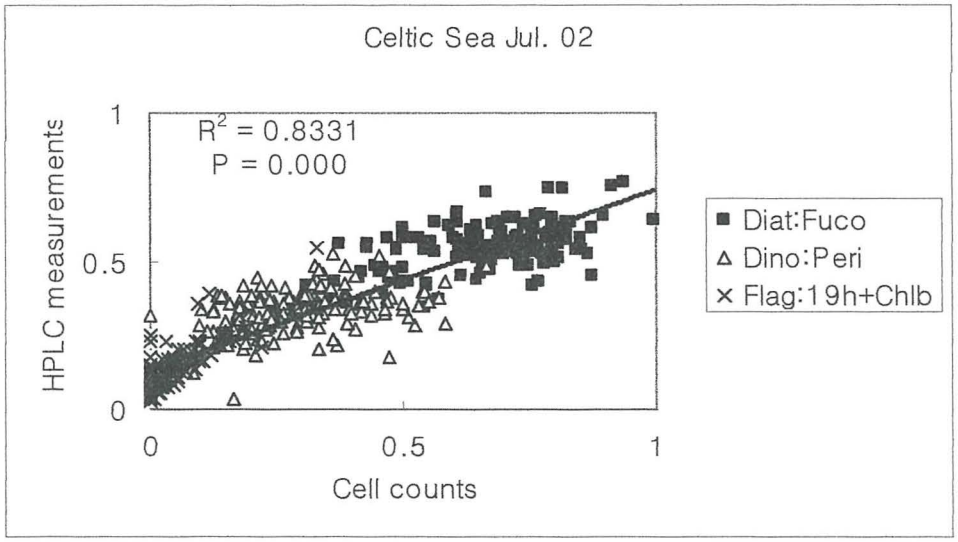

gure4.18 Comparison between HPLC pigment measurements and Taxonomic identification ata in the Irish Sea November 2001 (a), the Irish Sea April 2002(b) and the Celtic Sea ugust 2002(c). Algal groups divided into three groups and compared to their marker gments; diatoms vs. fucoxanthin, dinoflagellates vs. peridinin and flagellates vs. 19' exanolyloxyfucoxanthin with chlorophyll *b*.The scale of both axis were proportionalised to 1

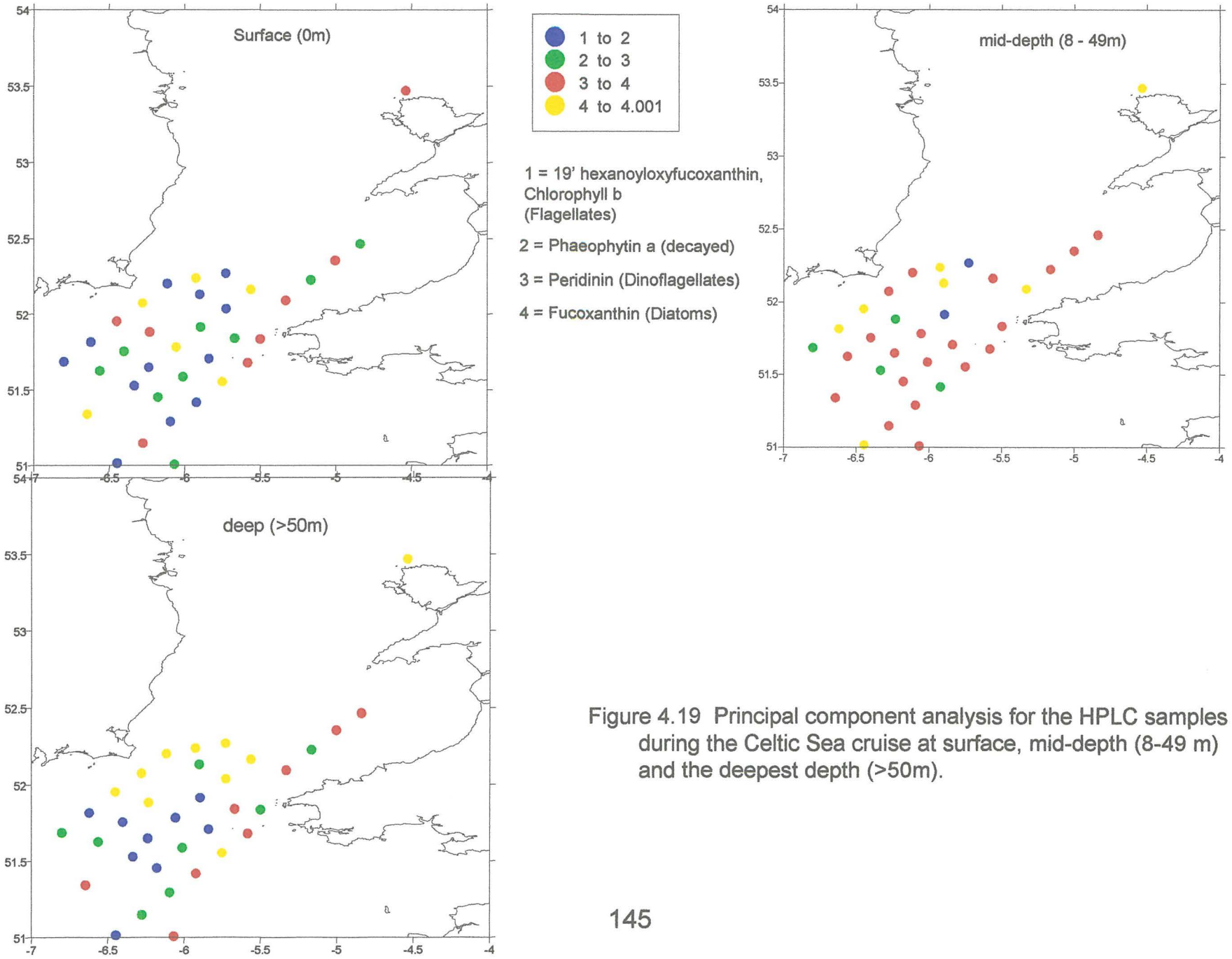

Figure 4.19 Principal component analysis for the HPLC samples during the Celtic Sea cruise at surface, mid-depth (8-49 m) and the deepest depth (>50m).

5. OPTICAL DETERMINATION OF PHYTOPLANKTON GROUPS

5.1 Introduction

This chapter presents the colour ratio algorithms, that were developed from the PRR-600 casts collected in the Menai Strait and on cruises around the U.K. shelf seas described in chapter 4. Phytoplankton group specific absorption spectra were classified according to the proportion of a marker pigment for diatom, fucoxantin, in the sum of all marker pigments used in this study; these were fucoxanthin, peridinin, 19'-hexanoloxyfucoxanthin and chlorophyll *b*. Modelled remote sensing reflectance were then developed, based on classified phytoplankton group specific absorption spectra, and were compared to the *in situ* remote sensing reflectance.

5.2 Colour ratio algorithms

The colour ratio algorithm (Morel, 1980; Gordon and Morel, 1983) to derive chlorophyll biomass was used in the Menai Strait and five cruises around the U.K. shelf seas: the Clyde Sea in April 2001; the Irish Sea in August and November 2001, and in April 2002; and the Celtic Sea in July 2002;

$$C = a(R(\lambda_1)/ R(\lambda_2))^b \qquad (5.1)$$

where C is the chlorophyll biomass in $\mu g\ l^{-1}$ measured by fluorometer and $R(\lambda_1)/ R(\lambda_2)$ is the irradiance reflectance ratio $((E_u(\lambda_1) / E_d(\lambda_1)) : (E_u(\lambda_2) / E_d(\lambda_2)))$ or remote

sensing reflectance ratio ((L_u (λ_1) / E_d (λ_1)) : (L_u (λ_2) / E_d (λ_2))). λ_1 = 443 or 490 nm and λ_2 = 555 nm. a and b are the constants. Logarithmic form of equation 5.1 is expressed;

$$\log C = b \log_{10} R + \log_{10} a \qquad (5.2)$$

where b is the gradient and $\log_{10} a$ is the intercept of regression between C and R. Table 5.1 and 5.2 shows chlorophyll algorithm coefficients using remote sensing reflectance rations of 443 nm : 555 nm and 490 nm : 555 nm respectively.

Table 5.1 Regression coefficients for chlorophyll algorithms from Menai Strait and five cruises with all data collected between 2001 and 2002. The remote sensing reflectance (R_{rs}) ratio of 443 nm and 555 nm was used. b and $\log_{10} a$ are the gradient and the intercept from the regression respectively with standard errors (s.e.) in brackets. The coefficient of determination (R^2), probability (p), and number of stations (n) are also given.

(Rrs 443 nm : Rrs 555 nm)						
Cruises	Periods	b (s.e.)	$\log_{10} a$ (s.e.)	R^2	p	n
Menai Strait	25/05/01-21/10/02	-0.898 (0.755)	0.022 (0.306)	0.086	0.253	17
Clyde Sea	23/04-27/04/01	-1.610 (0.244)	0.189 (0.107)	0.731	0.000	18
Irish Sea	06/08-10/08/01	-0.515 (0.323)	0.081 (0.097)	0.113	0.126	22
Irish Sea	26/11-30/11/01	-1.630 (0.250)	-0.479 (0.092)	0.668	0.000	23
Irish Sea	02/04-05/04/02	0.833 (0.228)	-0.018 (0.034)	0.471	0.002	17
Celtic Sea	13/07-20/0702	-1.790 (0.171)	-0.190 (0.028)	0.774	0.000	34
All	25/05/01-20/07/02	-1.150 (0.126)	-0.041 (0.039)	0.387	0.000	131

Table 5.2 Regression coefficients for chlorophyll algorithms from Menai Strait and five cruises with all data collected between 2001 and 2002. The remote sensing reflectance (R_{rs}) ratio of 490 nm and 555 nm was used. b and $\log_{10} a$ are the gradient and the intercept from the regression respectively with standard errors (s.e.) in brackets. The coefficient of determination (R^2), probability (p), and number of stations (n) are also given.

(Rrs 490 nm : Rrs 555 nm)						
Cruises	Periods	b (s.e.)	$\log_{10} a$ (s.e.)	R^2	p	n
Menai Strait	25/05/01-21/10/02	-1.712 (1.141)	0.128 (0.180)	0.131	0.154	17
Clyde Sea	23/04-27/04/01	-1.937 (0.343)	0.546 (0.063)	0.666	0.000	18
Irish Sea	06/08-10/08/01	-1.051 (0.423)	0.186 (0.037)	0.236	0.022	22
Irish Sea	26/11-30/11/01	-2.093 (0.305)	-0.096 (0.034)	0.691	0.000	23
Irish Sea	02/04-05/04/02	2.181 (0.943)	-0.152 (0.088)	0.263	0.035	17
Celtic Sea	13/07-20/0702	-2.451 (0.227)	0.089 (0.029)	0.785	0.000	34
All	25/05/01-20/07/02	-2.354 (0.178)	0.125 (0.023)	0.568	0.000	131

PRR measurements used were taken at 0.5 m below the surface. Remote sensing reflectance developed in this section are compared with modeled remote sensing reflectance in section 5.4.

Figure 5.1 and 5.2 show the regression line plots between *in situ* chlorophyll measurements and remote sensing reflectance ratios between 443 nm : 555 nm and 490 nm : 555 nm for the Menai Strait and five cruises around the U.K. shelf seas. Regressions of all data are also presented (Figure 5.1g and 5.2g). In all cases the regressions gave corresponding relationships for both ratios. During the Clyde Sea

cruise in April 2001, the Irish Sea cruise in November 2001, and the Celtic Sea cruise in July 2002, R^2 values were higher than 0.666 for both ratios with significant relationships ($p<0.001$). However, the rest of sampling points at the Menai Strait, and the Irish Sea cruise in August 2001 and in April 2002 showed lower R^2 values. R^2 vales for all sampling stations (n = 131) were 0.387 and 0.568 for both reflectance ratios respectively. Algorithms using remote sensing reflectance rations of 443 nm : 555 nm and 490 nm : 555 nm for all dataset were expressed as;

$$\log C = -1.150 \log_{10}((R_{rs}(443) / R_{rs}(555)) - 0.041 \quad (5.3)$$

$$\log C = -2.354 \log_{10}((R_{rs}(490) / R_{rs}(555)) + 0.125 \quad (5.4)$$

where R_{rs} is remote sensing reflectance.

5.3 Phytoplankton group specific absorption spectra

Using HPLC measurements, the particulate absorption spectra of phytoplankton, $a_{ph}(\lambda)$, obtained from the Menai Strait and five cruises around the U.K. shelf seas were grouped according to the proportion of a marker pigment for diatom, fucoxanthin in the sum of all marker pigments, fucoxanthin, peridinin, 19'- hexanoloxyfucoxanthin and chlorophyll *b*. A marker pigment fucoxanthin was used to divide spectra into four groups, as it was a predominant pigment for many sampling points during studies, while other pigments dominate no more than 50 % of the concentration of all marker pigments. In addition, fucoxanthin was the most commonly found marker pigment during studies as diatom was found all sampling stations. The proportions of fucoxanxanthin in the

sum of pigments were ranged between 23 % and 39 %; 40 % and 59 %; 60 % and 79 %, and over 80 %. Absorption spectra used were taken at the surface as the spectral shape of phytoplankton is usually lost at depth. At depth phytoplankton pigment concentrations and light levels are reduced, and the optical properties are influenced by pure water absorption.

Regressing the particulate spectra of phytoplankton, $a_{ph}(\lambda)$, against chlorophyll *a* concentration, a chlorophyll specific absorption spectra, $a_{ph}^{*}(\lambda)$, was derived (Morel and Bricaud, 1981; Bricaud *et al.*, 1983). The group of chlorophyll specific absorption spectra, $a_{ph}^{*}(\lambda)$, divided into four groups according to the proportion of fucoxanthin in the sum of all marker pigments, are presented in Figure 5.3a-d. Table 5.3 shows the classified phytoplankton group specific absorption coefficient, $a_{ph}^{*}(\lambda)$ at 443 nm and 490 nm, and the ratios $a_{ph}^{*}(443) : a_{ph}^{*}(555)$ and $a_{ph}^{*}(490) : a_{ph}^{*}(555)$.

Table 5.3 Chlorophyll *a* specific absorption spectra, $a_{ph}^{*}(\lambda)$ with standard errors (s.e.) in brackets. The ratios of specific absorption spectra $a_{ph}^{*}(443) : a_{ph}^{*}(555)$ and $a_{ph}^{*}(490) : a_{ph}^{*}(555)$ are presented with number of spectra (n). Groups of specific absorption spectra were classified according to the proportion of fucoxanthin in the sum of pigments, fucoxanthin, peridinin, 19'- hexanoloxyfucoxanthin and chlorophyll *b*, ranged between 23 % and 39 %; 40 % and 59 %; 60 % and 79 %, and over 80 %.

Proportion of fucoxanthin	$a_{ph}^{*}(443)$ (s.e.)	$a_{ph}^{*}(490)$ (s.e.)	$a_{ph}^{*}(443) : a_{ph}^{*}(555)$	$a_{ph}^{*}(490) : a_{ph}^{*}(555)$	n
23 – 39 %	0.047 (0.004)	0.024 (0.007)	9.642	4.918	21
40 – 59 %	0.043 (0.007)	0.0253 (0.014)	6.746	4.016	51
60 – 79 %	0.036 (0.006)	0.0246 (0.008)	4.138	2.828	32
> 80 %	0.030 (0.005)	0.020 (0.004)	3.392	2.255	31

All specific absorption spectra showed a typical shape, with maxima observed in the blue (around 440 nm) and red (around 670 nm) regions. The chlorophyll specific absorption coefficient, $a_{ph}^*(\lambda)$ at 443 nm, which corresponds to the maximum chlorophyll *a* absorption showed a smaller coefficient as the fucoxanthin concentration in the sum of all pigments had a bigger proportion (Table 5.3). $a_{ph}^*(\lambda)$ at 443 nm decreased from 0.047 m^2 mg^{-1} Chl *a* to 0.030 m^2 mg^{-1} Chl *a*, while the proportion of fucoxanthin in the sum of all pigments increased from 23-39 % to over 80 %. A similar pattern was found $a_{ph}^*(\lambda)$ at 490 nm. As a result, the chlorophyll specific absorption coefficient ratios $a_{ph}^*(443) : a_{ph}^*(555)$ and $a_{ph}^*(490) : a_{ph}^*(555)$ also had the smallest values (3.392 and 2.255, respectively) while the proportion of fucoxanthin was the biggest (>80%).

The small proportion of fucoxanthin means that there is a small number of diatoms in the phytoplankton population (Figure 5.3a). In other words, a number of flagellate groups including cryptophytes, prymnesiophytes and chlorophytes were present. There were small peaks around 480 nm and 545 nm in Figure 5.3a. These peaks might be the evidence of the presence of accessory pigments alloxanthin and phycoerythrin respectively, as both pigments are commonly found in cryptophytes (Gieskes and Kraay, 1983; Kirk, 1994)

The chlorophyll specific absorption spectra for the proportion of fucoxanthin ranged between 40% to 59% (Figure 5.3b), and between 60 % to 79% (Figure 5.4c) showed a shoulder between 470 nm and 490 nm, which may result from the pigment peridinin, which represents dinoflagellates. This shoulder is also found in Figure 5.3d. Figure 5.3d shows the specific absorption spectrum for the proportion of fucoxanthin over 80 %. The predominant group of phytoplankton in this spectrum was the diatoms.

As fucoxanthin produces a shoulder in the absorption spectrum at 460 to 470 nm, the group specific absorption spectra in Figures 5.3c and 5.3d might be enhanced signals in this area. In Figure 5.3d apart from the maximum absorption peak at 443 nm, there was a second peak at 410 nm. This peak may be the result of the presence of dinoflagellates and protozoa, which graze and succeed the diatom bloom. The grazing activity causes a phaeopigment peak at this wavelength. The grazing and sinking result in the decline of the spring diatom bloom (Mills *et al.*, 1994).

5.4 Comparison of modelled and *in situ* remote sensing reflectance

Using the chlorophyll specific absorption spectra, $a_{ph}^{*}(\lambda)$, the remote sensing reflectance, $R_{rs}(\lambda)$ was modelled. Equations 5.4 to 5.8 define all the parameters required for the calculation. A model developed by Gordon *et al.* (1988), and Garver and Siegel (1997) for the waters where the optical properties are dominated by the presence of phytoplankton is used to define the relationship between, $R_{rs}(\lambda)$, and absorption, $a(\lambda)$, and backscattering, $b_b(\lambda)$;

$$R_{rs}(\lambda) = L_u(\lambda) / E_d(\lambda) \cong \sum_{i=1}^{2} l_i [\, b_b(\lambda) / (b_b(\lambda) + a(\lambda))]^i \qquad (5.3)$$

where $L_u(\lambda)$ and $E_d(\lambda)$ are the upwelling radiance and the downwelling irradiance respectively. l_1 is 0.0945 steradian^{-1}, and l_2 is 0.0794 steradian^{-1} (Gordon *et al.*, 1988). Absorption coefficient, $a(\lambda)$ and backscattering coefficient, $b_b(\lambda)$ are expressed as follow;

$$a(\lambda) = a_w(\lambda) + a_{ph}(\lambda) \tag{5.4}$$

$$b_b(\lambda) = b_{bw}(\lambda) + b_{bph}(\lambda) \tag{5.5}$$

where $a_w(\lambda)$ and $a_{ph}(\lambda)$ are the absorption coefficients for pure seawater and phytoplankton respectively. $b_{bw}(\lambda)$ and $b_{bph}(\lambda)$ are the backscattering coefficients for pure sea water and phytoplankton respectively. The spectral values of absorption and scattering coefficients of pure sea water, $a_w(\lambda)$ and $b_w(\lambda)$, were measure by Morel (1974); Morel and Prieur (1977); Smith and Baker (1981), and Pope and Fry (1997). Absorption coefficients of pure sea water, $a_w(\lambda)$, were adopted from Pope and Fry (1997), while scattering coefficients of pure sea water, $b_w(\lambda)$ values, were adopted from Morel and Prieur (1977). The specific absorption coefficient of phytoplankton, $a_{ph}^*(\lambda)$, was determined from the following relation;

$$a_{ph}(\lambda) = a_{ph}^*(\lambda) \times \text{Chl } a \tag{5.6}$$

where Chl *a* is the Chlorophyll *a* concentration.

The backscattering coefficient $b_b(\lambda)$ is defined as follow;

$$b_b(\lambda) = 0.5b_w(\lambda) + (560 / \lambda)^{-1} (b_{bph}(\lambda)/b_{ph}(\lambda))b_{ph}(\lambda) \tag{5.7}$$

The phytoplankton backscattering ratio of $b_{bph}(\lambda)$ to $b_{ph}(\lambda)$, determined by Morel and Bricaud (1981) was 0.005. The scattering coefficient for phytoplankton, $b_{ph}(\lambda)$, is determined as function of chlorophyll *a* concentration and expressed;

$$b_{ph}(\lambda) = 0.3 \text{ Chl } a^{0.62} (560/\lambda)^n \tag{5.8}$$

At low chlorophyll *a* concentration (Chl *a* < 0.1 μg l^{-1}), n is -1. For higher concentrations, n is zero (Gordon *et al.*, 1988).

Figure 5.4 shows observed remote sensing reflectance ratio of $R_{rs}(490) : R_{rs}(555)$ from the Menai Strait and all cruises around the U.K. shelf seas. Modelled remote sensing reflectance ratio of $R_{rs}(490) : R_{rs}(555)$ are also shown on the plot based on the group specific absorption coefficients $a_{ph}^*(490)$ and $a_{ph}^*(555)$. The modelled and observed remote sensing data were classified according to the proportion of a marker pigment, fucoxanthin in the all marker pigments measured by HPLC. The proportion of fucoxanthin ranged between 23 % and 39 %; 40 % and 59 %; 60 % and 79 %, and over 80 % (Table 5.3).

The reflectance ratio, $R_{rs}(490) : R_{rs}(555)$, was used instead of $R_{rs}(443) : R_{rs}(555)$ as the waveband at 490 nm is better to cover absorption peaks of accessory pigments. In addition, $R_{rs}(\lambda)$ model values at low wavelengths including 443 nm can be altered due to the influence of CDOM in the absorption spectra. The wavelength at 490 nm and longer wavelengths have little or no effect of CDOM. The variability of chlorophyll specific absorption spectra, $a_{ph}^*(\lambda)$ divided into four groups due to the proportion of fucoxanthin should be differentiated on the plot using the ratio, $R_{rs}(490) : R_{rs}(555)$ (Figure 5.4). The classification of the ratio, $R_{rs}(490) : R_{rs}(555)$ was expressed as coloured lines for model and the shape of points for *in situ* data. The modelled and observed values showed an agreement where the chlorophyll *a* concentration value was over 0.6 in logarithmic scale (≈ 4 μg l^{-1}). Observed ratios of $R_{rs}(490) : R_{rs}(555)$ for the proportion of fucoxanthin between 60 % and 79 %, and over 80 % lay close to the modelled lines (green and blue) on this part of plot at high chlorophyll and low reflectance ratio. These observed data were mostly collected during the Clyde Sea

cruise in April 2001 when the large population of diatom was found. The rest of observed $R_{rs}(\lambda)$ ratios per Chl *a* were smaller than the modelled $R_{rs}(\lambda)$ ratios per Chl *a*. This may indicate the influence of SPM and CDOM, masking phytoplankton absorption signal. The model used in this study adopted absorption coefficient, $a(\lambda)$, which only included absorption coefficients for pure seawater $a_w(\lambda)$ and phytoplankton $a_{ph}(\lambda)$ because of the unavailability of absorption data for SPM and CDOM (Equation 5.4). The seasonal averages of Mineral Suspended Sediment (MSS) concentration at the surface of the Irish Sea as a whole over the period 1982 to 1988 were 5.39 mg l^{-1} in the winter and 2 mg l^{-1} in the summer (Bowers *et al.*, 1998). In other words, the absorption spectra of SPM and CDOM should be included to complete the absorption information, $a(\lambda)$ to derive more accurate modelled $R_{rs}(\lambda)$ ratios in the Irish Sea. Bowers *et al.*, (1996) modelled the blue-green reflectance ratio to predict chlorophyll concentration due to the range of MSS from 0 to 10 mg l^{-1}, which may cover most sampling points collected in the Irish Sea.

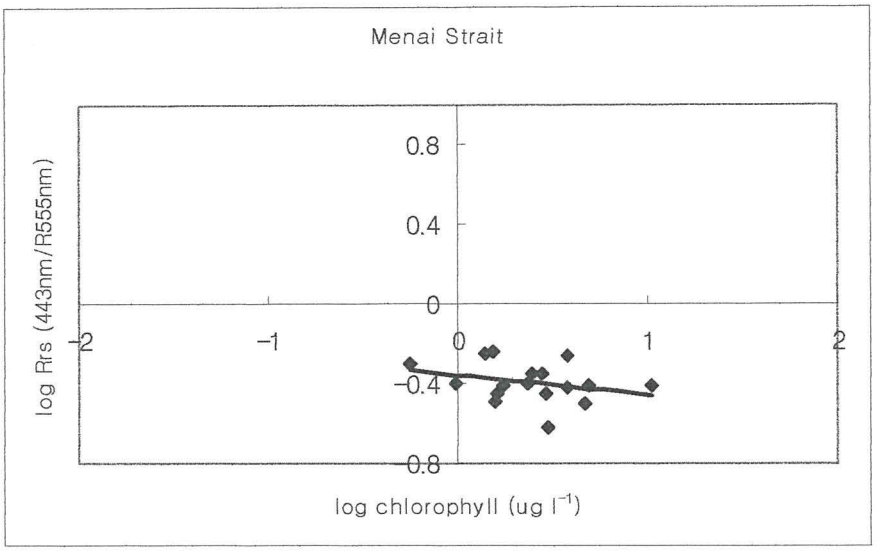

Figure 5.1a Regression of *in situ* chlorophyll measurement against remote sensing reflectance ratio between 443 nm and 555 nm in the Menai Strait from 25 May 01 to 21 October 02. Regression coefficient are given in Table 5.1

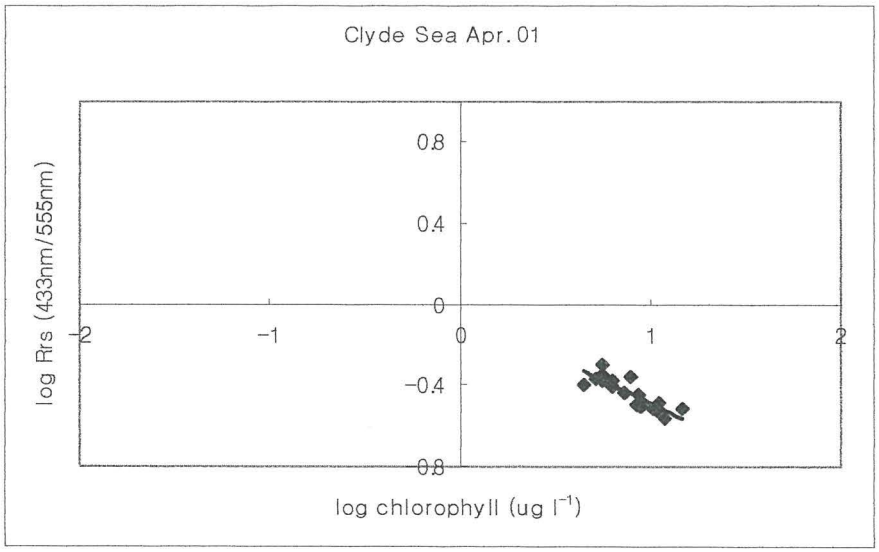

Figure 5.1b Regression of *in situ* chlorophyll measurement against remote sensing reflectance ratio between 443 nm and 555 nm during the Clyde Sea cruise in April 2001. Regression coefficient are given in Table 5.1

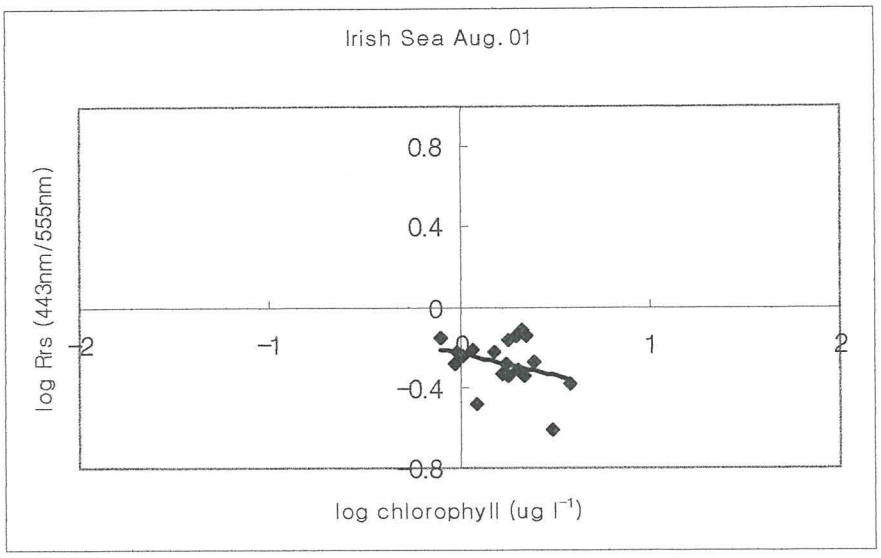

Figure 5.1c Regression of *in situ* chlorophyll measurement against remote sensing reflectance ratio between 443 nm and 555 nm during the Irish Sea cruise in August 2001. Regression coefficient are given in Table 5.1

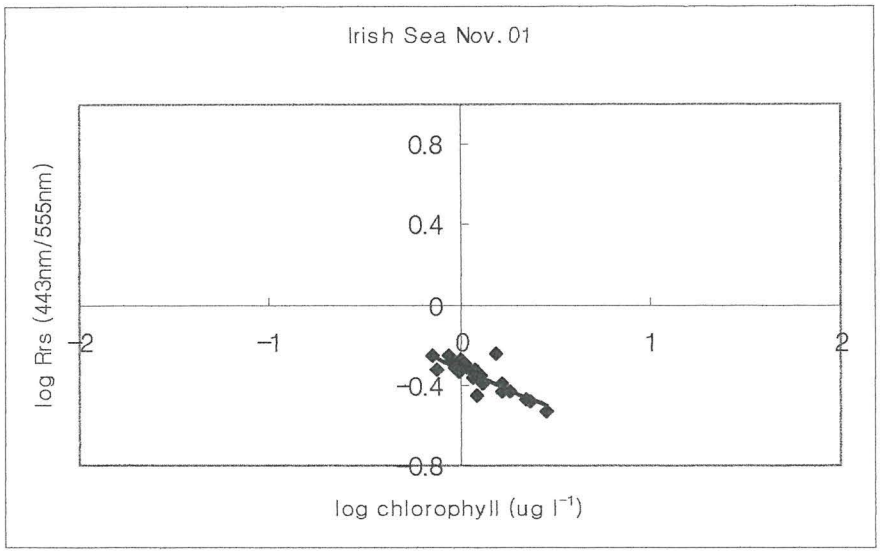

Figure 5.1d Regression of *in situ* chlorophyll measurement against remote sensing reflectance ratio between 443 nm and 555 nm during the Irish Sea cruise in November 2001. Regression coefficient are given in Table 5.1

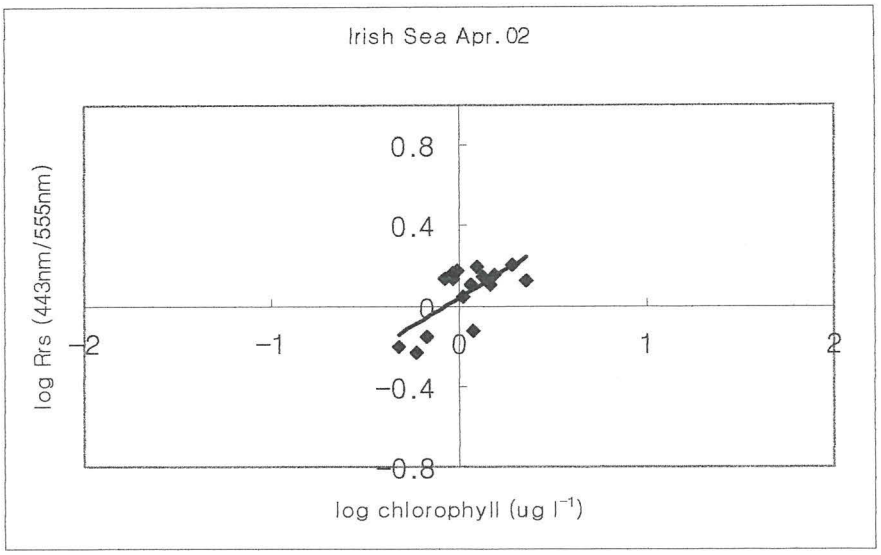

Figure 5.1e Regression of *in situ* chlorophyll measurement against remote sensing reflectance ratio between 443 nm and 555 nm during the Irish Sea cruise in April 2002. Regression coefficient are given in Table 5.1

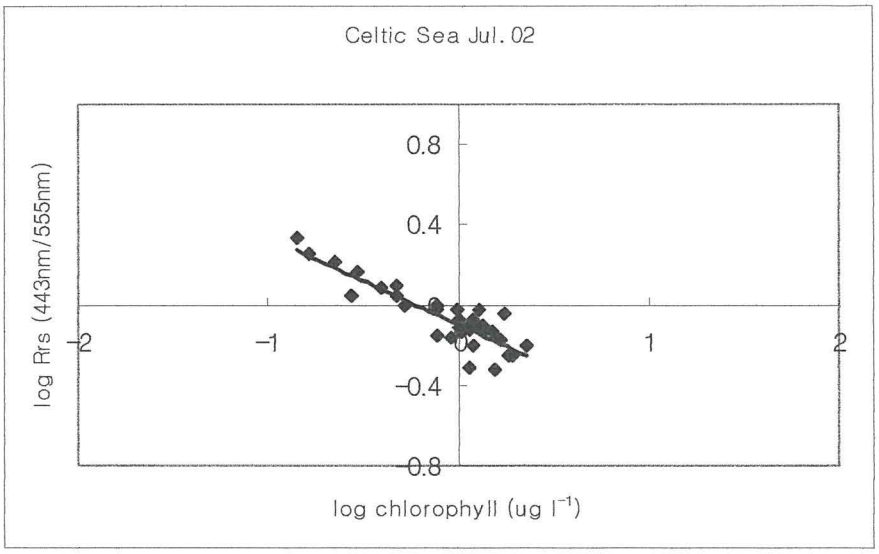

Figure 5.1f Regression of *in situ* chlorophyll measurement against remote sensing reflectance ratio between 443 nm and 555 nm during the Celtic Sea cruise in July 2002. Regression coefficient are given in Table 5.1

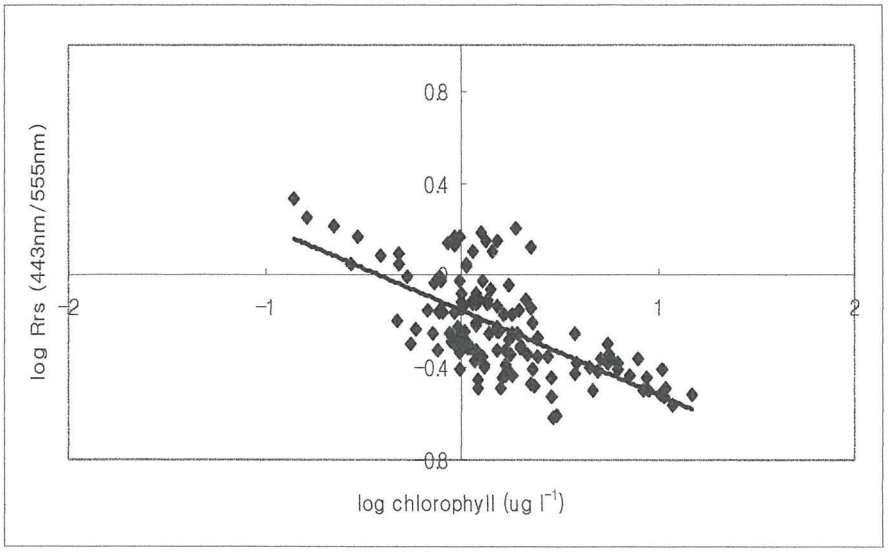

Figure 5.1g Regression of *in situ* chlorophyll measurement against remote sensing reflectance ratio between 443 nm and 555 nm in the Menai Strait and during five cruises around the U.K. shelf seas. Regression coefficient are given in Table 5.1

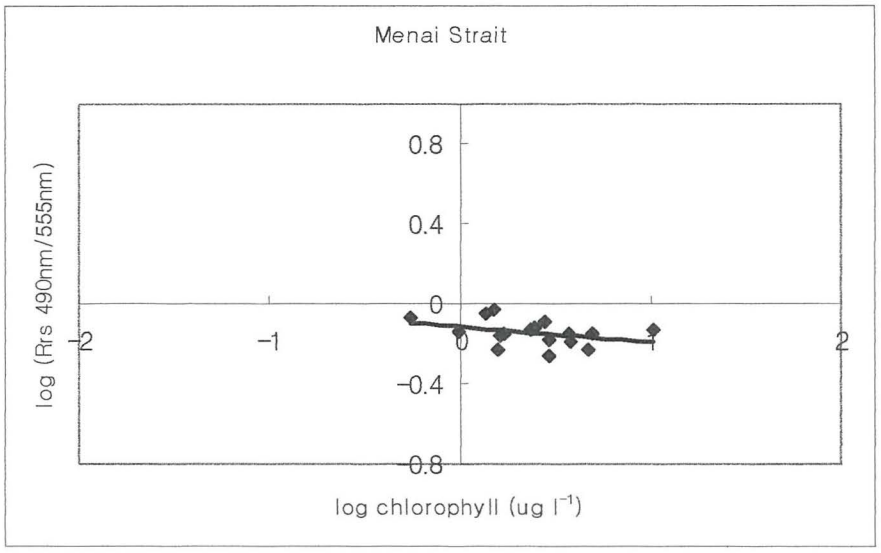

Figure 5.2a Regression of *in situ* chlorophyll measurement against remote sensing reflectance ratio between 490 nm and 555 nm in the Menai Strait from 25 May 01 to 21 October 02. Regression coefficient are given in Table 5.2

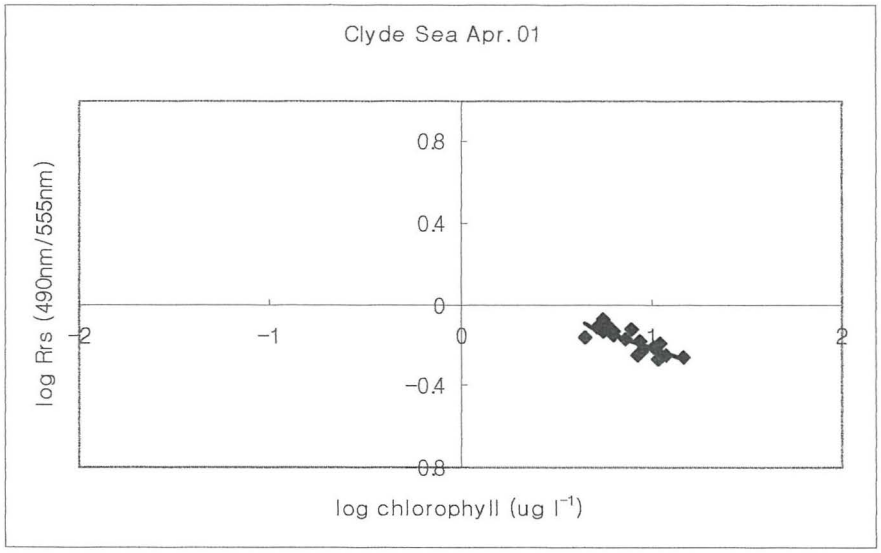

Figure 5.2b Regression of *in situ* chlorophyll measurement against remote sensing reflectance ratio between 490 nm and 555 nm during the Clyde Sea cruise in April 2001. Regression coefficient are given in Table 5.2

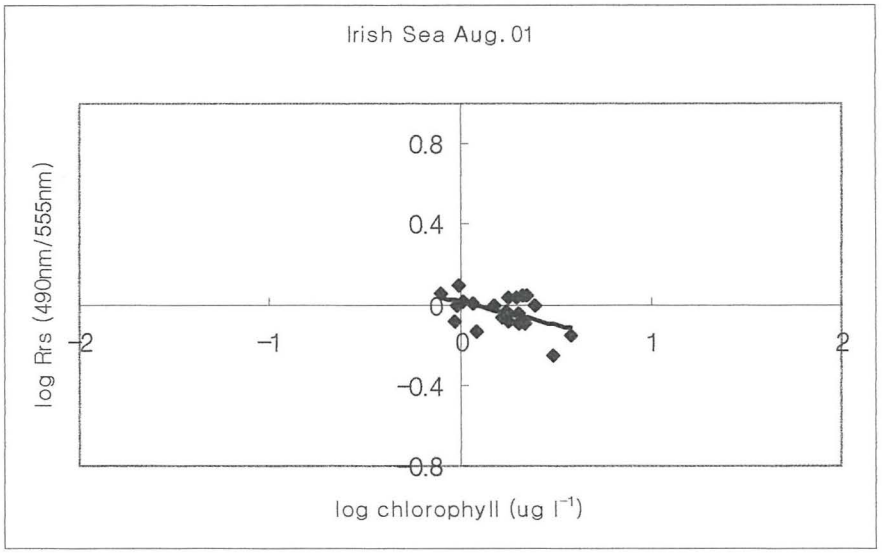

Figure 5.2c Regression of *in situ* chlorophyll measurement against remote sensing reflectance ratio between 490 nm and 555 nm during the Irish Sea cruise in August 2001. Regression coefficient are given in Table 5.2

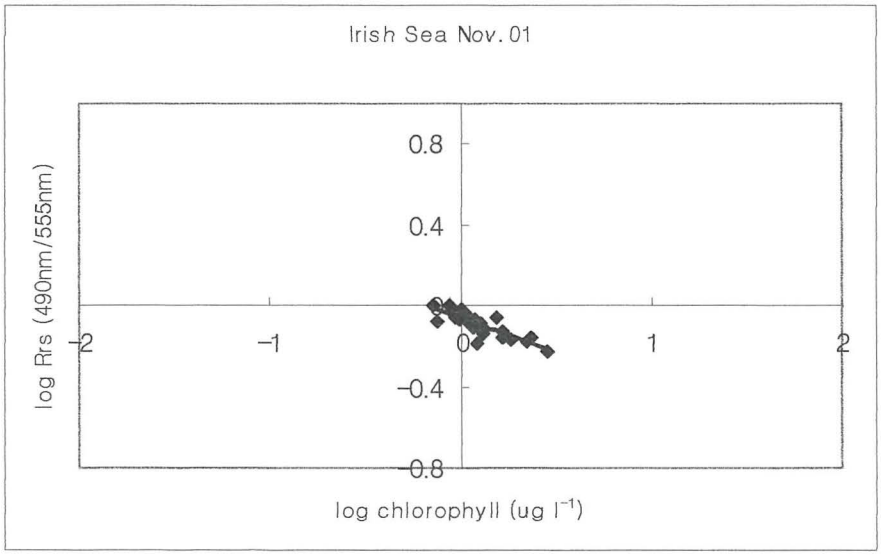

Figure 5.2d Regression of *in situ* chlorophyll measurement against remote sensing reflectance ratio between 490 nm and 555 nm during the Irish Sea cruise in November 2001. Regression coefficient are given in Table 5.2

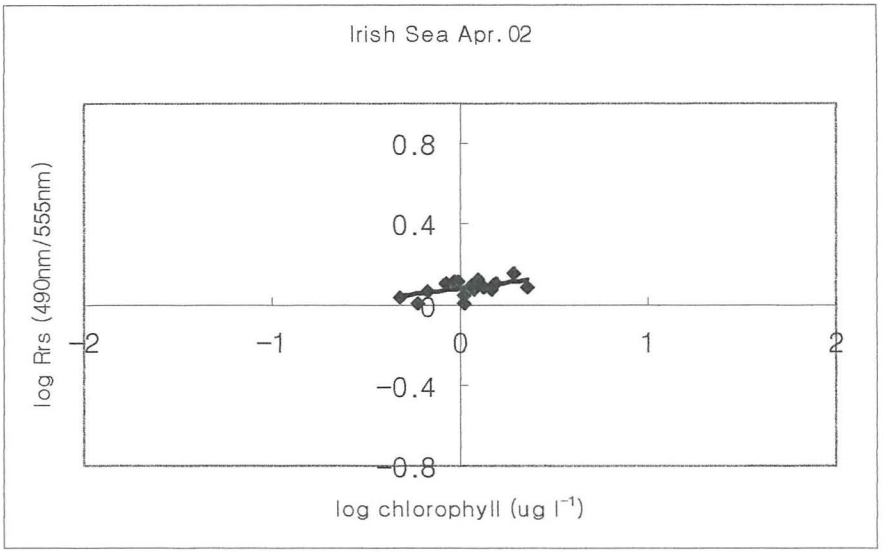

Figure 5.2e Regression of *in situ* chlorophyll measurement against remote sensing reflectance ratio between 490 nm and 555 nm during the Irish Sea cruise in April 2002. Regression coefficient are given in Table 5.2

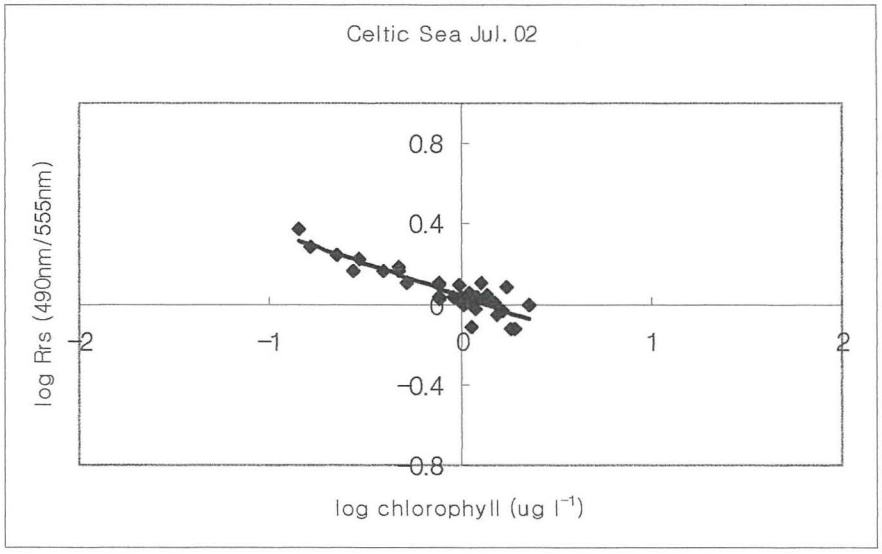

Figure 5.2f Regression of *in situ* chlorophyll measurement against remote sensing reflectance ratio between 490 nm and 555 nm during the Celtic Sea cruise in July 2002. Regression coefficient are given in Table 5.2

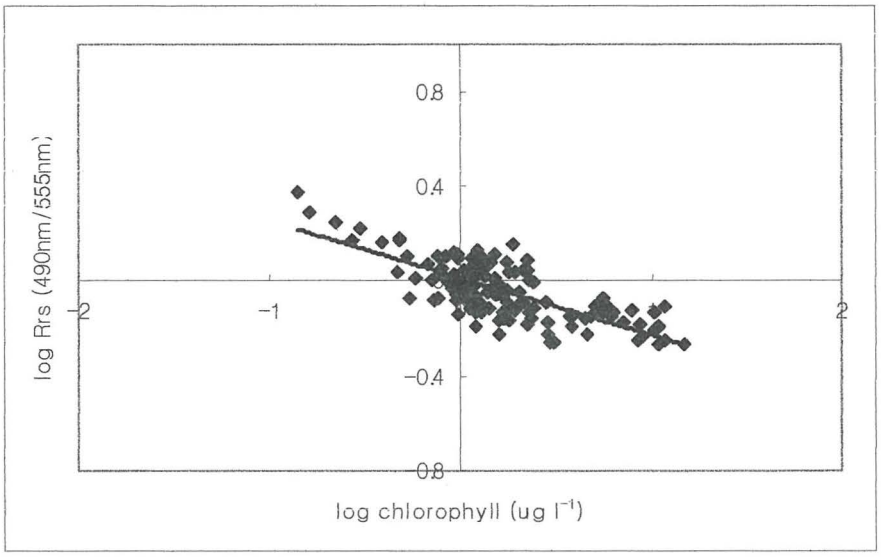

Figure 5.2g Regression of *in situ* chlorophyll measurement against remote sensing reflectance ratio between 490 nm and 555 nm in the Menai Strait and during five cruises around the U.K. shelf seas. Regression coefficient are given in Table 5.2

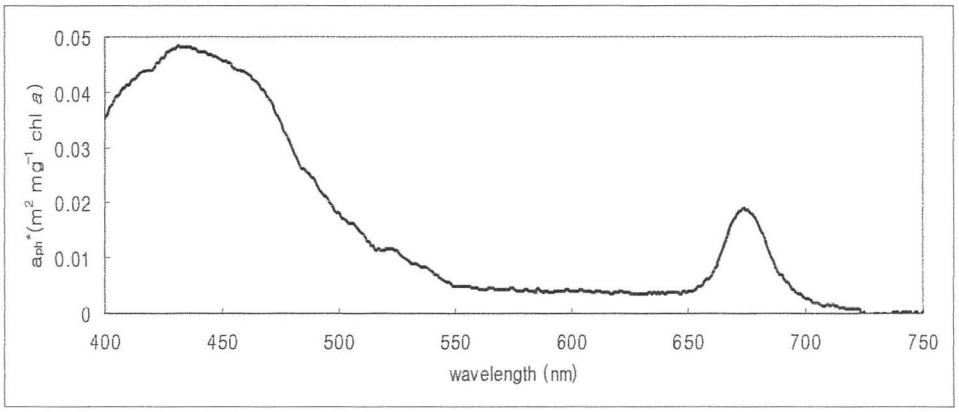

Figure 5.3a group specific absorption spectra of phytoplankton, $a_{ph}^*(\lambda)$, for the proportion of fucoxanthin ranged between 23 % and 39 % in the sum of pigments. The spectra ranged between 400 nm and 750 nm

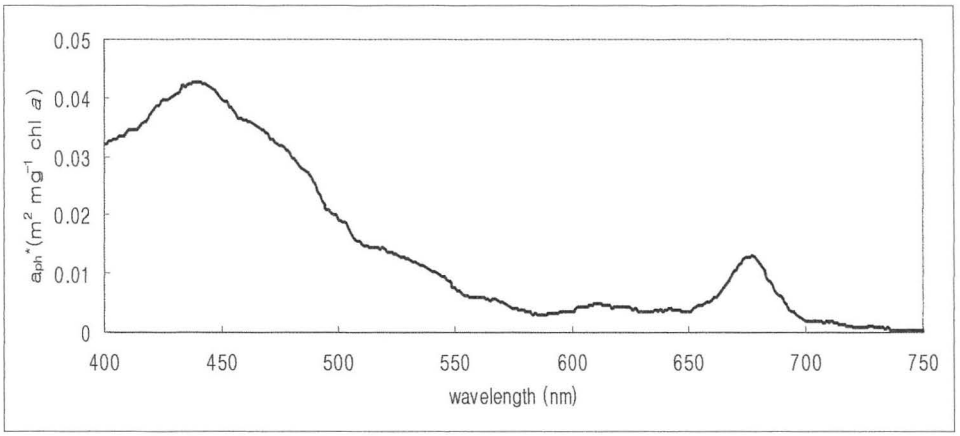

Figure 5.3b group specific absorption spectra of phytoplankton, $a_{ph}^*(\lambda)$, for the proportion of fucoxanthin ranged between 40 % and 59 % in the sum of pigments. The spectra ranged between 400 nm and 750 nm

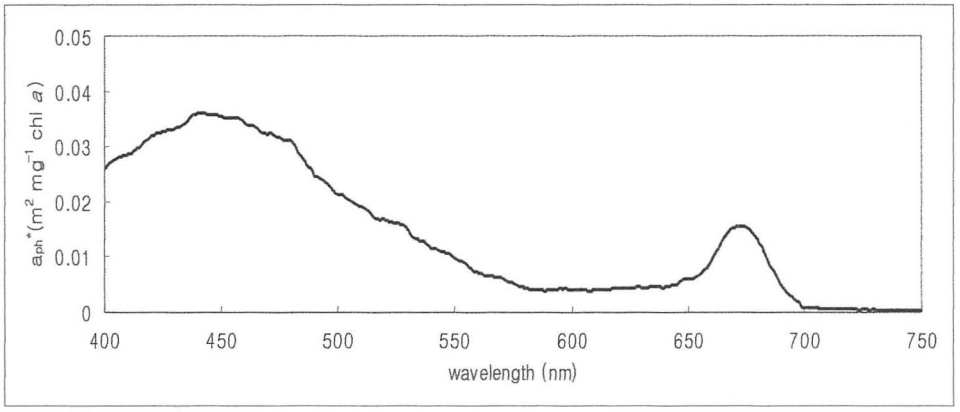

Figure 5.3c group specific absorption spectra of phytoplankton, $a_{ph}^*(\lambda)$, for the proportion of fucoxanthin ranged between 60 % and 79 % in the sum of pigments. The spectra ranged between 400 nm and 750 nm

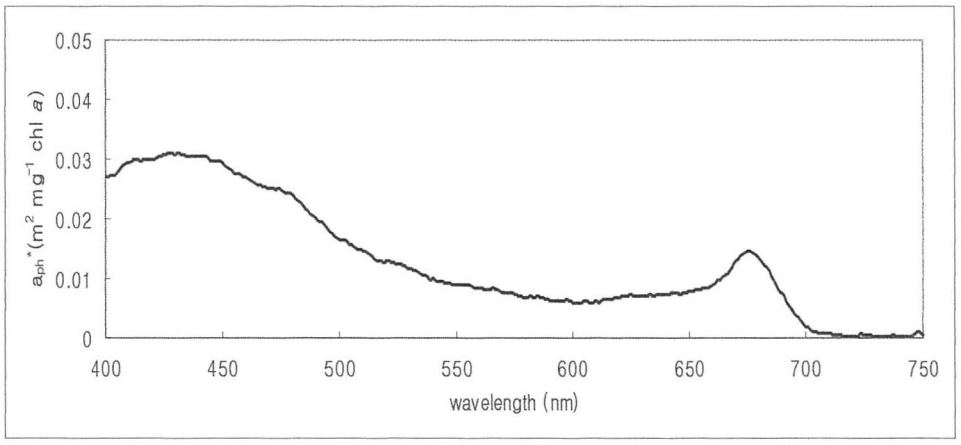

Figure 5.3d group specific absorption spectra of phytoplankton, $a_{ph}^*(\lambda)$, for the proportion of fucoxanthin over 80 % in the sum of pigments. The spectra ranged between 400 nm and 750 nm

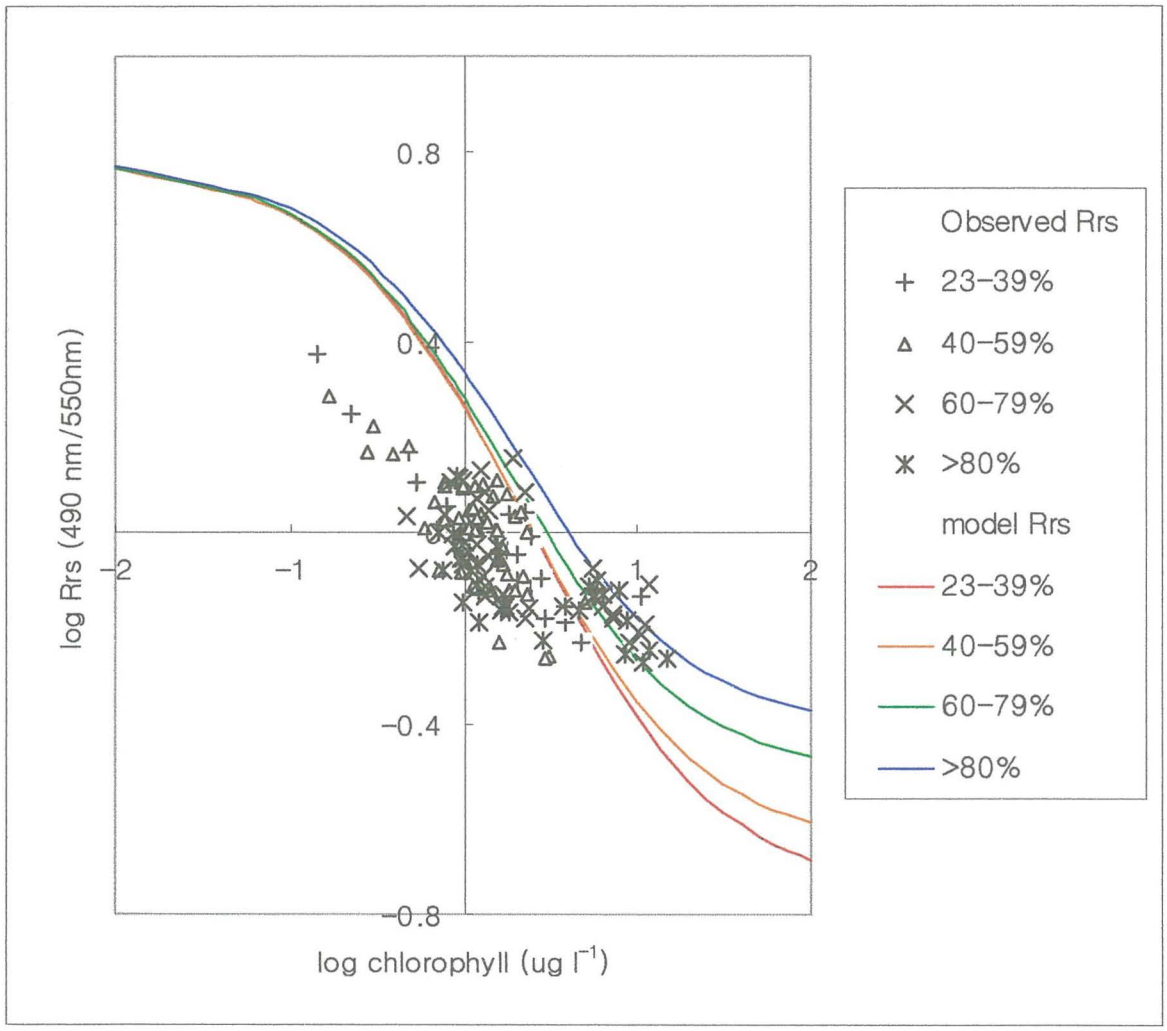

Figure 5.4 *In situ* and modelled remote sensing reflectance ratio of R_{rs}(490) : R_{rs}(555) against chlorophyll *a*. The modelled and observed remote sensing data were classified according to the proportion of a marker pigment, fucoxanthin in the sum of pigments, fucoxanthin, peridinin, 19'-hexanoloxyfucoxanthin and chlorophyll *b*. Classification ranges between 23 % and 39 %, 40 % and 59 %, 60 % and 79 %, and over 80 %

6. DISCUSSION AND CONCLUSIONS

6.1 Introduction

This chapter presents a general discussion of the comparison between phytoplankton taxonomic data and HPLC results. The relationship between phytoplankton group absorption spectra and modelled remote sensing reflectance spectra are reviewed. Finally, the main conclusions are summarised.

6.2 Phytoplankton taxonomic data and HPLC results

Phytoplankton samples collected in the Menai Strait during the study showed a seasonal variation. The diatom population was found all through the year 2001 and 2002. The fast growing small sized diatoms such as *Thalassiosira* species and *Skeletonema costatum*, which dominated the early spring bloom were replaced by medium sized and slow growing diatoms such as *Rhizosolenia* species and *Fragilaria oceanica* in the early summer. One of the prymnesiophytes, *Phaeocystis pouchetti*, succeeded the spring diatom bloom after depletion of silicate, and formed the largest bloom in the early summer in 2001 and 2002. Dinoflagellates became the dominant group of phytoplankton in September 2001 and August 2002 in Menai Strait. After the autumnal bloom the population decreased. Diatoms, *Coscinodiscus* and *Biddulphia* species, were dominant during the winter.

Diatoms, *Skeletonema costatum* and *Thalassiosira nordenskioldii*, were the predominant species at all stations during the Clyde Sea cruise in April 2001, while

Rhizosolenia species were the most commonly found diatoms during the Irish Sea cruise in August 2001. The phytoplankton population density reached over 1800 x 10^3 cells l^{-1} during the Clyde Sea cruise. Hannah and Boney (1983) observed the seasonal occurrence of the principal phytoplankton species between 1976 and 1978. They found that *Skeletonema costatum* was the most common species through the year and especially predominating phytoplankton population in late spring. During the August 2001 cruise dinoflagellates, *Ceratium* species and *Noctiluca scintillans*, were found at all sampling stations and *Gyrodinium aureolum* was found in the eastern Irish Sea. Raine and McMahon (1998) recorded the distribution of physical, chemical and biological characteristics for shelf waters off southwestern Ireland between 1992 and 1995. They found that dinoflagellates *Dinophysis acuminata* (125 x 10^3 cells l^{-1}) in July 1992 and *Gyrodinium aureolum* (up to 4300 x 10^3 cells l^{-1}) in August 1994 and 1995 were the most common species in the summer. *Gyrodinium aureolum* was found in the eastern Irish Sea during the August 2001 cruise with the cell densities of 20 –30 x 10^3 cells l^{-1}.

Diatoms, *Coscinodiscus* and *Biddulphia* species, were the major phytoplankton species found during the Irish Sea cruise in November 2001 where the sampling stations were located in Red Wharf Bay. During the Irish Sea cruise in April 2002, the commonly found phytoplankton at all sampling stations were diatoms, such as *Bacillaria paxillifer* and *Skeletonema costatum*. *Chaetoceros debilus* was one of the major diatoms in the Western Irish Sea, while *Thalassiosira decipiens* was the predominant phytoplankton species in Red Wharf Bay. Few dinoflagellates, such as *Ceratium* species, were also found during the Irish Sea cruise in April 2002. Rees *et al.* (1999) found the large numbers of *Nitzschia*, *Thalassionema* and *Chaetoceros* species at

the shelf edge region of the Celtic Sea in April and May 1994 with cell densities of 357 x 10^3 cells l^{-1}, 182 x 10^3 cells l^{-1} and 147 x 10^3 cells l^{-1} respectively.

Diatoms, *Nitzschia seriata* and *Rhizosolenia setigera*, dominated many sampling stations across the Celtic Sea front during the Celtic Sea cruise in July 2002. Dinoflagellates, *Ceratium* species and *Prorocentrum micans*, were also commonly found in the Celtic Sea during the study. The small number of flagellate cells, such as Chrysophytes (*Dictyocha speculum*, *Mallomonas* species) and prymnesiophytes (*Chrysochromulina species*), were found at most stations. Joint *et al.* (2001) found that most phytoplankton biomass was small unidentified flagellates with a diverse assemblage of dinoflagellates at cell densities of 100-200 cells l^{-1} in July 1993 in the Celtic Sea; the species included *Ceratium furca*, *Ceratium fusus*, *Ceratium lineatum*, *Gonyaulax polygramma*, and *Prorocentrum dentatum*. Joint *et al.* (2001) pointed out that diatoms, *Nitzschia seriata* and *Nitzschia delicatissima*, were the commonly found species through the year. The cell densities of these species closely agreed with those found in this study (around 100 x 10^3 cells l^{-1} to 300 x 10^3 cells l^{-1}). Phytoplankton samples collected by Pemberton *et al.* (2004) in the Celtic Sea in late May 2000 showed that diatom *Guinardia delicatula* and dinoflagellate *Gyrodinium spirale* were the most abundant phytoplankton species.

The slope of the regression of chlorophyll *a* concentration measured by the fluorometric method against the chlorophyll a concentration measured by HPLC showed generally good agreement. The chlorophyll *a* measurement by fluorometric method overestimated the values compared to the HPLC during the Irish Sea cruises in August 2001 and April 2002. The chlorophyll *a* samples taken at the Menai Strait were also overestimated by about 7 % by fluorometer compared to the HPLC. However, the

fluorometric measurement underestimated the chlorophyll *a* concentration during the Irish Sea cruise in November 2001 and the Celtic Sea cruise in July 2002. The all data from the Menai Strait and each cruise showed chlorophyll *a* measurement by HPLC averaging about 93 % of fluorometric method.

The conventional methods (fluorometry and spectrophotometry) to measure chlorophyll *a* use the wavelength at 665 nm where other green pigments such as chlorophyll *b* and *c*, chlorophyllides, allomers, and phaeopigments also absorb (Meyns *et al.*, 1994). As the HPLC separates individual pigments on the chromatography, other green pigments do not contribute to the chlorophyll *a* values. Therefore, the HPLC is regarded to be more accurate. Lower chlorophyll *a* measurements by HPLC have been reported by several authors (Mantoura and Llewellyn, 1983; Webb *et al.*, 1992; and Meyns *et al.*, 1994). Redden *et al.* (1993) found the fluorometric measurements of chlorophyll *a* in cultured *Thalassiosira weissflogii* were higher than HPLC measurements by an average of 9 % (91 % of fluorometric method). Gowen *et al.* (1983) estimated the proportion of chlorophyll *a*, chlorophyllide *a*, phaeophorbide *a* and phaeophytin *a* during the spring bloom of 1979 in two fjordic sea-lochs on the west coast of Scotland. The proportion of chlorophyllide *a* and phaeophorbide *a* were up to 30 % and 15 % of total pigment respectively at the beginning of bloom. They concluded that standard methods for measurement of 'chlorophyll' which do not distinguish between chlorophyll *a* and chlorophyllide *a* might significantly overestimate the photosynthetic potential of phytoplankton.

Meyns *et al.* (1994) found that HPLC yielded chlorophyll *a* values which were 36 to 75 % of the spectrophotometrically determined concentrations in Greifensee, a small eutrophic lake near Zürich, Switzerland. They pointed out that the large

discrepancies between spectrophotometer and HPLC results of chlorophyll *a* in Greifensee were due to the presence of allomers, which are believed to be closely related to the composition and senescence of algae, and the presence of humic substances, which absorb light at a range of 400 to 700 nm. However, there were no significant influences between samples with and without addition of humic acids neither by spectrophotometry nor by HPLC (Meyns *et al.*, 1994). They recommended that if exact information on chlorophyll *a* amount is required (e.g. for calculation of energy balances), HPLC is the only available method.

Pinckney *et al.* (1994) assessed the accuracy of spectrophotometry and fluorometry over HPLC. The spectrophotometric method overestimated the chlorophyll *a* concentration by 16% but the relationship between spectrophotometry and HPLC values was constant. The fluorometric method underestimated chlorophyll *a* concentrations by 3% and the relationship to HPLC determined values was also constant. The relationship between spectrophotometry and fluorometry was linear across a wide range of naturally occurring concentrations. They concluded spectrophotometry and fluorometry are suitable for showing relative differences in chlorophyll *a* concentrations, but should be corrected when absolute concentrations are important.

The presence of dominant groups of phytoplankton were determined using the marker pigments; these were peridinin (dinoflagellates), fucoxanthin (diatoms), 19' – hexanoyloxyfucoxanthin (prymnesiophytes) and chlorophyll *b* (green flagellates). Phytoplankton group division was simplified to diatoms, dinoflagellates and the rest of phytoplankton groups, classified as flagellates. The flagellate groups, which include cryptophytes, prymnesiophytes, green flagellates and so on, rarely represented a

significant proportion of the phytoplankton population during the study (below 20 % of the all population in most cases). As marker pigments for flagellates used in the study were 19' – hexanoyloxyfucoxanthin and chlorophyll *b* only, if there was the presence of flagellates other than prymnesiophytes and green flagellates, the determination of flagellate proportion using HPLC might underestimate its presence. As a result, the comparison between taxonomic cell identification data and HPLC pigment measurements showed a lesser agreement during the Irish Sea cruise in August 2001, the Irish Sea cruise in April 2002, and the Celtic Sea cruise in July 2002, when there was a mixed population of diatoms and dinoflagellates with few flagellates. In the summer, the mixed population contains a number of different accessory pigments, but occurs with a lower pigment concentration. During the Clyde Sea cruise in April 2001 and the Irish Sea cruise in November 2001, diatoms predominated the phytoplankton population, and the relationship between taxonomic data and HPLC measurements showed a better agreement.

The presence of few species, such as *Phaeocystis pouchetti* (prymnesiophyte) and *Gyrodinium aureolum* (dinoflagellate), may alter the estimation of marker pigment concentration to determine the phytoplankton population, as these species contain more than one marker pigment. After the spring diatom bloom, flagellates found in the Menai Strait were predominantly the prymnesiophyte, *Phaeocystis pouchetti*. The presence of this species may cause an over-estimation of the concentration of fucoxanthin as it contains both marker pigments, fucoxanthin and 19' – hexanoyloxyfucoxanthin. As a result, the estimation of diatom population using HPLC during the study was exaggerated. During the Irish Sea cruise in August 2001 and the Celtic Sea cruise in July 2002, *Gyrodinium aureolum* was found at many sampling stations. The

dinoflagellate, *Gyrodinium aureolum* contributed fucoxanthin rather than a marker pigment for dinoflagellate, peridinin. As a result, there were an over-estimation of diatom and under-estimation of dinoflagellate. However, the relationship between HPLC data and cell identification data showed generally good agreement.

6.3 Colour ratio algorithm, absorption and modelled remote sensing reflectance

The Gordon-Morel algorithm (Gordon and Morel, 1983) to derive chlorophyll biomass was used for all the sampling data. The coefficients derived here for this algorithm in the equation 5.1 were $a = 0.91$, $b = -1.15$ if the wavebands used were 443 nm and 555 nm. The coefficients a and b for the waveband ratio between 490 nm and 555 nm were 1.33 and –2.35 respectively. Bowers *et al.* (2001) developed the colour ratio algorithm for the samples collected at three diverse sites; a sea loch, the west Scottish shelf and the north Atlantic with *in situ* chlorophyll *a* concentration ranging from 0.01 to 50 $\mu g\ l^{-1}$. The log-log relation between the ratio of irradiance reflectance at 490 nm and 570 nm induced the coefficients $a = 1.87$ and $b = -1.81$. These coefficients are not greatly different from the coefficients developed by Gordon and Morel (1983) ($a = 1.71$ and $b = -1.82$). Many samples taken in this study, especially in the Clyde Sea and the Menai Strait with many sampling points in the Irish Sea, were regarded to have an influence of SPM and CDOM (case 2) (Mitchelson *et al.*, 1986), while the coefficients developed by Bowers *et al.* (2001) confirmed the effectiveness of estimation for chlorophyll concentrations in case 1 water with a minimum of calibration information.

The coefficients derived by Darecki *et al.* (2003) in case 2 water off the west coast of Ireland, using the remote sensing reflectance ratio between 490 nm and 550 nm,

showed no great differences with the coefficients derived in this study. These were a = 1.55 and b = -2.51 while the range of chlorophyll a concentration was from 0.6 to 3.23 $\mu g\ l^{-1}$. in April 1998. The coefficients in August 1998 were a = 1.32 and b = -2.95 while the concentration of chlorophyll a reached 14 $\mu g\ l^{-1}$. Mitchelson *et al.* (1986) collected samples in the Irish Sea (case 2 waters) and for comparison, in case 1 waters off the west coast of Scotland, and off the Isle of Ushant, Brittany. They generated the regression coefficients using the colour ration of upwelling irradiance between 440 nm and 550 nm for case 1 and case 2 waters. The coefficients a and b for case 1 waters were 0.78 and –2.254 respectively, and for case 2 waters were 0.45 and –3.921 respectively, which were lower than the coefficients derived in this study. Kratzer (2000) generated the regression algorithm between the concentration of chlorophyll a and upwelling irradiance ratio at 490 nm and 570 nm for case 1 waters. The samples were collected in the south west of Gran Canaria, Loch Striven in west Scottland and the Menai Strait with the cruises on the Malin Shelf, in the Irish Sea and the North Sea. The regression coefficients derived by Kratzer (2000) were a = 0.74 and b = -0.51. Kratzer (2000) and Kratzer *et al.* (2000) used log-log regression with the upwelling irradiance ratio between 670 nm and 550 nm to estimate the concentration of total suspended solids (TSS), mineral suspended solids (MSS), organic suspended solids (OSS) and Chlorophyll a. The red:green ratio gave good results for TSS and MSS but poor result for OSS and chlorophyll a.

A marker pigment fucoxanthin was used to divide absorption spectra into four groups, as it was a predominant pigment found for many sampling points during these studies. Fucoxanthin was the most commonly found marker pigment during studies as diatoms were found all sampling stations. The proportions of fucoxanxanthin in the sum

of all marker pigments, fucoxanthin, peridinin, 19'- hexanoloxyfucoxanthin and chlorophyll *b* ranged between 23 % and 39 %; 40 % and 59 %; 60 % and 79 %, and over 80 %.

As the proportion of fucoxanthin in all pigments was bigger, the absorption coefficients and ratios $a_{ph}^*(443) : a_{ph}^*(555)$ and $a_{ph}^*(490) : a_{ph}^*(555)$ became smaller. The variability in the shape of absorption spectra was mostly found in the blue-green region between 440 nm and 550 nm, where accessory pigments have their maximum absorption. The group specific absorption spectra, which have over 60 % of fucoxanthin in proportion, were mostly dominated by diatoms and showed a shoulder peak around 460 nm, according to the presence of the diatom marker pigment, fucoxanthin. The group specific absorption spectra, which have under 60 % of fucoxanthin in proportion, had mixed phytoplankton population, therefore, containing a number of different accessory pigments. The presence of many accessory pigments tends to overlap the absorption spectra. In addition, the mixed phytoplankton population may cause a low pigment concentration, resulting in the influence of the accessory pigments on the absorption signal being reduced.

The model developed by Gordon *et al.* (1988) and Garver and Siegel (1997) for the waters where the optical properties are dominated by the presence of phytoplankton was used to define the relationship between remote sensing reflectance, $R_{rs}(\lambda)$, and absorption, $a(\lambda)$, and backscattering, $b_b(\lambda)$. The model for case 1 waters assumes b_b is less than 1 to 2 % of the scattering coefficient, b. In other words, the absorption coefficient, a, is bigger than b_b for the moderate pigment concentration. Remote sensing reflectance, R_{rs}, is mainly influenced by absorption coefficient, a, and is supported by insignificantly low values of algal backscatter, b_b, for case 1 waters (Ahn *et al.*, 1992).

The magnitude of the backscattering may be influenced by the particulate type and size. Particles of 1 μm diameter and smaller are the major source of backscattering in the ocean (Garver and Siegel, 1997).

The reflectance ratio, $R_{rs}(490) : R_{rs}(555)$, was used instead of $R_{rs}(443) : R_{rs}(555)$ for the comparison between modelled and *in situ* remote sensing reflectance as the remote sensing reflectance at low wavelengths including 443 nm may be enhanced due to the CDOM. Wavelength at 490 nm and longer have little or no effect of CDOM. In addition, the 490 nm waveband was chosen as it is positioned in the centre of the carotenoid absorption band, which includes the diatom and dinoflagellate marker pigments, fucoxanthin and peridinin. The variability of the reflectance signal dominated by phytoplankton pigment composition should be sensitive to this wavelength.

The observed and modelled remote sensing reflectance showed a good agreement when the high concentration of chlorophyll *a* was observed during the Clyde Sea cruise in April 2001 and from the Menai Strait in summer 2001 and 2002. During the Clyde Sea cruise, diatoms predominated the population. As a result, modelled lines for the proportion of fucoxanthin over 60 % closely fitted the observed sample points where the concentration of chlorophyll *a* were over 4 μg l^{-1}. Observed and modelled remote sensing reflectance ratio of $R_{rs}(490) : R_{rs}(555)$ at low chlorophyll *a* concentration did not agree well as models may have neglected the influence of SPM and CDOM. Future bio-optical models should include absorption due to CDOM and SPM.

It would be also possible to take characteristic values of CDOM and SPM for the area of study from earlier works and test whether including these in the calculations make any improvements to the modelled reflectance ratios compared to the *in situ*

reflectance ratio. The specific absorption coefficient of MSS can be obtained from measurements by Bowers *et al.* (1998) in the Irish Sea, and is of the form;

$$a^*_m = 0.0205 + 0.038\, e^{-0.0055\,(\lambda - 440)} \qquad (6.1)$$

In the case of CDOM, absorption is represented by measured absorption at 440 nm, g_{440}, multiplied by a shape function, $a^*_y(\lambda)$, to give absorption at other wavelengths. The specific absorption by CDOM can be calculated from

$$a^*_y = e^{(-0.018\,(\lambda - 440)} \qquad (6.2)$$

using the mean decay constant –0.018 nm^{-1} in the Clyde Sea (Bowers *et al.*, 2000). The specific absorption coefficients, a^*_m and a^*_y from Bowers *et al.* (1998) and Bowers *et al.* (2000) at the wavelengths of 490 nm and 555 nm are as follow; $a^*_m(490) = 0.049\ m^2g^{-1}$ and $a^*_m(555) = 0.041\ m^2g^{-1}$ in the Irish Sea; and $a^*_y(490) = 0.41$ and $a^*_y(555) = 0.13$ in the Clyde Sea. The specific absorption coefficients a^*_m and a^*_y in the Irish Sea at the wavelength of 440 nm and 550 can be obtained from Bowers and Mitchelson-Jacob (1996). These are 0.042 and 0.027 for a^*_m at 440 nm and 550 nm respectively; and 0.007 and 0.005 for a^*_y at 440 nm and 550 nm respectively. The specific absorption coefficients of CDOM and MSS for the Menai Strait were derived and evaluated by Kratzer (2000). a^*_m at 490 nm and 570 nm were 0.055 and 0.045 respectively, while a^*_y at 490 nm and 570 nm were 0.533 and 0.174 respectively. The reflectance ratio model should improve its performance in case 2 waters including these a^*_m and a^*_y values.

6.4 Conclusions

The aim of this study was to optically differentiate phytoplankton groups classified due to the proportion of a marker pigment, fucoxanthin in the sum of all marker pigments used in the study. Phytoplankton samples were collected in the Menai Strait from 2001 to 2002 and during five cruises in the Irish Sea and Celtic Sea. The major phytoplankton groups found during the study were organised as diatoms, dinoflagellates and flagellates. The flagellate groups included the rest of phytoplankton groups, such as cryptophytes, prymnesiophytes and green flagellates, which rarely represented a significant proportion of the phytoplankton population as a single class during the study. The phytoplankton group was identified using the visual microscopy. The HPLC measured the concentration of accessory pigments, which represent the presence of major phytoplankton groups as markers. These were peridinin (dinoflagellates), fucoxanthin (diatoms), 19' – hexanoyloxyfucoxanthin (prymnesiophytes) and chlorophyll *b* (green flagellates).

Optical data, the absorption spectra and *in situ* remote sensing reflectance, were collected. Using HPLC, the particulate absorption spectra were divided into four groups according to the proportion of a marker pigment for diatom, fucoxanthin in the sum of all marker pigments, fucoxanthin, peridinin, 19'- hexanoloxyfucoxanthin and chlorophyll *b*. The proportions of fucoxanthin in the sum of all pigments ranged between 23 % and 39 %; 40 % and 59 %; 60 % and 79 %, and over 80 %. Chlorophyll specific absorption spectra, which regressed the particulate spectra of phytoplankton against chlorophyll *a* concentration were derived. These were used to model the remote sensing reflectance ratios based on the group chlorophyll specific absorption spectra

classified due to the proportions of fucoxanthin in the sum of all pigments. The highest specific absorption spectra ratio, $a_{ph}^*(490) : a_{ph}^*(555)$ resulted in the lowest modelled remote sensing reflectance ratio, $R_{rs}(490) : R_{rs}(555)$. The remote sensing reflectance ratio, $R_{rs}(490) : R_{rs}(555)$, was chosen over $R_{rs}(443) : R_{rs}(555)$ as the waveband at 490 nm is positioned in the centre of the carotenoid absorption band, which includes the diatom and dinoflagellate marker pigments, fucoxanthin and peridinin. In addition, $R_{rs}(\lambda)$ values at low wavelengths, including 443 nm were found to be altered due to the influence of CDOM in the absorption spectra. The wavelength at 490 nm and longer wavelengths show little or no effect from CDOM.

The variability of chlorophyll specific absorption spectra, $a_{ph}^*(\lambda)$ divided into four groups due to the proportion of fucoxanthin were differentiated on the plot using the ratio, $R_{rs}(490) : R_{rs}(555)$. The modelled and observed values showed an agreement at high chlorophyll *a* concentration (over 4 $\mu g\ l^{-1}$) and low reflectance ratio where the area on the plot (Figure 5.4) reflected the proportion of fucoxanthin in the sum of all pigments over 60 %. In other words, model and *in situ* results have a better agreement if diatoms dominate. However the rest of observed $R_{rs}(\lambda)$ ratios per Chl *a* were smaller than the modelled $R_{rs}(\lambda)$ ratios per Chl *a*. This may indicate the influence of SPM and CDOM, masking phytoplankton absorption signal. Future bio-optical models should include absorption due to CDOM and SPM to complete the absorption information, $a(\lambda)$ to derive more accurate modelled $R_{rs}(\lambda)$ ratios.

REFERENCES

Ahn, Y.H., Bricaud, A. and Morel, A., (1992). Light backscattering efficiency and related properties of some phytoplankters. *Deep-Sea Research*, **39**, 1835-1855.

Barlow, R.G., Mantoura, R.F.C., Gough., M.A. and Fileman, T.W., (1993). Pigment signatures of the phytoplankton composition in the northeastern Atlantic during 1990 spring bloom. *Deep-Sea Research*, **40**, 459-477.

Bidigare, R.R., (1991). Analysis of algal chlorophylls and carotenoids. In: *Marine Particles: analysis and characterization*, Hurd, D.H. and Spencer, D.W. (eds.), American Geophysical Union, Washington DC, U.S.A., p. 119-123.

Bidigare, R.R., Ondrusek, M.E., Morrow, J.H. and Kiefer, D.A, (1990). *In vivo* absorption properties of algal pigments. In: *Ocean Optics X, proceedings SPIE International Society of Optical Engineering*, **1302**, 290-302.

Bidigare, R.R., Smith, R.C., Baker, K.S. and Marra, J., (1987). Oceanic primary production estimates from measurements of spectral irradiance and pigment concentrations. *Global Geochemical Cycles*, **1** 171-186.

Blight, S. P., (1996) Microbial metabolism and temperature: comparative studies in the Southern Ocean and a temperature coastal ecosystem. Ph.D. Thesis, University of Wales, Bangor.

Blough, N.V. and Del Vecchio, R., (2002). Chromophoric DOM in the coastal environment. In: *Biogeochemistry of marine dissolved organic matter*, Hansell, D.A. and Carlson, C.A. (eds.), Academic Press, U.S.A., 774pp.

Bold, H.C. and Wynne, M.J. (1985). *Introduction to the algae* (2nd ed.), Prentice-Hall, New Jersey.

Boney, A.D., (1989). *Phytoplankton* (2nd ed.), Edward Arnold, London, 107p.

Bowers, D.G., Harker, G.E.L. and Stephen, B., (1996). Absorption spectra of inorganic particles in the Irish Sea and their relevance to remote sensing of chlorophyll.

International Journal of Remote Sensing, **17**, 2449-2460.

Bowers, D.G., and Mitchelson-Jacob, E.G., (1996). Inherent optical properties of the Irish Sea determined from underwater irradiance measurements. *Estuarine, Coastal and Shelf Science*, **43**, 433-447.

Bowers, D.G., Boudjelas, S. and Harker, G.E.L., (1998). The distribution of fine suspended sediments in the Irish Sea and its dependence on tidal stirring. *International Journal of Remote Sensing*, **19**, 2789-2805.

Bowers, D.G., Harker, G.E.L., Smith, P.S.D. and Tett P., (2000). Optical properties of a region of freshwater influence (The Clyde Sea). *Estuarine Coastal and Shelf Science*, **50 (5)**, 717-726.

Bowers, D.G., Kratzer, S., Morrison, J.R., Smith, P.S.D. and Tett, P., Walne, A.W., Wild-Allen, K., (2001). On the calibration and use of *in situ* ocean colour measurements for monitoring algal blooms. *International Journal of Remote Sensing*, **22 (2-3)**, 359-368.

Boxall, S. R., Chaddock, S. E., Matthews, A. and Holden, N., (1993). Airborne remote sensing of coastal waters. NRA & Southampton University. *NRA Research and Development report No.4.* ISBN 1 973160 305.

Bricaud, A., Morel, A. and Prieur, L., (1981). Absorption by dissolved organic matter of the sea (yellow substance) in the UV and visible domains. *Limnology and Oceanography*, **26**, 43-53.

Bricaud, A., Morel, A. and Prieur, L., (1983). Optical efficiency factors of some phytoplankters. *Limnology and Oceanography*, **28**, 816-832.

Bricaud, A., Bedhomme, A. and Morel, A., (1988). Optical properties of diverse phytoplanktonic species: experimental results and theoretical interpretation. *Journal of Phytoplankton Research*, **10**, 851-873.

Chretiennot - Dinet, M. (1990). *Atlas du phytoplancton marin Vol. 3. Chlorarachniophycees, Chlorophycees, Chrysophycees, Cryptophycees, Euglenophycees, Eustigmatophycees, Prasinophycees, Prymnesiophycees,*

Rhodophycees, Tribophycees, Editions du CNRS, Paris

Cleveland, J.S. and Weidemann, A.D., (1993). Quantifying absorption by aquatic particles: a multiple scattering correction for glass-fiber filters. *Limnology and Oceanography*, **38**, 1321-1327.

Cullen, J.J., Ciotti, A.M., Davis, R.F. and Lewis, M.R., (1997). Optical detection and assessment of algal blooms. *Limnology and Oceanography*, **42**, 1223-1239.

Darecki, M., Weeks, A., Sagan, S. and Kowalczuk, P., Kaczmarek, S., (2003). Optical characteristic of two contrasting Case 2 waters and their influence on remote sensing algorithms. *Continental Shelf Research*, **23**, 237-250.

Edler, L., (1979). Recommendations for marine biological studies in the Baltic Sea: phytoplankton and chlorophyll. *The Baltic Marine Biologist Working Group*, Volume 5, University of Lund, Sweden, p 38.

Embleton, K., (2000). Phytoplankton Images. (on-line). Available from: http://192.171.163.165/pil/phytoplankton_images.htm (Accessed 14 May 2001).

Esaias, W., Abbot, M.R., Barton, I., Brown, O.B., Campbell, J.W., Carder, K.L., Clark, D.K., Evans, R.L., Hoge, F.E., Gordon, H.R., Balch, W.P., Letelier, R. and Minnett, P.J., (1998). Overview of MODIS Capabilities for Ocean Science Observations, *IEEE Transactions on Geoscience and Remote Sensing*, **36**, 1250-1265.

Everitt, D., Wright, S., Volkman, J. and Thomas, D., Lindstrom, E., (1990). Phytoplankton community compositions in the western equatorial pacific determined from chlorophyll and caratenoid pigments distributions. *Deep-Sea Research*, **37**, 975-997.

Fasham, M.J., Holligan P.M. and Pugh P.R., (1983). The spatial and temporal development of the spring phytoplankton bloom in the Celtic Sea, April 1979. *Progress in Oceanography*, **12**, 87-145.

Forrest, E. and Nell, E., (1994). Field testing two instruments for Remote Sensing Water Quality in the Tennessee Valley, *Environ. Sci. Technol.*, **28**,16-25.

Garver, S.A. and Siegel, D.A., (1997). Inherent optical property inversion of ocean color spectra and its biogeochemical interpretation. 1. Time series from the Sargasso Sea. *Journal of Geophysical Research*, **102**, 18607-18625.

Gieskes, W.W.C. and Kraay, G..W., (1983). Dominance of Cryptophyceae during the phytoplankton spring bloom in the central North Sea detected by HPLC analysis of pigments. *Marine Biology*, **75**, 179-185.

Gordon, H.R., Brown, O.B. and Jacobs, M.M., (1975). Computed relationships between the inherent and apparent optical properties of flat, homogeneous ocean. *Applied Optics*, **14**, 417-427.

Gordon, H.R., Clark, D.K., Brown, J.W., Brown, O.B., Evans, R.H. and Broenkow, W.W., (1983). Phytoplankton pigment concentrations in the Middle Atlantic Blight: Comparison of ship determinations and CZCS estimations. *Applied Optics*, **22**, 20-36.

Gordon, H.R. and Morel, A.Y., (1983). *Remote Assessment of Ocean Colour for Interpretation of Satellite Visible Imagery. A review*. Springer-Verlag, New York, U.S.A., 114p.

Gordon, H.R., Brown, O.T., Evans, R.H., Brown, J.W., Smith, R.C., Baker, K.S. and Clark, D.K., (1988). A semianalytic radiance model of ocean color. *Journal of Geophysical Research*, **93**, 10909-10924.

Gowen, R.J., Tett, P. and Wood, B.J.B., (1983) Changes in the major dihydroporphyrin plankton pigments during the spring bloom of phytoplankton in two Scottish sea-lochs, *Journal of the Marine Biological Association of the United Kingdom*, **63**, 27-36.

Gower, J. F. R., (1979). Observation of *In situ* Fluorescence of Chlorophyll *a* in Saanich Inlet, In: *Passive Radiometry of the Ocean*, Gower, J. F. R., (ed.), D. Reidel publishing company, London 235-245 p.

Gower, J. F. R. and Borstad, G. A., (1990). Mapping of phytoplankton by solar-stimulated fluorescence using an imaging spectrometer. *International Journal of Remote Sensing*, **11**,313-320.

Hallegraeff, G. M., (1993). A review of harmful algal blooms and their apparent global increase. *Phycologia* **32**, 79-99.

Hannah, F.J. and Boney, A.D., (1983). Nanophytoplankton in the Firth of Clyde, Scotland: seasonal abundance, carbon fixation and species composition. *Journal of experimental Marine Biology and Ecology*, **67**, 105-147.

Helm, M.M., Hepper, B.T., Spencer, B.E. and Waine, P.R., (!974). Lugworm mortalities and a bloom of *Gyrodinium aureolum* Hulburt in the eastern Irish Sea, Autumn 1971. *Journal of the Marine Biological Association of the United Kingdom*, **54**, 857-869.

Hoek, C.V., Mann, D.G., and Jahns, H.M., (1995). *Algae, an introduction to phycology*. Cambridge University press, Cambridge, U.K

Hooker, S,B., Esaias, W.E., Feldman, G.C, Gregg, W.W. and McClain, C.R., (1992). An overview of SeaWiFS and ocean colour, In: *NASA Technical Memorandum 104566*, **1**, Hooker, S.B. and Clark, D.K. (eds.), NASA Goddard Space Flight Center, Greenbelt, Maryland, 24 p.

Hooks, C.E., Bidigare, R.B., Keller, M.D. and Guillard, R.R.L., (1988). Coccoid eukaryotic marine ultraplankters with four different HPLC pigment signatures. *Journal of Phycology*, **24**, 571-580.

Jeffrey, S.W., Sielicki, M., and Haxo, F.T., (1975). Chloroplast pigment patterns in dinoflagellates. *Journal of Phycology*, **11**, 374-384.

Jeffery, S.W. and Vesk, M., (1997). Introduction to marine phytoplankton and their pigment signatures. In: *Phytoplankton pigments in oceanography: Guidelines to modern methods*, Jeffrey, S.W., Mantoura, R.F.C.and Wright, S.W., (eds.), UNESCO, Paris, 37-84.

Jerlov, N.G., (1976). Marine optics (2nd ed.), Elsevier Oceanography Series, Number 14, Elsevier, Amsterdam, The Netherlands, 231 p.

JGOFS, (1994). Protocols for the Joint Global Ocean Flux Studies (JGOFS) core measurements. *JCOFS Report Number 19*, Scientific committee on Ocean Rrsearch,

210 p.

Johnsen, G., Sakshaug, E., Vernet. V., (1992), Pigment composition, spectral characterization and photosynthetic parameters in *Chrysochromulina polylepis*. *Marine Ecology Progress Series*, **83**, 241-249.

Johnsen, G., Samset, O., Granskog, L. and Sakshaug, E., (1994). *In vivo* absorption characteristics in 10 classes of bloom-forming phytoplankton: taxonomic characteristics and responses to photoadaptation by means of discriminant and HPLC analysis. *Marine Ecology Progress Series*, **105**, 149-157.

Johnson, M.P. and Costello,M.J., (2002). Local and external components of the summertime plankton community in Lough Hyne, Ireland a stratified marine inlet. *Journal of plankton research*, **24**, 1305-1315.

Joint, I., Wollast, R., Chou, L., Batten, S., Elskens, M., Edwards, E., Hirst, A., Burkill, P., Groom, S., Gibb, S., Miller, A., Hydes, D., Dehairs, F., Antia, A., Barlow R., Rees, A., Pomroy, A., Brockmann, U., Cummings D., Lampitt, R., Loijens, M., Mantoura, F., Miller, P., Raabe, T., Alvarez-Salgado, X., Stelfoxa, C., Woolfenden, J., (2001). Pelagic production at the Celtic Sea shelf break. *Deep-Sea Research II*, **48**, 3049-3081.

Jones, M. and C. P. Spencer (1970). The phytoplankton of the Menai Straits. *ICES Journal of Marine Science*, **33**, 169-180.

Kiefer, D. A. and SooHoo, J.B., (1982). Spectral absorption by marine particles of coastal waters of Baja California. *Limnology and Oceanography*, **27**, 492-499.

Kirk, J.T.O., (1994). *Light and photosynthesis in aquatic ecosystems* (2nd ed.), Cambridge University press, Cambridge, U.K.

Kishino, M., Takahashi, M., Okami, N., and Ichimura, S., (1985). Estimation of the spectral absorption coefficients of phytoplankton in the sea. *Bulletin of Marine Science*, **37**, 634-642.

Kratzer, S., (2000).Bio-optical studies of coastal waters. Ph.D. thesis, University of Wales, Bangor.

Kratzer, S., Bowers, D. and Tett, P.B., (2000). Seasonal changes in colour ratios and optically active contituents in the optical Case-2 waters of the Menai Strait, North Wales *International Journal of Remote Sensing*, **21 (11)**, 2225-2246.

Lalli, C.M. and Parsons, T.R., (1997). *Biological Oceanography, An introduction* (2nd ed.), Butterworth-Heinemann, Oxford, U.K.

Lennox, A., (1979). Studies on the ecology and physiology of *Phaeocystis*. Ph.D. thesis, University of Wales, Bangor.

Mantoura, R.F.C., Llewellyn, C.A., (1983). The rapid determination of algal chlorophyll and carotenoid pigments and their breakdown products in natural waters by reverse-phase high-performance liquid chromatography. *Analytica Chimica Acta*, **151**, 297-314.

Mantoura, R.F.C., Wright, S.W., Jeffrey, S.W. and Barlow, R.G.., Cummings D.E., (1997). Filtration and storage of pigments from microalgae. In: *Phytoplankton pigments in oceanography: Guidelines to modern methods*, Jeffrey, S.W., Mantoura, R.F.C.and Wright, S.W., (eds.), UNESCO, Paris, 283-305.

Martinjezequel, V. and Videau, C., (1992). Phytoplankton and bacteria over the transient area of the continental-slope of the Celtic Sea in spring .1. Vertical-distribution and productivity. *Marine Ecology-Progress Series*, **85(3)**, 289-301.

McKinney, E.S.A., Gibson, C. E. and Stewart, B. M., (1997). Planktonic diatoms in the north-west Irish Sea: a study by automatic sampler. *Biology and Environment*, **97B**, 197-202.

Meyns, S., Illi, R. and Ribi, B., (1994). Comparison of chlorophyll-*a* analysis by HPLC and Spectrophotometry – Where do the differences come from?. *Archiv fur Hydrobiologie*, **132 (2)**, 129-139.

Millie, D.F., Kirkpatrick G.J., and Vinyard B.T., (1995). Relating photosynthetic pigments and *in vivo* optical density spectra to irradiance for the Florida red-tide dinoflagellate *Gymnodinium breve*. *Marine Ecology Progress Series*, **120**, 65-75.

Millie, D.F., Schofield, O.M., Kirkpatrick, G.J., Johnsen, G., Tester, P.A. and Vinyard, B.T., (1997). Detection of harmful algal blooms using photopigments and absorption signatures. A case study of the Florida red tide dinoflagellate, *Gymnodinium breve*. *Limnology and Oceanography*, **42**, 1240-1251.

Mills, D.K., Tett, P.B., and Nobarino, G., (1994). The spring bloom in the south western North Sea in 1989. *Netherlands Journal of Sea Reasearch*, **33**, 65-80.

Mitchell, B.G., (1990). Algorithms for determining the absorption coefficient for aquatic particles using the quantitative filter technique. In: *Ocean Optics X, Proceedings SPIE International Society of Optical Engineering*, **1302**, 137-148.

Mitchell, B.G., and Kiefer, D.A., (1984). Determination of absorption and fluorescence excitation spectra phytoplankton. In: *Marine phytoplankton and productivity*, Holm-Hansen, O., Bolis, L. and Gilles, R. (eds.), Springer-Verlag, Berlin, Germany, p.157-169.

Mitchelson, E.G., Jacob, N.J. and Simpson, J.H., (1986). Ocean Colour algorithms from the case 2 waters of the Irish Sea in comparison to algorithms from case 1 waters. *Continental Shelf Research*, **5**, 403-418.

Morel, A., (1974). Optical properties of pure water and pure seawater. In*: Optical aspects of oceanography*, Jerlov, N.G. and Steeman Nielsen, E. (eds.), Academic Press, London, U.K., p. 1-24.

Morel A.Y., (1980). In-water and remote measurements of ocean colour. *Boundary-layer Meteorology*, **18**, 177-201.

Morel, A. and Prieur L., (1977). Analysis of variations in ocean colour. . *Limnology and Oceanography*, **22**, 709-722.

Morel, A. and Bricaud, A., (1981). Theoretical results concerning light absorption in a discrete medium, and application to specific absorption of phytoplankton. *Deep-Sea Research*, **28**, 1375-1393

Mueller, J.L. and Austin, R.W., (1995). Ocean Optic Protocols for SeaWiFS Validation, Revision 1. *NASA Technical Memorandum 104566*, **25**, Hooker, S.B., Firestone, E.R., and Acker, J.G. (eds.), NASA Goddard Space Flight Center, Greenbelt, MD, U.S.A., 67 p.

Nelson, N.B. and Siegel, D.A.., (2002). Chromophoric DOM in the Open Ocean. In: *Biogeochemistry of marine dissolved organic matter*, Hansell, D.A. and Carlson, C.A. (eds.), Academic Press, U.S.A., 774p.

Newton, A. (1986). Studies on phytoplankton succession. MSc. Thesis, University of Wales, Bangor.

Nova, E.M.M., Hansom, J.D. and Curran, P.J., (1989) The effect of sediment type on the relationship between reflectance and suspended sediment concentration. *International Journal of Remote Sensing*, **10**, 1283-1289.

Paerl, H.W. and Millie, D.F., (1991). *Evaluation of spectrophotomeric, fluorometric and High Performance Liquid Chromatographic methods for algal pigment determinations in aquatic ecosystems*. United States Environmental Protection Agency publication, Washington DC, U.S.A., 134 p.

Pemberton, K., Rees, A.P., Miller, P.I., and Raine, R., Joint, I (2004). The influence of water body characteristics on phytoplankton diversity and production in the Celtic Sea. *Continental Shelf Research*, **24**, 2011-2028.

Pinckney, J., Papa, R. and Zingmark, R., (1994). Comparison of High-Performance Liquid-Chromatographic, Spectrophotometric, and Fluorometric methods for determining chlorophyll *a* concentrations in estuarine sediments. *Journal of Microbiological Methods*, **19 (1)**, 59-66.

Pope, R. M. and Fry, E. S., (1997). Absorption spectrum (380-700nm) of pure water: II. Integrating cavity measurements. *Applied Optics*, **36**, 8710-8723.

Preisendorfer, R.W., (1976). *Hydrologic Optics volume 1: Introduction*. U.S. Department of Commerce, Washington DC, U.S.A., 218 p.

Prescott, G.W., (1969). *The algae: a review*. Nelson, U.K, 381 p

Prestidge, M.C. and Taylor, A.H., (1995). A modelling investigation of the distribution of stratification and phytoplankton abundance in the Irish Sea. *Journal of phytoplankton Research*, **17**, 1397-1420.

Prezelin, B.B. and Boczar, B.A., (1986). Molecular bases of cell absorption and fluorescence in phytoplankton: potential applications to studies in optical oceanography. In: *Progress in Phycological Research*, Round, F. and Chapman, D. (eds.), Elsevier, Amsterdam, The Netherlands, p. 350-465.

Prieur, L. and Sathyendranath, S., (1981). An optical classification of coastal and oceanic waters based on the specific spectral absorption curves of phytoplankton pigments, dissolved organic matter, and other particulate material. *Limnlogy and Oceanography*, **26**, 671-689.

Raine, R. and McMahon, T. (1998). Physical dynamics on the continental shelf off southwestern Ireland and their influence on coastal phytoplankton blooms. *Continental Shelf Research*, **18**, 883-914.

Rast, M., Bezy, J.L. and Bruzzi, S., (1999). The ESA Medium Resolution Imaging Spectrometer MERIS – a review of the instrument and its mission. *International Journal of Remote Sensing*, **20**, 1681-1702.

Redden, A.M., Thompson, R.J. and Deibeld, D., (1993). Effects of short-term and long-term freezing of chloropigments in cultured diatoms and bivalve digestive gland and feces as determined by standard fluorometry and HPLC. *Archiv fur Hydrobiologie*, **129 (1)**, 67-87.

Rees, A., Joint, I. and Donald, K.M., (1999). Early spring bloom phytoplankton-nutrient dynamics at the Celtic Sea Shelf Edge. *Deep-Sea Reseearch 1*, **46**, 483-510.

Ricard, M., (1987). *Atlas du phytoplancton marin Vol. 2. Diatomophycees*, Editions du CNRS, Paris

Sathyendranath, S., (1981). Influence des substances en solution et en suspension dans les eaux de mer sur l'absorption et la reflectance. Modelisation et applications a la teledetection. These de Docteur de Qeme cycle, Universite Pierre et Marie Curie, Paris.

Sathyendranath, S., Lazzara, L and Prieur, L., (1987). Variations in the spectral values of specific absorption of phytoplankton. *Limnology and Oceanography*, **32**(2), 403-415

Sathyendranath, S., Hodge, F.E., Platt, T. and Swift, R.N., (1994). Detection of phytoplankton pigments from ocean colour: improved algorithms. *Applied Optics*, **33** 1081-1098.

Savidge, G. and Kain, J.M., (1990). Ch. 2. productivity of the Irish Sea. In: *The Irish Sea, An environmental review, part 3*, Norton T.A. and Geffen A.J. (eds.), Liverpool University Press, Liverpool, U.K., p. 9-44

Schlens, J., (2003). A tutorial on Principal Component Analysis: Derivation, Discussion and Singular Value Decomposition (online). Available from: http://www.sul.sulk.edu/~shlens/pub/notes/pca.pdf. (Accessed 15 August 2004)

Simpson, J.H., (1971). Density stratification and microstructure in the western Irish Sea. *Deep Sea Research*, **18**, 309-319.

Simpson, J.H, Edelsten, D.J., Edwards, A., Morris, N.C.G. and Tett, P.B., (1979). The Islay Front: Physical structure and phytoplankton distribution. *Estuarine and Coastal Marine Science*, **9**, 713-726.

Smith, P.S.D. (1999).Bio-optical observations at the Hebridian shelf edge. Ph.D. thesis, University of Wales, Bangor.

Smith, R.C. and Baker, K.S., (1981). Optical properties of the clearest natural water. *Applied Optics*, **20**, 177-184.

Sournia, A. (1986). *Atlas du phytoplancton marin Vol.1. Cyanophycees, Dictyochophycees, Dinophycees, Raphidophycees*, Editions du CNRS, Paris

Spencer, C.P., (1988). *Algal blooms in Liverpool Bay and associated areas during 1987. Report to the Department of the Environment*, London. 17 p.

Sykes, J.B. (1981). An illustrated guide to the diatoms of British coastal plankton. *Field Studies*. **5**: 425-468.

Tangen, K. and Björnland, T., (1981). Observations on pigments and morphology of *Gyrodinium aureolum* Hulburt, a marine dinoflagellate containing 19' – hexanoyloxyfucoxanthin as the main carotenoid. *Journal of Plankton Research*, **3**, 389-401.

Tett, P., (1987). Plankton. In: *Biological Survey of Estuaries and Coasts*, Baker, J. and Wolff, W.J. (eds.), Cambridge University press, Cambridge, U.K., p. 280-341.

Tiffany, M.A. and Lange, C.B., (2000). The Diatom Flora of the Salton Sea, California. (on-line). Available from: http://www.sci.sdsu.edu/salton/SaltonSeaBenthicDiatoms.html (Accessed 28 June 2005)

Vernet, M., Neori, A., Haxo, F.T., (1989). Spectral properties and photosynthetic action in red-tide populations of *Prorocentrum micans* and *Gonyaulax polyedra*. *Marine Biology*, **103**, 365-371.

Voltolina, D., (1980). Phytoplankton of Liverpool Bay. Ph.D. Thesis. University of Wales, Bangor

Weaver, E.C. and Wrigley, R., (1994). Factors affecting the identification of phytoplankton groups by means of remote sensing. *NASA Technical Memorandum 108799*, Greenbelt, MD, U.S.A., 121 p.

Webb, D.J., Burnison, B.K., Trimbee, A.M. and Prepas, E. (1992). Comparison of chlorophyll *a* extractions with ethanol and dimethly sulfoxide/acetone, and a concern about spectrophotometric phaeopigment correction. *Canadian Journal of Fisheries and Aquatic Sciences*, **49**, 2331-2336.

Willén, T., (1976). A simplified method of phytoplankton counting. *British phycology Journal*, **11**, 265-278.

Wood, A.M., Phinney, D.A., and Yentsch, C.S., (1998). Water column transparency and the distribution of spectrally distinct forms of phycoerythrin-containing organisms. *Marine Ecology Progress Series*, **162**, 25-31.

Wright, S.W. and Jeffrey, S.W., (1987). Fucoxanthin pigment markers of marine phytoplankton analysed by HPLC and HPTLC. *Marine Ecology Progress Series*, **38**, 259-266.

Wright, S.W., Jeffrey, S.W., Mantoura, R.F.C., Llewellyn, C.A., Bjornland, T., Repeta, D. and Welschmeyer, N., (1991). Improved HPLC method for the analysis of chlorophylls and carotenoids from marlin phytoplankton. *Marine Ecology Progress Series*, **77**,183-196.

Young, G..A., (1993). The Menai Strait: a review and bibliography of literature from the Wolfson Library. University of Wales, Bangor.

APPENDIX

Appendix A-1 Menai Strait Taxonomic data (No. of cells l^{-1})

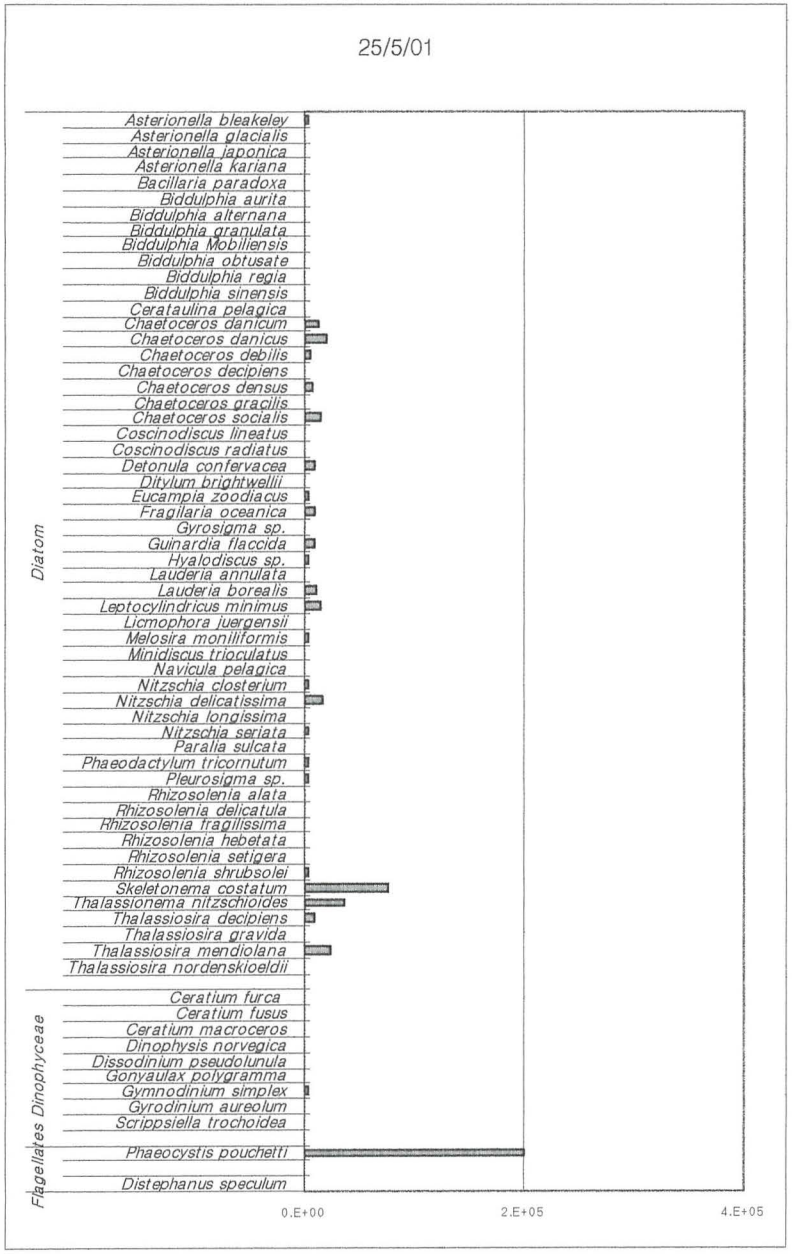

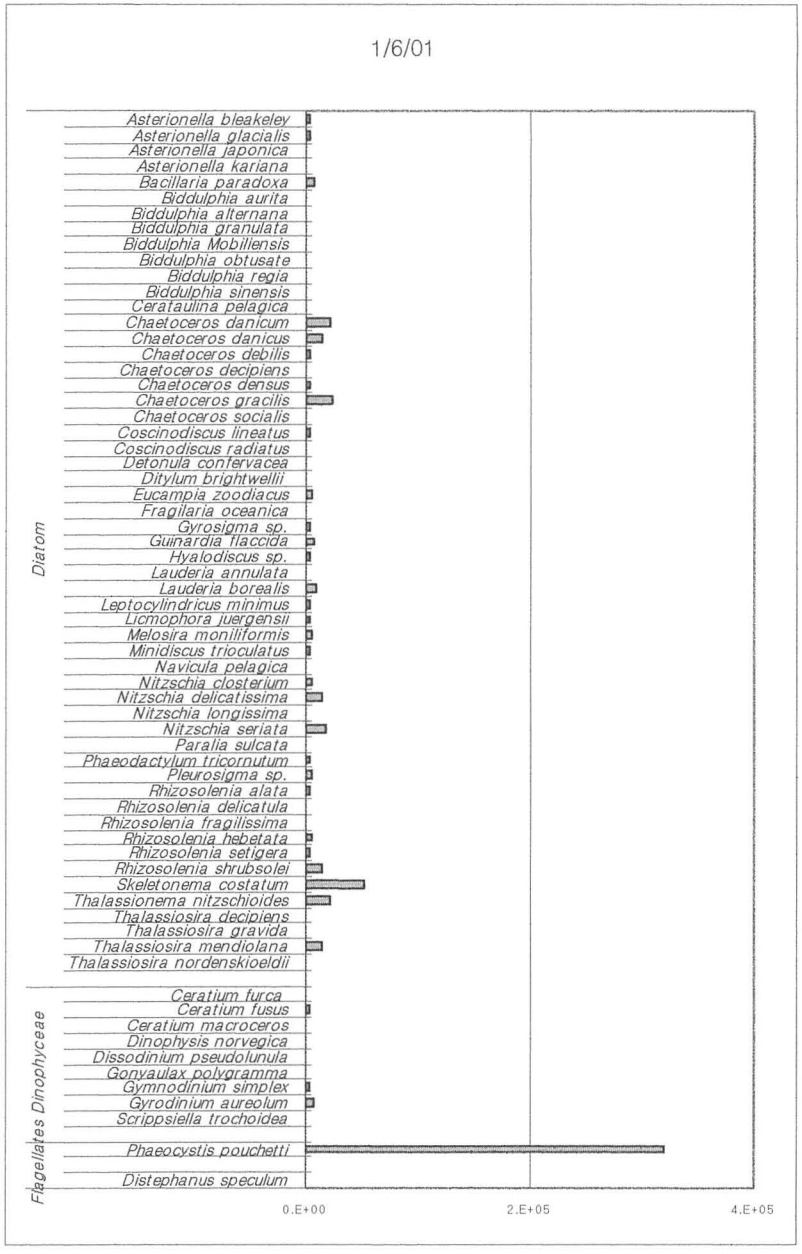

Appendix A-1 Menai Strait Taxonomic data (No. of cells l^{-1})

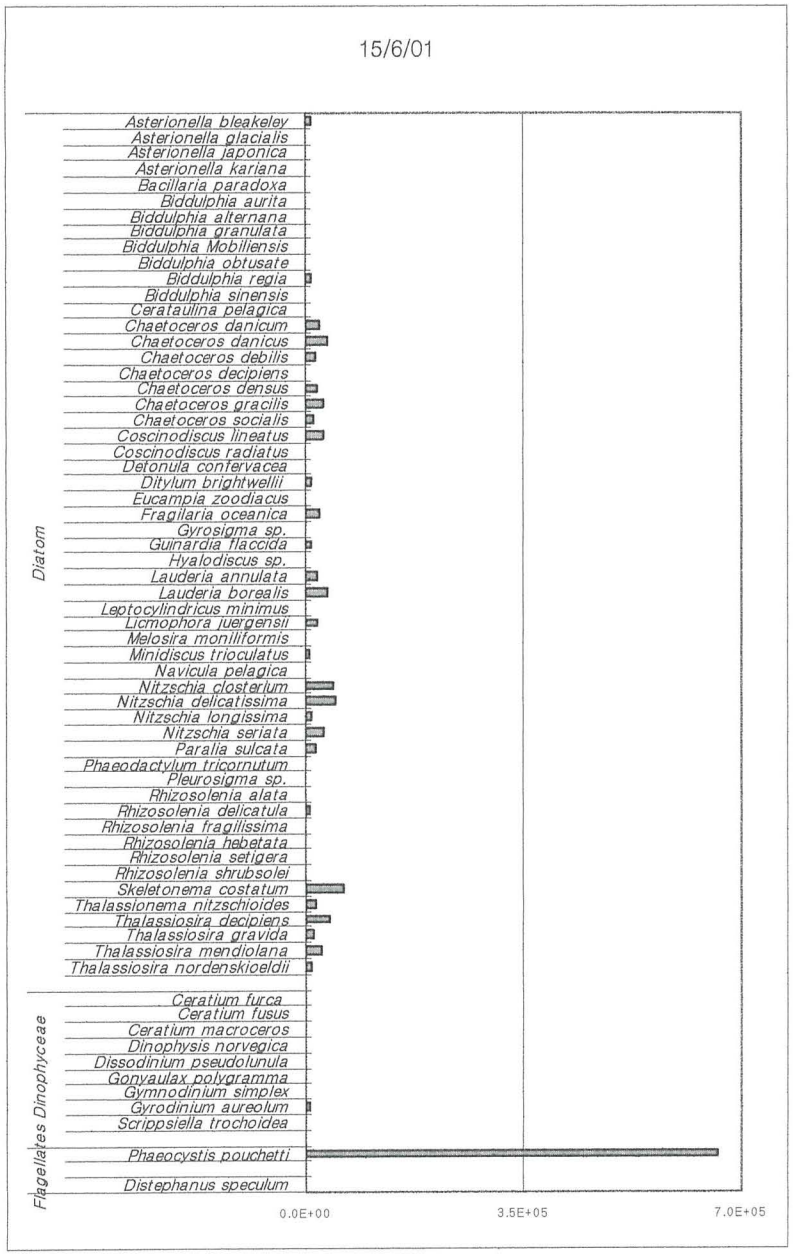

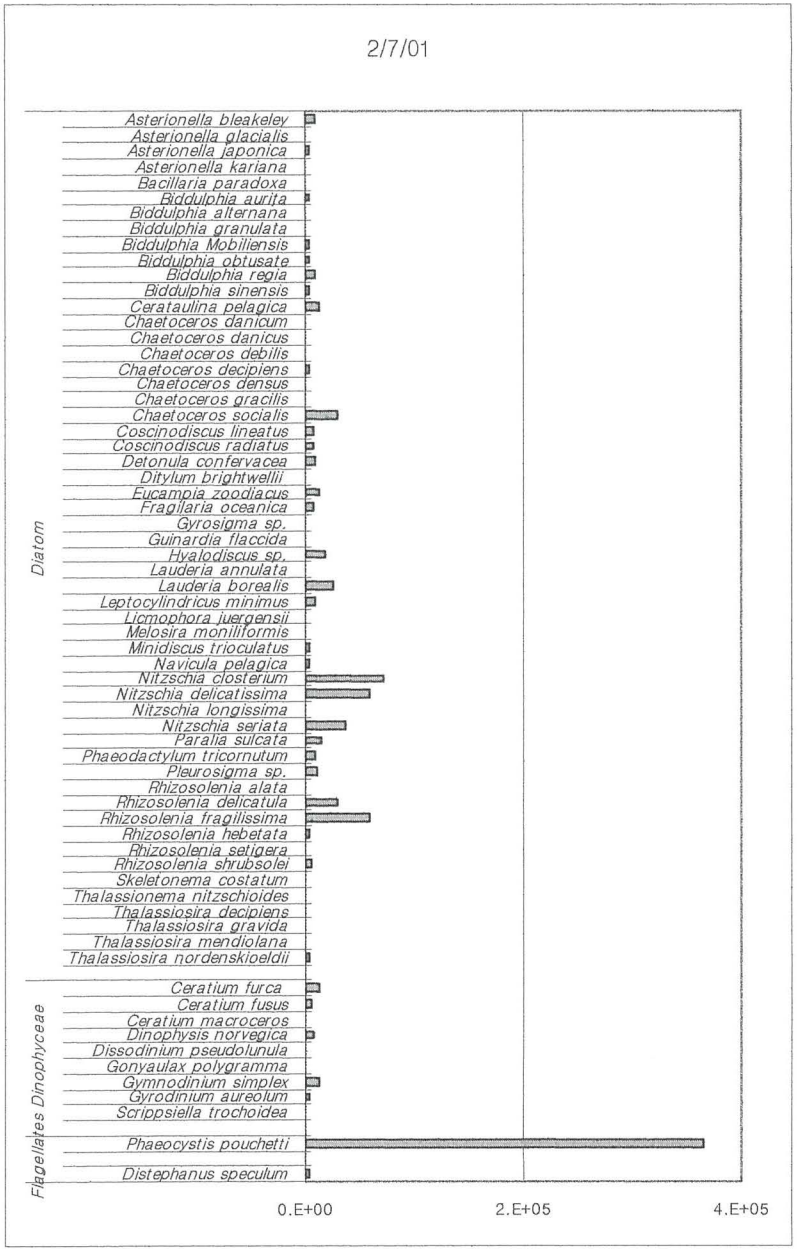

Appendix A-1 Menai Strait Taxonomic data (No. of cells l^{-1})

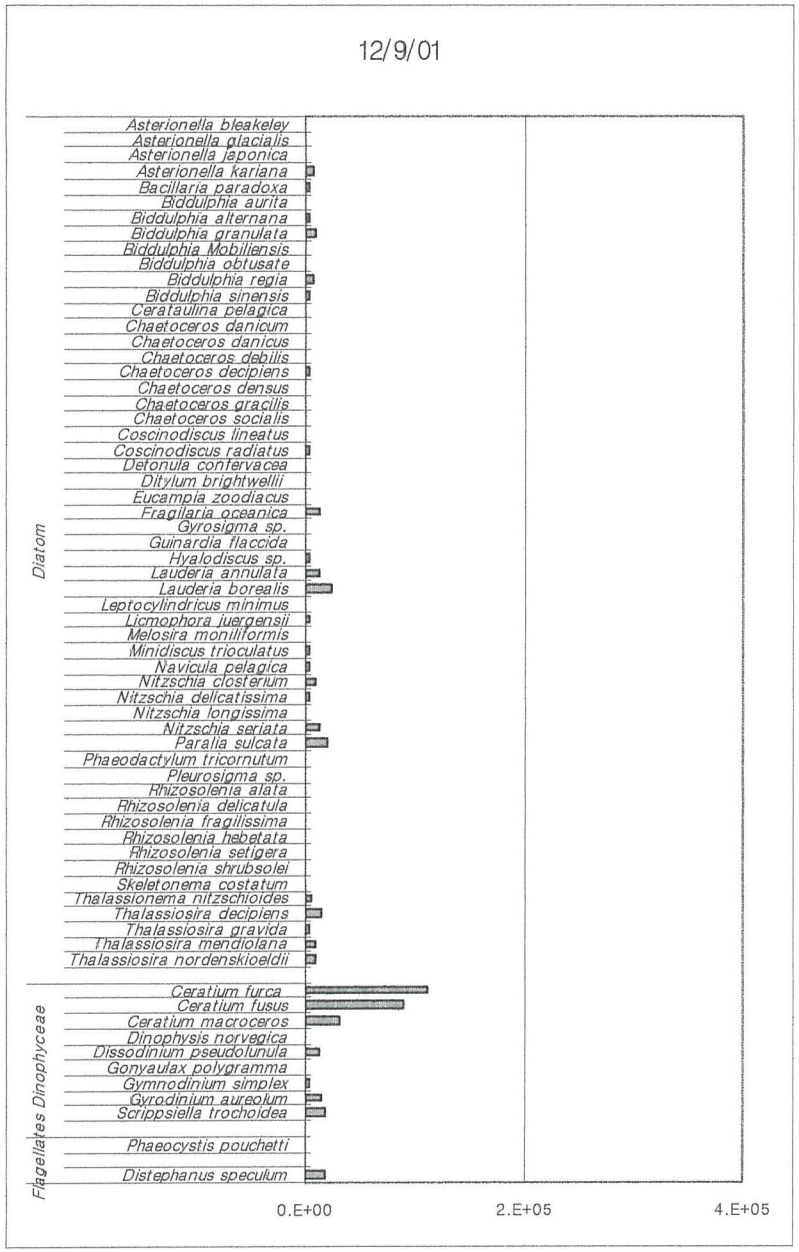

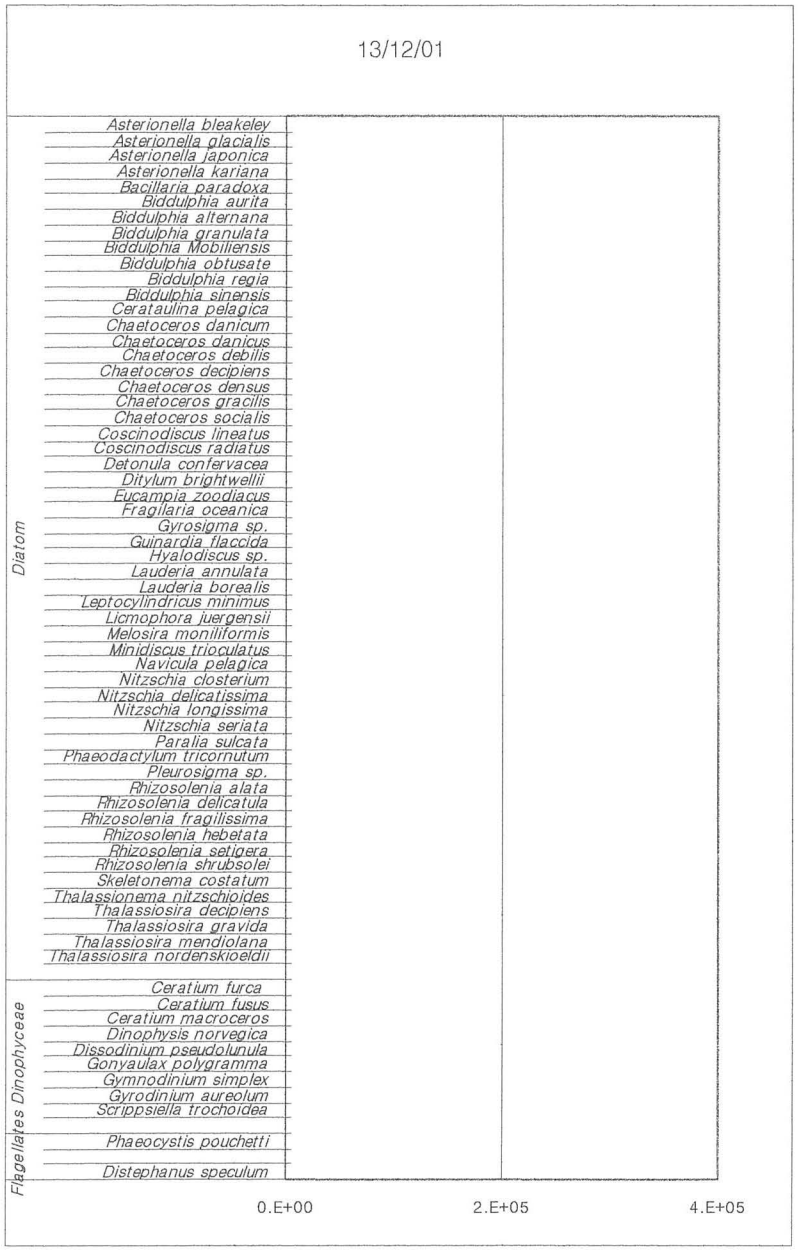

Appendix A-1 Menai Strait Taxonomic data (No. of cells l^{-1})

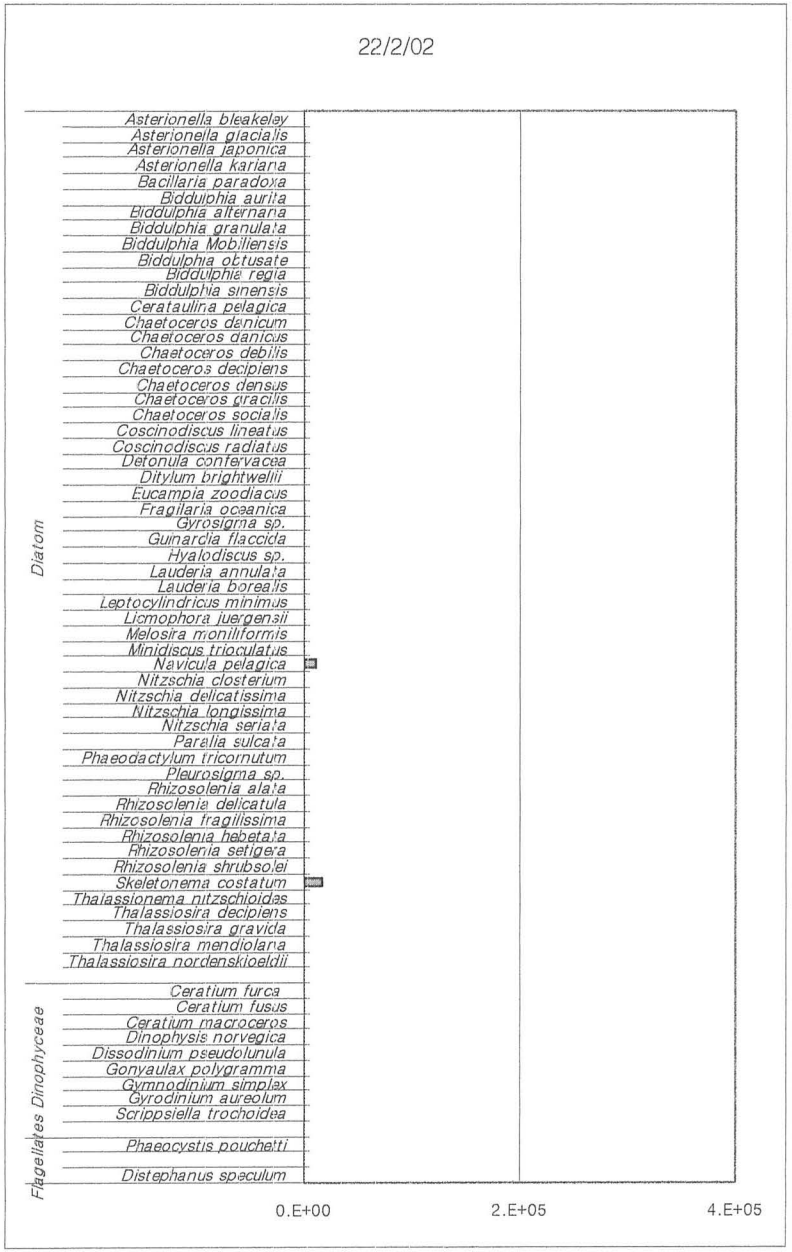

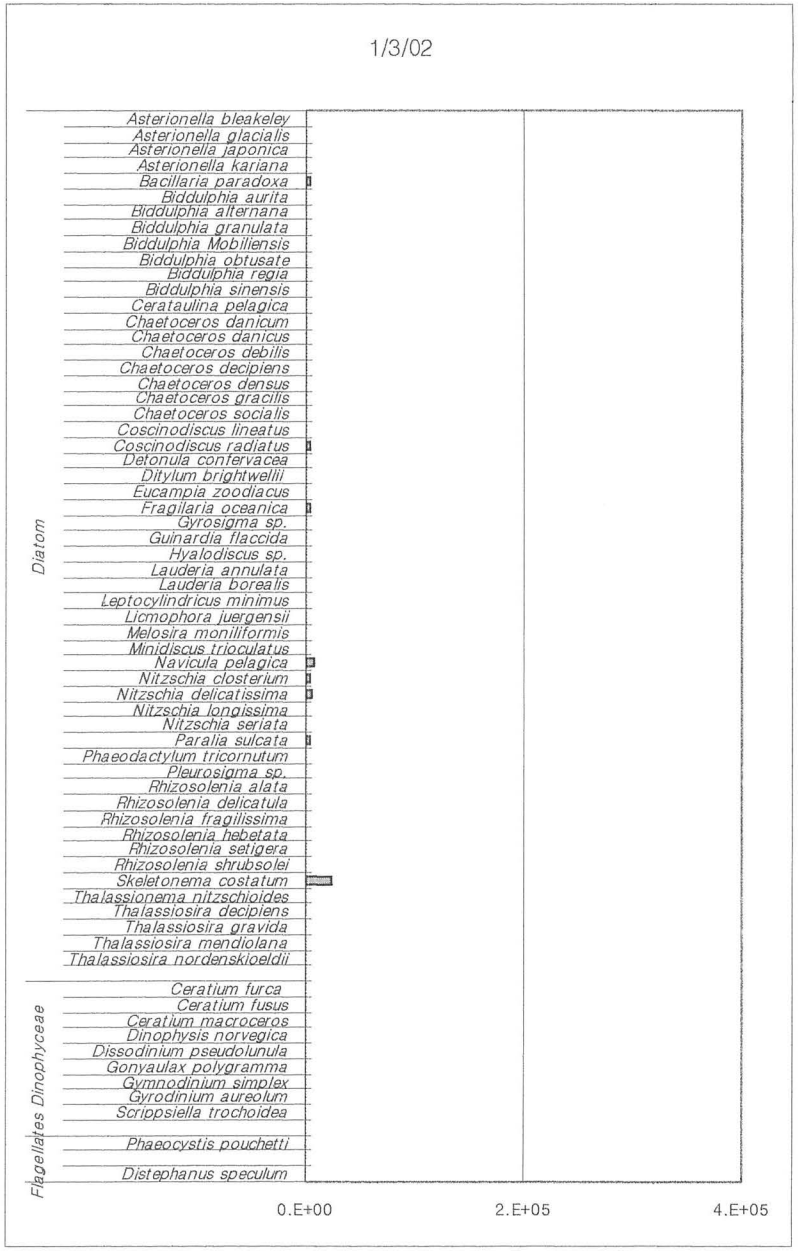

Appendix A-1 Menai Strait Taxonomic data (No. of cells l^{-1})

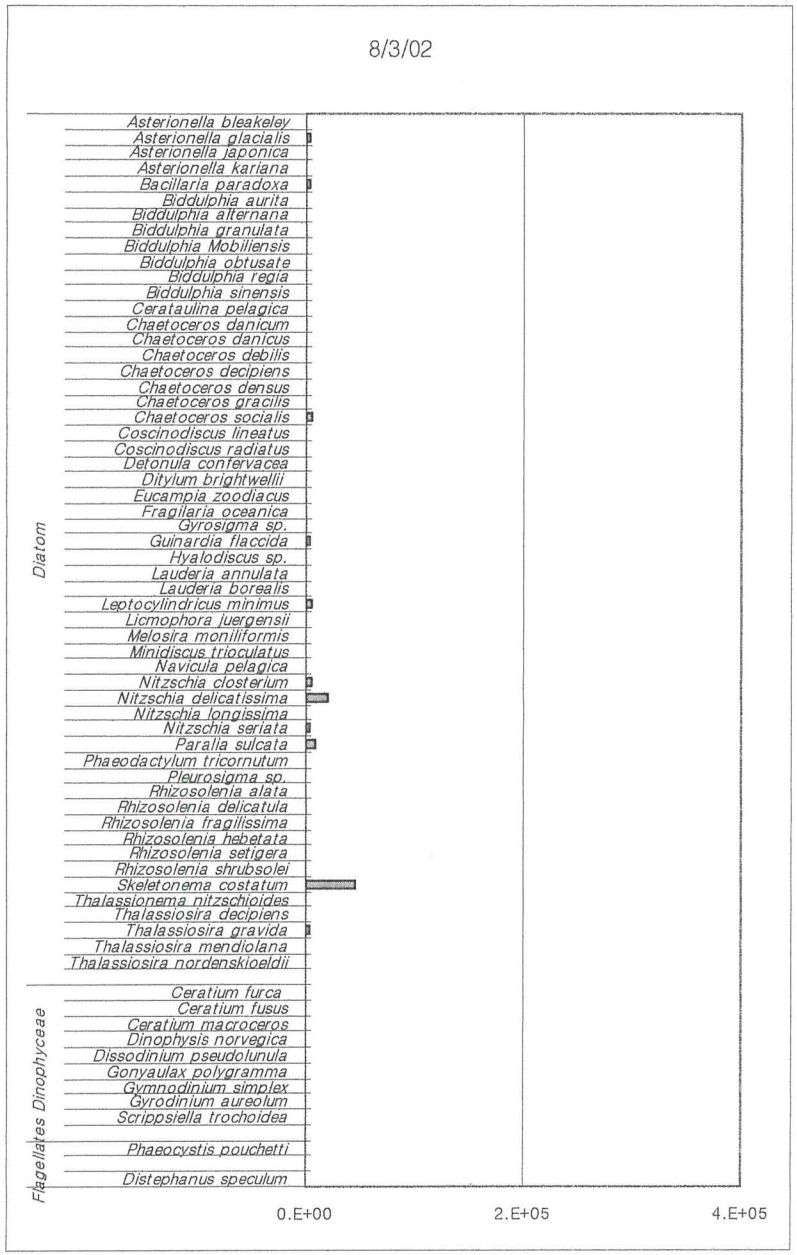

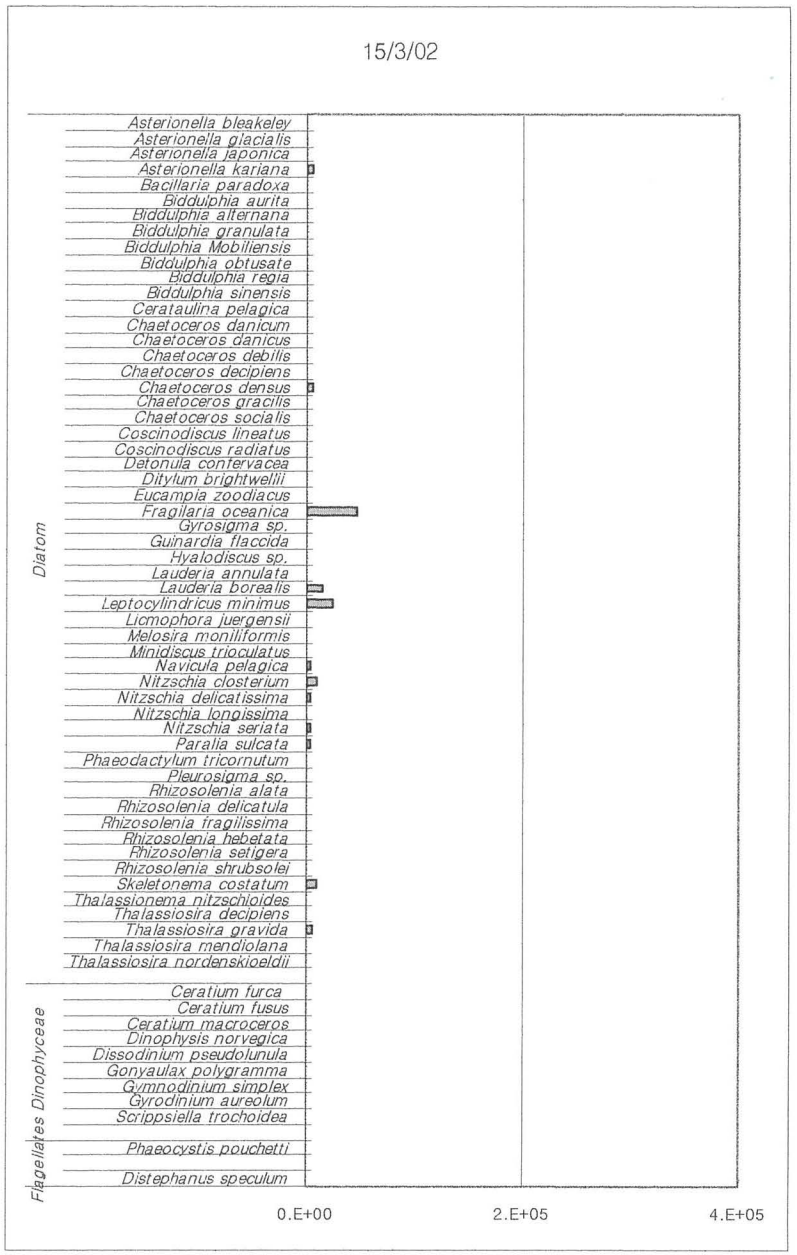

Appendix A-1 Menai Strait Taxonomic data (No. of cells l^{-1})

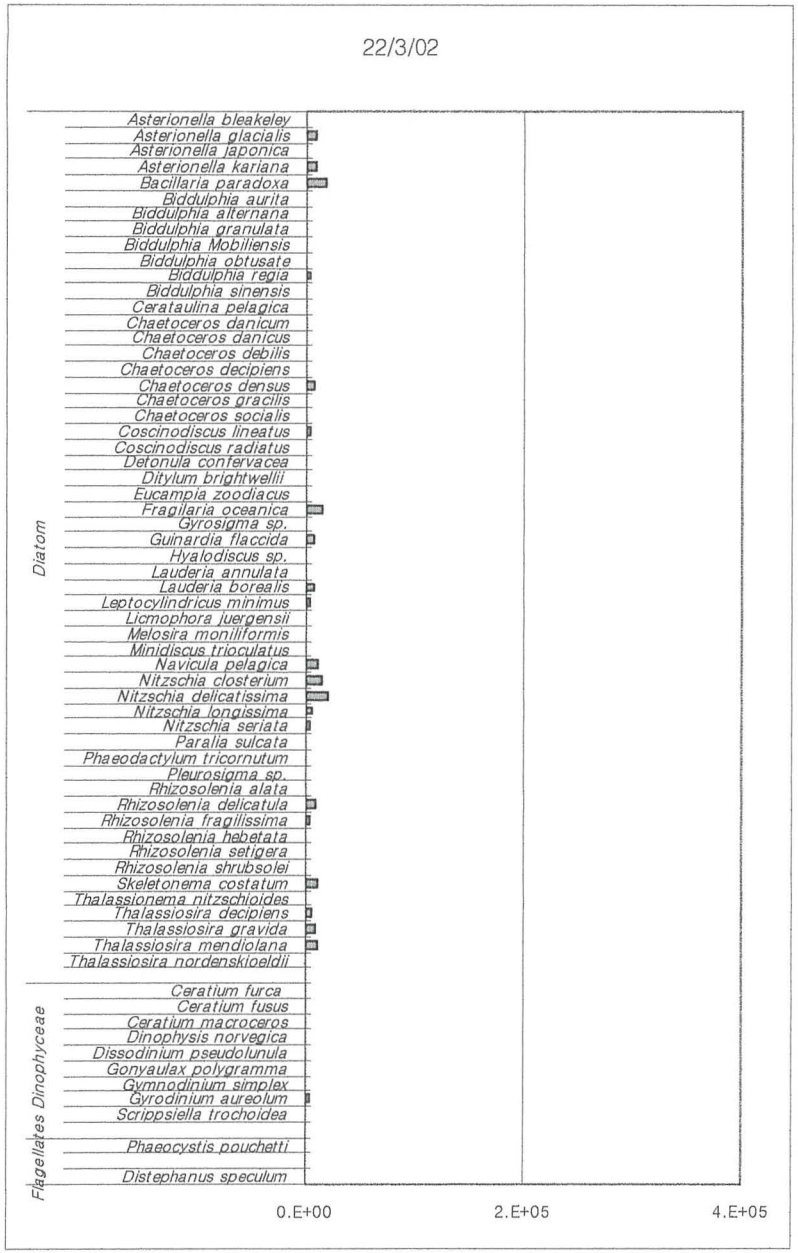

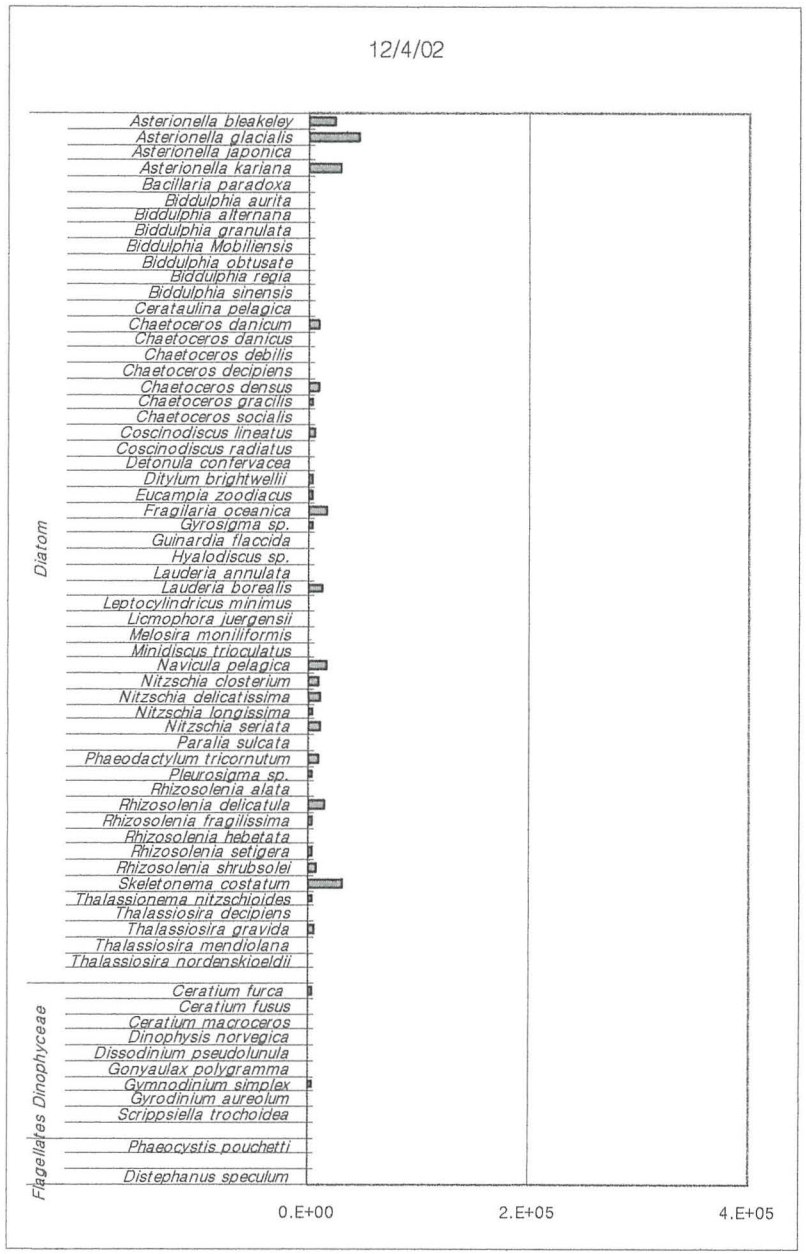

Appendix A-1 Menai Strait Taxonomic data (No. of cells l^{-1})

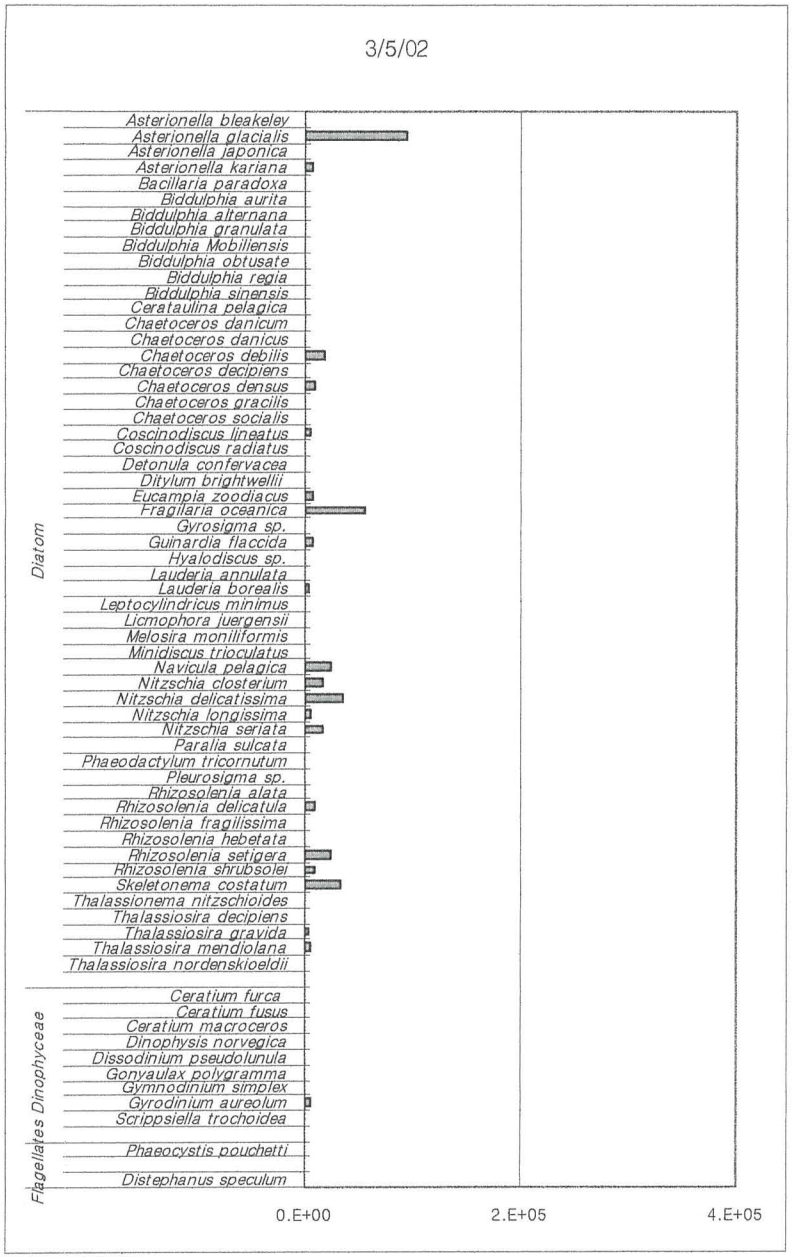

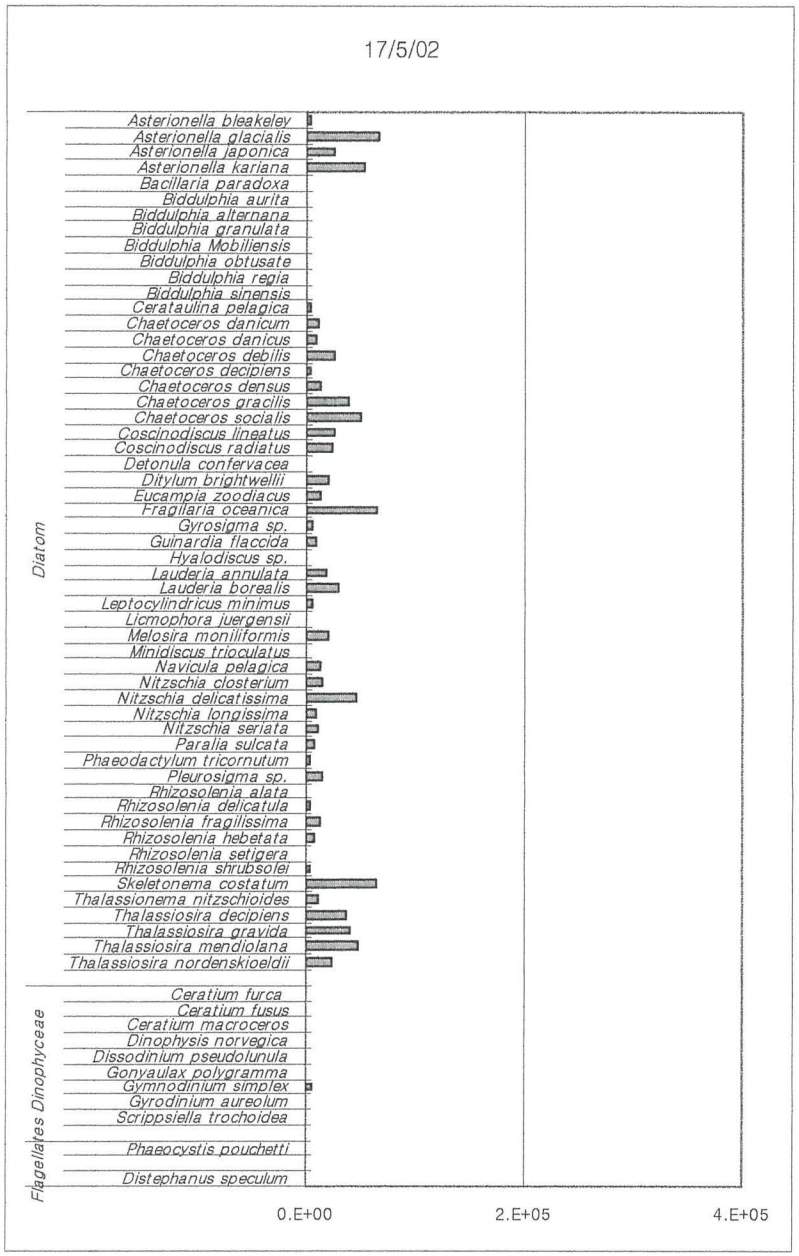

Appendix A-1 Menai Strait Taxonomic data (No. of cells l^{-1})

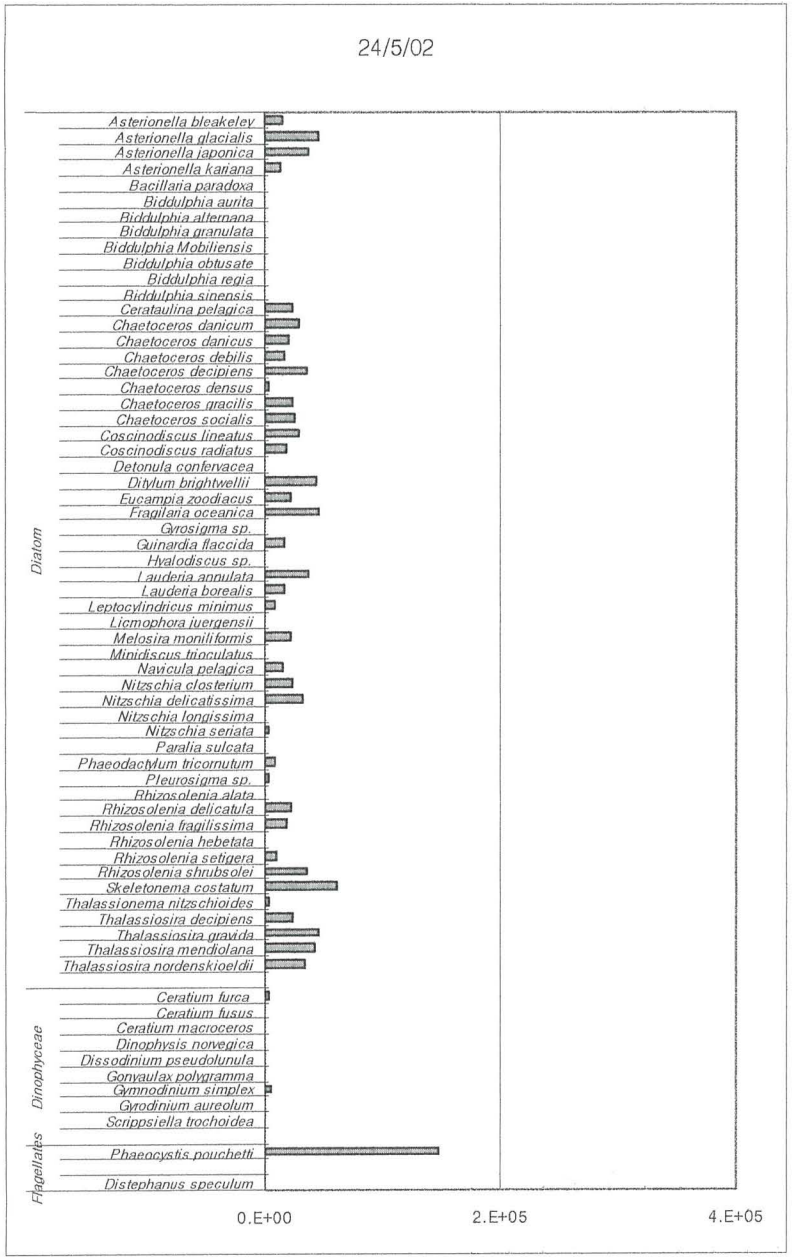

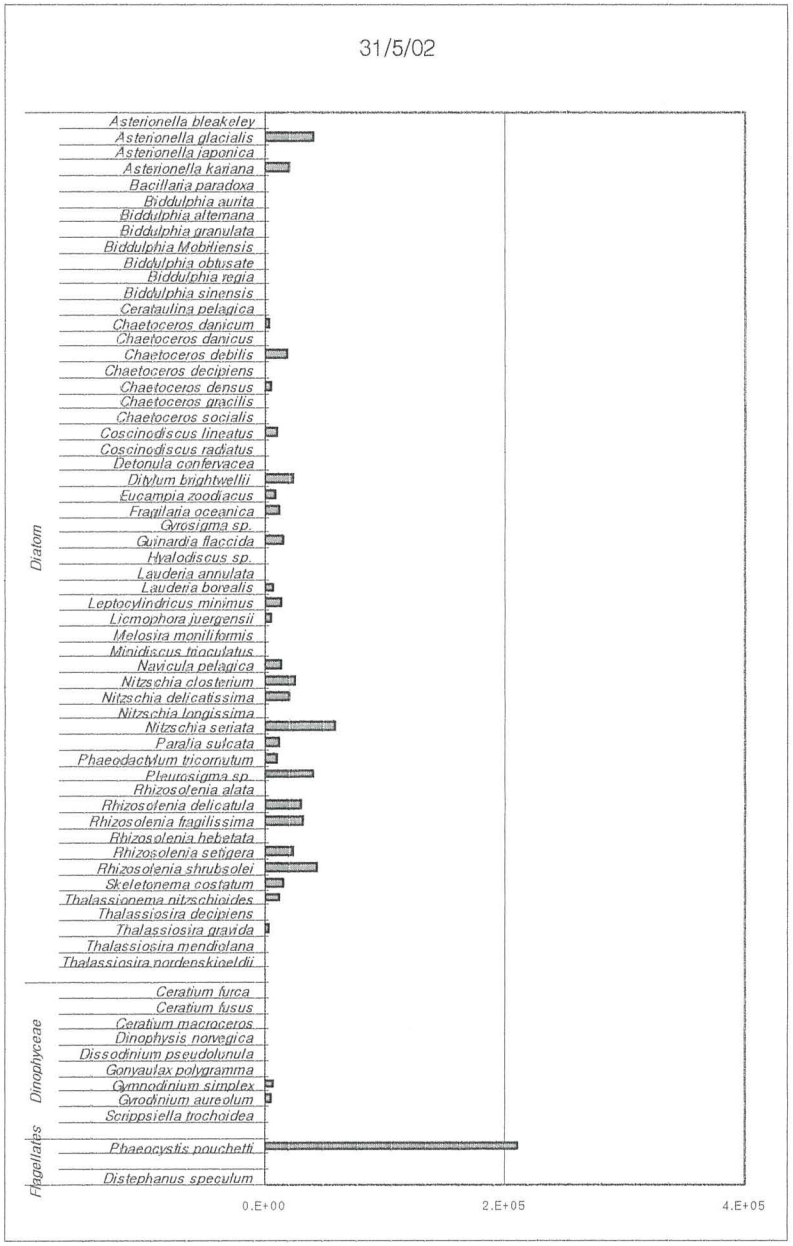

Appendix A-1 Menai Strait Taxonomic data (No. of cells l^{-1})

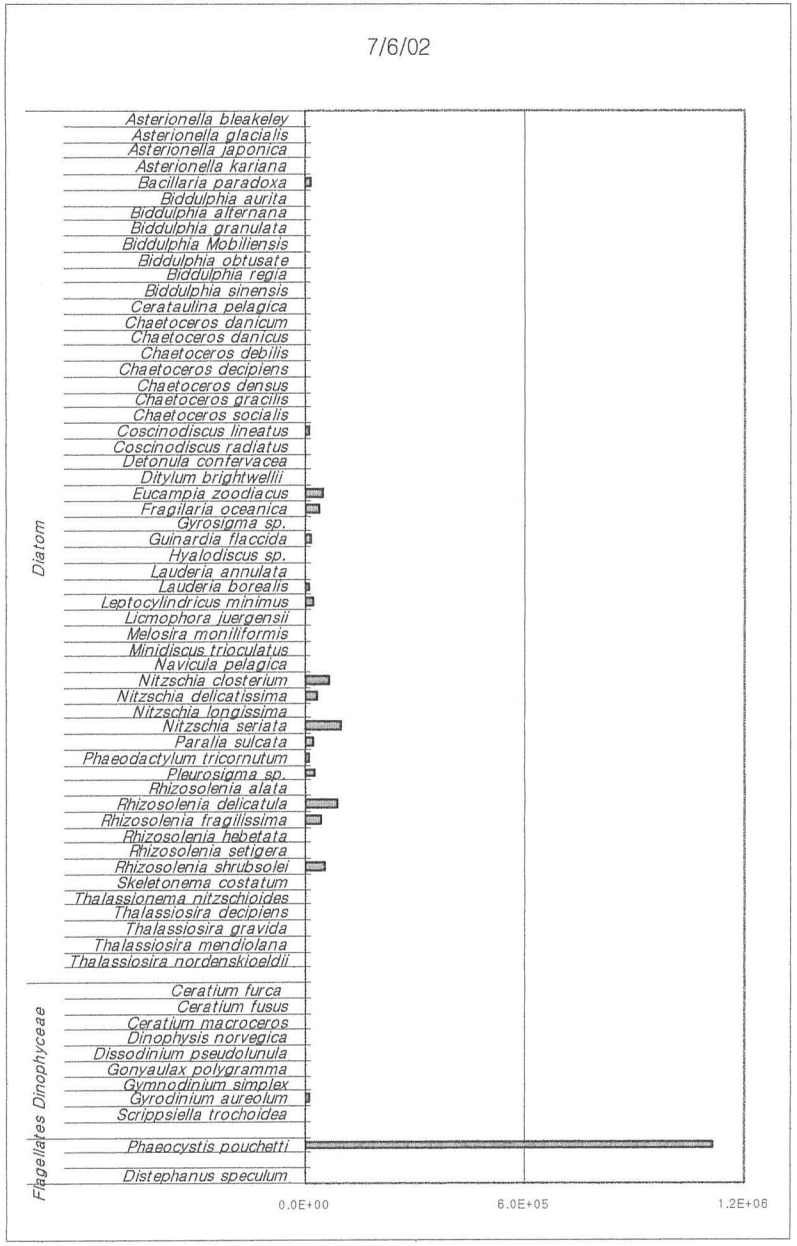

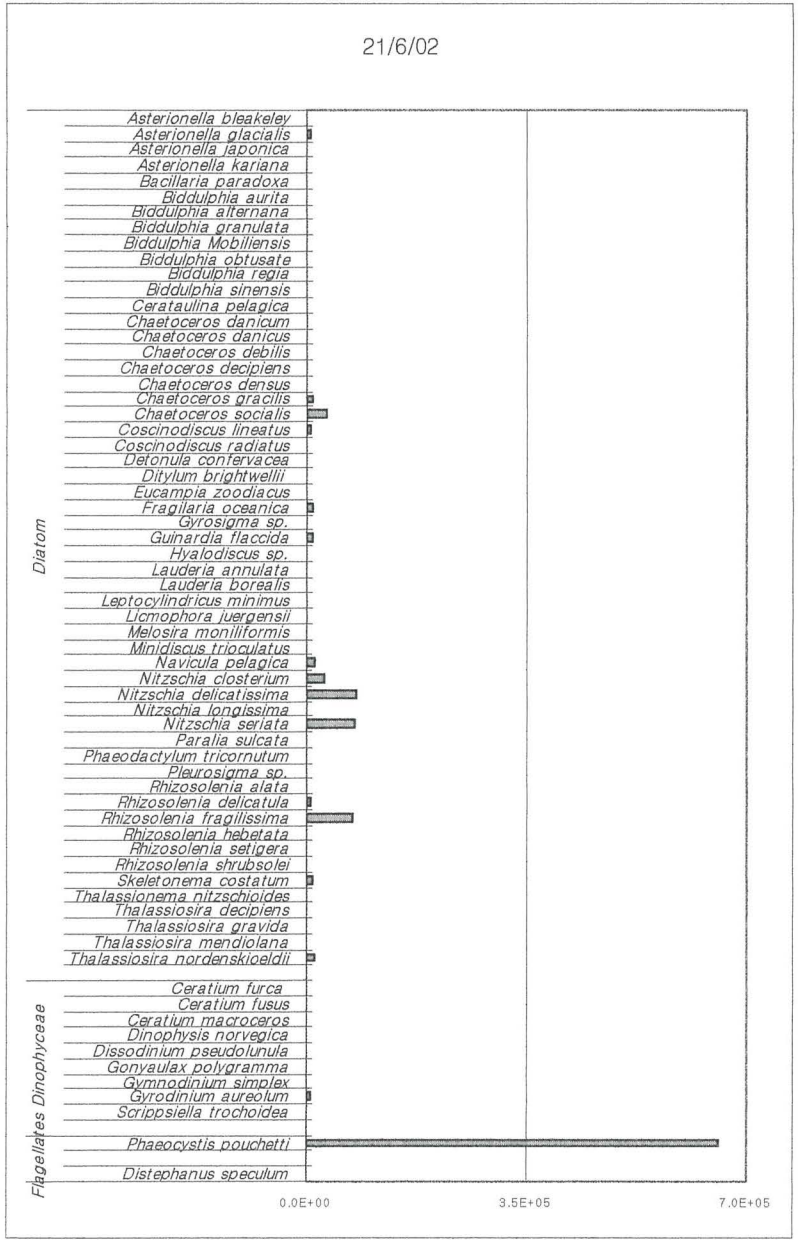

Appendix A-1 Menai Strait Taxonomic data (No. of cells l^{-1})

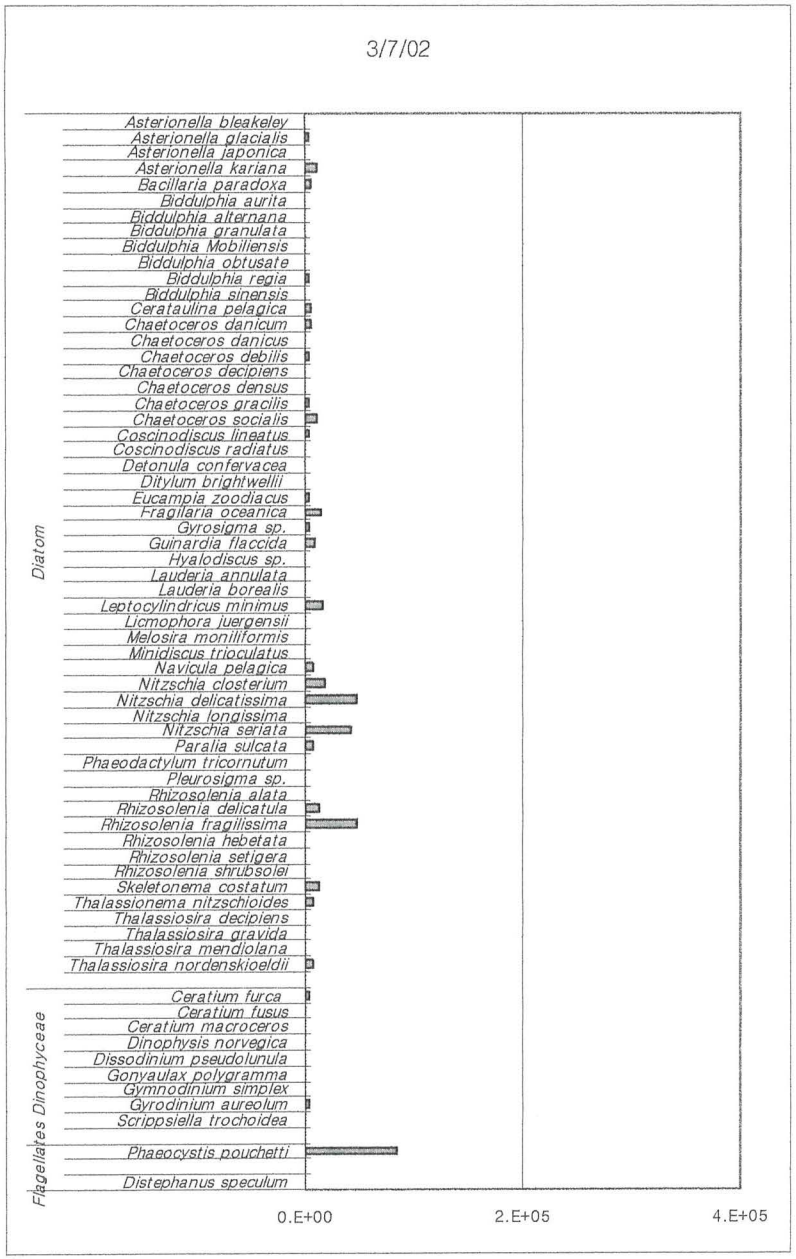

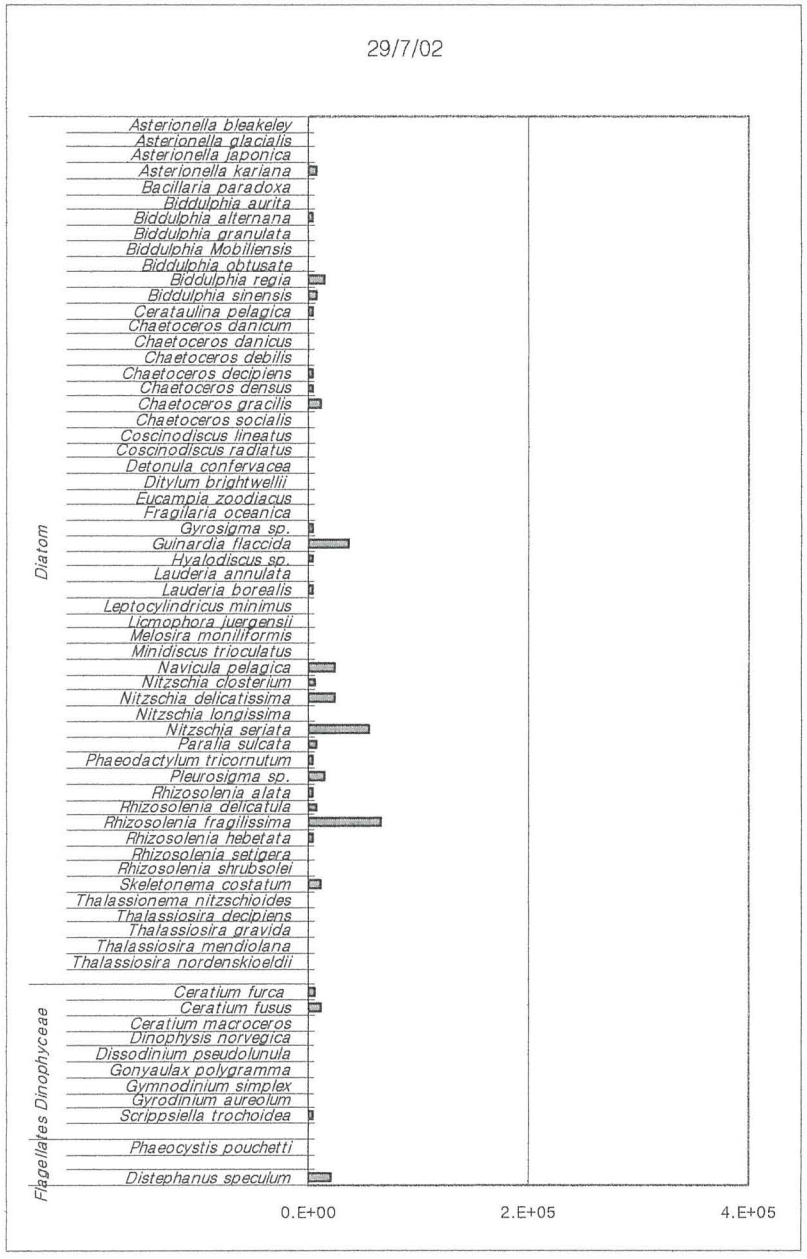

Appendix A-1 Menai Strait Taxonomic data (No. of cells l^{-1})

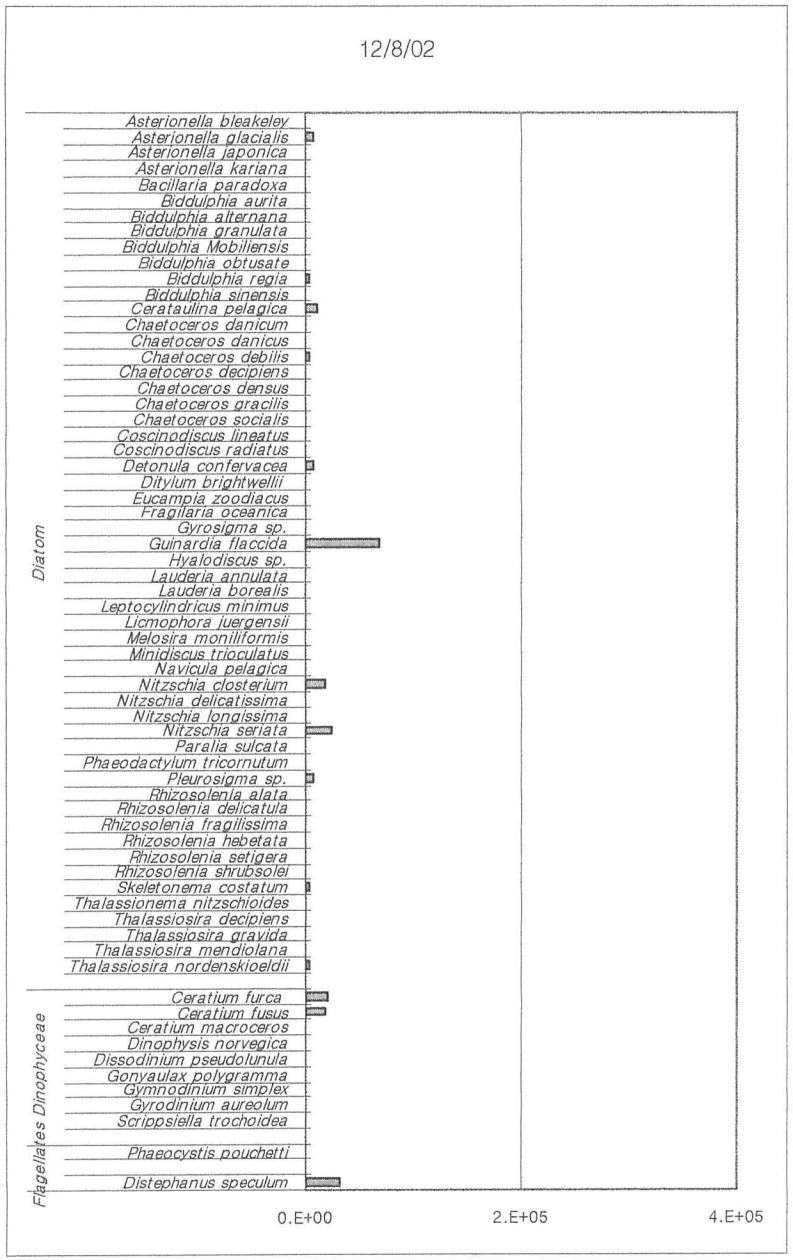

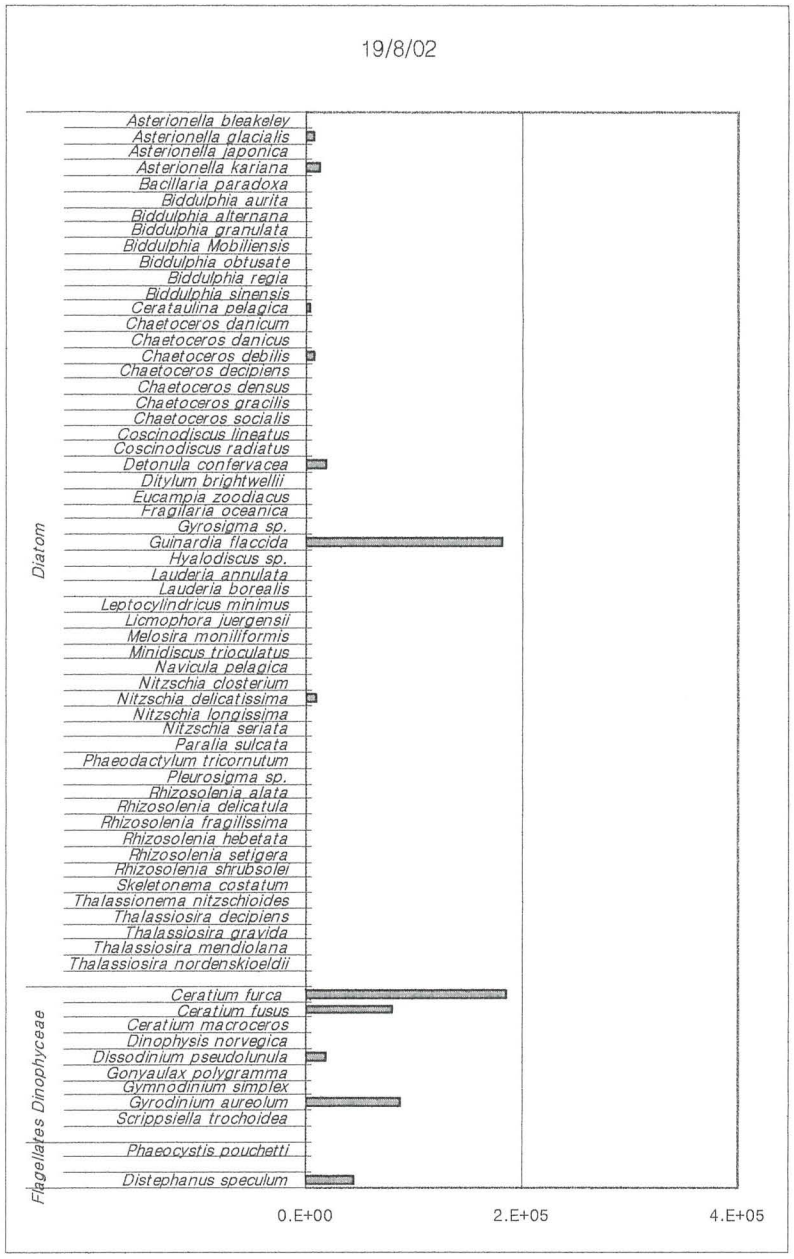

Appendix A-1 Menai Strait Taxonomic data (No. of cells l^{-1})

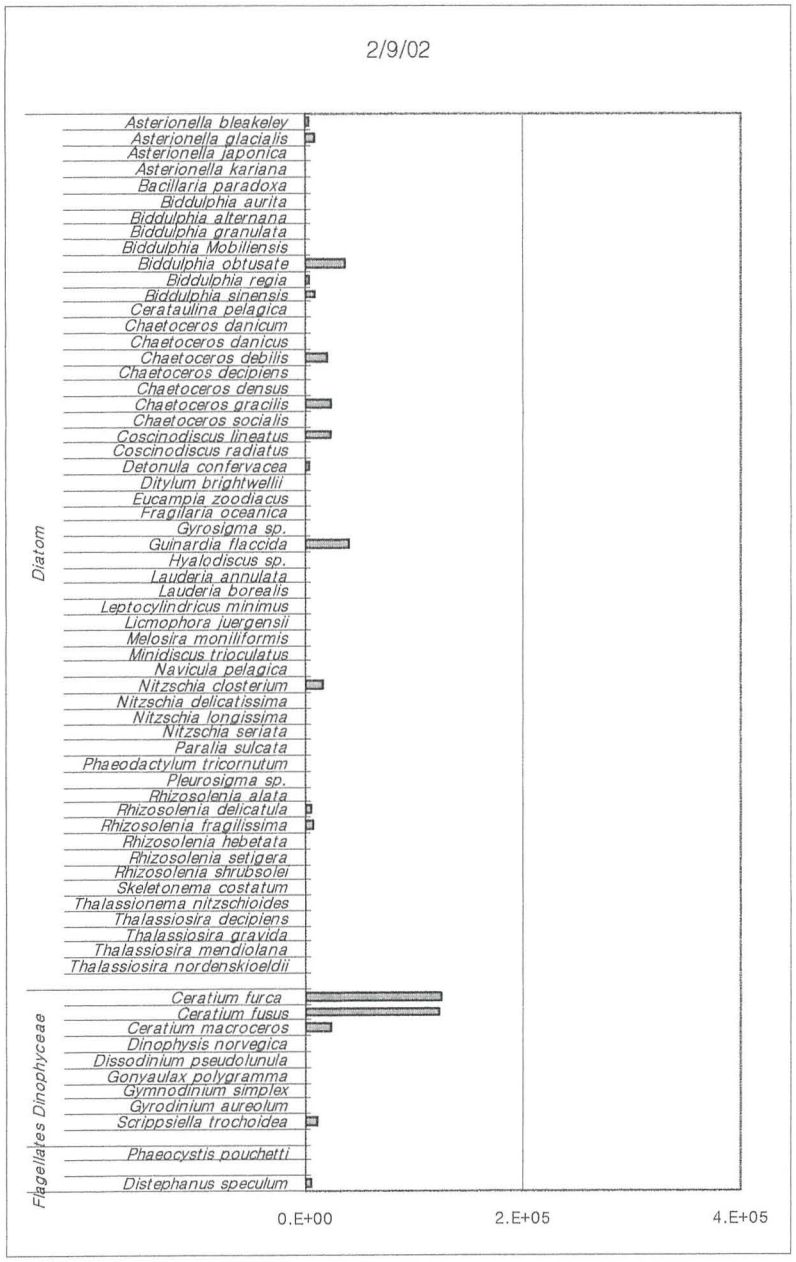

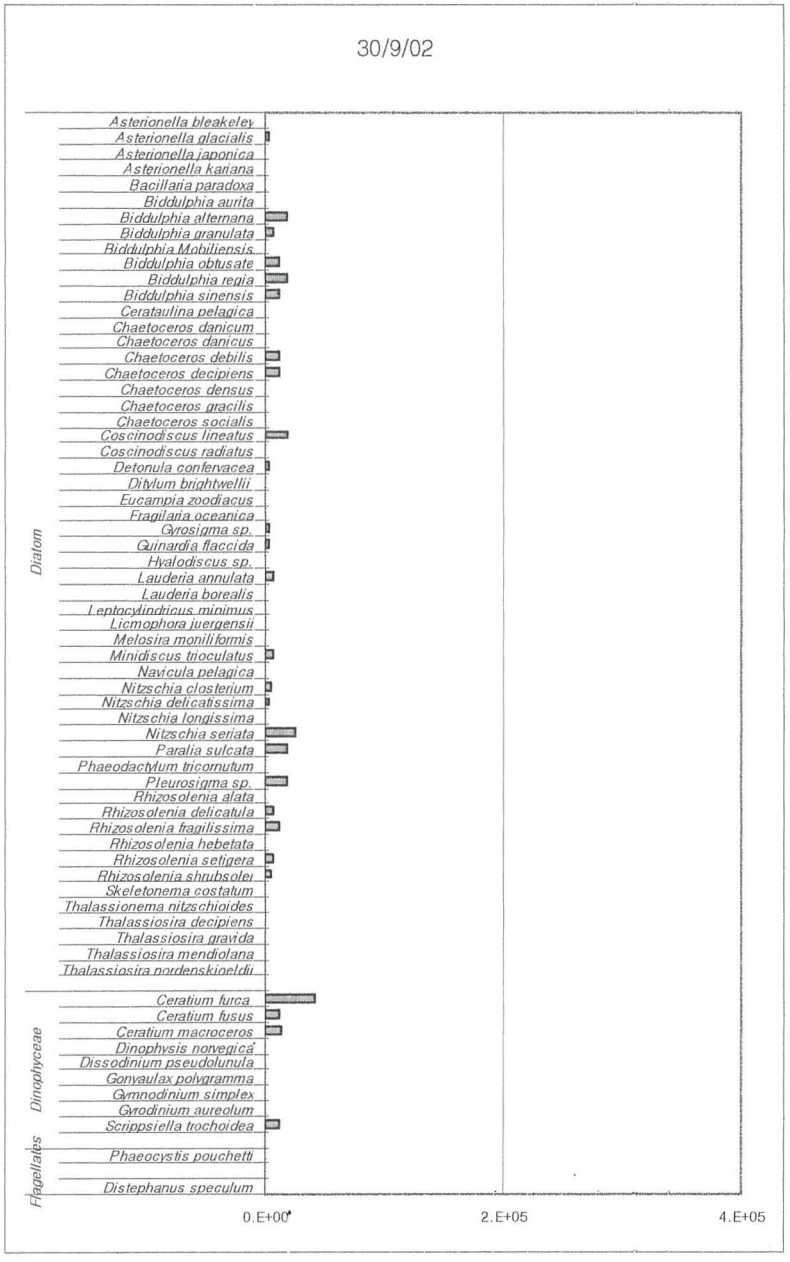

Appendix A-1 Menai Strait Taxonomic data (No. of cells l^{-1})

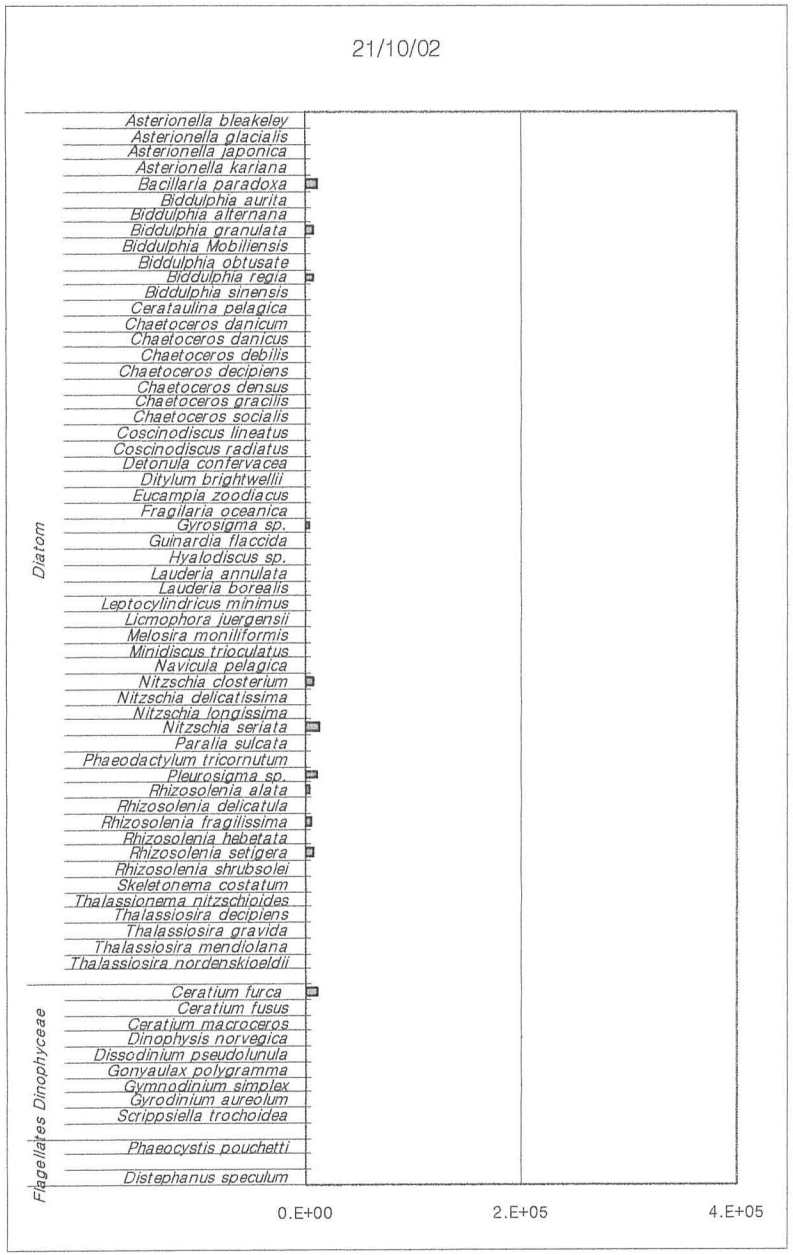

Appendix A-2 Clyde Sea Taxonomic data (No. of cells l^{-1}) 23-April-2001

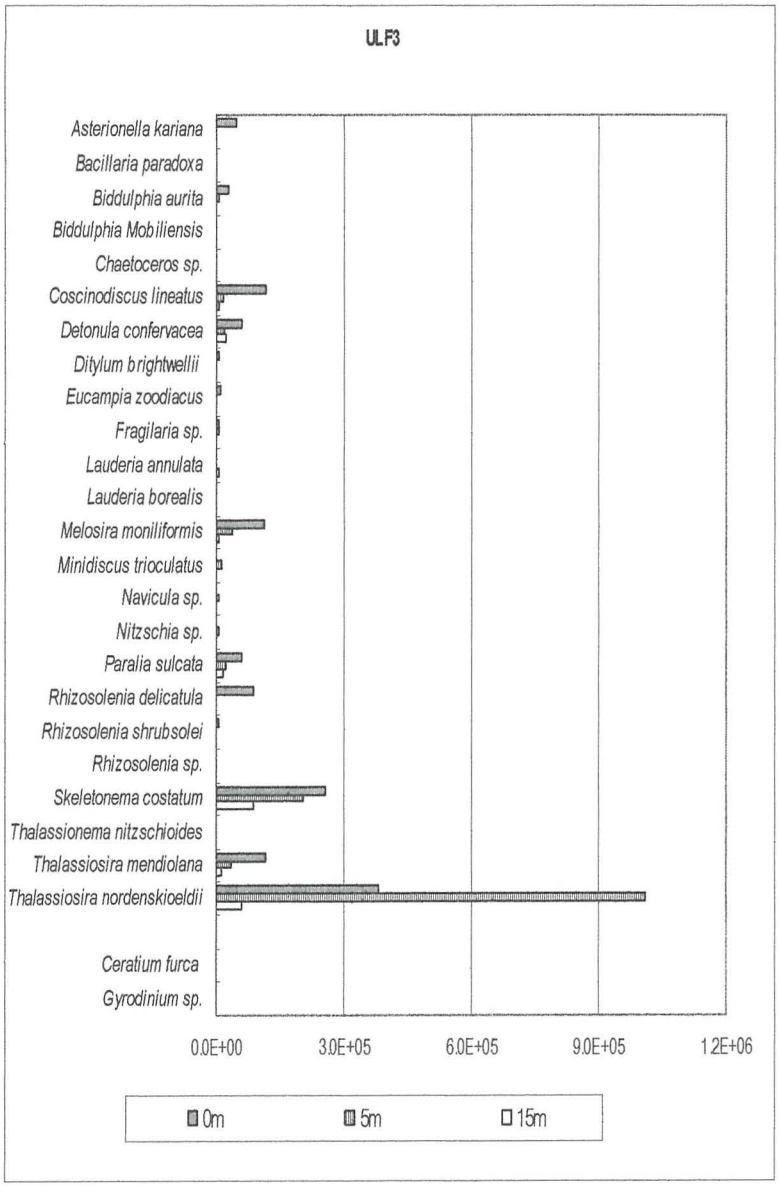

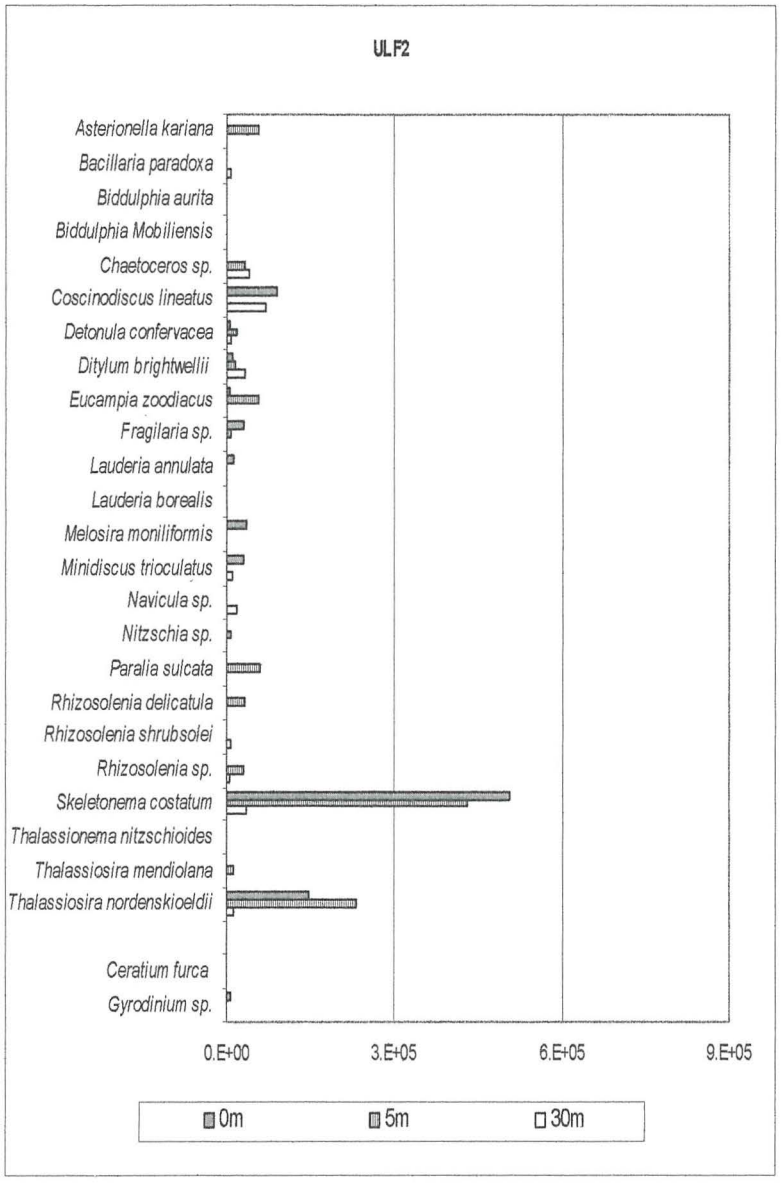

Appendix A-2 Clyde Sea Taxonomic data (No. of cells l^{-1}) 23-April-2001

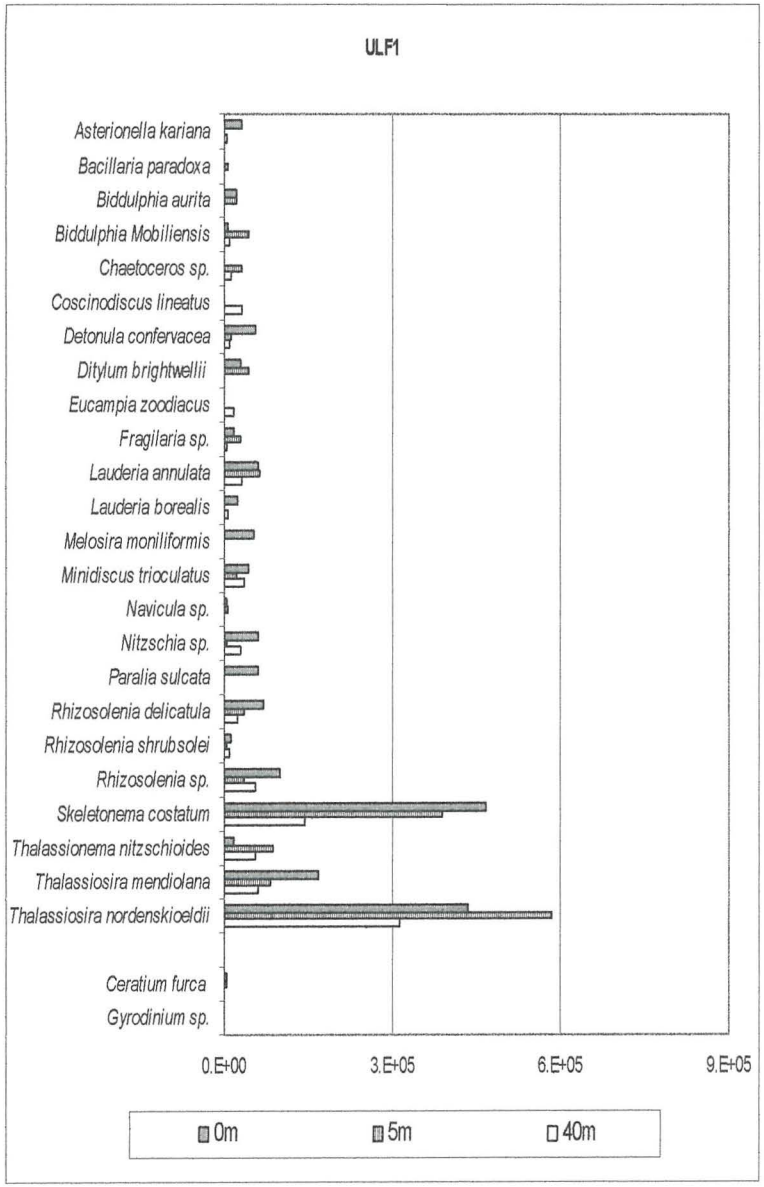

Appendix A-2 Clyde Sea Taxonomic data (No. of cells l^{-1}) 24-April-2001

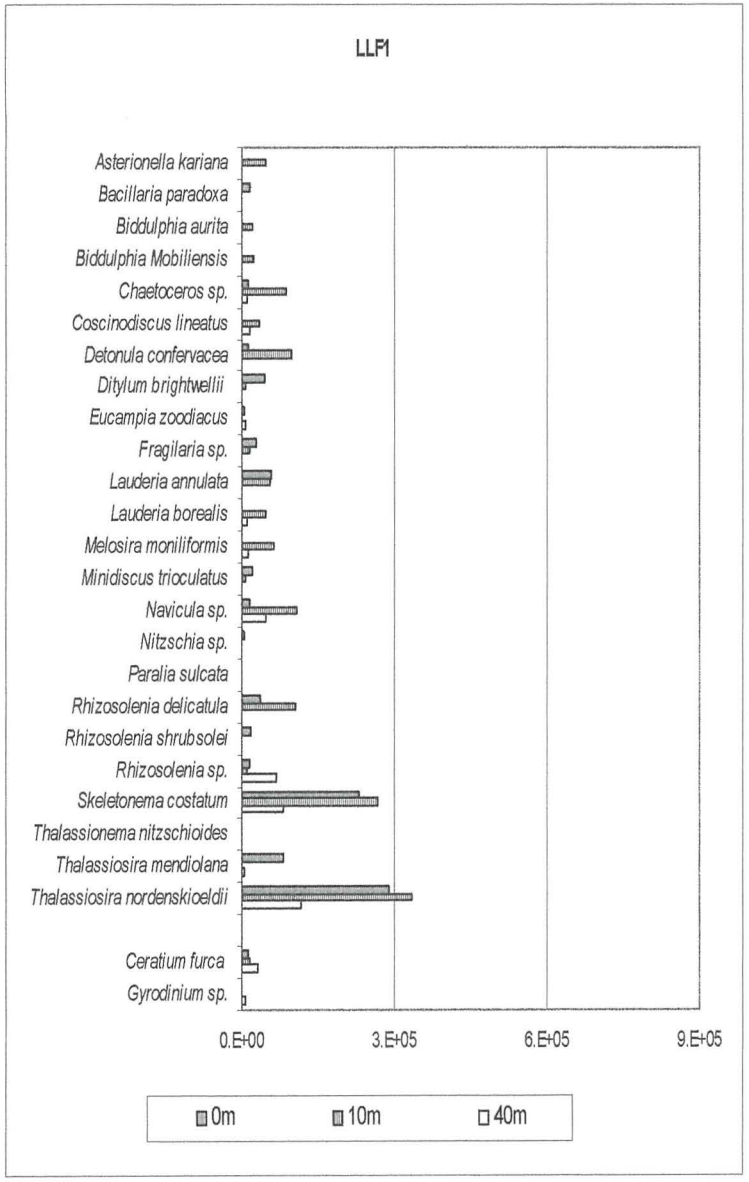

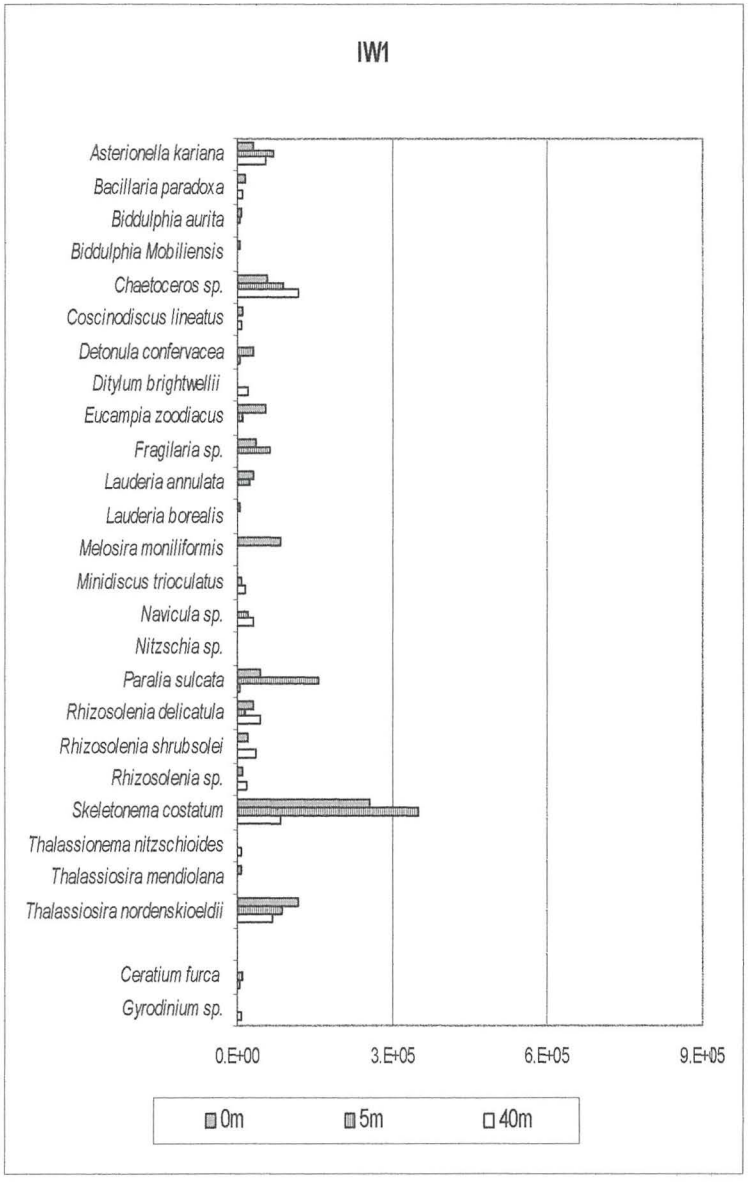

Appendix A-2 Clyde Sea Taxonomic data (No. of cells l^{-1}) 24-April-2001

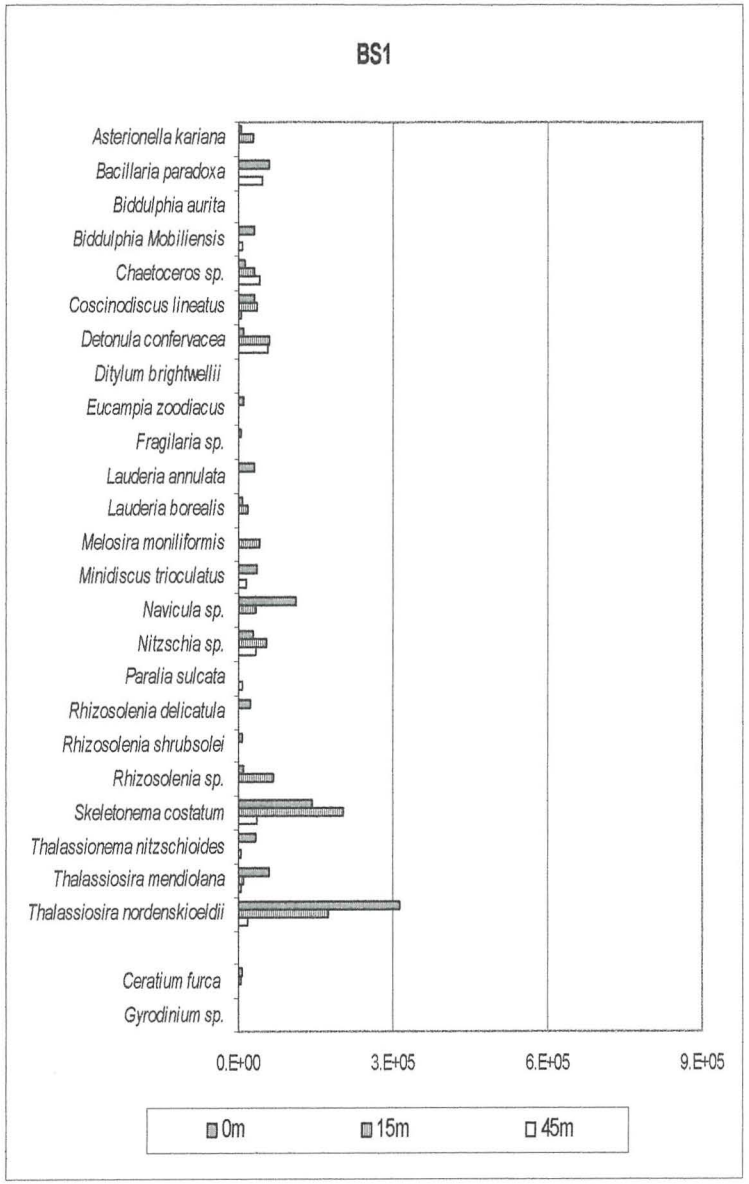

Appendix A-2 Clyde Sea Taxonomic data (No. of cells l^{-1}) 25-April-2001

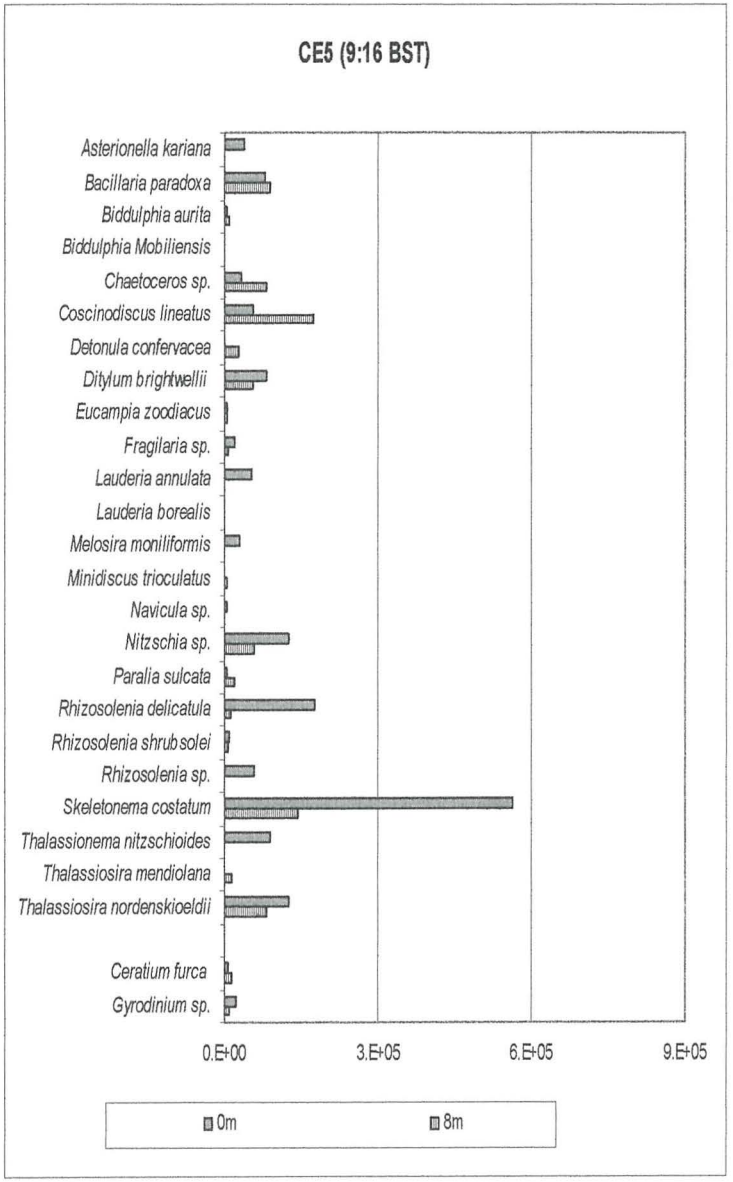

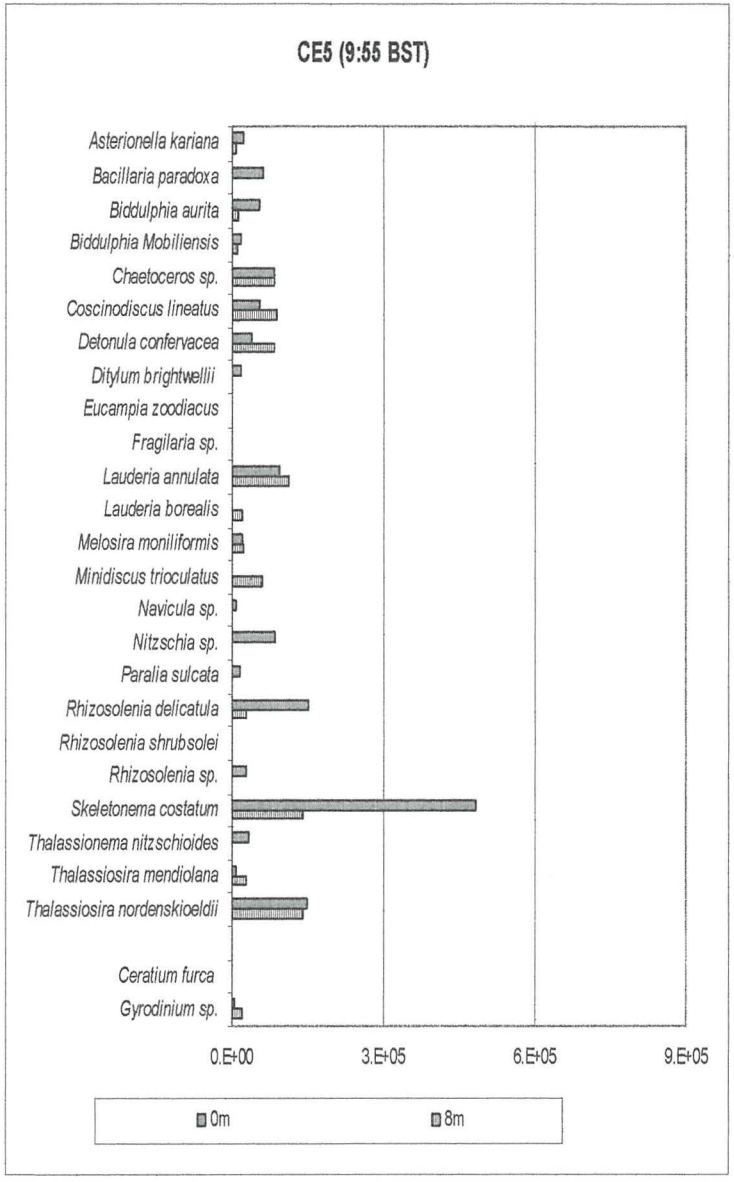

Appendix A-2 Clyde Sea Taxonomic data (No. of cells l^{-1}) 25-April-2001

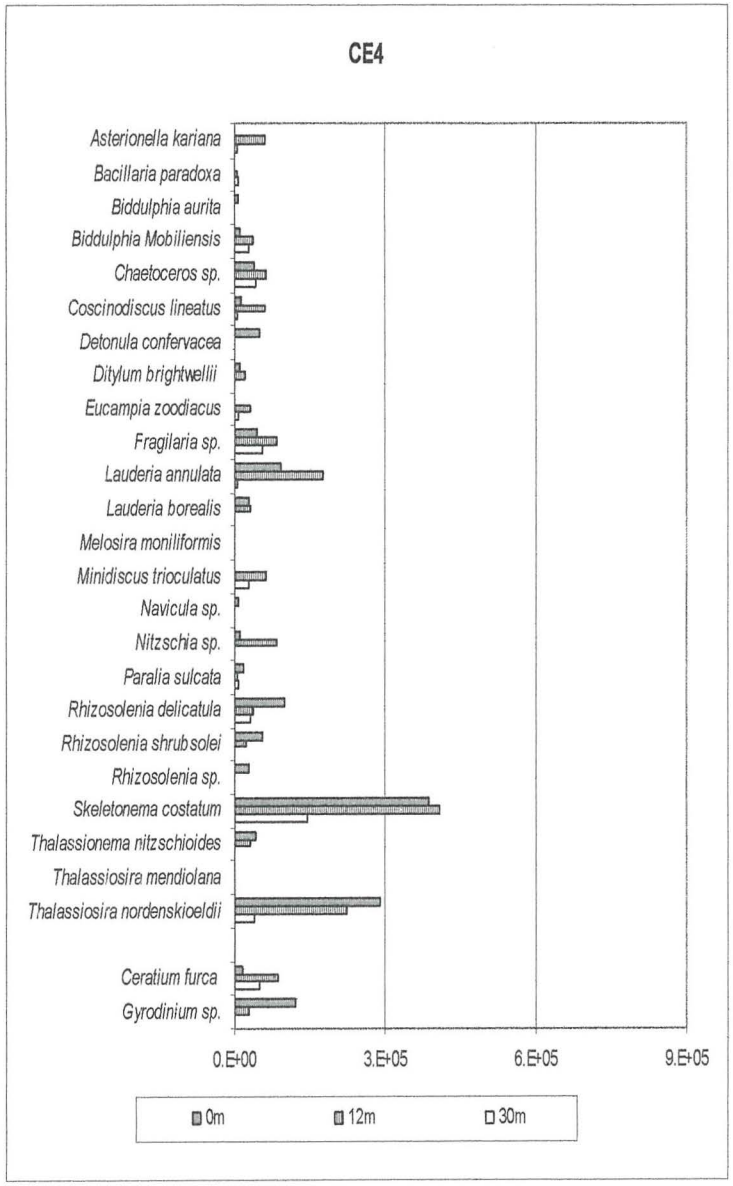

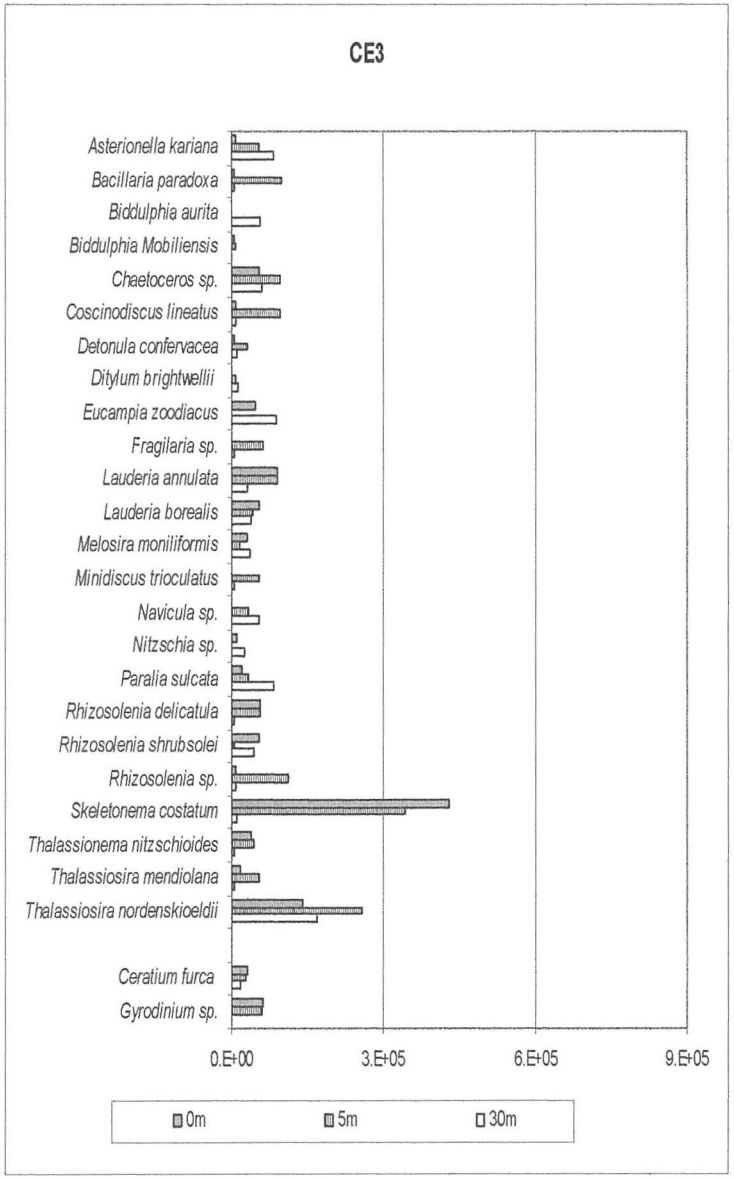

Appendix A-2 Clyde Sea Taxonomic data (No. of cells l^{-1}) 25-April-2001

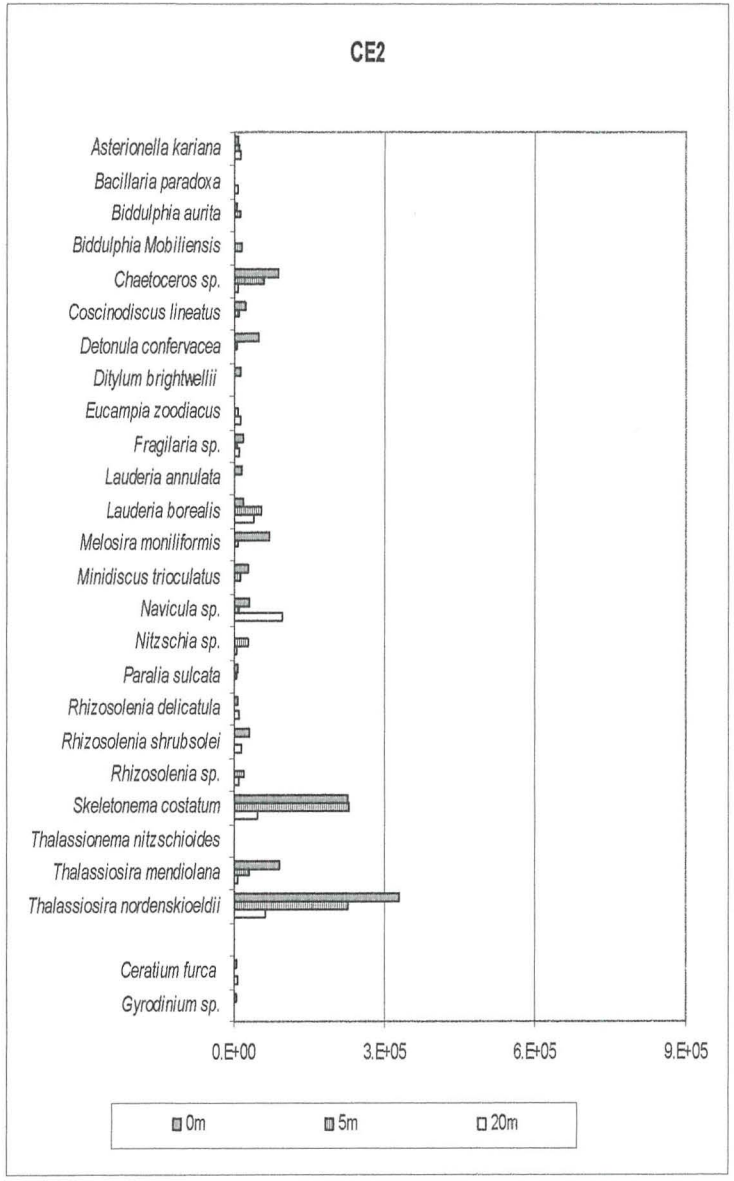

Appendix A-2 Clyde Sea Taxonomic data (No. of cells l^{-1}) 26-April-2001

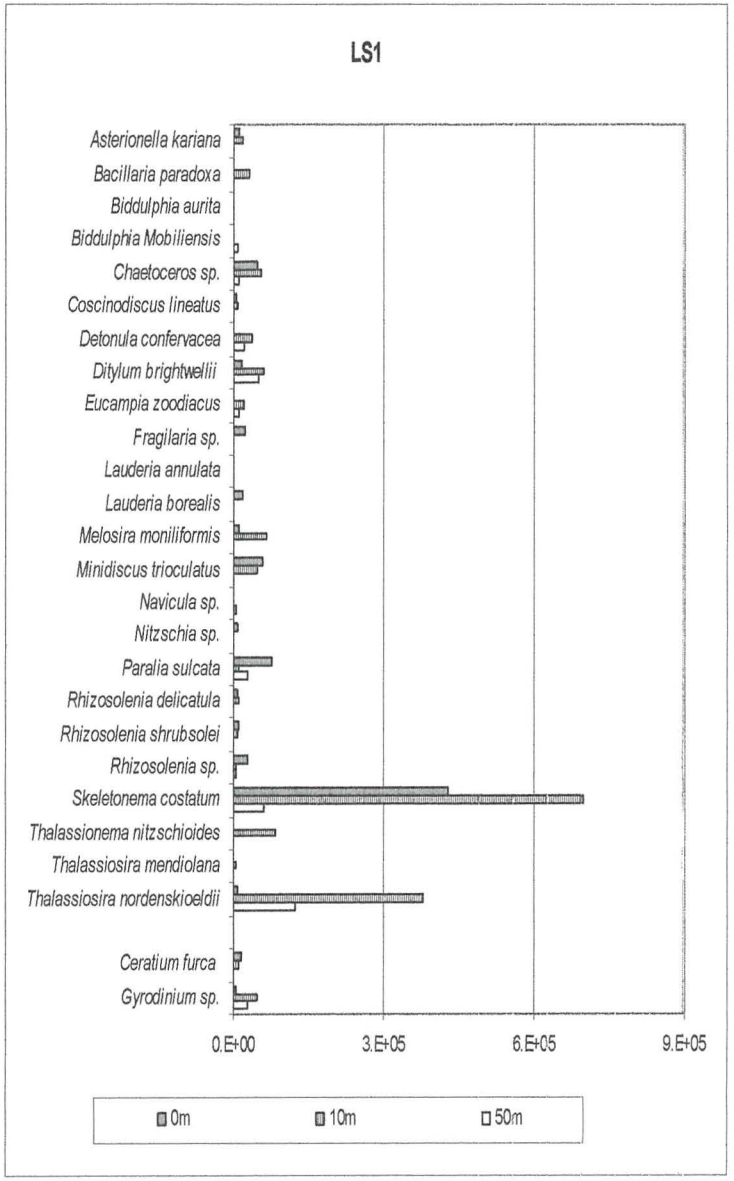

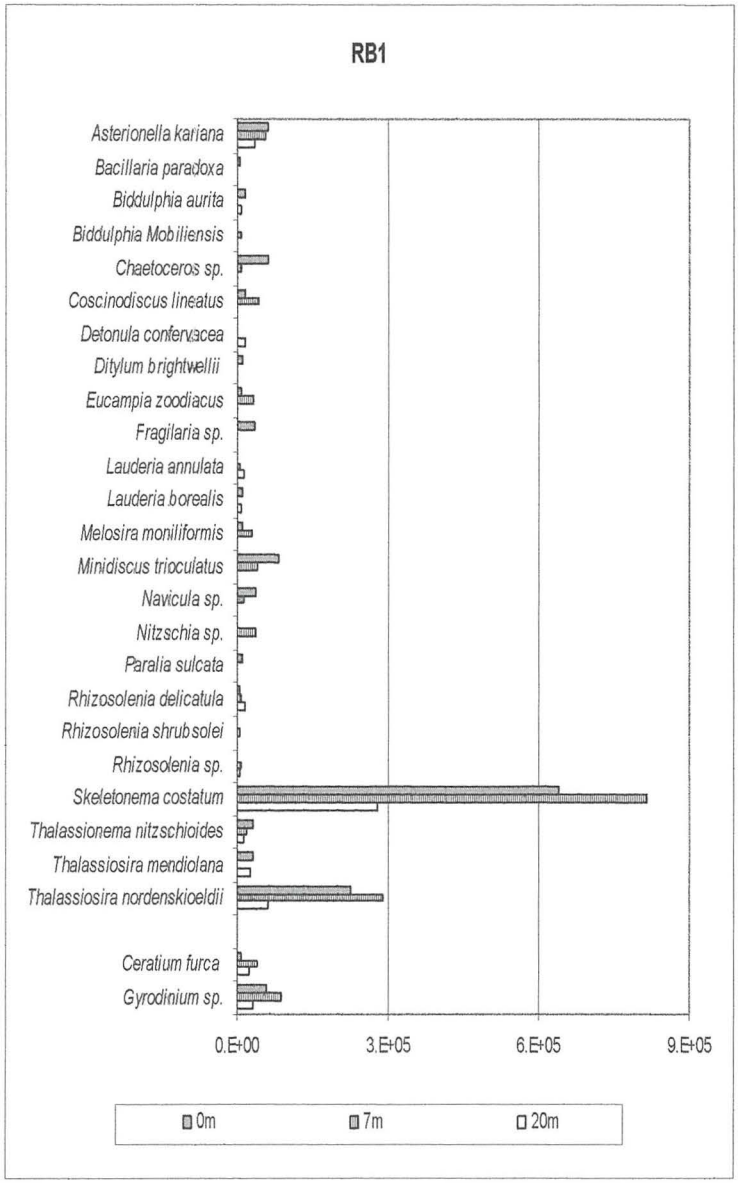

Appendix A-2 Clyde Sea Taxonomic data (No. of cells l^{-1}) 26-April-2001

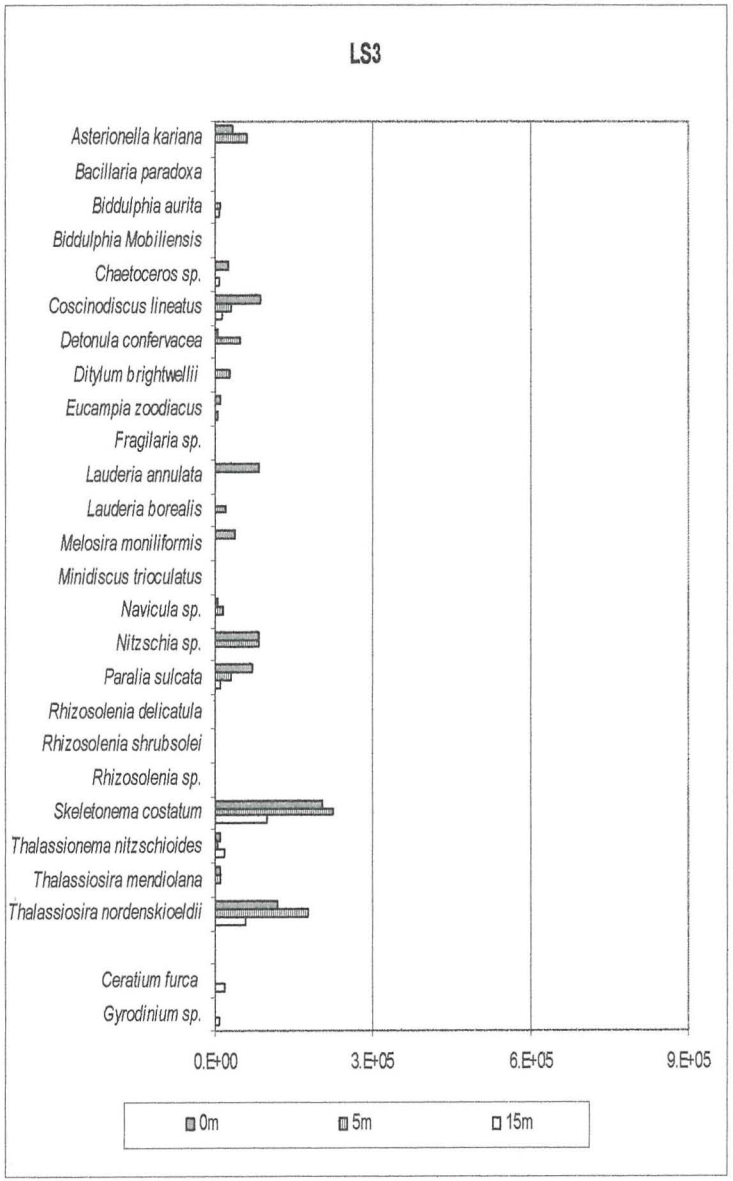

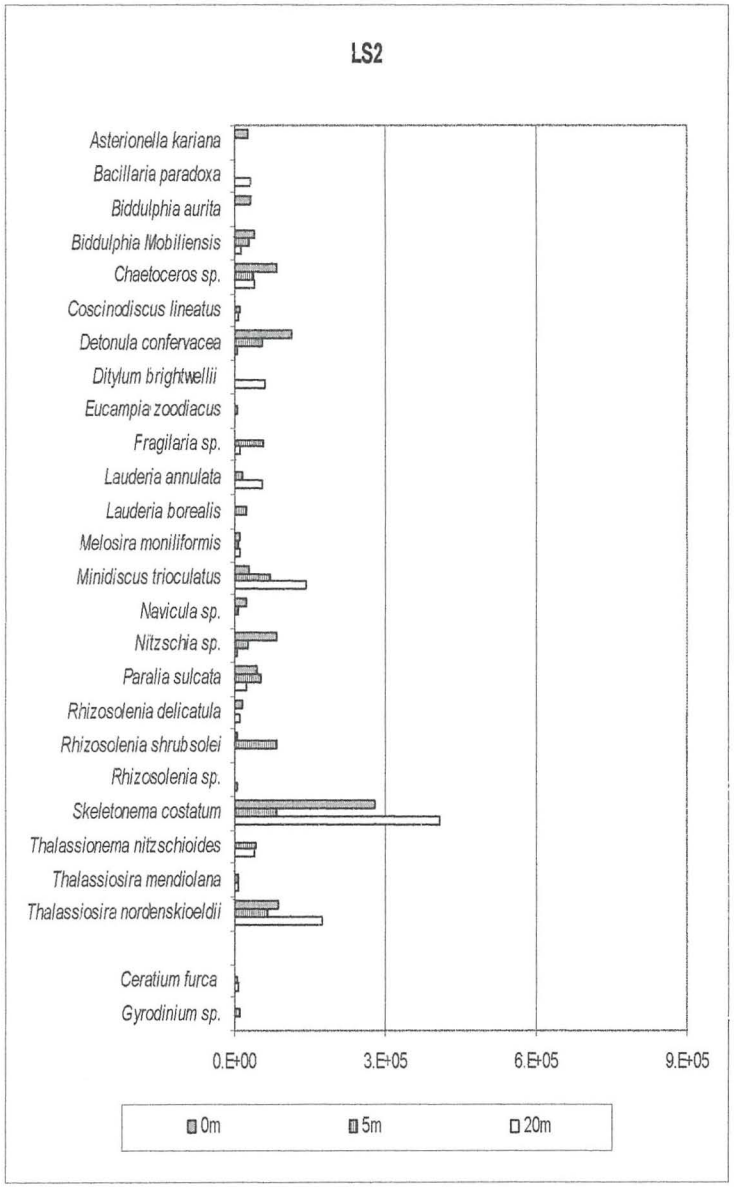

Appendix A-2 Clyde Sea Taxonomic data (No. of cells l^{-1}) 26-April-2001

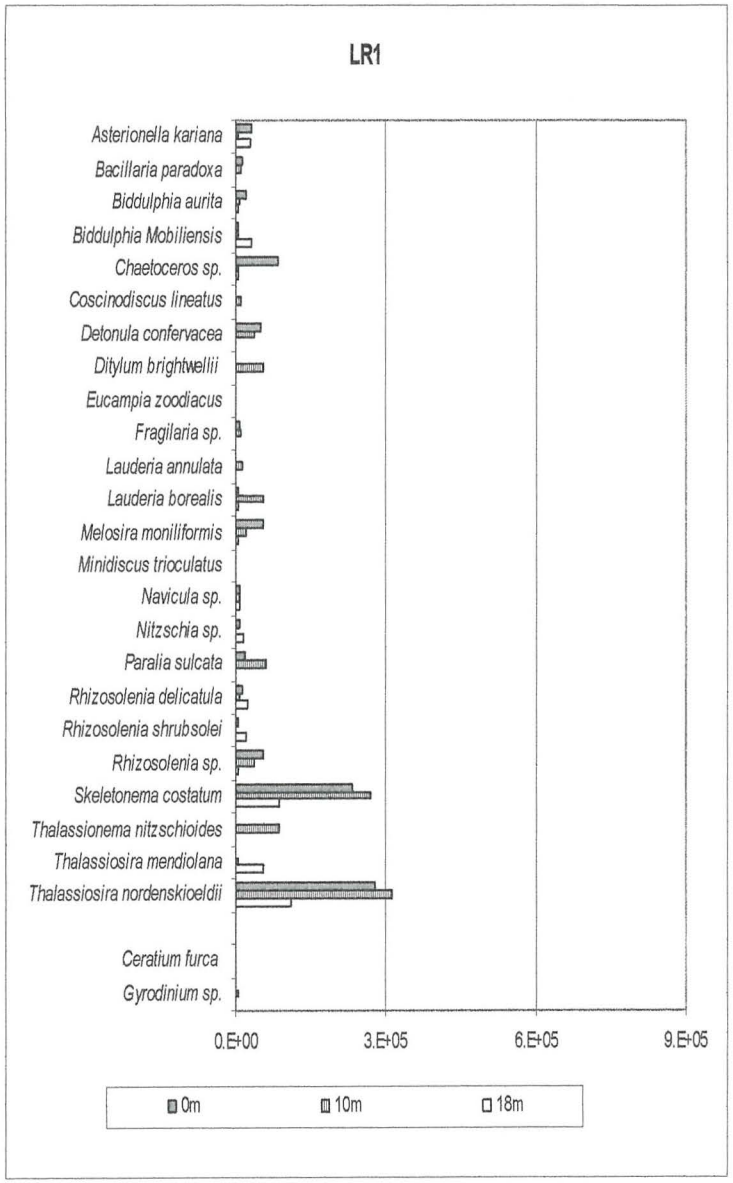

Appendix A-2 Clyde Sea Taxonomic data (No. of cells l^{-1}) 27-April-2001

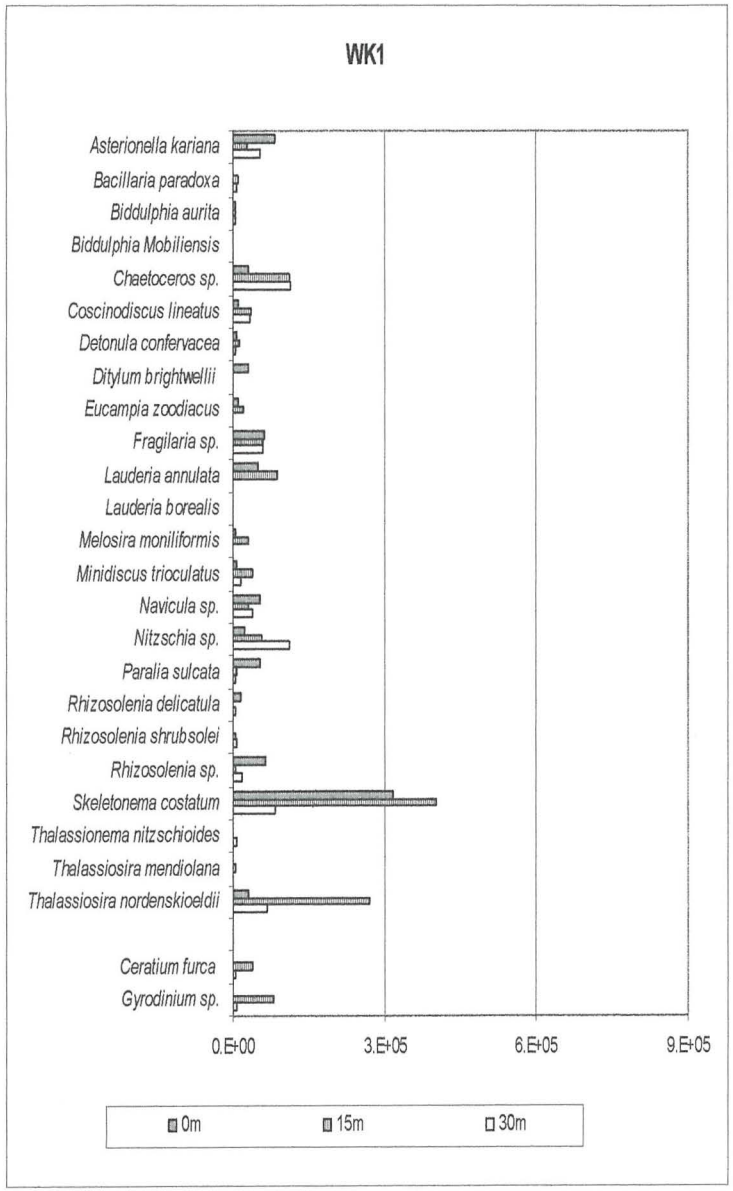

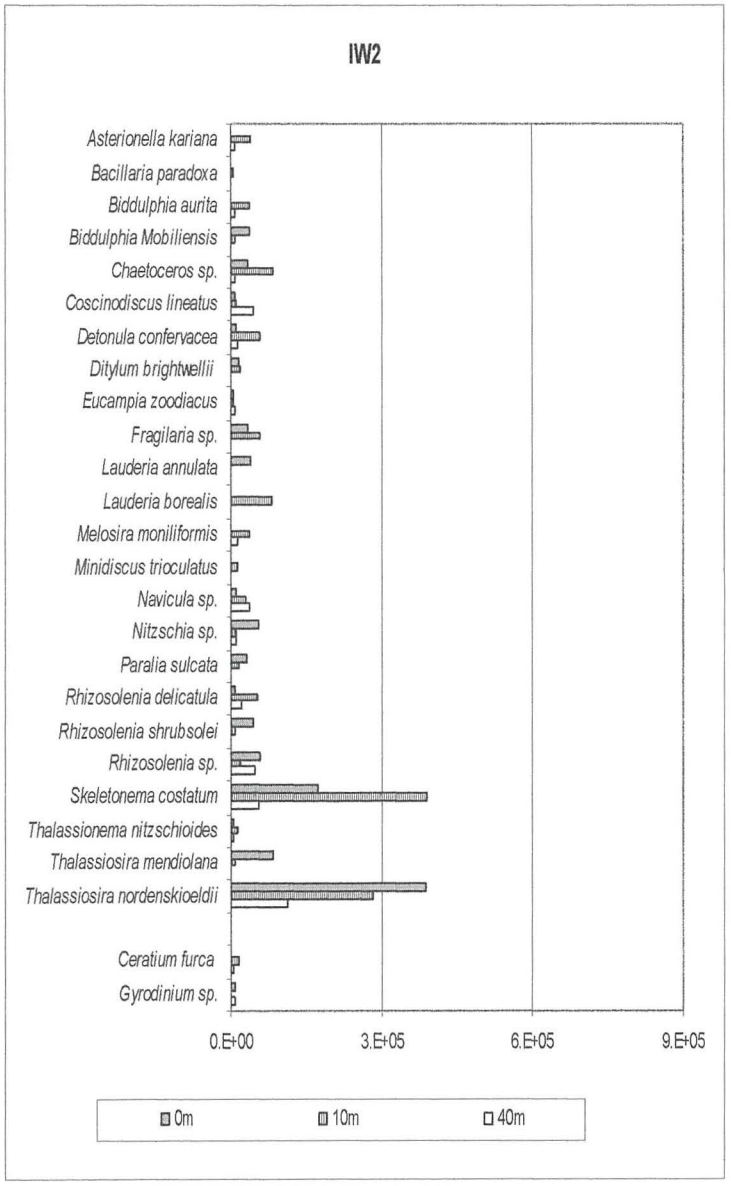

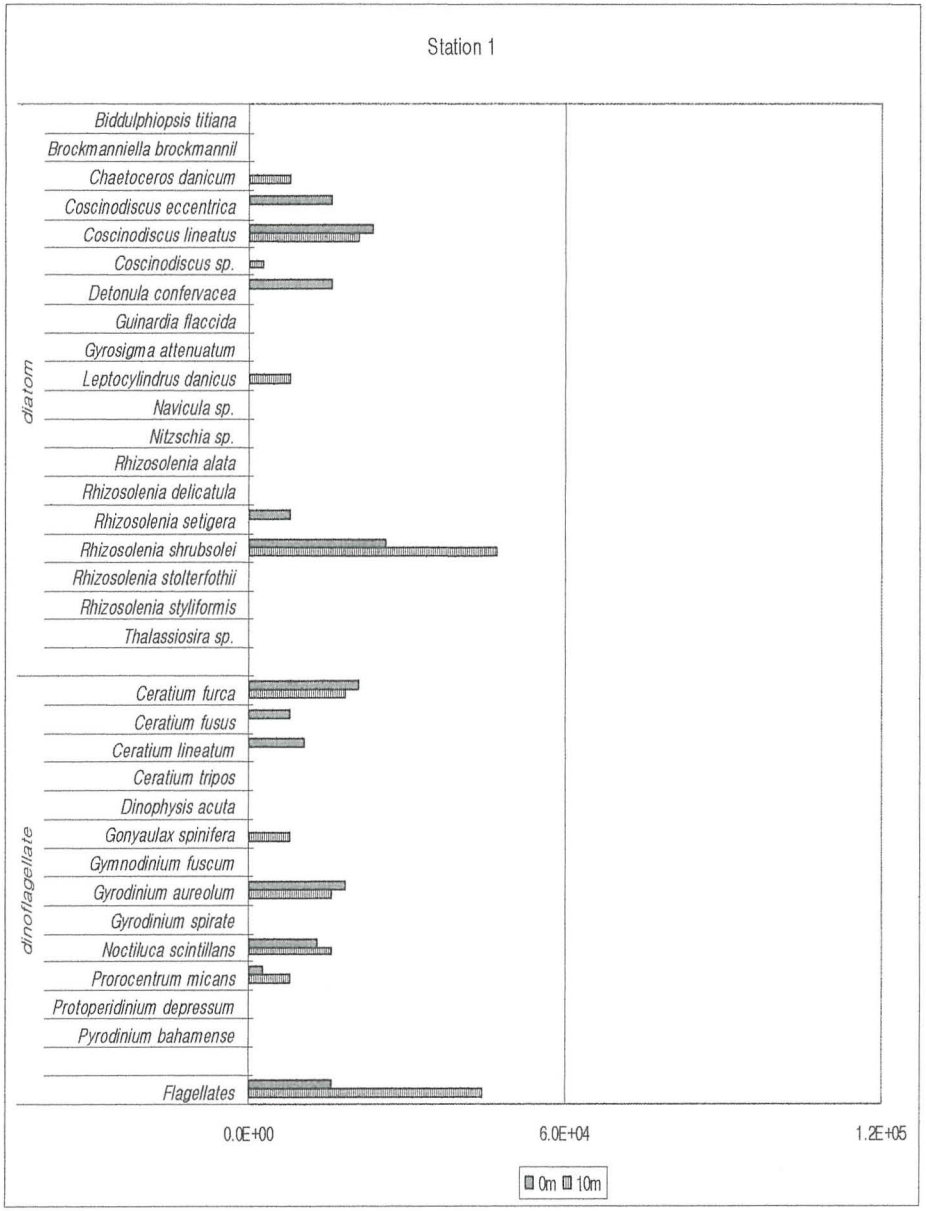
Station 1
Biddulphiopsis titiana
Brockmanniella brockmannil
Chaetoceros danicum
Coscinodiscus eccentrica
Coscinodiscus lineatus
Coscinodiscus sp.
Detonula confervacea
Guinardia flaccida
Gyrosigma attenuatum
Leptocylindrus danicus
Navicula sp.
Nitzschia sp.
Rhizosolenia alata
Rhizosolenia delicatula
Rhizosolenia setigera
Rhizosolenia shrubsolei
Rhizosolenia stolterfothii
Rhizosolenia styliformis
Thalassiosira sp.
diatom
Ceratium furca
Ceratium fusus
Ceratium lineatum
Ceratium tripos
Dinophysis acuta
Gonyaulax spinifera
Gymnodinium fuscum
Gyrodinium aureolum
Gyrodinium spirate
Noctiluca scintillans
Prorocentrum micans
Protoperidinium depressum
Pyrodinium bahamense
dinoflagellate
Flagellates
0.0E+00
6.0E+04
1.2E+05
0m
10m

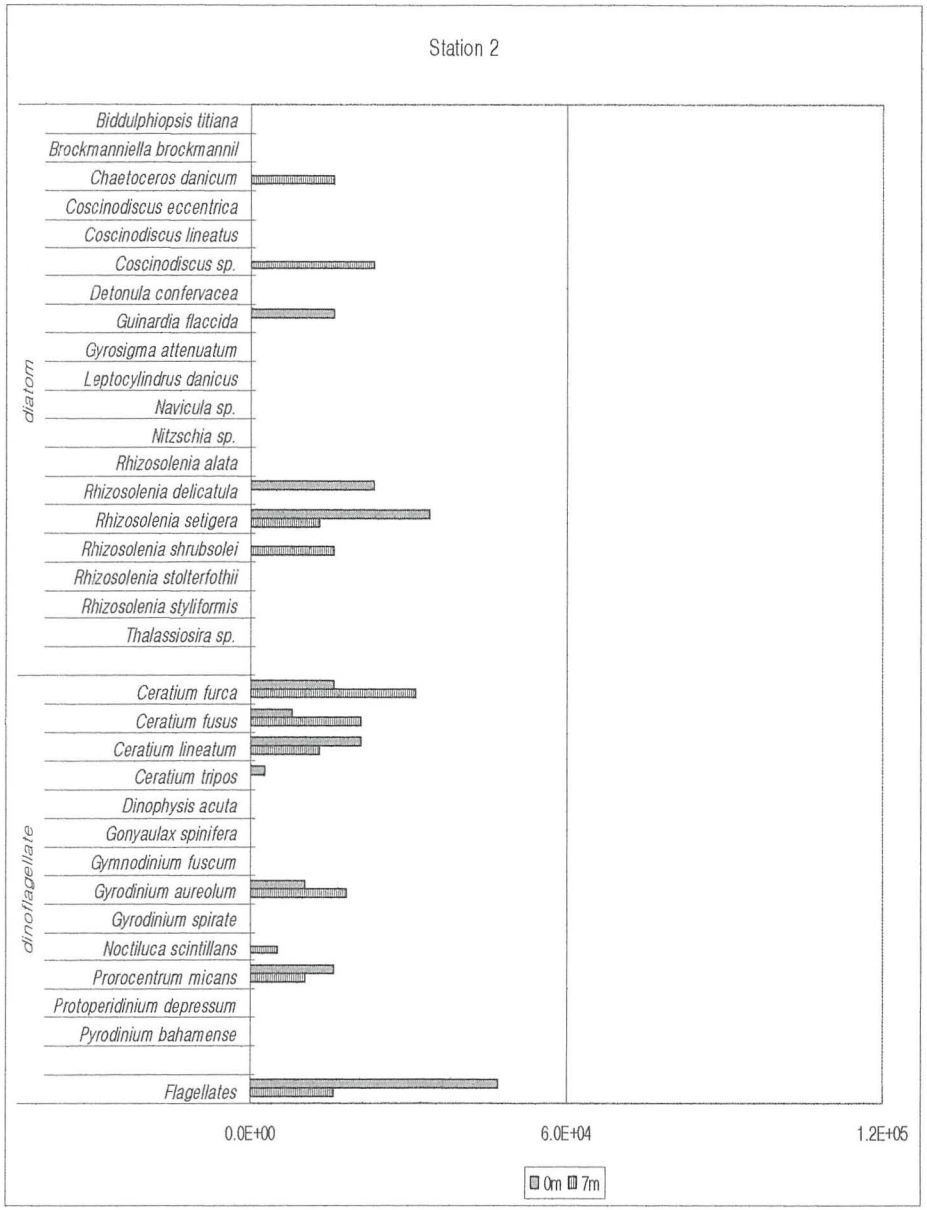
Station 2
Biddulphiopsis titiana
Brockmanniella brockmannil
Chaetoceros danicum
Coscinodiscus eccentrica
Coscinodiscus lineatus
Coscinodiscus sp.
Detonula confervacea
Guinardia flaccida
Gyrosigma attenuatum
Leptocylindrus danicus
Navicula sp.
Nitzschia sp.
Rhizosolenia alata
Rhizosolenia delicatula
Rhizosolenia setigera
Rhizosolenia shrubsolei
Rhizosolenia stolterfothii
Rhizosolenia styliformis
Thalassiosira sp.
diatom
Ceratium furca
Ceratium fusus
Ceratium lineatum
Ceratium tripos
Dinophysis acuta
Gonyaulax spinifera
Gymnodinium fuscum
Gyrodinium aureolum
Gyrodinium spirate
Noctiluca scintillans
Prorocentrum micans
Protoperidinium depressum
Pyrodinium bahamense
dinoflagellate
Flagellates
0.0E+00
6.0E+04
1.2E+05
0m
7m

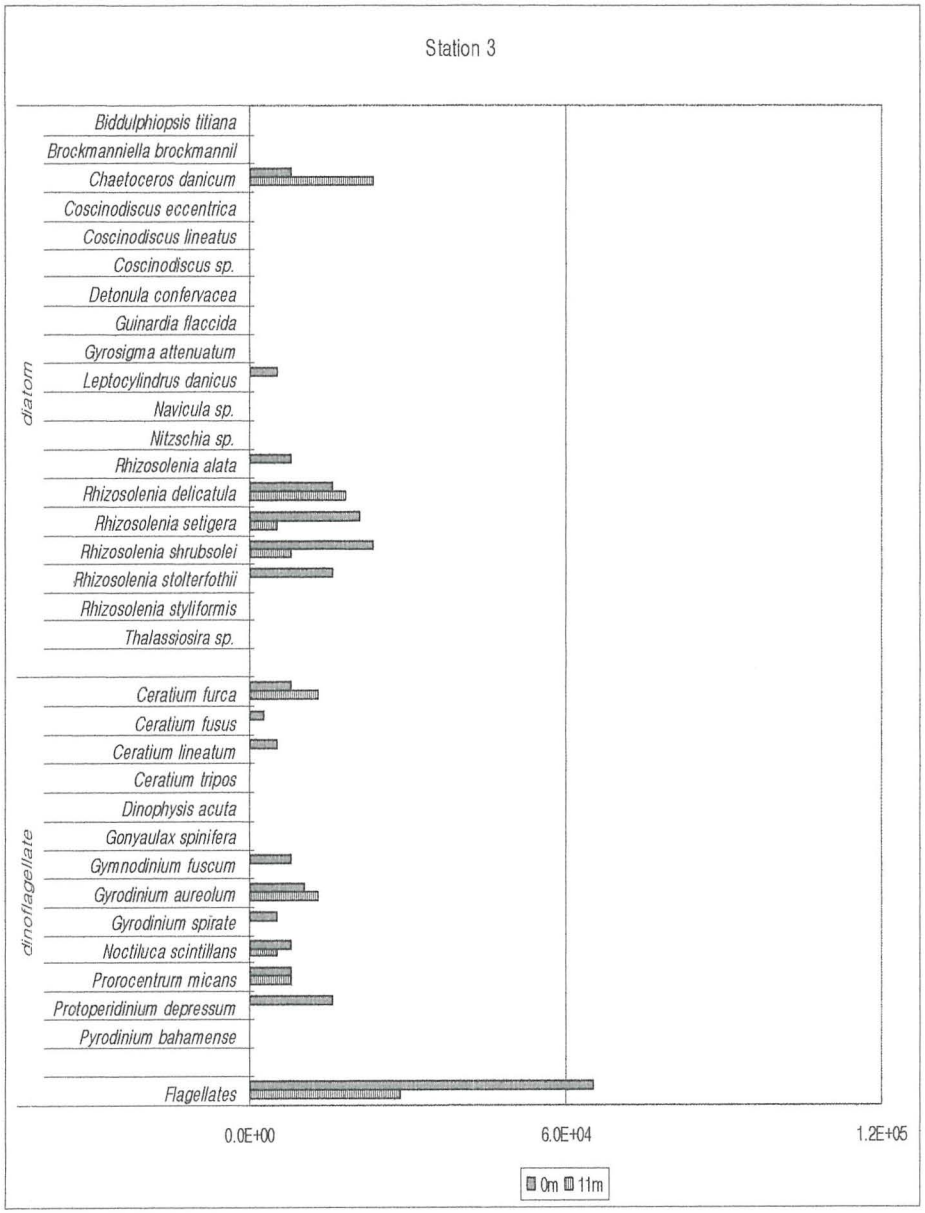
Station 3
diatom
Biddulphiopsis titiana
Brockmanniella brockmannil
Chaetoceros danicum
Coscinodiscus eccentrica
Coscinodiscus lineatus
Coscinodiscus sp.
Detonula confervacea
Guinardia flaccida
Gyrosigma attenuatum
Leptocylindrus danicus
Navicula sp.
Nitzschia sp.
Rhizosolenia alata
Rhizosolenia delicatula
Rhizosolenia setigera
Rhizosolenia shrubsolei
Rhizosolenia stolterfothii
Rhizosolenia styliformis
Thalassiosira sp.
dinoflagellate
Ceratium furca
Ceratium fusus
Ceratium lineatum
Ceratium tripos
Dinophysis acuta
Gonyaulax spinifera
Gymnodinium fuscum
Gyrodinium aureolum
Gyrodinium spirate
Noctiluca scintillans
Prorocentrum micans
Protoperidinium depressum
Pyrodinium bahamense
Flagellates
0.0E+00
6.0E+04
1.2E+05
0m
11m

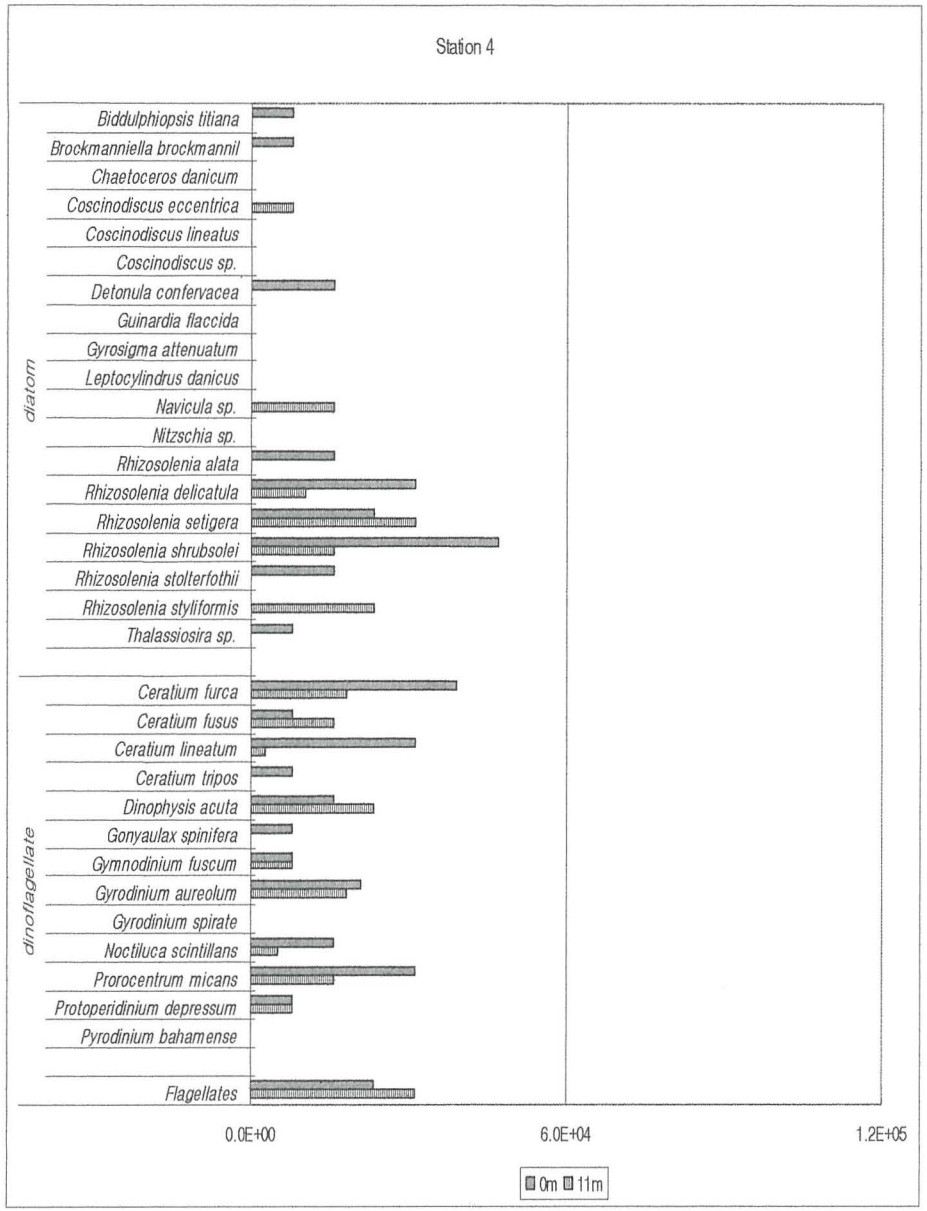
Station 4
diatom
Biddulphiopsis titiana
Brockmanniella brockmannil
Chaetoceros danicum
Coscinodiscus eccentrica
Coscinodiscus lineatus
Coscinodiscus sp.
Detonula confervacea
Guinardia flaccida
Gyrosigma attenuatum
Leptocylindrus danicus
Navicula sp.
Nitzschia sp.
Rhizosolenia alata
Rhizosolenia delicatula
Rhizosolenia setigera
Rhizosolenia shrubsolei
Rhizosolenia stolterfothii
Rhizosolenia styliformis
Thalassiosira sp.
dinoflagellate
Ceratium furca
Ceratium fusus
Ceratium lineatum
Ceratium tripos
Dinophysis acuta
Gonyaulax spinifera
Gymnodinium fuscum
Gyrodinium aureolum
Gyrodinium spirate
Noctiluca scintillans
Prorocentrum micans
Protoperidinium depressum
Pyrodinium bahamense
Flagellates
0.0E+00
6.0E+04
1.2E+05
0m 11m

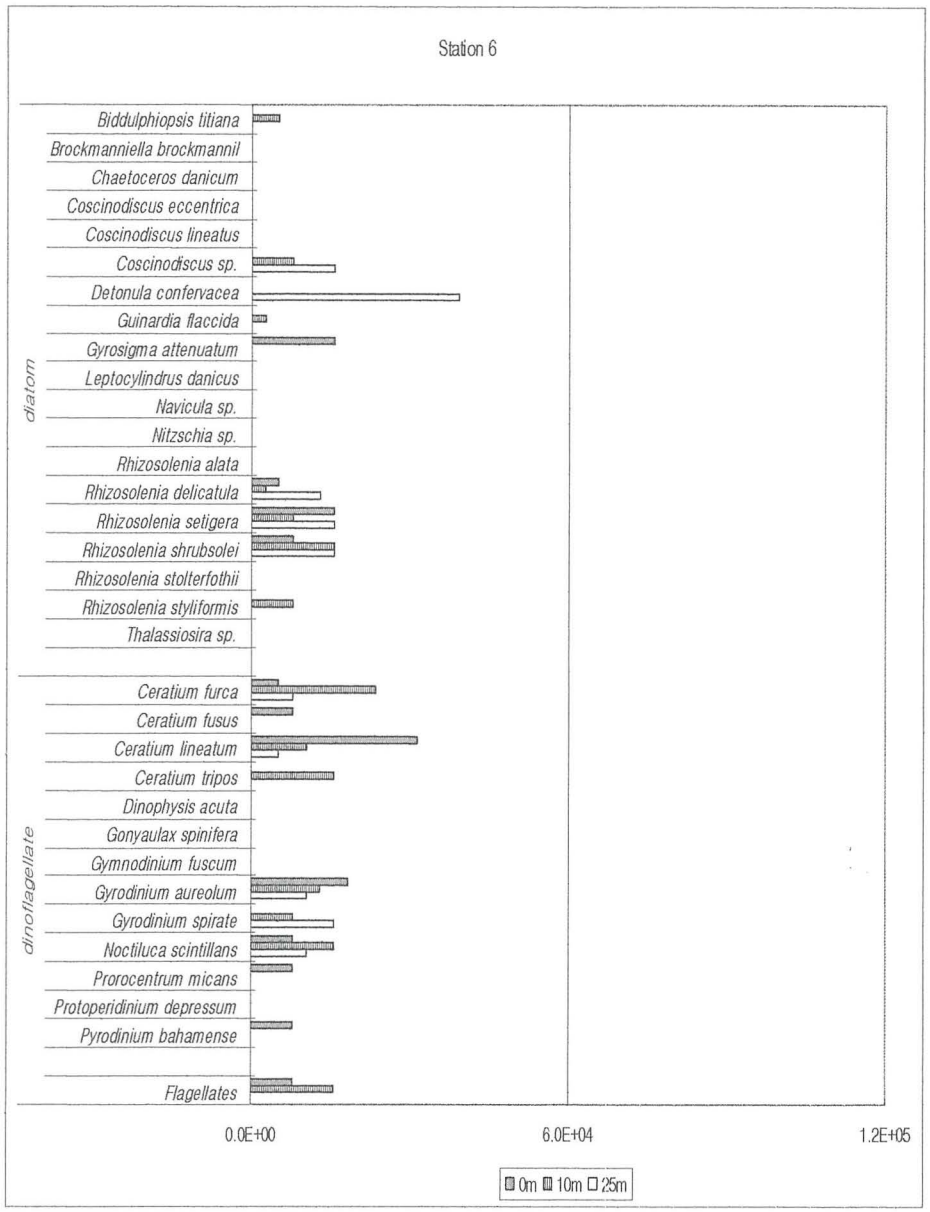
Station 6
diatom
Biddulphiopsis titiana
Brockmanniella brockmannil
Chaetoceros danicum
Coscinodiscus eccentrica
Coscinodiscus lineatus
Coscinodiscus sp.
Detonula confervacea
Guinardia flaccida
Gyrosigma attenuatum
Leptocylindrus danicus
Navicula sp.
Nitzschia sp.
Rhizosolenia alata
Rhizosolenia delicatula
Rhizosolenia setigera
Rhizosolenia shrubsolei
Rhizosolenia stolterfothii
Rhizosolenia styliformis
Thalassiosira sp.
dinoflagellate
Ceratium furca
Ceratium fusus
Ceratium lineatum
Ceratium tripos
Dinophysis acuta
Gonyaulax spinifera
Gymnodinium fuscum
Gyrodinium aureolum
Gyrodinium spirate
Noctiluca scintillans
Prorocentrum micans
Protoperidinium depressum
Pyrodinium bahamense
Flagellates
0.0E+00
6.0E+04
1.2E+05
0m 10m 25m

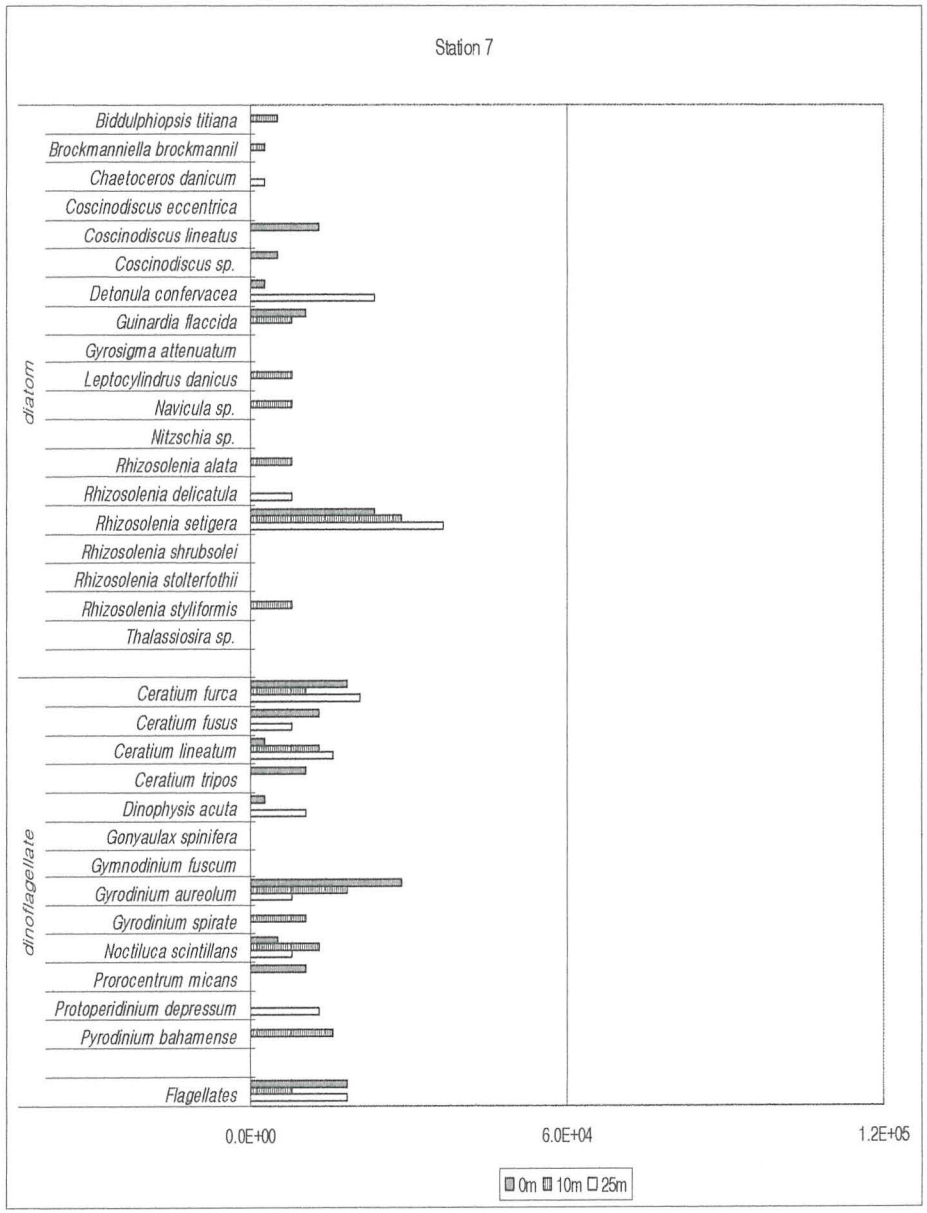
Station 7
diatom
Biddulphiopsis titiana
Brockmanniella brockmannil
Chaetoceros danicum
Coscinodiscus eccentrica
Coscinodiscus lineatus
Coscinodiscus sp.
Detonula confervacea
Guinardia flaccida
Gyrosigma attenuatum
Leptocylindrus danicus
Navicula sp.
Nitzschia sp.
Rhizosolenia alata
Rhizosolenia delicatula
Rhizosolenia setigera
Rhizosolenia shrubsolei
Rhizosolenia stolterfothii
Rhizosolenia styliformis
Thalassiosira sp.
dinoflagellate
Ceratium furca
Ceratium fusus
Ceratium lineatum
Ceratium tripos
Dinophysis acuta
Gonyaulax spinifera
Gymnodinium fuscum
Gyrodinium aureolum
Gyrodinium spirate
Noctiluca scintillans
Prorocentrum micans
Protoperidinium depressum
Pyrodinium bahamense
Flagellates
0.0E+00
6.0E+04
1.2E+05
0m 10m 25m

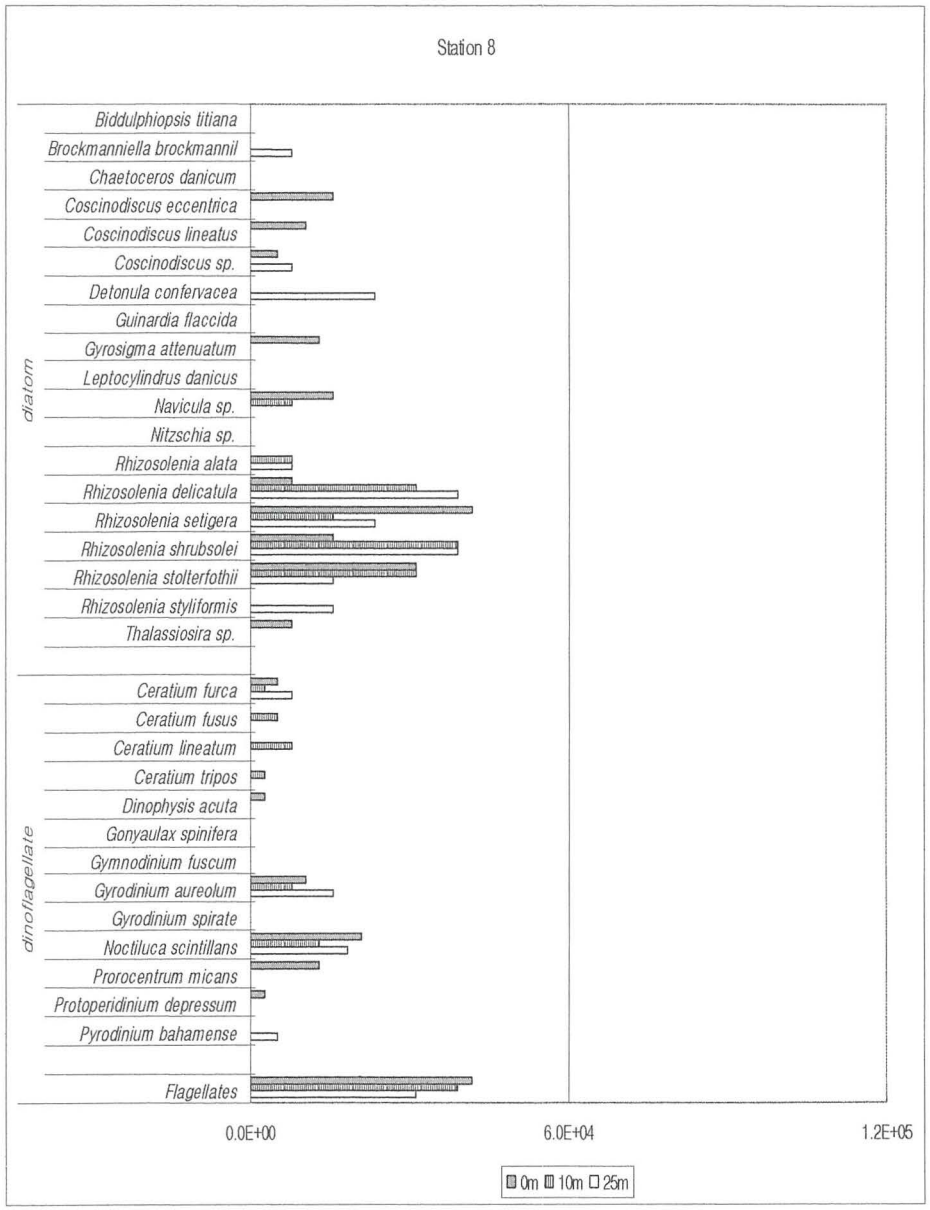
Station 8
diatom
Biddulphiopsis titiana
Brockmanniella brockmannil
Chaetoceros danicum
Coscinodiscus eccentrica
Coscinodiscus lineatus
Coscinodiscus sp.
Detonula confervacea
Guinardia flaccida
Gyrosigma attenuatum
Leptocylindrus danicus
Navicula sp.
Nitzschia sp.
Rhizosolenia alata
Rhizosolenia delicatula
Rhizosolenia setigera
Rhizosolenia shrubsolei
Rhizosolenia stolterfothii
Rhizosolenia styliformis
Thalassiosira sp.
dinoflagellate
Ceratium furca
Ceratium fusus
Ceratium lineatum
Ceratium tripos
Dinophysis acuta
Gonyaulax spinifera
Gymnodinium fuscum
Gyrodinium aureolum
Gyrodinium spirate
Noctiluca scintillans
Prorocentrum micans
Protoperidinium depressum
Pyrodinium bahamense
Flagellates
0.0E+00
6.0E+04
1.2E+05
0m 10m 25m

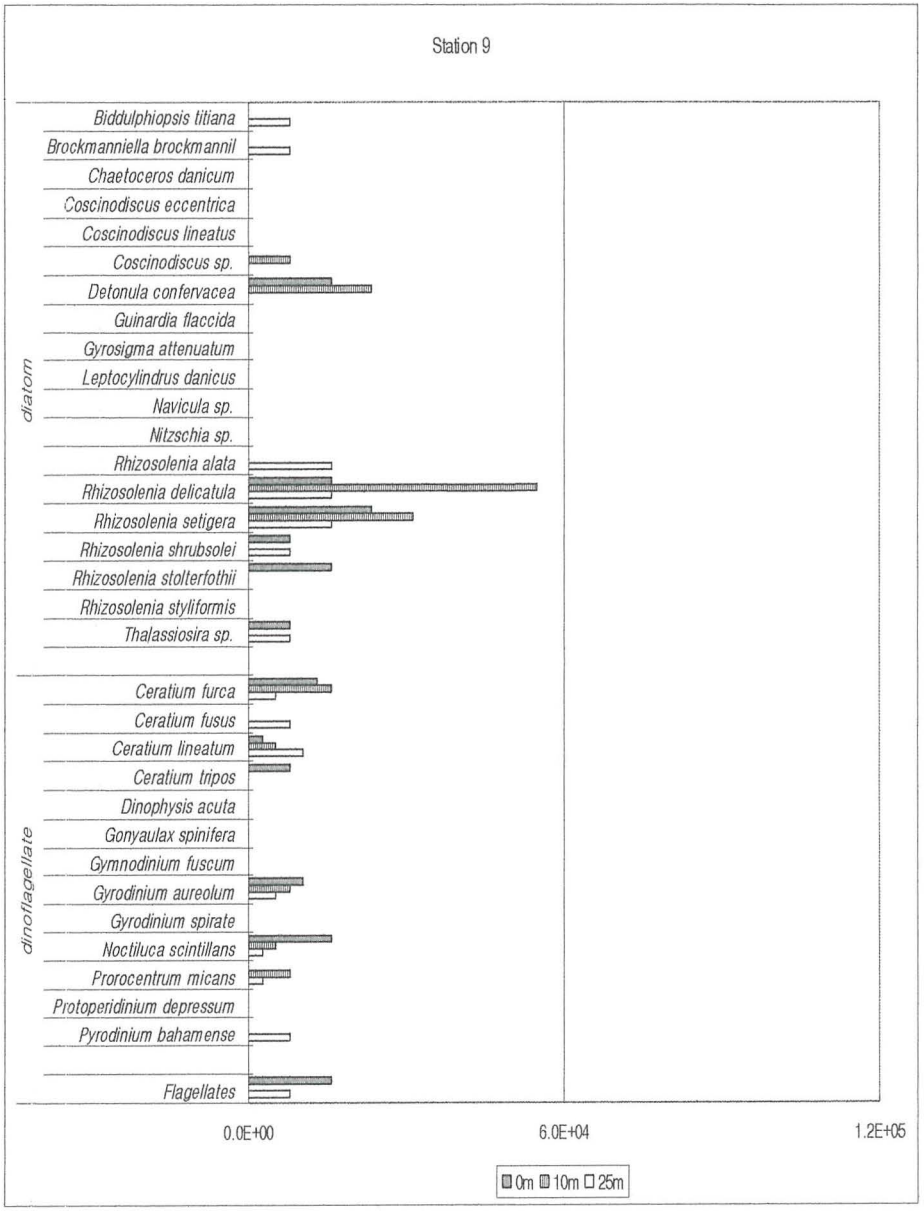
Station 9
diatom
Biddulphiopsis titiana
Brockmanniella brockmannil
Chaetoceros danicum
Coscinodiscus eccentrica
Coscinodiscus lineatus
Coscinodiscus sp.
Detonula confervacea
Guinardia flaccida
Gyrosigma attenuatum
Leptocylindrus danicus
Navicula sp.
Nitzschia sp.
Rhizosolenia alata
Rhizosolenia delicatula
Rhizosolenia setigera
Rhizosolenia shrubsolei
Rhizosolenia stolterfothii
Rhizosolenia styliformis
Thalassiosira sp.
dinoflagellate
Ceratium furca
Ceratium fusus
Ceratium lineatum
Ceratium tripos
Dinophysis acuta
Gonyaulax spinifera
Gymnodinium fuscum
Gyrodinium aureolum
Gyrodinium spirate
Noctiluca scintillans
Prorocentrum micans
Protoperidinium depressum
Pyrodinium bahamense
Flagellates
0.0E+00
6.0E+04
1.2E+05
0m 10m 25m

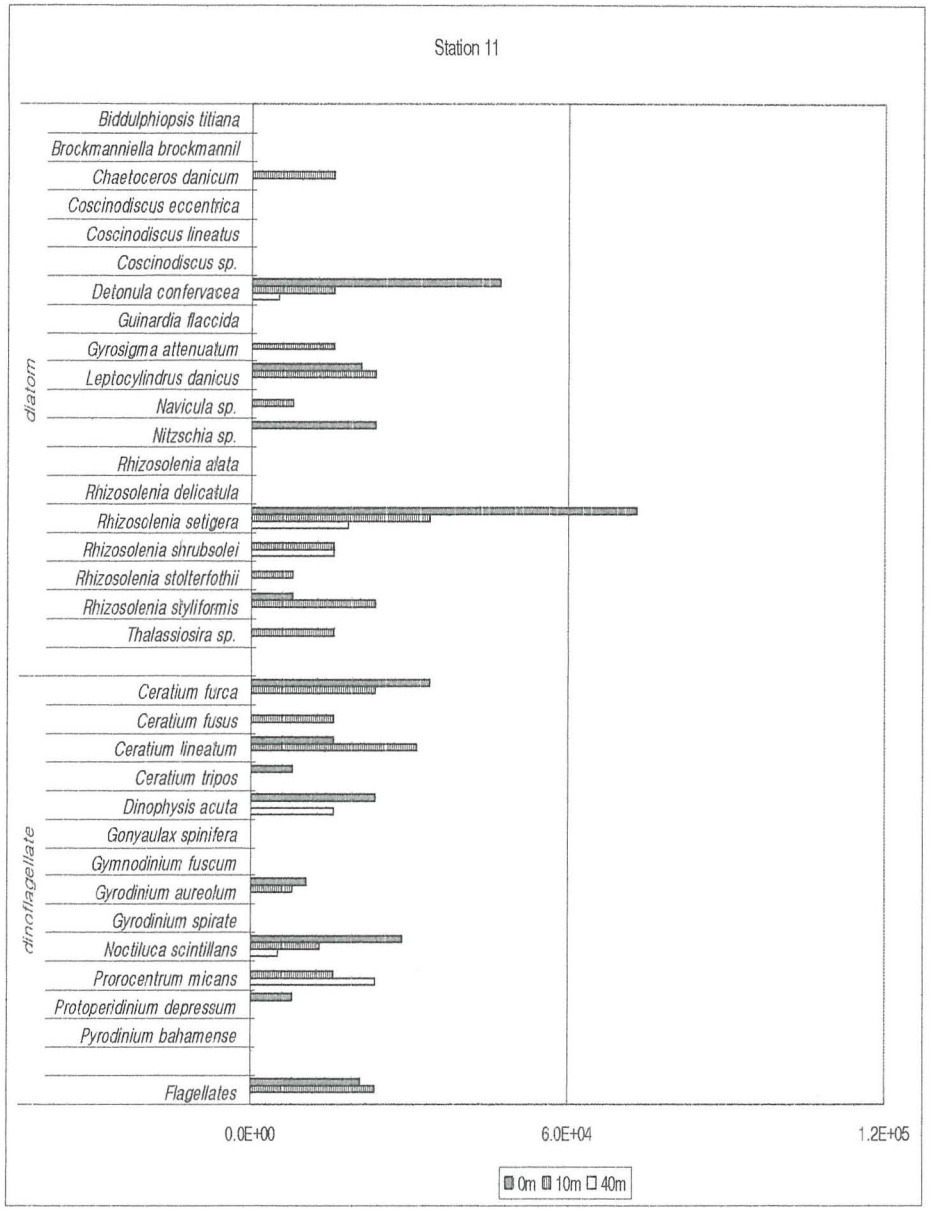
Station 11
diatom
Biddulphiopsis titiana
Brockmanniella brockmannil
Chaetoceros danicum
Coscinodiscus eccentrica
Coscinodiscus lineatus
Coscinodiscus sp.
Detonula confervacea
Guinardia flaccida
Gyrosigma attenuatum
Leptocylindrus danicus
Navicula sp.
Nitzschia sp.
Rhizosolenia alata
Rhizosolenia delicatula
Rhizosolenia setigera
Rhizosolenia shrubsolei
Rhizosolenia stolterfothii
Rhizosolenia styliformis
Thalassiosira sp.
dinoflagellate
Ceratium furca
Ceratium fusus
Ceratium lineatum
Ceratium tripos
Dinophysis acuta
Gonyaulax spinifera
Gymnodinium fuscum
Gyrodinium aureolum
Gyrodinium spirate
Noctiluca scintillans
Prorocentrum micans
Protoperidinium depressum
Pyrodinium bahamense
Flagellates
0.0E+00
6.0E+04
1.2E+05
0m 10m 40m

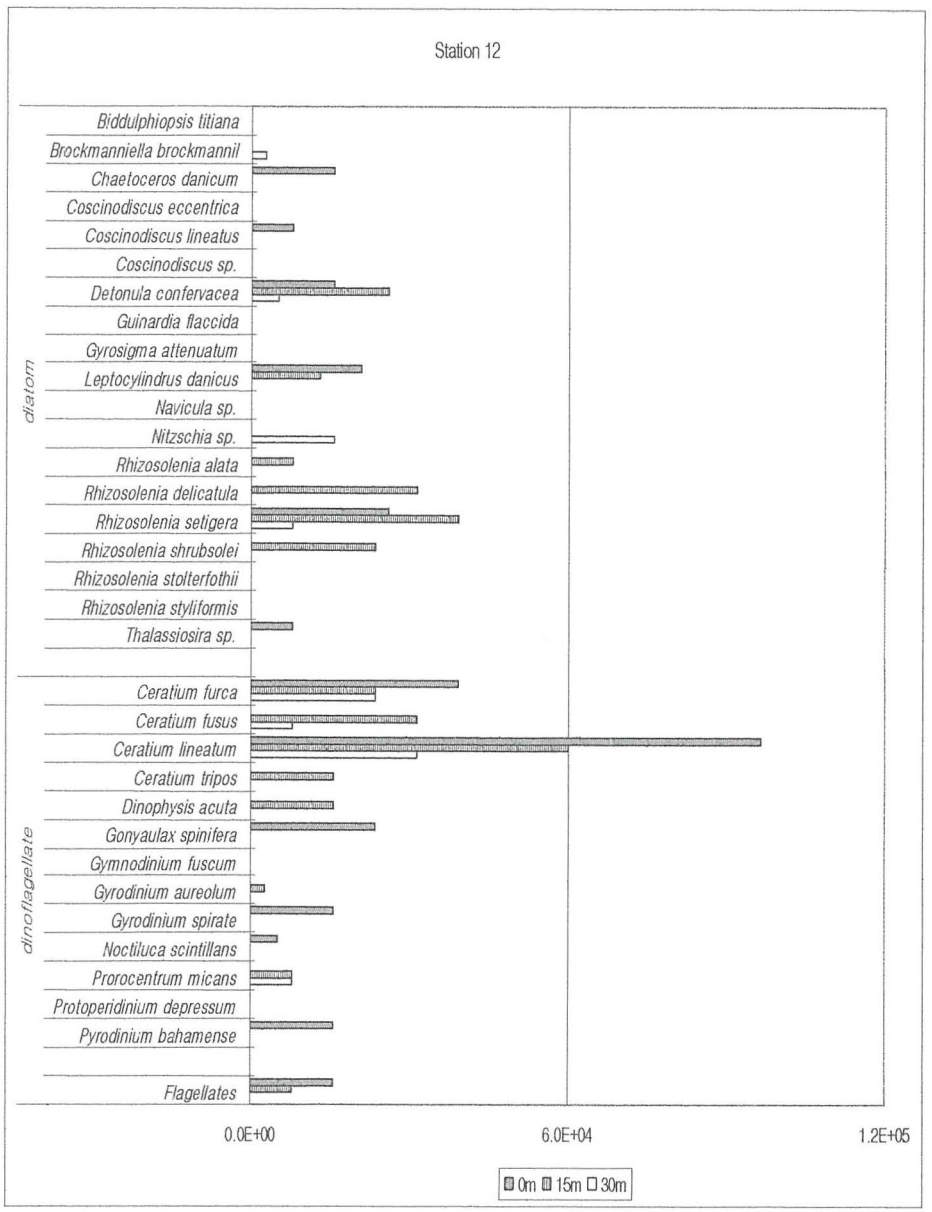
Station 12
diatom
Biddulphiopsis titiana
Brockmanniella brockmannil
Chaetoceros danicum
Coscinodiscus eccentrica
Coscinodiscus lineatus
Coscinodiscus sp.
Detonula confervacea
Guinardia flaccida
Gyrosigma attenuatum
Leptocylindrus danicus
Navicula sp.
Nitzschia sp.
Rhizosolenia alata
Rhizosolenia delicatula
Rhizosolenia setigera
Rhizosolenia shrubsolei
Rhizosolenia stolterfothii
Rhizosolenia styliformis
Thalassiosira sp.
dinoflagellate
Ceratium furca
Ceratium fusus
Ceratium lineatum
Ceratium tripos
Dinophysis acuta
Gonyaulax spinifera
Gymnodinium fuscum
Gyrodinium aureolum
Gyrodinium spirate
Noctiluca scintillans
Prorocentrum micans
Protoperidinium depressum
Pyrodinium bahamense
Flagellates
0.0E+00
6.0E+04
1.2E+05
0m 15m 30m

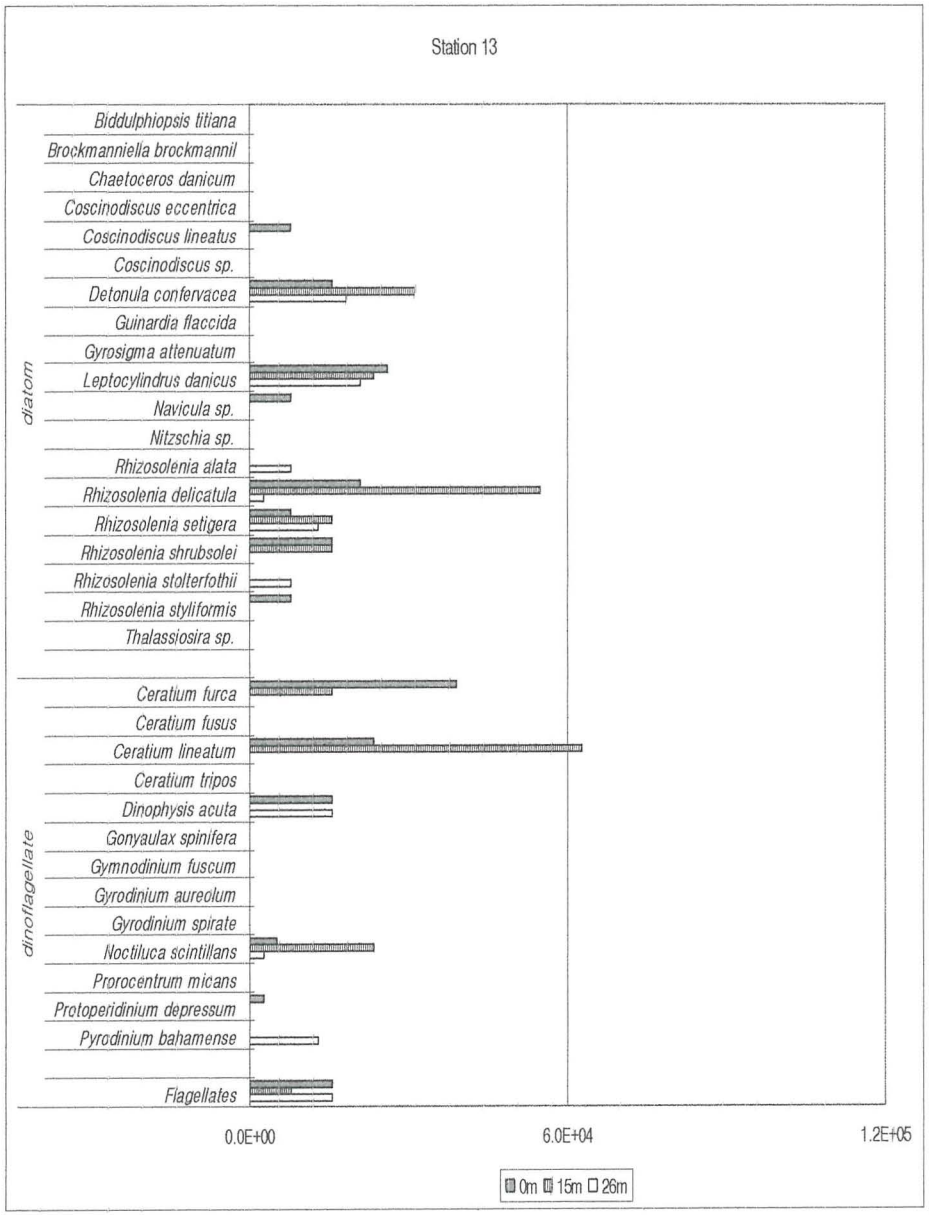
Station 13
diatom
Biddulphiopsis titiana
Brockmanniella brockmannil
Chaetoceros danicum
Coscinodiscus eccentrica
Coscinodiscus lineatus
Coscinodiscus sp.
Detonula confervacea
Guinardia flaccida
Gyrosigma attenuatum
Leptocylindrus danicus
Navicula sp.
Nitzschia sp.
Rhizosolenia alata
Rhizosolenia delicatula
Rhizosolenia setigera
Rhizosolenia shrubsolei
Rhizosolenia stolterfothii
Rhizosolenia styliformis
Thalassiosira sp.
dinoflagellate
Ceratium furca
Ceratium fusus
Ceratium lineatum
Ceratium tripos
Dinophysis acuta
Gonyaulax spinifera
Gymnodinium fuscum
Gyrodinium aureolum
Gyrodinium spirate
Noctiluca scintillans
Prorocentrum micans
Protoperidinium depressum
Pyrodinium bahamense
Flagellates
0.0E+00
6.0E+04
1.2E+05
0m 15m 26m

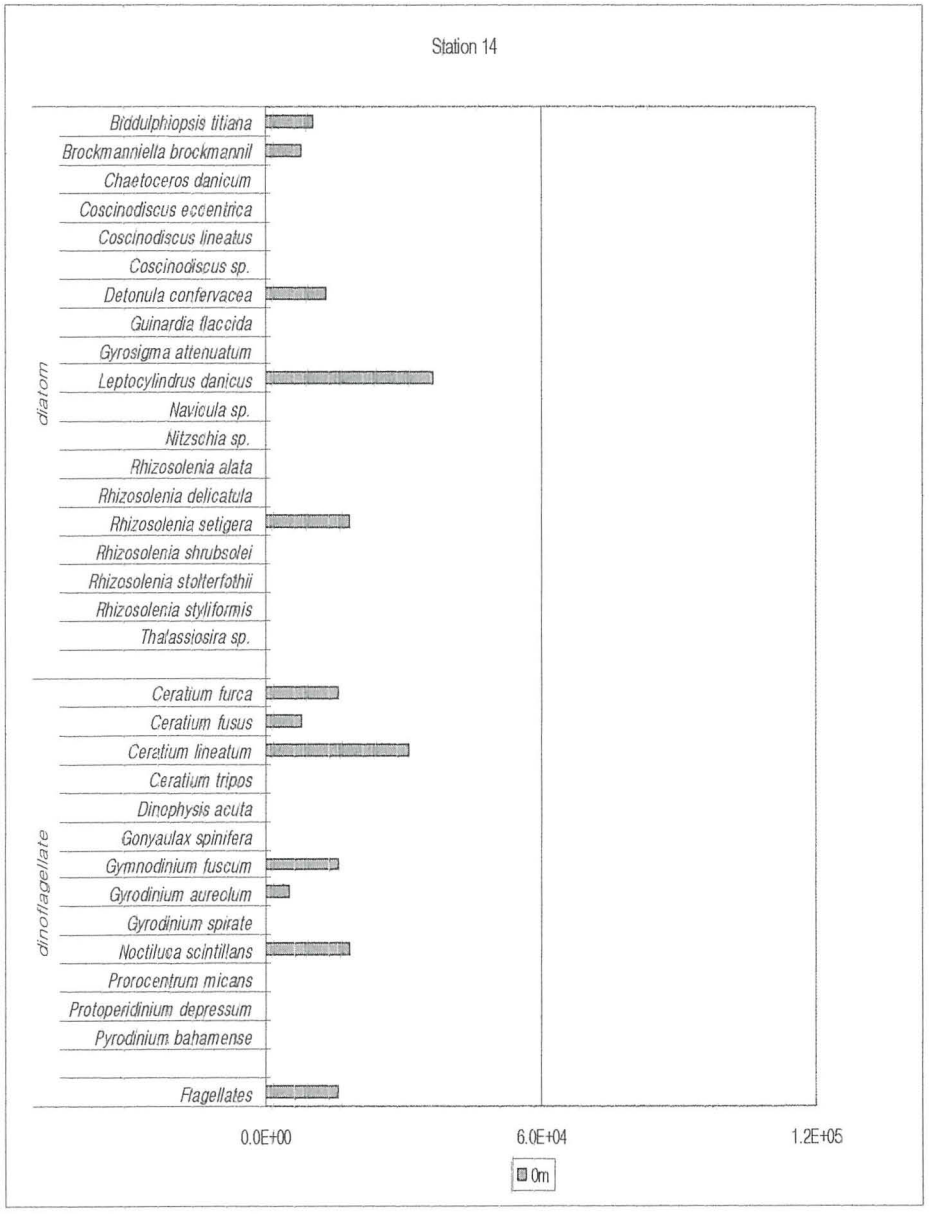
Station 14
diatom
Biddulphiopsis titiana
Brockmanniella brockmannil
Chaetoceros danicum
Coscinodiscus eccentrica
Coscinodiscus lineatus
Coscinodiscus sp.
Detonula confervacea
Guinardia flaccida
Gyrosigma attenuatum
Leptocylindrus danicus
Navicula sp.
Nitzschia sp.
Rhizosolenia alata
Rhizosolenia delicatula
Rhizosolenia setigera
Rhizosolenia shrubsolei
Rhizosolenia stolterfothii
Rhizosolenia styliformis
Thalassiosira sp.
dinoflagellate
Ceratium furca
Ceratium fusus
Ceratium lineatum
Ceratium tripos
Dinophysis acuta
Gonyaulax spinifera
Gymnodinium fuscum
Gyrodinium aureolum
Gyrodinium spirate
Noctiluca scintillans
Prorocentrum micans
Protoperidinium depressum
Pyrodinium bahamense
Flagellates
0.0E+00
6.0E+04
1.2E+05
0m


Station 15
diatom
Biddulphiopsis titiana
Brockmanniella brockmannil
Chaetoceros danicum
Coscinodiscus eccentrica
Coscinodiscus lineatus
Coscinodiscus sp.
Detonula confervacea
Guinardia flaccida
Gyrosigma attenuatum
Leptocylindrus danicus
Navicula sp.
Nitzschia sp.
Rhizosolenia alata
Rhizosolenia delicatula
Rhizosolenia setigera
Rhizosolenia shrubsolei
Rhizosolenia stolterfothii
Rhizosolenia styliformis
Thalassiosira sp.
dinoflagellate
Ceratium furca
Ceratium fusus
Ceratium lineatum
Ceratium tripos
Dinophysis acuta
Gonyaulax spinifera
Gymnodinium fuscum
Gyrodinium aureolum
Gyrodinium spirate
Noctiluca scintillans
Prorocentrum micans
Protoperidinium depressum
Pyrodinium bahamense
Flagellates
0.0E+00
6.0E+04
1.2E+05
0m

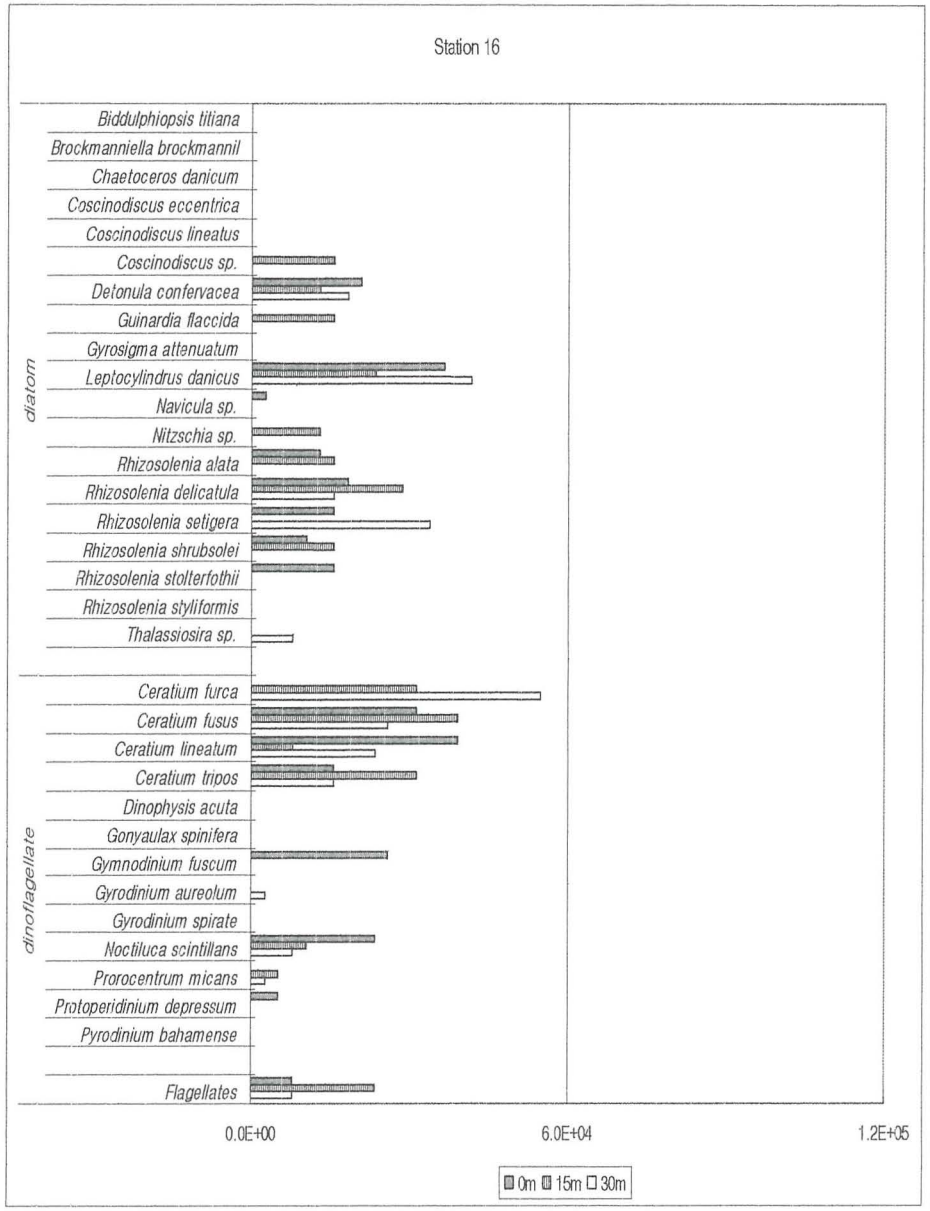
Station 16
diatom
Biddulphiopsis titiana
Brockmanniella brockmannil
Chaetoceros danicum
Coscinodiscus eccentrica
Coscinodiscus lineatus
Coscinodiscus sp.
Detonula confervacea
Guinardia flaccida
Gyrosigma attenuatum
Leptocylindrus danicus
Navicula sp.
Nitzschia sp.
Rhizosolenia alata
Rhizosolenia delicatula
Rhizosolenia setigera
Rhizosolenia shrubsolei
Rhizosolenia stolterfothii
Rhizosolenia styliformis
Thalassiosira sp.
dinoflagellate
Ceratium furca
Ceratium fusus
Ceratium lineatum
Ceratium tripos
Dinophysis acuta
Gonyaulax spinifera
Gymnodinium fuscum
Gyrodinium aureolum
Gyrodinium spirate
Noctiluca scintillans
Prorocentrum micans
Protoperidinium depressum
Pyrodinium bahamense
Flagellates
0.0E+00
6.0E+04
1.2E+05
0m 15m 30m


Station 17
diatom
Biddulphiopsis titiana
Brockmanniella brockmannil
Chaetoceros danicum
Coscinodiscus eccentrica
Coscinodiscus lineatus
Coscinodiscus sp.
Detonula confervacea
Guinardia flaccida
Gyrosigma attenuatum
Leptocylindrus danicus
Navicula sp.
Nitzschia sp.
Rhizosolenia alata
Rhizosolenia delicatula
Rhizosolenia setigera
Rhizosolenia shrubsolei
Rhizosolenia stolterfothii
Rhizosolenia styliformis
Thalassiosira sp.
dinoflagellate
Ceratium furca
Ceratium fusus
Ceratium lineatum
Ceratium tripos
Dinophysis acuta
Gonyaulax spinifera
Gymnodinium fuscum
Gyrodinium aureolum
Gyrodinium spirate
Noctiluca scintillans
Prorocentrum micans
Protoperidinium depressum
Pyrodinium bahamense
Flagellates
0.0E+00
6.0E+04
1.2E+05
0m 10m


Station 18
diatom
Biddulphiopsis titiana
Brockmanniella brockmannil
Chaetoceros danicum
Coscinodiscus eccentrica
Coscinodiscus lineatus
Coscinodiscus sp.
Detonula confervacea
Guinardia flaccida
Gyrosigma attenuatum
Leptocylindrus danicus
Navicula sp.
Nitzschia sp.
Rhizosolenia alata
Rhizosolenia delicatula
Rhizosolenia setigera
Rhizosolenia shrubsolei
Rhizosolenia stolterfothii
Rhizosolenia styliformis
Thalassiosira sp.
dinoflagellate
Ceratium furca
Ceratium fusus
Ceratium lineatum
Ceratium tripos
Dinophysis acuta
Gonyaulax spinifera
Gymnodinium fuscum
Gyrodinium aureolum
Gyrodinium spirate
Noctiluca scintillans
Prorocentrum micans
Protoperidinium depressum
Pyrodinium bahamense
Flagellates
0.0E+00
6.0E+04
1.2E+05
0m 15m 30m

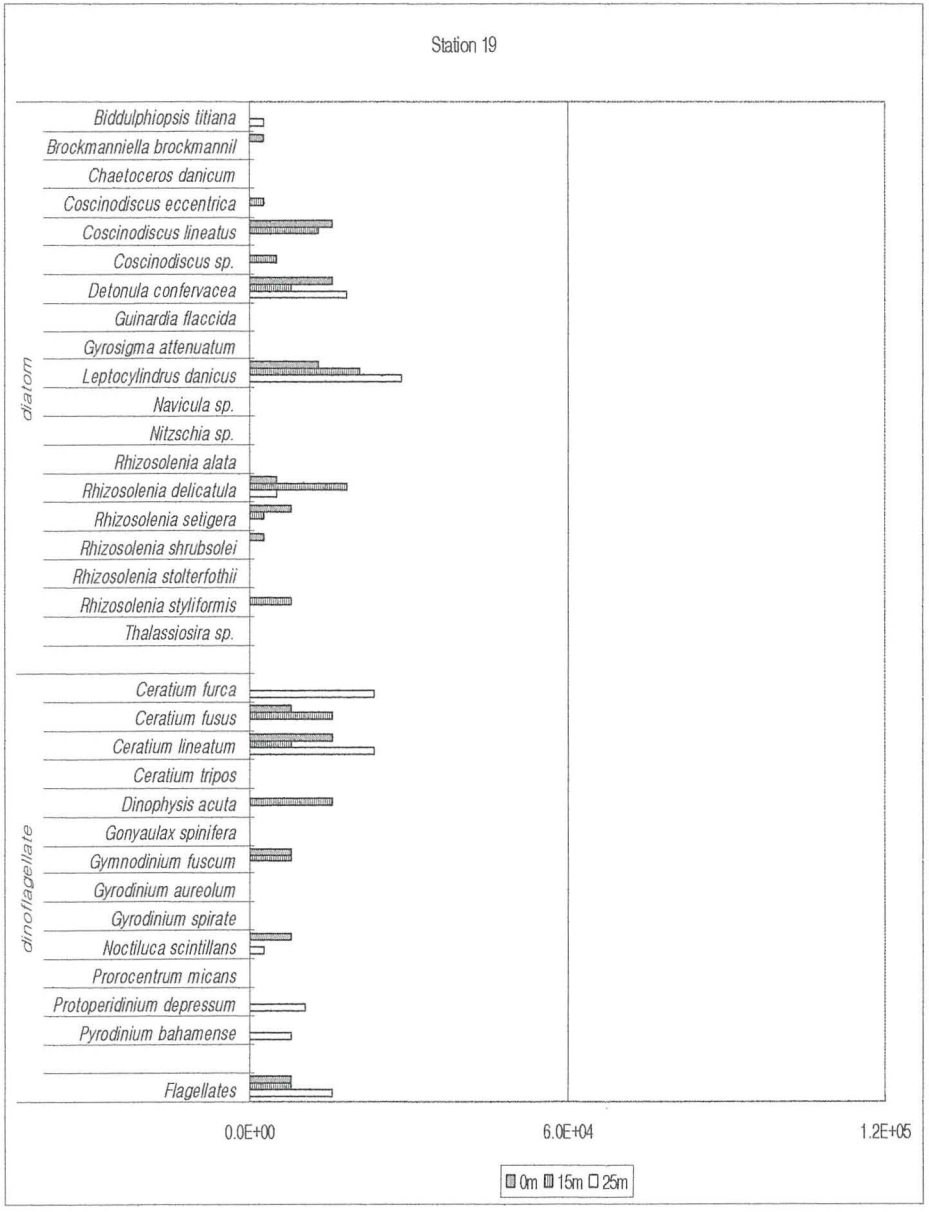
Station 19
diatom
Biddulphiopsis titiana
Brockmanniella brockmannil
Chaetoceros danicum
Coscinodiscus eccentrica
Coscinodiscus lineatus
Coscinodiscus sp.
Detonula confervacea
Guinardia flaccida
Gyrosigma attenuatum
Leptocylindrus danicus
Navicula sp.
Nitzschia sp.
Rhizosolenia alata
Rhizosolenia delicatula
Rhizosolenia setigera
Rhizosolenia shrubsolei
Rhizosolenia stolterfothii
Rhizosolenia styliformis
Thalassiosira sp.
dinoflagellate
Ceratium furca
Ceratium fusus
Ceratium lineatum
Ceratium tripos
Dinophysis acuta
Gonyaulax spinifera
Gymnodinium fuscum
Gyrodinium aureolum
Gyrodinium spirate
Noctiluca scintillans
Prorocentrum micans
Protoperidinium depressum
Pyrodinium bahamense
Flagellates
0.0E+00
6.0E+04
1.2E+05
0m 15m 25m


Station 20
diatom
Biddulphiopsis titiana
Brockmanniella brockmannil
Chaetoceros danicum
Coscinodiscus eccentrica
Coscinodiscus lineatus
Coscinodiscus sp.
Detonula confervacea
Guinardia flaccida
Gyrosigma attenuatum
Leptocylindrus danicus
Navicula sp.
Nitzschia sp.
Rhizosolenia alata
Rhizosolenia delicatula
Rhizosolenia setigera
Rhizosolenia shrubsolei
Rhizosolenia stolterfothii
Rhizosolenia styliformis
Thalassiosira sp.
dinoflagellate
Ceratium furca
Ceratium fusus
Ceratium lineatum
Ceratium tripos
Dinophysis acuta
Gonyaulax spinifera
Gymnodinium fuscum
Gyrodinium aureolum
Gyrodinium spirate
Noctiluca scintillans
Prorocentrum micans
Protoperidinium depressum
Pyrodinium bahamense
Flagellates
0.0E+00
6.0E+04
1.2E+05
0m 10m

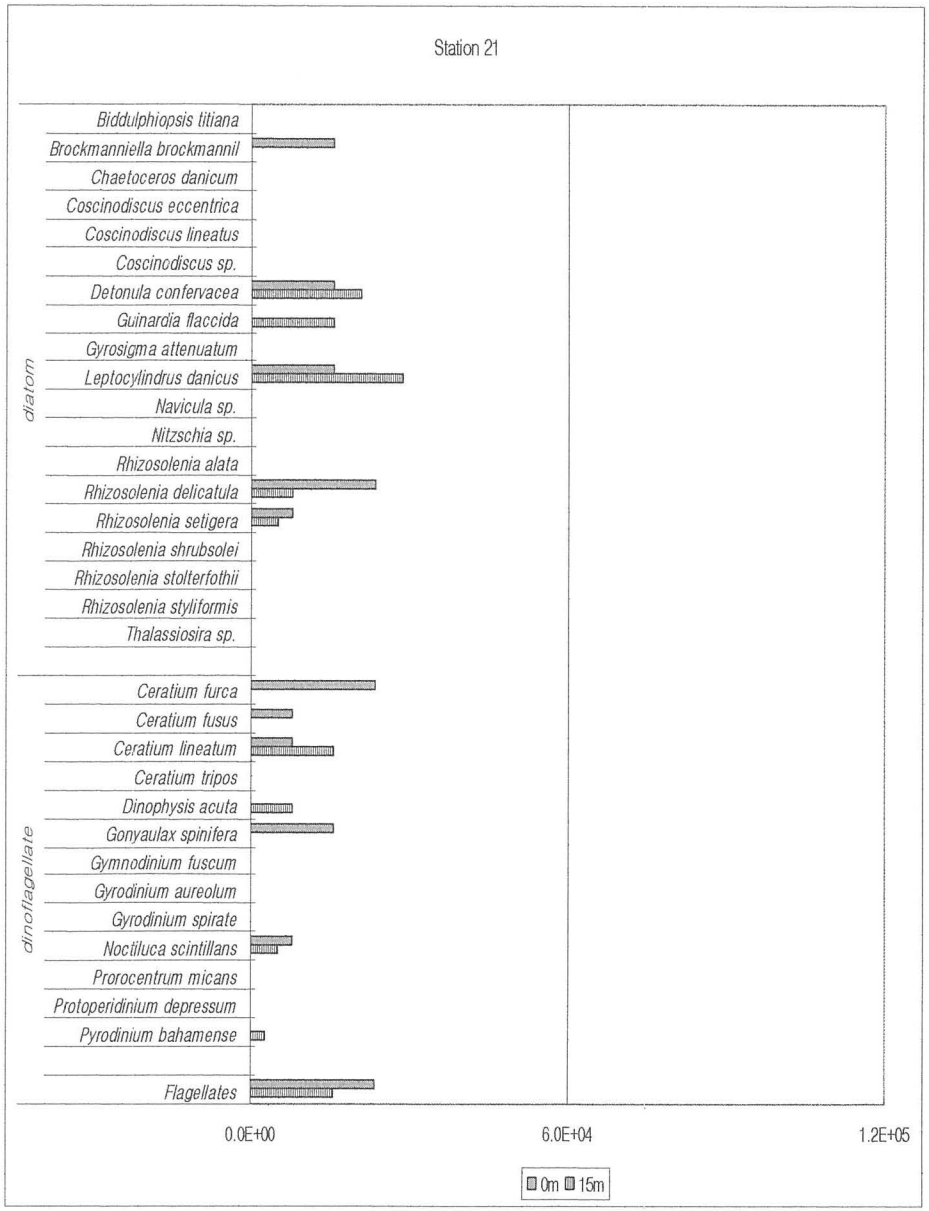
Station 21
diatom
Biddulphiopsis titiana
Brockmanniella brockmannil
Chaetoceros danicum
Coscinodiscus eccentrica
Coscinodiscus lineatus
Coscinodiscus sp.
Detonula confervacea
Guinardia flaccida
Gyrosigma attenuatum
Leptocylindrus danicus
Navicula sp.
Nitzschia sp.
Rhizosolenia alata
Rhizosolenia delicatula
Rhizosolenia setigera
Rhizosolenia shrubsolei
Rhizosolenia stolterfothii
Rhizosolenia styliformis
Thalassiosira sp.
dinoflagellate
Ceratium furca
Ceratium fusus
Ceratium lineatum
Ceratium tripos
Dinophysis acuta
Gonyaulax spinifera
Gymnodinium fuscum
Gyrodinium aureolum
Gyrodinium spirate
Noctiluca scintillans
Prorocentrum micans
Protoperidinium depressum
Pyrodinium bahamense
Flagellates
0.0E+00
6.0E+04
1.2E+05
0m 15m


Station 23
diatom
Biddulphiopsis titiana
Brockmanniella brockmannil
Chaetoceros danicum
Coscinodiscus eccentrica
Coscinodiscus lineatus
Coscinodiscus sp.
Detonula confervacea
Guinardia flaccida
Gyrosigma attenuatum
Leptocylindrus danicus
Navicula sp.
Nitzschia sp.
Rhizosolenia alata
Rhizosolenia delicatula
Rhizosolenia setigera
Rhizosolenia shrubsolei
Rhizosolenia stolterfothii
Rhizosolenia styliformis
Thalassiosira sp.
dinoflagellate
Ceratium furca
Ceratium fusus
Ceratium lineatum
Ceratium tripos
Dinophysis acuta
Gonyaulax spinifera
Gymnodinium fuscum
Gyrodinium aureolum
Gyrodinium spirate
Noctiluca scintillans
Prorocentrum micans
Protoperidinium depressum
Pyrodinium bahamense
Flagellates
0.0E+00
6.0E+04
1.2E+05
0m 10m 25m


Station 24
diatom
Biddulphiopsis titiana
Brockmanniella brockmannil
Chaetoceros danicum
Coscinodiscus eccentrica
Coscinodiscus lineatus
Coscinodiscus sp.
Detonula confervacea
Guinardia flaccida
Gyrosigma attenuatum
Leptocylindrus danicus
Navicula sp.
Nitzschia sp.
Rhizosolenia alata
Rhizosolenia delicatula
Rhizosolenia setigera
Rhizosolenia shrubsolei
Rhizosolenia stolterfothii
Rhizosolenia styliformis
Thalassiosira sp.
dinoflagellate
Ceratium furca
Ceratium fusus
Ceratium lineatum
Ceratium tripos
Dinophysis acuta
Gonyaulax spinifera
Gymnodinium fuscum
Gyrodinium aureolum
Gyrodinium spirate
Noctiluca scintillans
Prorocentrum micans
Protoperidinium depressum
Pyrodinium bahamense
Flagellates
0.0E+00
6.0E+04
1.2E+05
0m 15m 25m


Station 25
diatom
Biddulphiopsis titiana
Brockmanniella brockmannil
Chaetoceros danicum
Coscinodiscus eccentrica
Coscinodiscus lineatus
Coscinodiscus sp.
Detonula confervacea
Guinardia flaccida
Gyrosigma attenuatum
Leptocylindrus danicus
Navicula sp.
Nitzschia sp.
Rhizosolenia alata
Rhizosolenia delicatula
Rhizosolenia setigera
Rhizosolenia shrubsolei
Rhizosolenia stolterfothii
Rhizosolenia styliformis
Thalassiosira sp.
dinoflagellate
Ceratium furca
Ceratium fusus
Ceratium lineatum
Ceratium tripos
Dinophysis acuta
Gonyaulax spinifera
Gymnodinium fuscum
Gyrodinium aureolum
Gyrodinium spirate
Noctiluca scintillans
Prorocentrum micans
Protoperidinium depressum
Pyrodinium bahamense
Flagellates
0.0E+00
6.0E+04
1.2E+05
0m
5m

Appendix A-4 Irish Sea Taxonomic data (No. of cells l^{-1}) 26-November-2001

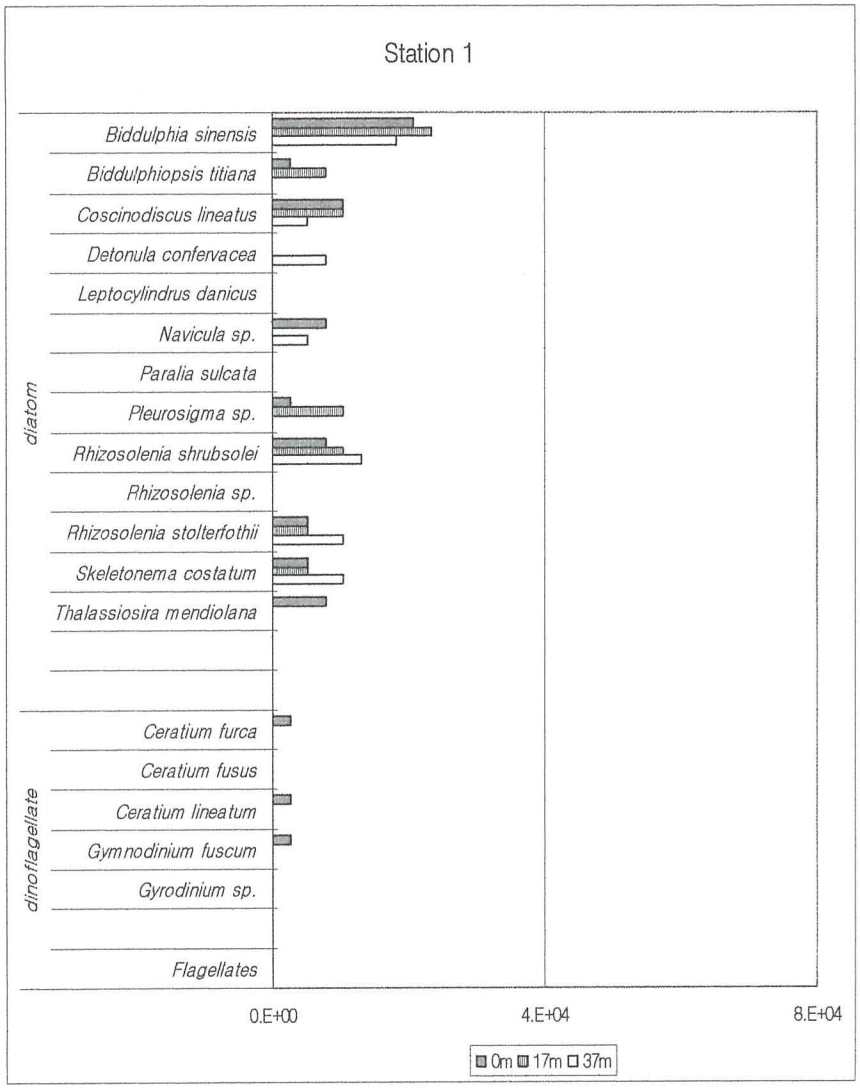

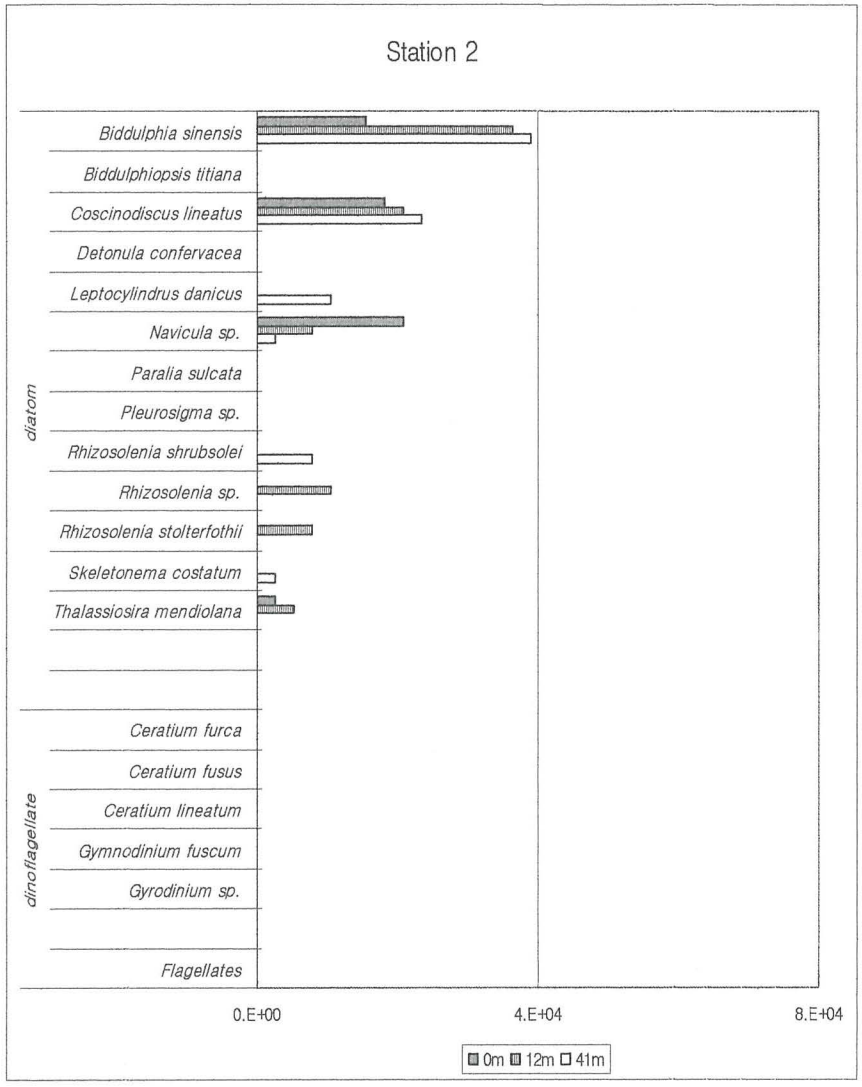

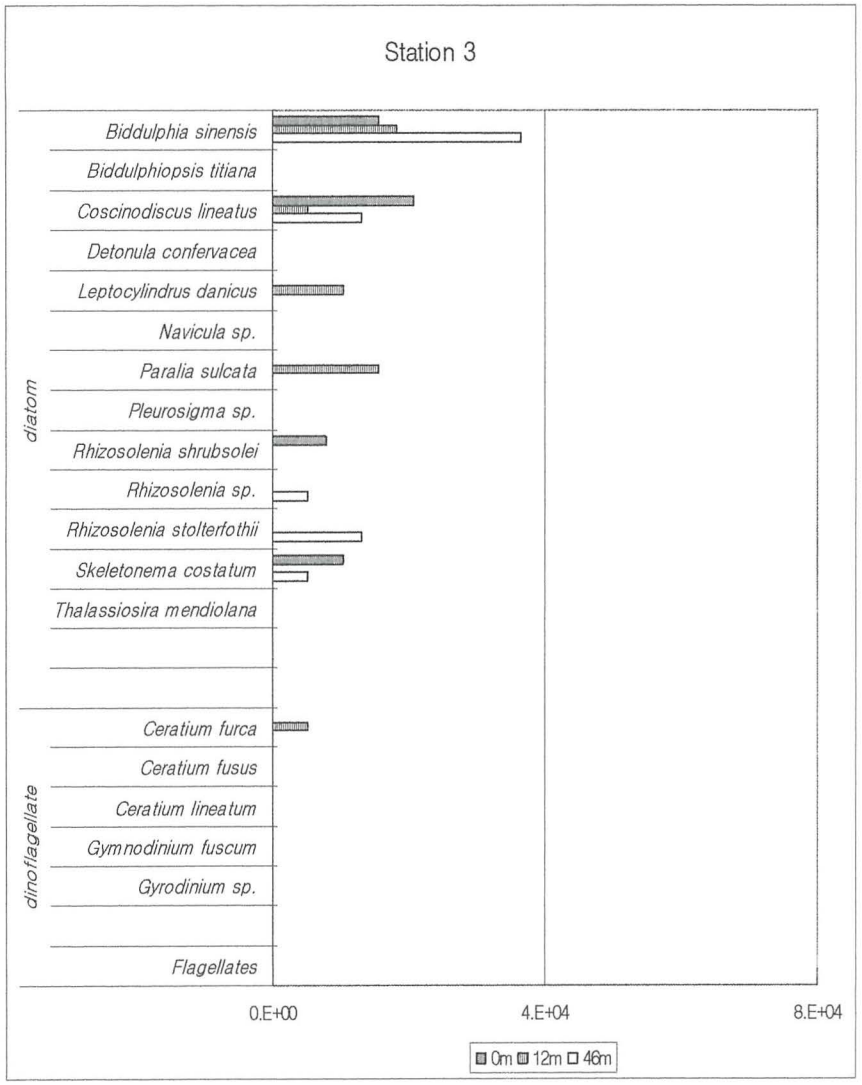
Station 3
Biddulphia sinensis
Biddulphiopsis titiana
Coscinodiscus lineatus
Detonula confervacea
Leptocylindrus danicus
Navicula sp.
Paralia sulcata
Pleurosigma sp.
Rhizosolenia shrubsolei
Rhizosolenia sp.
Rhizosolenia stolterfothii
Skeletonema costatum
Thalassiosira mendiolana
diatom
Ceratium furca
Ceratium fusus
Ceratium lineatum
Gymnodinium fuscum
Gyrodinium sp.
dinoflagellate
Flagellates
0.E+00
4.E+04
8.E+04
0m 12m 46m

Appendix A-4 Irish Sea Taxonomic data (No. of cells l^{-1}) 27-November-2001

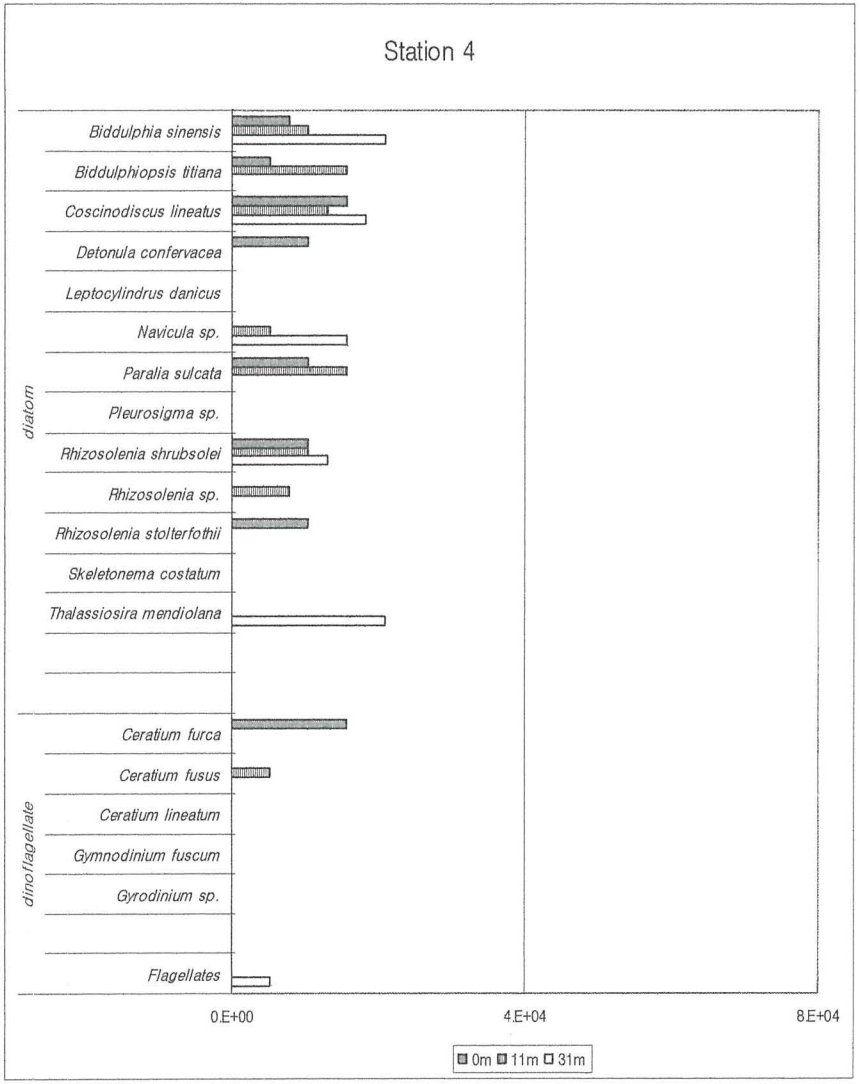

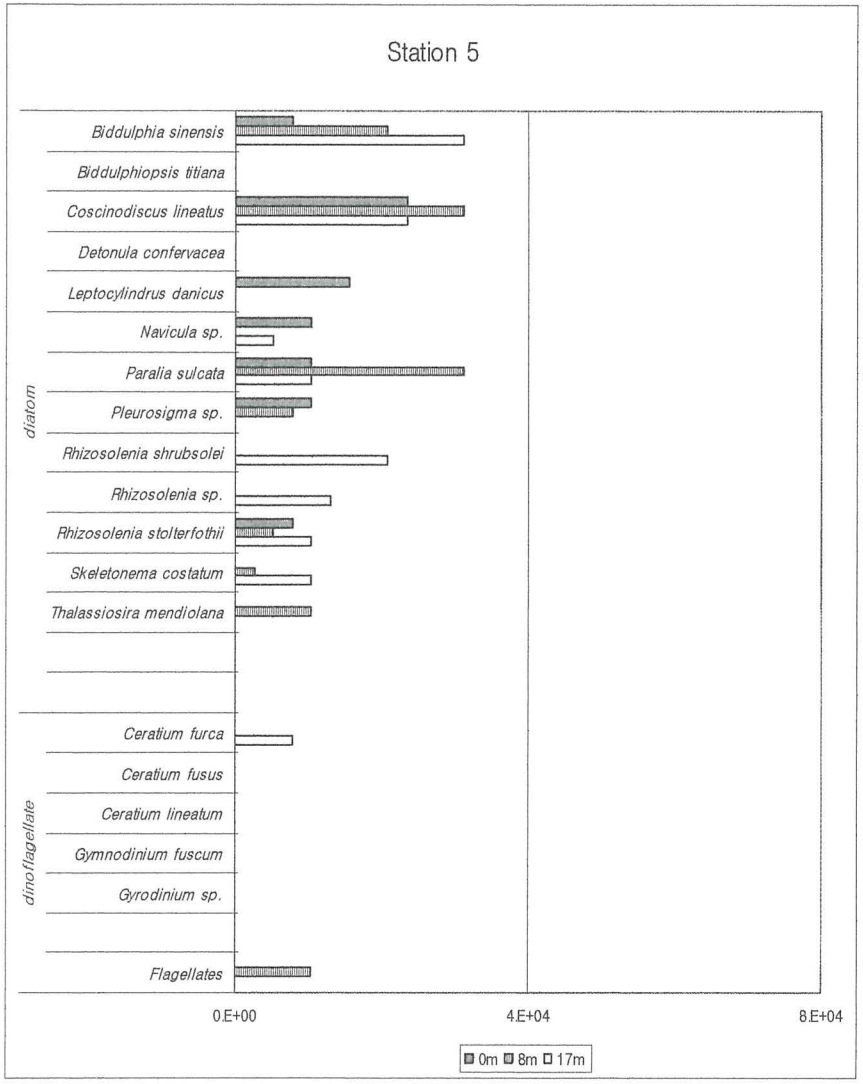

Appendix A-4 Irish Sea Taxonomic data (No. of cells l^{-1}) 27-November-2001

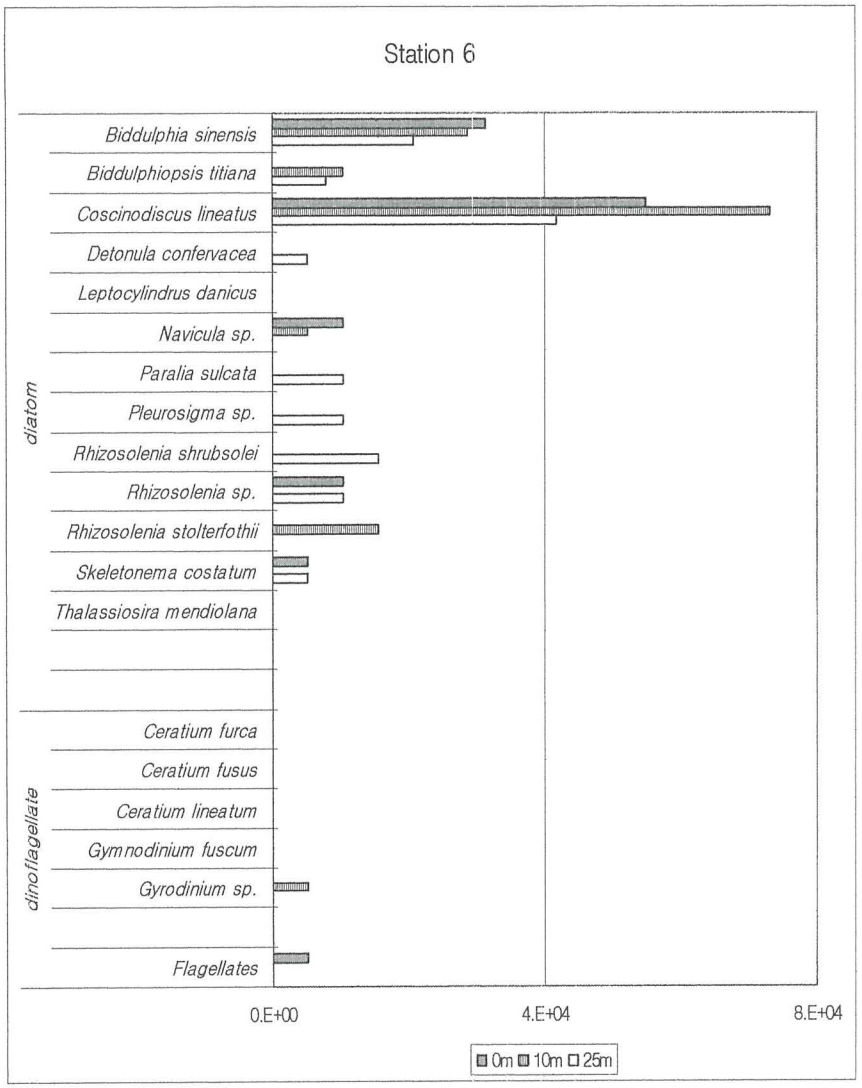

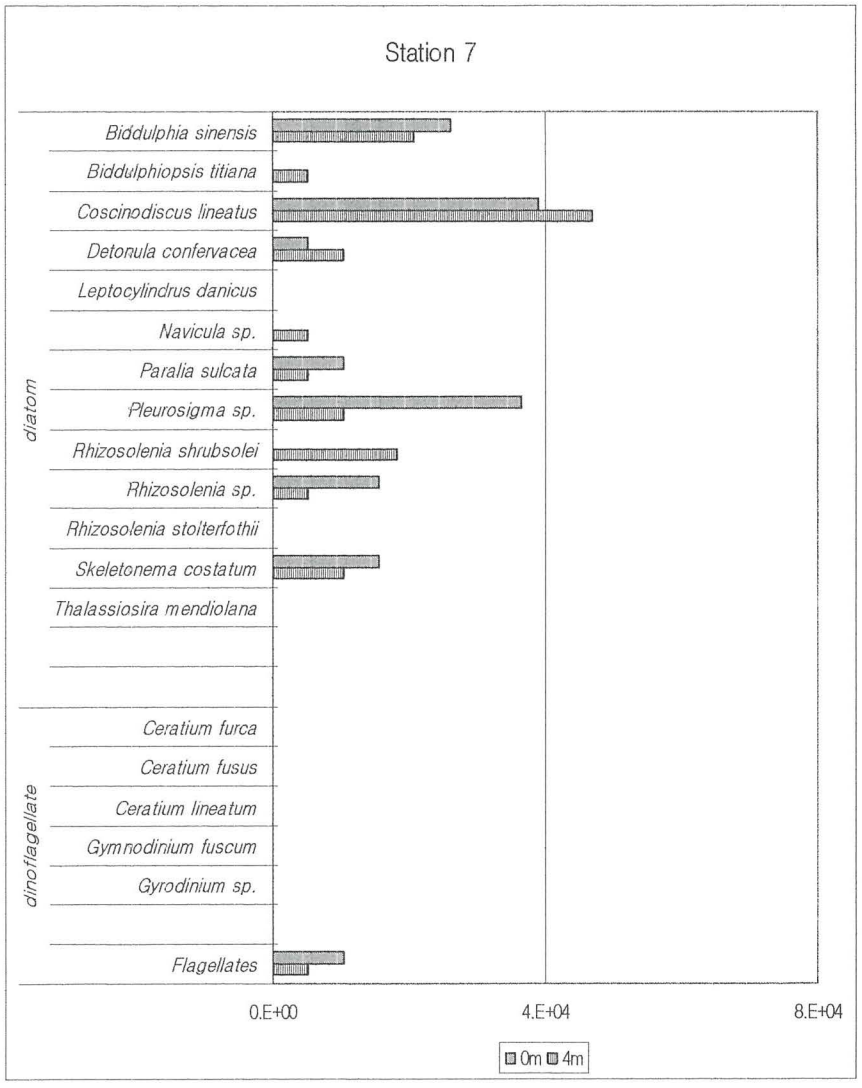

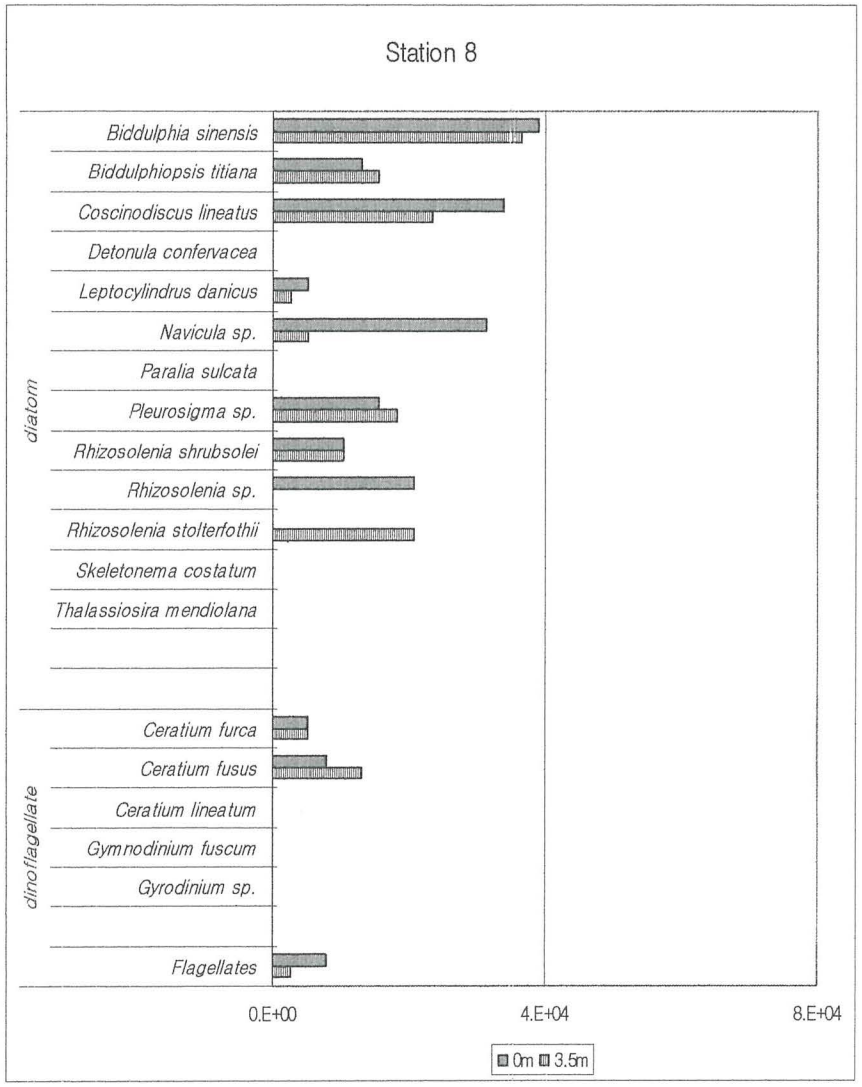
Station 8
diatom
Biddulphia sinensis
Biddulphiopsis titiana
Coscinodiscus lineatus
Detonula confervacea
Leptocylindrus danicus
Navicula sp.
Paralia sulcata
Pleurosigma sp.
Rhizosolenia shrubsolei
Rhizosolenia sp.
Rhizosolenia stolterfothii
Skeletonema costatum
Thalassiosira mendiolana
dinoflagellate
Ceratium furca
Ceratium fusus
Ceratium lineatum
Gymnodinium fuscum
Gyrodinium sp.
Flagellates
0.E+00
4.E+04
8.E+04
0m 3.5m

Appendix A-4 Irish Sea Taxonomic data (No. of cells l^{-1}) 28-November-2001

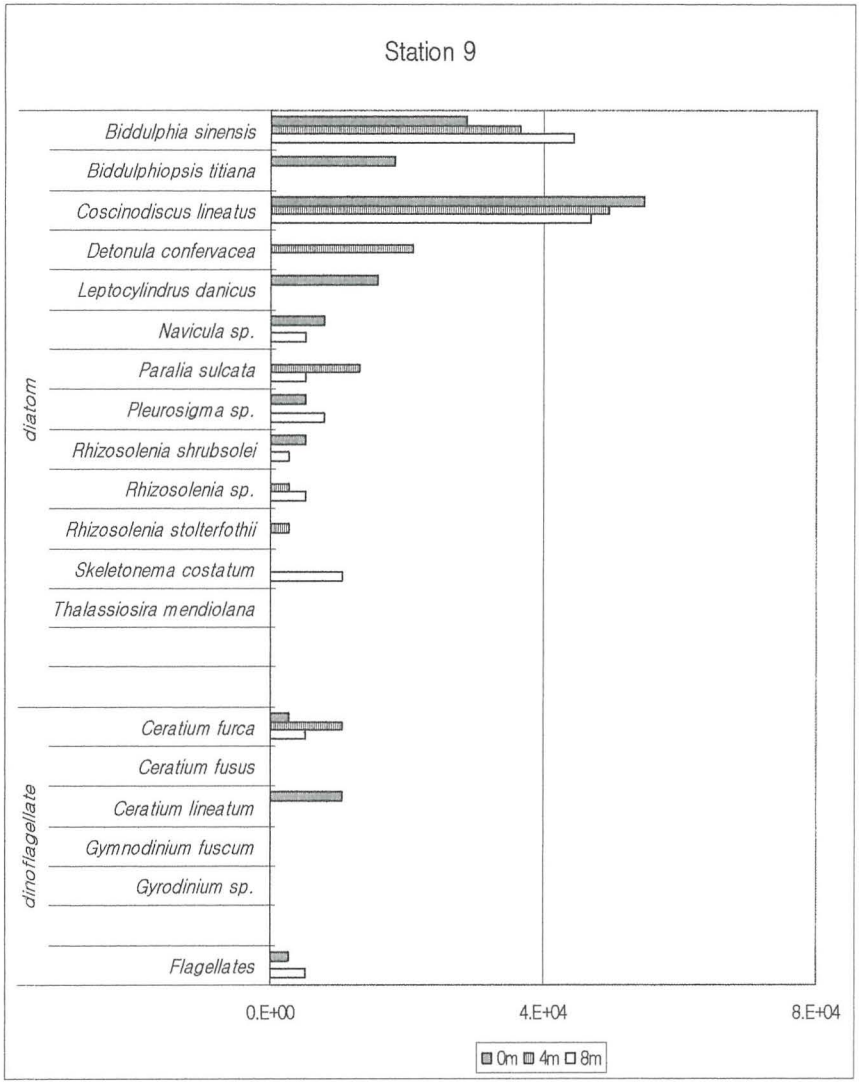

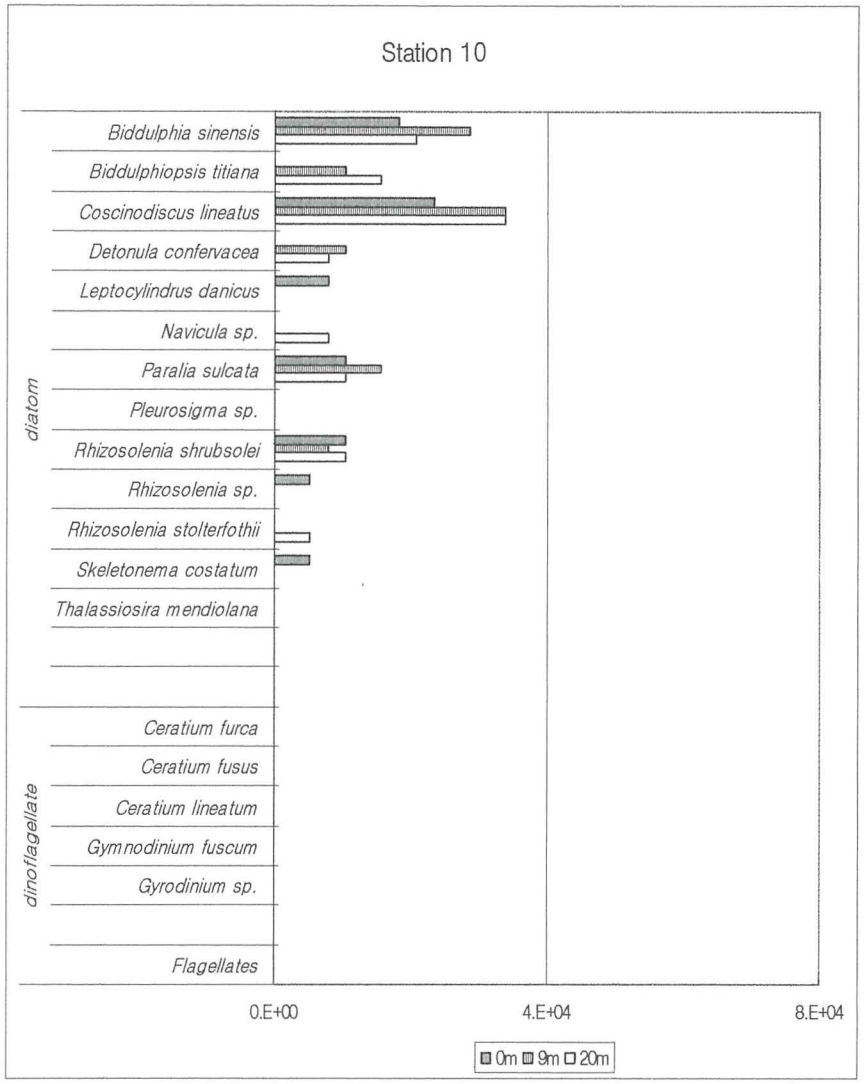

Appendix A-4 Irish Sea Taxonomic data (No. of cells l^{-1}) 28-November-2001

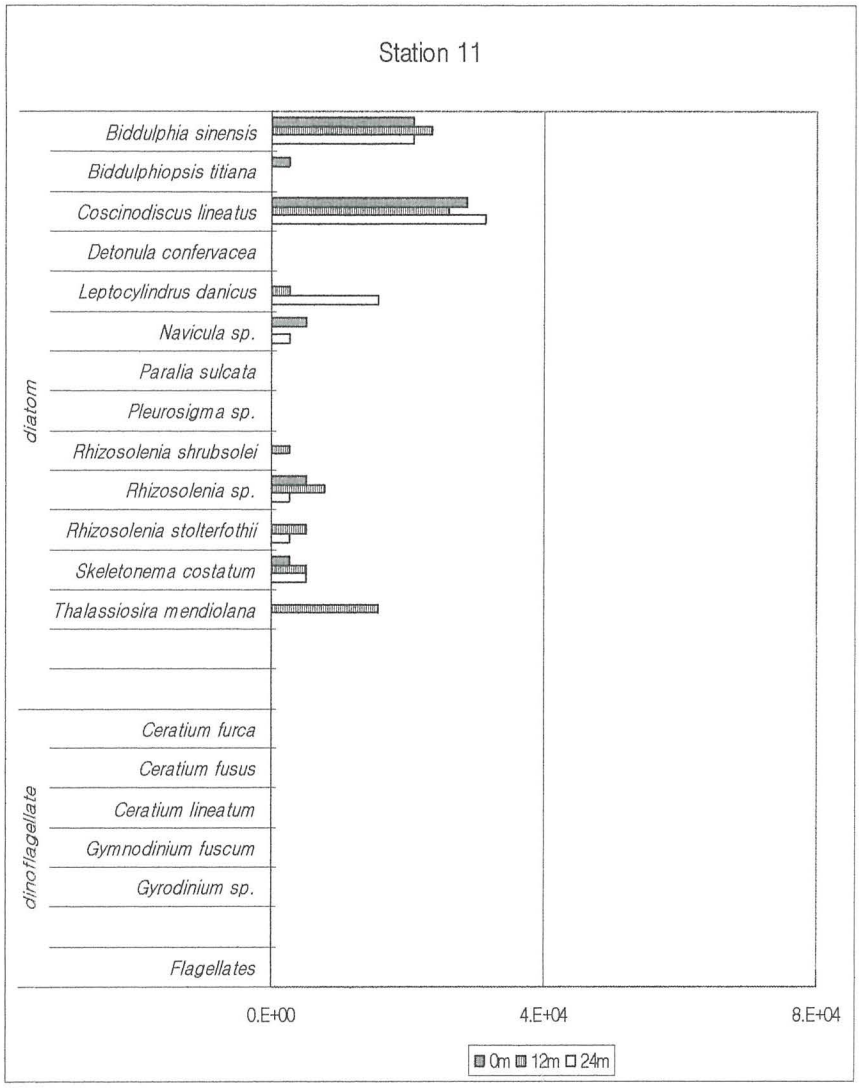

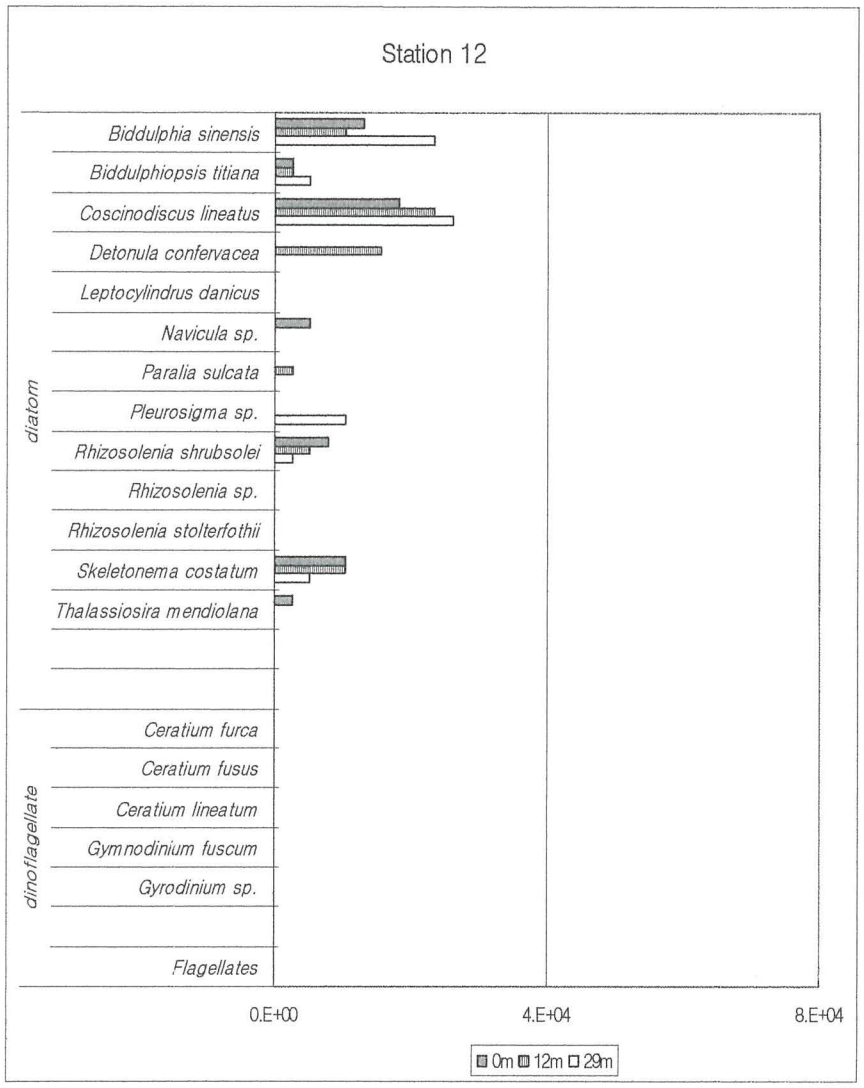

Appendix A-4 Irish Sea Taxonomic data (No. of cells l^{-1}) 28-November-2001

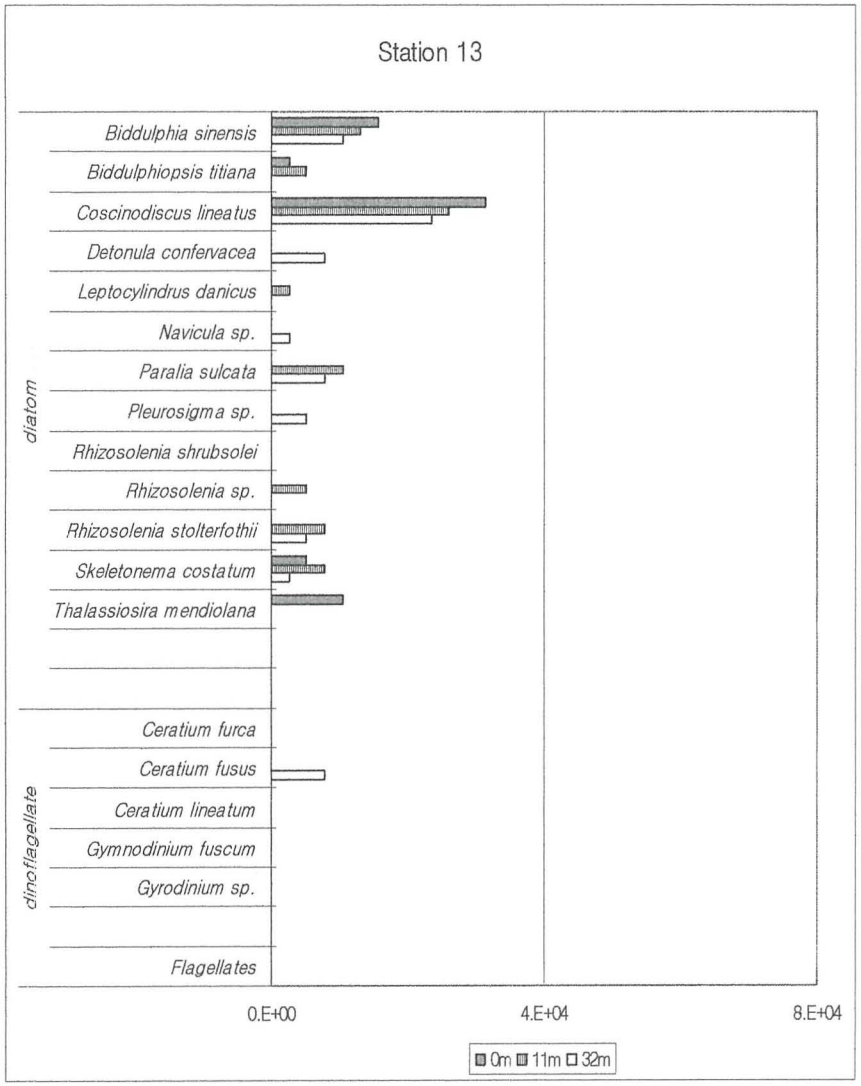

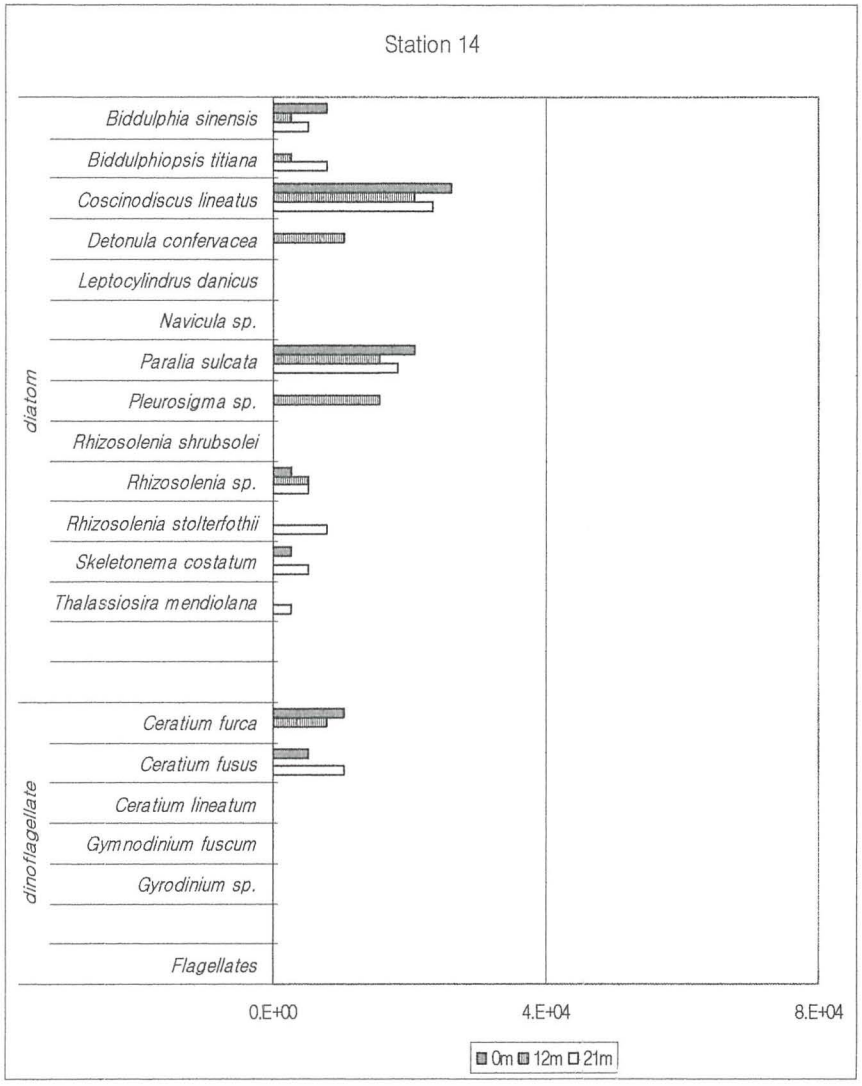

Appendix A-4 Irish Sea Taxonomic data (No. of cells l^{-1}) 29-November-2001

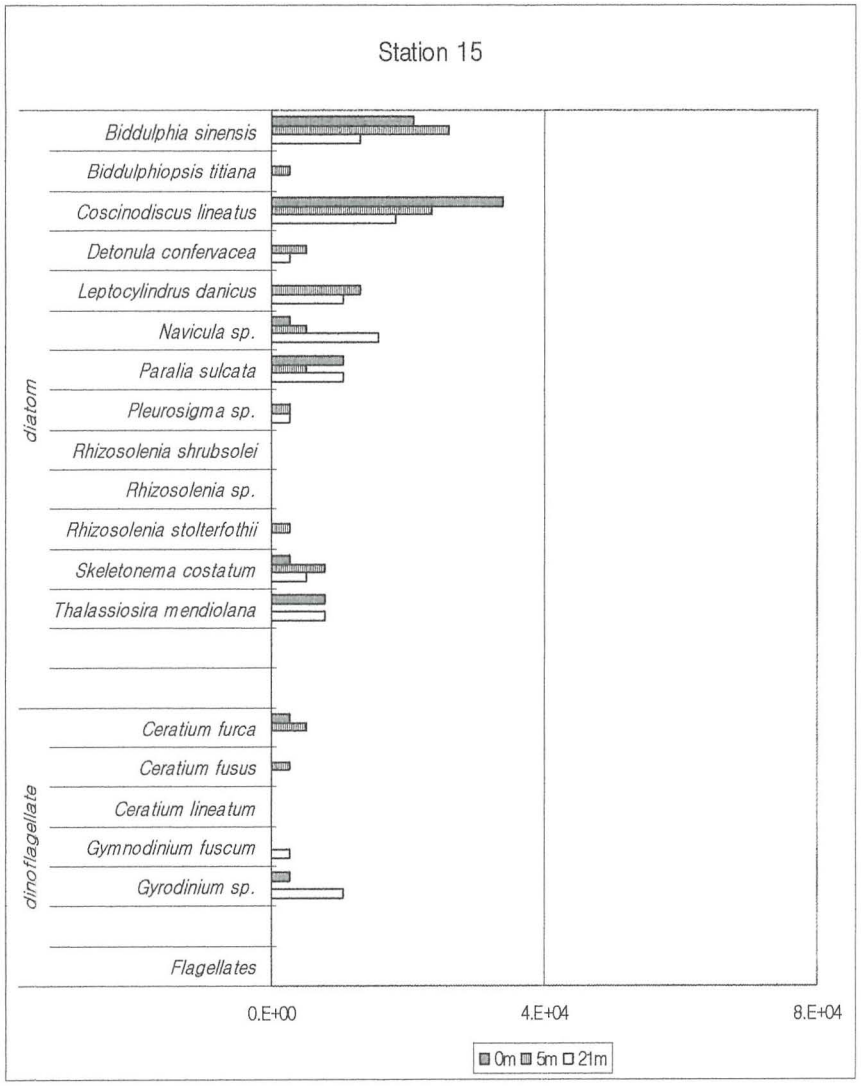

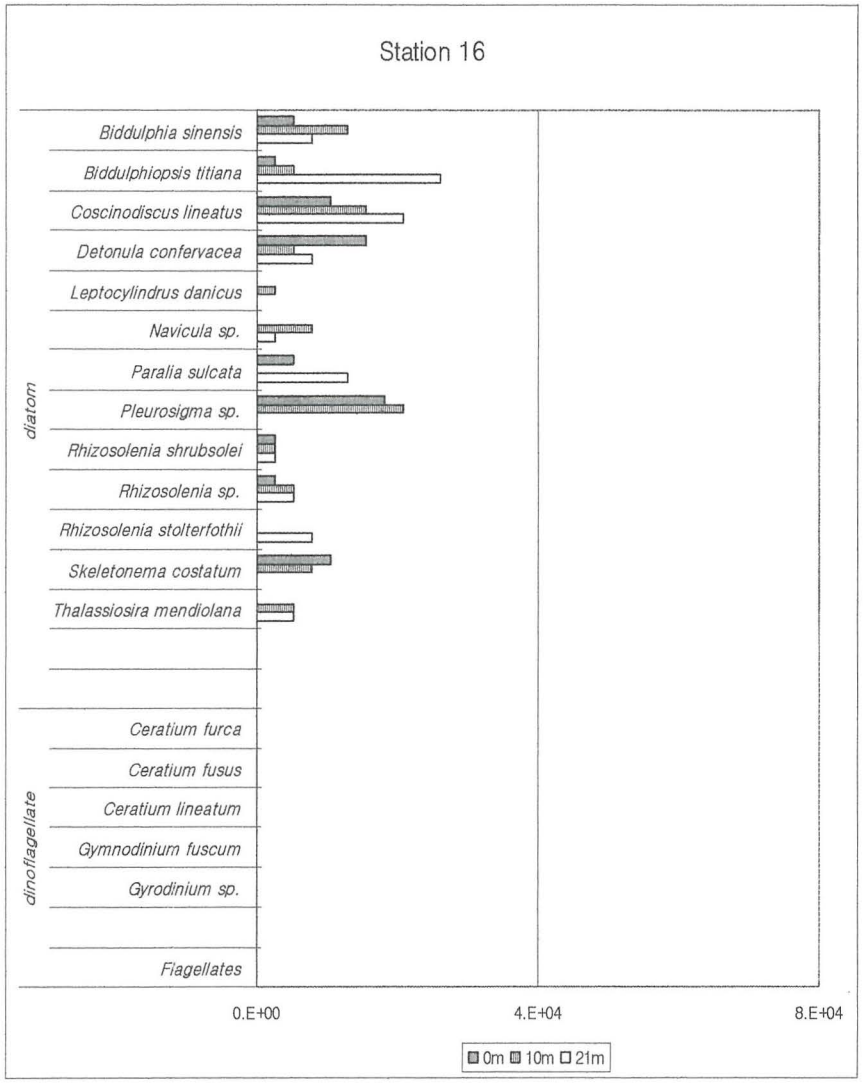

Appendix A-4 Irish Sea Taxonomic data (No. of cells l^{-1}) 29-November-2001

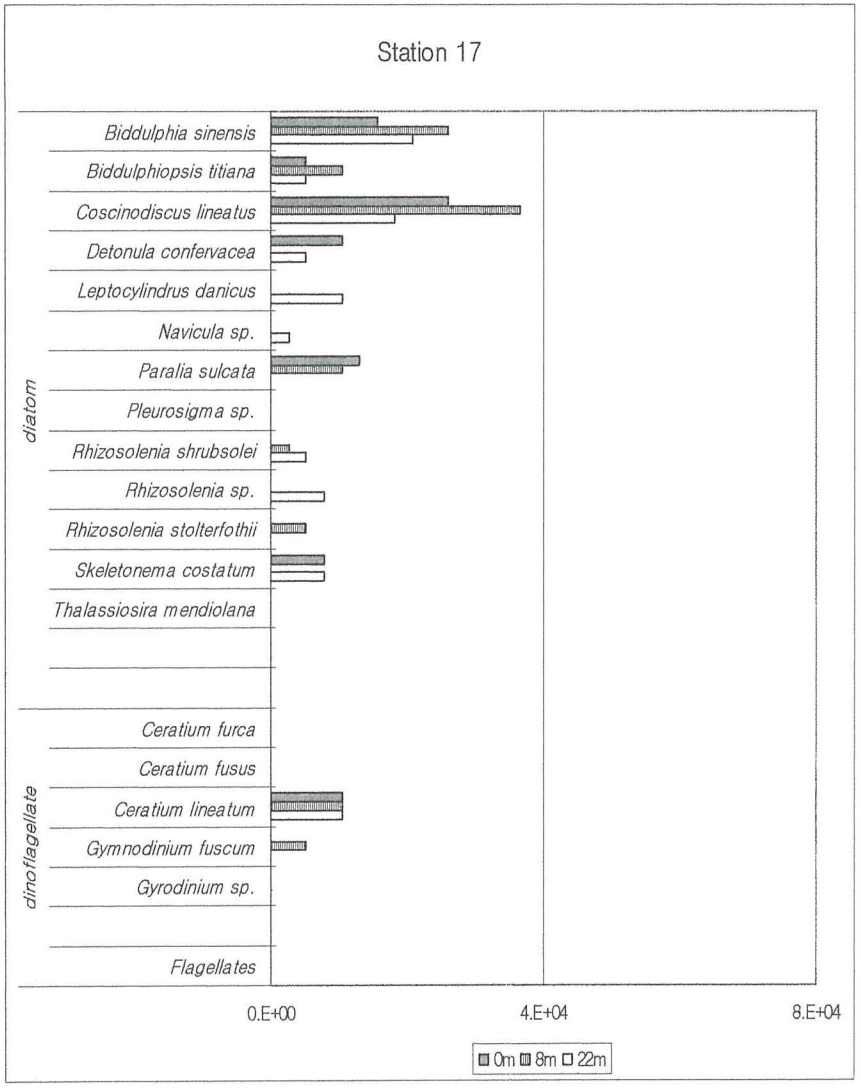

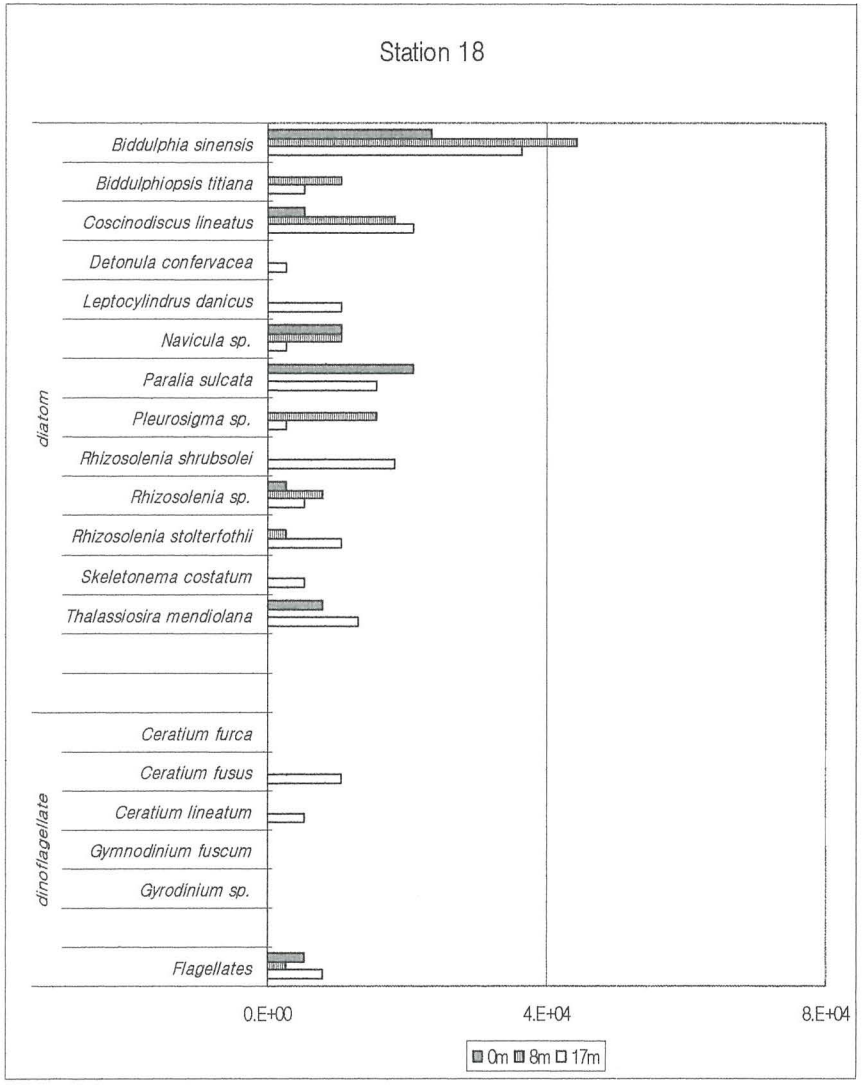

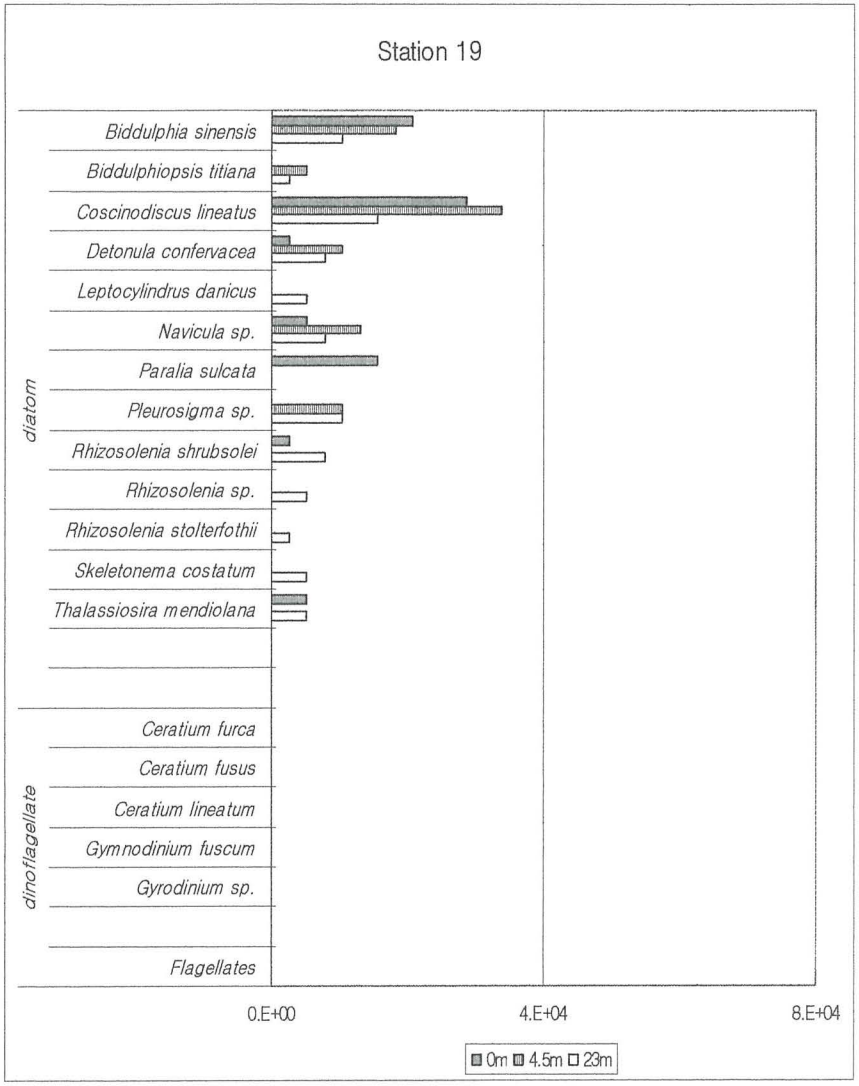
Station 19
diatom
Biddulphia sinensis
Biddulphiopsis titiana
Coscinodiscus lineatus
Detonula confervacea
Leptocylindrus danicus
Navicula sp.
Paralia sulcata
Pleurosigma sp.
Rhizosolenia shrubsolei
Rhizosolenia sp.
Rhizosolenia stolterfothii
Skeletonema costatum
Thalassiosira mendiolana
dinoflagellate
Ceratium furca
Ceratium fusus
Ceratium lineatum
Gymnodinium fuscum
Gyrodinium sp.
Flagellates
0.E+00
4.E+04
8.E+04
0m 4.5m 23m

Appendix A-4 Irish Sea Taxonomic data (No. of cells l^{-1}) 30-November-2001

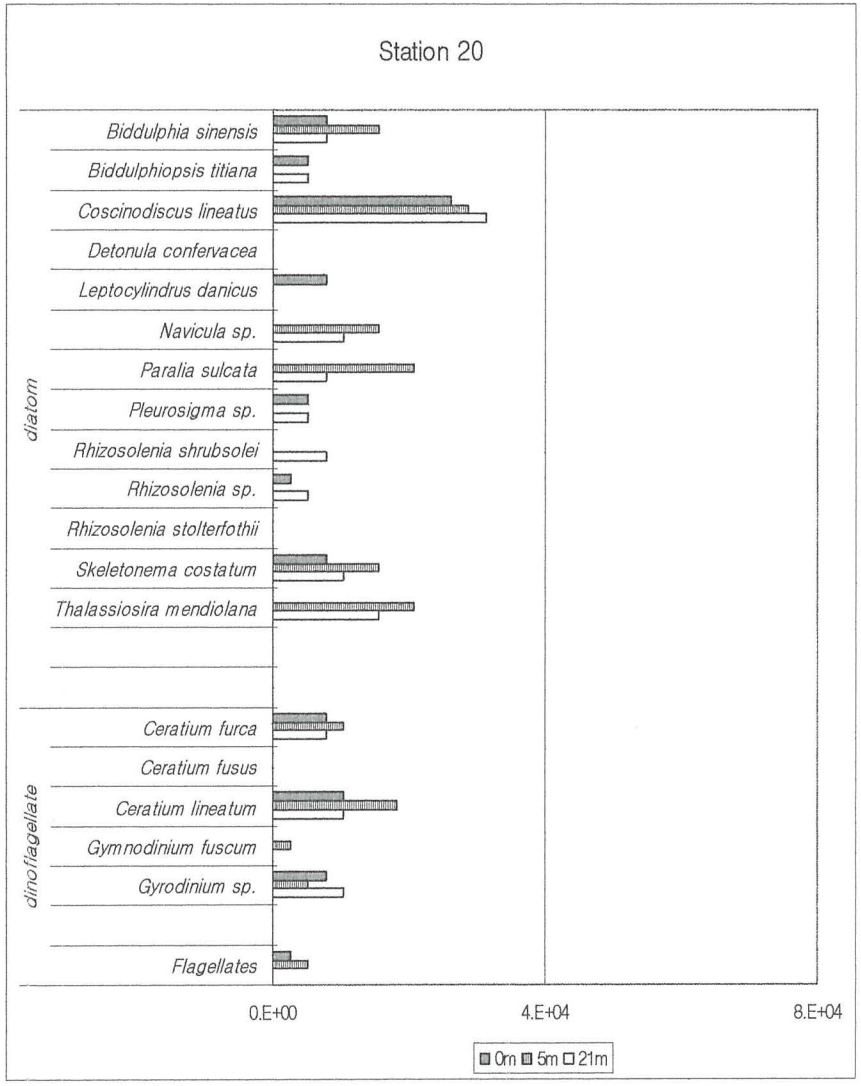

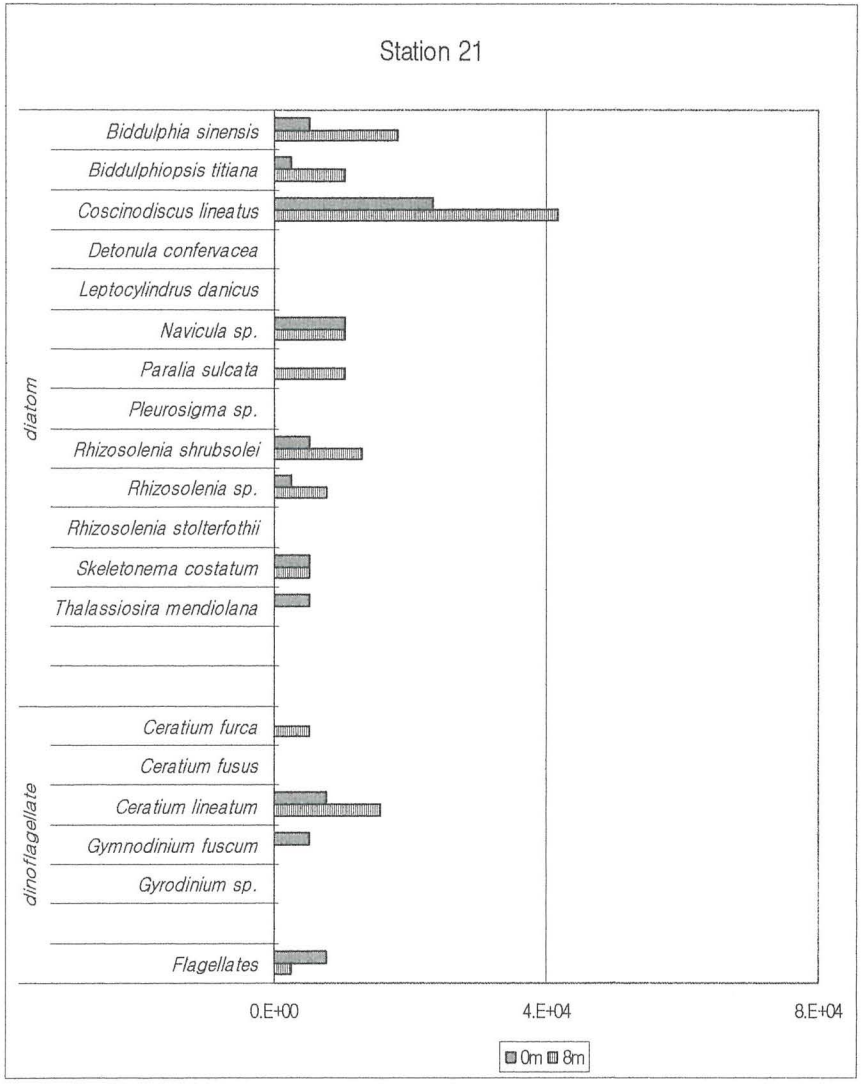

Appendix A-4 Irish Sea Taxonomic data (No. of cells l^{-1}) 30-November-2001

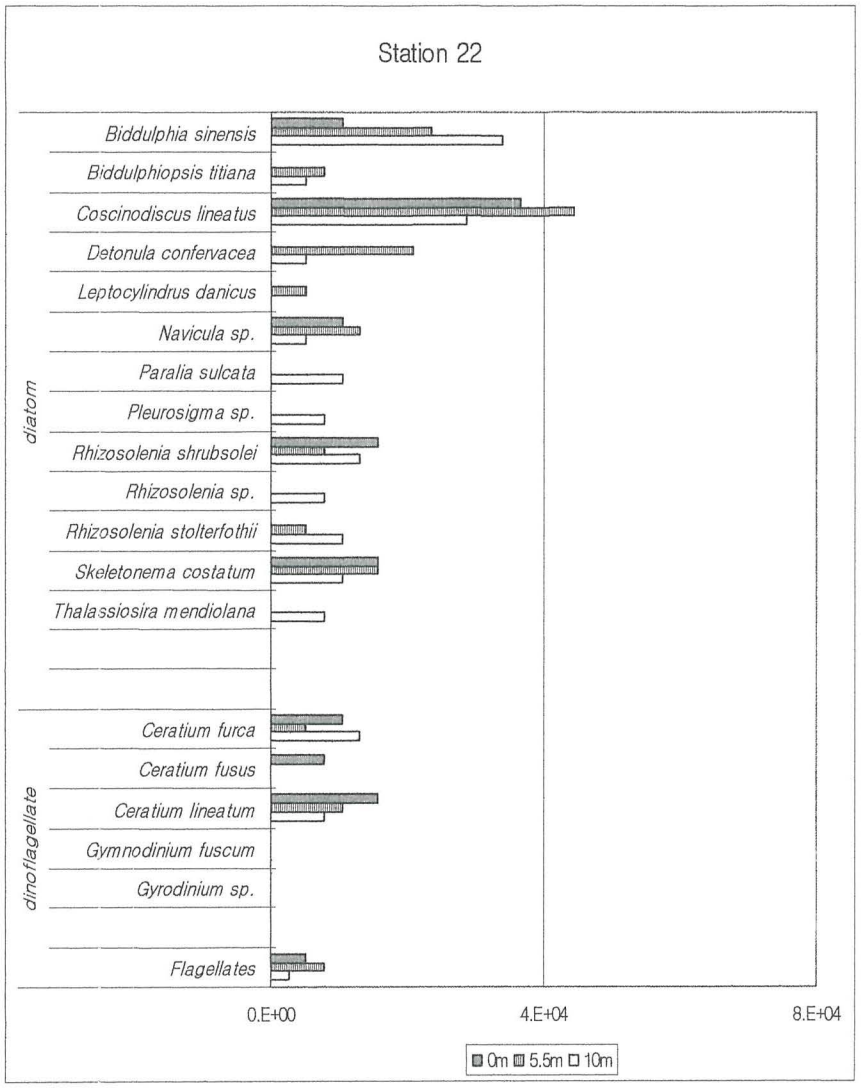

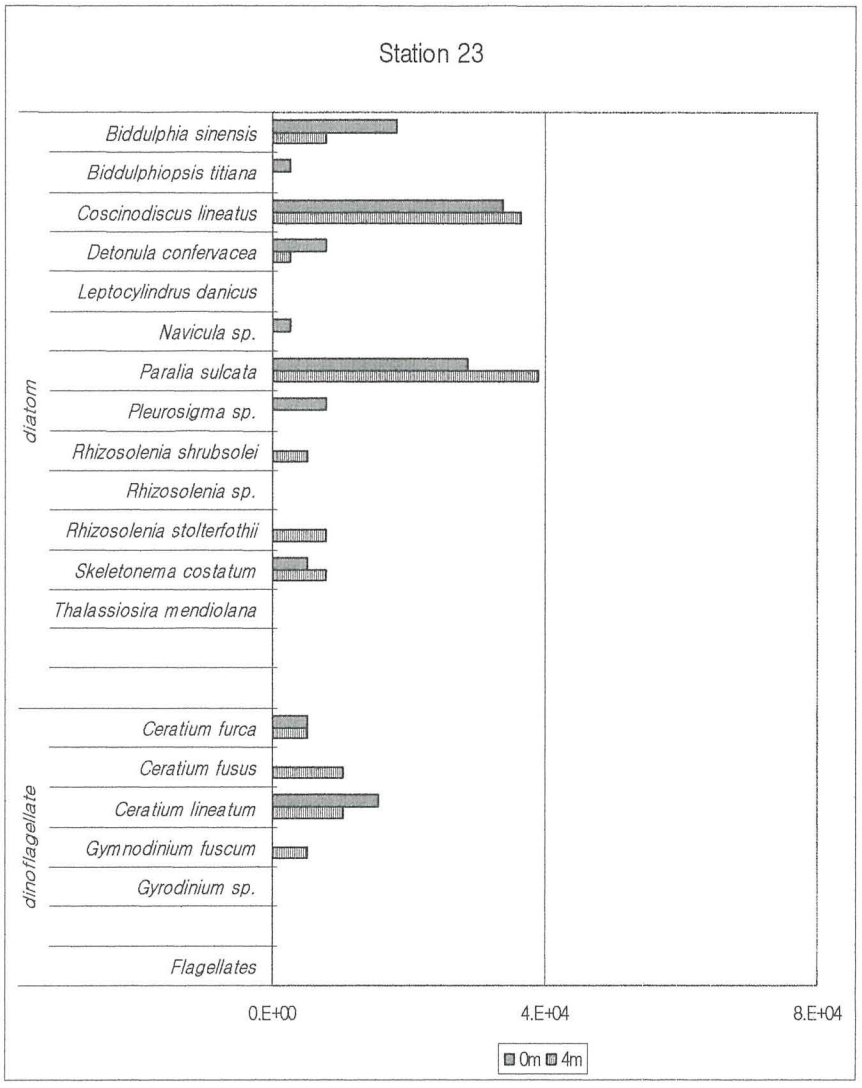

Appendix A-5 Irish Sea Taxonomic data (No. of cells l^{-1}) 02-April-2002

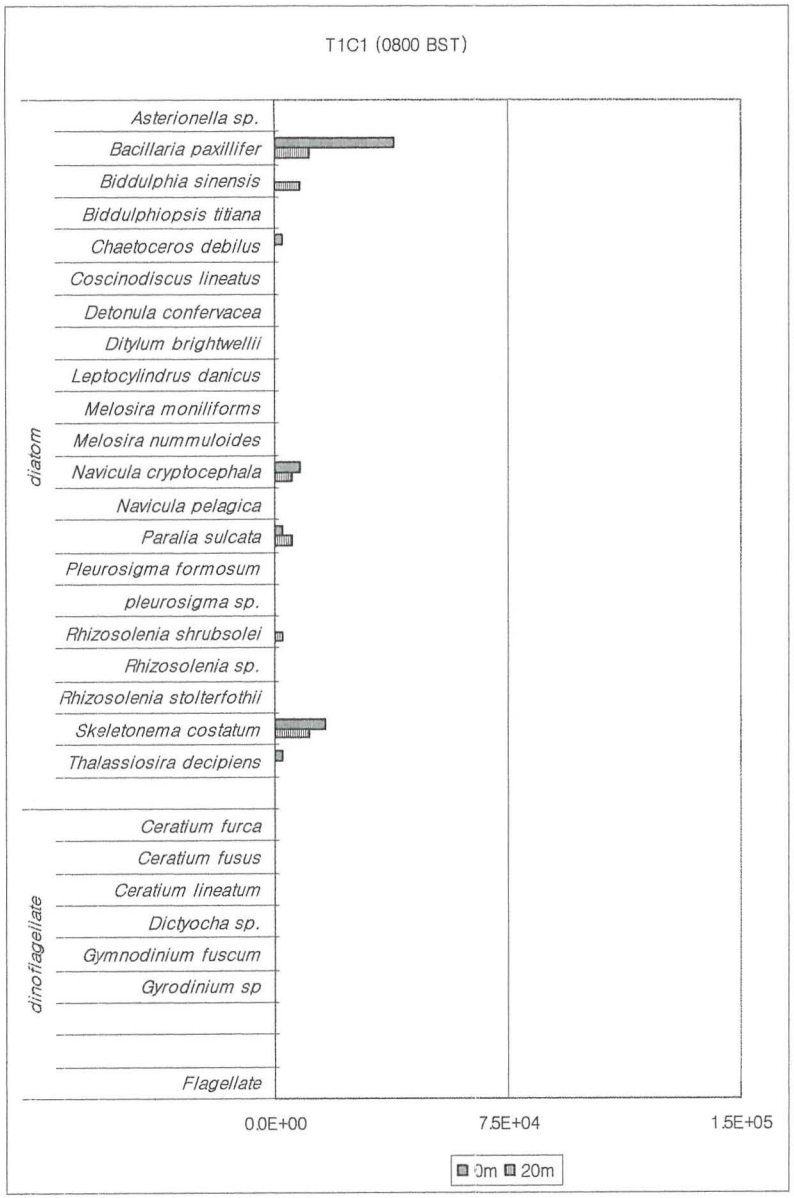

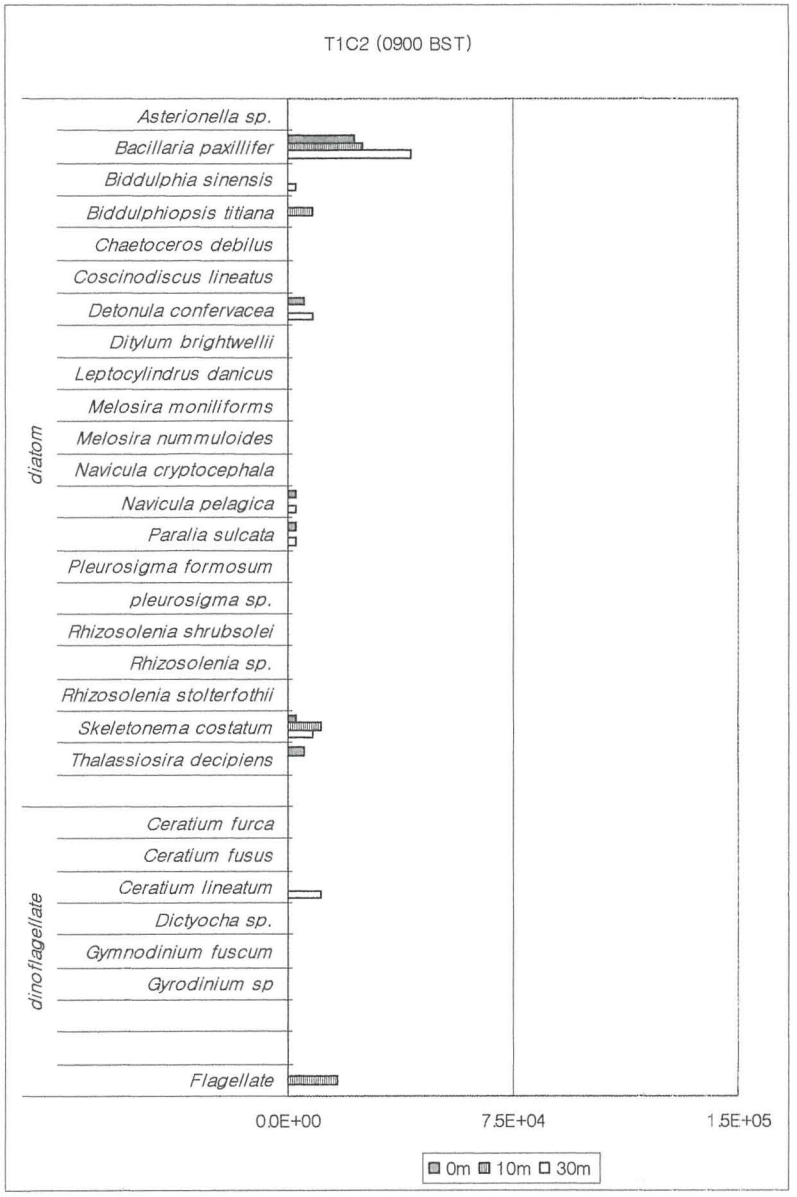

Appendix A-5 Irish Sea Taxonomic data (No. of cells l^{-1}) 02-April-2002

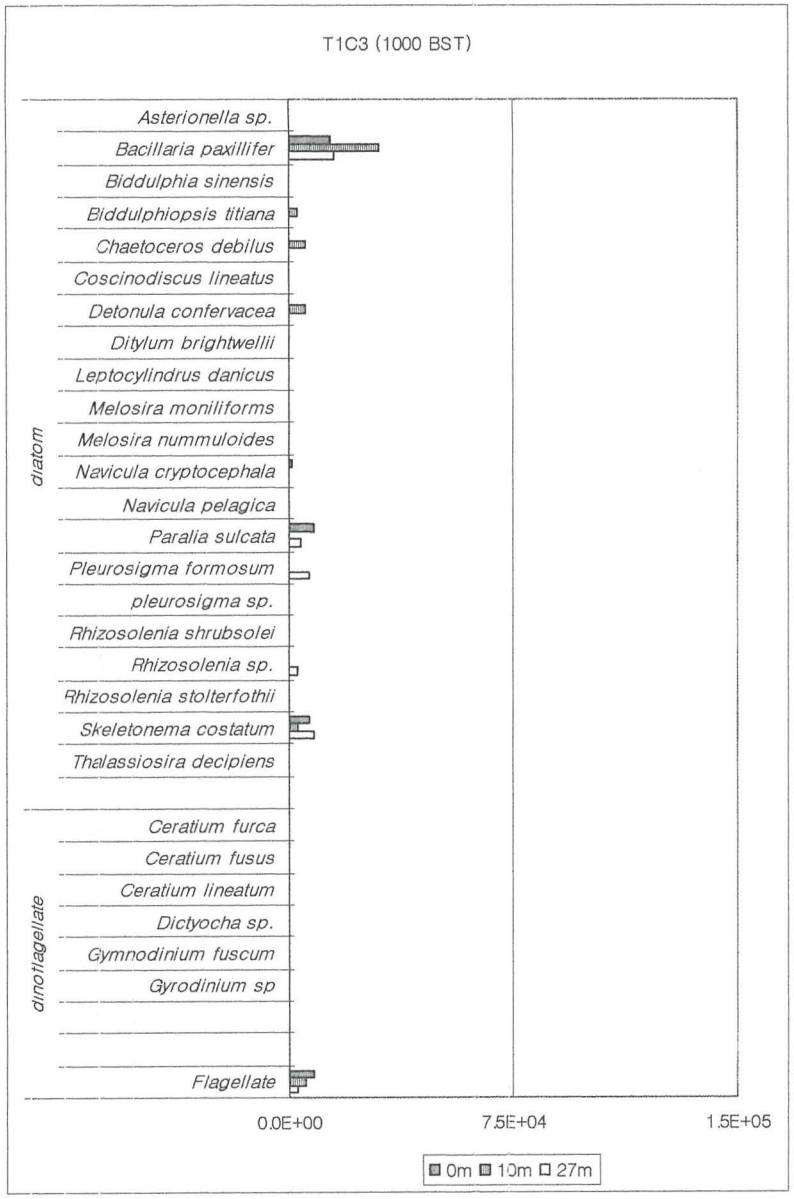

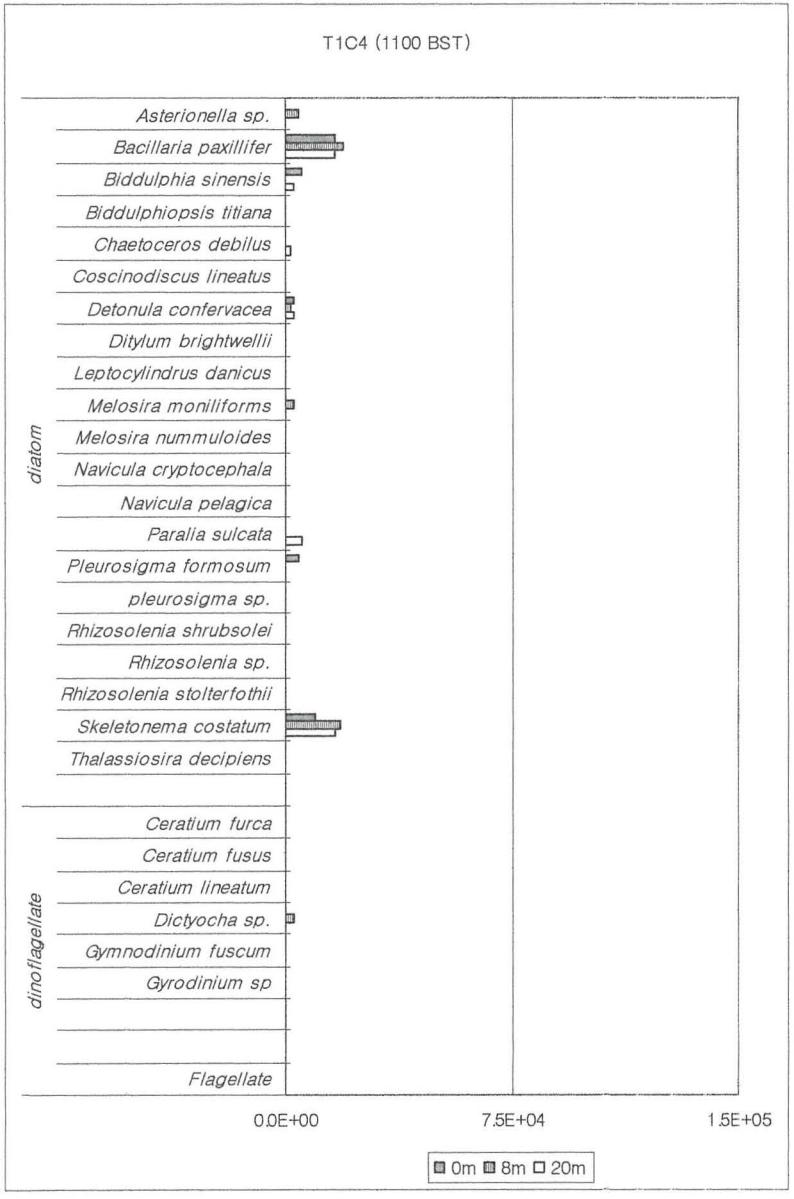

Appendix A-5 Irish Sea Taxonomic data (No. of cells l^{-1}) 02-April-2002

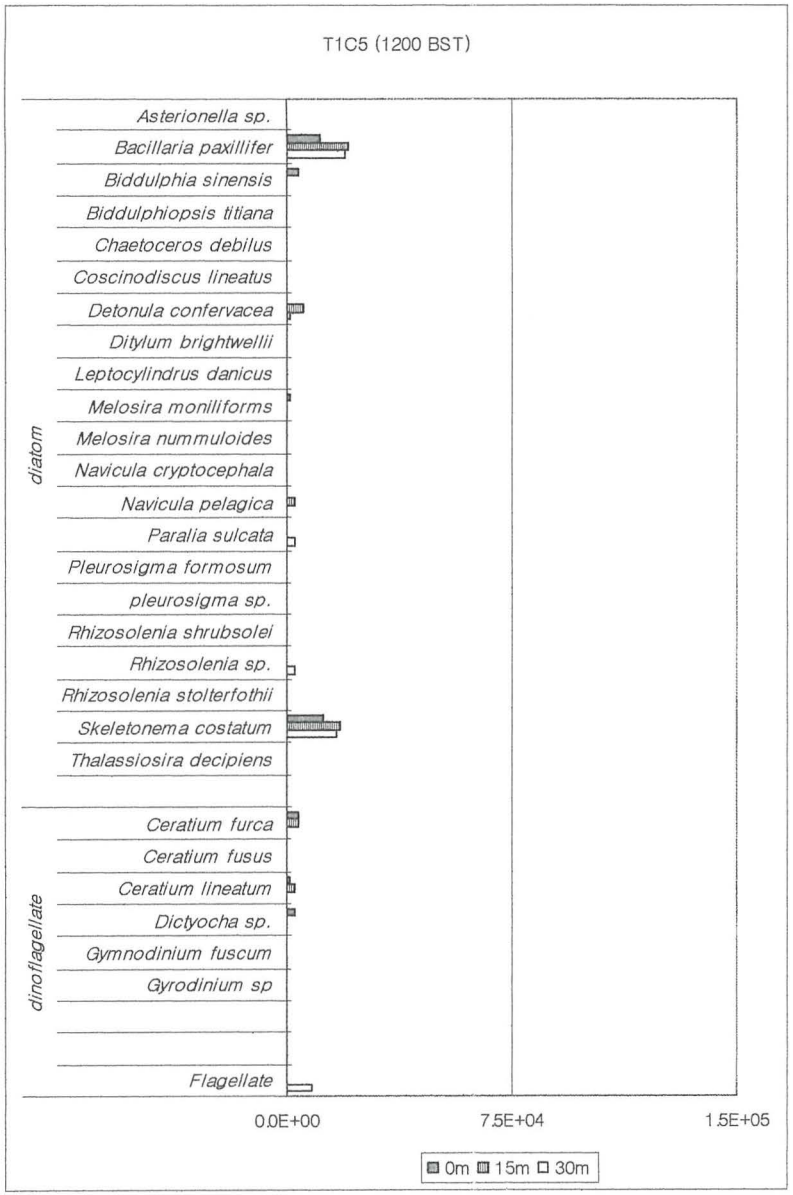

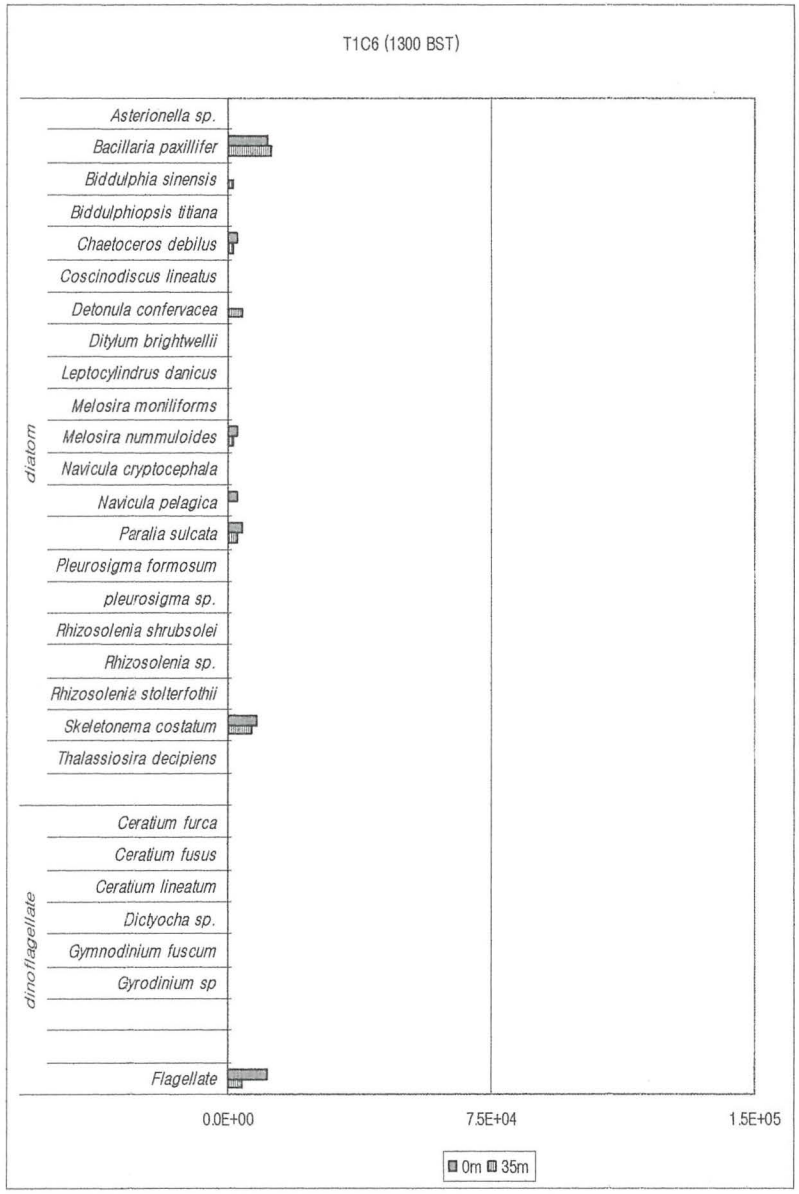

Appendix A-5 Irish Sea Taxonomic data (No. of cells l^{-1}) 02-April-2002

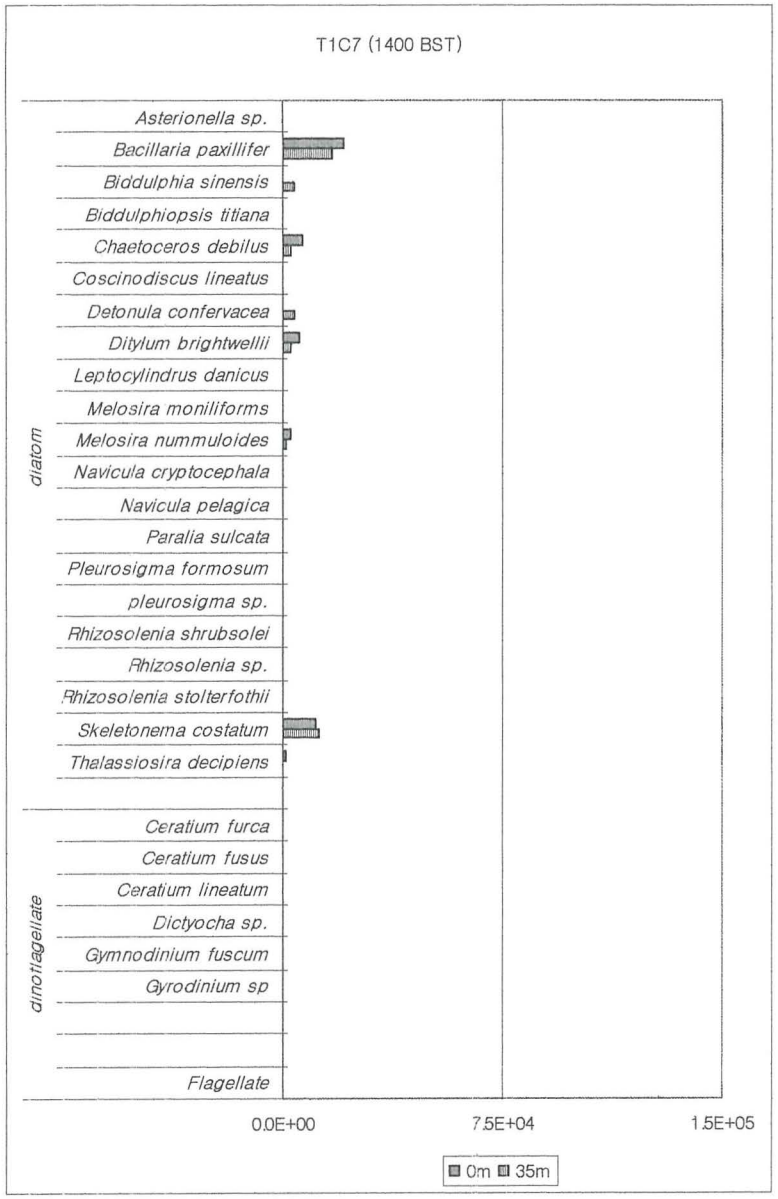

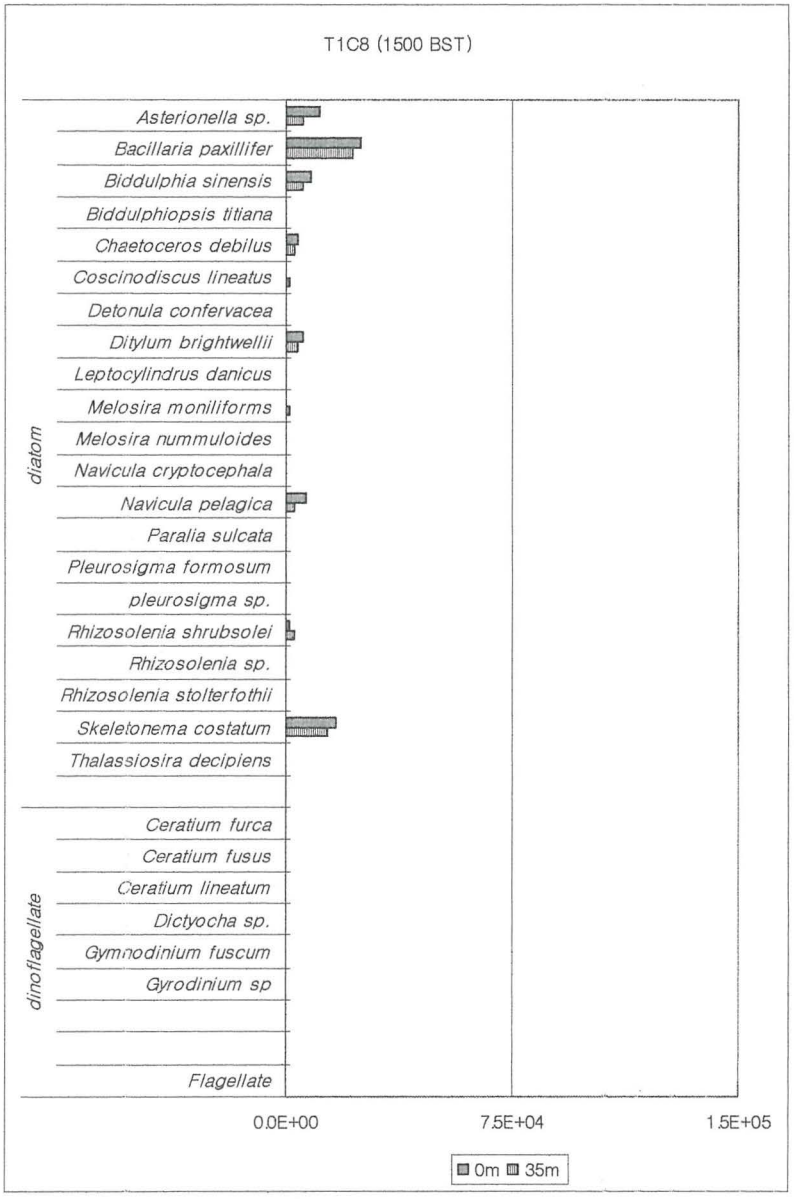

Appendix A-5 Irish Sea Taxonomic data (No. of cells l^{-1}) 02-April-2002

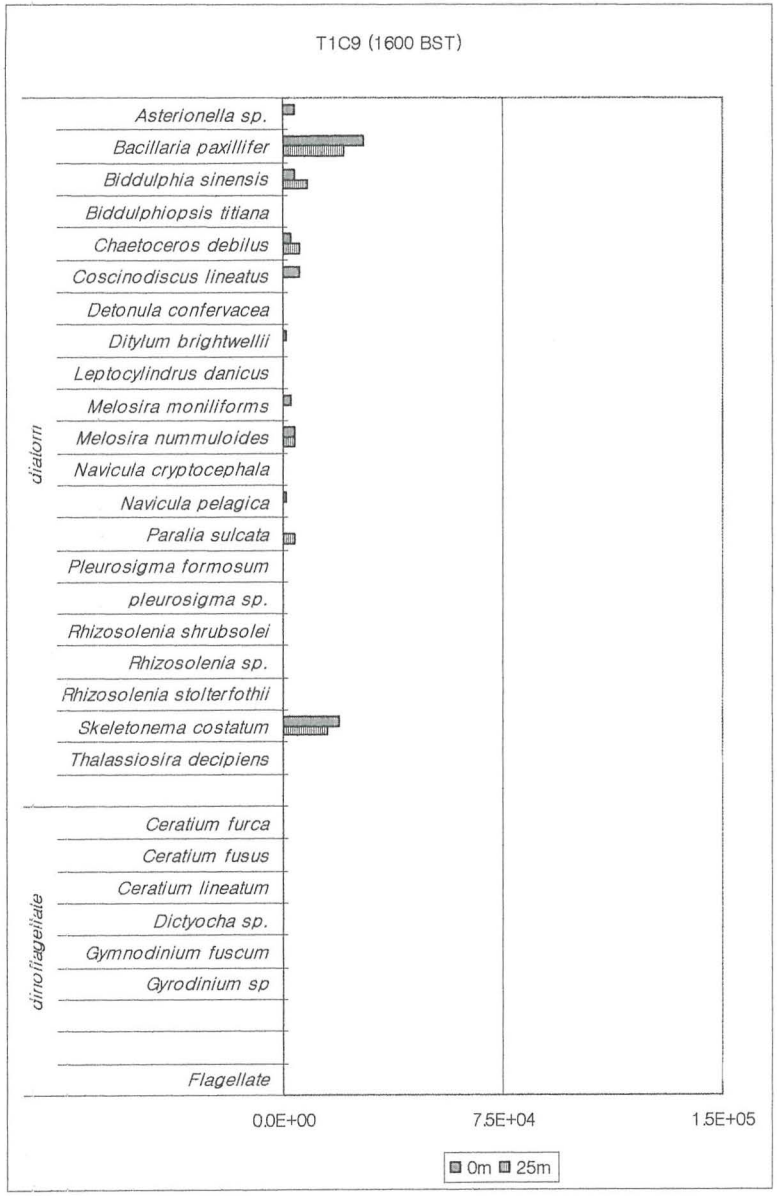

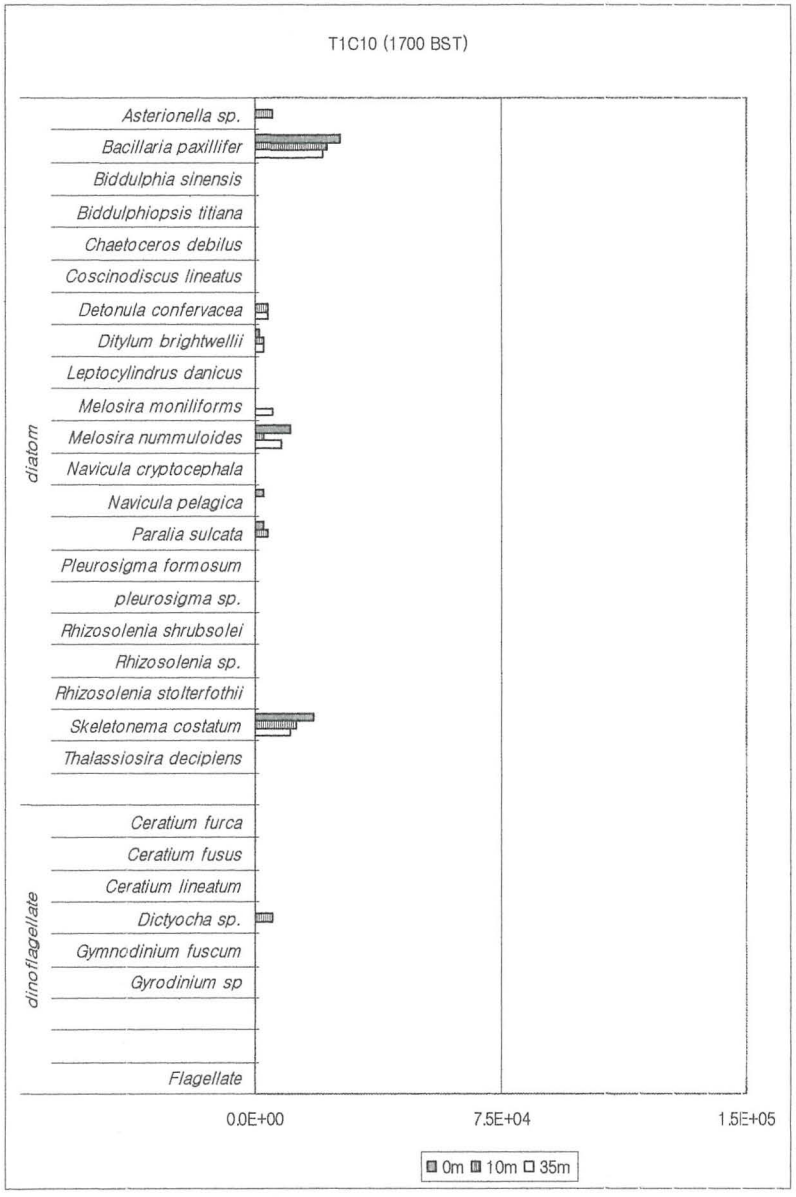

Appendix A-5 Irish Sea Taxonomic data (No. of cells l^{-1}) 02-April-2002

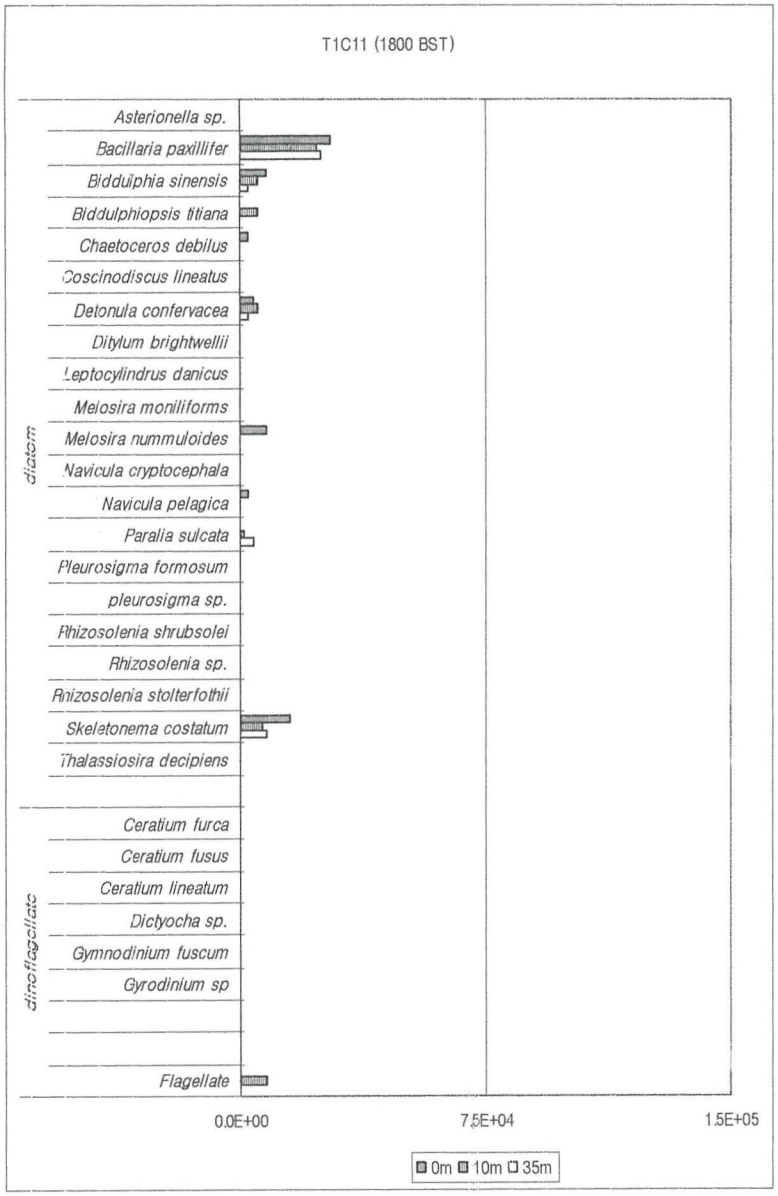

Appendix A-5 Irish Sea Taxonomic data (No. of cells l^{-1}) 03-April-2002

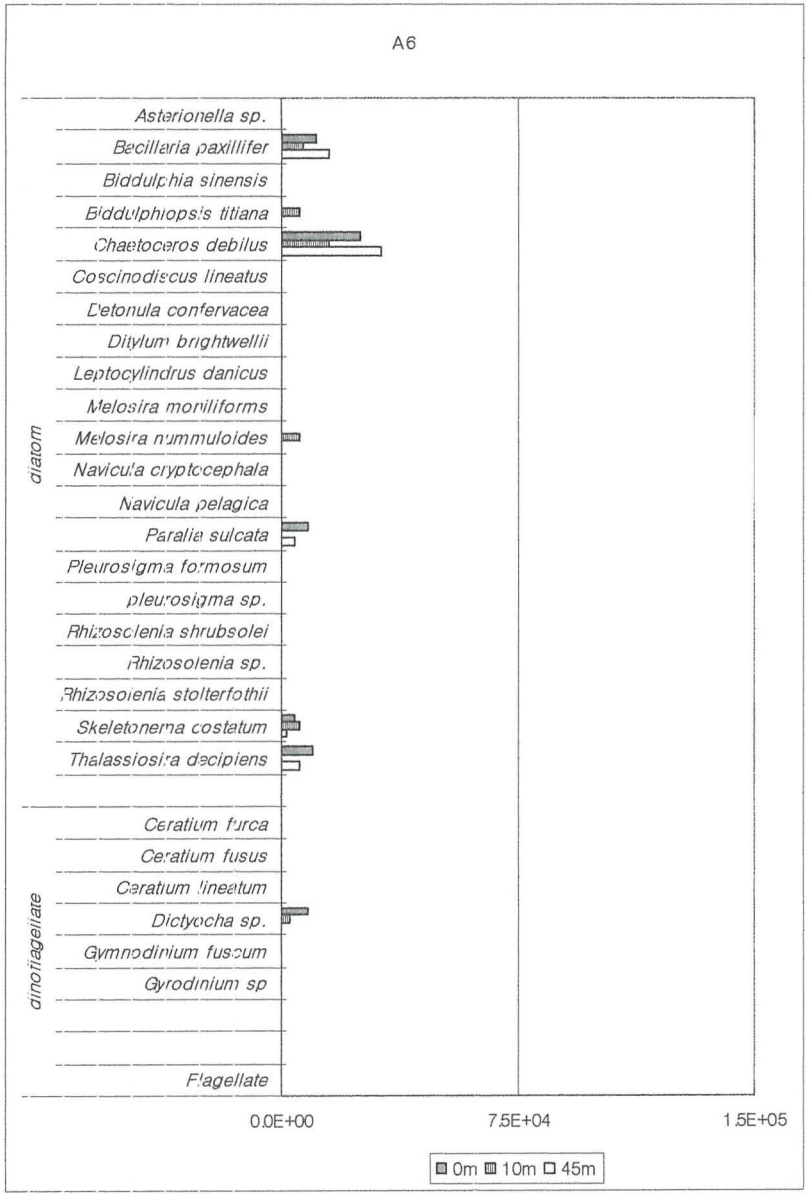

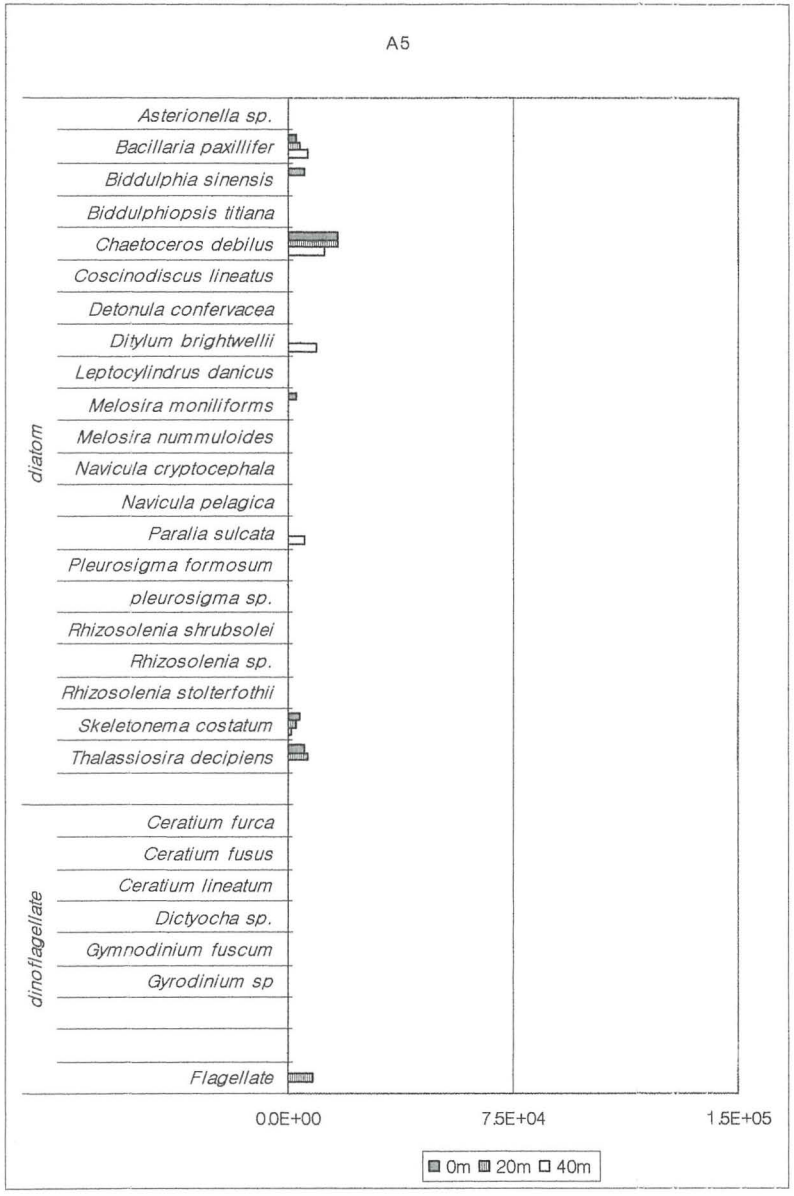

Appendix A-5 Irish Sea Taxonomic data (No. of cells l^{-1}) 03-April-2002

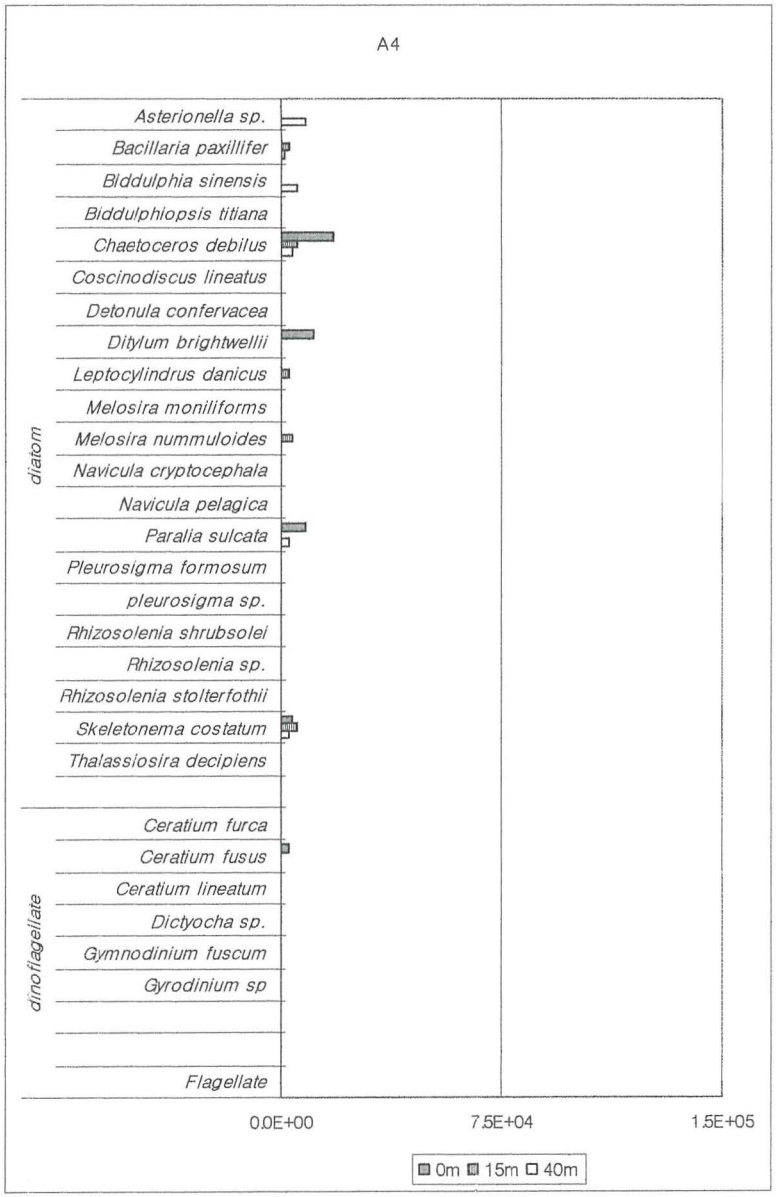

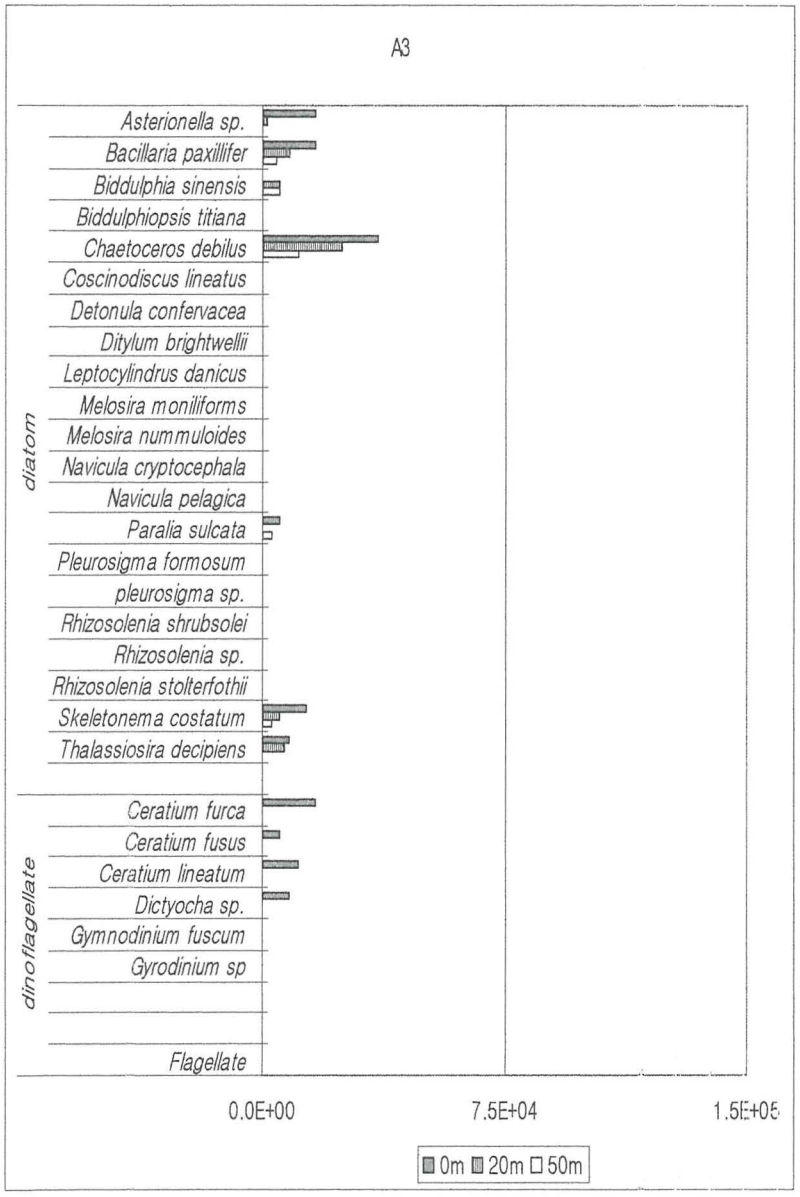

Appendix A-5 Irish Sea Taxonomic data (No. of cells l^{-1}) 03-April-2002

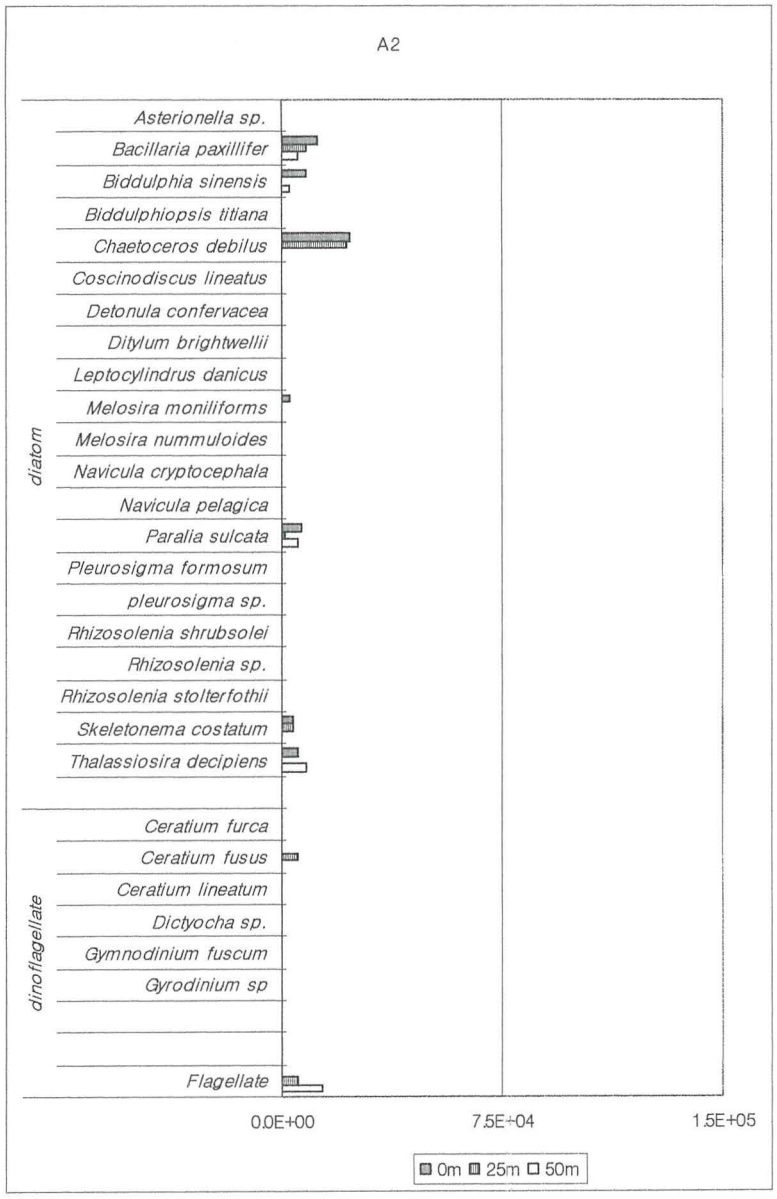

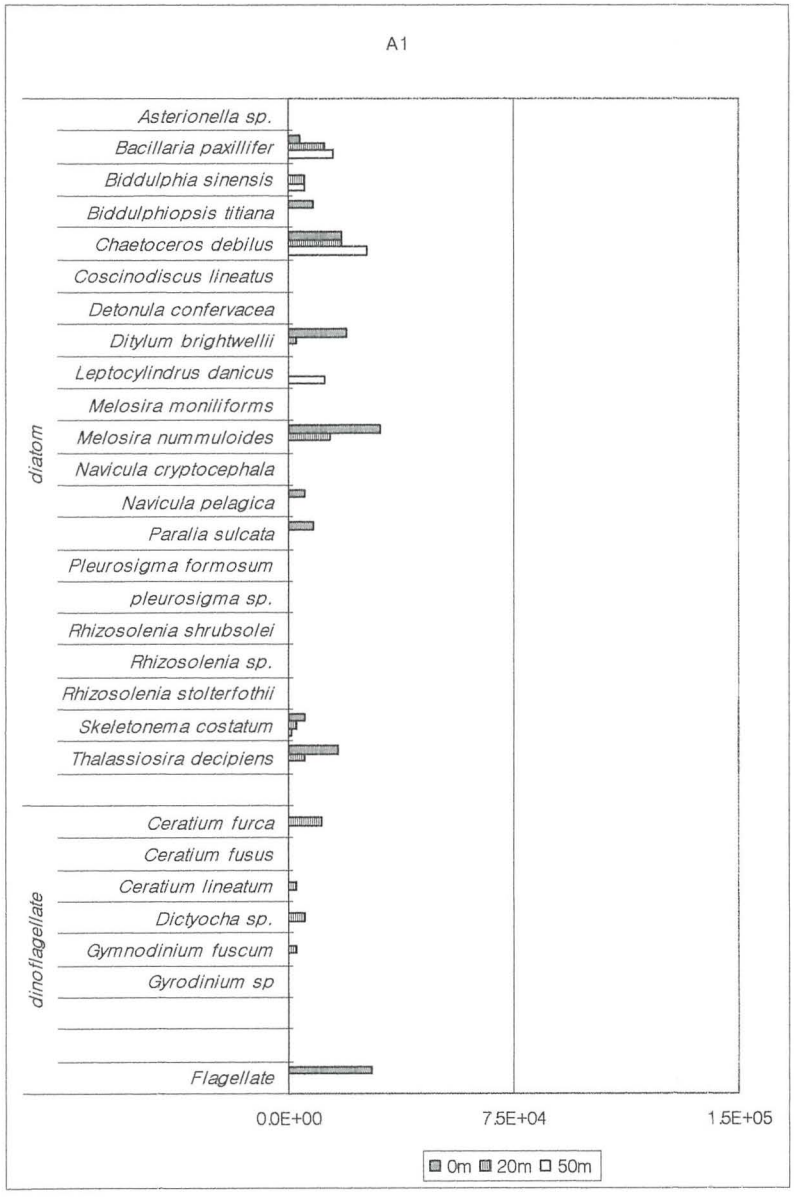

Appendix A-5 Irish Sea Taxonomic data (No. of cells l^{-1}) 03-April-2002

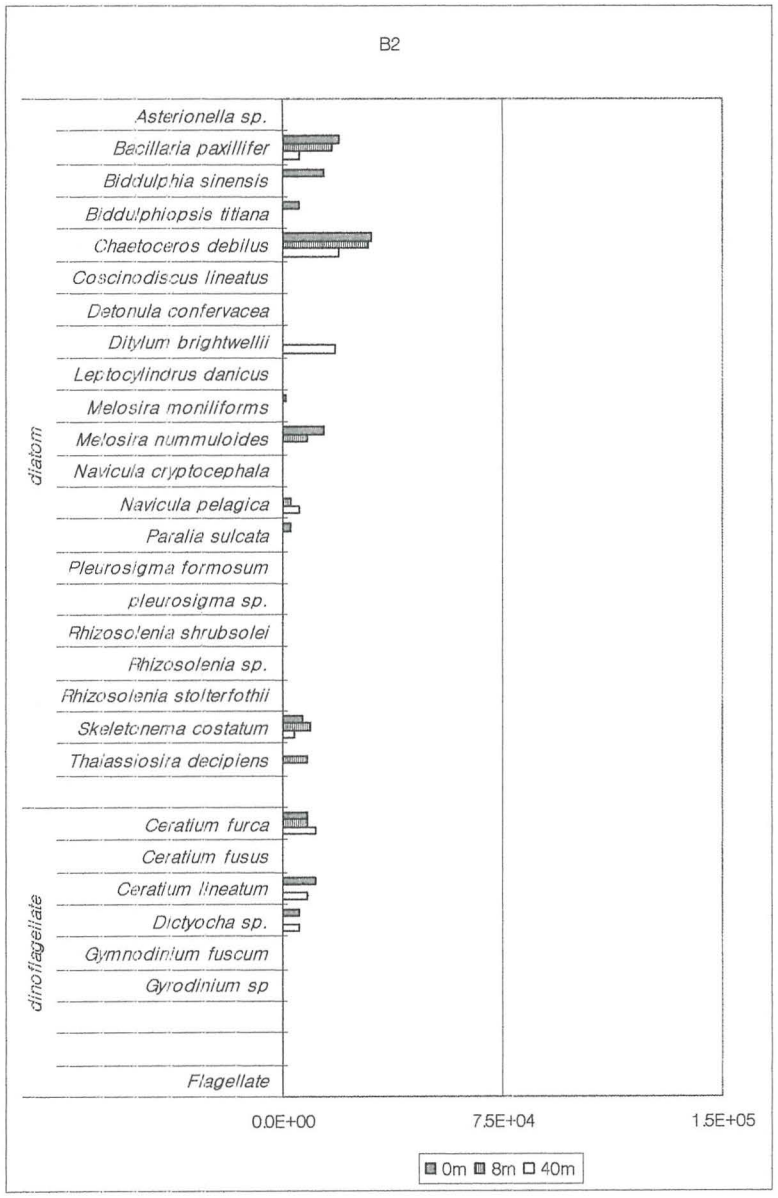

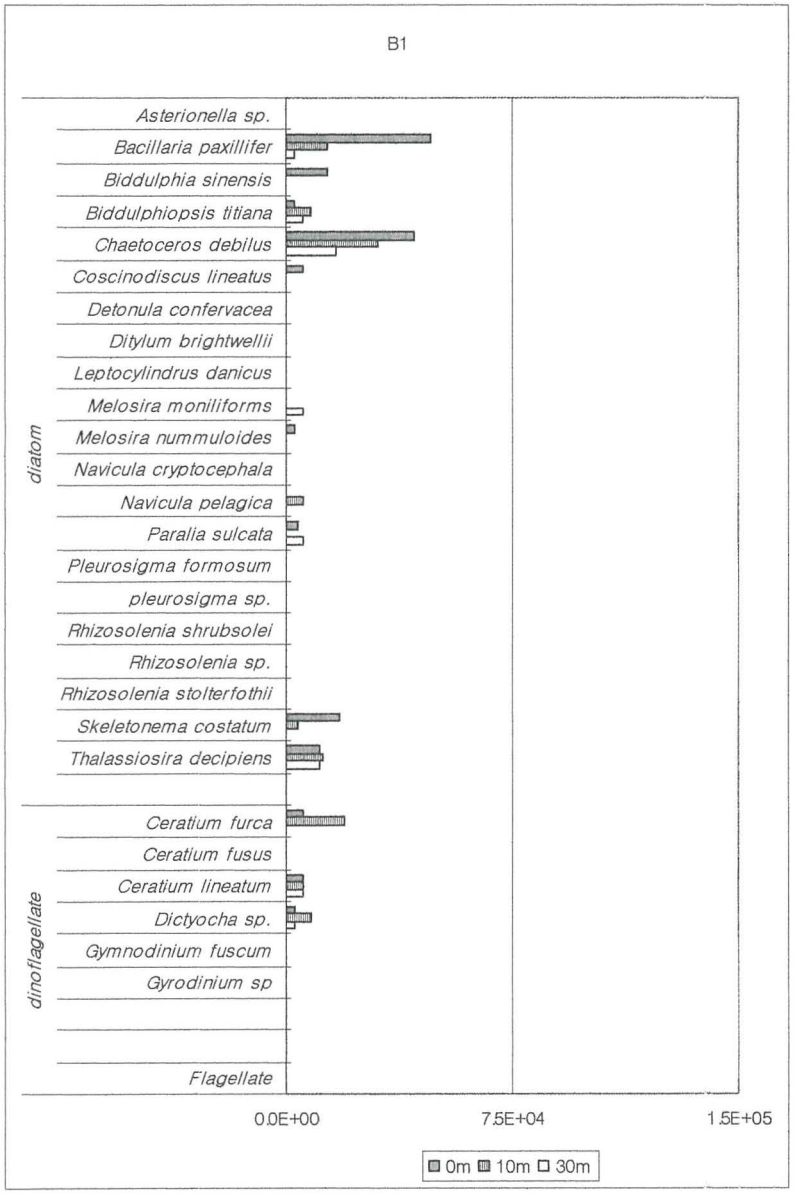

Appendix A-5 Irish Sea Taxonomic data (No. of cells l^{-1}) 03-April-2002

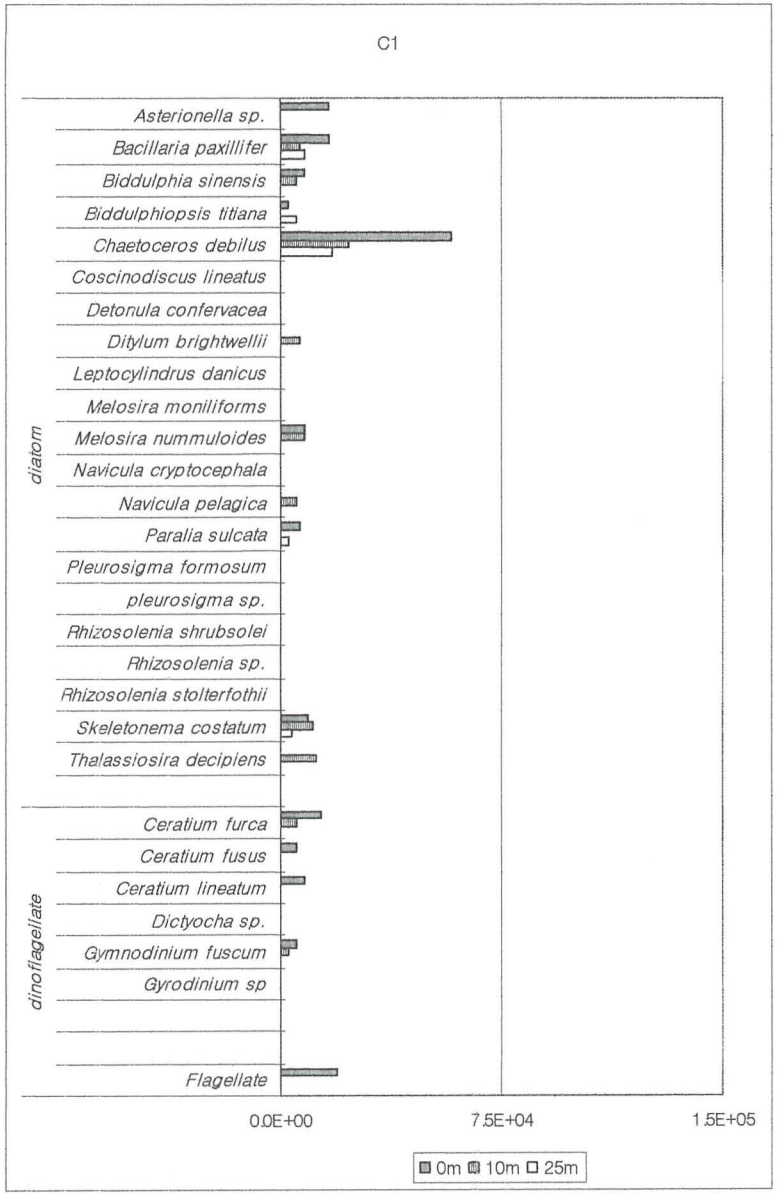

Appendix A-5 Irish Sea Taxonomic data (No. of cells l^{-1}) 04-April-2002

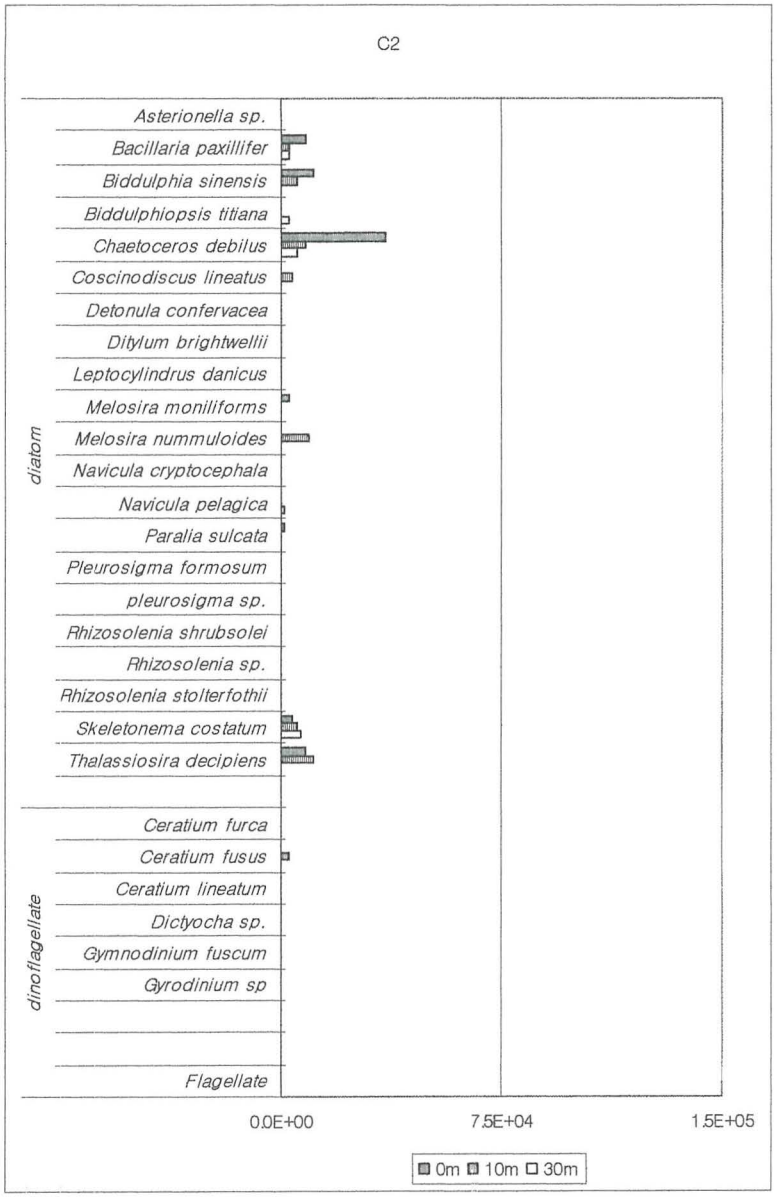

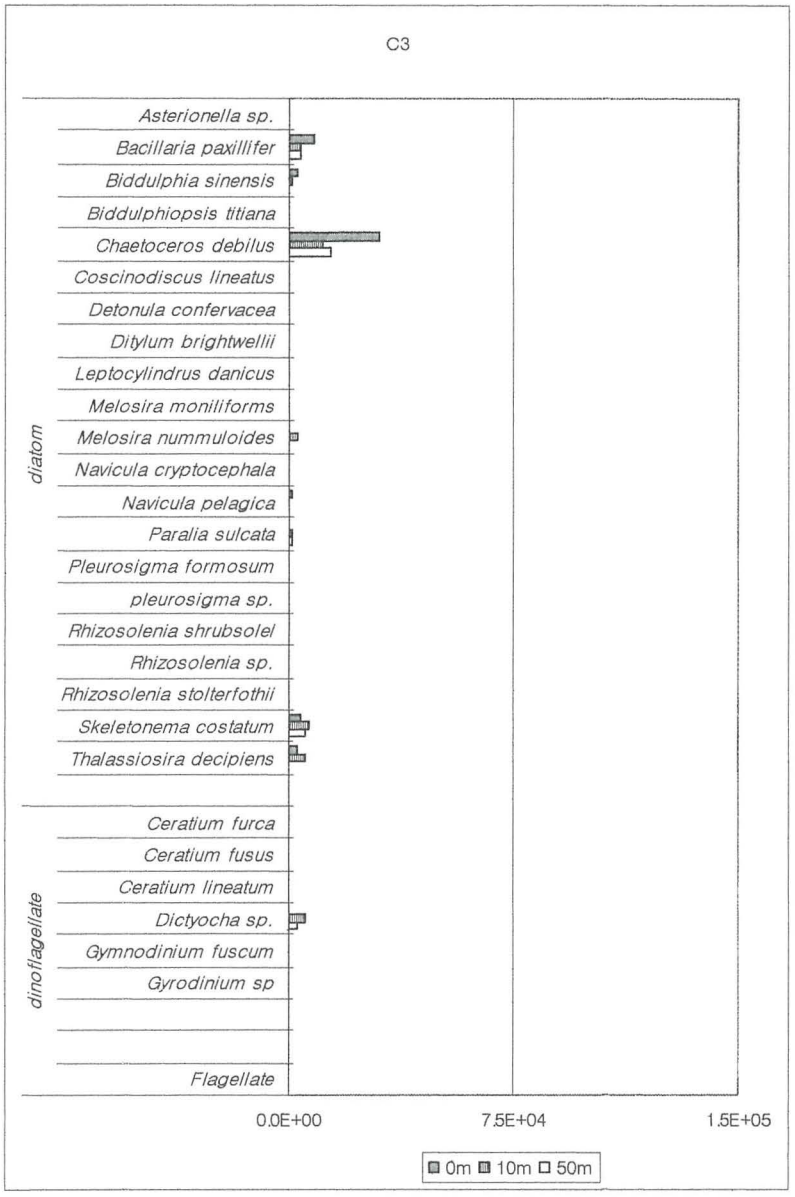

Appendix A-5 Irish Sea Taxonomic data (No. of cells l^{-1}) 04-April-2002

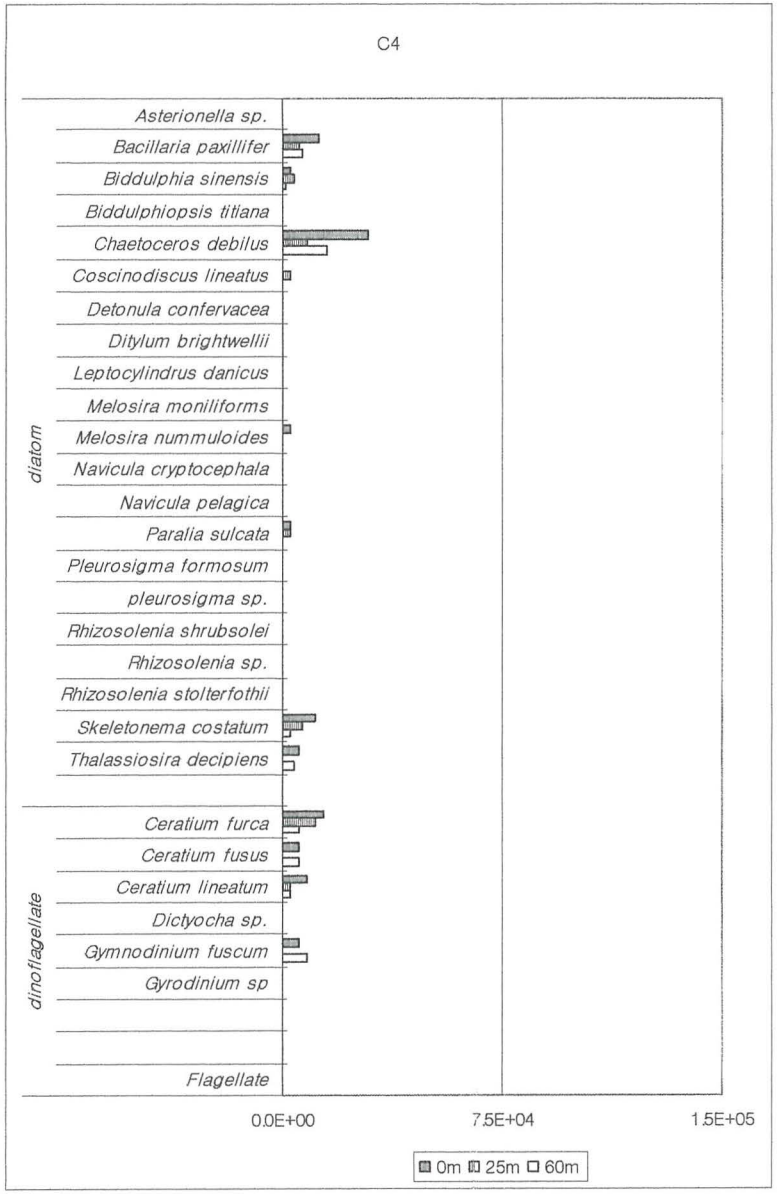

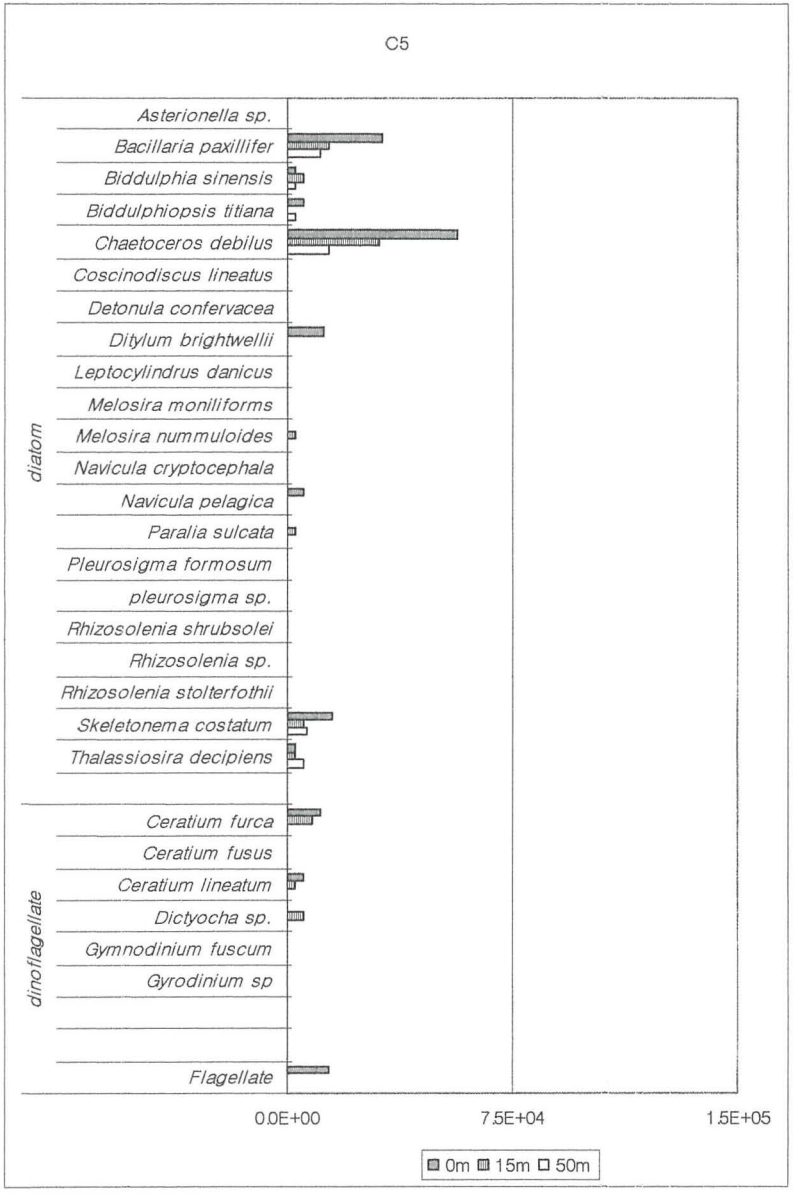

Appendix A-5 Irish Sea Taxonomic data (No. of cells l^{-1}) 04-April-2002

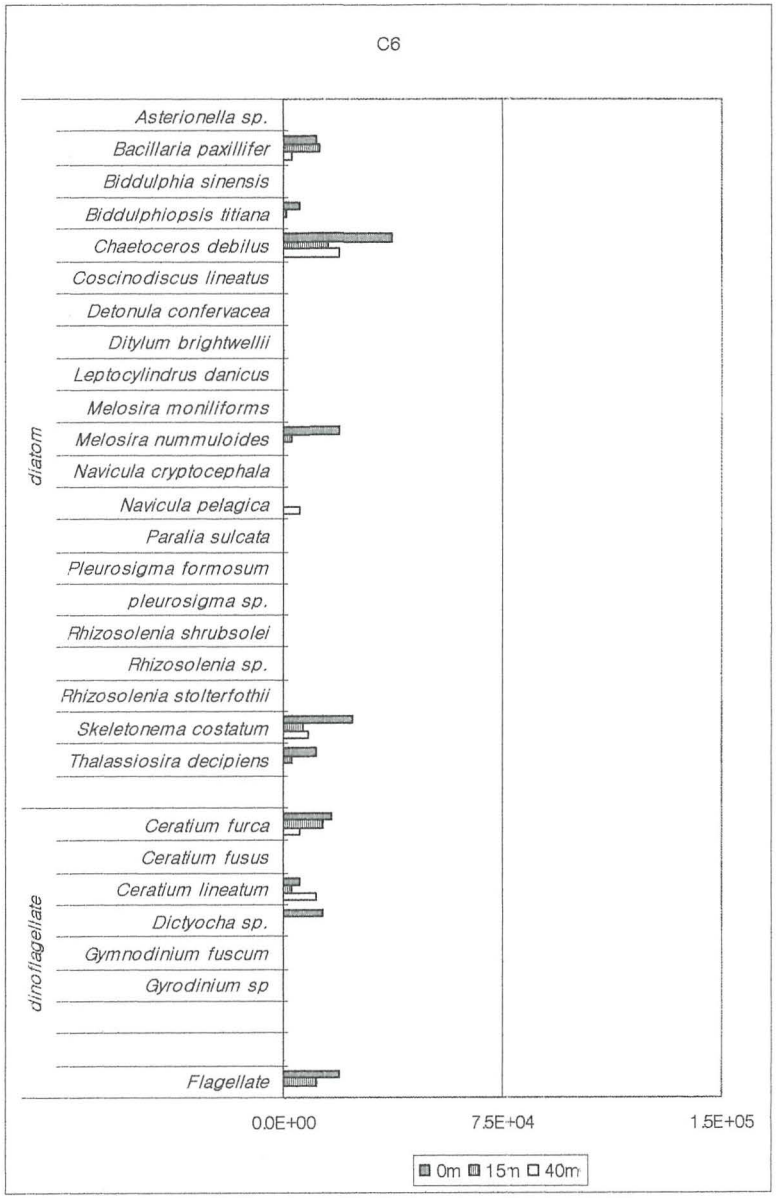

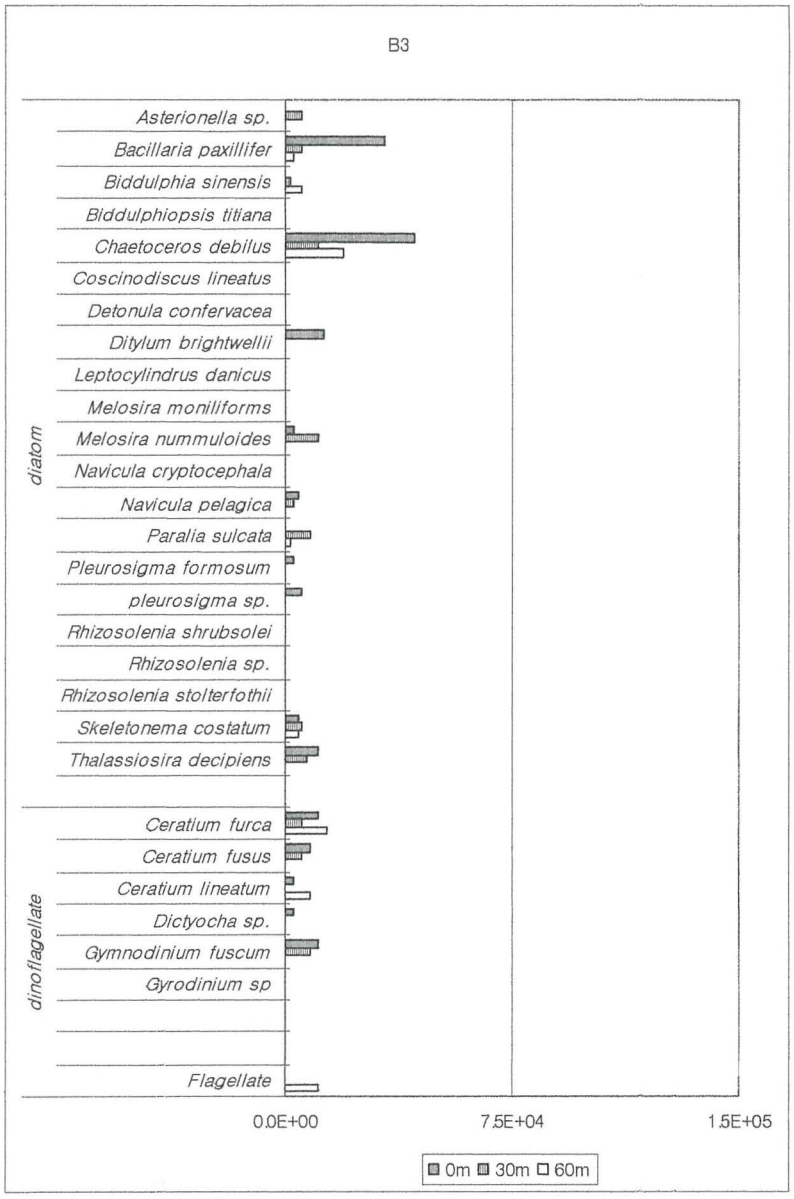

Appendix A-5 Irish Sea Taxonomic data (No. of cells l^{-1}) 04-April-2002

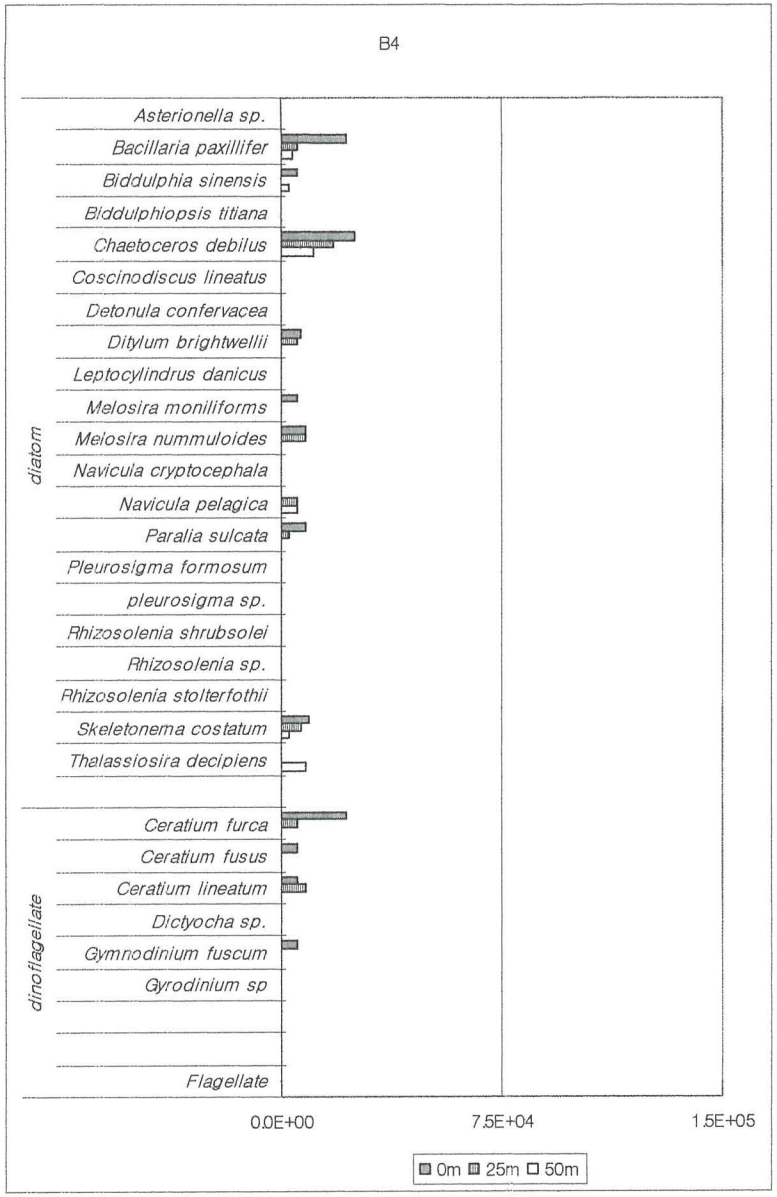

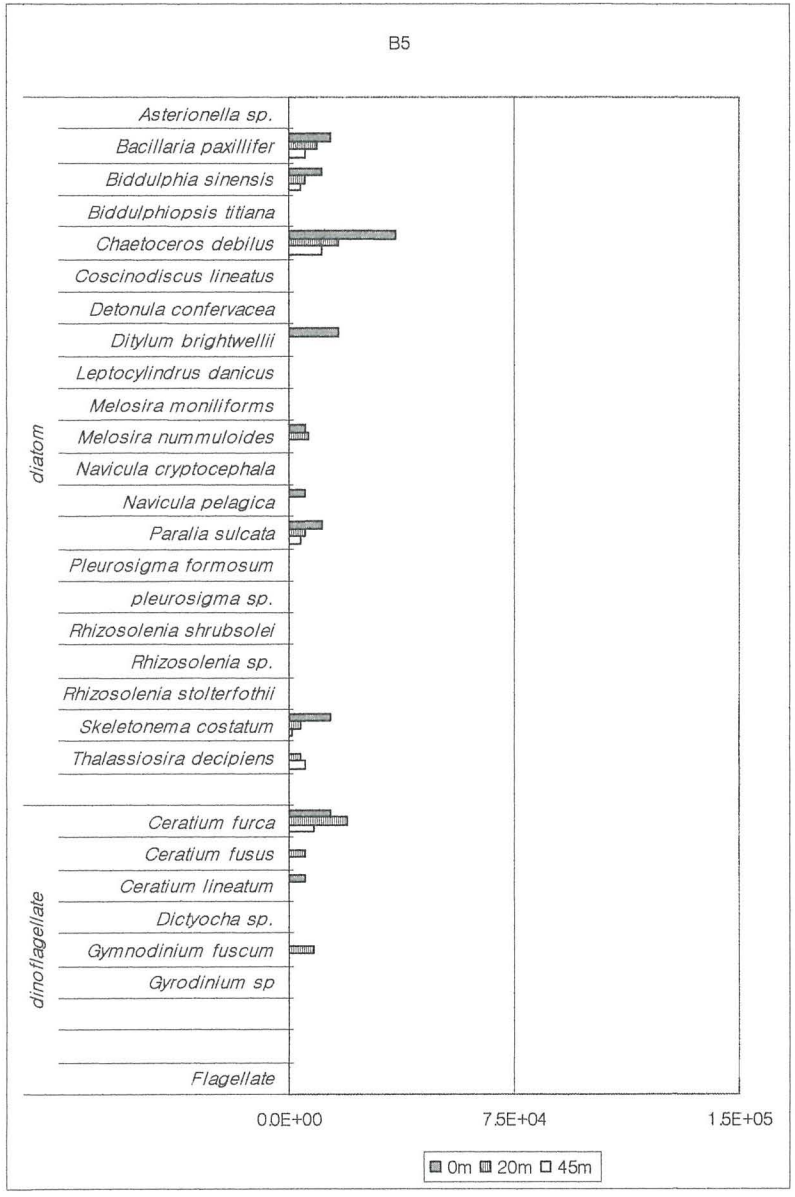

Appendix A-5 Irish Sea Taxonomic data (No. of cells l^{-1}) 04-April-2002

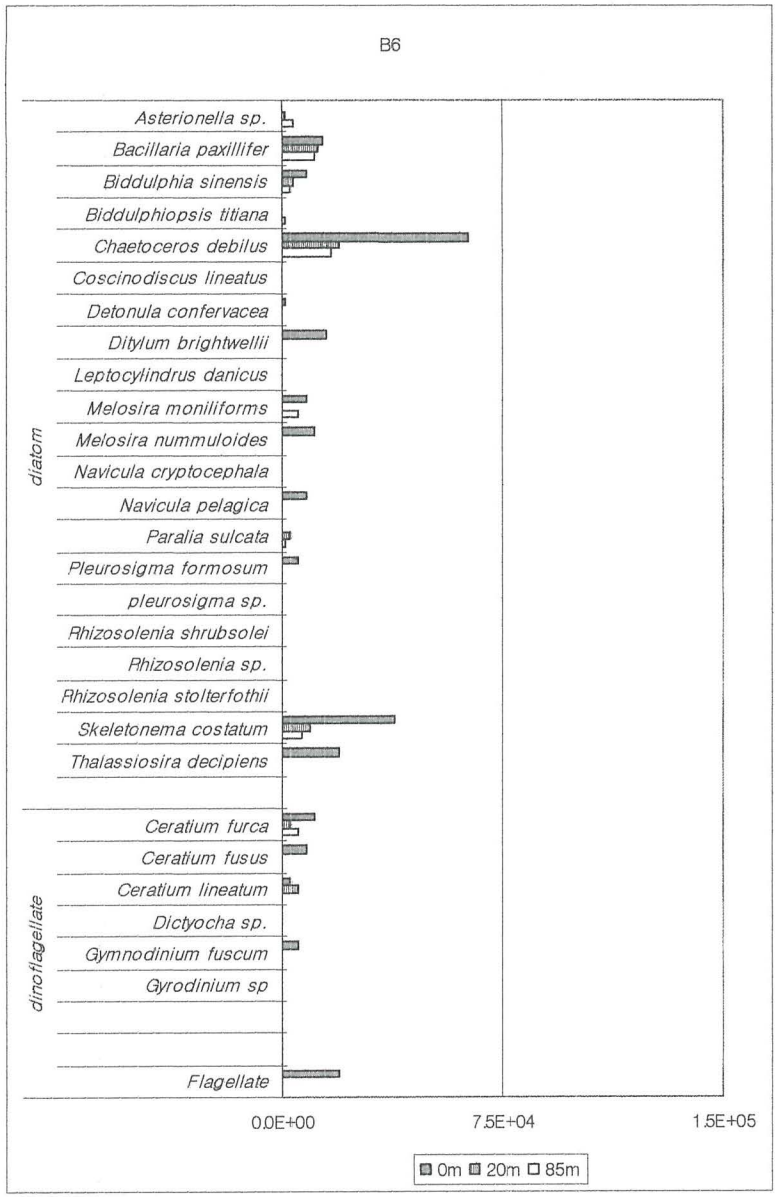

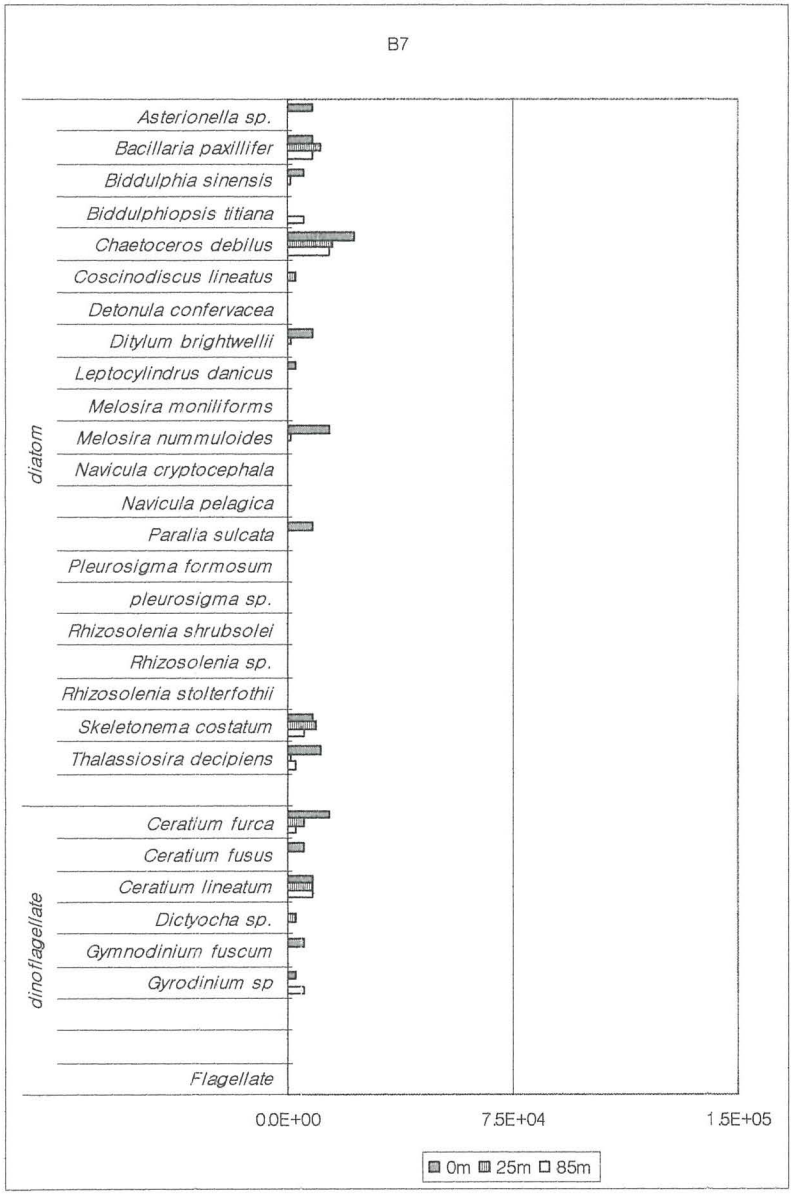

Appendix A-5 Irish Sea Taxonomic data (No. of cells l^{-1}) 05-April-2002

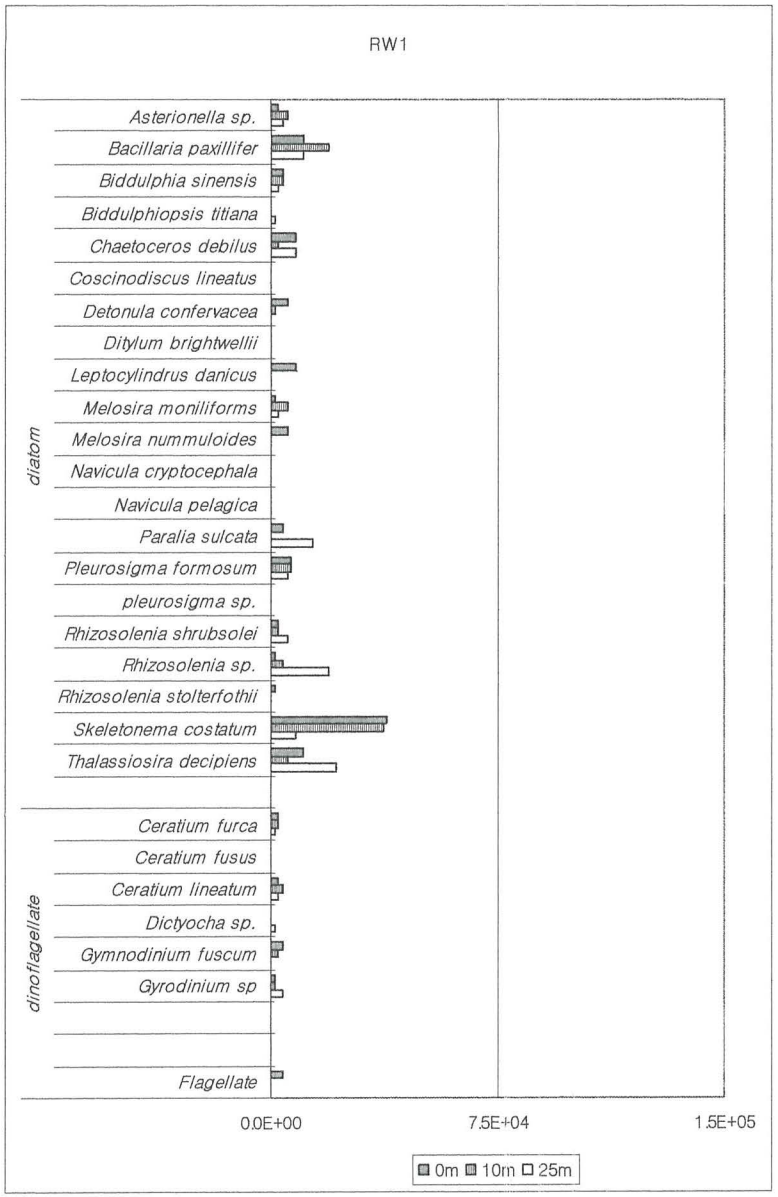

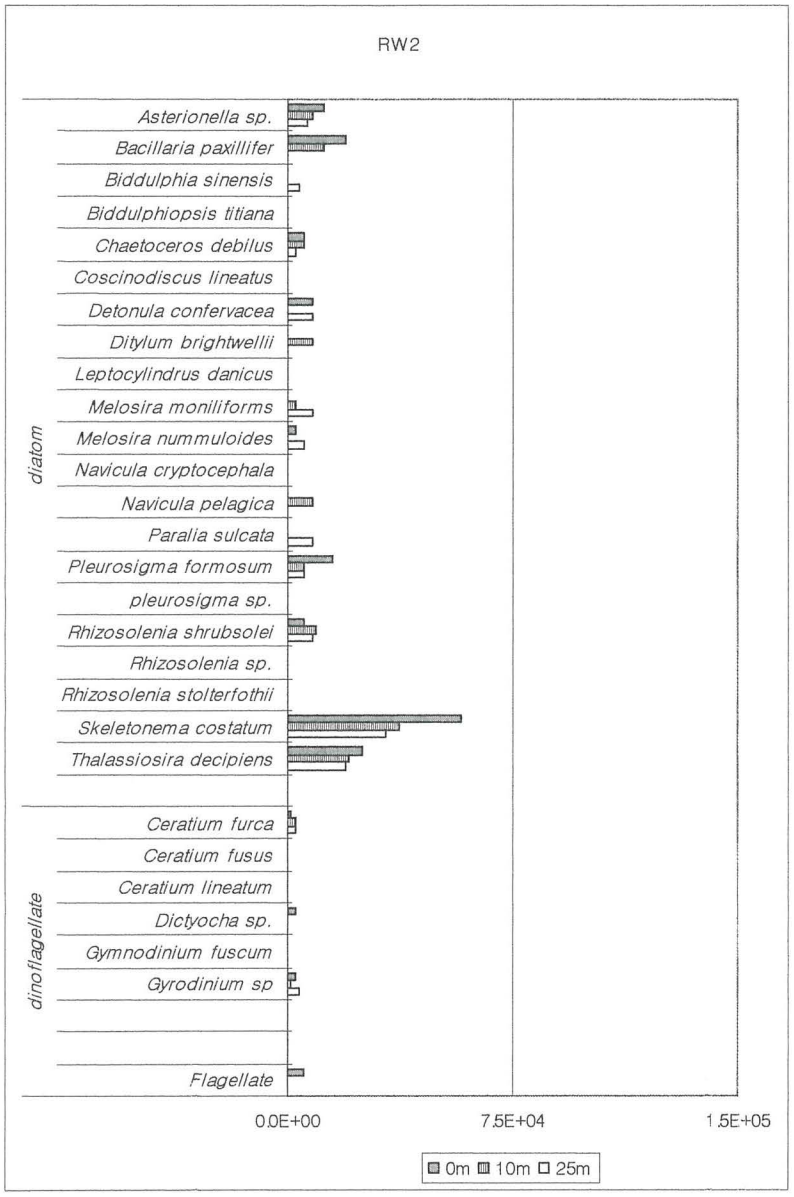

Appendix A-5 Irish Sea Taxonomic data (No. of cells l^{-1}) 05-April-2002

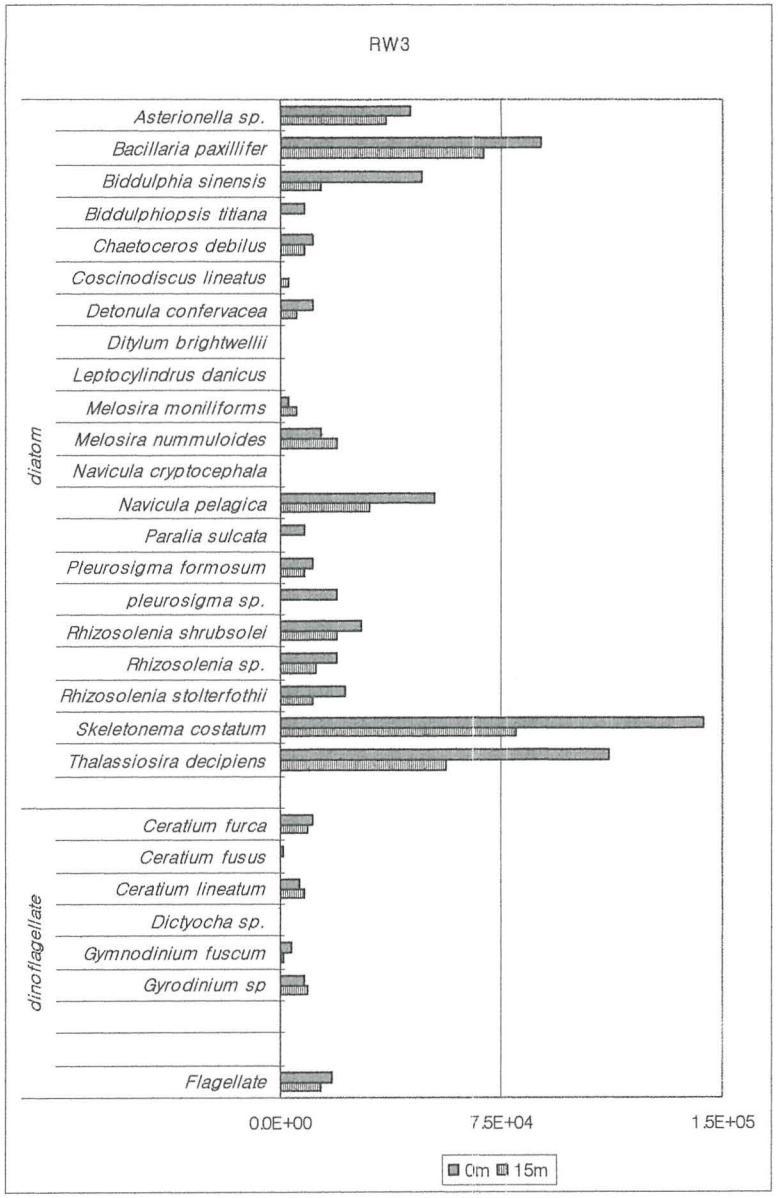

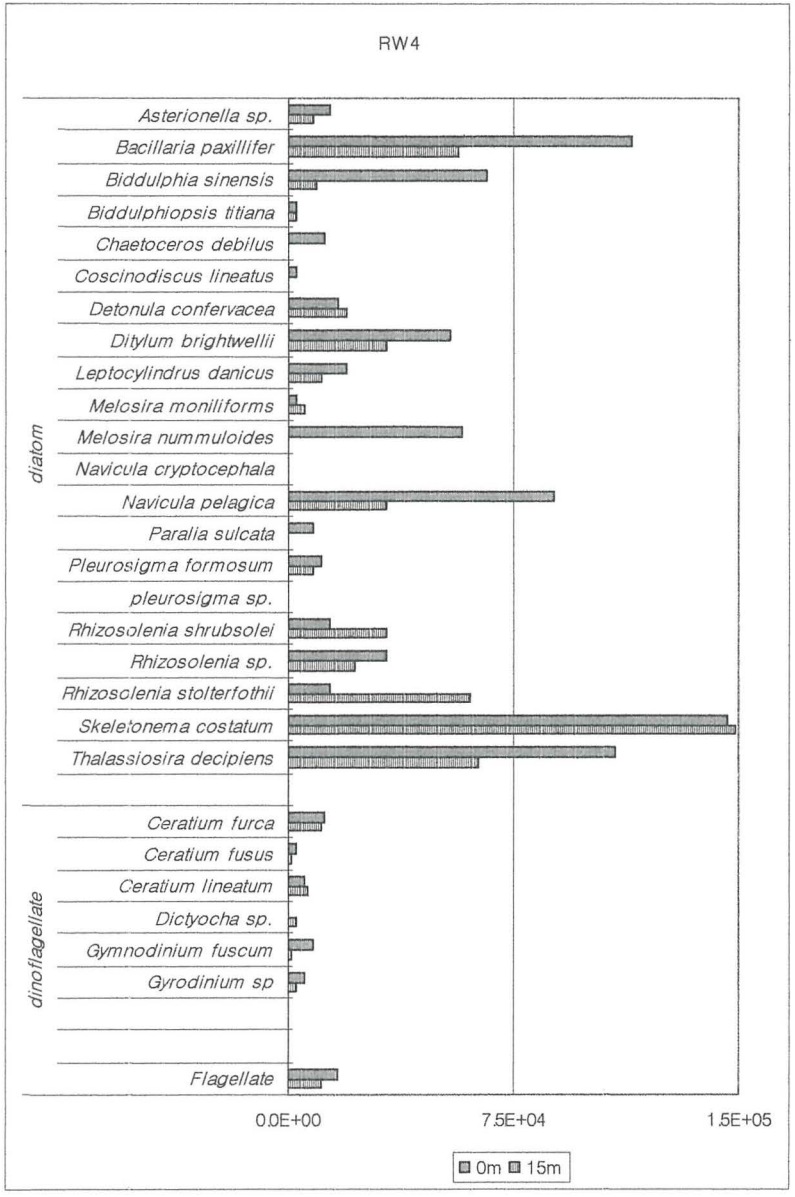

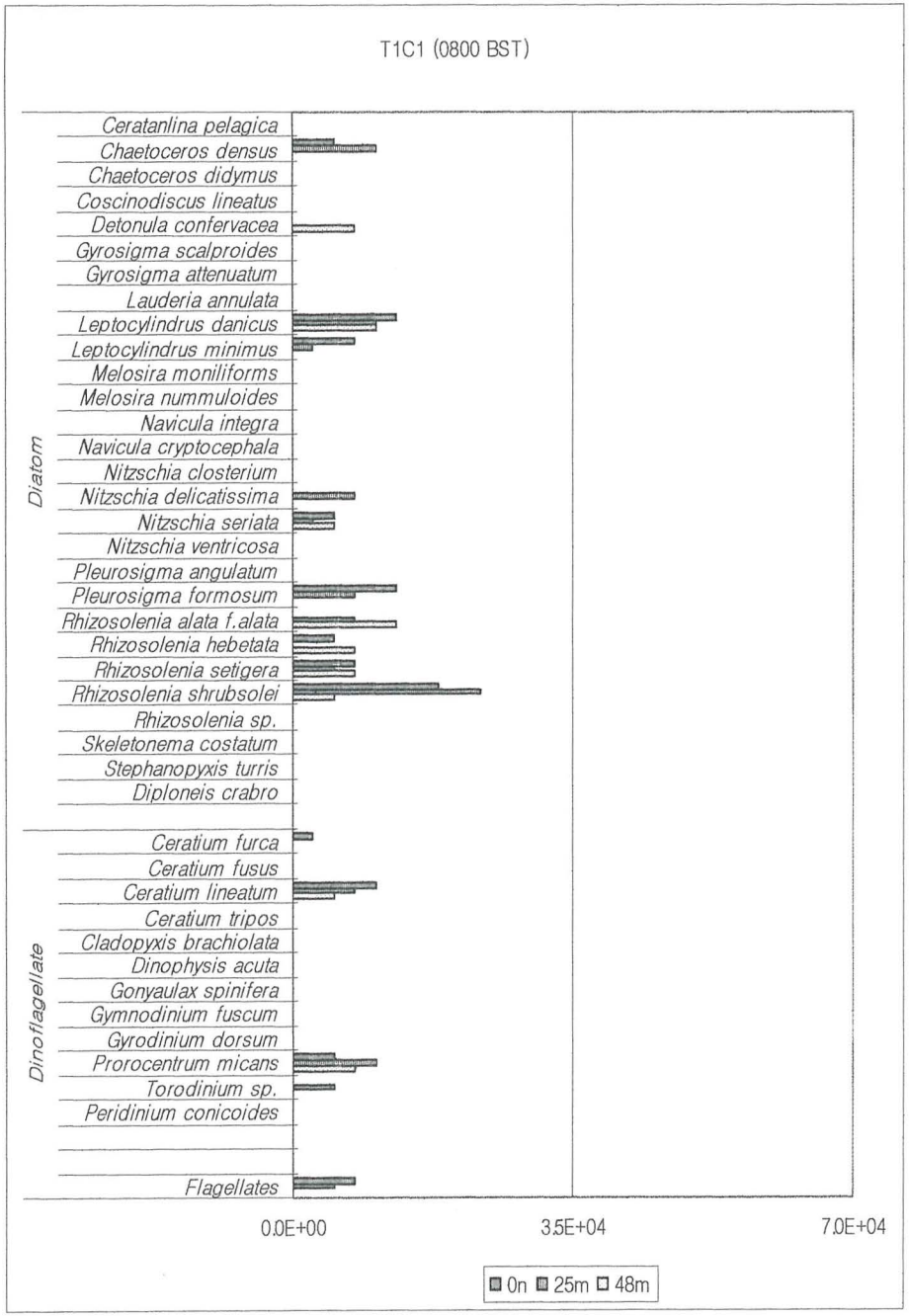
T1C1 (0800 BST)
Ceratanlina pelagica
Chaetoceros densus
Chaetoceros didymus
Coscinodiscus lineatus
Detonula confervacea
Gyrosigma scalproides
Gyrosigma attenuatum
Lauderia annulata
Leptocylindrus danicus
Leptocylindrus minimus
Melosira moniliforms
Melosira nummuloides
Navicula integra
Navicula cryptocephala
Nitzschia closterium
Nitzschia delicatissima
Nitzschia seriata
Nitzschia ventricosa
Pleurosigma angulatum
Pleurosigma formosum
Rhizosolenia alata f.alata
Rhizosolenia hebetata
Rhizosolenia setigera
Rhizosolenia shrubsolei
Rhizosolenia sp.
Skeletonema costatum
Stephanopyxis turris
Diploneis crabro
Diatom
Ceratium furca
Ceratium fusus
Ceratium lineatum
Ceratium tripos
Cladopyxis brachiolata
Dinophysis acuta
Gonyaulax spinifera
Gymnodinium fuscum
Gyrodinium dorsum
Prorocentrum micans
Torodinium sp.
Peridinium conicoides
Dinoflagellate
Flagellates
0.0E+00
3.5E+04
7.0E+04
0n 25m 48m

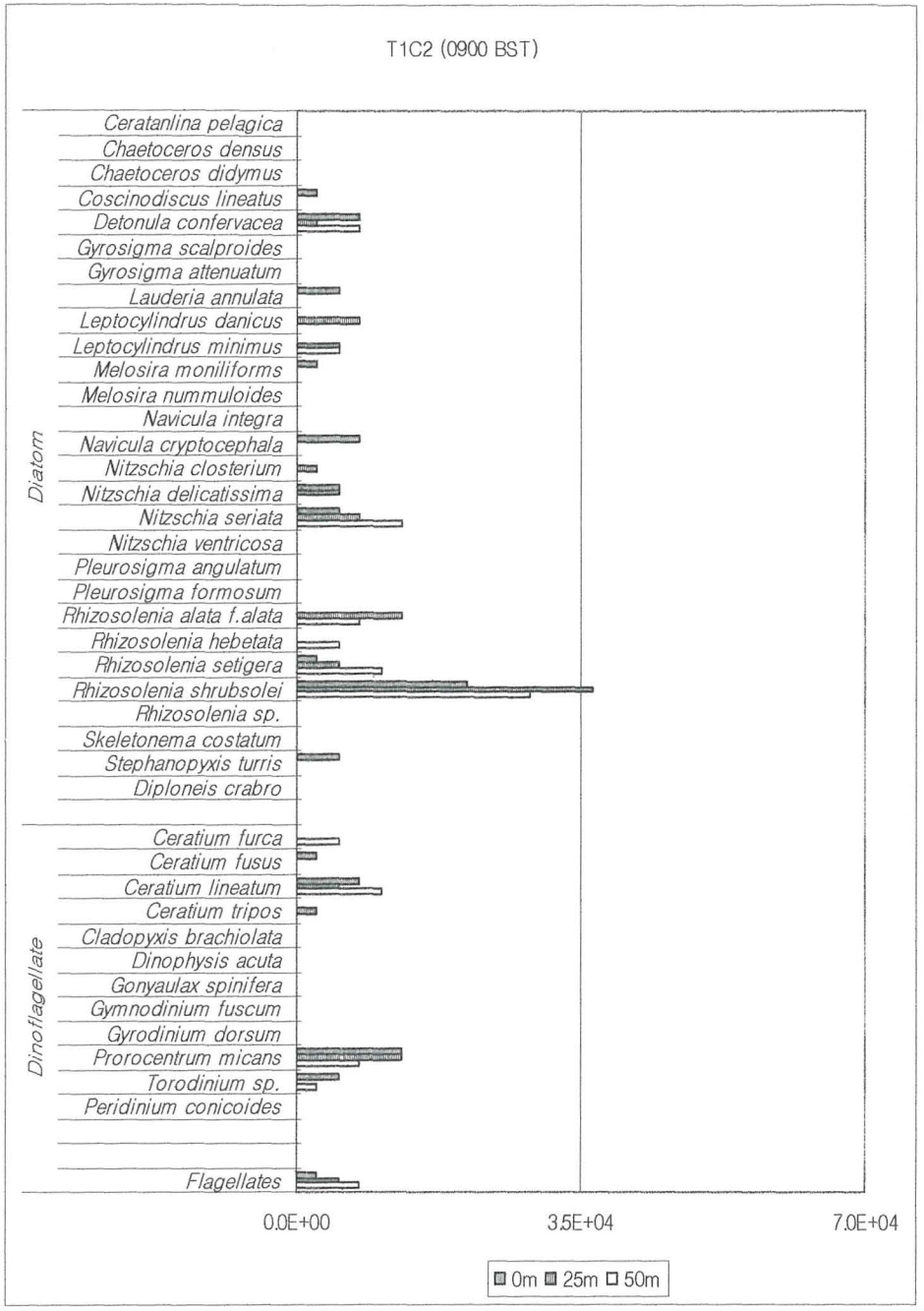
T1C2 (0900 BST)
Ceratanlina pelagica
Chaetoceros densus
Chaetoceros didymus
Coscinodiscus lineatus
Detonula confervacea
Gyrosigma scalproides
Gyrosigma attenuatum
Lauderia annulata
Leptocylindrus danicus
Leptocylindrus minimus
Melosira moniliforms
Melosira nummuloides
Navicula integra
Navicula cryptocephala
Nitzschia closterium
Nitzschia delicatissima
Nitzschia seriata
Nitzschia ventricosa
Pleurosigma angulatum
Pleurosigma formosum
Rhizosolenia alata f.alata
Rhizosolenia hebetata
Rhizosolenia setigera
Rhizosolenia shrubsolei
Rhizosolenia sp.
Skeletonema costatum
Stephanopyxis turris
Diploneis crabro
Diatom
Ceratium furca
Ceratium fusus
Ceratium lineatum
Ceratium tripos
Cladopyxis brachiolata
Dinophysis acuta
Gonyaulax spinifera
Gymnodinium fuscum
Gyrodinium dorsum
Prorocentrum micans
Torodinium sp.
Peridinium conicoides
Dinoflagellate
Flagellates
0.0E+00
3.5E+04
7.0E+04
0m 25m 50m

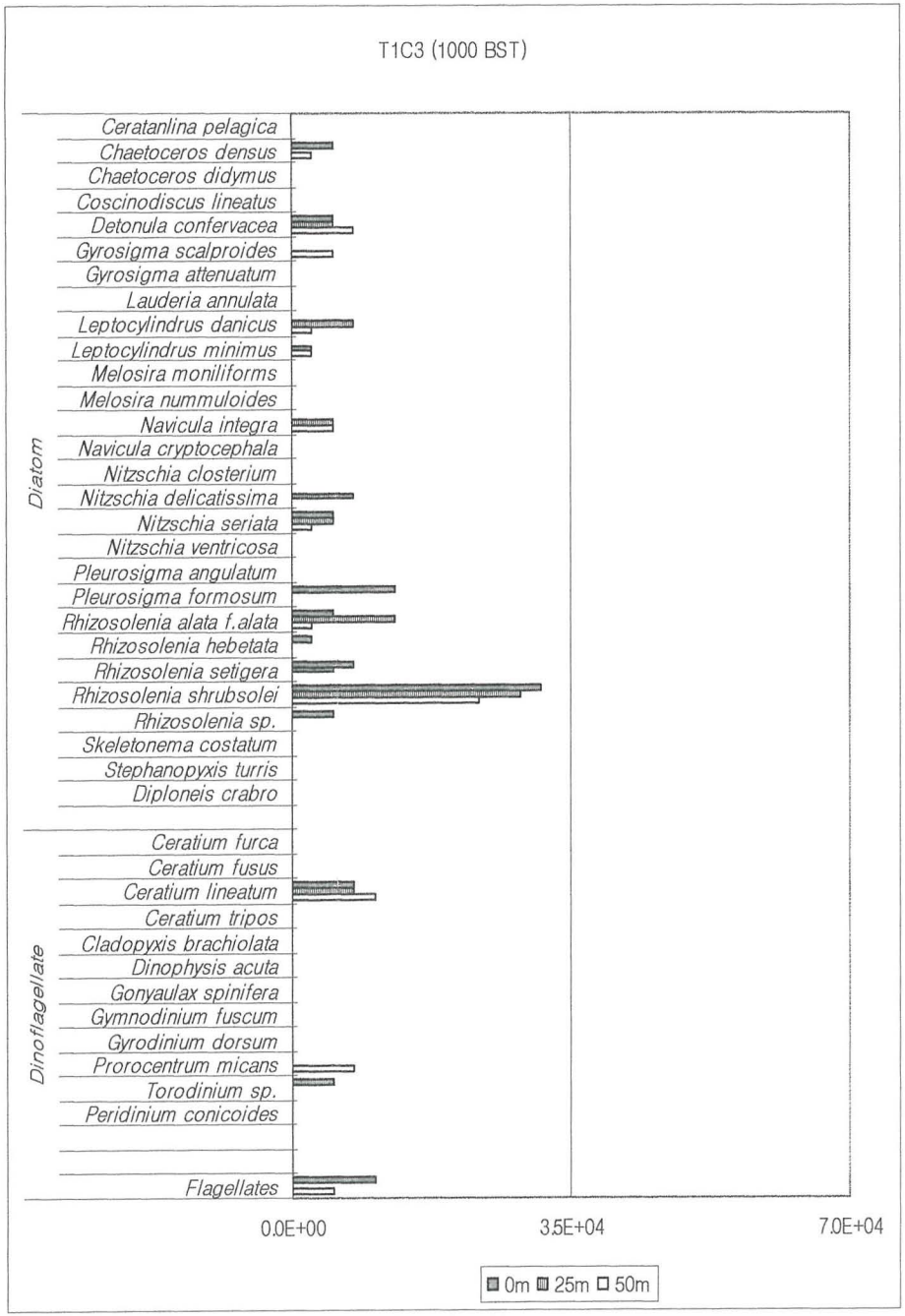
T1C3 (1000 BST)
Ceratanlina pelagica
Chaetoceros densus
Chaetoceros didymus
Coscinodiscus lineatus
Detonula confervacea
Gyrosigma scalproides
Gyrosigma attenuatum
Lauderia annulata
Leptocylindrus danicus
Leptocylindrus minimus
Melosira moniliforms
Melosira nummuloides
Navicula integra
Navicula cryptocephala
Nitzschia closterium
Nitzschia delicatissima
Nitzschia seriata
Nitzschia ventricosa
Pleurosigma angulatum
Pleurosigma formosum
Rhizosolenia alata f.alata
Rhizosolenia hebetata
Rhizosolenia setigera
Rhizosolenia shrubsolei
Rhizosolenia sp.
Skeletonema costatum
Stephanopyxis turris
Diploneis crabro
Diatom
Ceratium furca
Ceratium fusus
Ceratium lineatum
Ceratium tripos
Cladopyxis brachiolata
Dinophysis acuta
Gonyaulax spinifera
Gymnodinium fuscum
Gyrodinium dorsum
Prorocentrum micans
Torodinium sp.
Peridinium conicoides
Dinoflagellate
Flagellates
0.0E+00
3.5E+04
7.0E+04
0m 25m 50m

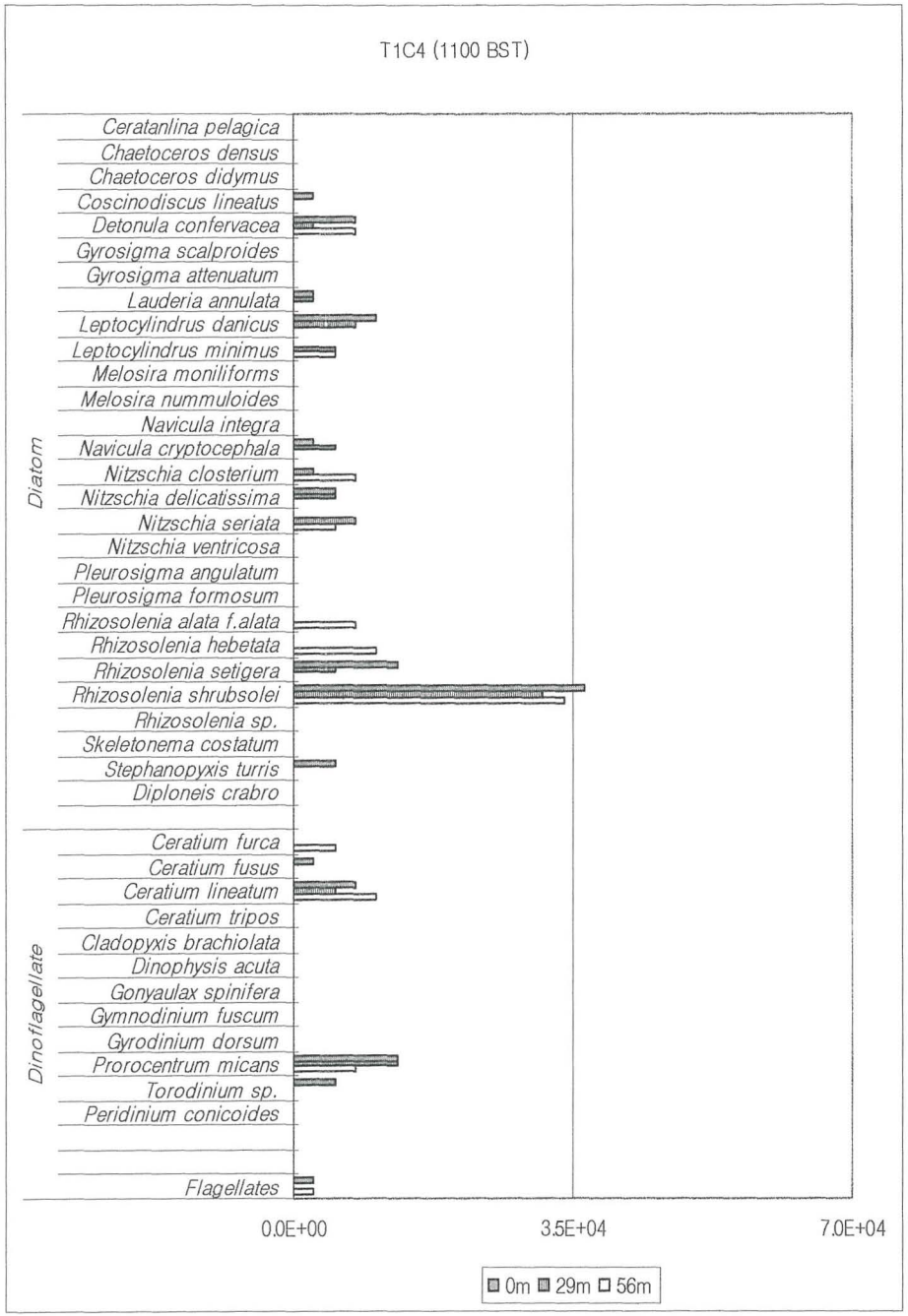
T1C4 (1100 BST)
Ceratanlina pelagica
Chaetoceros densus
Chaetoceros didymus
Coscinodiscus lineatus
Detonula confervacea
Gyrosigma scalproides
Gyrosigma attenuatum
Lauderia annulata
Leptocylindrus danicus
Leptocylindrus minimus
Melosira moniliforms
Melosira nummuloides
Navicula integra
Navicula cryptocephala
Nitzschia closterium
Nitzschia delicatissima
Nitzschia seriata
Nitzschia ventricosa
Pleurosigma angulatum
Pleurosigma formosum
Rhizosolenia alata f.alata
Rhizosolenia hebetata
Rhizosolenia setigera
Rhizosolenia shrubsolei
Rhizosolenia sp.
Skeletonema costatum
Stephanopyxis turris
Diploneis crabro
Diatom
Ceratium furca
Ceratium fusus
Ceratium lineatum
Ceratium tripos
Cladopyxis brachiolata
Dinophysis acuta
Gonyaulax spinifera
Gymnodinium fuscum
Gyrodinium dorsum
Prorocentrum micans
Torodinium sp.
Peridinium conicoides
Dinoflagellate
Flagellates
0.0E+00
3.5E+04
7.0E+04
0m 29m 56m

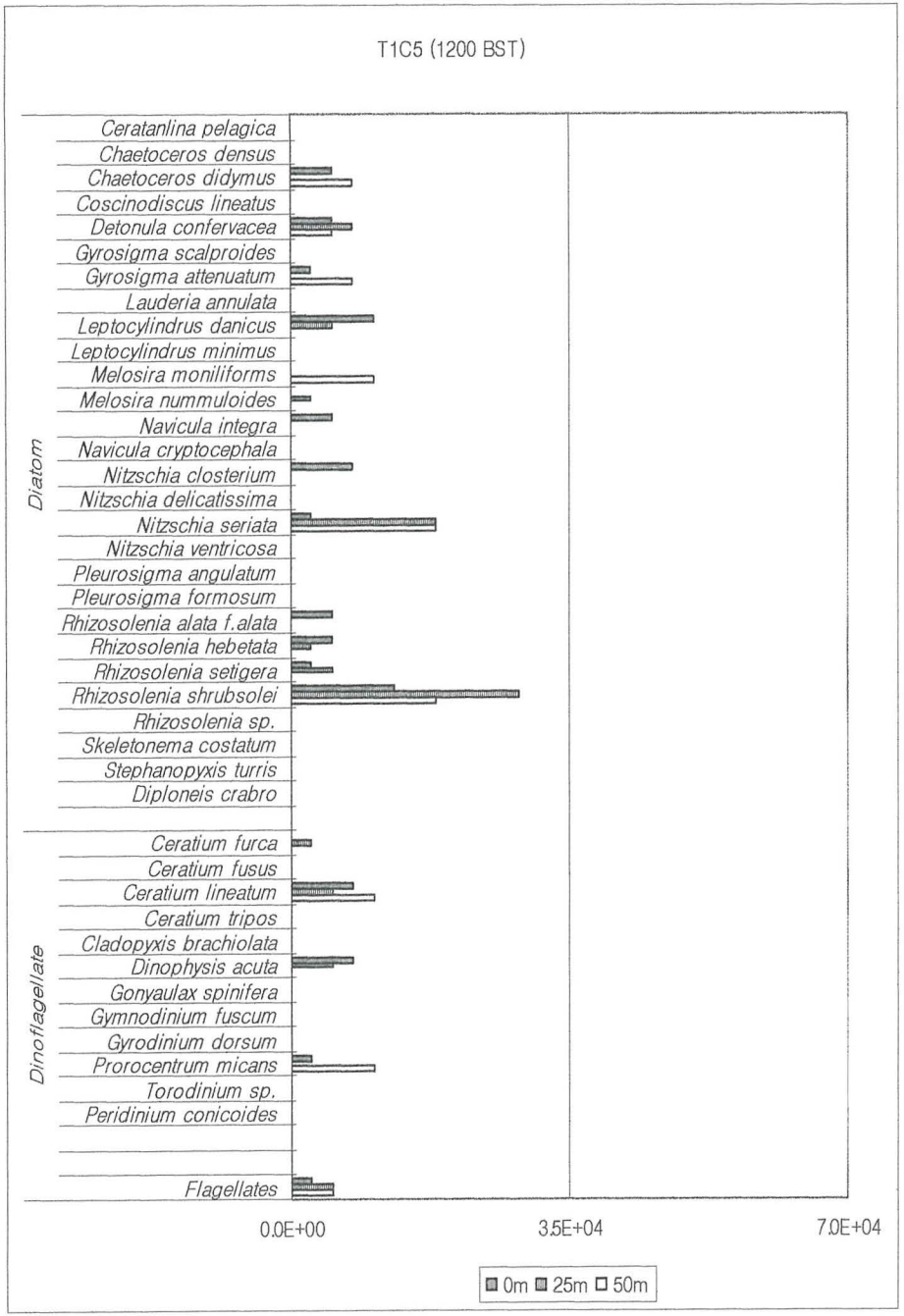
T1C5 (1200 BST)
Ceratanlina pelagica
Chaetoceros densus
Chaetoceros didymus
Coscinodiscus lineatus
Detonula confervacea
Gyrosigma scalproides
Gyrosigma attenuatum
Lauderia annulata
Leptocylindrus danicus
Leptocylindrus minimus
Melosira moniliforms
Melosira nummuloides
Navicula integra
Navicula cryptocephala
Nitzschia closterium
Nitzschia delicatissima
Nitzschia seriata
Nitzschia ventricosa
Pleurosigma angulatum
Pleurosigma formosum
Rhizosolenia alata f.alata
Rhizosolenia hebetata
Rhizosolenia setigera
Rhizosolenia shrubsolei
Rhizosolenia sp.
Skeletonema costatum
Stephanopyxis turris
Diploneis crabro
Diatom
Ceratium furca
Ceratium fusus
Ceratium lineatum
Ceratium tripos
Cladopyxis brachiolata
Dinophysis acuta
Gonyaulax spinifera
Gymnodinium fuscum
Gyrodinium dorsum
Prorocentrum micans
Torodinium sp.
Peridinium conicoides
Dinoflagellate
Flagellates
0.0E+00
3.5E+04
7.0E+04
0m 25m 50m

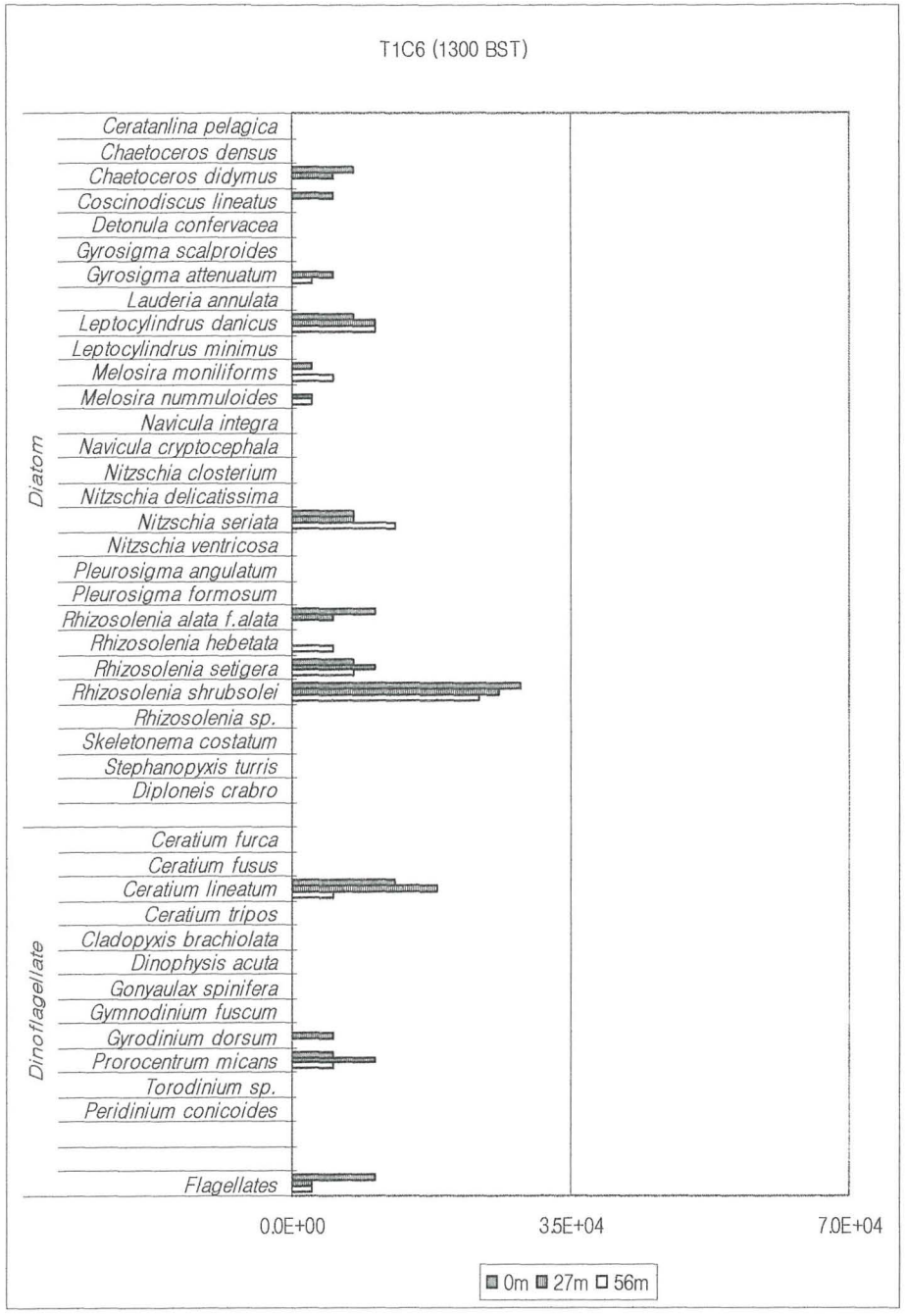
T1C6 (1300 BST)
Ceratanlina pelagica
Chaetoceros densus
Chaetoceros didymus
Coscinodiscus lineatus
Detonula confervacea
Gyrosigma scalproides
Gyrosigma attenuatum
Lauderia annulata
Leptocylindrus danicus
Leptocylindrus minimus
Melosira moniliforms
Melosira nummuloides
Navicula integra
Navicula cryptocephala
Nitzschia closterium
Nitzschia delicatissima
Nitzschia seriata
Nitzschia ventricosa
Pleurosigma angulatum
Pleurosigma formosum
Rhizosolenia alata f.alata
Rhizosolenia hebetata
Rhizosolenia setigera
Rhizosolenia shrubsolei
Rhizosolenia sp.
Skeletonema costatum
Stephanopyxis turris
Diploneis crabro
Diatom
Ceratium furca
Ceratium fusus
Ceratium lineatum
Ceratium tripos
Cladopyxis brachiolata
Dinophysis acuta
Gonyaulax spinifera
Gymnodinium fuscum
Gyrodinium dorsum
Prorocentrum micans
Torodinium sp.
Peridinium conicoides
Dinoflagellate
Flagellates
0.0E+00
3.5E+04
7.0E+04
0m 27m 56m

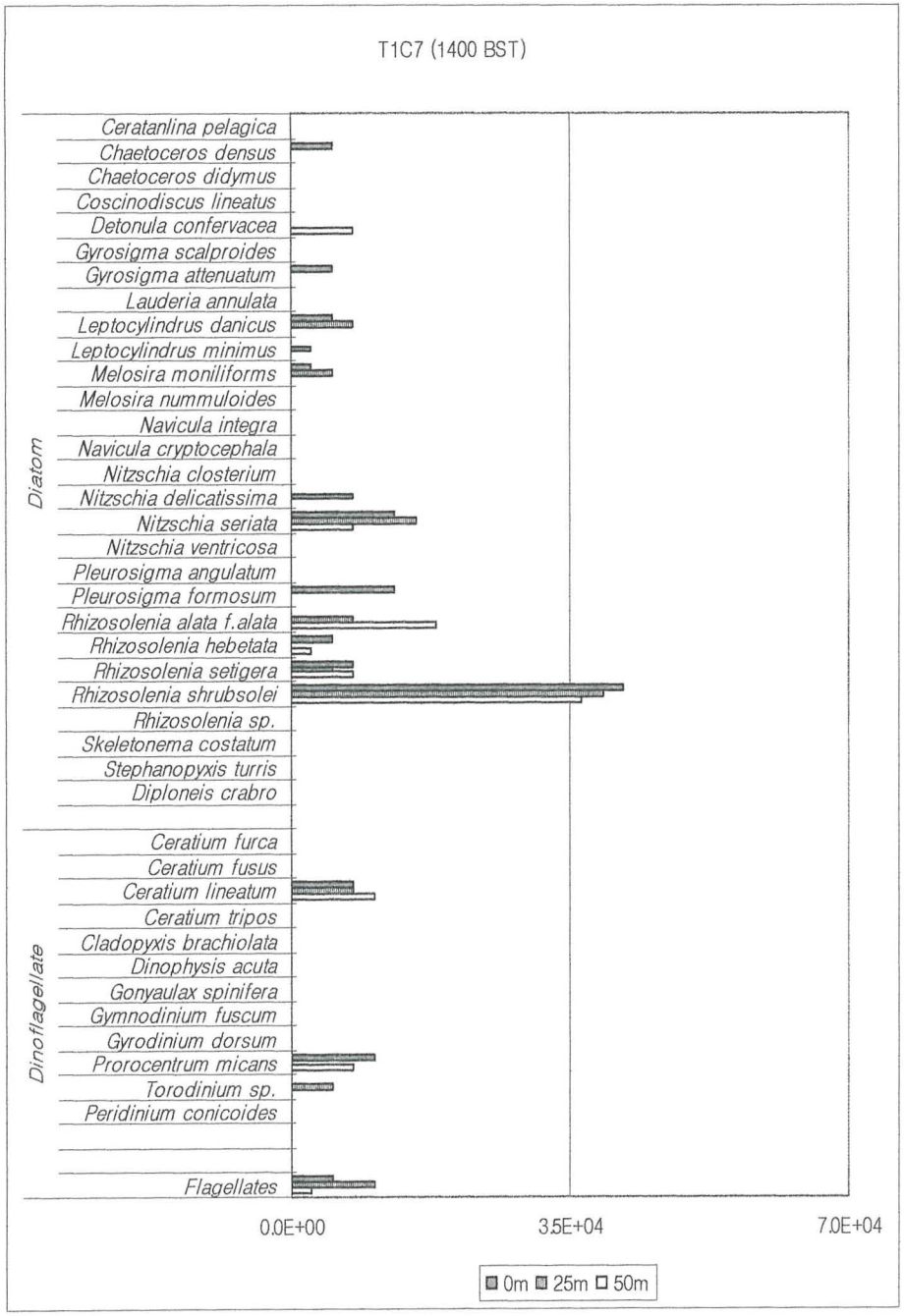
T1C7 (1400 BST)
Ceratanlina pelagica
Chaetoceros densus
Chaetoceros didymus
Coscinodiscus lineatus
Detonula confervacea
Gyrosigma scalproides
Gyrosigma attenuatum
Lauderia annulata
Leptocylindrus danicus
Leptocylindrus minimus
Melosira moniliforms
Melosira nummuloides
Navicula integra
Navicula cryptocephala
Nitzschia closterium
Nitzschia delicatissima
Nitzschia seriata
Nitzschia ventricosa
Pleurosigma angulatum
Pleurosigma formosum
Rhizosolenia alata f.alata
Rhizosolenia hebetata
Rhizosolenia setigera
Rhizosolenia shrubsolei
Rhizosolenia sp.
Skeletonema costatum
Stephanopyxis turris
Diploneis crabro
Diatom
Ceratium furca
Ceratium fusus
Ceratium lineatum
Ceratium tripos
Cladopyxis brachiolata
Dinophysis acuta
Gonyaulax spinifera
Gymnodinium fuscum
Gyrodinium dorsum
Prorocentrum micans
Torodinium sp.
Peridinium conicoides
Dinoflagellate
Flagellates
0.0E+00
3.5E+04
7.0E+04
0m 25m 50m

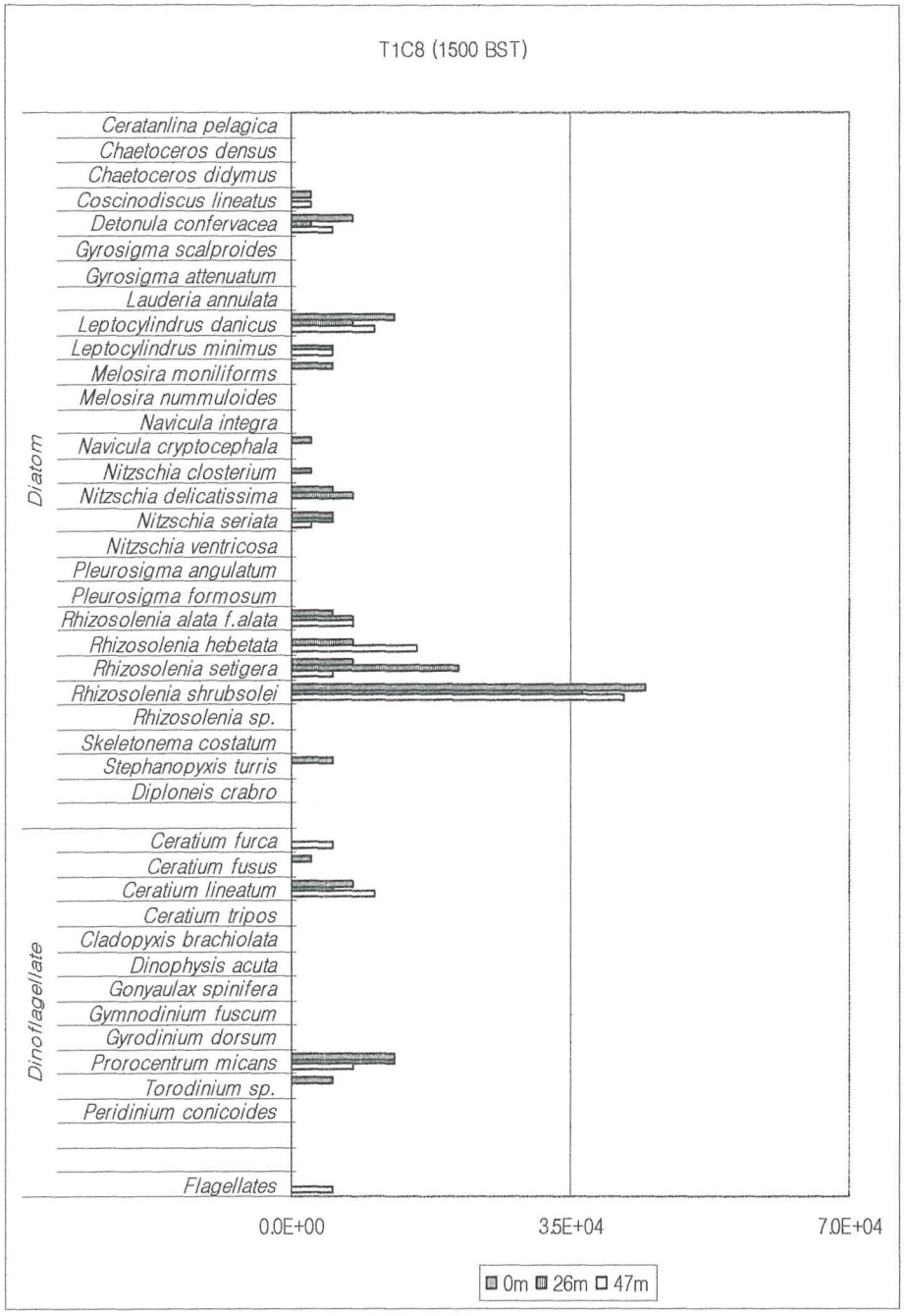
T1C8 (1500 BST)
Ceratanlina pelagica
Chaetoceros densus
Chaetoceros didymus
Coscinodiscus lineatus
Detonula confervacea
Gyrosigma scalproides
Gyrosigma attenuatum
Lauderia annulata
Leptocylindrus danicus
Leptocylindrus minimus
Melosira moniliforms
Melosira nummuloides
Navicula integra
Navicula cryptocephala
Nitzschia closterium
Nitzschia delicatissima
Nitzschia seriata
Nitzschia ventricosa
Pleurosigma angulatum
Pleurosigma formosum
Rhizosolenia alata f.alata
Rhizosolenia hebetata
Rhizosolenia setigera
Rhizosolenia shrubsolei
Rhizosolenia sp.
Skeletonema costatum
Stephanopyxis turris
Diploneis crabro
Diatom
Ceratium furca
Ceratium fusus
Ceratium lineatum
Ceratium tripos
Cladopyxis brachiolata
Dinophysis acuta
Gonyaulax spinifera
Gymnodinium fuscum
Gyrodinium dorsum
Prorocentrum micans
Torodinium sp.
Peridinium conicoides
Dinoflagellate
Flagellates
0.0E+00
3.5E+04
7.0E+04
0m 26m 47m

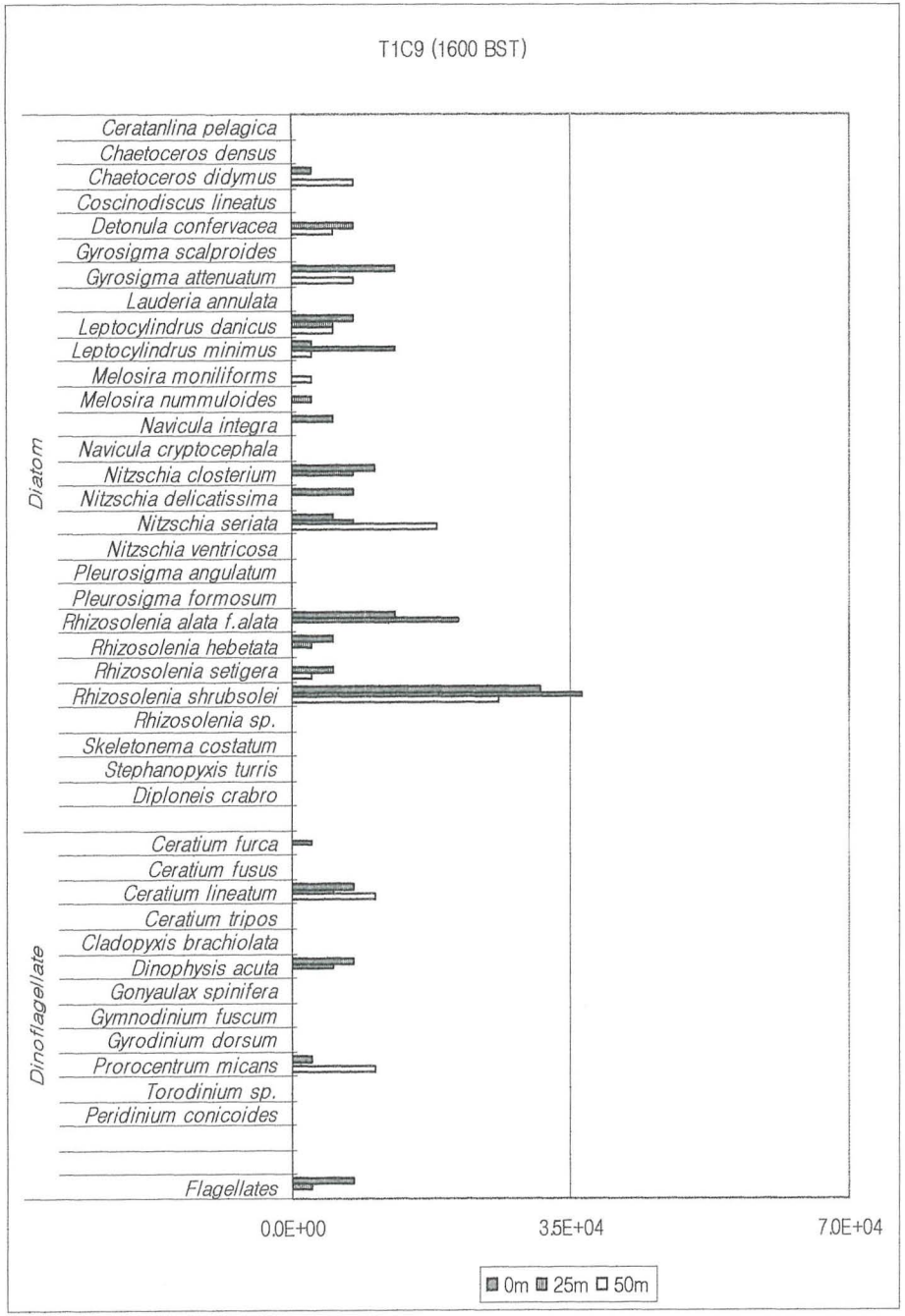
T1C9 (1600 BST)
Ceratanlina pelagica
Chaetoceros densus
Chaetoceros didymus
Coscinodiscus lineatus
Detonula confervacea
Gyrosigma scalproides
Gyrosigma attenuatum
Lauderia annulata
Leptocylindrus danicus
Leptocylindrus minimus
Melosira moniliforms
Melosira nummuloides
Navicula integra
Navicula cryptocephala
Nitzschia closterium
Nitzschia delicatissima
Nitzschia seriata
Nitzschia ventricosa
Pleurosigma angulatum
Pleurosigma formosum
Rhizosolenia alata f.alata
Rhizosolenia hebetata
Rhizosolenia setigera
Rhizosolenia shrubsolei
Rhizosolenia sp.
Skeletonema costatum
Stephanopyxis turris
Diploneis crabro
Diatom
Ceratium furca
Ceratium fusus
Ceratium lineatum
Ceratium tripos
Cladopyxis brachiolata
Dinophysis acuta
Gonyaulax spinifera
Gymnodinium fuscum
Gyrodinium dorsum
Prorocentrum micans
Torodinium sp.
Peridinium conicoides
Dinoflagellate
Flagellates
0.0E+00
3.5E+04
7.0E+04
0m 25m 50m

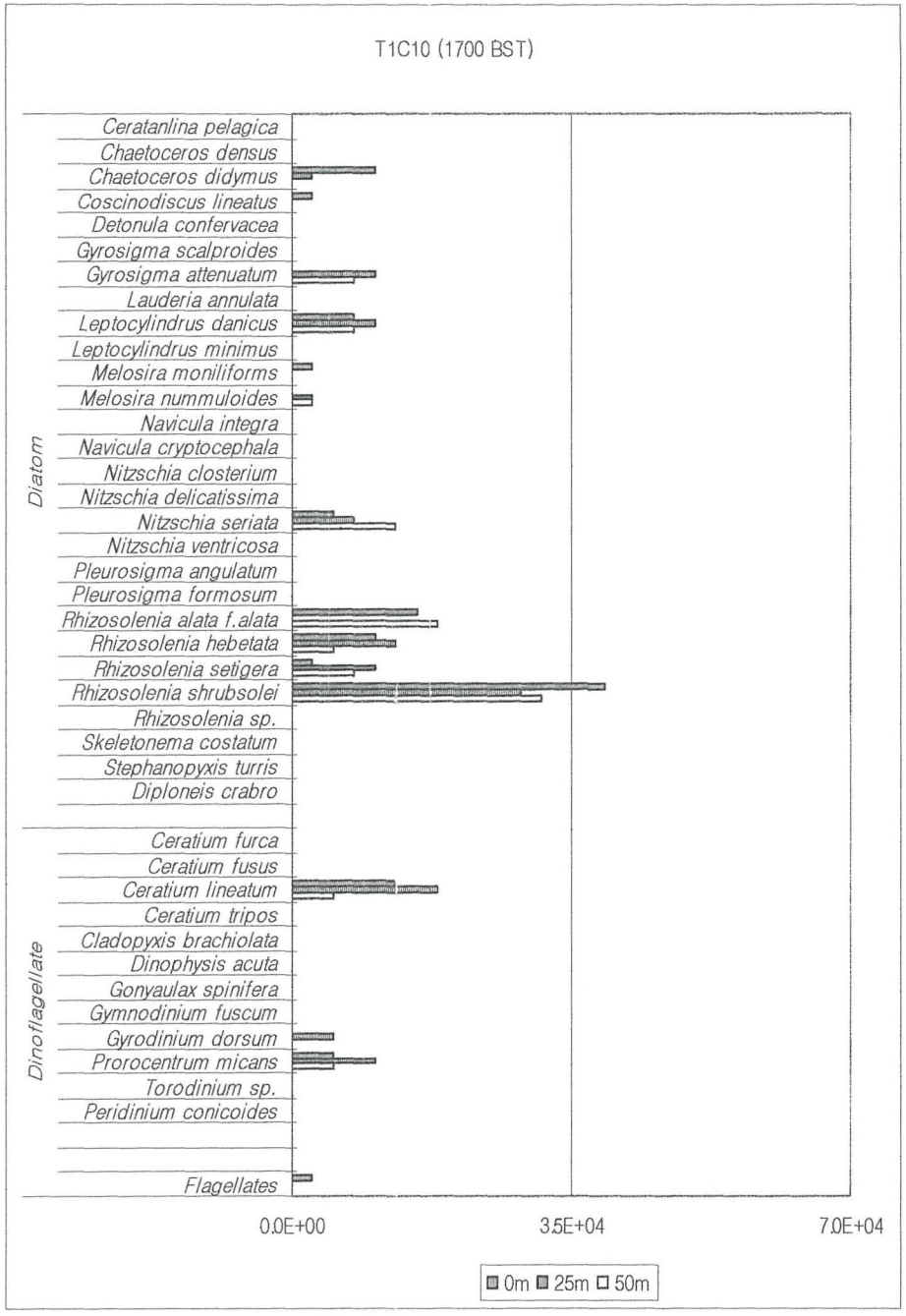
T1C10 (1700 BST)
Ceratanlina pelagica
Chaetoceros densus
Chaetoceros didymus
Coscinodiscus lineatus
Detonula confervacea
Gyrosigma scalproides
Gyrosigma attenuatum
Lauderia annulata
Leptocylindrus danicus
Leptocylindrus minimus
Melosira moniliforms
Melosira nummuloides
Navicula integra
Navicula cryptocephala
Nitzschia closterium
Nitzschia delicatissima
Nitzschia seriata
Nitzschia ventricosa
Pleurosigma angulatum
Pleurosigma formosum
Rhizosolenia alata f.alata
Rhizosolenia hebetata
Rhizosolenia setigera
Rhizosolenia shrubsolei
Rhizosolenia sp.
Skeletonema costatum
Stephanopyxis turris
Diploneis crabro
Diatom
Ceratium furca
Ceratium fusus
Ceratium lineatum
Ceratium tripos
Cladopyxis brachiolata
Dinophysis acuta
Gonyaulax spinifera
Gymnodinium fuscum
Gyrodinium dorsum
Prorocentrum micans
Torodinium sp.
Peridinium conicoides
Dinoflagellate
Flagellates
0.0E+00
3.5E+04
7.0E+04
0m 25m 50m

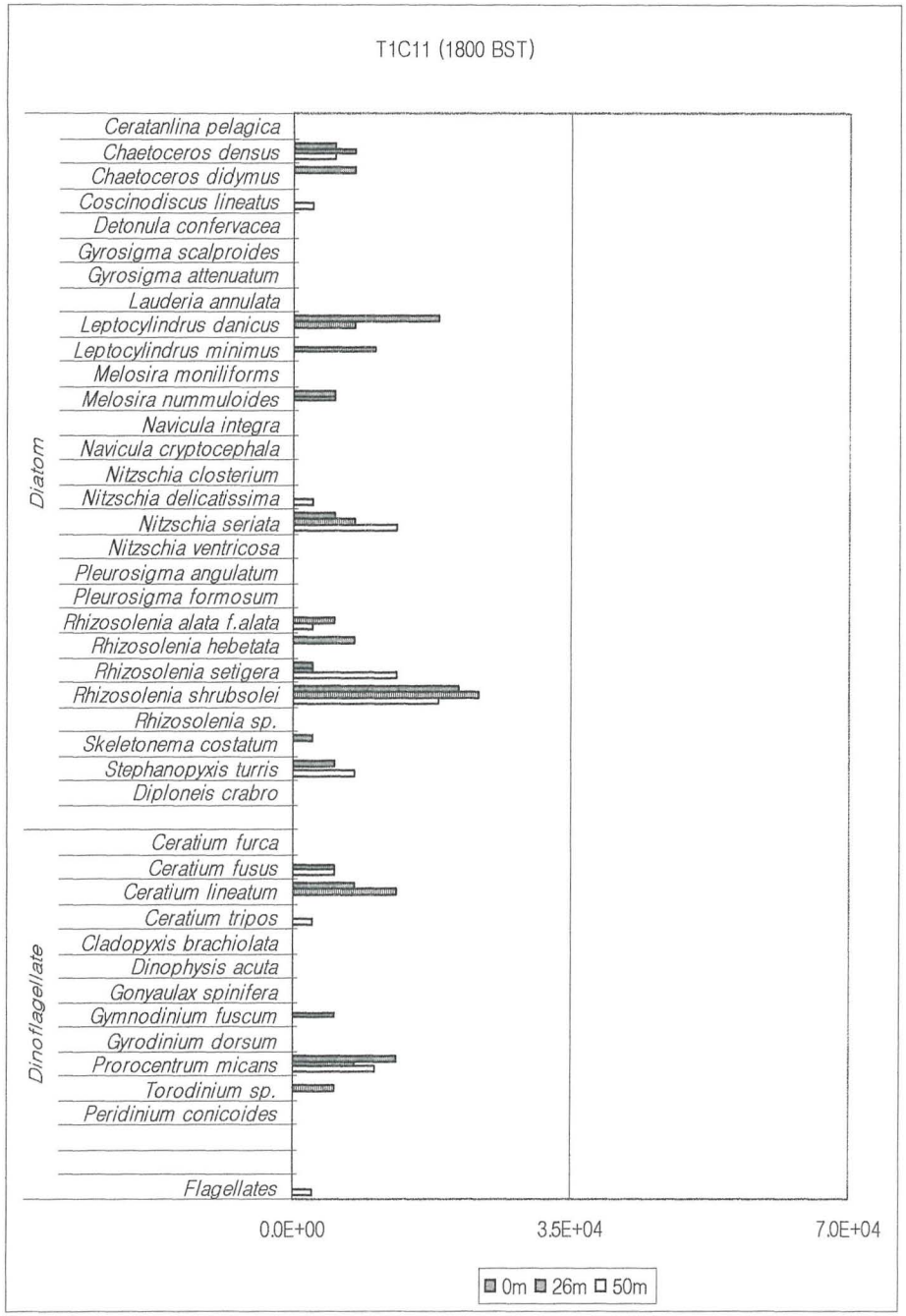
T1C11 (1800 BST)
Ceratanlina pelagica
Chaetoceros densus
Chaetoceros didymus
Coscinodiscus lineatus
Detonula confervacea
Gyrosigma scalproides
Gyrosigma attenuatum
Lauderia annulata
Leptocylindrus danicus
Leptocylindrus minimus
Melosira moniliforms
Melosira nummuloides
Navicula integra
Navicula cryptocephala
Nitzschia closterium
Nitzschia delicatissima
Nitzschia seriata
Nitzschia ventricosa
Pleurosigma angulatum
Pleurosigma formosum
Rhizosolenia alata f.alata
Rhizosolenia hebetata
Rhizosolenia setigera
Rhizosolenia shrubsolei
Rhizosolenia sp.
Skeletonema costatum
Stephanopyxis turris
Diploneis crabro
Ceratium furca
Ceratium fusus
Ceratium lineatum
Ceratium tripos
Cladopyxis brachiolata
Dinophysis acuta
Gonyaulax spinifera
Gymnodinium fuscum
Gyrodinium dorsum
Prorocentrum micans
Torodinium sp.
Peridinium conicoides
Flagellates
Diatom
Dinoflagellate
0.0E+00
3.5E+04
7.0E+04
0m 26m 50m

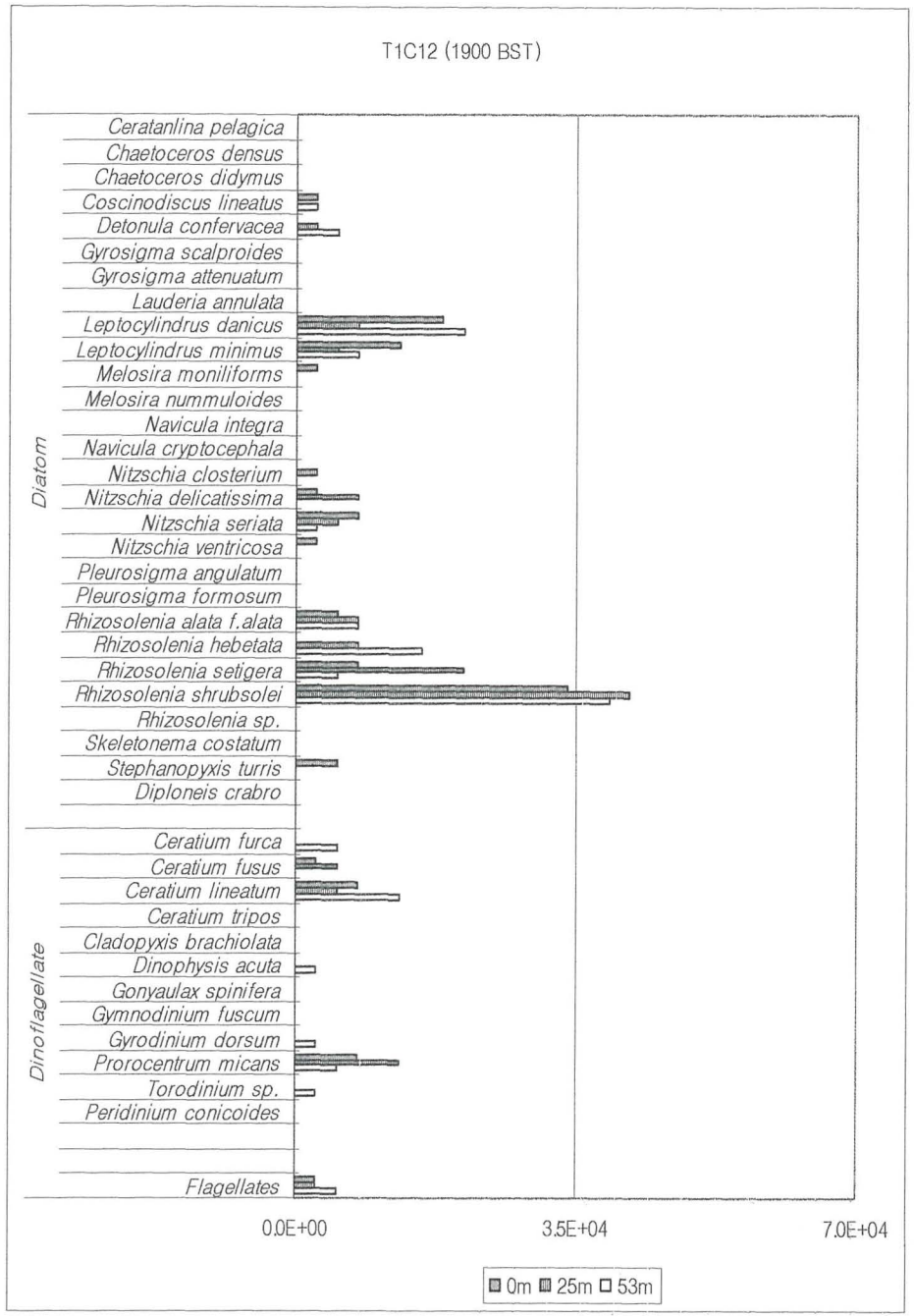
T1C12 (1900 BST)
Ceratanlina pelagica
Chaetoceros densus
Chaetoceros didymus
Coscinodiscus lineatus
Detonula confervacea
Gyrosigma scalproides
Gyrosigma attenuatum
Lauderia annulata
Leptocylindrus danicus
Leptocylindrus minimus
Melosira moniliforms
Melosira nummuloides
Navicula integra
Navicula cryptocephala
Nitzschia closterium
Nitzschia delicatissima
Nitzschia seriata
Nitzschia ventricosa
Pleurosigma angulatum
Pleurosigma formosum
Rhizosolenia alata f.alata
Rhizosolenia hebetata
Rhizosolenia setigera
Rhizosolenia shrubsolei
Rhizosolenia sp.
Skeletonema costatum
Stephanopyxis turris
Diploneis crabro
Ceratium furca
Ceratium fusus
Ceratium lineatum
Ceratium tripos
Cladopyxis brachiolata
Dinophysis acuta
Gonyaulax spinifera
Gymnodinium fuscum
Gyrodinium dorsum
Prorocentrum micans
Torodinium sp.
Peridinium conicoides
Flagellates
Diatom
Dinoflagellate
0.0E+00
3.5E+04
7.0E+04
0m 25m 53m

Appendix A-6 Celtic Sea Taxonomic data (No. of cells l^{-1}) 14-July-2002

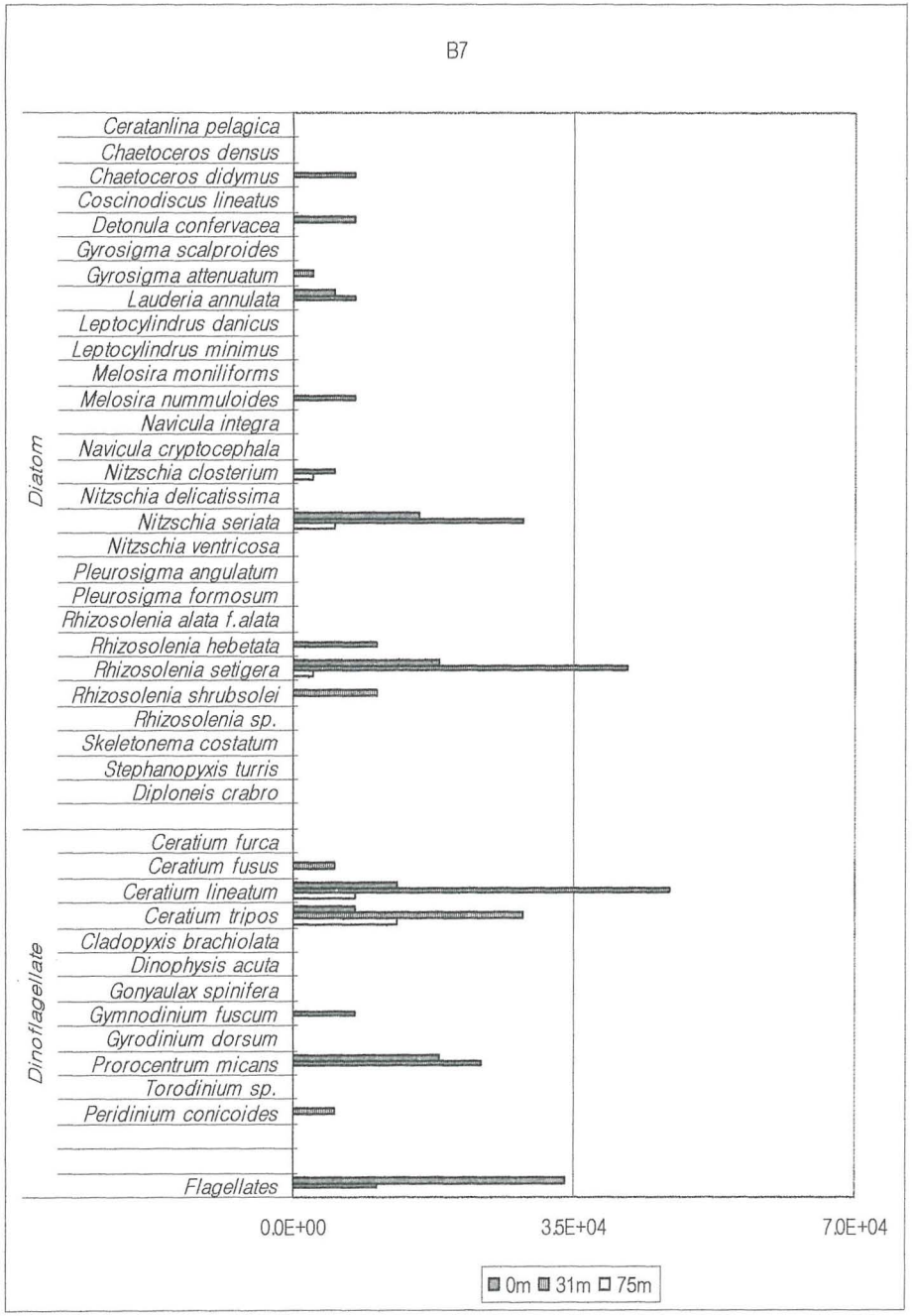

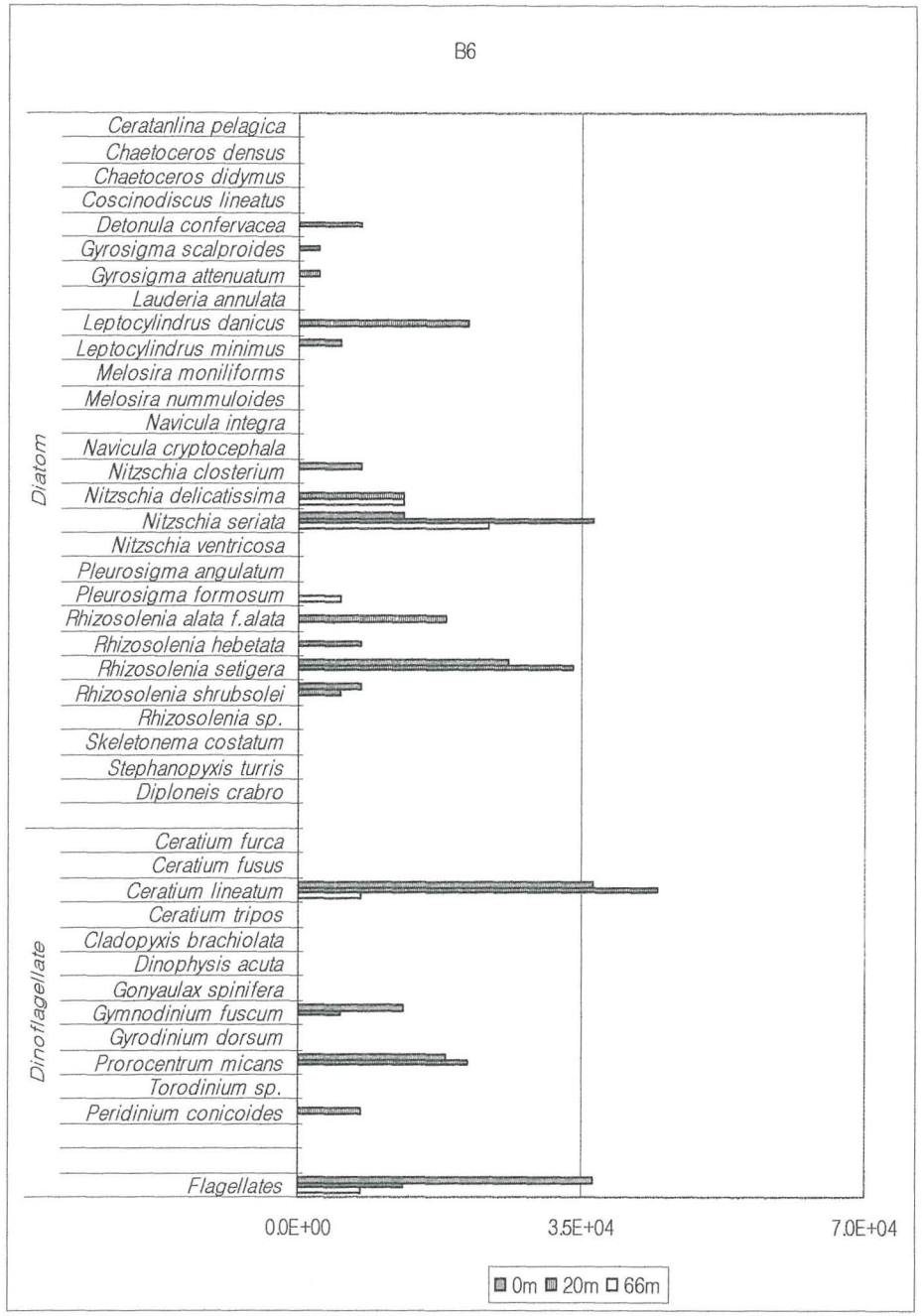

Appendix A-6 Celtic Sea Taxonomic data (No. of cells l^{-1}) 14-July-2002

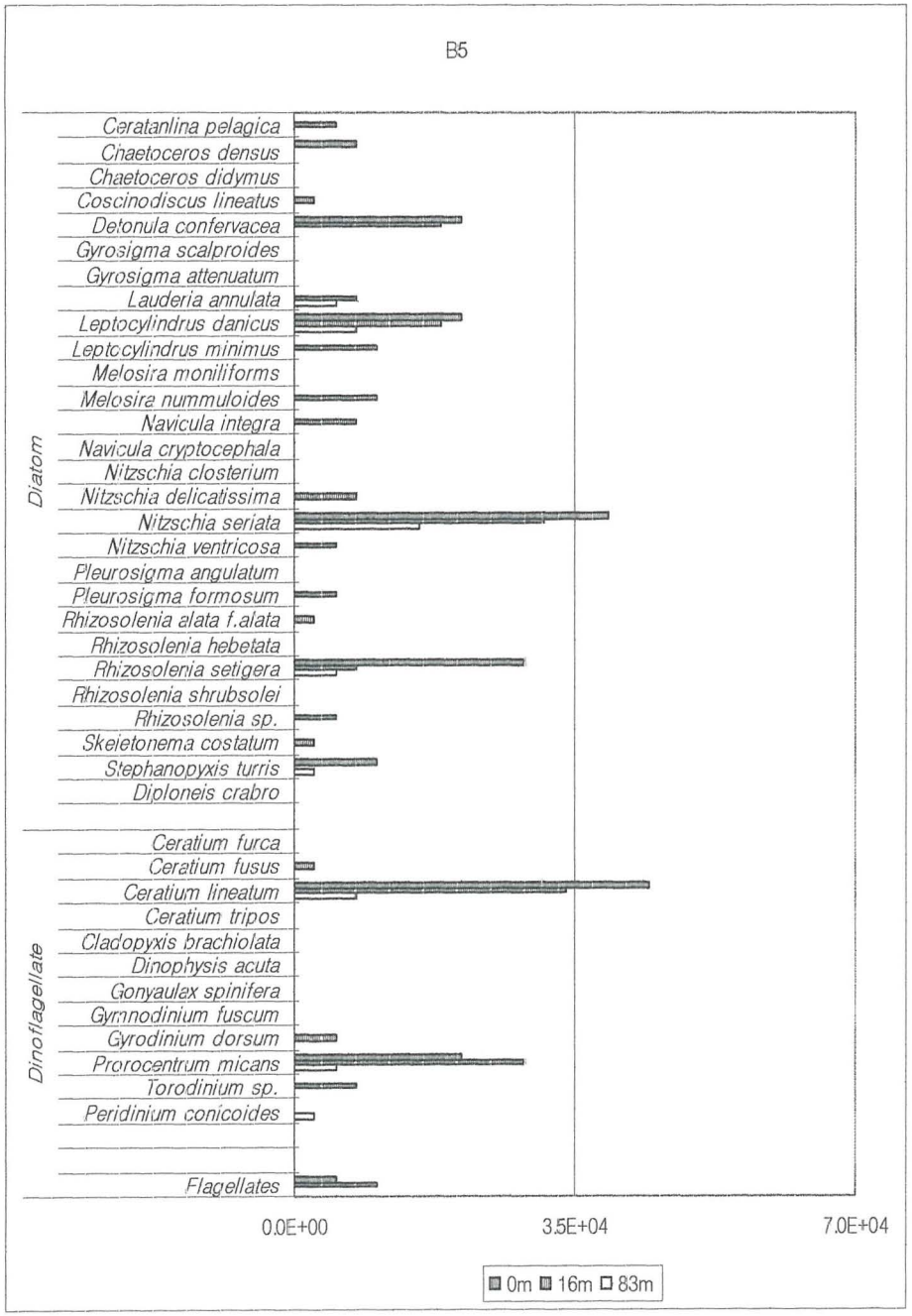

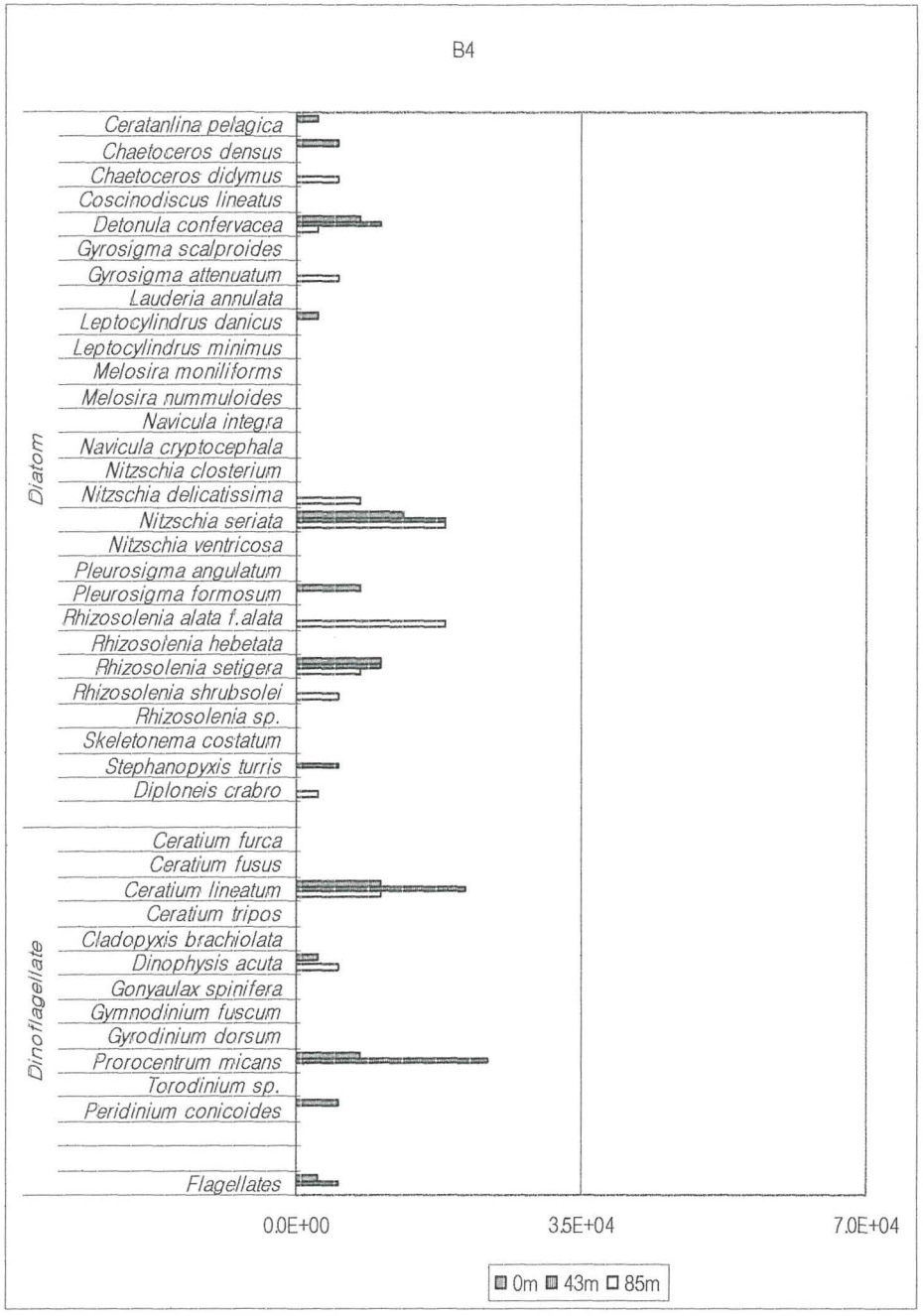

Appendix A-6 Celtic Sea Taxonomic data (No. of cells l^{-1}) 14-July-2002

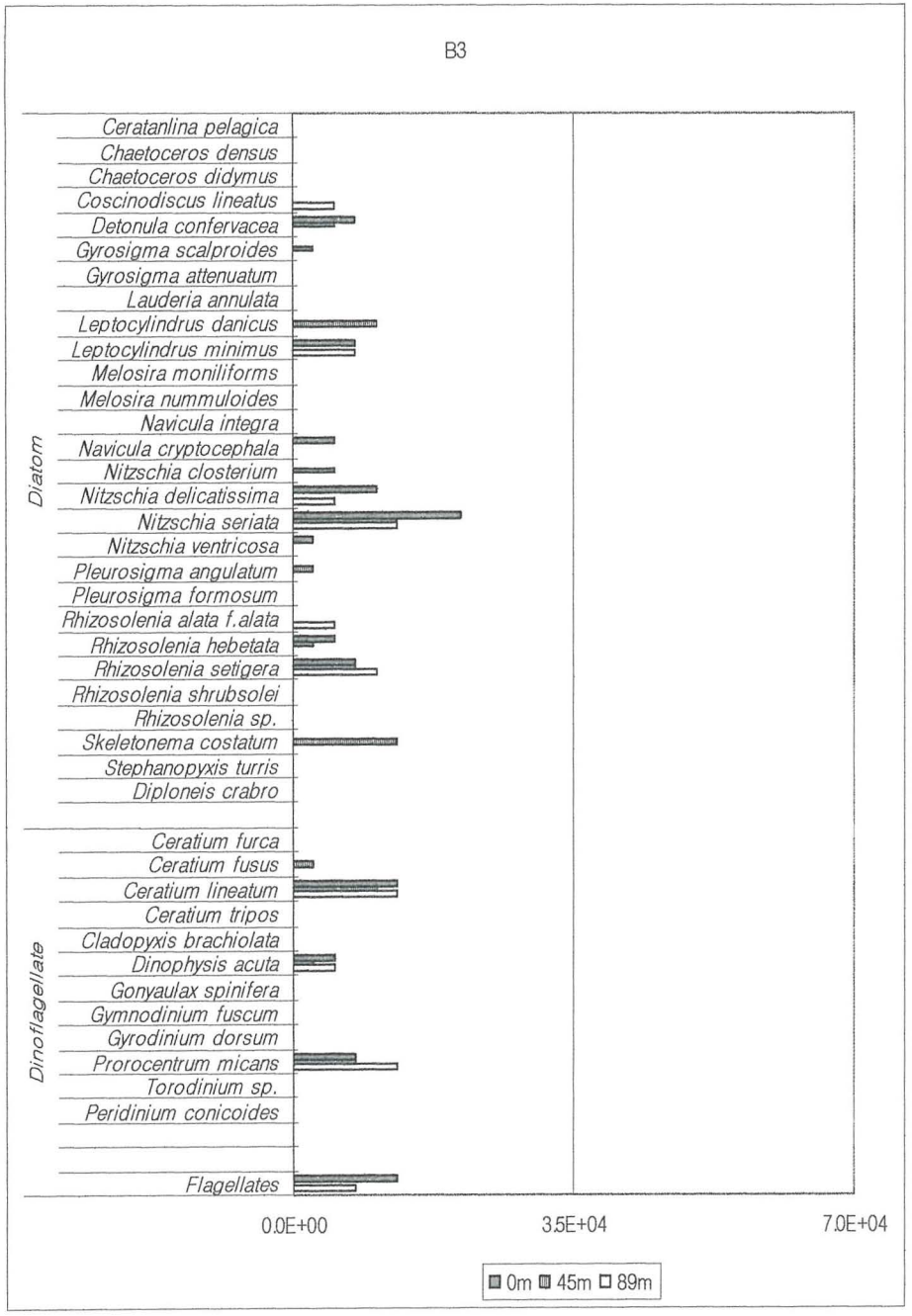

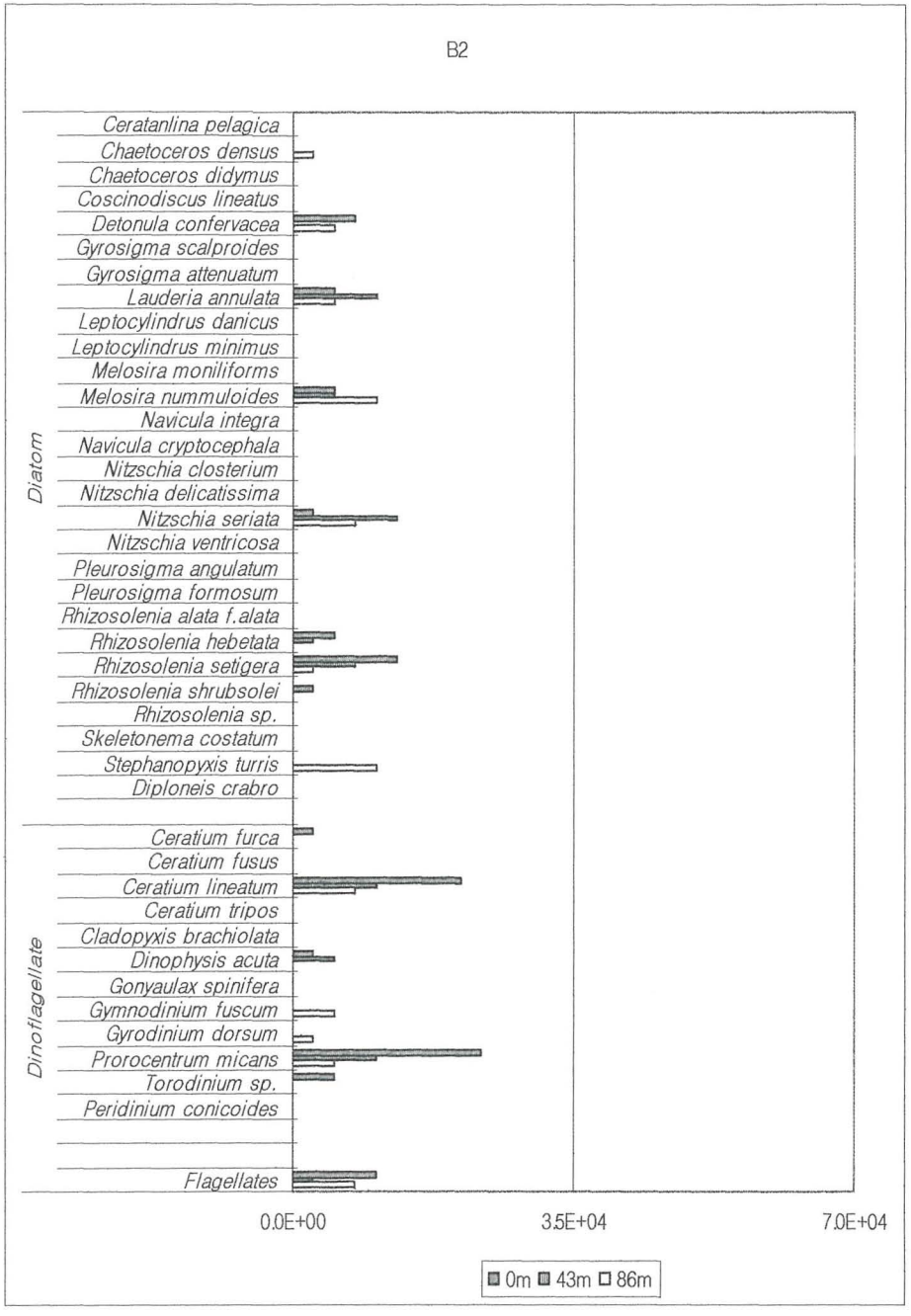

Appendix A-6 Celtic Sea Taxonomic data (No. of cells l^{-1}) 15-July-2002

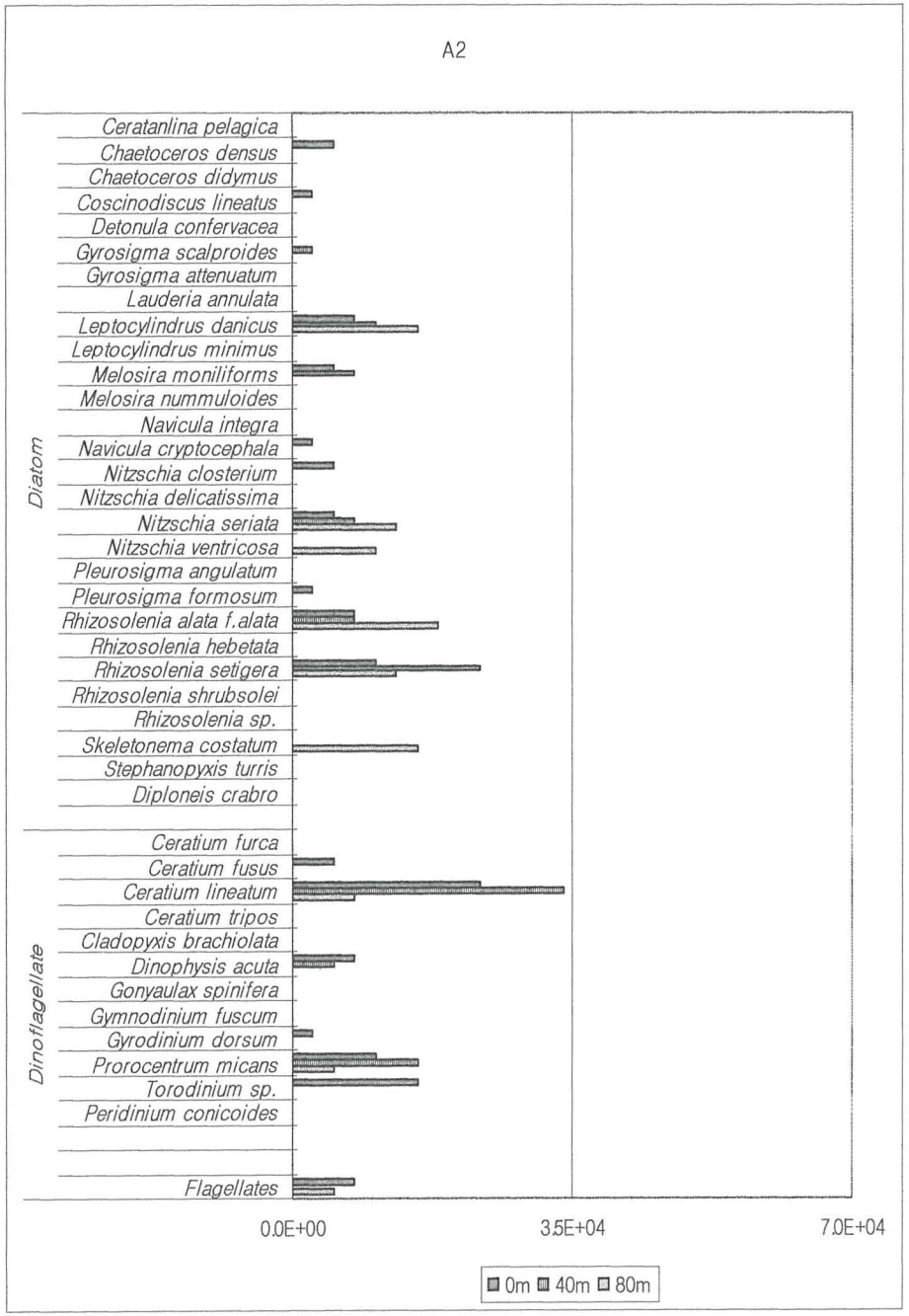

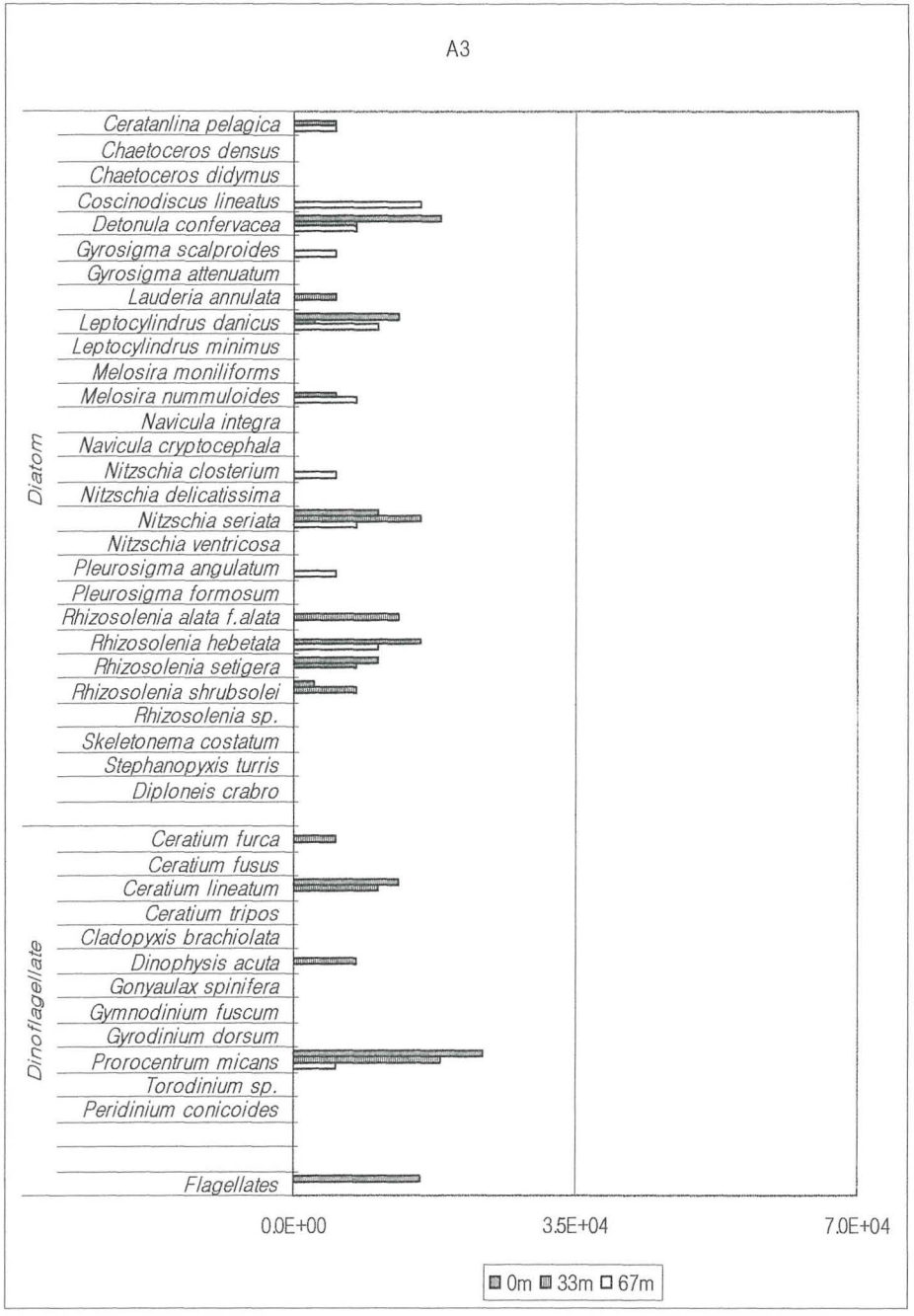

Appendix A-6 Celtic Sea Taxonomic data (No. of cells l^{-1}) 15-July-2002

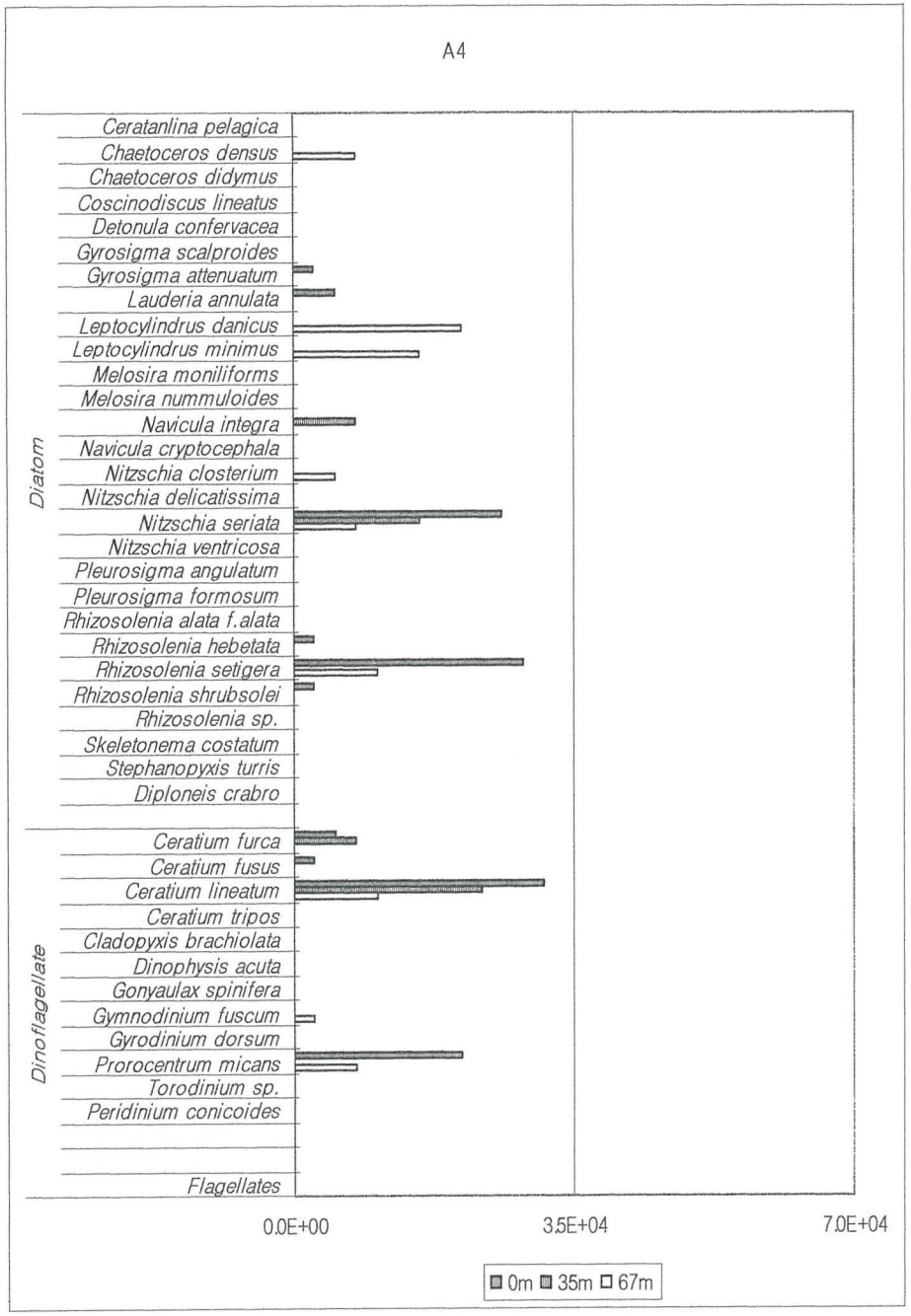

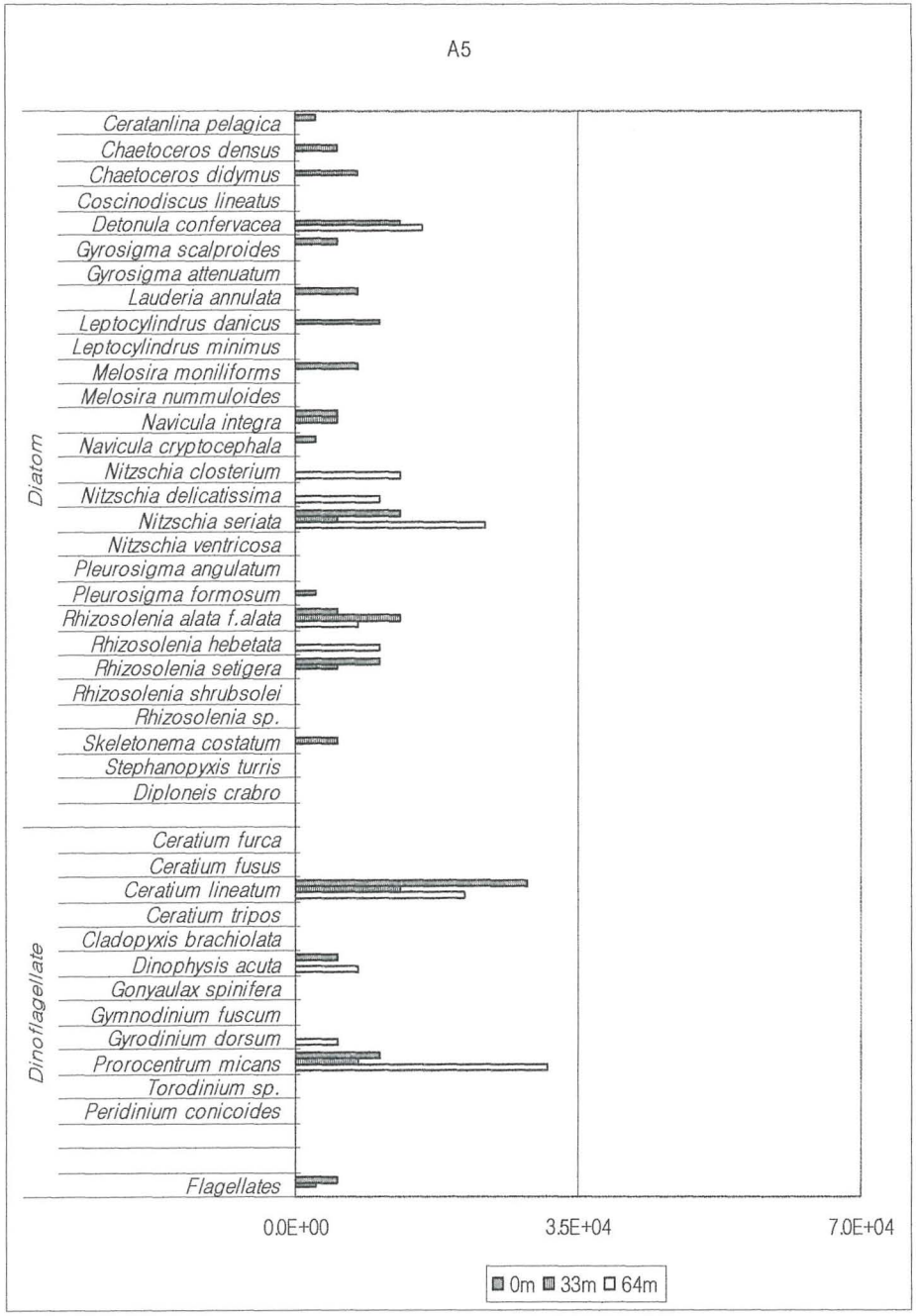

Appendix A-6 Celtic Sea Taxonomic data (No. of cells l^{-1}) 15-July-2002

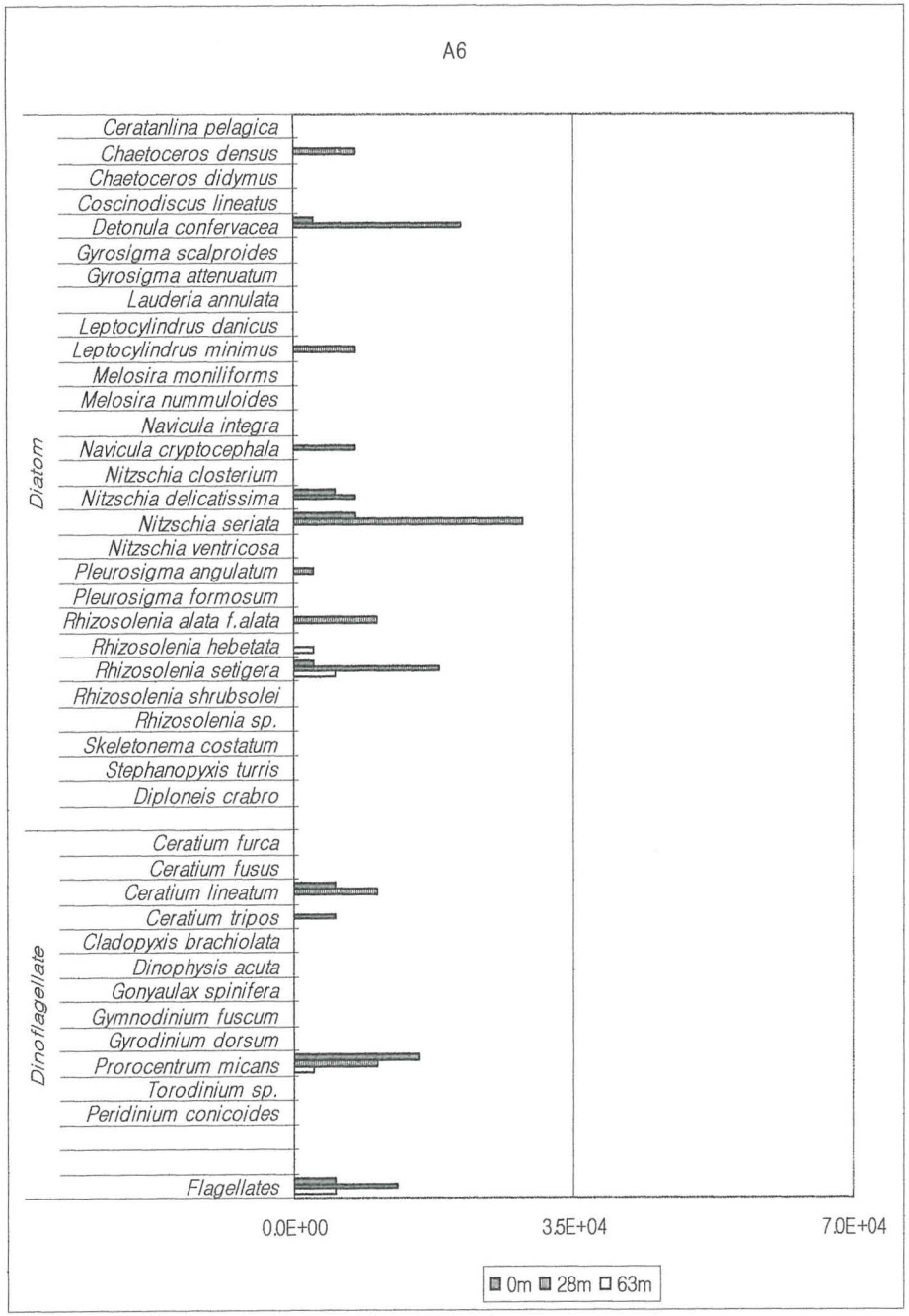

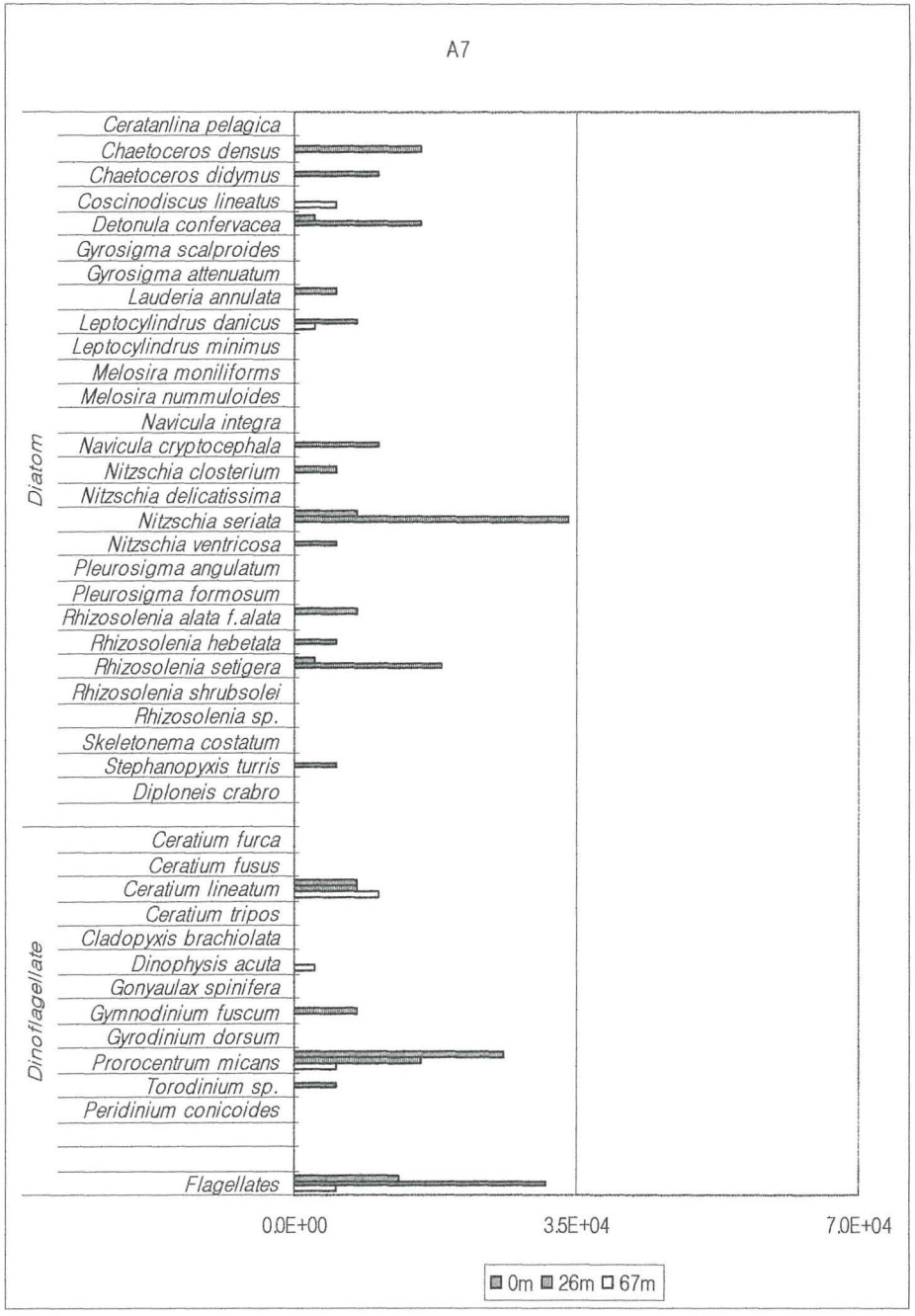

Appendix A-6 Celtic Sea Taxonomic data (No. of cells l^{-1}) 15-July-2002

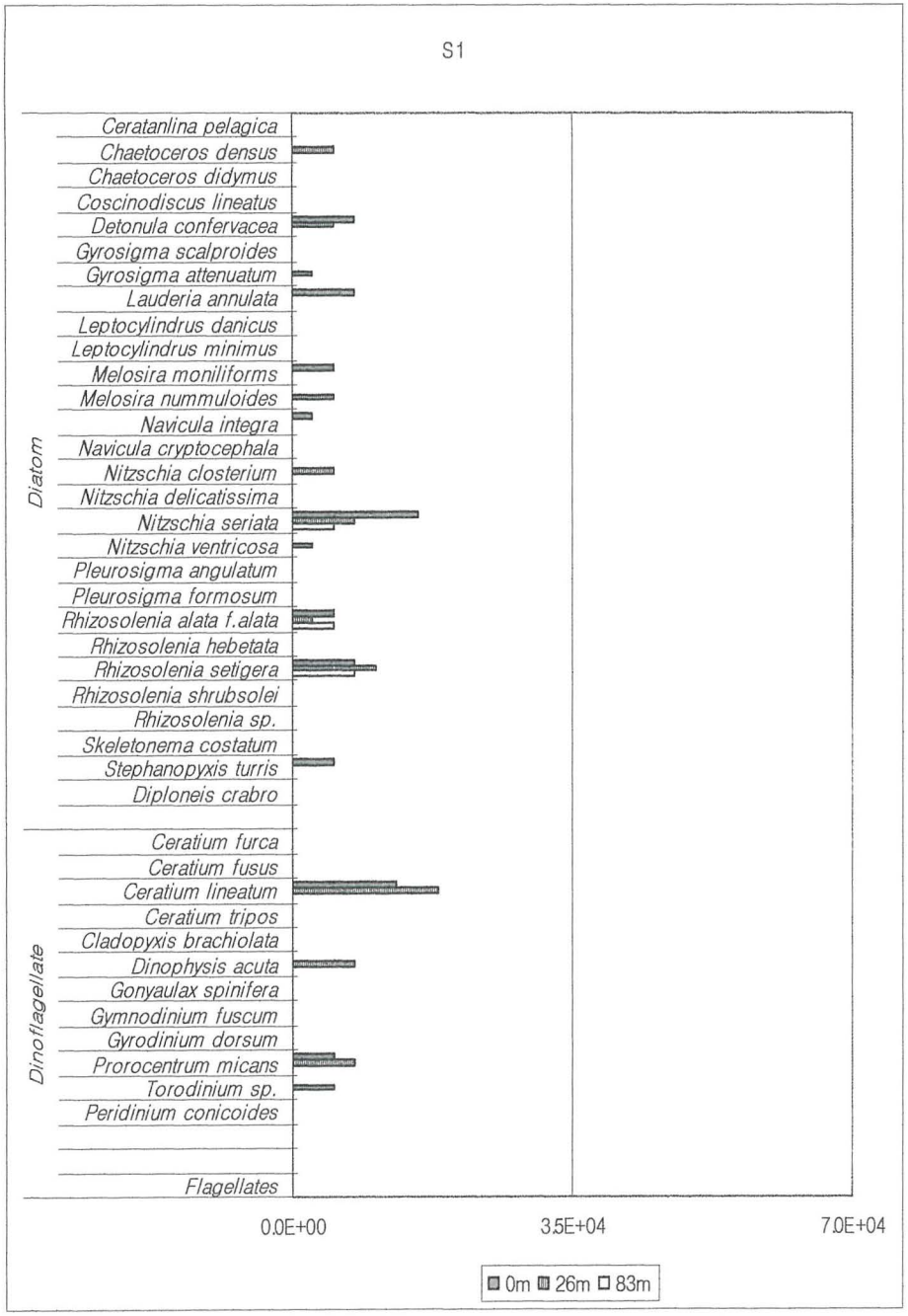

Appendix A-6 Celtic Sea Taxonomic data (No. of cells l^{-1}) 16-July-2002

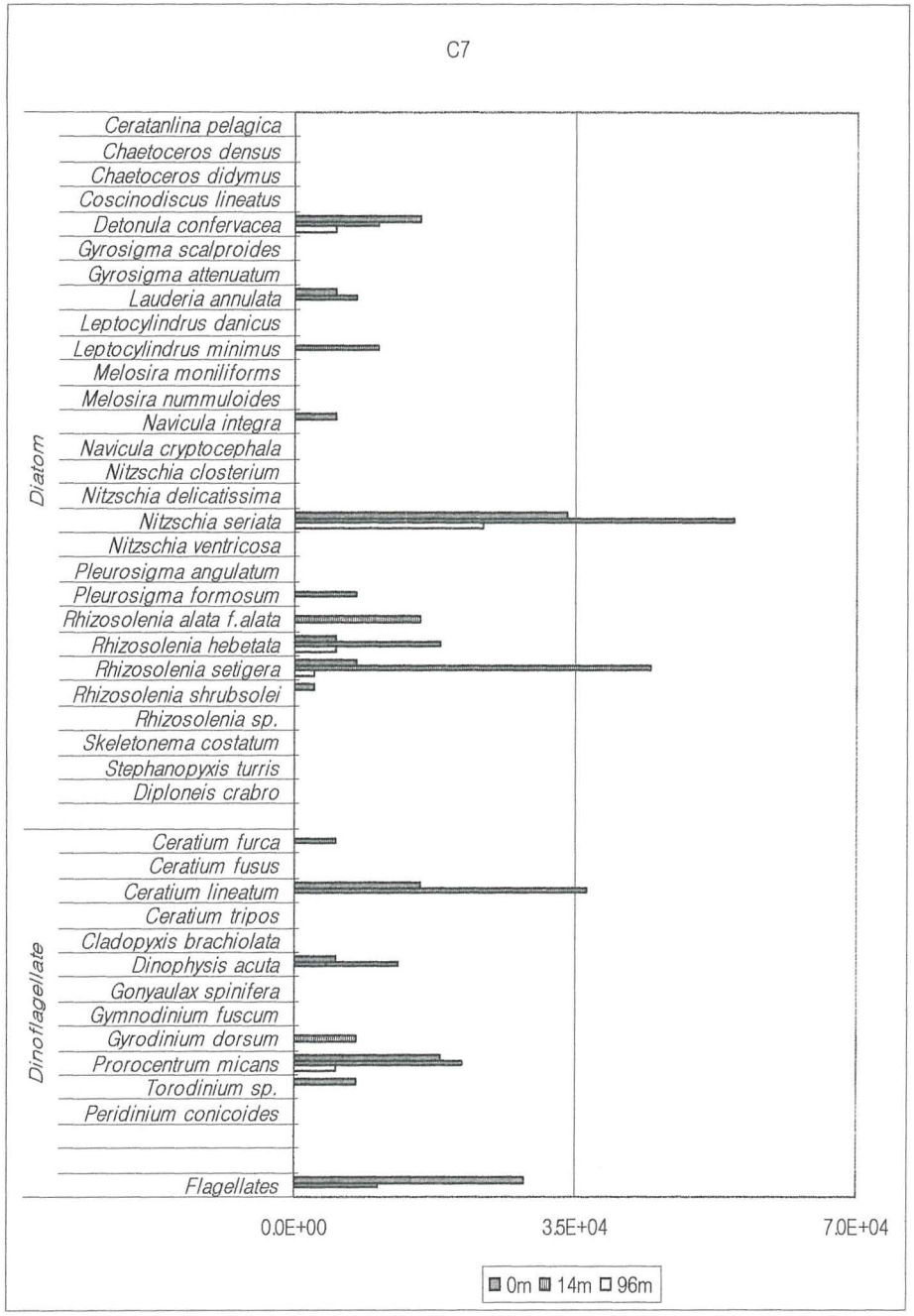

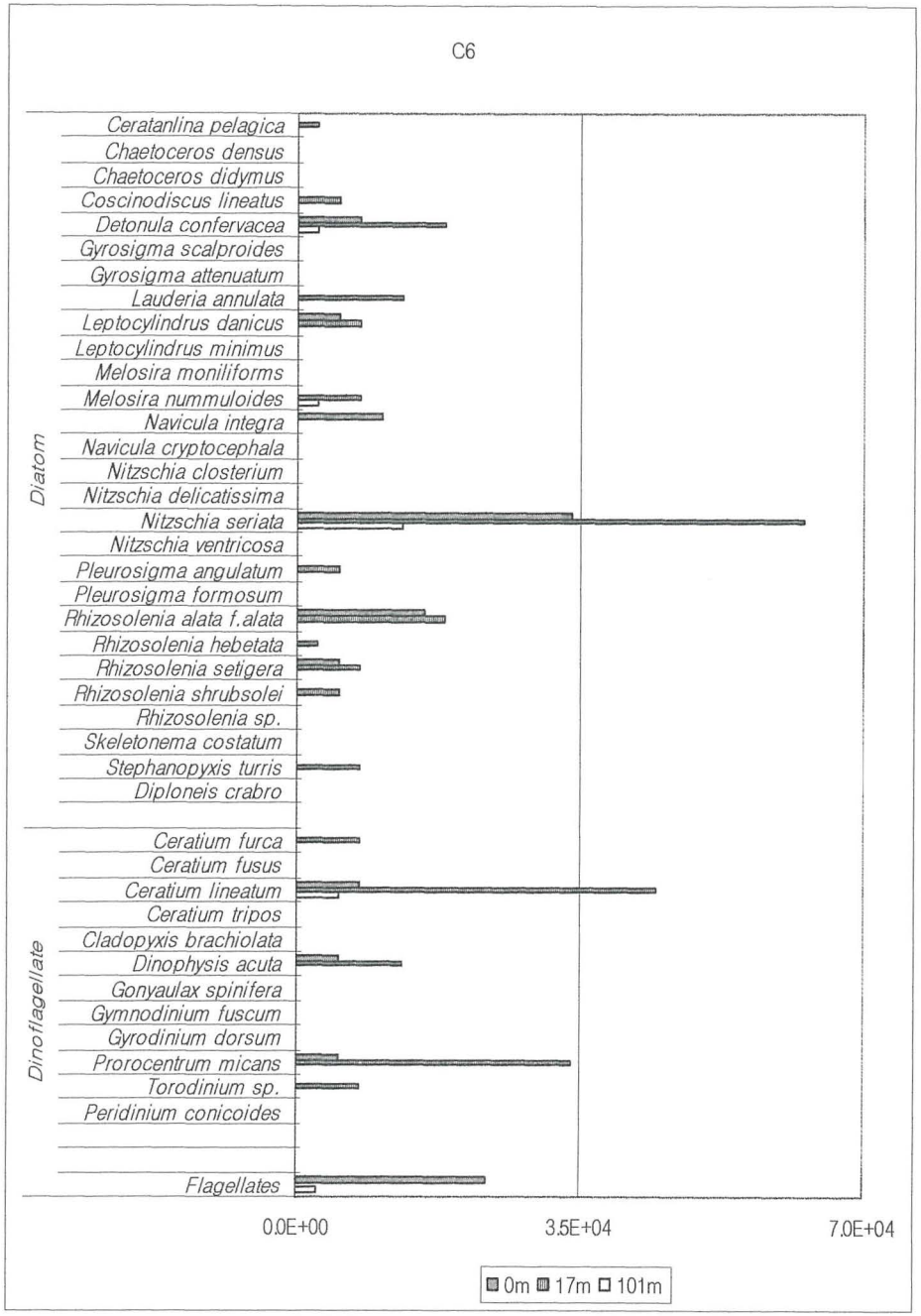

Appendix A-6 Celtic Sea Taxonomic data (No. of cells l^{-1}) 16-July-2002

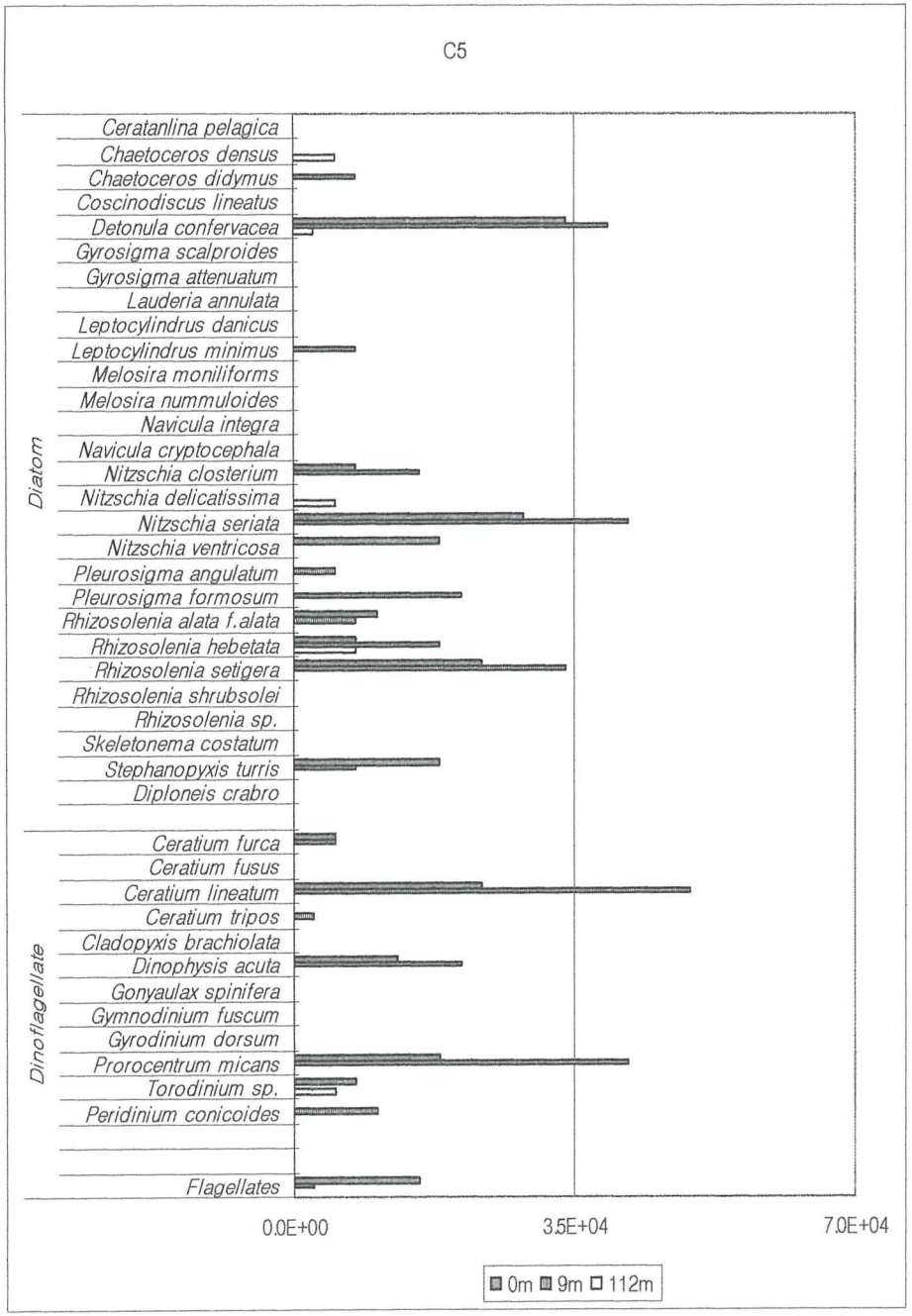

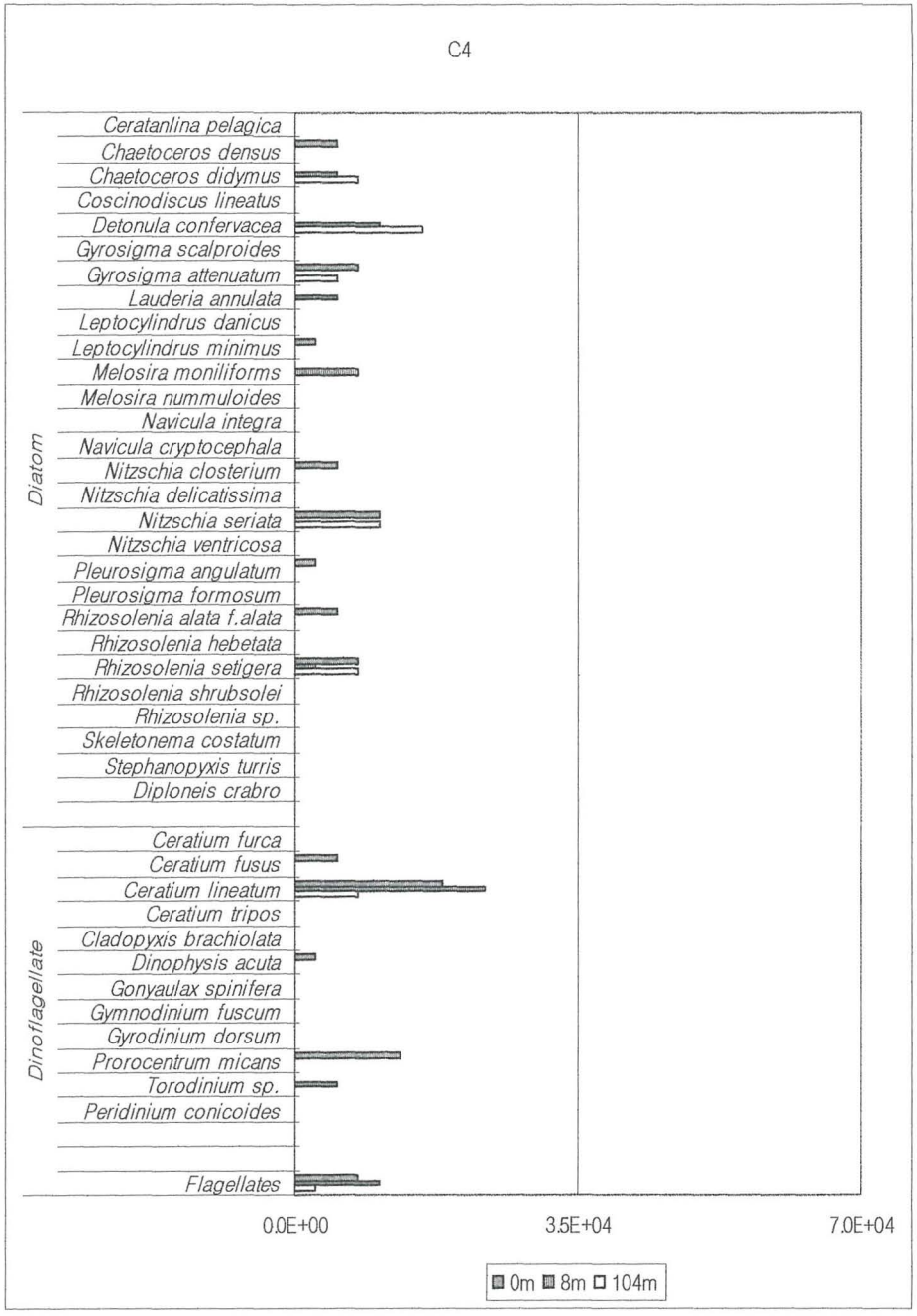

Appendix A-6 Celtic Sea Taxonomic data (No. of cells l^{-1}) 16-July-2002

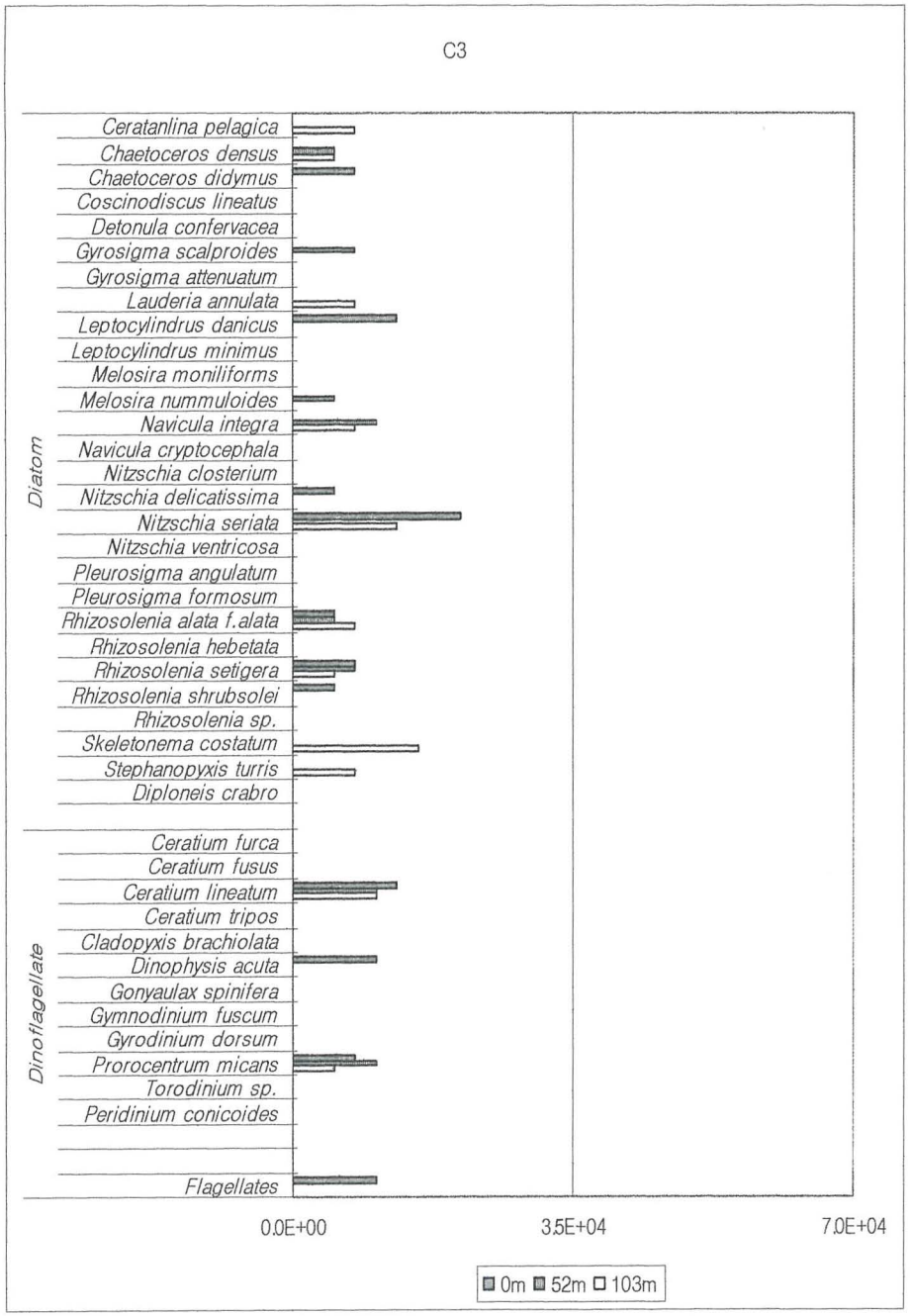

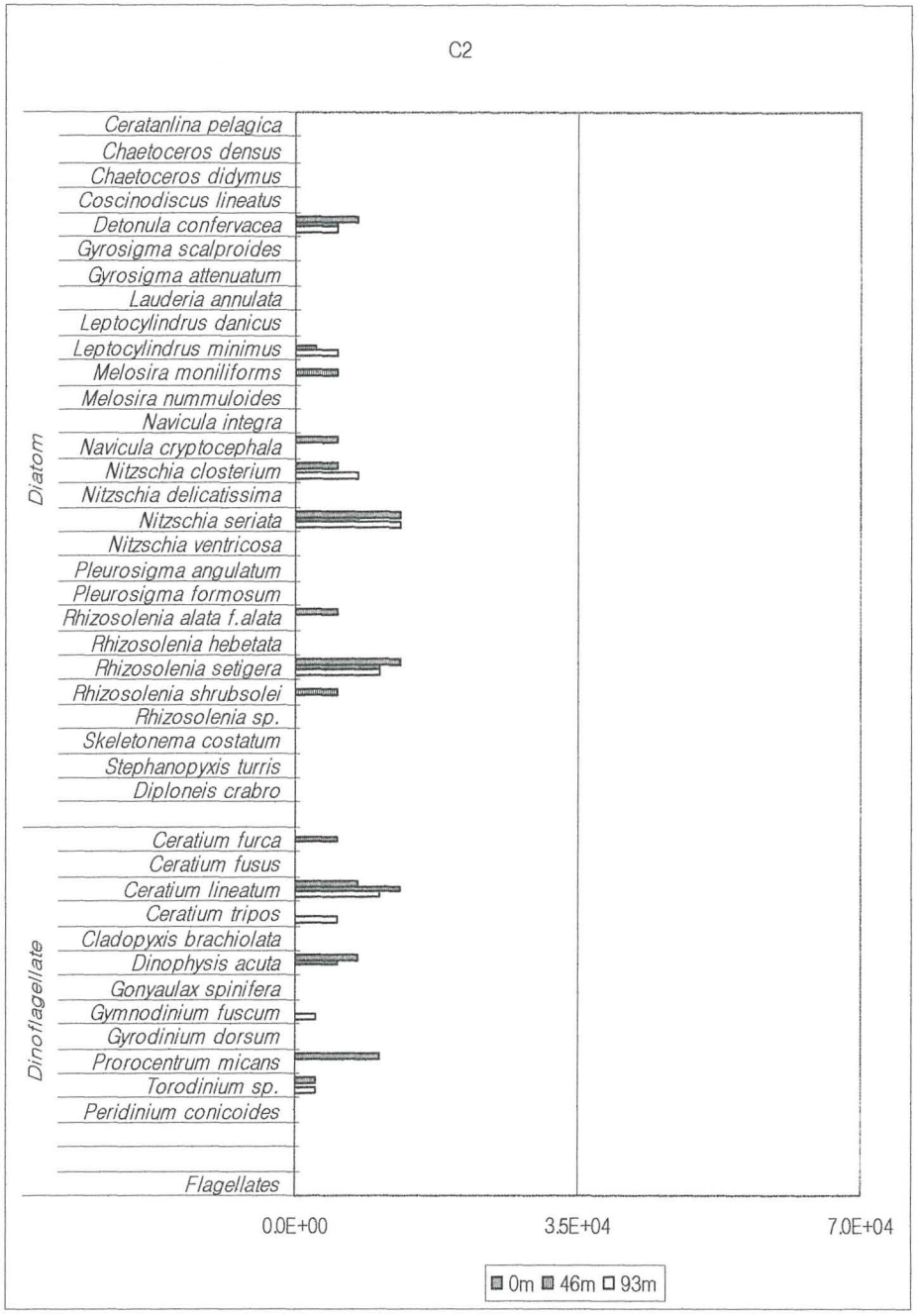

Appendix A-6 Celtic Sea Taxonomic data (No. of cells l^{-1}) 17-July-2002

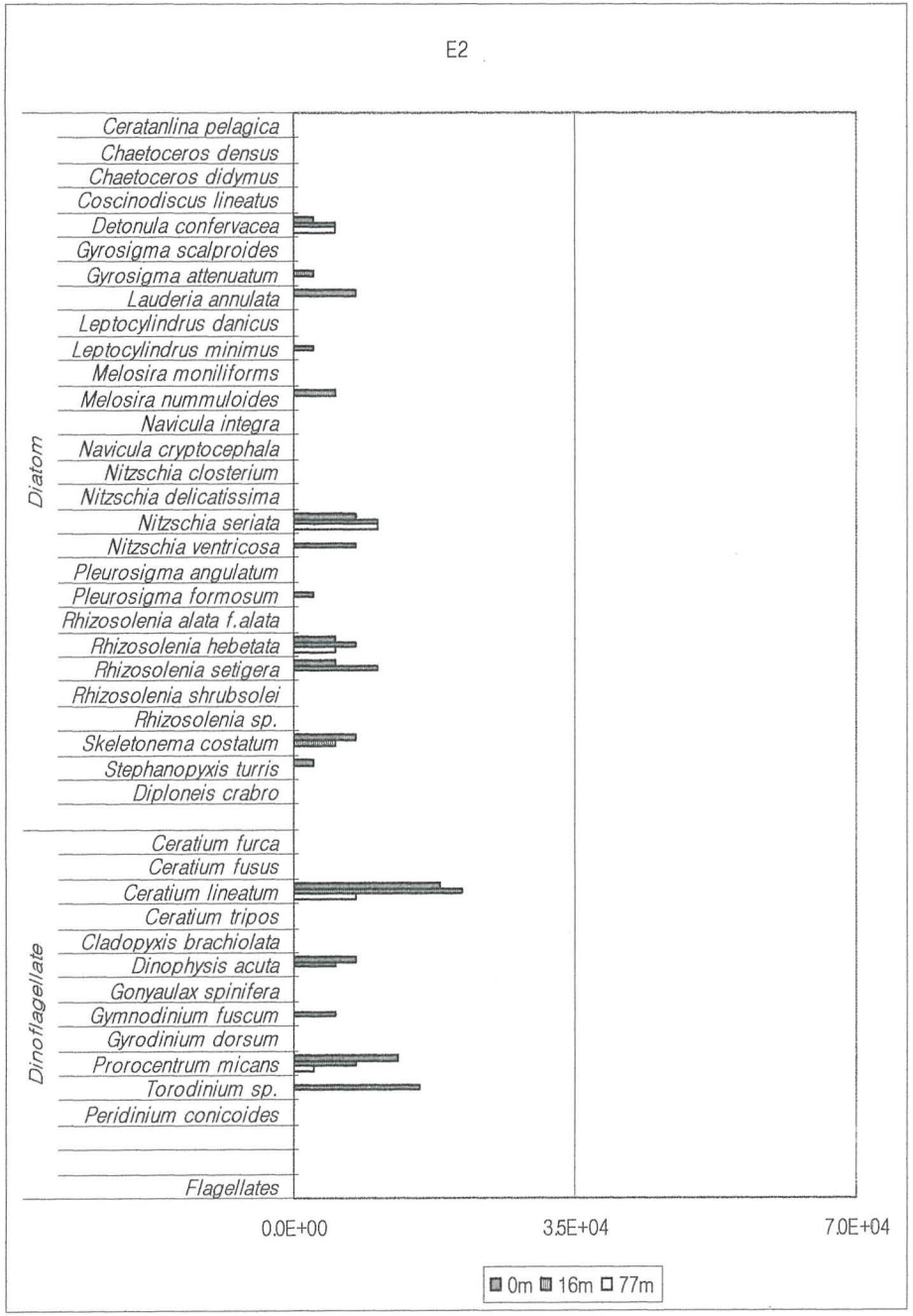

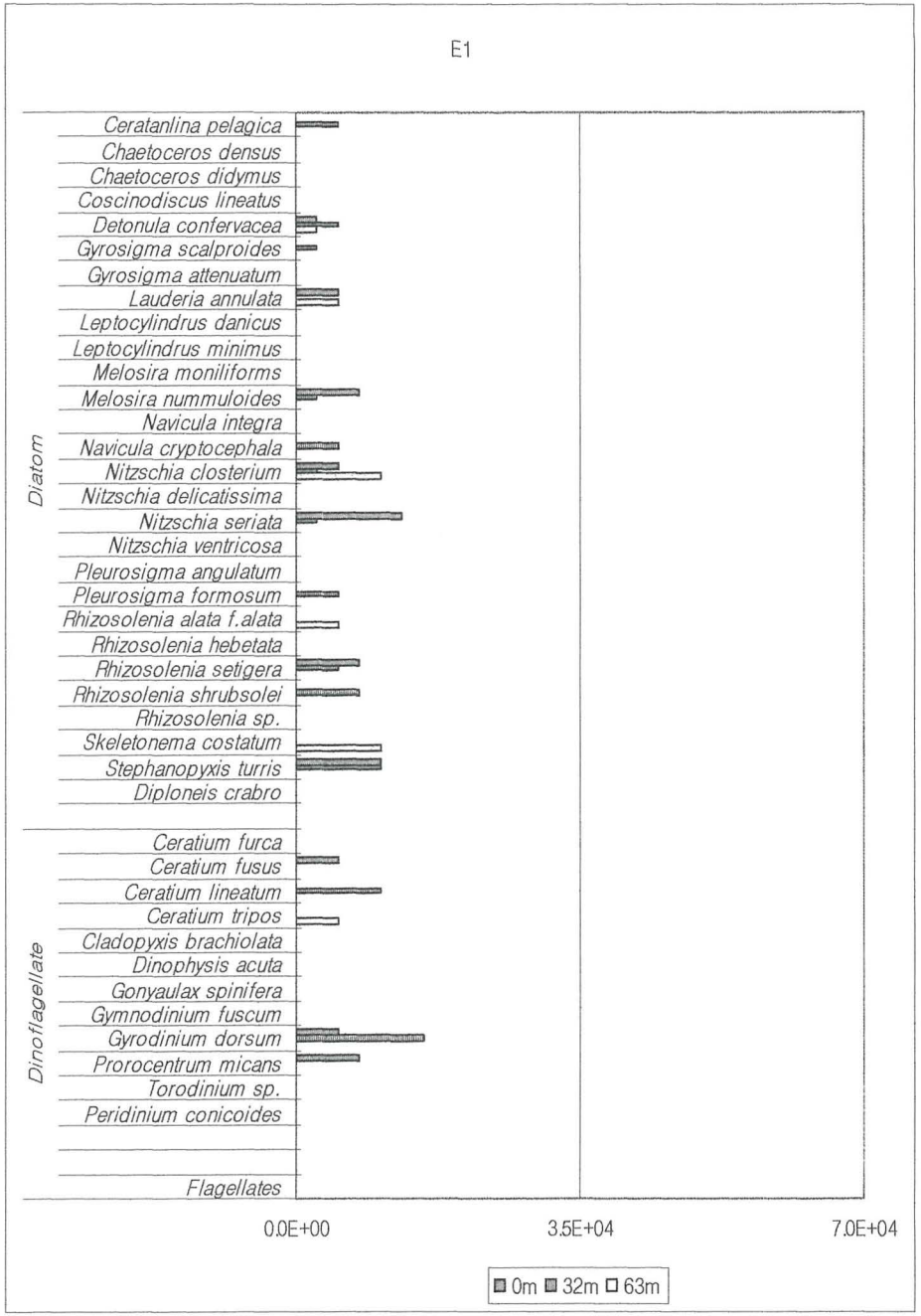

Appendix A-6 Celtic Sea Taxonomic data (No. of cells l^{-1}) 18-July-2002

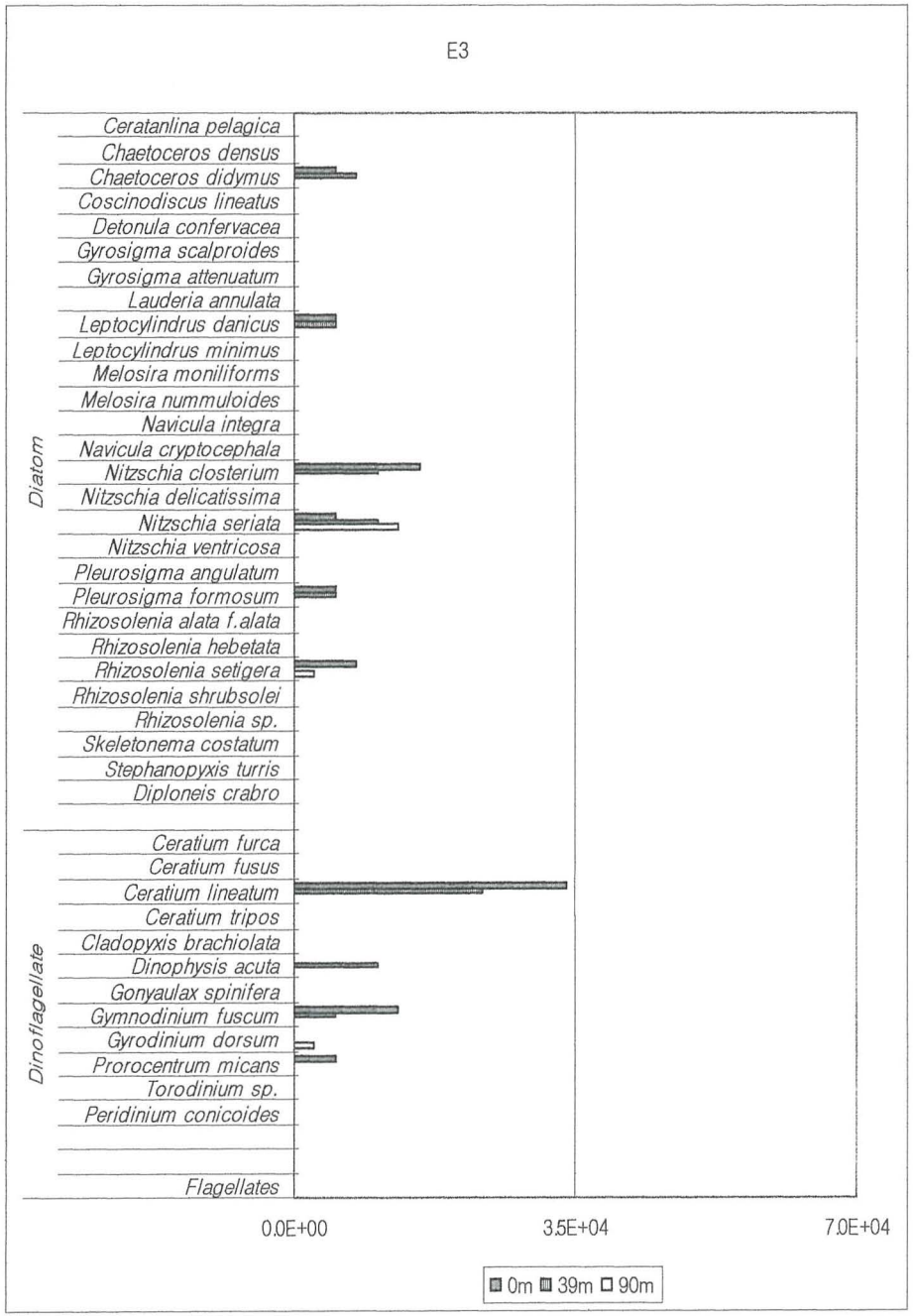

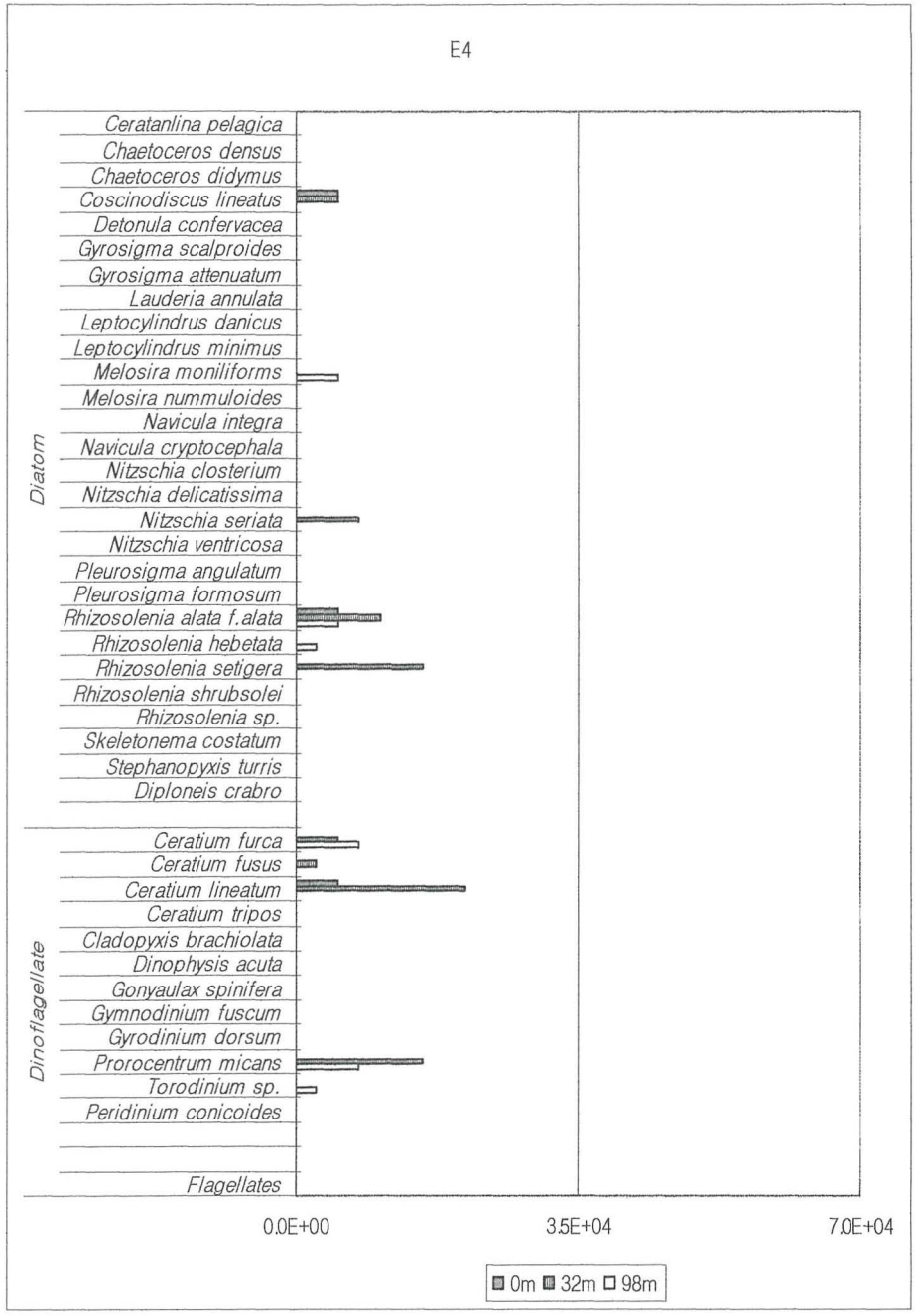

Appendix A-6 Celtic Sea Taxonomic data (No. of cells l^{-1}) 18-July-2002

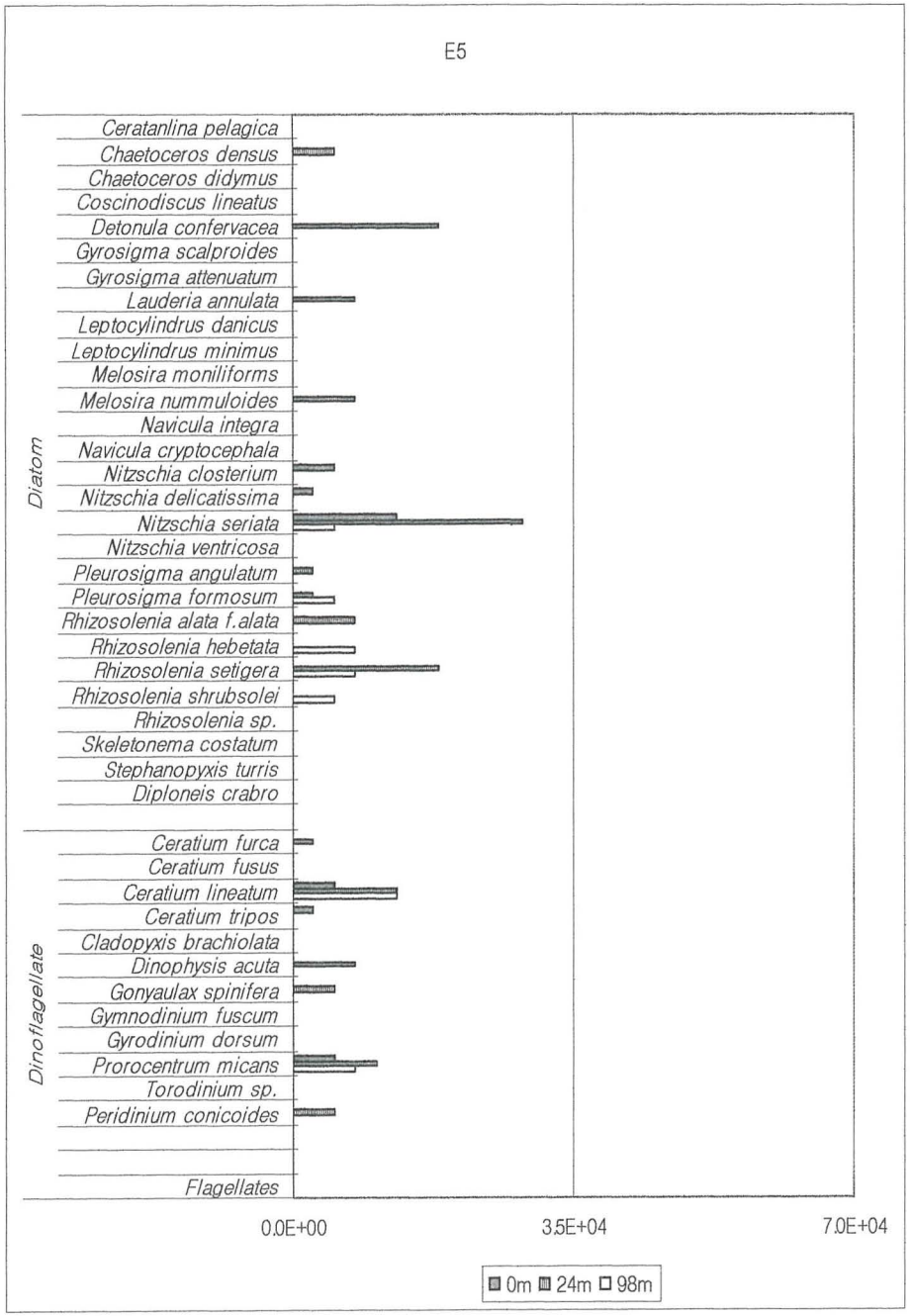

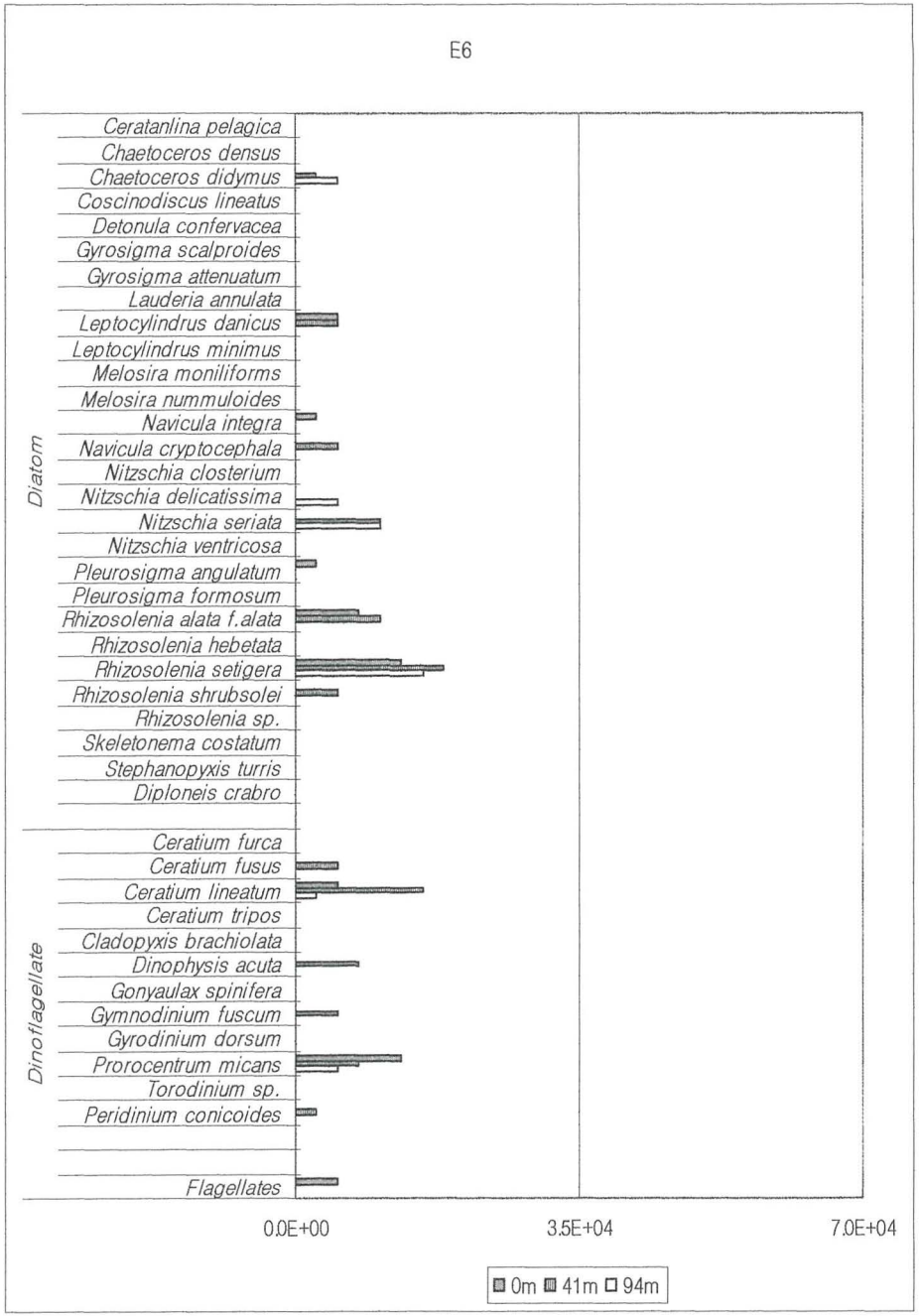

Appendix A-6 Celtic Sea Taxonomic data (No. of cells l^{-1}) 19-July-2002

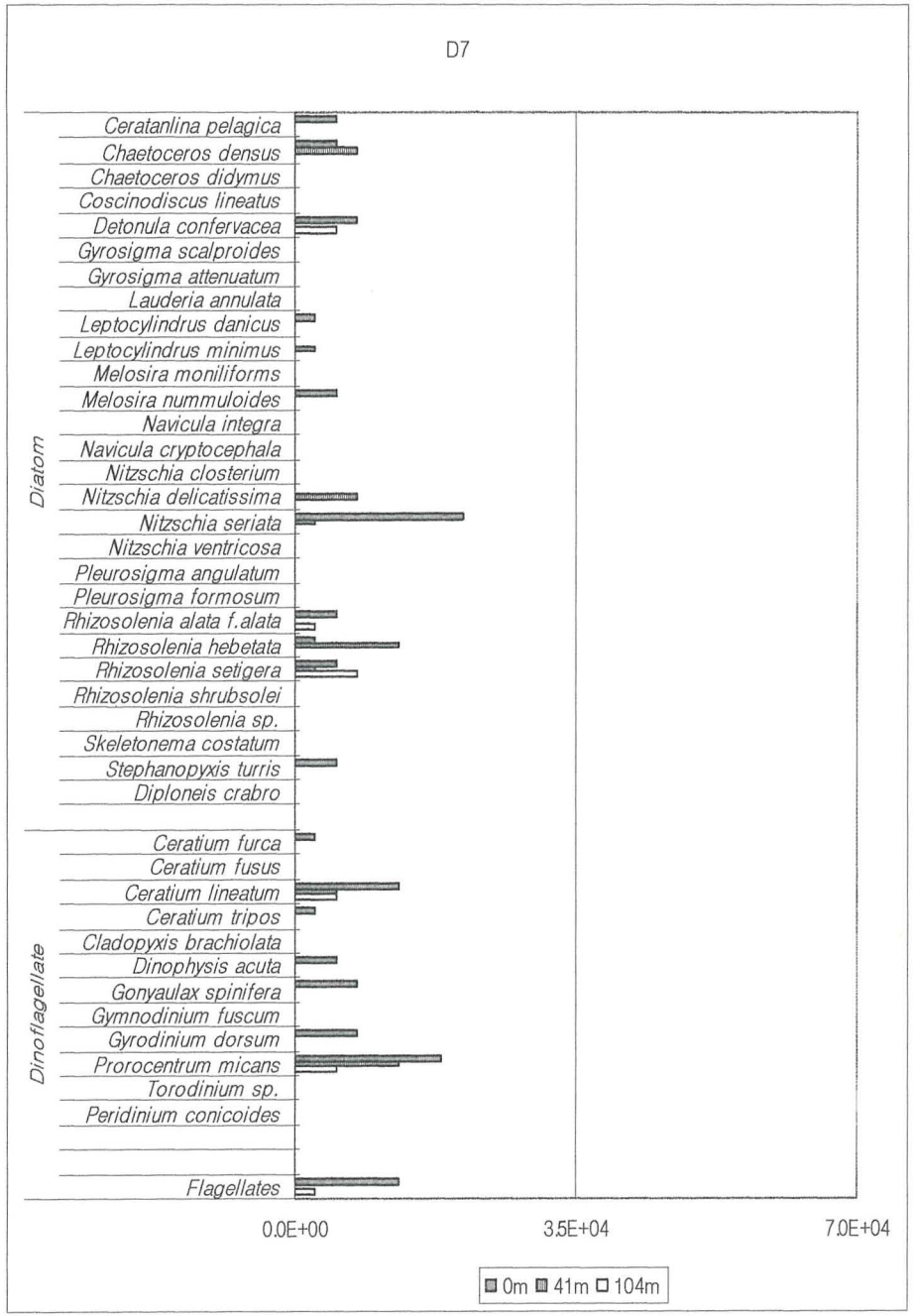

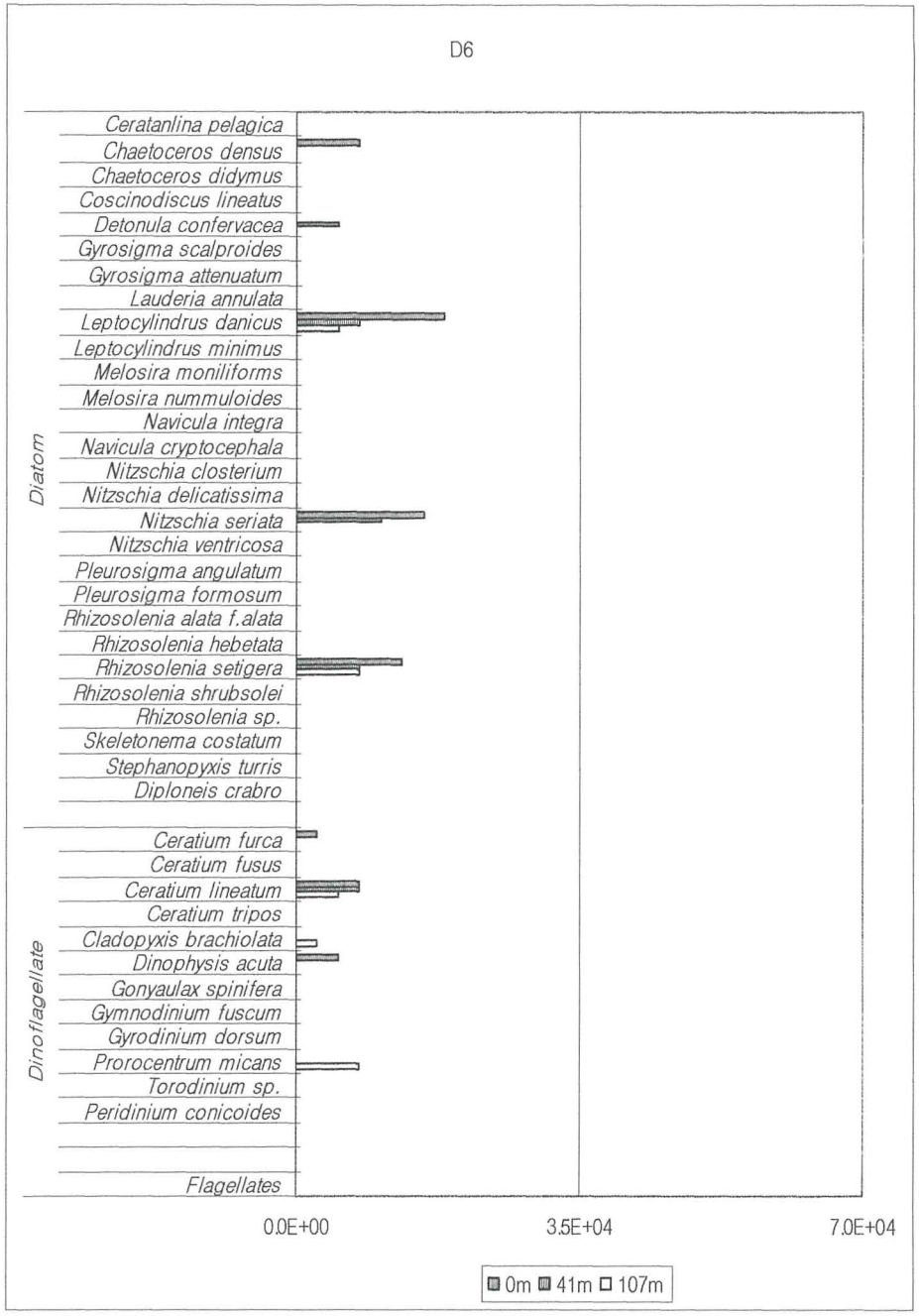

Appendix A-6 Celtic Sea Taxonomic data (No. of cells l^{-1}) 19-July-2002

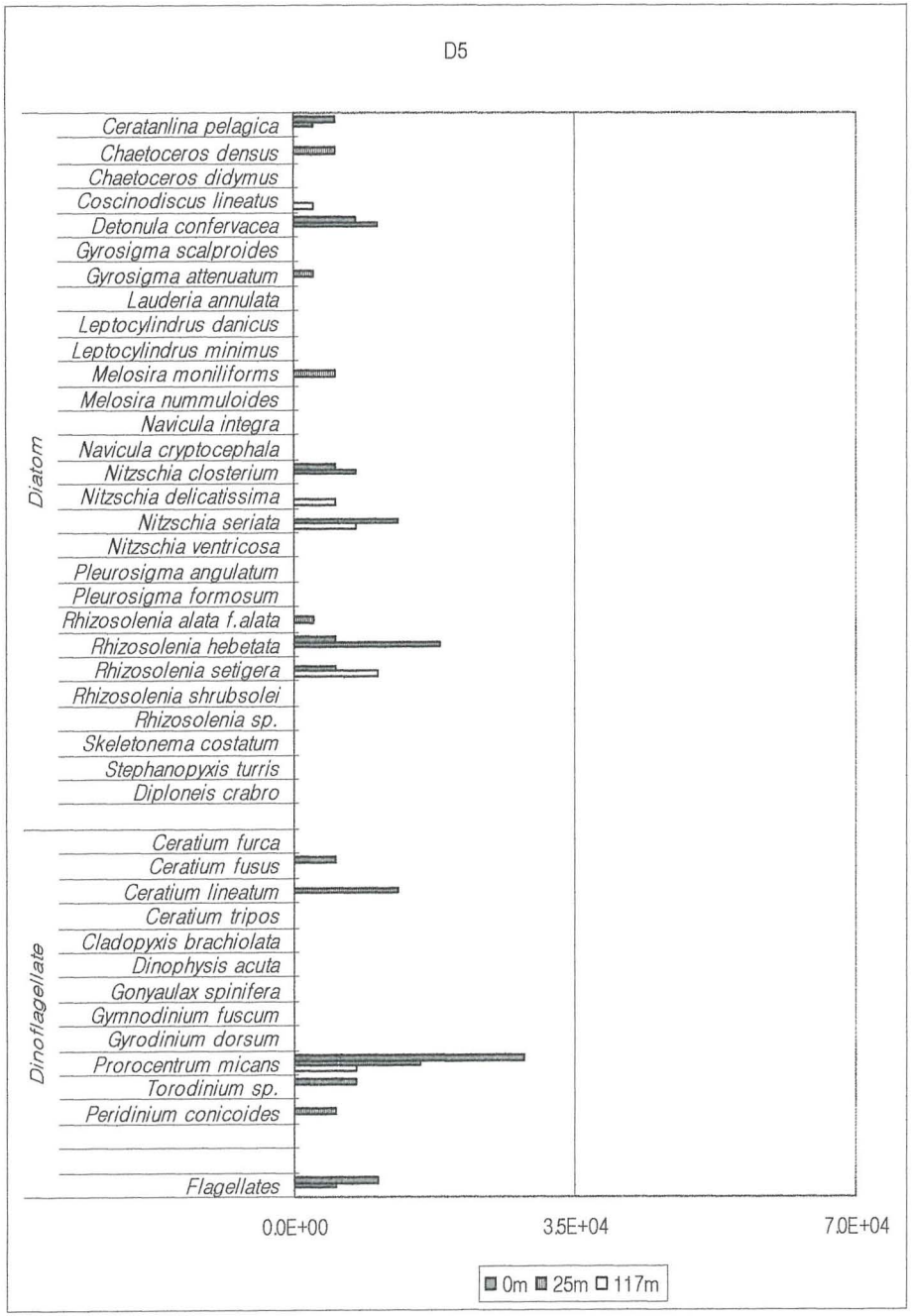

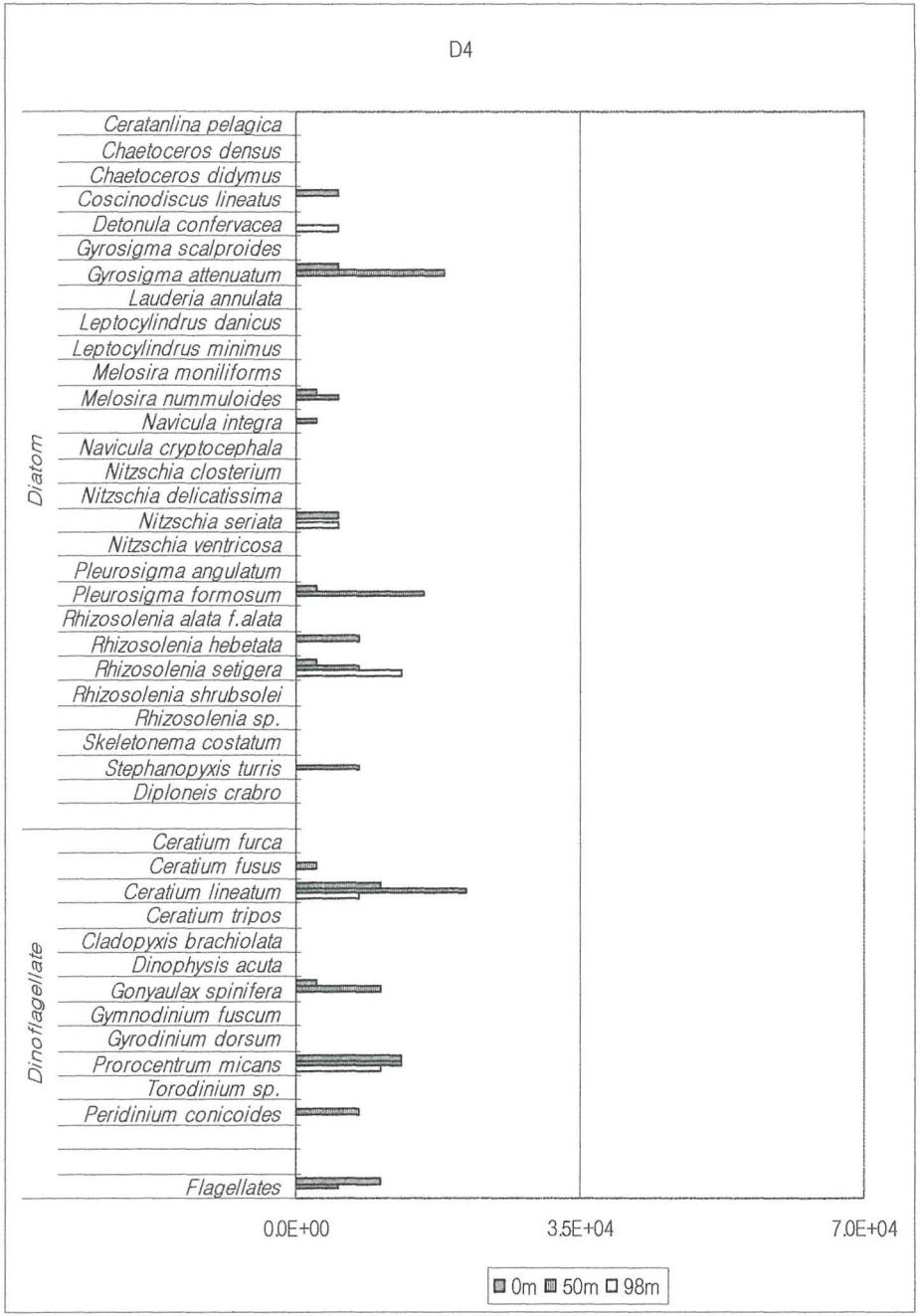

Appendix A-6 Celtic Sea Taxonomic data (No. of cells l^{-1}) 19-July-2002

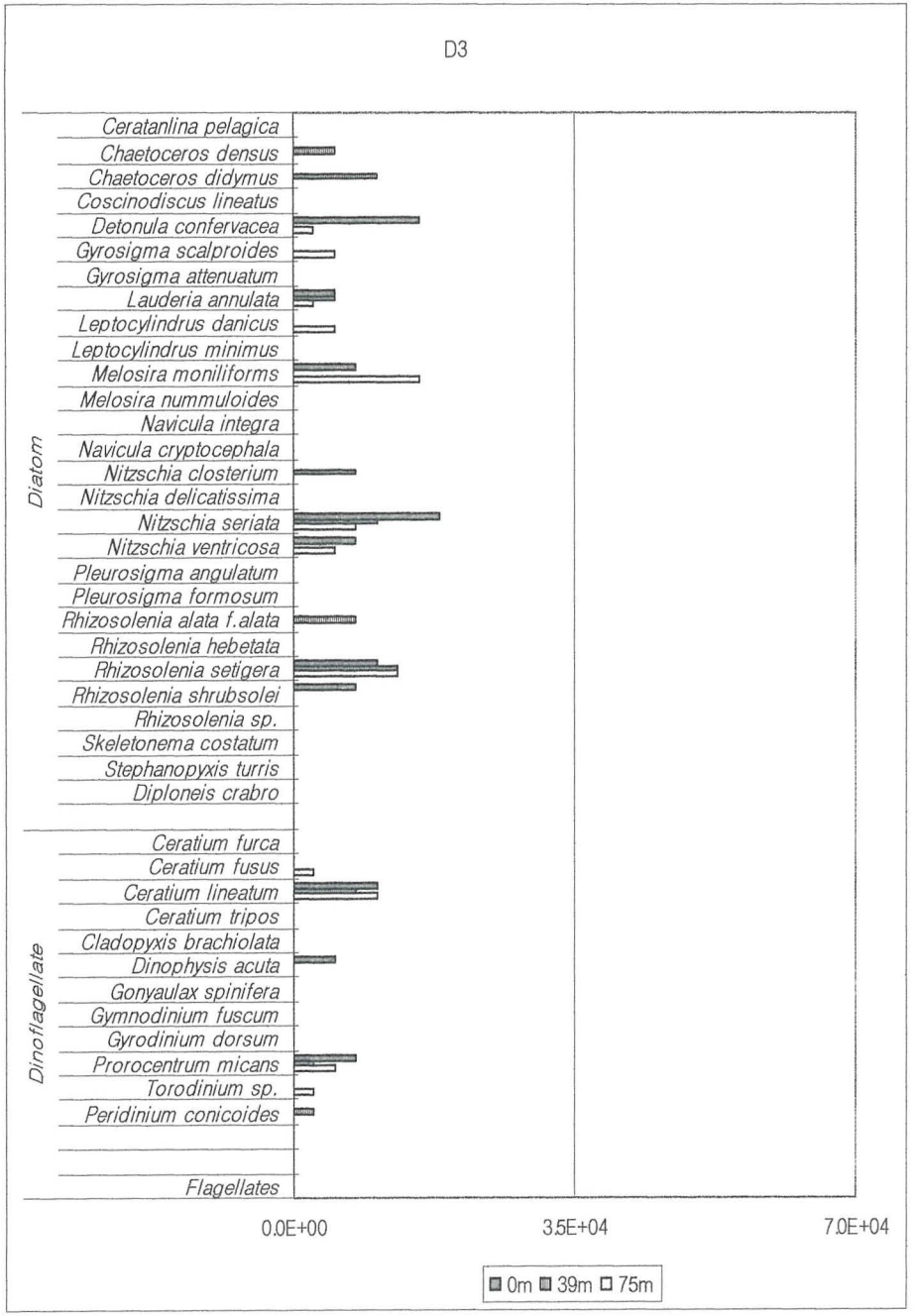

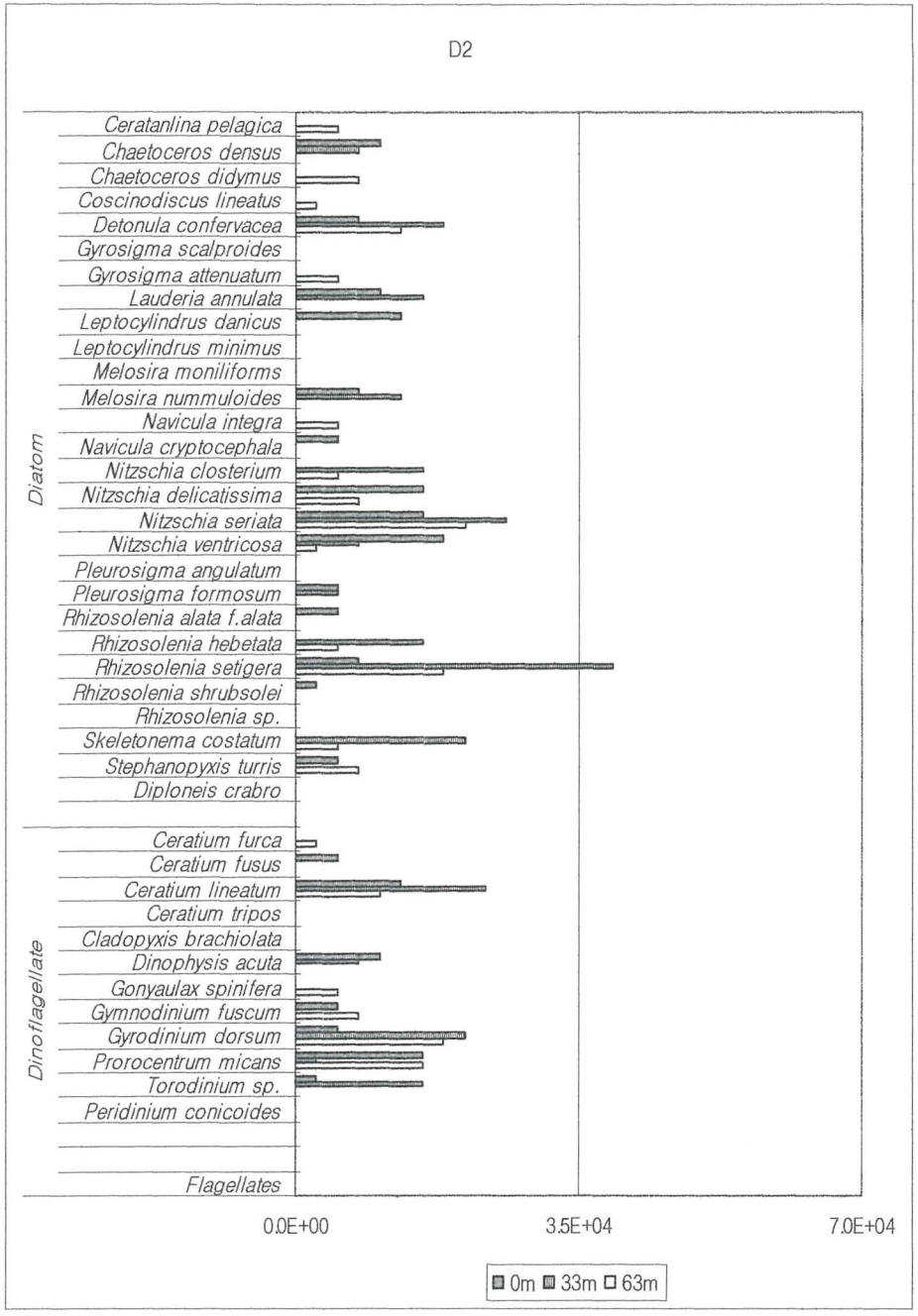

Appendix A-6 Celtic Sea Taxonomic data (No. of cells l^{-1}) 19-July-2002

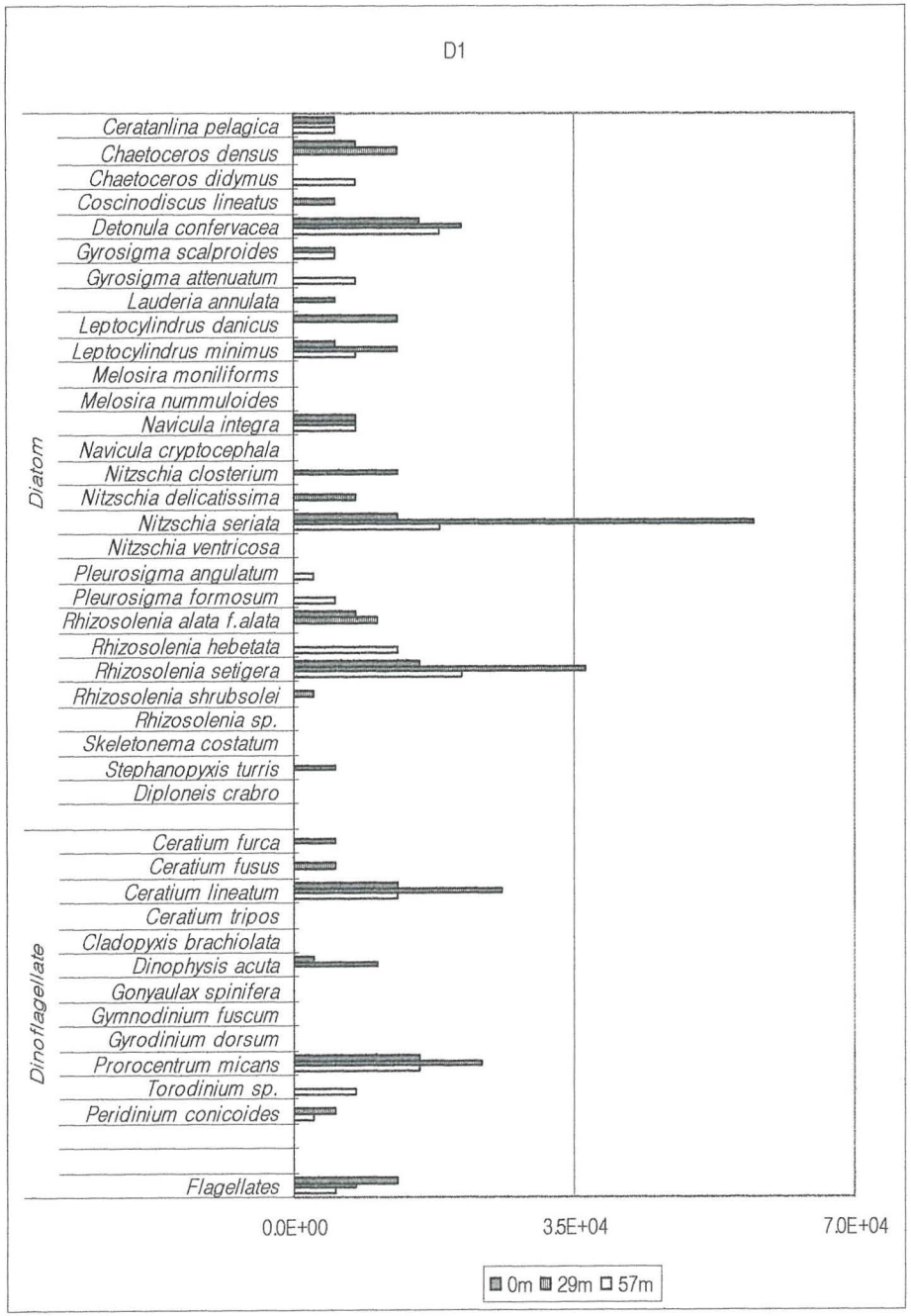

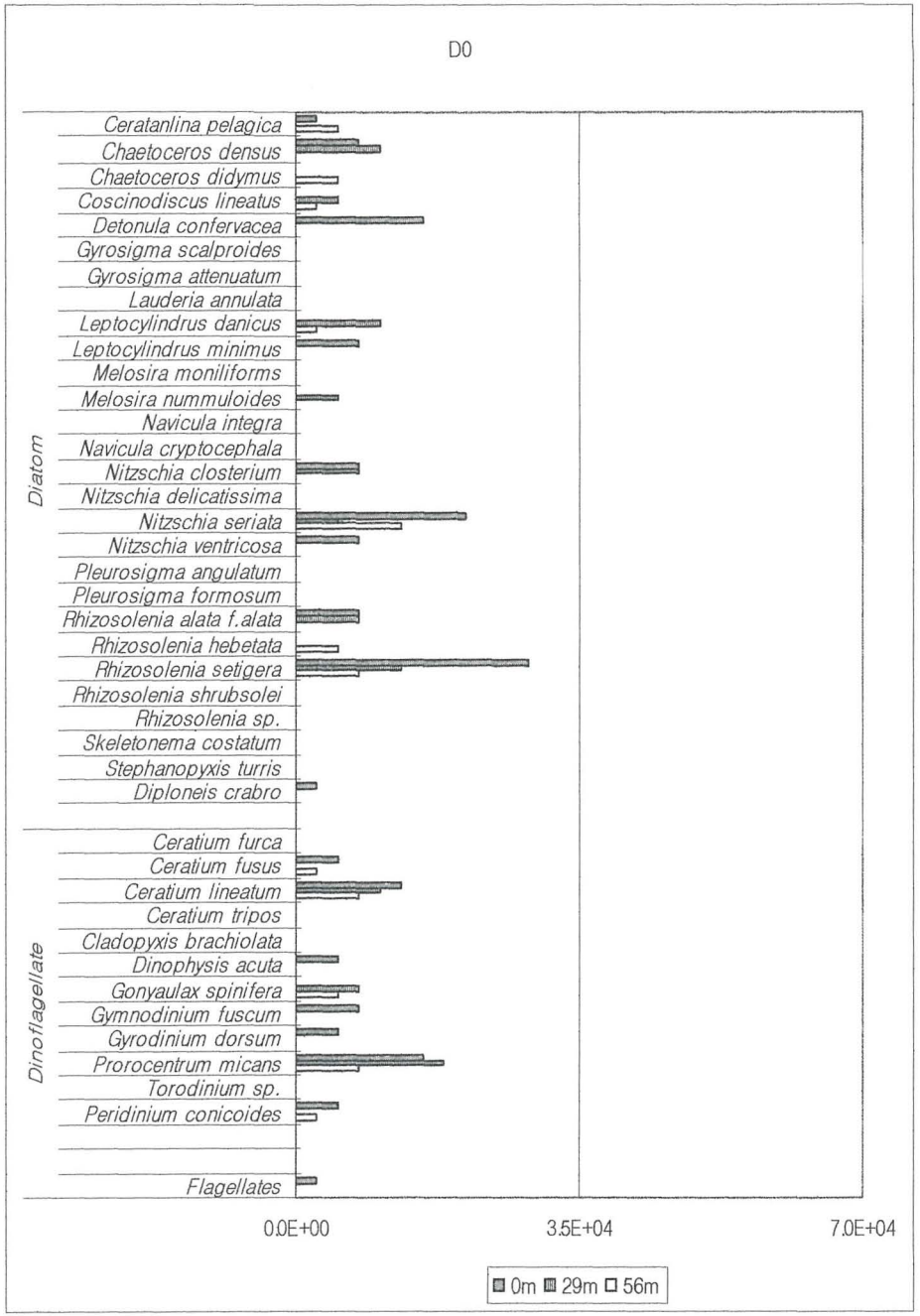

Appendix A-6 Celtic Sea Taxonomic data (No. of cells l^{-1}) 19-July-2002

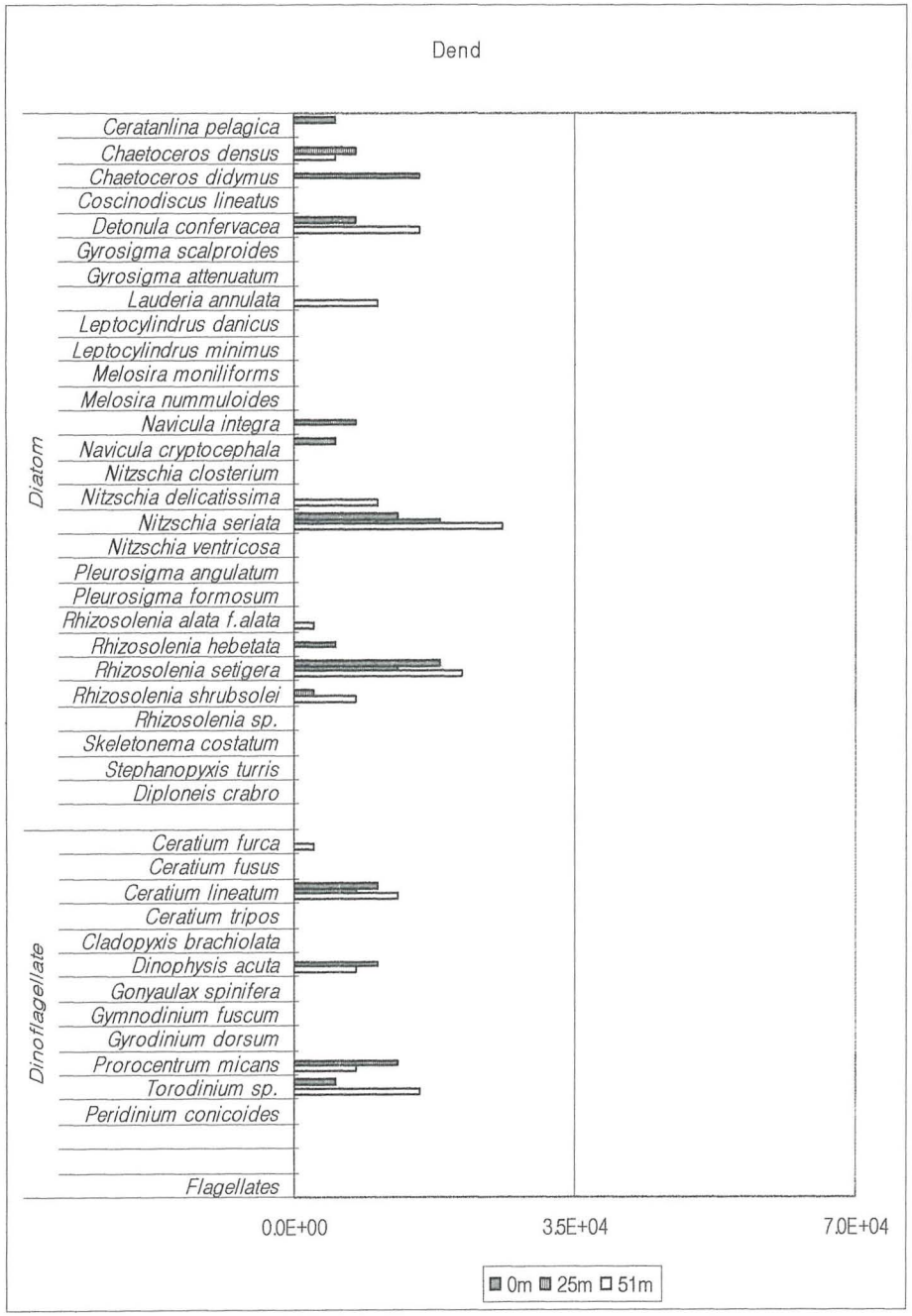

Appendix A-6 Celtic Sea Taxonomic data (No. of cells l^{-1}) 20-July-2002

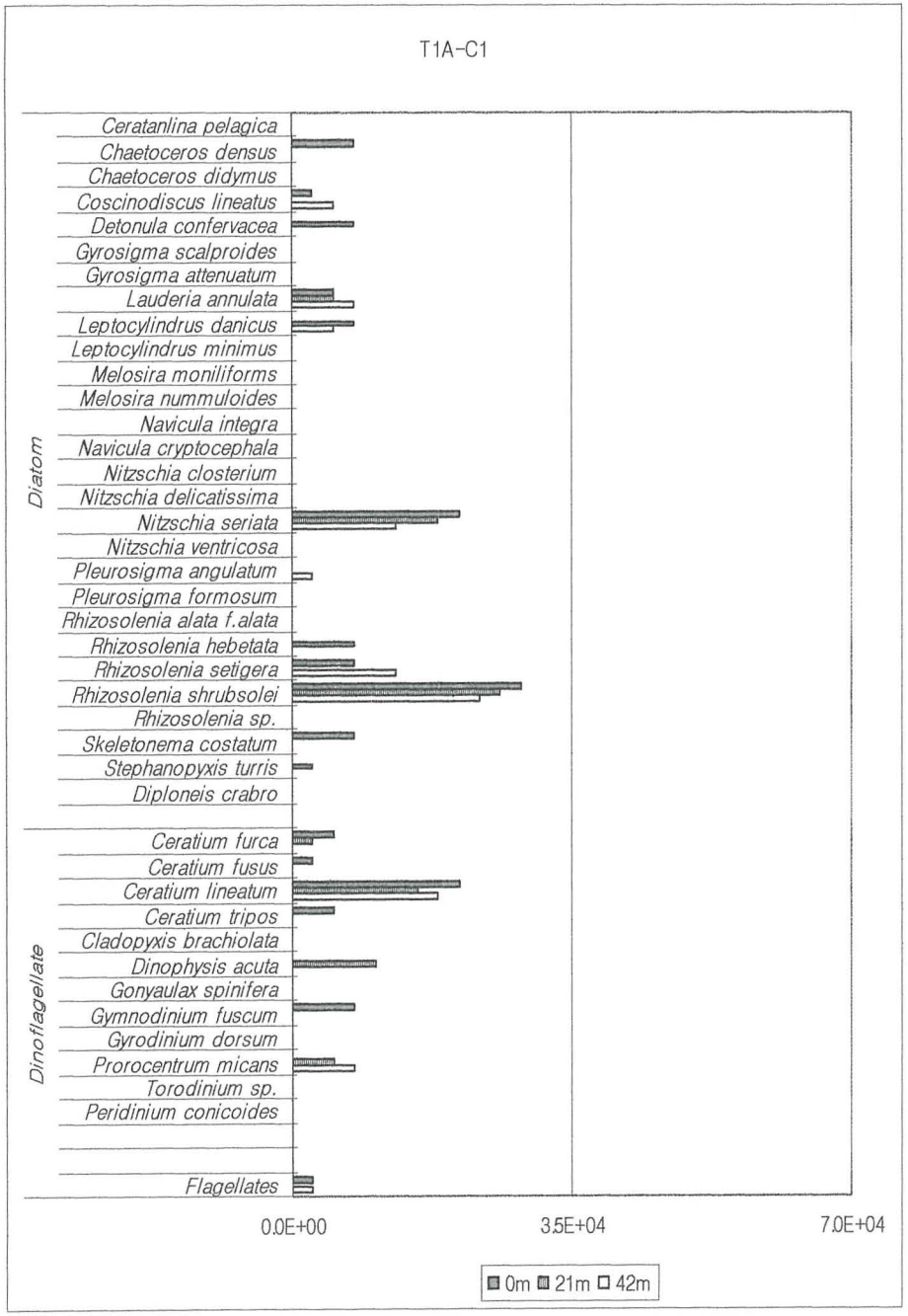

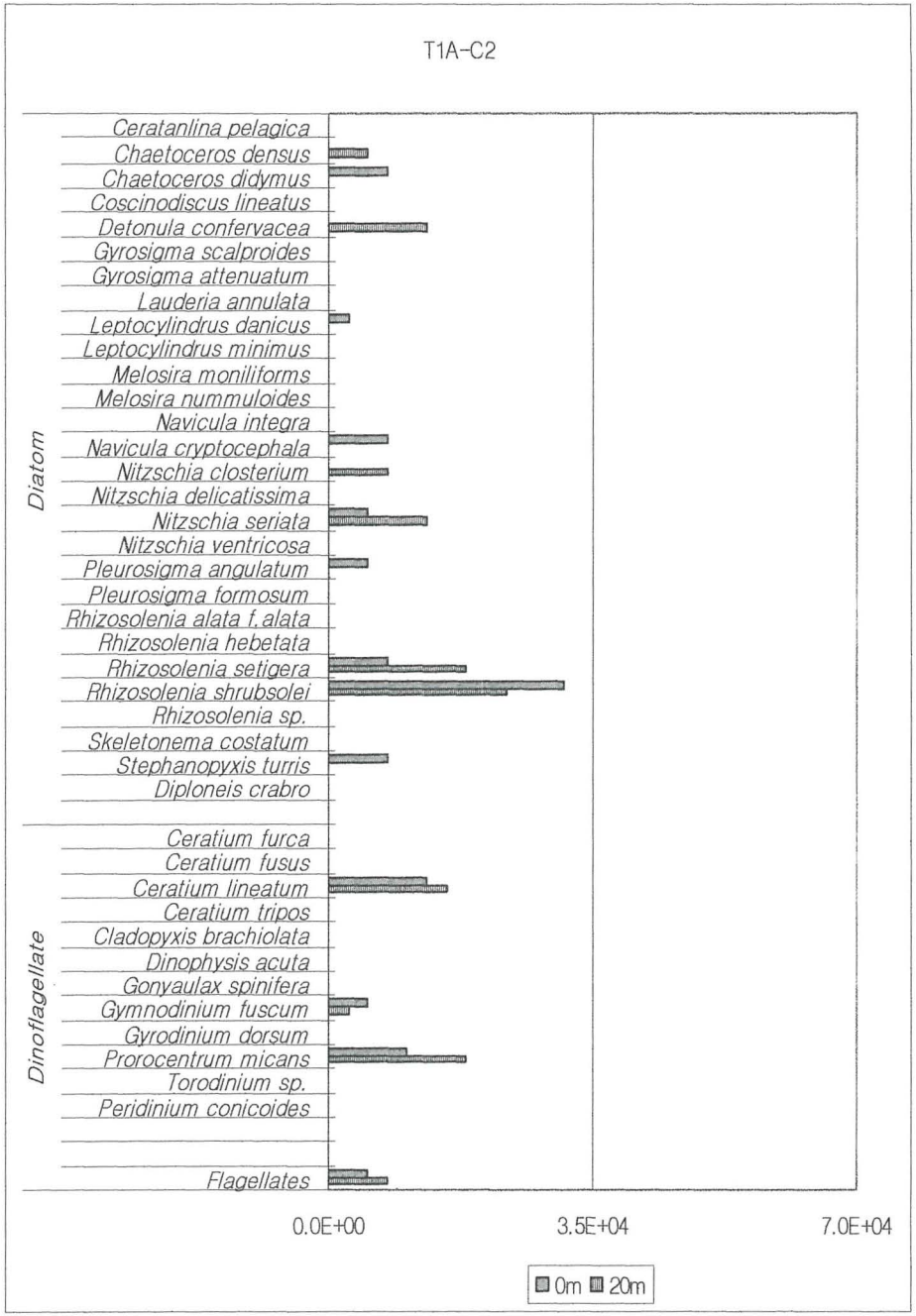

Appendix A-6 Celtic Sea Taxonomic data (No. of cells l^{-1}) 20-July-2002